The effect of transverse rotation and longitudinal translation between prosthetic components during the gait of unilateral trans-tibial amputees

M. TWISTE

Ph.D. Thesis   **2004**

The effect of transverse rotation and longitudinal translation between prosthetic components during the gait of unilateral trans-tibial amputees

MARTIN TWISTE

Institute for Health & Social Care Research

The School of Health Care Professions

University of Salford, United Kingdom

Submitted in partial fulfilment of
the requirements for the degree of
Doctor of Philosophy, May 2004

I.   <u>**TABLE OF CONTENTS**</u>

II.   LIST OF EQUATIONS

III.   LIST OF FIGURES

IV.   <u>**LIST OF TABLES**</u>

V.   ACKNOWLEDGEMENTS

In alphabetical order:

Alison Walker Twiste	-	General support
Bernard Noakes	-	Technical support
British Limbless Ex-Service Men's Association	-	Sponsorship
Chris Nester	-	Advisor & co-ordinator
Colin Smith	-	Technical support
Department of Health	-	Major funding source
Ernest Van Ross	-	Advisor
Jane Mickelborough	-	Information source
Jim Richards	-	Information source
John Bacon	-	Statistical support
Laurence Kenney	-	Advisor
Marianne Twiste	-	General support
North Sea Plastics Ltd	-	Sponsorship
Őssur Europe	-	Sponsorship
Peter Bowker	-	Co-supervisor
South Manchester University Hospital NHS Trust	-	Major funding source
Shyam Rithalia	-	Supervisor
Staff at Manchester Disablement Services Centre	-	Information source
Stefan Jedut	-	Technical support
Volunteering subjects	-	Test participants
William Walker	-	Technical support

amongst professions allied to medicine is a key part of the capability building component of those organisations' R&D strategy and the current study represents an emerging area of research that falls within that strategy.

The National Centre for Prosthetics is based at the University of Salford. Its geographical proximity to the local Manchester Disablement Services Centre (DSC), which is one of the largest facilities of this kind in the UK, allows existing research partnerships between trusts and universities to be strengthened for the development of clinically focused research. This is consistent with the two funding organisations' strategy to foster collaborations with other organisations, such as academic institutes, and they considered that the current study helped facilitate this process. Taking their limited budget into consideration, the NHS's commitment to funding this project demonstrates the need for research into prosthetics for evidence-based practice.

VI.   <u>DECLARATIONS</u>

This thesis contains part of the publications and presentations alphabetically listed below, whereby the corresponding authors and publishers gave permission for their material to be incorporated.

Mickelborough J. The biomechanics of gait initiation in normal elderly people and in patients with higher-level gait disorders associated with cerebral multi-infarct states. *PhD thesis*, University of Manchester, Manchester UK; 2001.

Twiste M, Kenney L, Smith C, Rithalia SVS. Measuring intersegmental prosthetic motion during gait using a cam. *International Society of Biomechanics XIXth Congress*, 2003 Jul 6-11; Dunedin, New Zealand.

Twiste M, Kenney L, Rithalia SVS. A cam design for measuring displacement between prosthetic segments. *Seventh International Symposium on the 3-D Analysis of Human Movement*, 2002 Jul 10-12; Newcastle upon Tyne, UK.

Twiste M, Rithalia SVS. Transverse rotation and longitudinal translation during prosthetic gait - a literature review. *J Rehab Res Dev* 2003;40(1):9-18.

Twiste M, Rithalia SVS, Kenney L. Displacement measurements at a torque-shock absorber during amputee gait. *The 11th World Congress of the International Society for Prosthetics & Orthotics*, 2004 Aug 1-6; Hong Kong, China (accepted).

Twiste M, Rithalia SVS, Kenney L. A cam-displacement transducer device for measuring bi-plane prosthetic motion. *Medical Engineering & Physics* 2004;26(4):335-40.

Twiste M, Rithalia SVS, Kenney L. An electromechanical device for measuring intersegmental prosthetic motion. In: Nester C, Kenney L, editors. *Proceedings of the Conference of Biomechanics of the Lower Limb in Health, Disease and Rehabilitation;* 2003 Sep 1-3; Salford, UK. ISBN: 0-902896-51-2 p. 14-5.

VII.   <u>ABBREVIATIONS</u>

The majority of abbreviations are defined in their singular form and those within the main body of this manuscript that are followed immediately by a small "s" should be interpreted in their plural form.

2D…3D	-	Two…Three Dimensions
ANOVA	-	Analysis Of Variance
ASIS	-	Anterior Superior Iliac Spine
A/D	-	Analogue/Digital
BAPO	-	British Association of Prosthetists and Orthotists
BNC	-	Bayonet Neill Concelman
BSK	-	Blatchford Stabilised Knee
CAST	-	Calibration Anatomical Systems Technique
c	-	Cosine
COM	-	Centre Of Mass
COP	-	Centre Of Pressure
COR	-	Centre Of Rotation
CsOP	-	Centres Of Pressure
DSC	-	Disablement Services Centre
EMG	-	Electromyographic
F	-	Foot
FSR	-	Force Sensing Resistor
GRF	-	Ground Reaction Force
GRM	-	Ground Reaction Moment
HPC	-	Health Profession Council
HS	-	Heel Strike
ISB	-	International Society of Biomechanics
ISO	-	International Standard Organisation
L	-	Left
LCD	-	Liquid Crystal Display
LED	-	Light Emitting Diode

LREC	-	Local Research Ethical Committee
LT	-	Longitudinal Translation
LTn	-	Longitudinal translation No
LTy	-	Longitudinal translation Yes
NHS	-	National Health Service
PC	-	Personal Computer
PCB	-	Printed Circuit Board
POA	-	Point Of Application
PsOA	-	Points Of Application
PSIS	-	Posterior Superior Iliac Spine
PTB	-	Patellar Tendon Bearing
PTFE	-	Polytetrafluoroethylene
PVC	-	Polyvinylchloride
QTM	-	Qualisys Track Manager
R	-	Right
R&D	-	Research And Development
RAM	-	Random Access Memory
RiiOG	-	Radii Of Gyration
RusOG	-	Radius Of Gyration
ROM	-	Range Of Motion
RMS	-	Root Mean Square
S	-	Shin
s	-	Sine
SACH	-	Soft Ankle Cushion Heel
SFESK	-	Stanceflex Endolite Stabilised Knee
T	-	Thigh
TO	-	Toe Off
TR	-	Transverse Rotation
TRn	-	Transverse Rotation No
TRy	-	Transverse Rotation Yes
TSV	-	Tab Separated Values
TSB	-	Total Surface Bearing
TT Pylon	-	Telescopic Torsion Pylon
VSP	-	Vertical Shock Pylon
+ve	-	Positive

VIII.   <u>UNITS</u>

°	-	degree
°C	-	degree Celsius
dB	-	decibel
g	-	gram
Hz	-	Hertz
kg	-	kilogram
kg	-	kilogram per millimetre
kHz	-	kilo Hertz
km/h	-	kilometers per hour
kΩ	-	kilo Ohm
kPa	-	kilo Pascal
lbin	-	pound inch
m	-	metre
$m^2...m^3$	-	square…cubic metre
ms^{-2}	-	metre per second squared
MB	-	megabytes
MHz	-	mega Hertz
MΩ	-	mega Ohm
µs	-	microsecond
mm	-	millimetre
m/s	-	metre per second
mW	-	milli Watts
Nm	-	Newton meter
Nm/°	-	Newton meter per degree
Ω	-	Ohm
pC	-	picocoulombs
pC/N	-	picocoulombs per Newton
pC/s	-	picocoulombs per second
s	-	second
V	-	Volt

IX. __ABSTRACT__

During stance phase of amputee gait, considerable forces are transmitted across the residual limb-socket interface. These loads and associated gait patterns can be altered by introducing compliant elements into the prosthesis. However, previous studies have failed to adequately describe the effects that components with such compliances have on amputee gait. In particular, despite manufacturers' claims, it was not yet clearly demonstrated that the use of those devices results in clinical improvements regarding the loads on the residual limb. This thesis addresses such a lack of evidence in order to establish whether or not compliant elements are beneficial for amputee gait and the reduction of residual limb-socket interface pressures.

Devices with compliant elements allow two types of motion including angular and linear displacements around and along the longitudinal axis of a prosthesis. Whether they affect the gait pattern and loads on the residual limb was determined by permitting these displacements separately, together and not at all during gait tests. Customised prostheses and measuring equipment were specifically designed and manufactured. Data were collected with regard to lower limb motion, ground reaction forces, displacements at the device with compliant elements and residual limb-socket interface pressures. Purpose-written programs served to process the data for calculating appropriate gait parameters.

The results showed that when mobility of the described device with the compliant elements was permitted, in-socket pressures were reduced. This demonstrated that both angular and linear displacements have a positive effect on amputee gait parameters, and this was even more beneficial when these two motions were combined. Particularly advantageous was the delay and decrease in peak ground reaction forces that consequently lowered shock impacts. In conclusion, the current investigation demonstrated that the two compliant elements have the potential for reducing the risk of damaging residual limb tissues.

CHAPTER 1.   <u>INTRODUCTION</u>

In addition to the restoration of aesthetic factors, the main goal for the majority of prostheses is to simulate the functional aspects of the missing limb. This requires components that allow motion between artificial segments as, for instance, mechanical ankle joints do, and this should also help to maintain forces within physiological limits. Companies producing prosthetic devices continuously release new hardware that permit and control passive motions with ever increasing complexity, but very few back their products' performance characteristics up with scientific findings. In a rehabilitation environment, prescriptions are therefore frequently based on intuition rather than rigorous research results, and this makes it difficult for clinicians to conduct evidence-based practice.

One type of component that flooded the prosthetic market over approximately the last ten years is often being referred to as a "torque-shock absorber". Its design introduces elastic elements into what is normally a rigid part of the artificial limb, namely the pylon or shin section that connects proximal parts of the prosthesis to the foot. The resultant compliance allows the socket, containing an amputee's residual limb, to displace relative to the replacement foot. The characteristics of a device with elastic elements seem to have the potential for amputees to benefit from due to more mobility within the prosthesis, and the low cost of such a device makes it an attractive alternative to other more expensive components.

Two types of motions are possible with such a device including angular displacements in a transverse plane and linear displacements in a combined sagittal and coronal plane. Instead of maintaining the same prosthesis alignment throughout stance phase, this sort of elasticity makes it more likely for the socket to follow the residual limb's natural tendency to move while carrying the body weight. Some manufacturers claim that the resultant dampening due to an increase in compliance within the prosthesis minimises movements between the socket and the residual limb. This is supposed to delay and therefore lower peak forces, thus reducing shear stresses and impact forces acting on the residual limb.

It is recognised that prolonged exposure to shear and/or compressive stresses can lead to tissue damage, so the goal of reducing these is justifiable. This is of particular importance to amputees who have lost a limb due to an underlying pathology rather than trauma, because these amputations are often associated with poor peripheral circulation and a loss of sensation in the residual limb. In these cases, the onset of tissue damage may occur earlier than in those related to trauma and they are often not easily recognised. This can lead to severe problems, including re-amputation. In other amputee populations such as the high activity group, the risk of tissue breakdown is also present due to the increased dynamic loads.

A prosthetic component that permits angular displacements in a transverse plane and linear displacements in a combined sagittal and coronal plane between the proximal parts of the prosthesis and the foot can, in a limited manner, replicate some of the kinematic freedom at joints in the anatomic foot. When studying the literature, it becomes clear that some design criteria for such prosthetic components were reported on for decades. Although a lot of newer devices have dual functions in that they allow angular or linear motion simultaneously, others exist that can only undergo one motion or the other, but rarely were any of these thoroughly assessed. Gait changes found in some studies that dealt with dual function adapters, have been attributed to the effect of linear displacements alone, but in the majority of cases were coupled interactions due to angular and linear motion neglected.

This demonstrates that there is a great need for further and in-depth research regarding compliant elements within prosthetic limbs. Whether prostheses with these adapters incorporated may be considered clinically more appropriate than more rigid designs can ultimately only be tested with a clinical trial. The underlying clinical benefit is otherwise purely an assumed mechanical property and assumed effect on gait. However, gait analysis could help identify non-optimal prosthetic gait patterns and excessive loads acting on the soft tissues inside the socket due to inappropriate componentry.

The purpose for the current study was to investigate the effects that angular displacements in a transverse plane and linear displacements in a combined sagittal and coronal plane have on amputee gait. Particular emphasis was put on an individual analysis of motions by permitting both types of motions separately, together and not at all during various set-ups. This was undertaken with an extra focus on differences due

to those set-ups with regard to sound and amputated side gait characteristics, kinematics of socket displacements and loads transmitted onto the residual limb.

The initial focus of this thesis is aimed at establishing relevant background information needed for the understanding of the overall research topic. The next part is a review of the literature related to this field in order to learn from work previously undertaken and to extract specific problem areas that have to be addressed during this investigation. Based on the conclusions of the literature review, the aims and objectives for this study are then stated. Subsequent Chapters detail the methods that were used and the assessment of these methods, and this is followed by the results and discussion related to the aims and objectives.

CHAPTER 2.   <u>BACKGROUND INFORMATION</u>

2.1.   <u>Definitions of segments, positions and motions</u>

The human body is composed of various inter-connected and chain-linked segments, meaning that analysing and interpreting the motion that is being generated at those segments is challenging. Developing an understanding about actions taking place during human movement requires sound definitions for orientations of body segments, directions of motion and timing events. During human motion, the interaction of the entire body plays a vital role in maintaining equilibrium and balance, and the integrity of cross-influences between inter-segmental motions are intricate. Motion analysis of the entire body would go far beyond the scope of this study, which is why body segments higher than the pelvis were excluded, so that the focus of this research project was limited to the lower extremities only.

2.1.1.   <u>Human segments</u>

The orientation of body segments can be derived from the anatomic position during human standing (Tortora 1992) where the feet are parallel to each other and the lower limbs and trunk are straight. The composition of segments that are located below the pelvis in the anatomic position will be referred to as the left and right lower extremity or limb. Each limb is composed of three main segments and these will be referred to in ascending order as the foot located between the ground and the ankle, the leg or shin located between the ankle and the knee and the thigh located between the knee and the hip (Tortora 1992).

2.1.2.   <u>Anatomic planes</u>

Body motion may be referred to as displacement of segments with respect to three orthogonal, anatomic planes. In the anatomic position the sagittal plane divides the body vertically into left and right aspects, the coronal plane vertically into front and back aspects and the transverse plane horizontally into upper and lower aspects (Tortora 1992).

2.1.3.   Segment locations

The adjectives "left", "right", "front", "back", "upper" and "lower" are fairly accurate as position descriptors during the anatomic position, but they may be confusing when body segments move away from this position. For instance, during the anatomic position the upper aspect of the leg is the knee, but when the leg is rotated at the knee by 90°, so that it is turned into a horizontal position, the calf would become the upper aspect of the leg although this, in turn, is the back aspect of the leg during the anatomic position.

In aircrafts and ships a similar scenario can be encountered for the description of the left and right side of a vessel, as this changes depending on the position of the viewer who may be looking forward or backward, hence the use of the nouns port and starboard. As with aviation and marine transport, suitable descriptors are required for an accurate identification of segment locations independent of their orientation in space. Further confusions may develop from the fact that most body segments are paired. For instance, the left front aspect of the left foot is the little toe, but the left front aspect of the right foot is the big toe.

Position descriptors are derived from the orientation of each segment during the anatomic position. Rather than using left and right as descriptors for a segment's side aspect, it is more appropriate to refer to its location with respect to the mid-line of the body. Therefore, a segment's landmark located toward the mid-line or away from the mid-line of the body is being referred to as medial or lateral, respectively; a landmark located at the front or back aspect of the segment as anterior or posterior, respectively; and a landmark located nearer the beginning of the segment where it is attached or nearer the end of the segment as proximal or distal, respectively (Blakinston's pocket medical dictionary). Implementing these definitions in the previous example when the leg was rotated at the knee by 90°, so that it was turned into a horizontal position, the calf is then the upper part of the leg, but in terms of position descriptors it is still the posterior aspect of the leg as it was during the anatomic position.

2.1.4.   Segment motions

Accurate terminology is not only needed for position descriptors, but also for motion descriptors to define both the direction and orientation of a segment during motion.

Such descriptors relate to motion in a particular plane and, as illustrated in Figure 2.1, they may vary depending on the segment that is being referred to. As with position descriptors, motion descriptors are defined in the anatomic position and the direction of motion is independent of the position from which the moving segment commences or finally reaches. In Figure 2.1, for instance, extension of the thigh appears as if the thigh is swinging backward around the hip. From a pure directional point of view this could be interpreted as correct during the anatomic position, but it is more appropriate to refer to the thigh as swinging posteriorly to make it applicable for any position a segment adopts.

2.2.   Definitions of walking events

Running and walking may be described as: "…a method of locomotion involving the use of two legs, alternately, to provide both support and propulsion…" (Whittle 1991). Both types of locomotion consist of complex, inter-linked motions occurring at various segments simultaneously. For reasons of simplicity and brevity only walking will be considered in this study.

2.2.1.   Stance phase

Walking may be broken down into a number of parts with stance phase being the longest in duration. It commences at heel strike, the initial contact of the foot with the ground at which stage the ankle is dorsiflexed, the knee extended and the hip flexed. For purposes of shock absorption the ankle instantly starts to plantarflex and the knee to flex until foot flat is reached when both the heel and the ball of the foot are in contact with the ground. Throughout stance phase the body shifts forward by progressively extending the hip and reaches mid-stance phase when it is located directly over the foot. At this stage the rate of forward propulsion increases and towards the end of stance phase the ankle actively plantarflexes, thereby initiating push off, which commences with heel off and terminates with toe off.

2.2.2.   Swing phase

Another part of walking, which is the second longest in duration, is swing phase and it starts at the instant the toe loses contact with the ground. Due to active hip flexion this is the time when knee flexion increases drastically as a result of the leg's inertial

Figure 2.1:   Anatomic planes, segment locations and segment motions
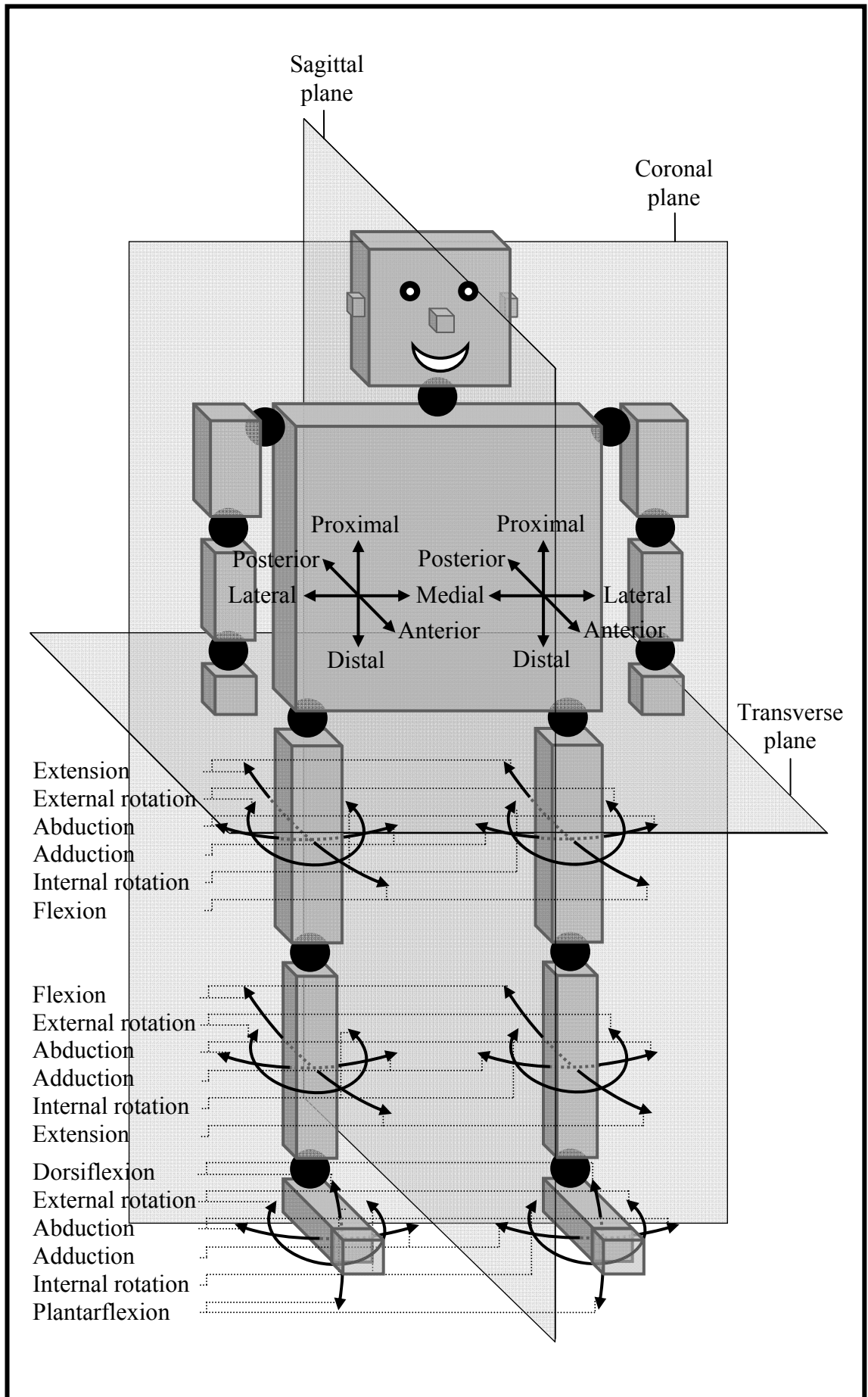
characteristics and the pull from the forward accelerating thigh. Mid-swing phase is the point in time during swing phase when the contra lateral stance side reaches mid-stance phase. Prior to mid-swing phase the foot starts to dorsiflex for toe clearance to avoid contact between the foot and the ground during swing phase and also to prepare for heel strike. Contraction of the gluteal muscles towards the end of swing phase decelerates hip flexion in anticipation of the beginning of stance phase and initiates knee extension due to the leg's momentum.

2.2.3. Double support phase

The third part of walking, which is the shortest in duration, is double support phase when both limbs are in contact with the ground simultaneously. No additional time is being taken up by this phase because double support phase is composed of part of both lower extremities' stance phase due to a slight overlap between stance phase of one limb and stance phase of the other, implying that heel strike of the swing limb takes place prior to toe off of the stance limb.

2.2.4. Gait cycle

A complete gait cycle consists of stance phase, swing phase and, due to both lower extremities stance phases' overlapping nature, double support phase. In normal human walking the gait cycle of both lower extremities is usually 180° out of phase. Sutherland et al 1994 reported that on level ground "during free (self selected) walking a cycle of repeated events has been consistenly observed". Under those circumstances, each gait cycle is composed of approximately 62% stance phase and 38% swing phase (Sutherland et al 1994). Part of stance phase also includes double support phase of approximately 12% of the entire cycle (Sutherland et al 1994). However, these figures have to be used with caution, as other variables, including different walking velocities, are likely to change the relationship between the various gait cycle phases, thus making inter-data comparisons problematic (Sutherland et al 1994). The main events during a human gait cycle are summarised in Figure 2.2.

Measuring temporal and spatial parameters of the gait cycle events helps in gaining an insight into someone's walking performance. In addition to the main gait cycle events described in Section 2.2.1 to Section 2.2.3, these parameters include the step phase commencing at heel strike of one side and terminating at heel strike of the opposite side,

and stride phase commencing at heel strike of one side and terminating at the next heel strike of the same side (Sutherland et al 1994). Normal human walking is characterised by an average of 90 to 100 steps taken per minute, a stride length of approximately 0.76 to 0.81m and a walking speed of around 4km/h or approximately 1.1m/s (Vitali et al 1986).

Figure 2.2:   Events during one full gait cycle
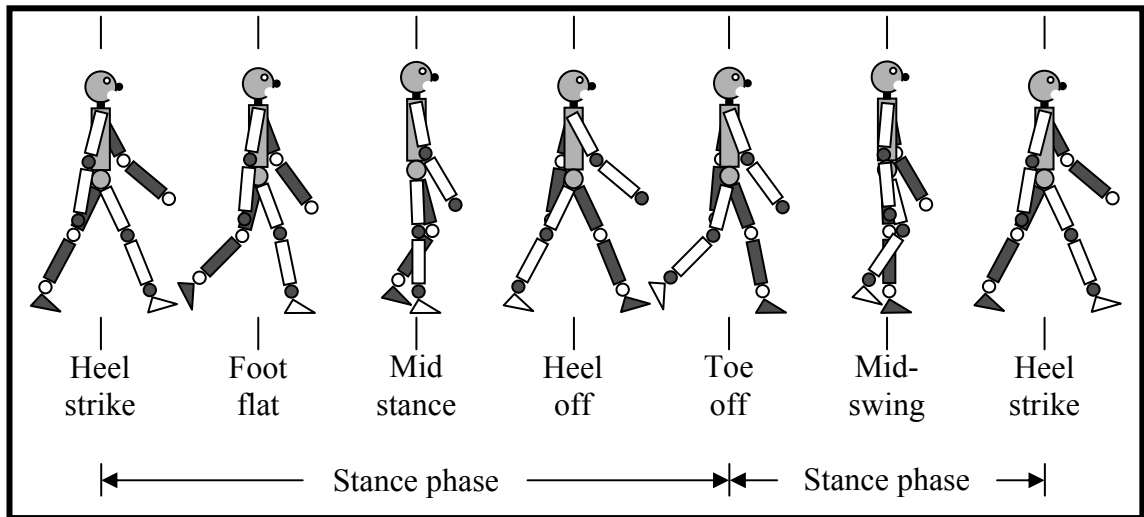
2.3.   <u>Levels of amputations</u>

2.3.1.   <u>Considerations for levels of amputations</u>

The level of lower limb amputation varies depending on the goal for the rehabilitation process. The power an amputee can generate by transmitting forces from the residual limb onto the prosthesis is greater with a long than a short residual limb due to greater leverage and a greater number of muscle fibres that are still connected to the bone of the residual limb for generating a contraction and therefore motion.

A long residual limb has a larger surface area than a short one and forces acting on it from the prosthesis are distributed more evenly, thus reducing peak forces, making the prosthesis more comfortable and reducing the likelihood for skin trauma. In turn, a long residual limb has a greater bulk than a short one, and from a cosmetic point of view a prosthesis to accommodate a long residual limb may not be as pleasing or inconspicuous as a prosthesis for a short residual limb.

Additional complications may arise during manufacture of a prosthesis for a long residual limb due to a short distance between the residual limb's distal end and the joint

centre distal to that. This is a scenario that can make it difficult to fit appropriate prosthetic hardware in between, thus limiting the range of prescription options available.

2.3.2.   Factors for determining levels of amputations

The level of amputation is determined by factors that permit a good level of healing. The residual limb in amputees who suffer, for instance, from peripheral vascular disease may have a poor blood supply. If the level of amputation is kept too far distal, this can either prolong or even hinder healing of the wound, so that re-amputation at a higher level may be necessary at a later stage. This is similar for people who suffered, for instance, an amputation due to trauma where the level of amputation must be kept sufficiently proximal to prevent complicated fractures from being incorporated in the residual limb or scarring making the wear of a prosthesis unacceptable. The level of amputation is therefore a compromise between the most proximal level necessary to remove factors like an insufficiently oxygenated residual limb or an irreparable wound, and the most distal level acceptable to provide sound control over a prosthesis without compromising the cosmetic appearance.

Trans-tibial or below-knee amputation is the level chosen for investigation during the current study. It is one of the most common levels of lower extremity amputation performed and from the prosthetic point of view one of the most interesting levels. This is so, because unlike, for instance, partial foot amputations, there is sufficient space to provide the option for prosthetic hardware to be fitted in between the distal end of the residual limb and the ground. In turn, from the biomechanical point of view, trans-tibial amputations are not over complicated by the introduction of a series of artificial joints, as can be the case in trans-femoral or above-knee amputations, hip disarticulations or hemipelvectomies.

2.4.   General functions of prostheses

2.4.1.   Evolution of prostheses

The purpose of prostheses is to act as a substitute for the amputated limb by replacing both its functional and cosmetic aspects. The emphasis in early designs was less on the cosmetic aspects but almost entirely on the functional aspects of artificial replacements,

because an amputee's main concern was to regain mobility for work, finding food and literally survival. Such designs were very basic and primarily consisted of a socket in which the residual limb was embedded, some type of suspension system to anchor the socket to the limb and a post to act as an extension from the socket to the ground for level walking. This type of limb is often referred to as a "Chelsea" peg (Vitali et al 1986) due to its narrow appearance at the distal end.

As time progressed, prostheses became more advanced and had an artificial foot fitted to allow an amputee to wear a shoe, firstly for improved cosmetic appearance by hiding the prosthesis, but also for increased functionality due to a larger weight bearing area and therefore balance and greater friction with the ground. The role of the post as an extension from the socket to the ground therefore changed to a connection between the socket and the foot. Current standard prostheses are still composed of the same basic elements, but technological advances over the years led to improved materials, which reduced irritation in areas of skin contact, made prostheses lighter and their appearance cosmetically more realistic.

Even in the early days of prosthetic replacements, efforts were made to introduce articulations for mimicking motion at the anatomic joints. Initially, such inter-segmental mobilisations were limited to the sagittal plane only because this was where the human extremities undergo angular displacement of largest magnitude and single axis joints were more durable and simpler to manufacture. The inherent practical implications that came with the introduction of joints had a particularly big impact amongst the amputee population who lost their limb proximal to the knee. Even today, someone with a similar level of amputation may not be safe to walk with a free swinging artificial knee and therefore locks the knee for walking. The option is, however, available to unlock the knee for sitting purposes to reduce the overall length of the prosthesis, an issue that had then, and still has today, huge advantages over stiff prostheses, for accessing confined spaces, such as a car or just behind a table.

The benefit of articulations became more apparent and also led to the introduction of joints in prostheses for people with more distal amputations. Research findings established that anatomic joints rarely move in just one plane (Nester 2000, Nester et al 2002) and technological advances provided a basis for constructing multi-axial joints that simulate passive motion similar to that of the anatomic joints.

2.4.2. Modern prostheses

Until approximately fifty years ago prostheses were predominantly made of leather, metal, rubber and wood. But with the development of new materials, the last few decades have seen engineering and design aspects evolve, leading to the provision of prostheses for otherwise healthy amputees that enabled them to regain a degree of mobility similar to that of non-amputees. Lighter materials, such as titanium-aluminium alloys, reduce the inertial characteristics of prostheses, making them less cumbersome to handle yet very durable for prolonged usage. Soft and pliable substances, such as silicone, can be used for better suspension systems, thus creating greater comfort. Others have stiff properties and when used in, for instance, leaf spring designs (Hsu et al 1999), can provide amputees with great energy returning properties during gait, thus allowing them to increase their activity level and even to participate in sports.

In more recent years, the introduction of microchips also had a great impact on the functional aspects of prostheses. They can be used, for instance, to measure amputees' walking speed, so that a pneumatic or hydraulic unit located together with the control circuitry inside the artificial knee can be electronically adjusted for tuning the rate of swing of the prosthetic leg and foot.

Today, designing more natural looking prostheses seems a common task. In addition to technological advances that not only contribute toward better functionality, but also improve the gait pattern and therefore indirectly enhance the cosmetic appearance, the introduction of artificial skins made from, for instance, silicone or polyvinylchloride (PVC) together with real body hair and natural looking nails, makes some modern prostheses appear stunningly real.

2.4.3. Residual limb-prosthesis interfaces

Despite evolution in the field of prosthetics, the socket remains essential. However, research is currently being conducted in the area of osseo-integration, a method based on locking the prosthesis to a rod that is embedded in the bone of the distal aspect of the residual limb. This makes the need for a socket superfluous (Brånemark et al 2001), but the principle behind it is not yet widely accepted for a number of reasons. Not only is the residual limb prone to infection due to the trans-cutaneous location of the rod, the challenge of creating a bond between the rod and the bone of sufficient strength to

sustain the forces exerted on it by the body over a prolonged period has still to be overcome.

Some amputees may not feel comfortable with the fact that they have a permanent fixture protruding from their residual limb, and such a pointed object needs covering up at night time to reduce the risk of injuring the contra-lateral sound side. In prostheses with a socket, forces are being transmitted onto the body via soft tissues, and in prostheses based on osseo-integration principles, forces are transmitted directly onto the bone making the control over a prosthesis feel more direct, but also reducing the impact absorbing elements from soft tissues. Due to its, until now, rare application, osseo-integration will be disregarded for this study and, to persevere with the statement made at the beginning of this Section, this leaves the socket as the necessary means of creating an interface between the residual limb and the prosthesis.

Improved materials and a better understanding of the underlying anatomy and physiology of the skin provide a basis for creating a drastically improved environment inside the socket. Also, the introduction of articulations made prostheses appear more natural, allowing segments to conform multi-directionally to opposing forces from the artificial limb and the ground, thereby reducing stresses transmitted to the body. In turn, such high performance technology may have an adverse effect that allows amputees to go beyond their usual activity level, thus creating additional stresses acting on the residual limb, and therefore negating the positive results described earlier in this Section.

Forces acting on the residual limb in a perpendicular and non-perpendicular fashion are the sources for shear stresses and peak impacts and these will ultimately be the main causes of skin breakdown. Excessive angular and linear displacement between the socket and the residual limb can be regarded as the trigger for these forces. Currently, there is speculation that by reducing residual limb-socket motion, the likelihood for skin problems may be reduced. This can be achieved in two ways. Firstly, securely locking the residual limb into the socket using appropriate socket designs and suspension systems should minimise motion between the two surfaces. Secondly, introducing appropriate prosthetic articulations to increase mobility between the socket and the prosthetic foot and allowing the socket to move with the residual limb for synchronised

residual limb-socket motion should also minimise motion at the residual limb-socket interface.

2.5.   Sockets and suspension systems

2.5.1.   Classic sockets and suspension systems

A secure locking of the residual limb into the socket for minimising motion between the two surfaces is dependent on the socket fit and the type of suspension system used. Both aspects are to some extent inter-linked in that the socket shape is dictated by the way the prosthesis is fastened to the residual limb.

2.5.1.1.   *Exoskeletal constructions*

Less common nowadays are trans-tibial prostheses that are manufactured with a leather, metal or wooden socket. This type of prosthesis was predominantly based on an exoskeletal construction with an outer weight bearing structure that simultaneously serves as cosmesis to resemble the shape of an anatomic limb.

Cotton or wool socks can be worn for greater comfort and reduced perspiration, whereby the required amount of socks may vary depending on the residual limb volume, which can fluctuate depending on a number of factors including the amputee's level of water retention and the length of time the prosthesis is being worn per day. Suspension systems for these types of artificial replacements are limited in choice and usually consist of a leather corset with bilateral side steels including joints at knee level and possibly additional support from a waist or shoulder strap.

2.5.1.2.   *Endoskeletal constructions*

Exoskeletal prostheses were succeeded by the endoskeletal type with an internal weight-bearing structure based on individual prefabricated modular components. These make the prosthesis far easier to assemble and to adjust compared to exoskeletal designs, but they require an additional, outer foam cosmesis to make it resemble the shape of an anatomic limb.

Endoskeletal prostheses are usually manufactured with an acrylic or thermoplastic socket and an inner soft liner or a flexible inner socket. They are usually worn with

cotton or wool socks for the same reasons as with the exoskeletal type. Acrylic sockets are laminated by impregnating a variety of overlaying materials including carbon fibre, fibre glass and perlon with acrylic resin. Thermoplastic sockets are thermoformed from a preheated sheet of co-polymer or similar material. The exact type of socket that is required for a certain prosthesis depends on a number of factors, which are determined by the prescription criteria.

The choice of suspension systems varies greatly. A standard endoskeletal prosthesis is secured to the residual limb just proximal to the knee using a cuff or by extending the medial and lateral socket trimline proximally and therefore taking advantage of the bone lock, as the femoral condyles are bulkier compared to the slim femoral shaft.

The shape of the socket is usually based on the patellar tendon bearing (PTB) style. This is a principle that reduces forces acting on the distal end of the residual limb by relying on a protrusion from the socket wall to create a weight-bearing surface for the soft tissue just distal to the patella to rest against (Radcliffe & Foort 1961). The remaining part of the socket is modelled to resemble the shape of the residual limb, except that it has areas that apply forces of greater magnitude on soft tissues and forces of lesser magnitude on bone prominences.

To create a model for socket manufacture, the residual limb is simply wrapped in plaster of Paris bandages and these are massaged into soft tissue areas. After additional alterations or rectifications of the model as described by prosthetists, the socket's topography becomes an exaggeration of the residual limb's topography. Part of this principle is conceived as an inhibitor for rotational motion. It could be argued, though, that even slight motion of the socket may displace the areas designed to apply large forces onto soft tissue areas. This, in turn, then increases the forces exerted onto the areas less tolerant to forces of great magnitude, namely bone prominences.

2.5.2.　　　Modern sockets and suspension systems

The types of prostheses based on principles that involve wearing socks for creating a contact surface with the skin are still regularly prescribed and predominantly used as the initial artificial replacement for primary amputees.

2.5.2.1.   Liners as residual limb-socket interfaces

More established and highly active amputees may benefit from prostheses that don't utilise these principles, but involve wearing liners made out of materials like silicone and urethane. During donning, those liners are inverted to allow them to be rolled onto the residual limb (Vandeven 1999).

While the liner is inverted, the material is being elongated at the radius where the liner overlaps with itself. Contraction of the material while rolling the liner onto the residual pre-stretches the skin distally to reduce piston action, which is a relative displacement in proximal-distal direction between the bone anatomy and the outer tissues (Kristinsson 1993). The intimate fit of the liner "creates a negative atmospheric pressure and an adhesive bond to the skin so it moves with the tissue" (Boonstra et al 1996).

2.5.2.2.   Locking pin suspension for liners

There are a number of suspension methods available including the use of a locking pin (Heim et al 1997). This principle was introduced by Fillauer et al 1989. To utilise such a method, it is necessary to have a liner with an "umbrella", which is a reinforcement at the distal aspect of the liner with a central thread located away from the skin into which the locking pin is attached. With the liner donned, the residual limb can be inserted into the socket until the locking pin reaches the lock at the distal aspect of the socket. There are a number of locks available and the type that is designed to give amputees an audible input as to how far they have gone into the socket is used in conjunction with a notched pin.

On insertion of the residual limb into the socket, engagement of the pin's first notch will create a clicking sound from the lock's mechanism. In addition to the pre-stretched tissues from donning the liner as explained in Section 2.5.2.1, engagement of the pin will stretch the tissue and the liner further. The resulting tissue displacement reduces the residual limb's distal diameter, allowing amputees to push themselves deeper into the socket, thereby engaging the pin's second notch and so on. This process is being repeated until an equilibrium is reached between reduction in distal residual limb diameters and distal stretch.

Unlike pins without notches that engage with a lock based on a clutch type, counting the amount of clicks generated by engaging the notched pin into its lock is a useful indicator as to the depth the residual limb has reached inside the socket. For both types of pins, namely with and without notches, upon doffing of the prosthesis these pins can be taken out by pressing a release button at the side of the lock. Other types of locks exist with an external winding mechanism (Otto Bock Orthopädische Industrie GmbH & Co, Duderstadt, Germany), so that the pin can be pulled further into the socket for additional tension. To withstand the tension created between the residual limb and the socket, some liners have a reinforcing distal matrix, as in Iceross silicone liners (Kristinsson 1993). This permits circumferential expansion and reduces distal stretch of those liners to minimise piston action.

2.5.2.3.   *Suction suspension for liners*

Another method of suspending prostheses that are worn in conjunction with a liner is based on suction. The aim is to provide an airtight environment between the liner and the socket. During donning of the prosthesis, a one way valve at the distal aspect of the socket allows the air inside the socket to be expelled. Rolling an external sleeve out of urethane or a similar non-breathable material over the socket and thigh not only helps in suspending the prosthesis by anchoring it to the thigh, it predominantly acts as a seal to prevent air from entering the socket. (Board et al 2001) demonstrated that the negative pressure inside the socket helps in reducing residual limb shrinkage over the course of a day by minimising the amount of fluid embedded in the residual limb tissues to be pumped into proximal parts of the lower limb. This is an advantage for amputees who wear their prostheses over prolonged periods of time in that they may not have to compensate for a possible reduction in residual limb volume by adding socks between the liner and the socket.

To maintain an airtight environment, the liners to be worn in conjunction with this sort of suspension system do not have a locking pin. It could therefore be argued that, unlike locking liners, prostheses with suction sockets do not stretch the tissues distally during the donning process. The piston action as a result of relative motion between the tissues and the underlying bone anatomy might consequently be less in magnitude when wearing prostheses with locking liners.

2.5.2.4.   *Sockets for liners*

A model to be used for the manufacture of sockets worn in conjunction with a locking liner can be created from a cast that was moulded by applying external pressure from an inflatable bladder onto plaster of Paris bandages wrapped around the residual limb (Kristinsson 1993). Unlike casts based on the PTB principle, models created from the pressure casting technique require no further rectifications. The resultant socket's topography becomes rather round in cross-section without compensation for areas more tolerant or less tolerant to forces of great magnitude.

Models obtained with the pressure casting technique can be used for manufacturing total contact sockets. Compared to sockets like the PTB in where some areas are off-loaded, a Total Surface Bearing (TSB) environment distributes forces over the entire residual limb surface area, thus reducing the overall pressure (Carlson 1997). Trieb et al 1999 claimed that silicone suspension systems "…diminish or eliminate pistoning of the residual limb…", but this was not substantiated by any research findings. In turn, Narita et al 1997 demonstrated that the suspension effect with a TSB socket in conjunction with an Iceross silicone liner (Össur hf, Reykjavik, Iceland) is superior to the suspension effect of a PTB prosthesis, which was reflected by less relative motion between the socket and the residual limb in proximal-distal direction. This study also revealed that the angle between the tibia and the socket during heel strike and toe off changed less in TSB prostheses than it did in PTB prostheses, which meant that the extent of overall motions between the socket and residual limb is likely to be reduced with the former.

The principle of suspending the prosthesis from the distal aspect of the residual limb, rather than from segments proximal to it, pulls the residual limb deeper into the socket and creates great tension due to the pre-stretched tissue thus reducing piston action. Pressure casting develops a hydrostatic equilibrium from the residual limb and displaces the tissues fairly uniformly. This creates an intimate fit that in itself acts as an inhibitor for rotational motion without the need to create a socket environment based on an exaggeration of a non-pressurised residual limb's topography. Unlike socks, liners' pliable and elastic properties allow them to distort and stretch between the socket and the residual limb (Sepin 1993), and the assumption is that this may reduce the amount of skin distortion and stretch of tissues.

2.6.　　　Prosthetic alignments

The prosthesis alignment is a vital stage during assembly and fitting of the prosthesis. It affects the stability an amputee will experience from the limb and influences the overall performance during gait. Adjusting the angular and linear relationship between the socket and the foot is the key to accomplishing a good alignment.

2.6.1.　　　Ankle alignments

Adjusting the ankle angle is necessary to make the prosthesis suit the heel height of the amputee's shoe to prevent the prosthesis from leaning too far forward or backward, whereby the goal for this adjustment varies depending on the manufacturer's stipulations. In "Endolite" endoskeletal prostheses (Chas A Blatchford & Sons Ltd, Basingstoke, UK), for instance, the shin tube, which is a modular component that acts as a connection between the socket and the foot, is supposed to be vertical in the sagittal and coronal plane, while the artificial limb is standing upright. Also, with respect to the transverse plane, rarely is the anatomic foot pointing straight forward, but it is usually characterised by slight external rotation, and the orientation of the prosthetic foot should match the sound side.

2.6.2.　　　Socket alignments

The alignment of the socket depends on its design characteristics. It is generally aimed at matching the amputee's residual limb angle, whereby the flexion angle can be increased by approximately 5-7° to create a larger weight-bearing area and less shear forces. Locating the socket correctly with respect to the prosthetic foot is vital, so that the forces from the residual limb can be transferred to the foot via the socket and shin tube without triggering major turning moments of the prosthesis.

Off-setting the socket can have additional effects, in that it may influence motion at the knee due to a displaced centre of gravity, thereby provoking early knee flexion or hyperextension (May 1996), an indicator for the extent of cross-influences simple alignment changes can have. The prosthesis alignment is generally aimed at locating the socket in a position that allows forces to be transmitted between the posterior and middle third of the foot. However, this may vary slightly depending on the type of prosthetic foot to be used (May 1996). The length of the prosthesis needs adjusting to

match the contra lateral sound side. Some amputees find it easier to walk with the prosthetic side slightly shorter than the sound side, but this may have adverse effects on the spine due to pelvic obliquity.

2.7. Prosthetic articulations

2.7.1. General considerations

When taking synchronised residual limb-socket motion into consideration as a mean to minimise angular and linear displacement at the residual limb-socket interface for a reduction in peak impacts and shear stresses, it is necessary to establish the direction of motion required to achieve the desired effect. Motions in three dimensions (3D) can be either angular to take place in the sagittal, coronal and transverse plane or linear to take place in an anterior-posterior, medial-lateral and proximal-distal direction. It seems excessive to permit all six degree of motion, and it is debatable whether this may even have detrimental impacts on the gait due to possible instabilities triggered by a lack of proprioceptive feedback and balance as a result of a repeated, momentary misalignment of the prosthesis. Instead, determining only inter-segmental motions that will be beneficial for a reduction in shear stresses and peak impacts, and isolating them from those that can be considered unnecessary, appears more appropriate.

Trans-tibial residual limbs are conical, cylindrical or bulbous in shape with a relatively circular cross-section. Their anterior, posterior, medial and lateral surface areas are therefore similar in size and considerably larger than the distal aspect, whereby both the anterior, lateral and distal aspects can be considered more sensitive to high forces than the others due to a superficially located underlying bone anatomy.

2.7.2. Considerations for angular displacements

Angular displacements in the sagittal and coronal plane between the socket and the prosthetic foot allow the prosthesis to reach full foot contact with the ground. This seems more important for the sagittal than for the coronal plane, because, as mentioned in Section 2.4.1, the human extremities undergo angular displacements of largest magnitude in this plane, particularly at the knee. Despite surfaces of similar sizes, the forces exerted onto the more sensitive, anterior aspect of the residual limb may be less

tolerable without angular inter-segmental sagittal plane motion than the forces exerted onto the medial or lateral aspects without coronal plane motion.

Therefore, angular coronal plane displacements appear less vital than sagittal plane angular displacements. Also, the dimensions of the prosthetic foot represent an additional factor that reinforces this theory in that they are larger anterior-posteriorly than medial-laterally. The lever arm between the foot's point of contact with the ground and the centre of the residual limb is, for most parts of the gait cycle, consequently much larger in the sagittal plane than in the coronal plane. This is, for instance, the case during push off when ground reaction forces (GRFs) are acting through the anterior aspect of the foot, namely through the toes. The resultant moment gives the socket the tendency to rotate around the residual limb, thus exerting large forces onto the residual limb due to a large lever arm and the residual limb's resistance against the moment, as shown in Figure 2.3. Angular sagittal plane displacements should therefore be permitted to reduce the forces exerted onto the residual limb.

Figure 2.3:   Angular socket displacements responsible for moments
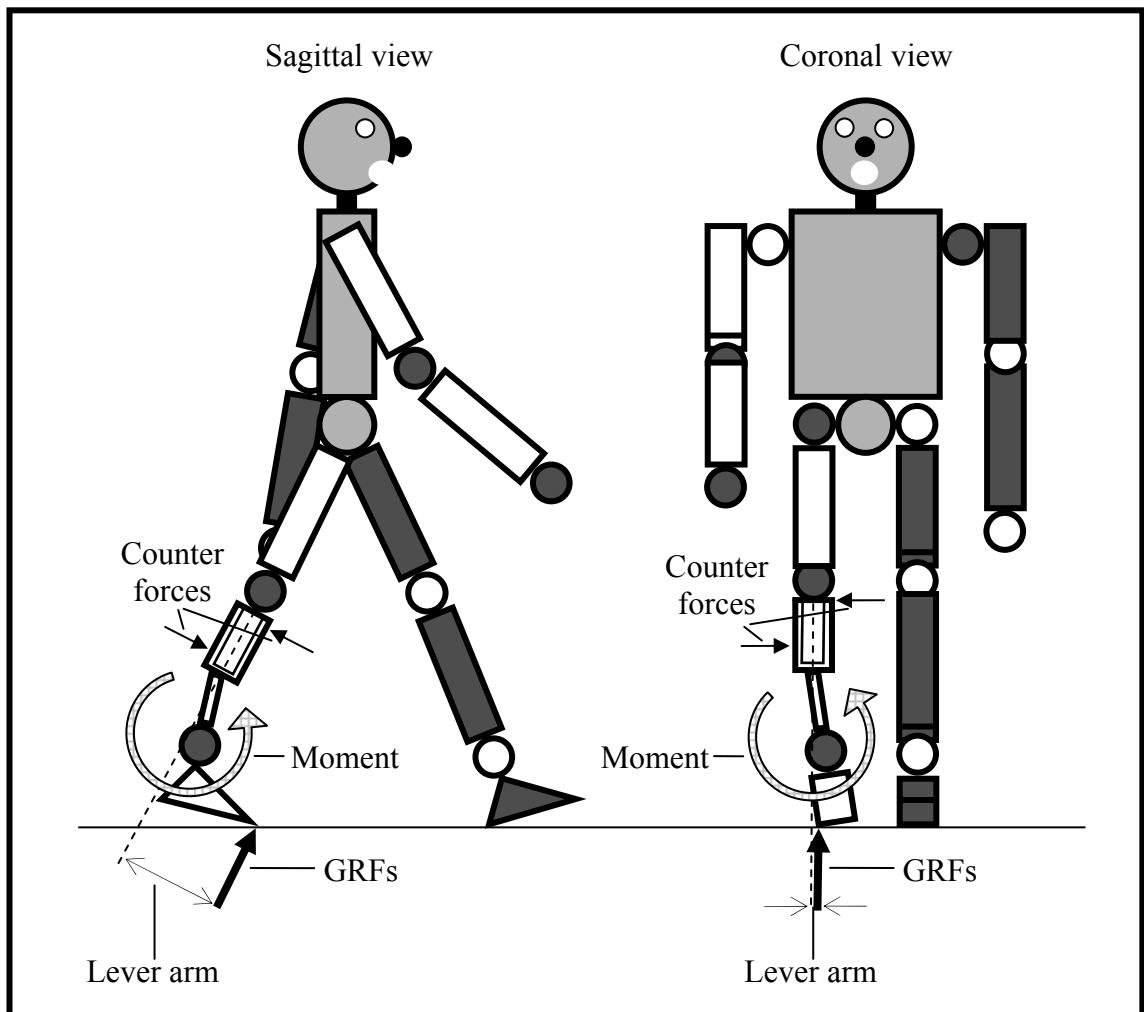
Angular displacements in the transverse plane do not contribute to the prosthesis reaching full foot contact with the ground, but can nevertheless be considered vital during gait due to the following reasons. Without articulations between the socket and the prosthetic foot, forces exerted by the residual limb onto the socket would be transmitted directly onto the foot. Neglecting air friction, gravity and inertial characteristics, during swing phase, the prosthesis is free to follow the residual limb's movements due to absent GRFs, but during stance phase, friction between the foot and the ground would limit motion of the prosthesis.

The transverse plane cross-section radius of the residual limb is smaller than its overall length, so that the lever arm in that plane is relatively small. In addition to that, this cross-section is, as mentioned in Section 2.7.1, relatively circular and therefore provides very little surface area where the socket can perpendicularly act against for reducing angular displacements. Even a snug fitting socket may not generate sufficient resistance to restrain angular transverse plane motion of the residual limb, and this can trigger tissue distortion and shear stresses, both due to forces acting in a non-perpendicular fashion and due to friction between the socket and the skin. It is therefore justifiable to introduce angular displacements in the transverse plane.

2.7.3.   Considerations for linear displacements

In addition to angular displacements, human joints are also capable of allowing linear displacements. The knee, for instance, is capable of approximately 6mm displacement in anterior-psoterior direction (Daniel et al 1985). However, whether linear displacements in the sagittal or coronal plane affect gait positively is debatable. However, taking the alignment procedures for trans-tibial prostheses described in Section 2.6 into consideration, it is reasonable to assume that it is more than likely for both types of motion to affect gait adversely. Anterior-posterior and medial-lateral GRFs represent only a fraction of the total body weight, and the resultant magnitudes of motions triggered at articulations that permit linear displacements in the sagittal and coronal plane in response to those GRFs would be relatively small.

Even though such relatively small forces would keep a shift of the socket with respect to the prosthetic foot to a minimum and would only cause a temporary shift, it would alter the prosthesis alignment and offset the forces exerted by the residual limb via the socket onto the prosthetic foot. Such an offset creates a moment at the prosthesis that would be

opposed by the residual limb resulting in an altered force pattern, as shown in Figure 2.4 or affecting motion at the knee, as mentioned in Section 2.6. Also, allowing the socket to be momentarily displaced in a linear fashion may be the equivalent of losing balance on a slippery surface, therefore making the gait very unbalanced and unstable. This emphasises the need to prevent these types of displacements.

Figure 2.4:   Linear socket displacements responsible for moments
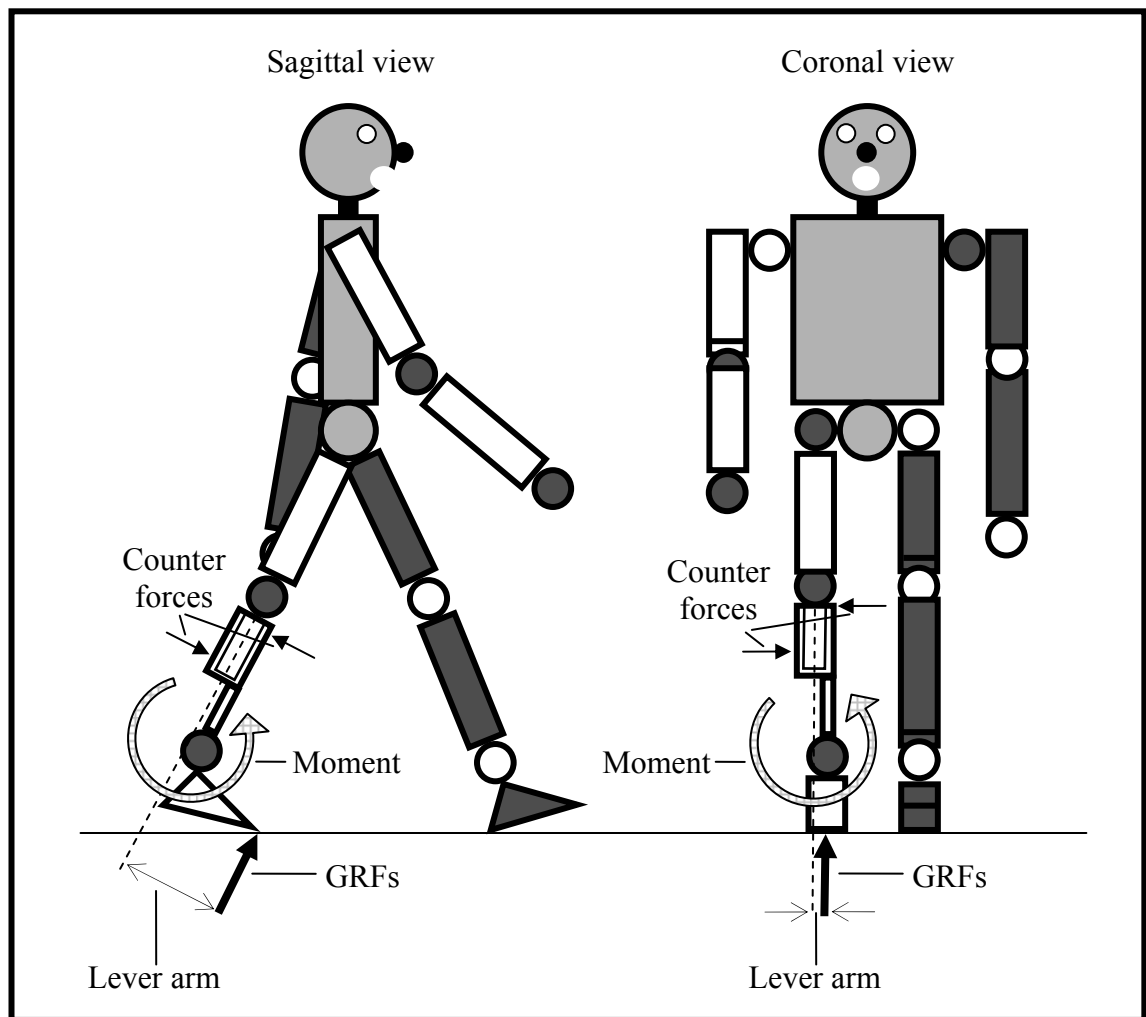
Unlike anterior-posterior and medial-lateral GRFs, vertical GRFs are very large in magnitude and even exceed body weight during the initial and final stages of stance phase (Meglan & Todd 1994). As mentioned earlier in Section 2.7.1, the distal aspect of the residual limb is relatively small compared to its anterior, posterior, medial and lateral surfaces. Also, the nature of the amputation requires cutting through the bones and nerves. Both these factors give rise to some degree of hypersensitivity rendering this part of the limb less tolerant to weight bearing. It is therefore necessary to redistribute GRFs over the residual limb's other surfaces to increase the area, thus reducing force concentrations.

The anatomic foot's fairly large surface area allows GRFs to act upon it in a near perpendicular fashion. However, GRFs transmitted by the socket onto the residual limb's anterior, posterior, medial and lateral surfaces act obliquely upon the skin, thereby giving rise to increased forces as well as shear stresses. This scenario is exacerbated if the residual limb is not conical but instead cylindrical or bulbous in shape, so that the degree of obliquity rises and the magnitude of shear forces increases. As the residual limb has the tendency to travel distally during stance phase, it appears logical for the socket to follow the residual limb's motion, so that the inherent impact between the prosthesis and the ground may be reduced and the forces acting on the residual limb become less severe.

2.8.   <u>Deciding on the types of displacements</u>

In conclusion, from the six degree of motion possible in 3D space, three types of motions were identified that seemed beneficial for prosthetic gait. This includes angular displacements in the sagittal plane, whereby modern prostheses are already designed with incorporated articulations that produce such motions, as explained in Section 2.4.1.

The two types of motions that are not regularly incorporated in prostheses are angular displacements in the transverse plane and linear displacements in proximal-distal direction between the socket and the prosthetic foot. Both these motions seem to have the potential for reducing the forces exerted onto the residual limb tissues. Prosthetic components that are capable of permitting these motions already exist. With the amount of these components produced by different manufacturers of prosthetic hardware continuously increasing, so does the number of prescriptions for these devices. Although Section 2.7 identified why such components may be beneficial for amputee gait, whether the theoretical basis for those devices provides actual benefits in a real world scenario has not been established. Investigating these components will show whether their predicted effects on the gait and residual limb are therefore required and if their prescription is justifiable.

Prior to a formal investigation of whether these components do have beneficial effects as is assumed, it was necessary to search the literature for evidence from related research studies that might inform on an appropriate methodology. The following Chapter therefore focuses on a literature review with regard to all relevant aspects that

involve angular displacements in a transverse plane and linear displacements in proximal-distal direction. It also concentrates on possible means for reducing forces transmitted onto the body.

CHAPTER 3.   <u>LITERATURE REVIEW</u>

3.1.   <u>Definitions of nomenclature</u>

3.1.1.   <u>Considerations for nomenclature</u>

Appropriate terminology will be required for a clear description of motions in the transverse plane and in the proximal-distal direction, as well as for prosthetic components that permit such motions. An attempt was made to derive these from the definitions in Table 3.1.

Table 3.1:   Literature terminology for components with elastic elements

•   Adapter   - "One who fits or suits one thing to another."   Oxford English Dictionary
•   Longitudinal - "Extending…in the direction of the length of a body…"   Oxford English Dictionary
•   Rotation   - "…moving round a centre, or of turning round…an axis…"   Oxford English Dictionary
•   Translation - "Onward movement without (or…apart from) rotation…"   Oxford English Dictionary
•   Transverse   - "…at right angles to the longitudinal axis of the body…"   Blakinston's pocket medical dictionary

Motions in the proximal-distal direction can be regarded as longitudinal motions. This also identifies motion in the transverse plane, because it occurs in a plane perpendicular to the longitudinal axis. Consequently, motion around and along the longitudinal axis can be described as transverse rotation and longitudinal translation, respectively.

3.1.2.   <u>Component mobility for dynamic set-ups</u>

To refer back to the problem previously described in Section 2.7.2 and Section 2.7.3 regarding excessive angular and linear motions of the residual limb within the socket, articulations that possibly accommodate those motions would have to allow relative transverse rotation and longitudinal translation of the socket with respect to the foot.

Terminologies for the description of prosthetic components are generally derived from the components' corresponding anatomic counterpart as in foot, knee, hip etc, their mechanical application as in adapter, socket, suspension etc or from both as in toe section, shin tube, thigh section etc. Whether prosthetic components that permit transverse rotation or longitudinal translation in lower limb replacements are located in the shin or thigh section, they also serve as a connection between the foot and socket, foot and knee, knee and socket or knee and hip.

Table 3.2: Literature terminology for transverse rotation

- "Drehung um die vertikale Achse" (rotation around the vertical axis)
  L Roeser, Essen, Germany

- "Internal-external rotation"
  Lafortune et al 1994, Lamoureux & Radcliffe 1977

- "Rotation movement in the long axis of the leg"
  Schmidl 1979

- "Torsion absorption"
  Schuch 1989

- "Transverse motion"
  Staros & Peizer 1973

- "Transverse plane motion"
  Fergason & Boone 2000

- "Transverse plane rotation"
  Nester 2000

- "Transverse rotation"
  Esquenazi 1991, Levens et al 1948, Twiste et al 2001, Twiste et al 2001

- "Twisting motion"
  Össur hf, Reykjavik, Iceland

According to the definitions in Table 3.1, these components can therefore be regarded as transverse rotation adapters or as longitudinal translation adapters. Some manufacturers produce components that permit both types of motion and these can therefore be regarded as transverse rotation and longitudinal translation adapters, which for the purposes of brevity in this document may sometimes be referred to as dual function adapters. Whether an adapter permits only one or both types of motion, if no

further clarifications regarding the types of motion permitted are required, then such components will in this study generally be referred to as motion adapters.

3.1.3.   Component mobility for static set-ups

Other types of adapters exist with articulations that are only mobile during assembly or alignment of the prosthesis by qualified personnel. After that those adapters are rigidly locked for ambulation purposes. Alternatively, some adapters that facilitate transverse rotation can be operated by amputees themselves, as often used for cross-legged sitting purposes in levels of amputation proximal to the knee (Chakraborty & Patil 1994, Chaudry et al 1982). These types of adapters are also rigid for ambulation purposes and require the angular relationship between the socket and the prosthetic foot to be returned manually back to the neutral position, as, for instance, with the "Endolite Turntable" (Chas A Blatchford & Sons Ltd, Basingstoke, UK) and the "Rotation Adapter" (Otto Bock Orthopädische Industrie GmbH & Co, Duderstadt, Germany). However, none of the adapters described in this paragraph are designed to permit motion during gait and will therefore not be taken into consideration for this study.

Table 3.3:   Literature terminology for longitudinal translation

• "Ability to elastically compress at impact"   Buckley et al 2002
• "Telescoping action"   DiAngeleo 1989
• "Vertical motion"   Staros & Peizer 1973
• "vertikale Stoßdämpfung" (vertical impact damper)   Biedermann Motech, Villingen-Schwenningen, Germany

3.2.   Variations in nomenclature

3.2.1.   Variations found in the literature

As may be seen in Table 3.2 to Table 3.6, terminologies for transverse rotation and longitudinal translation, as well as for prosthetic components that permit these motions, vary tremendously and some are ambiguous or even imprecise. Variations were encountered in both peer reviewed literature and in commercial literature. The majority

of descriptors used for these terminologies can be allocated into the categories which follow.

Table 3.4:   Literature terminology for transverse rotation adapters

---

- "Ankle rotator"
  Mulby & Radcliffe 1960

- "Axial rotation device"
  Lamoureux & Radcliffe 1977

- "Demountable Torque Absorber"
  Chas A Blatchford & Sons Ltd, Basingstoke, UK

- "Integrated rotation unit"
  Knoche 1979

- "Radix$^®$ Torsion Absorber"
  Ambroise UK Ltd, Somerset, UK

- "Rotator"
  Fergason & Boone 2000, Kaphingst 1977, Staros & Peizer 1972

- "Torque absorbing device"
  Kaphingst 1977

- "Torque rotation unit"
  Schmidl 1979

- "Torsion Adapter"
  Otto Bock Orthopädische Industrie GmbH & Co, Duderstadt, Germany

- "Transverse rotation system"
  Staros & Peizer 1972

3.2.2.   Types of names

Some terminologies encountered for describing prosthetic components that permit transverse rotation, longitudinal translation, or both, do not clearly define the function of those components. This is because the manufacturers advertised them by the components' brand names, like, for instance, "Total Shock™" or "Ultimate Pylon II™" (Table 3.6), which can be misleading. Instead, brand names together with descriptive appendices give the products individuality, but they also clarify to some extent the functional aspects of those products, as in "Radix$^®$ Torsion Absorber" (Table 3.4).

3.2.3.   Types of axes or planes

Although some terminologies refer to the type of motion, as in "rotator" or "integrated rotation unit" (Table 3.4), they fail to address the plane in which that motion occurs. In turn, attempts are sometimes being made to address the plane in, or the axis around, which motions occur as in "rotation around the vertical axis" (Table 3.2) or "vertical shock absorbing pylon" (Table 3.5). However, vertical is defined as "placed or extending at right angles to the plane of the horizon; perpendicular; upright" (Oxford English Dictionary) and as "pertaining to the position of the long axis of the human body in the erect posture" (Blakinston's pocket medical dictionary). If the axis around or along which motions occur is vertical with respect to, for instance, the prosthetic foot, any motion at the ankle would alter this angular relationship.

Even during standing, it would be very difficult to position the prosthesis in such a way that the axis of concern would be perpendicular to the horizon or parallel with the long axis of the human body. During ambulation this would be virtually impossible due to the motion of the whole body. This is why it would be more appropriate to define the actual anatomic plane in which motion occurs rather than to describe angular displacement with regard to an inappropriate axis or even no axis or no plane.

3.2.4.   Types of displacements

Some terminologies define the plane in which motions occur as in "transverse plane motion" (Table 3.2). Others are, to a certain extent, descriptive by insinuating that motions of some kind take place as in "ability to elastically compress at impact" (Table 3.3) or "shock torque suppresser" (Table 3.6). But all three examples fail to specify the exact type of motion, namely angular or linear. On the other hand, considering that certain mechanical applications can operate in an angular or linear mode, terminologies like "telescoping action" (Table 3.3) or "spring loaded telescoping mechanism" (Table 3.5) not only lack a description of the type of motion they also fail to address the plane in which that motion occurs.

Terminologies that are used to describe transverse rotation and transverse rotation adapters frequently include words such as torque or torsion. Torque is defined as "the twisting or rotary force in a piece of mechanism…; the moment of a system of forces producing rotation", and torsion as "the action of twisting, or turning a body spirally by

the operation of contrary forces acting at right angles to its axis; also the twisted condition produced by this action; twist" (Oxford English Dictionary).

Table 3.5: Literature terminology for longitudinal translation adapters

- "Automated spring pylon"
  Hsu et al 2000

- "Icon"
  Össur hf, Reykjavik, Iceland

- "Shock absorbing pylon"
  Gard & Konz 2001, Fergason & Boone 2000

- "Shoky Federstoβdämpfer" (Shoky spring impact damper)
  Biedermann Motech, Villingen-Schwenningen, Germany

- "Spring loaded telescoping mechanism"
  Martel et al 1986

- "Spring loaded telescoping shank"
  DiAngeleo et al 1989, Miller et al 1997

- "Telescoping mechanism"
  Gard & Konz 2001

- "Telescoping pylon"
  Fergason & Boone 2000

- "Vertical compliance mechanism"
  Miller & Childress 1995

- "Vertical shock absorbing pylon"
  Ross et al 2003

- "Vertical shock pylon"
  Össur hf, Reykjavik, Iceland

Considering that quite a few of the terminologies found in Table 3.2, Table 3.4 and Table 3.6 incorporate either the word torque or torsion, it is difficult to determine the exact meaning of these terminologies without receiving further clarification. It is consequently important to see them in context rather than analysing them on their own. For instance, forces acting at the residual limb-socket interface can be considered to rotate and distort the skin of the residual limb. Therefore, according to the above definitions for torque and torsion, terminologies like "torsion absorption" (Table 3.2) and "torque absorbing device" (Table 3.4) would be appropriate if they referred to

motion at the residual limb-socket interface. However, neither of these terminologies would be applicable with regard to motion at the transverse rotation adapter, because it is not absorption that takes place, but rotation that is being permitted.

Table 3.6:   Literature terminology for dual-function adapters

- "Ceterus"
  Össur hf, Reykjavik, Iceland

- "DeltaTwist"
  Otto Bock Orthopädische Industrie GmbH & Co, Duderstadt, Germany

- "Modular-Stoßdämpfer mit Torsion" (modular shock absorber with torsion)
  Gömed$^®$ Orthopädie Service GmbH, Herzberg am Harz Pöhlde, Germany

- "Rotation shock absorber"
  Stauf 2000

- "Rotationsstoßdämpfer" (rotation-shock absorber)
  medipro Technik, Bayreuth, Germany

- "Shock and torque absorbing device"
  USMC$^®$ Zinco Orthomedics, Pasadena California, USA

- "Shock torque suppressor"
  Century XXII Innovations Inc, Jackson Michigan, USA

- "Total Shock"
  Century XXII Innovations Inc, Jackson Michigan, USA

- "TT Pylon" (telescopic and torsional pylon)
  Chas A Blatchford & Sons Ltd, Basingstoke, UK

- "Ultimate Pylon II$^{™}$"
  USMC$^®$ Zinco Orthomedics, Pasadena California, USA

Also, when regarding the prosthesis as a whole entity, according to Kaphingst 1977, transverse rotation can be described as "torsion" of the prosthesis, because of its distortion induced by relative angular displacements between the socket and the prosthetic foot. Such angular displacements, however, do not alter the linear distance between the socket and the prosthetic foot. Those displacements only allow the socket to rotate, but not to spiral with respect to the prosthetic foot. This is why it would be incorrect, taking the above definitions into account, to describe transverse rotation as torsion of the prosthesis.

As mention in Section 2.5.1.2, modular prostheses are generally covered by a foam-based cosmetic finish that is attached to the socket and the prosthetic foot. While they undergo relative transverse rotation without longitudinal translation, the cosmetic finish will stretch despite a constant linear distance between the socket and the prosthetic foot. This is because the rotation will cause the cosmetic finish to be wrapped around the prosthesis, thus increasing the distance between one arbitrary point of attachment to the socket and another to the prosthetic foot. Such an increase in length spirals the cosmetic finish, which can therefore be regarded as torsion.

A similar effect can be observed during motion at the return unit. This is a mechanism that permits transverse rotation adapters to be returned back to their neutral state following relative displacement between the proximal and distal part of the adapter. Some return units are being truly twisted during transverse rotation and this is why the noun "torsion" would be appropriate to describe this action. In fact, the return unit in two types of transverse rotation adapters manufactured by Chas A Blatchford & Sons Ltd, Basingstoke, UK and called "Demountable Torque Absorber" and "TT Pylon" (Telescopic Torsion Pylon), is based on a cylindrical stem that is exposed to exactly this type of action during transverse rotation. This return unit is correctly termed "torsion rod".

3.2.5.   Types of component installations

Although a fair amount of the terminology encountered in the literature was lacking important aspects necessary for a thorough description of the type of activity that takes place, other terms were composed in quite the opposite way and contain irrelevant information that exceeded the necessary level of detail required. For instance, most prosthetic components are, unless permanently bonded, easily accessible so they can be repaired or replaced if necessary. Therefore, considering that lengthy and complicated terminology is more cumbersome to remember and to use, "Demountable Torque Absorber" (Table 3.4) and "Modular-Stoßdämpfer mit Torsion" (modular shock absorber with torsion) (Table 3.6) are examples that incorporate additional descriptions with perhaps lower priority for inclusion than those discussed throughout Section 3.2.

3.2.6.   Considerations for terminology

The amount of variation amongst terminology encountered in the literature demonstrates a general lack of consensus, which can be explained in various ways. Considering that the importance of transverse rotation (Mulby & Radcliffe 1960) and longitudinal translation (Martel 1986) during prosthetic gait is not a recent establishment, there might simply be a general lack of interest for research in this field.

Terminology used for specific prosthetic components, which have pure mechanical applications that exceed the purpose of, for instance, basic adapters, is generally fairly uniform amongst the literature, as in swing phase control, dorsiflexion stop etc. Although adapters that permit transverse rotation, longitudinal translation, or both, can be regarded as components of the same category, the terminology for these components and their function obviously varies. Therefore, due to the relatively small number of studies conducted with these types of components, the assumption can be made that manufacturers of prosthetic components possibly based their terminology on intuition or on brand names rather than on rigorous research findings.

3.3.   Considerations for lower limb motions

One of the main problems associated with the design of prostheses is to create an interface, which allows GRFs that usually act through the anatomic foot in non-amputees to be transmitted via the prosthesis onto the residual limb. Implications that angular and linear motions at the residual limb-socket interface have on the development of non-perpendicularly orientated forces were explained in Section 2.7.2 and Section 2.7.3. This emphasised the need for permitting transverse rotation and longitudinal translation of the socket in an attempt to reduce circumferentially and longitudinally directed shear and/or compressive stresses.

Another difficulty encountered in the design of artificial limbs is the assimilation of prosthetic gait to that of non-amputees in order to restore both aesthetic and functional aspects of the missing limb (DiAngelo 1989). From the aesthetic point of view, prostheses that appear, in terms of exterior modelling and gait performance, like an anatomic limb can be considered an accurate replica of the absent limb. With respect to functional maximisation, a number of authors have reported on differences in prosthetic designs and the influence of those designs on the gait parameters. In the majority of

cases, minimisation of energy consumption was considered one of the most advantageous effects on prosthetic gait (Buckley et al 2002, Gailey et al 1993). It is debatable, though, whether a gait pattern similar to that of non-amputees is the most appropriate type for amputees. At this stage, however, this will be assumed to be the case. Consequently, taking into account that, as mentioned above, transverse rotation and longitudinal translation is assumed to be beneficial for the reduction of shear and/or compressive stresses acting on the residual limb, the same motion must occur during non-pathological gait of non-amputees, in order for prosthetic gait to be similar.

The following two headings 3.4 and 3.5 contain Sections, which are a continuation of the literature review that forms part of the current Chapter. They represent an introduction into areas of relevance for a comprehensive collection of related topics that are necessary to trigger an understanding of this study. These Sections are based on a peer-reviewed publication by Twiste & Rithalia 2003 in the Journal of Rehabilitation Research and Development. Parts of the report were either copied in their entirety or adapted and updated as appropriate. The journal gave consent for the described publication to be integrated as part of this thesis.

3.4. Anatomic lower limb motions

3.4.1. Transverse rotation

3.4.1.1. *Motions of non-amputee anatomic segments*

A study by Levens et al 1948 revealed that transverse rotation of the tibia, femur, and pelvis occurs throughout swing and stance phase. However, no analyses were given for possible implications of that motion on the gait except that it can be regarded as "an important factor in the ease and rhythm of walking". Lafortune et al 1994 found that during peak knee flexion, the amount of internal rotation of the tibia was greatest when shoes with a valgus wedge were used and smallest when shoes with a varus wedge were used. However, the presence or the type of wedge neither affected transverse rotation of the tibia during the remaining part of stance phase that followed peak knee flexion nor did it affect the tibio-femoral joint throughout stance phase. From their findings, Lafortune et al 1994 concluded that changes in the magnitude of transverse rotation of the tibia must therefore affect transverse rotation at the hip. However, no evidence was given to substantiate their assumption. Also, changes in transverse rotation of the tibia could possibly trigger compensatory motions further proximal to the hip.

This hypothesis was supported by Nester et al 2001 who found that, despite significant effects on the rear foot complex motion, medially and laterally wedged foot orthoses have a negligible influence on transverse rotation at the knee, hip, and pelvis. Because of skin movements relative to the underlying bone (Cappozzo 1991, Cappozzo et al 1996), Steinman traction pins more accurately identify anatomic landmarks than skin markers do. These were used in the study by Levens et al 1948. However, drastic changes in the angular relationship of the lower limb segments with respect to the cameras can cause errors, because of perspective and parallax. Levens et al 1948 made corrections to compensate for these errors, but because available technology was less advanced when this study was conducted, the accuracy with regard to camera equipment during the study by Lafortune et al 1994 is likely to be greater. Nevertheless, both studies demonstrated that transverse rotation of the tibia is characterised by two main events. These involve progressive internal rotation during the initial part of stance phase, followed by progressive external rotation during the remaining part of stance phase.

Unlike Levens et al 1948 whose results involved transverse rotation of the tibia, femur, and pelvis and at both intersegmental joints throughout the gait cycle, Lafortune et al 1994 limited their results to transverse rotation of the tibia and at the tibio-femoral joint for the stance phase only. Therefore, because of limited information in the study by Lafortune et al 1994, the data by Levens et al 1948 were considered more useful as they addressed a wider range of segments and joints over a longer duration of the gait cycle. However, those results were only used as a general guide for gross motion rather than for a detailed motion analysis. Some of the data published by Levens et al 1948 were adapted for incorporation in this study in Figure 3.1.

During swing phase, without a mobile, anatomic structure that allows relative motion between the shin and the foot, transverse rotation of the shin would cause transverse rotation of the foot. But, as briefly mentioned in Section 2.7.2, because of the presence of GRFs during stance phase, lack of transverse rotation of the foot as a result of friction with the ground would also limit transverse rotation of the shin, if intersegmental mobility would not exist. Manter 1941 studied articulations that allow the necessary intersegmental mobility. This author established the orientations of axes and the types of motion that occur at the subtalar and transverse tarsal joint. Building on these concepts, McPoil & Knecht 1985 and Subotnick 1975, amongst others, elaborated on

the intricate action of pronation and supination at these joints and the relationship between those triplanar motions and transverse rotation of the shin.

Figure 3.1:   Lower limb transverse rotation relative to the ground

This diagram was adapted from Levens et al 1948
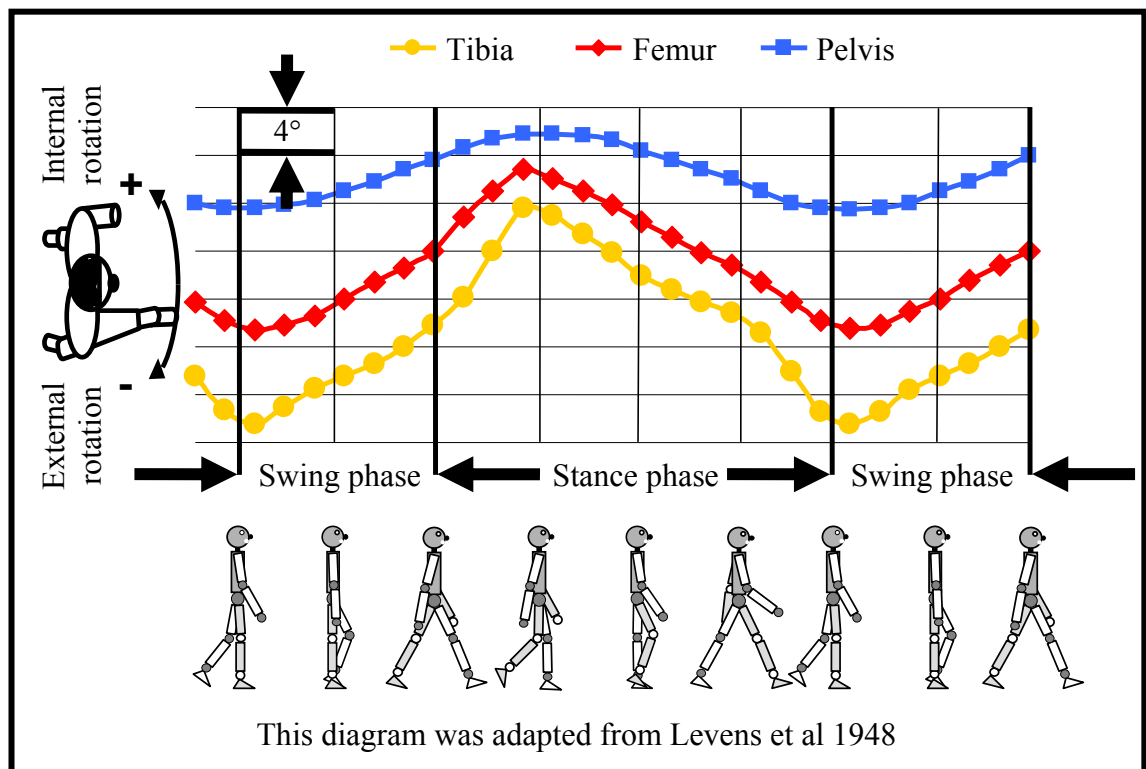
In turn, Reischl et al 1999 established that magnitude and temporal characteristics of peak transverse rotation of the tibia and femur could not be predicted from the magnitude and temporal characteristics of peak foot pronation. However, motions of body segments were referred to the global reference system. Nester 2000 described this as ambiguous, because motions between segments are, in a clinical situation, generally referred to as joint motions, thus to the anatomic reference system. In this study, Nester 2000 demonstrated that the magnitude and temporal characteristics of transverse plane motion at the hip and knee could not be directly correlated with rear foot complex motion.

Nevertheless, the authors of both studies agreed that, because of the interaction between joints, the extent of variability between subjects might contribute to a lack of correlation between intersegmental motions, but a relationship must obviously still exist to prevent the anatomic foot from rotating together with proximal segments. Also, in addition to pronation and supination, another motion that helps to prevent the foot from rotating with the shin is the ankle joint, which can undergo as much as 15° of transverse rotation

(Nester et al 2003). Although it is difficult to predict the exact interactions between joints of the foot and the remaining lower limb segments, the representations of likely relationships that Inman & Mann, 1978 described, seem plausible to use as a rough guide for supporting theories of correlated segment motions. An adaptation of these can be found in Figure 3.2.

Figure 3.2:   Relationship between displacements at the shin and foot

Orientation of shin: Orientation of shin: Orientation of shin:
Neutral   Internal rotation   External rotation

Orientation of foot: Orientation of foot: Orientation of foot:
Neutral   Pronation   Supination

This diagram was adapted from Inman & Mann 1978
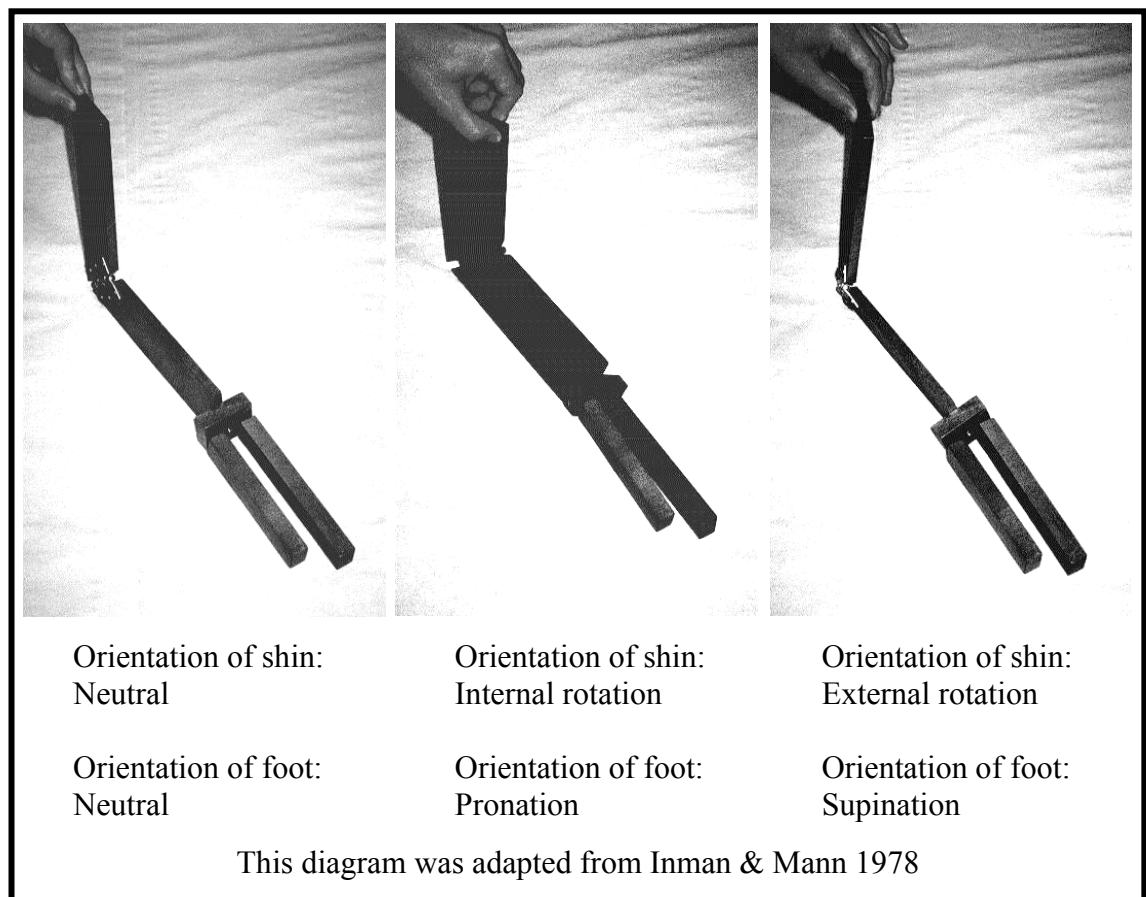
3.4.1.2.   *Motions of amputee anatomic segments*

Lamoureux & Radcliffe 1977 investigated the effects of a locked and unlocked transverse rotation adapter on trans-femoral gait, thus simulating the absence and presence of such a device, respectively. They not only found that the amount of transverse rotation of the pelvis was greater with the transverse rotation adapter unlocked compared to when it was locked, but they also found that the relative amount of transverse rotation between pelvis and socket increased and the torque at the adapter decreased. Internal and external rotation of the socket with respect to the pelvis reached a maximum at the beginning of swing phase and during mid-stance phase, respectively.

In turn, the study by Levens et al 1948, which was used as a general guide only, as previously suggested in Section 3.4.1.1, showed that internal and external rotation of the femur with respect to the pelvis reached a maximum at the beginning of stance phase and at the beginning of swing phase, respectively. Therefore, with the residual limb embedded in the socket, the incorporation of a transverse rotation adapter does not cause the socket to undergo transverse rotation similar in amount or pattern to that of the femur during non-amputee gait. The reason for this could be that the amount or pattern of transverse rotation of the femur during non-amputee gait is different to that of the residual femur in amputees.

Figure 3.3: Trans-femoral prosthesis rotated by thigh muscles

This diagram was adapted from Lamoureux & Radcliffe, 1977
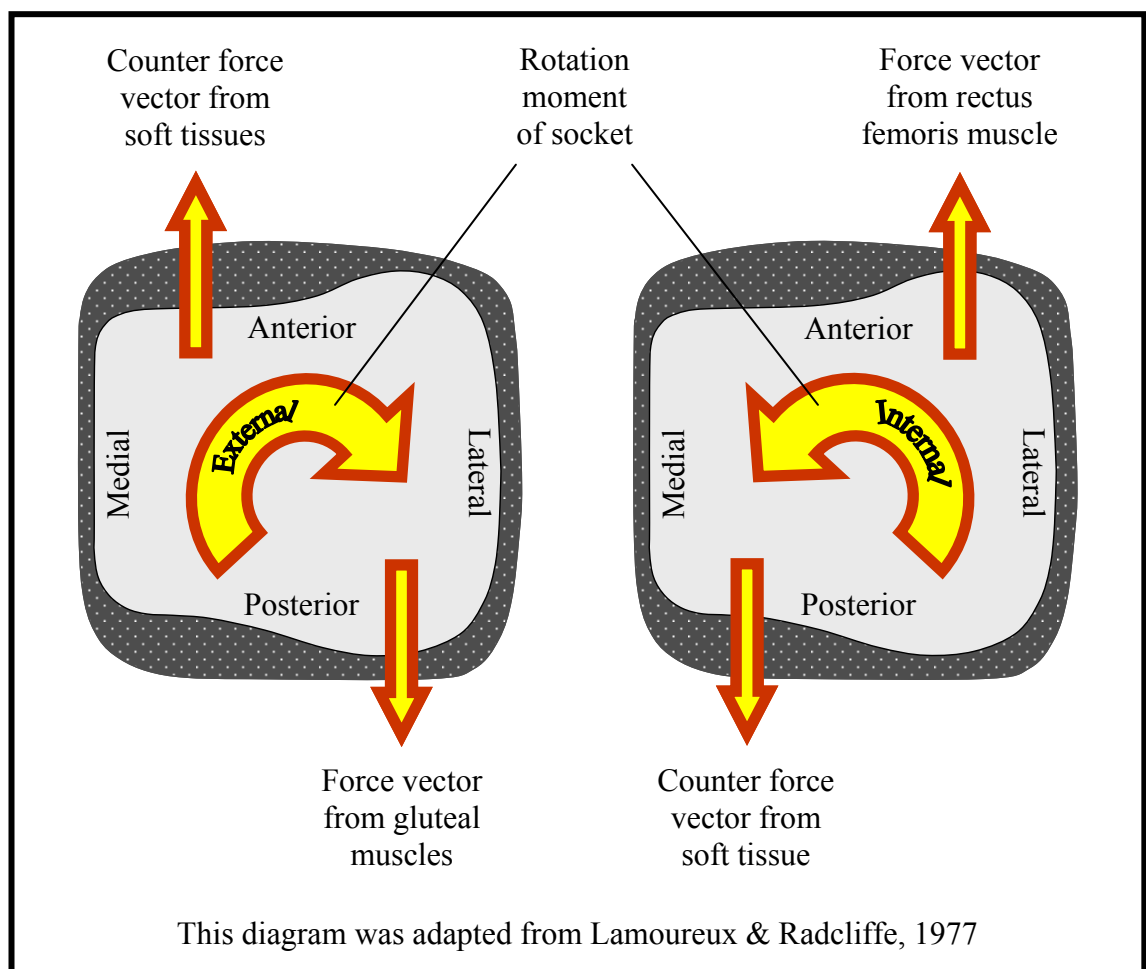
Alternatively, Lamoureux & Radcliffe 1977 suggested that contractions of the rectus femoris muscle and gluteal muscles may apply a transverse rotation moment on the socket, because of bulging of those muscles during hip flexion and extension, as indicated in an adaptation of one of their diagrams in Figure 3.3. Whether the characteristics of soft tissue properties are the sole influence on transverse rotation of the socket or whether the encapsulation of the bones inside the socket also affects

motion of the socket remains open. What is shown, though, is that non-amputee gait is clearly characterised by transverse rotation and that this motion still has an effect on the prosthesis during amputee gait, which demonstrates the need for a transverse rotation adapter. However, as explained in Section 2.7.2 and Section 3.4.1.1, the socket is not restricted to undergo transverse rotation during swing phase, because GRFs are absent and so is the resultant friction between the prosthetic foot and the ground. This is why a transverse rotation adapter can be considered necessary for stance phase only.

3.4.2.   Longitudinal translation

3.4.2.1.   *Motions due to compressions*

Extending the duration of collision time is a means of dissipating energy and helps reduce shock impact (Jøergensen & Bojesen-Møller 1989). This is a process that is based on a number of mechanisms in the anatomic lower limb, including soft tissues, bones, and motion at the joints (Noe et al 1993). Such a process changes the force-time ratio by allowing the body's centre of mass (COM) to decelerate gradually rather than abruptly, because of a relative shortening of the lower limbs.

Linear translation can be regarded as one of the causes for a relative shortening of the lower limbs. Responsible for a large reduction of the acceleration experienced by the lower limb, the heel pad represents one of the most important shock absorbers due to its spongy characteristics (Nack & Phillips 1990, Noe et al 1993). Because its absorbency depends on its thickness (Kinoshita 1992), wear, as a result of repetitive impact, may compromise the absorbing characteristics by triggering degenerative changes. However, additional shock absorbers including shock absorbing shoes and shoe inserts can be worn, which help to prevent or compensate for excessive wear of anatomic shock absorbers (Cook et al 1985, Jøergensen & Bojesen-Møller 1989, Wosk et al 1984).

3.4.2.2.   *Motions due to angulations*

Angular displacements between segments of the lower limbs are another cause for shortenings that can be observed at both the ankle and knee. Lafortune et al 1994 demonstrated that following heel strike, the knee joint flexes before returning to nearly full extension during the second half of stance phase.

In addition to heel pad absorbency, the foot, as a whole, may be considered a shock absorber, because of the relative displacements of the bones as a result of the elastic properties of tendons, ligaments, and muscles, which allow the foot to deform and by doing so, to store and release energy (Ker et al 1987). Regardless of whether angular displacement or longitudinal translations take place between segments of the anatomic lower limb, the fact that the body possesses numerous mechanisms to permit such motions demonstrates that shock impact needs to be reduced in prostheses also.

3.5.   Prosthetic lower limb motions

3.5.1.   Transverse rotation

3.5.1.1.   Motions of prosthetic segments

Multiaxial mobility is a design characteristic incorporated in a number of prosthetic feet to simulate motion at the joints of the anatomic foot. Some designs are based on compression and deflection of elastic materials and others on mechanisms with rotation axles. However, despite no obvious technical restrictions and despite the possibility to permit motion in any direction, the use of transverse rotation in prosthetic feet is limited.

According to Thomsen 1959, an early design of a prosthetic foot permitting transverse rotation was patented in 1921 and was later incorporated in the design of the "Roesser-Gummiblock-Gelenkfuß" (Roesser, Essen, Germany). More recent developments include the "Multiflex foot" (Chas A Blatchford & Sons Ltd, Basingstoke, UK) and "Greissinger foot" (Otto Bock Orthopädische Industrie GmbH & Co, Duderstadt, Germany), which allow motion in all three planes. Boonstra et al 1993 investigated motions of the Multiflex foot, but measured angular displacements in the sagittal and coronal plane only.

Buchgold 1991 investigated the design characteristics of, and maintenance procedure for, the Multiflex foot but, despite describing transverse rotation as an unusual feature in prosthetic feet, the author did not elaborate any further on this matter. Edelstein 1991 described some features of the Multiflex foot and Greissinger foot, and explained that motion in all three planes not only helps those feet to conform to the ground, but also reduces shear stresses transmitted to the residual limb.

Esquenazi & Torres 1991 listed some design characteristics of a number of prosthetic feet that permit transverse rotation, but failed to elaborate on the possible benefits of such motion on the gait. Incorporating a mechanism for transverse rotation in the prosthetic foot rather than providing an additional mechanism to provide such motion proximal to the foot may be advantageous, because of a possible reduction in space requirements and weight. However, this may be achieved at the expense of reduced durability and a foot with such a mechanism incorporated may not be the most suitable type for a particular amputee. The choice of suitable prosthetic components therefore is greater when deciding on separate parts.

3.5.1.2.   *Motions of transverse rotation adapters*

Mulby & Radcliffe 1960 suggested that the socket during trans-femoral gait undergoes 3° of internal and 10° of external rotation with up to 75lbin (approximately 8.48Nm) of torque acting on the lower limb. Amputees with skin problems or with a range of motion exceeding 5° of transverse rotation between the pelvis and the foot were defined as those who would benefit from such a design, but no explanations were given as to how any of the figures were derived. Staros & Peizer 1973 described a transverse rotation adapter, which permitted 7° of angular displacement and, unlike current designs, in one direction only (Lord Corp. of Erie, Erie Pennsylvania, USA). From this finding, one can assume that the authors were not referring strictly to unidirectional motion, but to either internal or external rotation, with the device subsequently returning to its neutral state. Whether transverse rotation in only one direction provided any advantage over devices with bidirectional motion was not clarified. Another, more recently developed transverse rotation and longitudinal translation adapter called "Delta Twist" (Otto Bock Orthopädische Industrie GmbH & Co, Duderstadt, Germany) allows motion in one or both directions to be suppressed. However, the justification in the company's promotional literature for this feature seems rather non-scientific in that it represents nothing but "a great addition for special patient needs".

Housing two ball bearings and an elastomer torsion spring, the "UC-BL shank axial rotation device" (Biomechanics Laboratory University of California, Berkeley California, USA) was tested by Lamoureux & Radcliffe 1977 on trans-femoral amputees who, with the device incorporated in the prosthesis, experienced a reduction in skin problems. Despite positive results, the authors suggested that trans-tibial amputees might be less in need for such a device, because of a normal hip and the

resultant freedom for transverse rotation. Firstly, however, no evidence was given that motion at the hip in trans-tibial amputees is what they described as "normal". Secondly, the authors considered transverse rotation adapters less critical for trans-tibial amputees, as they probably assumed that the resultant freedom for transverse rotation in response to a "normal hip" counteracts and therefore neutralises to a certain extent the rotation occurring at the pelvis.

It can be seen from the study by Levens et al 1948, which is used as a general guide only, as discussed in Section 3.4.1.1, that transverse rotation of the femur was shown to be greater than, and in phase with, transverse rotation of the pelvis. This demonstrates that transverse rotation of the femur does not counteract transverse rotation of the pelvis, but that it occurs in addition to it. Therefore, if the assumption is true that for trans-tibial amputees, transverse rotation at the hip is similar to that of non-amputee gait, this stresses the need to utilise a transverse rotation adapter for trans-tibial amputees despite this being considered less critical by Lamoureux & Radcliffe 1977.

Schmidl 1979 recorded the absolute values for transverse rotation during trans-tibial and trans-femoral gait, but without relating these data to temporal gait characteristics. It was shown, however, that the sum of internal and external rotation was approximately 14-15°. This was similar for both levels of amputation and greater in symmetry with respect to the neutral position in trans-tibial amputees. Therefore, despite the assumptions made by Lamoureux & Radcliffe 1977 that, as explained previously in this Section, trans-tibial amputees may be less in need for a transverse rotation adapter, findings by Schmidl 1979 demonstrate that the need for such a device is of similar importance for trans-tibial and trans-femoral amputees.

3.5.2.   Longitudinal translation

3.5.2.1.   Motions of prosthetic segments

Prosthetic knee joints may be flexed during swing phase but remain fully extended throughout stance phase to create sufficient stability within the prosthesis (Radcliffe 1970, Radcliffe 1977, Radcliffe 1994). This, however, not only prevents shock absorption, because of the lack of compliance from the prosthesis, but it also prevents the prosthetic gait pattern from being assimilated to that of non-amputees.

A weight activated mechanism, the "bouncy knee", stabilises the joint while a rubber bush, in which its single axle is embedded, permits some degree of rotation and therefore controls knee flexion (Fisher & Judge 1985, Fisher & Lord 1986). This was based on a modified "Blatchford Stabilised Knee" (BSK) and later led to a design with similar features, the current "Stanceflex Endolite Stabilised Knee" (SFESK) (Chas A Blatchford & Sons Ltd, Basingstoke, UK). Polycentric mechanisms represent an alternative solution, such as the "3R60" knee (Otto Bock Orthopädische Industrie GmbH & Co, Duderstadt, Germany). Part of the linkage arrangement was designed to permit stance phase knee flexion during which the instantaneous centre of rotation (COR) shifts further posteriorly to maintain stability of the knee (Blumentritt 1997). With the 3R60 knee, shortening of the shin section during knee flexion (Blumentritt et al 1997), as is characteristic for polycentric knees with a certain geometry (Gard et al 1996, Greene 1983), occurs in addition to a relative shortening of the whole prosthesis, as with the bouncy knee. Therefore, with both the bouncy knee and 3R60 knee undergoing the same amount of flexion, the overall relative shortening and shock absorption should theoretically be greater with the latter.

Also, prosthetic feet that permit motion in the sagittal plane and in particular plantarflexion or simulation of plantarflexion by compressing the heel, as in the Soft Ankle Cushion Heel (SACH) (Goh et al 1984, Stein & Flowers 1987), dampen impact at heel strike, because of the shortening of the prosthesis length, as with the anatomic ankle and heel pad (Edelstein 1991, Esquenazi & Torres 1991). However, it is debatable whether the amount of dampening is sufficient without some degree of knee flexion from artificial limbs, as in joints described previously in this Section.

3.5.2.2.   *Motions of longitudinal translation adapters*

The Terry Fox jogging prosthesis is a spring-loaded telescopic unit incorporated in the shin section (DiAngeleo et al 1989, Martel 1986). It facilitates longitudinal translation and is designed not only to absorb shock impact during compression of the spring, but also to release the energy stored later during stance phase. However, DiAngelo et al 1989 found that, because of a spring mechanism with an inappropriate amount of resistance, as well as a pneumatic damper, which seemed to counteract the decompression of the spring, the desired extent of shock absorption and energy release was not achieved.

Flex-Foot Inc, Aliso Viejo California, USA incorporated the concept of energy storage and shock absorption in the design of prosthetic feet. In addition to carbon fibre leaf spring technology, as used in all of their Flex-Foot designs, the "Reflex VSP" (Vertical Shock Pylon) foot comprises a telescopic shin section with an external carbon fibre leaf spring to control longitudinal translation. Research into this foot demonstrated that neither permitting nor restricting longitudinal translation greatly affected its influence on the gait parameters (Miller & Childress 1995, Miller & Childress 1997). However, the findings may be influenced by lack of statistical power, as only two subjects were considered. In turn, research into trans-tibial gait using a SACH foot, a Flex-Foot and a Reflex VSP foot revealed that the latter improved gait efficiency and reduced energy expenditure and exercise intensity (Hsu et al 1997, Hsu et al 1999, Hsu et al 2000). However, no explanations were given as to what type of SACH or Flex-Foot was being used. Yack et al 1999 demonstrated that with trans-tibial amputees ascending stairs using the same prosthetic feet, the work done by the hip on the amputated side was greatest using the SACH foot, which indicates that energy storage can have a positive effect on prosthetic gait.

Fergason & Boone 2000 also elaborated on the importance of longitudinal translation to reduce shock impact by using a telescopic shin section. These authors pointed out that the amount of longitudinal translation is adjustable in the majority of such devices, but no examples were given. Instead, what is adjustable in most adapters examined for this study is the resistance to longitudinal translation, which, in turn, will consequently affect the amount of travel, providing that the same amount of force is applied. Changing the amount of travel without altering the resistance to longitudinal translation can have detrimental effects. For instance, a reduction in the amount of travel possible may cause longitudinal translation to halt abruptly when the mechanical stops inside the adapter are hit, making the use of such devices pointless, because shock impact would still occur.

3.5.3.   Transverse rotation and longitudinal translation

3.5.3.1.   Motions of combined adapters

Staros & Peizer 1973 reported on a device called the "S.P.T. Limb" (Een-Holmgren, Uppsala, Sweden) that provided, in addition to transverse rotation, longitudinal translation also to simulate knee flexion. The authors gave no descriptions on the type

of design or the actual effects of such a device on the gait. In turn, research into the "TT Pylon" (Chas A Blatchford & Sons Ltd, Basingstoke, UK) was conducted by a number of authors, but its effects on gait were interpreted primarily because of longitudinal translation rather than transverse rotation, as elaborated on in the following paragraphs.

Buckley et al 2002 reported on the gait of six trans-tibial amputees who, with the TT Pylon incorporated in their prostheses, experienced a reduction in energy expenditure when travelling at 130% and 160% of their normal walking velocity. Despite the lack of significant findings encountered during normal walking velocity, transverse rotation was not being considered as the source for the effects found at higher speeds. Whatever the actual reasons were for those findings, three of the subjects who benefited most from the TT Pylon also had this device incorporated in their own prosthesis. This is why those authors considered it possible that increased familiarity with the device may maximise its effects on gait.

Gard & Konz 2001 found that incorporating a TT Pylon (Blatchford & Sons Ltd, Basingstoke, UK) in a trans-tibial prosthesis caused a decrease in the initial vertical GRFs. Although this effect may be the result of longitudinal translation, the authors did not elaborate on whether transverse rotation of the device was possible or whether it was locked. It would therefore be speculation to assume that only longitudinal translation was responsible for such effects. A later publication by Gard & Konz 2003 reported on similar findings with regard to the initial vertical GRFs. In this study, the motion adapter that was being used was again the TT Pylon, and both its transverse rotation and longitudinal translation elements were being permitted simultaneously. The authors did address that transverse rotation may also have an effect on amputee gait, but they assumed that such influences had not contributed to changes in gait due to longitudinal translation. Again, assumptions were made without substantiating any conclusions.

Ross & McLaren 2001 analysed the gait of ten trans-femoral amputees with two different lower limb set-ups, namely a TT Pylon with longitudinal translation permitted and with this motion restricted. However, the results were unclear in that the authors reported a change in the vector profiles, but did not elaborate on what measurements these profiles represent. Also, as with the study by Gard & Konz 2001, Ross &

McLaren 2001 did not clarify whether transverse rotation was possible or not, which is why an interpretation of the results is similarly speculative.

Using the "OS1" and "US1" adapter (medipro Technik, Bayreuth, Germany, designed by Century XXII Innovations Inc, Jackson Michigan, USA), the study by Stauf 2000 was, unlike studies described throughout Section 3.4, based on gait analysis regarding both transverse rotation and longitudinal translation. Tests were conducted with only one trans-femoral and one trans-tibial amputee, thus demonstrating lack of statistical power. Also, in addition to insufficient clarity concerning the description of technical details for the collection and analysis of the data, the relationship between the torque around a vertical axis and transverse rotation appeared to be based on a static rather than dynamic situation, which may falsify the results. In turn, with regard to longitudinal translation, the results showed a reduction of the force-time ratio for the early parts of stance phase by 25% and 20% for the trans-femoral and trans-tibial amputee, respectively. This indicates positive shock absorbing characteristics from those adapters.

3.5.3.2.   *Motion adapter design criteria*

A number of authors reported on design criteria that motion adapters should either possess or that future models would benefit from. However, these publications all focused on purely the transverse rotational aspect, and no literature was found that investigated suitable design characteristics with regard to longitudinal translation. Only transverse plane motion therefore is described here.

To design motion adapters with suitable characteristics concerning transverse rotation, one must consider the type of mechanical features that need to be incorporated. Lamoureux & Radcliffe 1977 suggested a small and lightweight mechanism that would fit into a variety of prostheses to reduce the inertia of the limb. A dampening mechanism was proposed to prevent excessive vibrations, caused when the adapter returned back to its neutral state too quickly. These authors considered transverse rotation of up to 20° in each direction to be a sufficient range. They recommended mechanical stops and a unit to return the adapter to its neutral state that can be customised for each amputee. However, no reasons were given for these considerations. Also, despite their recommendations with regard to adjustments of the return unit, a resistance of about 0.23Nm/° was suggested. This was, without substantiation,

considered low enough not to exceed the friction at the residual limb-socket interface and high enough to permit the adapter to return back to its neutral state. The authors also proposed rotation that does not occur purely in the transverse plane and considered asymmetrical, nonlinear forces from the return unit.

Asymmetrical resistance is a feature incorporated in the recently released transverse rotation and longitudinal translation adapter "Delta Twist" (Otto Bock Orthopädische Industrie GmbH & Co, Duderstadt, Germany), but the company's promotional literature includes no scientific explanation for incorporating such a feature. Kaphingst 1977 analysed a variety of resistances to transverse rotation including 0.15Nm/°, 0.23Nm/° and 3.9Nm/° and considered the first and the last figure as quite "soft" and quite "hard", respectively. However, neither were the sources of those figures defined nor were the assessments of those figures substantiated. This author also suggested a design, which allows the motion adapter to be converted into a rigid device, if required, by manually locking it in its neutral state for security on different ground surfaces.

As to the location of a motion adapter within trans-femoral and hip disarticulation prostheses, Knoche 1979 considered it to be irrelevant whether transverse rotation occurs proximally or distally, but without backing up this assumption scientifically. More recent studies revealed that in trans-femoral prostheses the amounts of transverse rotation between the socket and pelvis were larger with the motion adapter incorporated than without it (Twiste et al 2001, Twiste et al 2001), as was the case in the study by Lamoureux & Radcliffe 1977. However, with a motion adapter incorporated in the shin section and later in the thigh section, the tests were inconclusive regarding the adapter's location, possibly because of lack of statistical power resulting from research into the gait of two subjects only.

Prescribing motion adapters can be confusing and misleading when the decision is made based on commercial literature that is often designed according to marketing strategies rather than validated scientific evidence. Some authors reported on specialised activities as a criterion for transverse rotation and they emphasised the importance of such a displacement for torsional tasks including golf (Fergason & Boone 2000, Schuch 1989). This is also an activity probably used as one of the most frequently encountered prescription guidelines in commercial literature but, in most cases, lacking scientific backup. Quesada et al 2000 and VanNess et al 2000 analysed the performance of golf

swings when amputees were using a prosthesis without a transverse rotation adapter. They found, amongst other deviations from motion patterns in non-amputee gait, a reduction in the amount of hip rotation and club swing as well as speed of hip and shoulder rotation. Their findings consequently indicated that there is less freedom of motion amongst the amputee population.

3.5.3.3.   Current adapter designs

Transverse rotation adapters, longitudinal translation adapters and combined transverse rotation adapter and longitudinal translation adapters are predominantly designed to be integrated into endoskeletal constructions, presumably because this is the type of structure used for the majority of modern prostheses. Also, due to the outer, weight bearing shell of exoskeletal constructions that simultaneously serves as cosmesis to resemble the shape of an anatomic limb, as described in Section 2.5.1.2, integration of such adapters in prostheses of this type of structure would spoil the appearance of the limb.

Currently available adapters are typically based on a proximal and distal housing, with a return unit located in between. Return units permit adapters to be returned back to their neutral state following relative displacement between the proximal and distal parts of the adapter, as already explained in Section 3.2.4 concerning transverse rotation. The purpose of such a mechanism is also the same for longitudinal translation. During transverse rotation or during longitudinal translation the return unit will be distorted or compressed while the two housings are being rotated or telescopically displaced in opposite directions to one another, respectively. Because of the elastic properties of the return unit, distorting or compressing it generates resistance to those motions and allows such adapters to return back to their neutral or fully elongated state upon removal of opposing forces. The mechanical representation of such units is based, amongst others, on elastomers, coil springs, or as mentioned in Section 3.5.2.2, on leaf springs, whereby the density, thickness and width determines the resistance to that motion.

3.6.   <u>Aims and objectives for the current study</u>

Clearly, there is the potential for compliant materials or components in prosthetic limbs to accommodate rotation and translation between the socket and foot. However, the field of prosthetics is awash with adapters that are regularly prescribed to patients,

despite a lack of structured and focused research into the mechanical and clinical value of those devices. In the short term, the dissemination of results from research into transverse rotation and longitudinal translation would provide practitioners with the opportunity to utilise evidence-based practice in the prescription of possibly the most effective equipment currently available. In the long-term, research results could be used to develop prosthetic equipment for more efficient healthcare practice and therefore to optimise amputees' rehabilitation processes.

It was hypothesised that the gait parameters and/or the loads exerted onto the residual limb may vary depending on whether transverse rotation and/or longitudinal translation is permitted singularly or in combination. If this was the case, then it might be possible to predict whether the introduction of adapters with these characteristics would provide a reduction or prevention of tissue damage on the residual limb.

The aim was therefore to carry out a biomechanical study on the effects of introducing the described compliant elements into trans-tibial prostheses. The adapters that permit these compliances are widely used devices. They are claimed to reduce the stresses on the residual limb and may to some degree mimic the kinematics of the anatomic foot. The current study addressed these claims and in particular investigated whether the motions at the adapter:

1)   have a major effect on the sound and amputated side gait parameters;
2)   change the kinematics between socket and prosthetic foot;
3)   reduce the loads on the residual limb.

Tests were conducted while permitting transverse rotation and longitudinal translation separately, together and not at all. These four test procedures consisted of recording the gait of amputees who were recruited as volunteers to walk on customised test-prostheses in a gait laboratory. This facilitated a process of elimination to determine the effects of these motions on unilateral trans-tibial amputee gait.

As this type of investigation had not previously been undertaken, an existing method for conducting the required tests could not be found. Some of the equipment needed was already available within the department at the University of Salford, where the current study was undertaken. However, some instrumentation had to be developed and then

subsequently manufactured, so that prosthetic hardware as well as customised measuring devices were available. The following Chapters report on all necessary equipment used during the current study by detailing design characteristics, manufacturing procedures, testing methods and data processing algorithms. This is followed by the results and discussion, a general discussion and finally by the conclusions.

CHAPTER 4. <u>PROSTHESES AND SUBJECTS</u>

4.1. <u>Customised prostheses</u>

4.1.1. <u>Justifications for test-prostheses</u>

Prosthetic components have to be easily interchangeable to create a sequence of set-ups that result in four types of test procedures to permit transverse rotation and longitudinal translation separately, together and neither of them, as described in Section 3.6. Using the prostheses that belong to the subjects, whose recruitment strategy for participation in the tests will be elaborated on in the Section 4.2, was not an option. This is because, following disassembly of their own prostheses for the purpose of interchanging components, it may not have been possible to fully restore the alignment back to its original state.

Dealing with amputees and prostheses in the UK is governed by regulatory authorities including the Health Professions Council (HPC) and the British Association of Prosthetists and Orthotists (BAPO). This ensures that the health and wellbeing of people who need, or use services regarding their amputation, will be protected. Also, companies that design and manufacture prosthetic components need to have their products tested over a set number of cycles to comply with a level of quality stipulated by the International Standards Organisation (ISO). Whoever adjusts, maintains, repairs or supplies prostheses has to inspect the appliances for safety and is liable for any harm inflicted upon amputees as a result of the prostheses breaking down or fitting inappropriately. Interchanging intrinsic components alters the original state of prostheses and therefore voids the warranty given by whoever undertook the required safety checks. This transfers the liability to the last person involved in changing the structural integrity of the prostheses, even if the original state of those limbs was fully restored.

Due to different individual needs, it is unlikely that the subjects' own prostheses are all based on the same prescription of components. Apart from difficulties that may arise from incompatibility of already fitted components with other components that need to

be incorporated for the tests, it was considered vital for subjects to wear a prosthesis with the same types of incorporated components as all the others had. This lends the tests consistency to make inter-subject comparisons more accurate. Therefore, each subject had a test-prosthesis manufactured that permitted easy exchangeability of components without the need to use the subjects' own prostheses at all.

4.1.2.   Structures for test-prostheses

As explained in Section 3.5.3.3, transverse rotation adapters, longitudinal translation adapters and combined transverse rotation and longitudinal translation adapters are predominantly designed for prostheses of endoskeletal construction. Consequently, because it is easier to use commercially available adapters rather than to specifically design and manufacture customised ones for the tests that may not function as well as those already available, an endoskeletal construction was the type of structure chosen for the test-prostheses assembly.

By using the same types of components, the completed test-prostheses were all identical, except for the sockets, which were customised in terms of shape and alignment for each subject. Although the prosthetic foot and shin tube were of the same type for all subjects, they represented additional factors that distinguished one test-prosthesis from another in that their length differed depending on the length of the subjects' contra lateral non-amputated foot and leg.

4.1.3.   Suspension systems for test-prostheses

4.1.3.1.   Considerations for choices of suspension

As mentioned in Section 2.8, the two types of motions that will be the source of this investigation are based on angular displacement in the transverse plane and linear displacement in proximal-distal direction between the socket and the prosthetic foot. Part of the current study concentrated on findings encountered in the literature that gave rise to speculation that these types of motions may be, as explained in Section 3.3, beneficial for the reduction of circumferentially and longitudinally directed shear stresses.

Measuring transverse rotation and longitudinal translation between the socket and the prosthetic foot was determined as one of the areas of data to be collected in order to

establish the extent of displacements that typically occur at motion adapters. Only if the residual limb is sufficiently embedded into the socket, to minimise relative motion between an amputee's anatomy and prosthesis, can the information regarding socket displacements relative to the prosthetic foot be related to residual limb displacements.

4.1.3.2. *Deciding on the type of suspension*

The chosen suspension system used during the current investigation was based on locking liners for reasons that are related to this system's superior interfacing characteristics, as explained in Section 2.5.2. Compared to more traditional ways of suspending prostheses, as outlined in Section 2.5.1, with locking liners, motion at the residual limb-socket interface could be assumed to be minimised. This justified the speculation that the extent of transverse rotation and longitudinal translation of the socket and the residual limb relative to the prosthetic foot would be similar.

The brand of liner chosen for this study was an Iceross silicone liner (Össur hf, Reykjavik, Iceland), because of its reinforcing distal matrix that permits circumferential expansion and reduces distal stretch of the silicone to minimise piston action. Also, the fact that the department at the University of Salford, where the current investigation was undertaken, had a large range of these liners readily available supported this choice.

4.1.3.3. *Deciding on the type of liner*

As one of the aims of this study was to measure the loads exerted onto the residual limb, cushioning effects from thick liners would reduce the force-time ratio at the residual limb-socket interface. This would make it less accurate to establish the magnitude of residual limb pressures. Taking into consideration that Iceross liners are available in different thicknesses, it was decided to choose the Iceross Original Two Colour, which is the thinnest type produced by Össur hf, Reykjavik, Iceland. Unlike cushion liners, as with the Iceross Comfort for instance, which has a thickness of 6mm proximally, 7mm distally and 16.2mm at the distal end, the Iceross Original Two Colour measures 2mm proximally, 4.5mm distally and 12.5mm at the distal end.

The reinforcing distal matrix varies in length between 90-140mm depending on the sizes of Iceross liners required, which range from 160-450 and this corresponds to the residual limb's circumference in mm as measured 40mm proximal to its distal end. The

smaller sizes are generally designed for upper limb amputees and the larger sizes for trans-femoral amputees leaving the mid-range predominantly for trans-tibial amputees, for whom the matrix sizes are fairly similar in length between 90-100mm. Iceross liners are available with customised matrices, but these are costly and would have had to be specially purchased for this study. This appeared unnecessary as for this level of amputation differences between large and small Iceross liners of only 10mm matrix length were considered to have only a negligible impact, if any, on the tests results.

4.1.4.   Locks and sockets for test-prostheses

4.1.4.1.   *Considerations for choices of locks*

Some commercially available locks have no function other than to grip the locking pin at the distal aspect of the liner. This type of construction requires an inner socket that contains the lock and an outer socket that contains a connecting system for linking proximal parts of the prosthesis to distal parts. Other commercially available locks have a dual function in that they simultaneously act as a gripping device as well as a connecting system. The advantage of this type of lock over the type that acts solely as a gripping device is that it only requires one socket, which reduces the weight of the prosthesis and makes its manufacture less costly and time consuming.

Despite those advantages, a dual function adapter may not be ideal for amputees whose residual limb orientation requires excessive socket angulations, because the lock's aspect that acts as a connecting system is similar in design to standard adapters without a lock and limited only to normal adjustment ranges. If excessive socket angulations were required, it would be more appropriate to use the other type of lock that does not contain an integrated connecting system. The desired alignment with this sort of device can be achieved during manufacture of the prosthesis by altering the relative orientation between the inner and outer socket. However, such measures are rarely required. Also, in prostheses with a lock that has an integrated connecting system, the distance between the distal end of the connecting system and the ground is greater than in prostheses with the other type of lock that has no integrated connecting system. The former therefore provides more space for all other components that need to be incorporated as part of the test-prostheses' assembly, which is why a lock with integrated connecting system was the choice for this study.

4.1.4.2.   *Deciding on the type of lock*

As mentioned in Section 2.5.1.2, prostheses of endoskeletal construction are usually manufactured with an acrylic or thermoplastic socket. Locks with an integrated connecting system are available for both types of socket. The department at the University of Salford, where the current investigation was undertaken, had one "PyraLok" (OrthoEurope Ltd, Abingdon, UK) with integrated connecting system readily available, which is a locking system based on a notched pin. As is the case with the majority of commercially available locks, upon doffing of the prosthesis the pin can be pulled out of the PyraLok by pressing a release button at the side of the lock housing, as explained in Section 2.5.2.2.

4.1.4.3.   *Deciding on the type of socket*

When using an acrylic socket, the manufacturing process requires the lock to be laminated into the socket and removal of the lock is only possible upon destruction of the socket. This was considered a disadvantage, because the number of PyraLoks available was less than the number of subjects due to be tested. Therefore, in cases where test procedures or raw data might appear dissatisfactory, subjects involved in those tests would need to be retested and their previous sockets renewed, which would be an exceedingly costly and time consuming process. Unlike acrylic sockets, the draping process for thermoplastic designs does not require the lock to be integrated during socket manufacture. Instead, the lock can be mounted into the socket using an inner and outer plate that sandwich the distal aspect of the socket by holding it securely with four bolts. The process of removing and reinserting the lock into the socket can therefore be repeated as often as required. A PyraLok for thermoformed sockets therefore became the lock of choice for the current study. In turn, this also determined the method for manufacturing the test-sockets.

Despite advantages of PyraLoks for thermoformed sockets over PyraLoks for acrylic sockets, the methods used for bonding each type of lock to their respective socket type have further implications on socket manufacture. Because PyraLoks for acrylic sockets are laminated in, no further means for bonding the lock to the socket are required. This means that the diameter of the lock's housing is designed to be minimal. In turn, due to the inner and outer plate of the PyraLok that sandwich the distal aspect of thermoplastic sockets, the overall lock housing diameter is larger than it is in PyraLoks for acrylic

sockets. This is to accommodate the four bolts that hold the inner and outer plate of the PyraLok together. In turn, the larger lock housing diameter therefore requires the distal outer walls in thermoplastic sockets to be further away from the lock centre. In amputees with very conically shaped residual limbs, this can lead to loss of contact around distal regions of the socket. This will have an impact on the overall socket fit in that proximal residual limb parts have to bear more weight than if total contact would have been maintained.

Instead of using just one outer socket, a thin, inner, total contact socket could be draped with its distal, outer parts being built up by extending them circumferentially with rigid polyurethane foam, so that this region is no smaller in diameter than the inner plate of the lock. With the outer socket draped over both the inner socket and the build-up, the polyurethane foam acts like a filler for the void between the two sockets, as displayed in Figure 4.1. Upon weight bearing, the distal parts of the inner socket cannot therefore be pushed outward against the outer socket and this ensures maintenance of a constant volume inside the socket. Because the diameter of the polyurethane foam build-up has to be at least the size of the inner plate of the lock, the internal dimensions of the outer socket are of sufficient size to allow easy access to its distal regions for insertion and removal of the inner plate.

The inner socket has no structural integrity other than being held by the outer socket and by the rigid, yet very light, polyurethane foam. This minimises the overall weight increase and makes this construction still lighter than those based on two sockets for locks without an integrated connecting system. Standard co-polymer sheets for draping the inner and outer sockets were readily available at the University of Salford's department where the current study was undertaken and so was the polyurethane foam.

4.1.4.4. *The lock's connecting system*

The aspect of the PyraLok that acts as a connecting system is based on what is known as a pyramid system. Displayed in Figure 4.1, it is an adjusting device for aligning the socket relative to the distal components of the prosthesis. Such a device consists of a dome and a pyramid that is embedded into a concave recess like a ball in a ball-and-socket joint. The concave recess forms the proximal part of a tube clamp that is located distal to the PyraLok and connected to the shin tube. It governs the angular orientation relative to its dome-shaped counterpart.

The apex of both the dome and the pyramid are joined together. The base of the pyramid inserts into a central, circular cut-out within the concave recess. Four equidistantly spaced grub screws are located circumferentially around the circular cut-out. They point centrally and have a slight orientation away from the dome and towards the base of the pyramid. Their flat end therefore corresponds with the four flat sides of the pyramid. Due to the expanding cross-section of a pyramid from its apex to its base, tightening all four grub screws firmly against the pyramid's flat sides forces the dome against the concave recess and therefore bonds the PyraLok to its distally located tube clamp.

Turning one grub screw outward releases the pyramid's corresponding flat side. Therefore, by turning the opposite grub screw inward, the pyramid is forced into the space created by turning the other grub screw outward. Changing the position of the pyramid means that the dome slides inside the concave recess. This alters the angle between the PyraLok and its distal tube clamp. Because the pyramid is held by all four grub screws, adjusting the angular orientation of the lock in this way is easier if the other two grub screws are also being loosened off to release the tension they created between those grub screws and the pyramid. With the PyraLok's alignment range of approximately 10° in anterior, posterior, medial and lateral direction each, this extent of mobility was considered to be sufficient for trans-tibial amputees with a normal residual limb alignment. The dome and pyramid are generally being referred to as a male pyramid connector and the concave recess as a female pyramid receiver.

4.1.4.5.   *The lock's pin*

The volume of the residual limb can fluctuate as a result of fluid loss or retention. If the volume is increased, amputees may have difficulties in donning their prosthesis. Because it is vital with locking liners to be able to engage the pin's first notch into the lock to pre-stretch the tissues, as explained in Section 2.5.2, an increased residual limb volume can prevent this from happening. Repeatedly pushing downwards is unlikely to achieve engagement of the pin's first notch, because the tissues will just bulge and stop the residual limb's distal parts from sliding further into the socket. With ten notches, the PyraLok's standard pin, as displayed in Figure 4.1, is approximately 50mm long and when fully inserted into the PyraLok the pin is about level with the base of the lock's pyramid at its distal connecting system.

Figure 4.1:   Cross-section of sockets and PyraLok with pyramid attachment

Inner socket

Outer socket

Polyurethane build-up

Locking pin with notches

Inner attachment plate

Release button

Outer attachment plate

Dome / concave recess

Grub screw

Male pyramid connector

Female pyramid receiver

Tube clamp

Shin tube
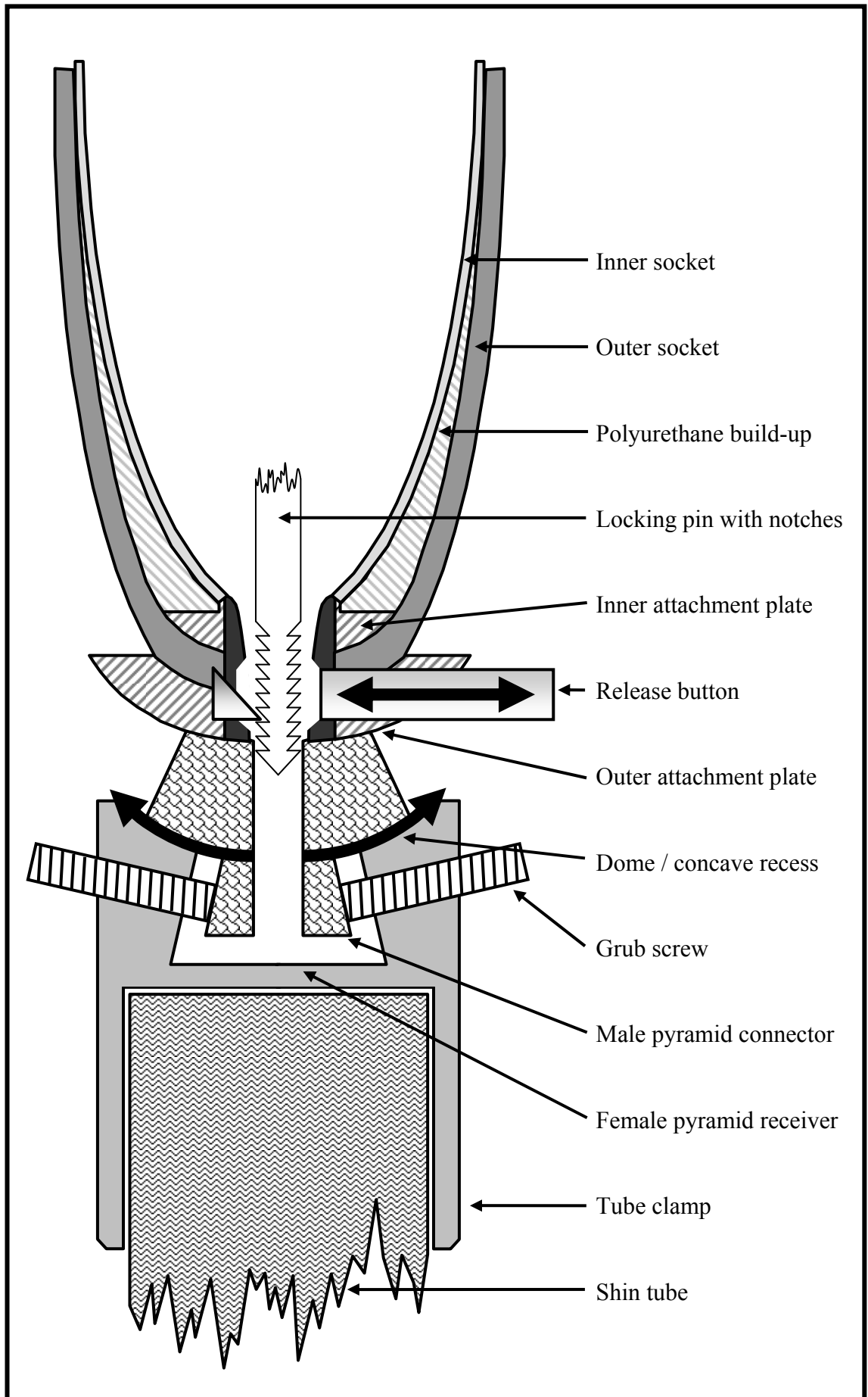
Two additional pins were manufactured with identical dimensions as the original pin apart from length, with one pin 10mm longer and the other 20mm longer. With the same number of notches as the original pin, the extended part of the two longer pins was therefore located between the threaded end for screwing them into the liner and the notched end. Depending on the extent of residual limb volume increase, either extended pin could be used to ensure that the subjects manage to engage the first notch, thus helping them to get into the socket. Inserting an extended pin fully into the PyraLok would make it protrude distally from the base of the lock's pyramid, so that it may interfere with tube the clamp that is connected to the pyramid. Therefore, once the residual limb volume decreased and it became easier to engage several notches within the lock, the socket could be removed to exchange the liner's extended pin with a standard pin.

4.1.5.   **Motion adapters and shin tubes for test-prostheses**

4.1.5.1.   *Considerations for choices of motion adapters*

As mentioned in Section 3.6, a sequence of set-ups will be created that results in four types of test procedures. The extent and type of mobility varies between transverse rotation adapters, longitudinal translation adapters and combined transverse rotation and longitudinal translation adapters. This implies that the internal mechanisms that are responsible for permitting and damping these motions must differ. When deciding what type of motion adapter to use for the tests, it may prove sensible to consider practical aspects for interchanging components between set-ups, as this may have an impact on the choice of motion adapter to be used during the gait laboratory tests.

External dimensions vary between different motion adapters, and so do their connecting systems for linking them proximally and distally to other prosthetic components. This can cause complications during the exchange of motion adapters between set-ups, in that extensions or converter adapters may be required to compensate for different lengths of components and incompatibilities in inter-connecting them. Using a number of different components may not only change the weight of test-prostheses, it can also affect their weight distribution. This may influence the gait characteristics, thus making comparisons between set-ups difficult and potentially inaccurate.

Changes to be undertaken between set-ups should be as straight forward as possible without the need to use a large variety of different components. Those changes should certainly only have minimal, if any, effects on aspects concerning the weight, so that the test-prostheses remain as near as identical between set-ups, except for the different types of motions to be introduced. Instead of using different adapters to create the four set-ups, the easiest approach seemed to be to aim for a solution that involves the incorporation of only one and the same motion adapter that can be modified to permit or restrict the necessary motions by simply exchanging the adapter's internal components. To permit both types of motions, it would be possible to use a transverse rotation adapter as well as a longitudinal translation adapter, but it is less obtrusive just to opt for one motion adapter namely a combined transverse rotation and longitudinal translation adapter, due to space restrictions between the PyraLok and the ground.

4.1.5.2. *Deciding on the type of motion adapter*

Motion adapters to be used during the current study that contain an integrated shin tube can be disadvantageous for customising the lengths of test-prostheses. This is so, because each subject's shin tube length is likely to be different, due to variations in socket-to-ground measurements. A large number of motion adapters would be required to correct for discrepancies in shin tube lengths between subjects, thus increasing the costs of the project. The aim was, therefore, to identify a more versatile type of motion adapter that can be adjusted for customising shin tube lengths to suit several subjects.

A number of motion adapters exist with an integrated tube clamp adapter, rather than an integrated shin tube, for connecting them to standard shin tubes. However, their overall height was rather large, and taking the factors regarding space restrictions described in Section 4.1 into consideration, those adapters were therefore deemed inappropriate for this study.

In turn, the TT Pylon (Blatchford & Sons Ltd, Basingstoke, UK) is one of the shortest commercially available motion adapters, but its disadvantage is that it has an integrated shin tube. Nevertheless, the tube is exchangeable, and due to continuous collaboration between the University of Salford and Blatchford & Sons Ltd, Basingstoke, UK, it was possible to obtain sponsorship in the form of one TT Pylon mechanism and a sufficient number of TT Pylon shin tubes. As this was one of the most suitable motion adapters for the tests, because of its short height, being provided with those components was of

tremendous help and it reduced the costs of the project drastically, thus leaving more funding available for other equipment. The TT Pylon was therefore an appropriate and cost effective option for incorporation into the test-prostheses and it became the choice of motion adapter for this study.

With the housing of the TT Pylon mechanism at one end and the shin tube at the other end, linking the TT Pylon to other prosthetic components required different connecting systems. There are two options available for the housing end and the particular one chosen for the test-prostheses contained a female pyramid receiver, previously described in Section 4.1.4.4. This was ideal for connection it to the male pyramid connector on the PyraLok. The shin tube end was an open ended pipe and connected to a tube clamp adapter.

Manufactured out of light-weight carbon fibre and with an external diameter of 35mm, shin tubes for the TT Pylon are similar to the same company's standard shin tubes without motion adapter. One of the differences is a shoulder at the housing end of the TT Pylon shin tube. Slightly larger in diameter than the shin tube itself, this shoulder acts as an extension and retraction stop to limit longitudinal translation to 13mm. It is not completely circular as it extends over only approximately 280° around the shin tube. In addition to the missing part of the shoulder, there is also a protrusion located inside the TT Pylon housing that extends over approximately 20° of the shin tube diameter. The missing part of the shoulder and the protrusion therefore act as a stop that limits transverse rotation to approximately 60° or 30° of each internal and external rotation.

Also, a Polytetrafluoroethylene (PTFE) surface extends circumferentially over approximately 55mm from the shoulder of the shin tube. It helps in maintaining the alignment between the shin tube and the TT Pylon housing, while these two parts are being displaced relative to one another during both transverse rotation and longitudinal translation.

4.1.5.3.   The motion adapter's return units

As explained in Section 3.5.3.3, motion adapters, including the TT Pylon, contain one, or several, return units to bring their proximal and distal parts, which undergo relative displacement during transverse rotation and longitudinal translation, back into a neutral state. The TT Pylon's return unit for elastically controlling transverse rotation is, as

explained in Section 3.2.4, based on a cylindrical stem or torsion rod that is being twisted during this type of motion. It is made out of thermoplastic, which allows it to store energy while being twisted. Upon reducing the transverse rotation moment, the rod releases the energy, so that the material's memory allows the proximal and distal parts of the adapter to return back to their position prior to rotation.

The torsion rod's main body is a solid cylinder, approximately 50mm long with a diameter of 12mm. One end of the torsion rod is characterised by a shoulder with four equidistantly spaced bores and the other end by a quadrant with dimensions of approximately 12×12mm in a transverse plane cross-section. The shoulder of the rod is firmly bolted through its bores to the TT Pylon housing. In turn, the quadrant inserts into its counterpart, which is a similarly dimensioned central, square cut-out inside a solid core at the shoulder end of the shin tube. Transverse rotation of both the adapter's housing and shin tube in opposite directions relative to one another forces the rod's shoulder to rotate with the adapter's housing to which it is bonded. This forces the rod's quadrant to rotate with the shin tube's matching, central, square cut-out and this twists the rod's cylindrical body.

Although the rod's quadrant and the central, square cut-out have matching and interlinked geometries that hold these two parts together, the adapter is still free to permit its housing and shin tube to undergo longitudinal translation in opposite directions relative to one another. Such a process is possible, because the quadrant is free to move longitudinally along the central, square cut-out. This is so, because the shin tube's core is a guide or female receptacle that slides along a male shaft represented by the rod's quadrant.

The TT Pylon's return unit for elastically controlling longitudinal translation is based on a metal coil spring. Being compressed during this type of motion, the coil spring stores energy and upon reducing the force that triggers longitudinal translation, the energy is being released. Like the torsion rod, the spring's memory allows the proximal and distal parts of the adapter to return back to their position prior to linear displacements. Located against the torsion rod's shoulder and against the shin tube's core, the spring has its outside perimeter positioned against the TT Pylon's housing and its inside perimeter positioned against the centrally protruding torsion rod. A threaded locking ring that slides along the shin tube's PTFE surface seals the adapter's housing and

maintains a straight alignment between shin tube and the adapter's housing. Tightening up the locking ring pushes the torsion rod's shoulder and the shin tube's core closer together, thereby ever so slightly compressing the coil spring, so that this pretension allows the adapter to be fully extended during its neutral state.

Figure 4.2: Torsion rod's de-rotationally aligned quadrants
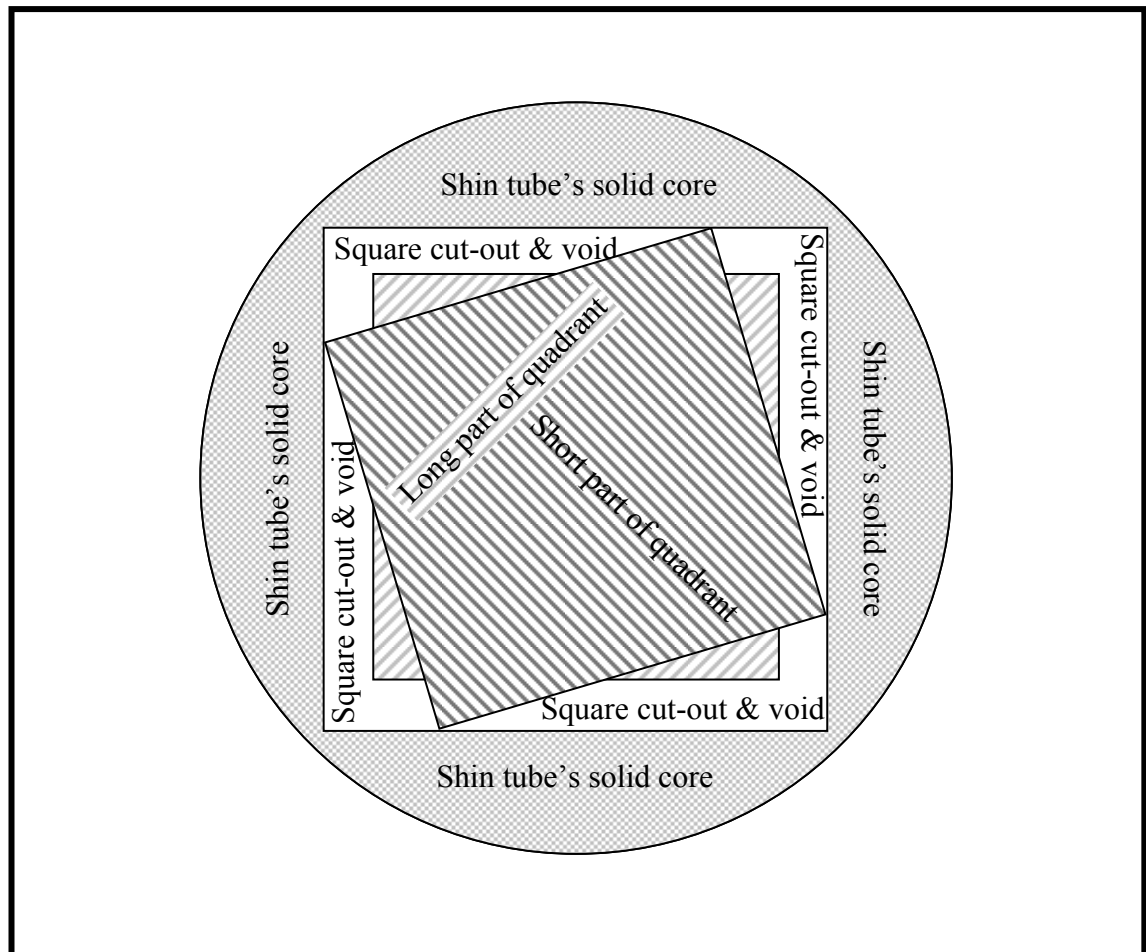
Due to the sliding action between the torsion rod and the shin tube's core, and due to the torsion rod's relatively soft material properties that allow it to distort, the quadrant perimeter can wear and this leads to play inside the central, square cut-out. As a result of this, the TT Pylon may not fully return back to its neutral state following transverse rotation. To overcome this problem, the quadrant, approximately 10mm long, is split up into a main, long part of approximately 6mm length and a second, short part of approximately 2mm length. They are both interconnected by a very short, solid cylinder of approximately 2mm length and 6mm diameter. Because the long and short quadrants are slightly rotated with respect to one another, inserting the torsion rod into the central, square cut-out lines the two quadrants up. Their de-rotational alignment, while inside the central, square cut-out, twists the short cylinder and leaves it under tension, as

illustrated in Figure 4.2. Therefore, the tendency for the two quadrants to rotate with respect to one another is constantly present. Even after some degree of unavoidable wear, the tension between the two quadrants takes up some of the void between the torsion rod and the central, square cut-out, thus allowing the adapter to fully return back to its original orientation prior to transverse rotation.

4.1.5.4. *Deciding on the type of return unit*

Because the manufacturer of the TT Pylon stipulates that the extent of adapter motion depends on the amputees' weight and activity level, specific types of torsion rods and coil springs can be selected from a range of return units to vary the resistances accordingly. The choice of resistances are 0.5Nm/°, 0.6Nm/° and 0.7Nm/° for torsion rods and 8kg/mm, 11kg/mm and 14kg/mm for coil springs. To obtain reasonable data the resistances of both types of return units have to be low enough, so that the proximal and distal parts of the TT Pylon undergo a reasonable amount of relative displacements.

As explained before in Section 4.1.5.2, transverse rotation and longitudinal translation are limited by mechanical stops. Because the tests entailed no activities other than normal walking, with transverse rotation of approximately 60° or 30° in each internal and external rotation direction, it was considered unlikely for subjects to exceed these limits. It was therefore decided that it would be justifiable to use a torsion rod with the lowest resistance to transverse rotation, namely 0.5Nm/°.

The maximum in longitudinal translation of approximately 13mm appeared to be a figure that was more likely to be reached than the maximum in transverse rotation. However, the manufacturer stipulated the displacement during normal walking to be approximately only half the maximum range, namely 5-8mm. It was therefore assumed that a coil spring with resistance of medium magnitude to longitudinal translation, namely 11kg/mm, would be appropriate. As it was considered to be unreasonable to choose subjects with hugely different weights and activity levels, the resistances selected for both return units were decided to be the same throughout the tests, to make comparisons between subjects easier and potentially more accurate.

Despite having decided to use a torsion rod with the lowest resistance, namely 0.5Nm/°, preliminary tests showed that the magnitude of transverse rotation was exceedingly

small. This was taken as an indicator that an even smaller resistance would be required for obtaining data that contain parameters with the potential to have a reasonable impact on the interpretation of transverse plane motion. The torsion rod's resistance is governed by a number of factors, including its length, thickness and the density of its material. The easiest way of undertaking adjustments for lowering its resistance was to reduce the diameter of the solid cylinder that forms the torsion rod's main body. Using a lathe for an even reduction from a 12mm to a 10mm diameter, the torsion rod's resistance to transverse rotation was reduced from 0.5Nm/° to approximately 0.3Nm/°. This was simply checked with a torque wrench. After further preliminary trials, the obtained resistance to rotation proved to be sufficiently small for obtaining an output of reasonable magnitude.

4.1.5.5.   *Deciding on the type of substitute return unit*

It is possible to create a sequence of set-ups that results in four types of test procedures by modifying the adapter's internal mechanism to permit or restrict the necessary motions. Either both types of motions or only one but not the other can be restricted by replacing the return unit with a rigid substitute that is otherwise identical to the return unit's dimensions, to allow it to fit into its position inside the motion adapter. Using a rigid substitute return unit means that the return unit's elastic properties have been removed from the adapter. The return unit therefore no longer controls the now locked motion it previously was responsible for.

In order to lock transverse rotation, the torsion rod was replaced with a near identical substitute that only differed from the original one by the material it was made out of and by the design of the quadrant. Because it was necessary to create a rigid substitute, splitting the quadrant up into two parts that are elastically rotated relative to one another, as with the original torsion rod, would have been a contradiction in itself. However, the fact that a quadrant without this feature would experience some play inside the central, square cut-out was difficult to avoid. Precise machining lent the quadrant dimensions of high accuracy, so that the play was only fractional and unlikely to increase drastically over the course of the study as the quadrant was made out of mild steel. This is a lot more hardwearing a material than the original torsion rod's thermoplastic material.

Due to its relatively heavy weight, mild steel was used in low quantities only. With the remaining parts of the substitute torsion rod being made out of aluminium, this metal's lightweight properties made it possible to assimilate the weight of the substitute torsion rod (32g) to that of the original torsion rod (11g) with reduced diameter (10g). Also, the stiffness of aluminium is greater than that of thermoplastic, thus giving the replacement rod virtually non-elastic characteristics for creating the required rigidity.

To lock longitudinal translation, the coil spring was replaced with a near identical substitute that only differed from the original one by the material it was made out of and by the fact that it was a hollow cylinder or pipe and not a coil. Although the substitute cylinder has the same height as the coil spring, as well as a matching internal and external diameter, the overall volume of material that was required to compose the cylinder's structure is larger than that of the coil spring due to the nature of these two geometrical shapes.

Figure 4.3:   TT Pylon return units and substitute return units
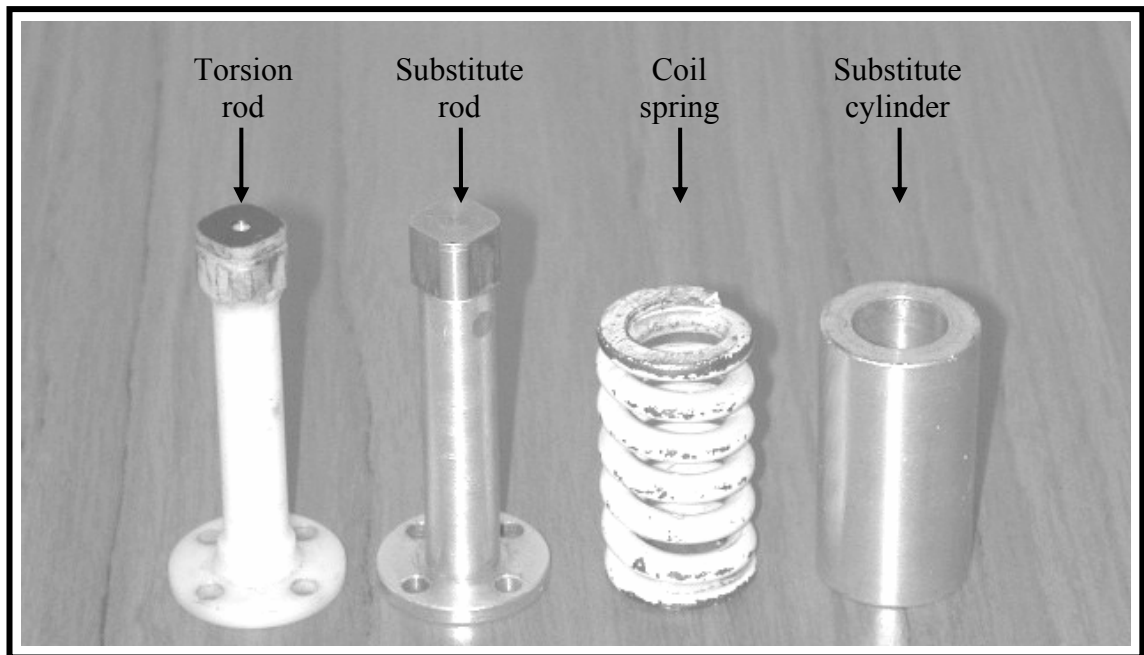
As the coil spring was made out of fairly heavy spring steel and the substitute cylinder out of comparatively light aluminium, the difference between the mass properties of those two metals was nearly compensated for by the difference in volume of material required to compose both structures. This helped in assimilating the substitute cylinder's weight (34g) to that of the coil spring (49g). With the threaded locking ring that slides along the shin tube's PTFE surface tightened up, it was possible to clamp the

substitute cylinder between the torsion rod's shoulder or substitute torsion rod's shoulder and the shin tube's core. Because the replacement is a cylinder and not a coil, its comparatively non-compressible structure prevents the shin tube and the TT Pylon housing from undergoing relative longitudinal translation. Both types of return units and their substitutes are illustrated in Figure 4.3.

4.1.5.6.   *Deciding on the length of test-prostheses*

Providing that the subjects' test-prostheses and their contra lateral sound side are of equal length, when longitudinal translation is permitted, compression of the coil spring during stance phase creates an height imbalance between the left and right side, but this would not happen during set-ups without longitudinal translation. As a result of this, amputees might increase sound side hip, knee and/or ankle motion to prevent the anatomic foot from cuffing the ground.

In turn, lengthening the shin tube by the approximated amount of maximum shortening at the motion adapter would make it possible for the amputated side, during set-ups with longitudinal translation being permitted, to acquire virtually the same height as the contra lateral sound side. This, however, would only occur at the instant of maximum adapter displacement. Lengthening the test-prostheses could therefore make subjects stumble, because the likelihood for the prosthetic foot to cuff the ground during the middle part of swing phase increases when the amputated side is longer than the contra lateral sound side.

A way of preventing this would be to increase motion on the amputated side in a similar manner as previously described in this Section for the contra lateral sound side. Unfortunately such action is impossible, at least with respect to ankle motion, because the artificial ankle can only be moved passively in response to GRFs, which are absent during swing phase. Therefore, the risk for amputees to cuff the ground with the amputated side is greater than for the sound side. To prevent subjects from injuring themselves, it was decided that it would be safer for the test-prostheses to have the same height throughout all set-ups. In particular, whether longitudinal translation was restricted or permitted, the test-prostheses were adjusted to match the contra lateral sound side during non-weight bearing scenarios.

4.1.6.   Ankles and feet for test-prostheses

4.1.6.1.   *Considerations for choices of ankle and foot*

Due to space restrictions between the socket and the ground, prosthetic components chosen to be used for the test-prostheses should be the least obtrusive types available with minimal dimensions to ensure that all the other components that need to be incorporated can fit in without exceeding the artificial limbs' overall build height. As can be seen from Section 4.1.4 and Section 4.1.5, decisions made for choosing previously selected components were based on the same criteria and these should also apply for the identification of an appropriate ankle and foot.

4.1.6.2.   *Deciding on the type of foot*

A large range of currently available prosthetic feet consist of multi-axial articulations that simulate some of the motions at the joints of the anatomic foot, as explained in Section 3.5.1.1. In addition to a slightly flexible keel and a pliable cosmetic shell for providing the prosthetic foot with some degree of conformity to the ground, multi-axial mobility stems from a mechanism that forms an intrinsic part of the majority of such components, but it also increases their overall build height.

An exception to these is the Multiflex foot (Blatchford & Sons Ltd, Basingstoke, UK), as this type of design has a separate mechanism, namely the Multiflex ankle that can be completely detached from the actual foot. In addition to motion in the sagittal and coronal plane, multi-axial mobility usually also involves transverse plane motion, as is the case with the Multiflex ankle. However, this may counteract motion at the transverse rotation adapter. Because the aim was to measure motion at those motion adapters, using prosthetic feet with multi-axial mobility including transverse rotation would therefore be inappropriate, as this can have an impact on the experimental data. Due to the exceedingly low build height of the Multiflex foot, its design without the Multiflex ankle conforms to the selection criteria regarding space restrictions within the test-prostheses.

In addition to matters regarding dimensional limitations, not incorporating the Multiflex ankle would also eliminate potential problems associated with additional articulations, including transverse rotation, as this is possible with those ankle mechanisms. With this in mind and taking into consideration that a whole range of Multiflex feet were readily

available from the department at the University of Salford where the current study was being conducted, it was decided that this is the foot of choice for this investigation.

4.1.6.3.   *The foot's connecting system*

The connecting system for the Multiflex foot is based on a concave, serrated surface that forms the counterpart of a convex, serrated surface at the distal aspect of the Multiflex ankle, which is illustrated in Figure 4.4. Due to the surfaces' curved appearances, locating the ankle forward or backward changes its angular relationship relative to the foot for adjusting the appropriate degree of plantarflexion or dorsiflexion, respectively. Once in the correct position, the ankle and foot's matching serrated surfaces can be tightened together using a bolt. Inserted into the plantar aspect of the foot, the bolt extends through the central slot along the foot's serrated surface and into the thread inside the middle of the ankle's serrated surface thus securing both Multiflex components together. Such a unique connecting system makes the Multiflex foot without its Multiflex ankle incompatible with other prosthetic components. To take full advantage of the foot's low build height characteristics, it was necessary to customise existing components, so they could be used for linking proximal structures of the test-prostheses to the Multiflex foot.

Figure 4.4:   Proximal connection of Multiflex foot via serrated surface
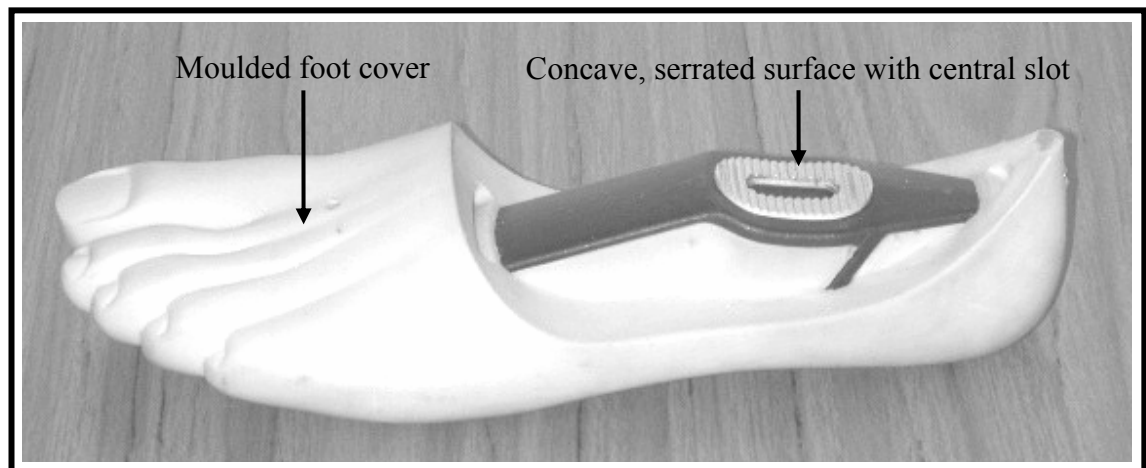
As explained in Section 4.1.5.2, the shin tube end of the TT Pylon is an open ended pipe that can be connected to a tube clamp adapter. These connectors are of standard construction and contain a circular recess of 35mm internal diameter to match the shin tube's external dimensions. By tightening a pinch bolt, that due to its bridging location narrows a longitudinal slot along the 34mm deep recess, the internal diameter is

decreased for securely gripping the shin tube. Increasing friction with the tube clamp adapter by roughening up the shin tube's shiny surface using sand paper, as stipulated by the manufacturer, improves the grip.

The connecting systems on the other side of tube clamp adapters vary. The most basic type is often used for bonding it to SACH feet via a single bolt inserted into the plantar aspect of the foot and tightened into the adapter's central thread. Although the bonding system for the Multiflex foot and ankle is similar in that it is, as described before in this Section, also based on just a single bolt, a tube clamp adapter of this construction is, in addition to its threaded connection, glued to the flat, proximal surface of SACH feet. Conversely, gluing the tube clamp adapter to the Multiflex foot would be difficult without further modifications, due to the foot's concave and serrated surface.

Distortion of a Multiflex foot's flexible keel and pliable cosmetic shell is difficult and, unlike SACH feet, its contribution to simulating motions of the anatomic foot's intrinsic joints is therefore minimal. It must be emphasised that, in addition to the facilities for adjusting the sagittal plane angular orientation between the Multiflex foot and ankle as described previously in this Section, this type of foot is designed to passively conform to the ground due to its interaction with the Multiflex ankle. Not incorporating the Multiflex ankle, but instead creating a rigid connection by using a single bolt and glue would limit the angular adjustments between the tube clamp adapter and foot. Its plantar surface may therefore not be flat on the floor during standing or mid-stance phase, thus making an upright posture, and the gait, unstable.

4.1.6.4.   *The foot's alternative connecting system*

Alternatively, it would be possible to use a tube clamp adapter that does not require a single bolt, but instead possesses a female pyramid receiver for attaching it to the prosthetic foot, whereby the principle behind this type of connection system was previously described in Section 4.1.4.4. Such an assembly would slightly increase the overall build height between the end of the shin tube and the ground. However, it would make the connection far more versatile due to the pyramid system's inherent angular adjustment characteristics.

In order to make the foot compatible with a female pyramid receiver, it would require a male pyramid connector. These can be attached to prosthetic feet using a single, central

bolt, as with tube clamp adapters based on the same bolt attachment principle. For a temporary assembly of only one provisional test-prosthesis, the convex, serrated surface was cut off a spare Multiflex ankle. It was then used as an interface between the flat, distal side of the male pyramid connector and the concave, serrated surface of a Multiflex foot. A single, central bolt extended from the foot through the convex, serrated and now detached surface of the ankle and into the threaded bore inside the pyramid itself. Two additional threaded bores were created in the base of the anterior and posterior aspect of the pyramid and in the convex, serrated and detached ankle surface. Two small bolts were tightened into these bores to prevent the male pyramid connector from unthreading itself due to rotation around the central, single bolt relative to the foot.

Preliminary trials proved that removal of the Multiflex ankle made the test-prosthesis far too stiff, so that the duration of foot flat was miniscule. It only occurred for a fraction of time during mid-stance phase exactly at the instant when the shin tube was vertical within the sagittal plane. Data analyses demonstrated that it was virtually impossible to detect any pattern indicating the occurrence of transverse rotation at the motion adapter. This was contributed to a lack of ankle motion and the near absent foot flat period. Therefore, any degree of transverse rotation of the socket was more likely to occur between the heel and the ground and between the ball of the foot and the ground, as the resistance for these motions was probably less than for motions at the transverse rotation adapter.

4.1.6.5.   *Considerations for choices of ankle mechanisms*

To increase the magnitude of angular displacements at the motion adapter, it was necessary to prolong the duration of foot flat to ensure that both the heel and the ball of the foot are in contact with the ground simultaneously for increased friction over a longer duration. The aim was therefore to create greater sagittal plane motion, but using the Multiflex ankle as a means for achieving this was not an option, as it permits motion in all three planes including transverse rotation.

An ideal solution to the problem was a single axis joint for pure sagittal plane motion. A number of commercially available feet exist that contain an integrated mechanism for creating this type of displacement. Like before, space restrictions and the research budget were dominant criteria for selecting appropriate components. Purchasing

commercial feet with such a mechanism incorporated and with low enough a build height for them to be an acceptable choice is costly. Also, the department at the University of Salford where the current study was conducted did not store a large enough range of such feet to cover all necessary sizes.

Following examination of a number of different feet, it was possible to determine a single axis mechanism with a low build height that could be adapted for linking it to a Multiflex foot. This mechanism was extracted from a "1H38 single axis foot" (Otto Bock Orthopädische Industrie GmbH & Co, Duderstadt, Germany). It was based, as implied by its name, on rotation around one axle, and contained two low friction bearings for holding the axle parallel to the coronal plane of the prosthetic foot. The single axis mechanism, when incorporated in the original Otto Bock foot, is illustrated in Figure 4.5.

Figure 4.5:   Otto Bock single axis foot 1H38
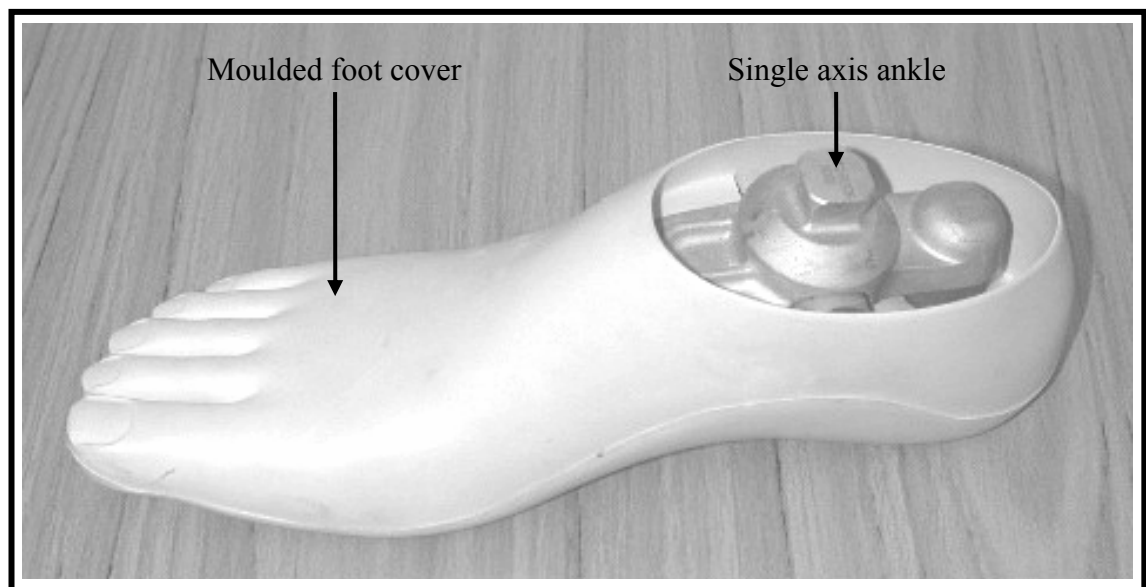
Sagittal plane motion is limited by two compressible blocks or bumpers. These are wedged between recesses in the proximal part of the foot and the anterior and posterior extension plates that form part of the housing in which the bearings are imbedded. A male pyramid connector at the proximal aspect of the housing proved ideal for attaching the mechanism to a tube clamp adapter with a female pyramid receiver. Two threaded protrusions extending distally from the axle served as the mechanism's connecting system to its foot. After feeding them through the bores in the foot's rigid keel, those protrusions can be secured by tightening two nuts against the foot's plantar surface.

4.1.6.6.   *The foot's connection system with the ankle*

Connecting the mechanism to a Multiflex foot was based on a 10mm thick aluminium plate. This plate acted as an interface that is strong, yet light-weight, and low in build height. The central slot extending in the anterior-posterior direction along the foot's concave, serrated surface was long enough to contain not just the usual one, but two bolts. These were tightened into their respective threaded bores along the mid-line of the aluminium plate. Bridged across the concave, serrated surface of the foot, the flat aluminium plate had its edges wedged between the teeth of the serration, thus preventing it from moving once the two bolts were tightened up.

Aligned in medial-lateral direction, the orientation of the two threaded protrusions that extended from the axle through two holes in the aluminium plate would not interfere with the two threaded bores for the bolts. The mechanism was secured in place using two nuts, which needed to be countersunk by milling a groove into the aluminium plate's distal face, as the space between the bridging aluminium plate and the foot's concave serrated surface was too small to let the nuts stick out from underneath the plate. The central part of the plate needed to maintain its full thickness, so that the threads that held the two central bolts were sufficiently strong. In turn, creating grooves at the sides of the plate did not weaken its structure, because the two threaded protrusions could not be fastened with threads inside the plate, so that the strain needed to be taken by the countersunk nuts.

Because Multiflex feet do not possess the necessary recesses for containing the two bumpers that limit the amount of sagittal plane motion, it was necessary to design a tailor made dampening system. Such a system should have similar characteristics to that of the original single axis foot, so that it can be integrated to work in conjunction with the anterior and posterior extension plates of the ankle mechanism. The new system was, like the previous one, based on two bumpers. However, instead of holding both of them in place by modifications undertaken at the proximal aspect of the Multiflex foot, it seemed less time consuming to devise an alternative attachment, so that it would not be necessary to alter every single Multiflex foot to be used for the tests.

The alternative attachment was made out of approximately 4mm thick, semi rigid leather. It had a cut-out to fit around the thick part of the aluminium plate. This flap-like attachment was bolted against the distal face of the plate and served as a platform for

the two bumpers to be glued onto. Once secured in their respective positions, the bumpers were then ground down to gain a shape that gave their rubber structure the appropriate amount of resistance to compression from the anterior and posterior extension plates. This was adjusted in such a way that the prosthetic foot reached a degree of plantarflexion and dorsiflexion sufficient in magnitude to maintain it flat on the ground throughout the majority of stance phase, but without letting it slap down too easily after heel strike. Also, upon swing phase the decompression of the bumpers should allow the feet to fully return back to their plantigrade position. Figure 4.6 shows the Otto Bock single axis mechanism in its new position mounted on top of the Multiflex foot.

Figure 4.6:   Single axis mechanism mounted onto a Multiflex foot
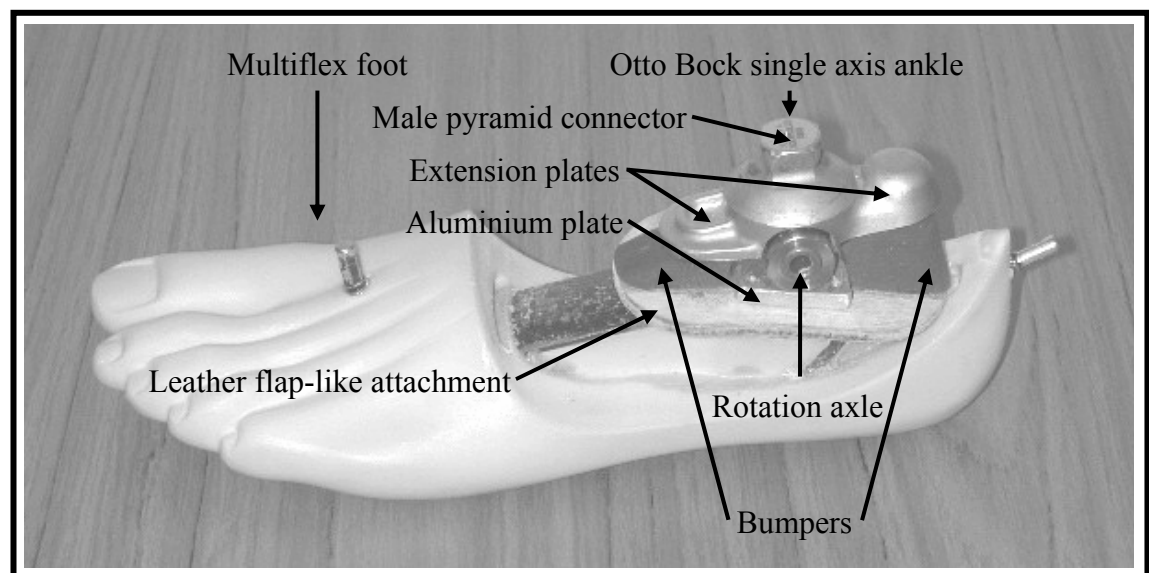
Having rectified problems encountered during the preliminary trials, subsequent definitive tests proved that the introduction of sagittal plane motion had beneficial effects on transverse rotation. This made it possible for patterns indicating the occurrence of transverse rotation at the motion adapter to emerge. As the duration of foot flat was longer with the new single axis mechanism than without it, the assumption was made that, once the foot reached a flat position, it retained the same transverse plane orientation relative to the ground. This would therefore imply that the extent of transverse plane socket rotation relative to the foot and ground were equal. However, due to footwear with a loose fit or an internal, low friction lining, it may be possible for the prosthetic foot, despite it being in a flat position, to rotate inside its shoe, which would decrease the amount of motion at the transverse rotation adapter. This would

falsify the information regarding transverse plane angular displacements of the socket relative to the ground. In turn, the data would be more likely to represent the true extent of motions, if subjects walked barefoot on their amputated side.

Manufactured to consist of an external, cosmetic shell out of relatively pliable and non-slippery materials, prosthetic feet, when in a flat position, experience good adhesion with the ground, even without shoes. The resultant friction therefore provides sufficient stability without putting subjects at risk of falling. As they were still supposed to wear shoes on their contra lateral sound side to prevent themselves from sustaining injuries, such as skin damage or other tissue traumas, it was necessary to lengthen the test-prostheses by the heel height of their shoes for levelling the left and right side up.

4.2.   **Subjects**

In addition to the need for test-prostheses to establish the effect of transverse rotation and longitudinal translation on unilateral trans-tibial amputee gait, it was necessary to recruit amputees who would participate as volunteers in walking trials using the customised test-prostheses that were previously described in Section 4.1. Because of existing research partnerships between one of the local NHS Trusts and the University of Salford, it was decided to further collaboration with staff from the Manchester DSC. They were asked to help select subjects who were, at the time of the study, registered at that centre as regularly attending amputees for treatment regarding their amputation and prostheses.

4.2.1.   **Ethical approval**

Prior to subject recruitment it was necessary to obtain ethical approval to comply with the "Declaration of Helsinki and the Committee For Proprietary Medicinal Products Note for Guidance on Good Clinical Practice for Trials of Medicinal Products 1990". The Manchester Local Research Ethical Committee (LREC) is divided into three sections, namely Central Manchester, North Manchester and South Manchester. The Manchester DSC falls within the jurisdiction of South Manchester LREC. Although the subjects were to be tested at the University of Salford, which is located outside the area covered by Manchester LRECs and falls under the jurisdiction of Salford & Trafford LREC, a second ethical approval was not required. In addition to the legal implications involved in testing human subjects, candidates for NHS Training Fellowships receive

funding only if ethical approval is granted. This required a successful application for ethical approval to be confirmed prior to the commencement of the project, so not to delay the schedule of the protocol.

Applications for ethical approval consist of the protocol of the study and details regarding the background of the study. There are other documents that also undergo inspection for suitability by the LREC. These include a letter requesting approval for subject recruitment from the subjects' consultant, a letter of invitation to potential subjects to act as volunteers, a recruitment information sheet for the subjects and a consent form that needs to be signed by the subjects for participation in trials. Examples of all of these are incorporated in Appendix 1 to Appendix 4 of this thesis.

All the documents to be given to potential subjects needed to be written in plain English, avoiding nomenclature including specific terminologies that people unrelated to science may not be familiar with, thus ensuring that everything is expressed clearly without being misleading. The subjects who agreed to participate in the study were not eligible to receive compensation other than for travel expenses to ensure their participation is entirely voluntary. They were free to withdraw from the trials at any time for any reason. To maintain anonymity, none of the subjects' personal details that disclose their identity will be revealed in this study. For future reference and to comply with the code of conduct stipulated by South Manchester LREC, each subject's data will be stored in their records at the Manchester DSC.

4.2.2.   Selection criteria for subjects

Subject selection criteria for potential volunteers, who may participate in gait laboratory tests, were diverse to obtain a range of amputees with very similar characteristics, thus making inter-subject comparisons easier for more precise data analyses. For this reason and this reason alone, it was decided to select subjects of the same gender. Also, due to the selection criteria that are outlined as follows, the majority of subjects who fell within those categories turned out to be male, so that it was logical for this to become the gender of choice to allow a sufficient number of subjects to be gathered.

Subjects had to be adult, unilateral, trans-tibial amputees with no history of strokes or heart attacks. They had to have good general health that enabled them to perform their walking tasks over the entire duration of the tests. The amputation side was irrelevant,

because in a left or right handed trans-tibial amputee, whether the missing lower limb was on the same side as the dominant, or the recessive upper limb side was not considered to affect the gait to an extent that it would be noticeable during normal walking. Externally mounted equipment that needed to be visibly exposed, as this formed part of the motion capture system, was the same in quantity and similarly located for the prosthetic foot and socket as it was for the contra lateral anatomic foot and shin. However, there may be circumstances when the spatial gait laboratory arrangements do not allow the motion capture system to be evenly distributed around a subject, thus causing the extent of visible exposure of externally mounted equipment to be different for the prosthetic and sound side. This was the case in the laboratory used for the current study at the University of Salford, which is why the side that was less visibly exposed as a result of spatial gait laboratory arrangements was less likely to be fully captured. Whether this involved the amputated or non-amputated side was irrelevant, because data was captured on both sides without prioritising one side over the other.

Potential subjects had to be good walkers and demonstrate a fairly symmetrical gait without the need for a walking aid, because this may reduce the quality of gait and interfere with data capturing equipment. Subjects with amputations as a result of diabetes or vascular disease were excluded from the study. This was to ensure that the residual limb and the contra lateral foot on the non-amputated side were in good condition, fully sensate and without ulcers to enable subjects to walk over prolonged periods without risking skin damage. Trauma or carcinoma was preferred as causes for amputation due to absent underlying pathologies other than those that led to the amputation. However, the topography of the residual limb had to be smooth without excessive scarring to ensure total contact with the socket.

To provide sufficient space for prosthetic components to fit into the test-prostheses, a minimum of 240mm clearance was required between the distal end of the residual limb and the ground, as measured with the subjects standing up straight and the pelvis level. The subjects also required a good range of motion (ROM) at all major lower limb joints. The residual limb should be fairly in line with the thigh on the amputated side and without excessive knee contractures. This was important, because contractures at the knee require an increase in socket angulation to accommodate the inclination of the residual limb, which in turn would affect the socket's weight bearing characteristics.

Because it was decided that the test-prostheses should be worn in conjunction with an Iceross locking liner, as explained in Section 4.1.3, this type of interfacing suspension was also supposed to be part of the subjects' prescription for their own, current prosthesis, even if the liner was not an Iceross, but a different brand. Being used to wearing a locking liner should make the test-prostheses feel more familiar to their own artificial limbs. Also, assuming that the gait with their own prostheses is of sufficiently high standard, the gait performance with the test-prostheses should, at least from the residual limb-socket interface point of view, be similarly high, although other aspects of prosthesis design may also have an influence on this. If subjects are used to wearing an Iceross liner or other types of locking liners, the likelihood for them to develop allergic reactions to the liner's material is low, even if their own liners are composed of different substances than Iceross liners are. Also, the sweat ducts in their residual limb should have adapted to the non-absorbent environment of a liner, which should prevent subjects from perspiring excessively, as often encountered in amputees who are new to this concept of interfacing suspension.

4.2.3.   Recruitments of subjects

With over three thousand amputees registered at the Manchester DSC and 52% of those amputated at trans-tibial level, the above, relatively strict selection criteria narrowed the total number of subjects that fell within these remits down to three females and thirteen males. Despite the majority of registered patients being trans-tibial amputees, the main reason that the number of subjects who met the selection criteria was so low was because most of them lost part of their limb due to diabetes and vascular disease. Another reason was because a lot of amputees' walking performances were not of high enough a standard. Also, although the concept of locking liners is around since the mid-eighties (Kristinsson 1993), the majority of trans-tibial amputees still have prostheses based on prescriptions other than locking liners.

With their consultant's permission, all thirteen male amputees were approached once, and if no reply was obtained, only one further approach was made. That way, despite a lack of feedback from them, the subjects would not have been pushed into volunteering in response to multiple, repetitive enquiries that may have a persuasive influence. Because some people may not feel comfortable with refusing to participate in the trials when being approached in person, all invitations were sent out by post, so that the subjects could consider their response without feeling pressurised.

From all thirteen subjects, eleven returned their agreement to participate in the tests shortly after having received the invitations. One subject could not participate due to injury and another subject did not respond. It was necessary to run preliminary trials, as explained in Section 4.1.6.4, to establish the suitability of test-prostheses and equipment for data gathering. This also helped to ensure that the set-ups and actual conduct of the trials ran smoothly, so that any problems, leading to non-optimised testing conditions, could be ironed out. Subjects were asked to attend the University of Salford twice: first for assessing, measuring and casting; and a second time for the tests. One of the eleven volunteers was asked to participate in the preliminary trials, which meant that this person could not be asked to participate in the definitive tests, as this would have been the third attendance. The number of subjects who agreed to participate was therefore reduced by one, so that the total number of subjects to be contacted for participation in the definitive tests was ten.

4.2.4.   Assessing, measuring and casting of subjects

Having received consent, the subjects could finally be contacted in person to arrange an appointment that suited them for their first attendance at the University of Salford. In addition to information received from prosthetists at the Manchester DSC and from medical records of their patients, recent changes or updates were established verbally and noted if this may affect the subjects' participation in the tests. Angular and length measurements were taken with a goniometer and tape measure, respectively. For reasons that will be outlined in Section 4.2.5, the subjects were not weighed on this occasion, but on the day of the actual tests instead.

Once the routine examinations of subjects were completed, it was time to proceed to the casting stage. The Iceross was rolled over their residual limb, while making sure that its distal umbrella was perpendicular with respect to the longitudinal axis of the residual limb. This was important to ensure that the pin reached the correct angle, thus allowing easy engagement with the lock. Gently pulling the pin distally served to establish the amount of stretch the residual limb tissues could tolerate. With a thin stockinet pulled on, anatomic landmarks could be identified by outlining them with an indelible pencil, whereby a layer of cling film underneath the stockinet prevented the marks from permanently staining the Iceross.

Plaster of Paris impregnated bandages were soaked in water and then wrapped around the subjects' residual limbs by applying them up to the proximal margins of the patella, using figures of eight to prevent the borders of bandages from digging into the tissues. As soon as the bandages were in place and the plaster of Paris was smoothed up, it was necessary for the lock inside the pump of the already pre-inflated and inverted bladder, described in Section 2.5.2.4, to be engaged with the pin. Pulling the pump and hence the pin distally pre-stretched the residual limb by the previously determined amount. It was important to act quickly, so that the plaster did not start to set before the bladder was rolled over the residual limb and inflated up to the recommended pressure of approximately 13.3-14.7kPa.

After approximately five minutes, with the knee on the amputated side fully extended and the bladder resting horizontally, it was time to reduce the pressure, thereby allowing the bladder to be removed and the negative cast to be pulled off the residual limb. Having doffed the Iceross, the subjects were then able to revert back to their own prostheses. Because it would take some time to manufacture all of the sockets and to prepare the necessary data capturing equipment, it was not possible at this stage to give subjects an appointment for the tests. It was explained that they would be contacted again as soon as the preparations were completed, so that a date for the tests could be arranged at their convenience.

4.2.5.   Non-identity disclosing personal details of subjects

To demonstrate the range of subjects recruited and their conformity to the selection criteria that were previously outlined in Section 4.2.2, some non-identity disclosing personal details are listed in Table 4.1. Also, Table 4.2 illustrates some of the subjects' anthropometric data to identify the range of prosthetic components required for manufacturing the test-prostheses. The information contained in those tables was, as explained in Section 4.2.4, obtained from the subjects' records stored at the Manchester DSC and by asking and assessing the subjects in person.

It was vital that information regarding the subjects' weight was exact, so that the processing of the data would lead to as accurate results as possible. Instead of weighing the subjects during their first appointment when they were invited to the University for assessing, measuring and casting, it was considered more reliable to establish their

Table 4.1:   Subjects' histories and current prescriptions

Sub-ject	Side of ampu-tation	Reason for ampu-tation	Age of subject	Age at ampu-tation	Years since ampu-tation	Current locking liner	Current foot	Current motion adapter
A	Left	Trauma	49	10	39	Tec [I]	SACH [1]	None
B	Left	Trauma	64	21	43	Iceross [II]	Multifl. [2]	None
C	Left	Trauma	42	28	14	Iceross [II]	Mod.III [3]	None
D	Right	Trauma	49	3	46	Iceross [II]	Multifl. [2]	None
E	Right	Trauma	27	22	5	Iceross [II]	Allurion [3]	None
F	Right	Trauma	43	30	13	Iceross [II]	Sin.axis [1]	None
G	Right	Cancer	61	54	7	Alpha [III]	Re.VSP [3]	Shock
H	Right	Trauma	63	30	33	Iceross [II]	Multifl. [2]	None
I	Right	Trauma	54	42	12	Iceross [II]	Varifl. [3]	None
J	Right	Trauma	71	41	30	Iceross [II]	Multifl. [2]	None
		Minimum						
			27	3	5			
		Maximum						
			71	54	46			
		Difference as in max-min						
			44	51	41			
		Mean						
			52.3	28.1	24.2			
		Standard deviation						
			13.1	15.2	15.6			

I	-	TEC Interface Systems, Waite Park Minnesota, USA
II	-	Össur hf, Reykjavik, Iceland
III	-	The Ohio Willow Wood Company, Mt Sterling Ohio, USA
1	-	Otto Bock Orthopädische Industrie GmbH & Co, Duderstadt, Germany
2	-	Blatchford & Sons Ltd, Basingstoke, UK
3	-	Össur hf, Reykjavik, Iceland

Table 4.2:   Subjects' anthropometric details

Sub-ject	Weight (kg)	Height (mm)	Residual limb length (mm)	Residual end to ground (mm)	Residual limb flexion (°)	Residual limb adduct. (°)	Iceross size (mm)	Foot length (mm)
A	95.3	1854	125	395	0	0	235	280
B	79.4	1702	135	325	5	5	250	270
C	85.7	1727	170	300	0	5	250	280
D	85.7	1905	170	360	0	0	220	290
E	63.6	1727	140	280	0	0	235	270
F	79.4	1823	80	400	5	0	280	280
G	70.0	1651	140	280	5	5	250	250
H	95.3	1855	105	405	5	0	280	260
I	82.7	1803	105	375	0	0	280	270
J	88.9	1752	130	340	5	5	300	270
	Minimum							
	63.6	1651	80	280	0	0	220	250
	Maximum							
	95.3	1905	170	405	5	5	300	290
	Difference as in max-min							
	31.7	254	90	125	5	5	80	40
	Mean							
	82.6	1779.9	130	346	2.5	2	258	272
	Standard deviation							
	10.1	80.4	28.3	48.5	2.6	2.6	25.6	11.4

weight on the day of the tests. This prevented any gain or loss of weight between those two occasions rendering previously obtained information obsolete and false. Such an approach was supported by the likelihood for their own prostheses and clothing to be different in weight than those they were to wear during the trials. The subjects were therefore weighed just prior to starting the actual tests while wearing the test-prostheses equipped with all the necessary data capturing devices. Their overall weight also included a light-weight attire that was provided for them, including one shoe on the

non-amputated side only and not on the test-prostheses for reasons previously described in Section 4.1.6.6. As the heaviest subject weighed 95.3kg, none of them exceeded the usual 100kg mark, as this is the standard weight limit to which the majority of commercially available components are tested, so that they conform to the safety requirements outlined in Section 4.1.1.

The majority of subjects lost their limb on the right side due to trauma. Amputations occurred at various stages of their lives ranging from early childhood to older middle age. Although the current prescriptions for their artificial feet varied, most of these subjects wore the same type of locking liner, namely Iceross. Only one of them had a motion adapter incorporated, and this was based on a longitudinal translation device as an integrated part of the Reflex VSP foot. All of the subjects had common body heights and they therefore fell within the dimensional limits that were stipulated in the selection criteria. This ensured that the residual limb lengths, circumferences and angulations as well as foot lengths suited the components chosen for the tests.

4.3.   Manufacture of sockets for tests

4.3.1.   Preparing the plaster cast

After the casting stage was completed, with the distal end sealed and the proximal trimline slightly extended, the negative cast was set up on a jig by aligning it in accordance with the subjects' residual limb angle. Secured in place to prevent it from moving and with a mandrel inserted that served as an alignment reference, the negative cast was then filled with liquid plaster of Paris.

Once it had set, the bandages of the outer, negative cast were removed to expose the inner, positive impression of the residual limb. Due to the moist environment, the indelible pen marks were transferred onto the positive model, and were used as an orientation aid for cast rectification, so that areas sensitive or tolerant to forces can be identified. Although the pressure casting technique with a bladder, as previously described in Section 4.2.4, does not require any further rectifications other than smoothing of the model, as explained in Section 2.5.2.4, the indelible pen marks served in establishing where to locate the sockets' proximal trimlines.

The anterior trimline is, predominantly for cosmetic purposes, usually low and exposes at least more than half of the patella, to prevent the socket from sticking out too far during sitting. To permit sufficient amounts of knee flexion, the posterior edge is generally lowest reaching the distal margins of the popliteal fossa with two additional cut-outs for the medial and lateral hamstring tendons. Medially and laterally, the socket trimlines usually extend proximally much further than the anterior and posterior trimlines up to at least mid-femoral condyle level, thus providing more knee stability and putting less strain on the medial and lateral collateral ligaments.

4.3.2.   Draping the inner socket

It was important to let the casts dry out completely, because heat retention during socket manufacture can lead to evaporation of trapped moisture, thus allowing water bubbles to form pockets between the socket and the cast, thereby increasing the socket volume. In addition to such water pockets, air can also get trapped while applying a vacuum for sucking the drape towards the cast, which can be prevented by using a stockinet to act as a wick during socket manufacture. This, however, can have adverse effects in that the stockinet's texture leaves an impression in the socket wall, therefore roughening the socket's inside surface and making it difficult for the residual limb to slide in.

The thin, inner, total contact socket, previously described in Section 4.1.4.3, was made out of a 5mm thick co-polymer sheet (North Sea Plastics Ltd, Glasgow, UK) that was draped directly over the cast. Due to the stretching process during draping, the walls of the inner sockets were reduced to only approximately 2mm. No other separating agent was used than talcum powder, to ensure that the internal aspect of the socket was smooth. However, talcum powder is not a very effective wick substitute. Therefore, to prevent air from getting trapped, a hole was drilled through the entire length of the cast, so that the vacuum could spread more easily, even up to the distal end of the cast. Drilling in an area that will be in contact with the Iceross would have left a dimple in the wall of the inner socket, thus making it uncomfortable to wear. The distal exit hole was therefore located in an area where the inner socket needed opening up to let the pin reach the lock. The resultant dimple would therefore be removed during the process of creating this opening.

4.3.3.   Shaping the distal build up

Once the drape cooled down, the polyurethane build-up could be manufactured, which, as explained in Section 4.1.4.3, was necessary to increase the outer sockets' distal dimensions for accommodating the PyraLok's inner attachment plate. A thick polythene sheet was wrapped around the inner socket while it was still on the cast to create a distal cylinder slightly larger in diameter than the inner plate. This formed a mould into which the liquid polyurethane foam was poured. Prior to that, roughening up the outer surface of the inner socket using sand paper helped to improve the bondage with the polyurethane foam. Once the liquid foam was poured in and had set, it was left for at least twenty-four hours before grinding it down to reduce the amount of toxins released during this process.

With the mandrel set in the positive cast and the non-adhering polythene sheet removed, the foam was ground down flat, so that it was level with the distal end of the inner socket and perpendicular to the long axis of the mandrel. This outlines the importance of a reference line, namely the mandrel, because flattening the foam in the way it was just described ensured that the PyraLok was orientated in accordance with the required socket alignment, as governed by the subjects' residual limb angles. The perimeter of the foam was reduced to match the diameter of the PyraLok's inner attachment plate and blended in to conform to the inner sockets' larger proximal dimensions. It was important during this procedure to shape the foam in such a way that the centre of the inner plate would be in line with the centre of the mandrel, as this determined the alignment of the test-prostheses. Failing to do so would result in an offset between the inner plate and the centre of the mandrel, thereby shifting the shin tube and prosthetic foot relative to the socket, as pictured in Figure 2.4, causing an altered force pattern to act on the residual limb.

4.3.4.   Draping the outer socket

Having achieved the appropriate shape for the polyurethane foam build up, the next step was to drape the outer socket. For these to conform to the dome-shaped, inner attachment plate of the PyraLok, it was necessary to locate a dummy, with identical dome dimensions as those of the inner attachment plate, onto the flat, distal aspect of the foam build up. Using double sided tape to fix the dummy to the foam prevented it from being displaced during the draping process. The dome side of the dummy

contained five spikes. Four of them corresponded with the four attachment bolts for sandwiching the outer socket between the PyraLok's inner and outer attachment plate. The fifth spike corresponded with the centre of the lock where the pin needed to be located. It was important that the PyraLok's pyramid system was aligned appropriately with the sides of the pyramid parallel to the coronal and sagittal planes, as depicted in Figure 4.7, to facilitate easy socket adjustments. This alignment was governed by the orientation of the spikes, which emphasised the need for the dummy to be affixed to the foam at the correct angle.

Figure 4.7:   Alignment of PyraLok attachment plate and pyramid system
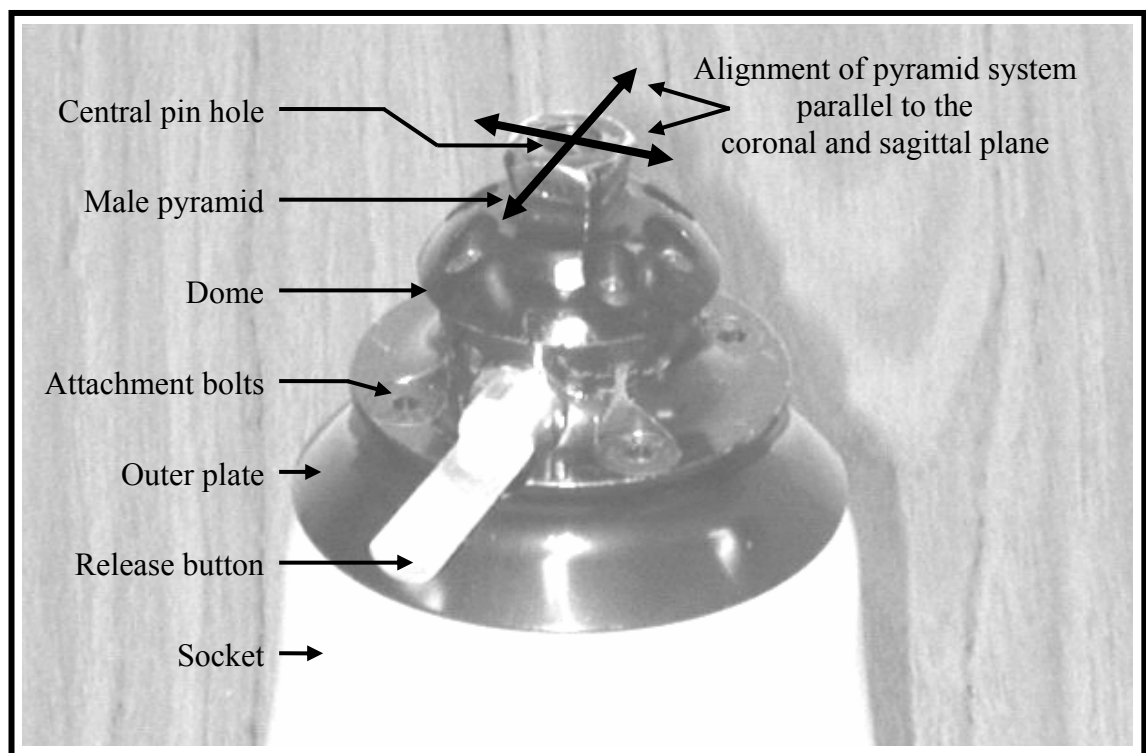
After heating a 12mm thick co-polymer sheet (North Sea Plastics Ltd, Glasgow, UK), the pliable material was draped over the combined dummy, foam, inner socket and cast. Due to contractions of most warm substances while dissipating stored heat, it was important for the co-polymer to cool down completely before removing the positive plaster model, to prevent the outer socket from shrinking. Having broken up the plaster using a pneumatic chisel, the inner socket with the polyurethane foam build up could be pulled out of its now rigid outer socket. Following extraction of the dummy from the outer socket, the impressions left by the spikes of the dummy helped in identifying the exact location of the holes for the four bolts and the pin. Because the pin had to pass through both the inner and outer socket, the position of the central hole was transferred

onto the inner socket for creating an opening that allowed the pin to reach its lock, as previously mentioned in Section 4.3.2.

The thickness of the outer sockets was reduced, as with the inner socket, due to the inherent stretch during the draping process. Because the outer sockets' structural integrity has to be sufficient to bear the subjects' weight, it was vital that the amount of stretch was kept low, so that the walls of the sockets remained thick, thus ensuring a strong design. The general guideline for trans-tibial, co-polymer, outer sockets is a minimum of 6mm thickness between the inner and outer attachment plates and at least 2.5mm of wall thickness for the distal third of sockets (Blatchford & Sons Ltd, Basingstoke, UK). Checking that the required construction criteria were achieved by measuring socket dimensions using a thickness gauge with extra depth of bow for easy insertion into the sockets, gave the research project assurance for a safe conduct of experiments.

Because only one PyraLok was available for all ten test-prostheses, the process of manufacturing the outer sockets was rather lengthy as the plaster had to be removed from the previous one to retrieve the dummy, before the next one could be draped. Having transferred the trimlines between draping processes from the cast onto the inner socket and from there onto the outer socket, it was then possible to cut off any excess material and grind the sockets down to the required level. With the trimlines of the outer socket approximately 5mm further distally than those of the inner sockets, to prevent subjects' skin from getting pinched, all rough edges were removed by buffing them until they were smooth.

CHAPTER 5.   MAIN CAPTURING EQUIPMENT

5.1.   Considerations for main capturing equipment

Clinical trials are effective ways for establishing the outcome of treatments that patients receive. They are possibly the only reliable approach for identifying viable long-term solutions that lead to a successful rehabilitation process. In the short term, however, one has to be aware that patients may be biased towards treatment regimes and possibly not fully objective in their approach to reach the full potential of the research protocol.

Instead of relying on outcomes that can be observed over prolonged periods of time, it may be more efficient to identify the potential some treatments have to offer by gathering quantitative data. Analysing those data may then give an impression whether these treatments have a beneficial effect. This was the chosen method for the current study to establish what aspects of trans-tibial amputee gait, if any, are influenced by the introduction of transverse rotation and longitudinal translation between the socket and the prosthetic foot. Measurable aspects of gait exist in abundance, which makes it necessary to concentrate on those that have the greatest potential for revealing parameters with interpretable properties from which conclusive evidence can be drawn regarding the benefit from these motions. As this study is limited in terms of duration and budget, it seemed logical to take advantage of already available equipment that on previous occasions proved useful for gathering high quality data.

5.1.1.   Computerised motion analysis system

5.1.1.1.   Functional background

Based on cameras that capture the position of markers, computerised motion analysis systems are extremely useful tools for recording movements. They are probably the most vital equipment in fields that require measuring of parameters under dynamic conditions. The ProReflex[TM] system (Qualisys AB, Sävedalen, Sweden) utilises these technological principles and it was part of the gait laboratory equipment within the department at the University of Salford where the current study was undertaken. This

system became, due to its versatility, the main data acquisition facility for the current research project.

To understand how the ProReflex^{TM} system captures the position of markers, it may be useful to explain the way in which it operates. The mechanism involved in detecting markers is based on recording light. The underlying problem involved in this process is that of distinguishing between light from markers and light from other sources. Because the frequencies of light fall within a bandwidth of fairly broad range, by eliminating certain parts of this range to detect only light with frequencies specific to the ProReflex^{TM} system, is it possible to capture purely the light from markers. The system's sensitivity is aimed at detecting light with frequencies encountered in the infrared part of the spectrum. The actual sources of light are the cameras themselves from which rays of infra red light travel away from a set of light emitting diodes (LEDs) located around each camera's lens. The markers, whose positions are to be captured, have a highly retro reflective coating. Their spherical shape allows the infrared rays to be returned back to each respective camera and pass through its lens to hit a photosensitive filament. Due to the nature of single lenses, the image received by each camera extends in two dimensions (2D) only.

When using such a system, the aim is to gain a more complex impression of marker locations. The advantage of computerised motion analysis systems over less sophisticated data acquisition facilities is the way information can be manipulated for combining images in 2D from a number of cameras into an overall image in 3D. As each camera's image in 2D is defined by the height and width of the image, the additional dimension required to create an image in 3D is the depth. This implies that a minimum of at least two cameras is required. The space around which the cameras are distributed to record marker positions is dependent on the distance necessary for completing the required manoeuvres. This space is generally referred to as the capture volume.

5.1.1.2. Camera positions

Each camera has a field of vision of up to 45°, so that a marker that is not immediately in front of a camera can be moved over a fair distance from side to side or up and down before it disappears from a camera's view. When elaborating on camera positions, it is important not only to consider the angle between one camera and the next, but also to

note the angle between one camera, a target marker and the second camera, which is sometimes referred to as the camera-marker-camera angle.

For instance, two cameras are exactly opposite or at 180° to one another, and a marker is located equidistantly from both cameras, but slightly offset at an angle of, say, 22° to either camera. Due to those cameras' field of vision of up to 45°, the marker can just about remain detected. Although the cameras oppose one another, the camera-maker-camera angle is therefore not 180°, but 136°. This implies that the aspect regarding depth of the capture volume for converting images recorded in 2D into an image in 3D is accounted for.

In turn, such a conversion would not be the possible if the marker was not slightly offset, but instead located exactly between the two cameras. In such a situation the aspect regarding depth is not accounted for, because the camera-maker-camera angle would be 180°. A similar scenario is applicable if the two cameras are located closely together with only a small angle between them. The camera-maker-camera angle is therefore very small. Also, the image captured by the two cameras would be very similar for both of them. However, this would be the reverse for one camera compared to the other if both of them were opposite each other. In summary, either scenario is lacking the aspect regarding depth. Therefore, in an ideal scenario, two cameras should be located perpendicular to one another, as this provides the greatest insight into the third dimension.

Another aspect worth considering is that obstructed markers will disappear from a camera's view. To avoid this, it may be better to set up more than two cameras, as the computerised motion analysis system will otherwise not be able to process an image in 3D for the duration the markers fail to be detected by at least two cameras. It is obviously impossible to locate each camera perpendicular to their adjacent two cameras if there are more than four in total. However, spacing them out fairly evenly around the markers to be captured should not only improve the cameras' angular relationships, the greater the number of cameras that are being used, the greater the likelihood for all markers to be detected. Also, when using, for instance, eight evenly spaced cameras, although the angle between one camera and the next is only 45°, a perpendicular relationship can still be found between every other camera.

Also, when two cameras are located at, for instance, 100° to one another with a target marker at the same height as the cameras and exactly straight ahead of them, moving the target marker vertically up or down increases its distance to the cameras. Despite the cameras themselves not being moved, displacing the marker reduces the camera-marker-camera angle to perhaps only 90°. Such a reduction would occur, because moving the marker relative to the stationary cameras changes the direction of the reflected infra red beams, which therefore do not enter the cameras from straight ahead anymore.

This example demonstrates that under dynamic conditions, the angle at which a marker is being detected by the cameras changes all the time, even with a near optimal camera arrangement. It is obviously not always possible to arrange cameras exactly perpendicularly. However, as long as markers are being captured from a variety of views, so that at least some of the camera-marker-camera angles approach 90°, then this should suffice to ensure the aspect concerning depth is taken into account.

5.1.1.3. *Calibration procedure*

For the cameras' 2D images to be converted into an image in 3D, it is necessary to complete a calibration procedure by recording frame-mounted markers that are positioned at known locations and distances with respect to one another. Calibrating the ProReflex^{TM} system is undertaken in conjunction with two of those frames. Carrying a total of four markers, one of the frames is L-shaped and rests flat on the floor. Its first marker is located in the corner of the L, its second and third marker at the end of the L's long and short bar, respectively, and its fourth marker between the first and second marker. The second frame is T-shaped and referred to as a wand, because it is moved relative to the L-shaped frame. It carries a total of two markers located on the ends of the T's cross-arm. The T's other arm serves as a handle for waving the wand around. Depending on the distances necessary for capturing motions, both the frame and wand are available in different sizes for different capture volumes.

The actual numeric information regarding the location of markers on the frame and wand has to be entered into the software that controls the capture process. The images in 2D, as detected by each camera, are then mathematically converted to define inter-marker distances in 3D. Each marker's location in space is expressed as co-ordinates within a Cartesian reference system, which consists of three orthogonal

axes X, Y and Z. Those co-ordinates depend on the orientation of the L-shaped calibration frame, the location of the co-ordinate system's origin and the arrangement of axes. For example, the marker co-ordinates required for defining a reference system with its origin at marker 1 and its X-axis pointing forward, its Y-axis pointing upward and its Z-axis pointing to the right, can be allocated as displayed in Figure 5.1. The orientation of the frame itself can be changed. However, this obviously requires the actual numeric information regarding the location of markers on the static L-shaped frame to be rearranged accordingly within the software.

Figure 5.1:   Marker locations as entered into the processing software

This diagram was adapted from a ProReflex™ instruction manual
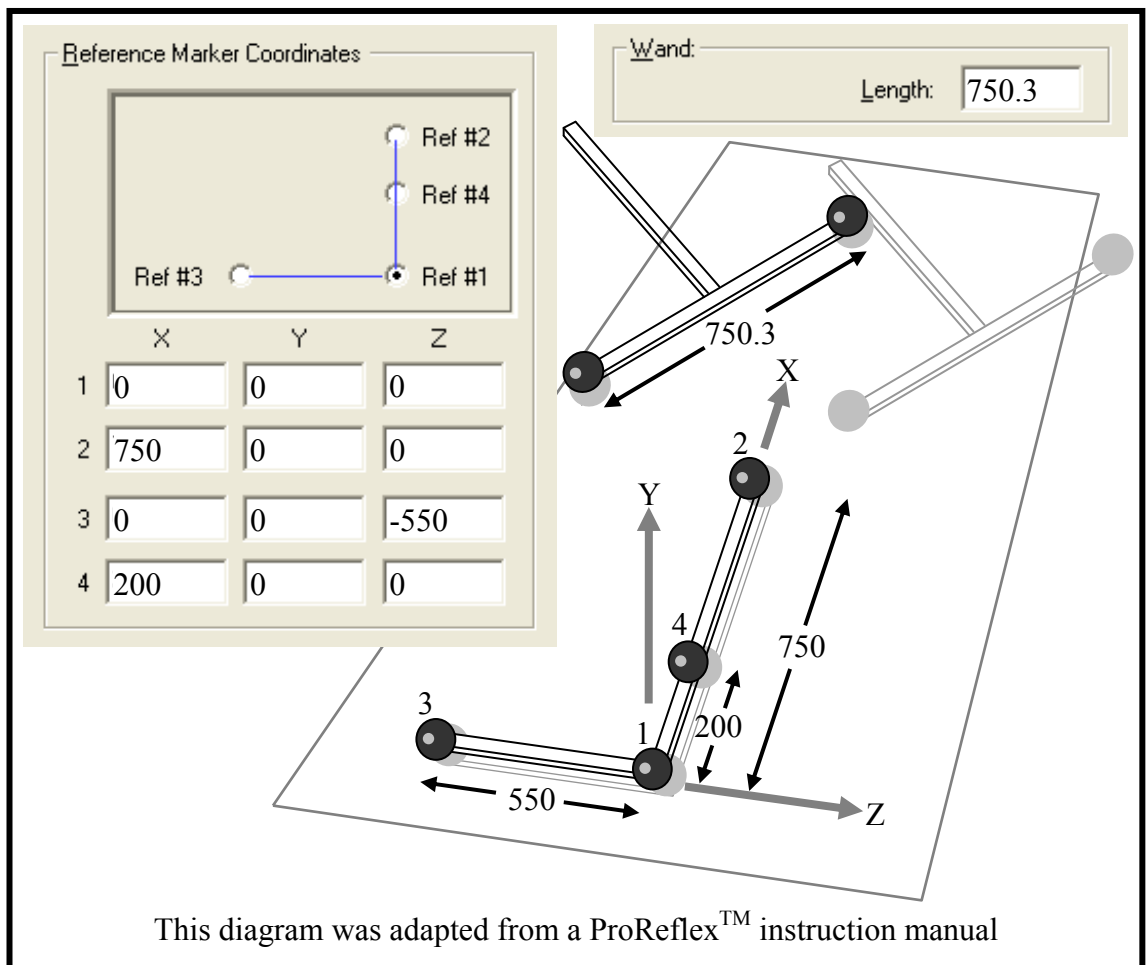
During the actual calibration process, which takes no longer than a few seconds, it is important to move the wand around the entire capture volume. That way the software can calculate the relative position between frame and wand markers over large distances. This is necessary in order to obtain precise measurements throughout the capture volume including its perimeter regions. However, despite the necessity to approach the borders of the capture volume, to prevent the wand markers from momentarily not being detected, motions of the wand should be limited to a slightly

lesser volume than the capture volume. Such a volume is generally referred to as the calibration volume.

In turn, if the wand was being moved solely within the proximity of the L-shaped frame, then the software would have to extrapolate wand marker positions near the frame or from a relatively small calibration volume to outer areas of the comparatively large capture volume. This reduces not only the accuracy of the calibration process, but the accuracy of the subsequent definitive recordings also. If the camera positions need to be changed then the system has to be recalibrated, so that the software can calculate the cameras' new location relative to the calibration frame and wand.

5.1.1.4.   *Calibration results*

Having finished calibrating, the software reports whether or not the process has been successful. If successful, the software then calculates the success rate, which is defined by the average residual of each camera. The average residual is the mean value by which infra red beams from each camera are deviated from their intended direction, or in other words, the difference between measured static marker co-ordinates and the actual marker co-ordinates in 3D as entered into the software. The lower these values are, the more accurate the calibration process becomes. However, care must be taken when interpreting the values, because very low average residuals can be achieved by moving the wand solely around the proximity of the frame. This, in turn, has implications for the accuracy in outer regions of the capture volume, as described previously in Section 5.1.1.3.

Another aspect that influences the accuracy of the calibration process is the quality of the linearisation. The procedure for the linearisation involves taking recordings while a camera faces an accurate, rectangular array of markers. The rows and columns that can be seen in the obtained image of the marker array will not necessarily produce straight and parallel lines of markers, because of errors from lens distortions and non-linearities in electronic components. To overcome this problem, a correction procedure in the form of linearisation algorithms implemented in the system's software can be used to remove the errors inherent in each camera, so that the processed data are not flawed by hardware imperfections, but represent true information. This procedure is rather complex due to the high level of accuracy that is required. Therefore, linearisation files are usually produced by the manufacturer.

Accomplishing an accurate calibration by using updated linearisation files is obviously mandatory for achieving high quality results. Once this procedure is completed, the calibration frame and wand can be removed to commence with the actual recordings. In addition to factors regarding camera angles as well as the calibration procedures, described in Section 5.1.1.3, the accuracy of the ProReflex^{TM} system also depends on a number of other criteria, including the size of the capture volume. As stipulated by the manufacturer, an accuracy of ±0.2mm is quite feasible for a volume of 1m^3. However, imprecise marker surfaces may not necessarily reflect a light beam back in exactly the correct direction. Because the cameras are further away from the centre of a large capture volume than they are from a smaller one, the angular deflections that result from slightly incorrect light reflections amplify the actual offset of the returning light beams as a result of the longer distance they have to travel. Also, an environment with restricted dimensions can prevent the cameras from being shifted far enough away from markers that are to be captured, thus limiting the view, so that only part of a large capture volume falls within the cameras' field of vision.

5.1.1.5.   *Marker specifications*

When capturing the position of spherical markers, the actual image of those markers makes them appear disc-shaped, because recordings can only be taken in 2D. Due to imprecise marker surfaces, for reasons explained before in Section 5.1.1.4, slight angular deflections from the reflected light's ideal direction can lead to miscalculations in determining the centre of the captured markers. In such a situation, the actual location of a marker and the image of its disc do not exactly coincide. The algorithms within the software, for converting individual camera images in 2D into an image in 3D, combine the information regarding disc locations from each of the cameras in order to calculate the centroid of a marker. As the curvature of larger markers is shallower, the direction a reflected light beam is travelling along is more likely to approach an ideal pathway than it would be for smaller markers with a deeper curvature. The accuracy of recordings therefore increases with larger markers. Also, the amount of light that enters the cameras from larger markers is greater than it is from smaller markers, as the reflected light disperses less due to smaller angles between individual light rays, as illustrated in Figure 5.2.

The likelihood for large markers to become obstructed by other large markers is, however, greater compared to smaller ones. If a particular set-up would require several

markers to be clustered closely together, it may therefore be less appropriate to use large markers. Although small markers may be better for such a clustered set-up, it can be difficult for them to be detected by the cameras if the capture volume is large, because the intensity of light reflected from smaller markers may be insufficient over longer distances. As a general rule, large markers are more suitable for a large capture volume when all the markers can be spread out, and small markers are more suitable for a small capture volume when markers are clustered together. Therefore, the size of markers should be proportional to the calibration volume and the proximity of inter-marker locations and distances.

Figure 5.2:   Reflected light beam dispersion due to small and large markers
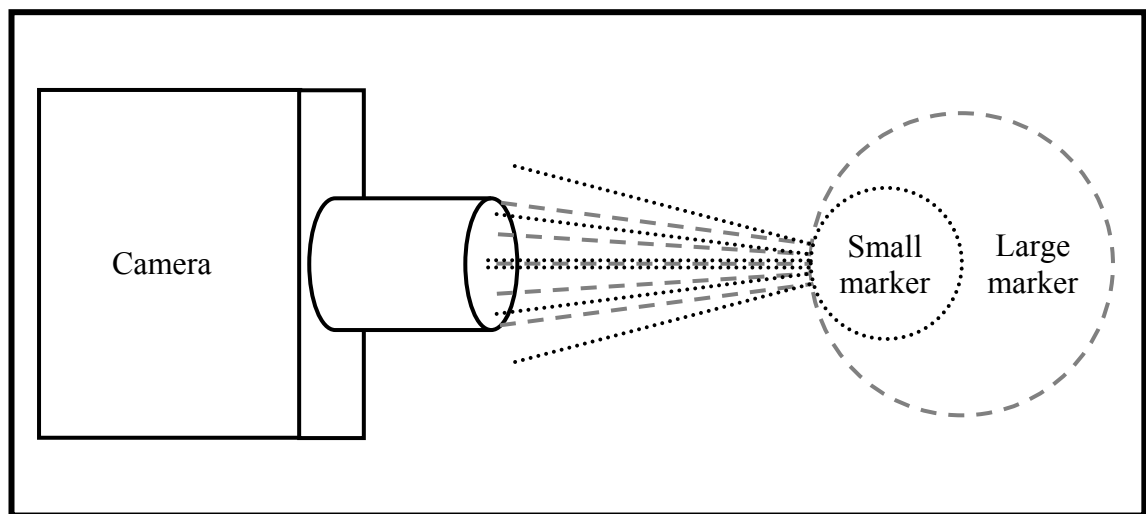
Adjusting a camera's aperture is, in addition to choosing suitable marker sizes, another method for improving accurate marker detection. It controls the amount of light passing through the camera's lens and helps to avoid the image from being too bright or too dark. Prior to taking recordings, opening or closing the aperture can be visibly monitored by observing changes in the disc sizes as seen on the screen. Opening the aperture too far not only causes adjacent discs from overlapping or even joining together as one, it also increases the system's sensitivity, so that other objects with reflective properties may also be picked up by the cameras, even if those objects are not as reflective as the markers themselves. In turn, when the aperture is closed too far, it may still be possible to observe all the markers that are being used while they are in the centre of the capture volume, but they may not be detected anymore when being moved further away from the camera whose aperture was adjusted. In addition to visibly monitoring disc sizes on the screen, another way of checking whether the setting of an aperture is appropriate is by comparing the amount of markers that are actually being

used with the number of markers or discs that the cameras detect, as indicated on each camera's light emitting diode (LED) display.

5.1.1.6.   *Current system set-up*

The ProReflex^{TM} system at the University of Salford consists of six cameras and to make it easier for them to be arranged around the capture volume without having to deal with excessive amounts of wiring, all cameras are inter-connected and plugged into the computer that runs the system's software using only one data transmission cable. Because the source of the cameras' power supply is not the computer, mains sockets in the vicinity of each camera could be used, which, again, reduces the extent of cable trailing between cameras.

The number of frames that can be captured per unit time determines how detailed the data recordings will be and this particular system can collect marker positions at a frequency of up to 240Hz. Capturing data at this sort of rate would be beneficial for recording fast movements with abrupt changes in the directions in which marker displacements are occurring. However, if the required manoeuvres are being performed fairly steadily with smooth transitions between multi-directional marker displacements, it might be advantageous to adjust the software to a lower frame setting, because high frequency recordings increase subsequent computation time for data processing and they require larger sizes of files on the computer's hard drive where the recorded data are being stored.

5.1.1.7.   *Processing the data*

Once the data have been captured, the information recorded by each camera needs to be processed to convert images in 2D into the required image in 3D. Such a data processing procedure is based on mathematical algorithms that rely on a number of factors. These factors are responsible for affecting the accuracy of the required mathematical conversions, during which the software calculates the co-ordinates in 3D for each marker during each frame. Stringing all the frames together, like in a cartoon, creates a continuous story. However, for the software to decide that the co-ordinates of a certain marker in two adjacent frames actually represent the same marker requires extra computational input, because the movement of that marker causes its co-ordinates to be different between those two frames. The aim is therefore to obtain the trajectory of each

marker throughout the recording period. Although this can be difficult to achieve, it should at least be possible to form a number of smaller trajectories or marker segments that can subsequently be strung together.

The predictor error is one of the factors for helping to foresee where about in the next frame a certain marker could be found. As can be seen in Figure 5.3, predictor errors create a conical volume ahead of that marker, so that during future frames, the software is restricted to search for the same marker within that particular space only. Deciding on the size of the cone by stipulating the radius of its base is dependent on the capturing frequency, the regularity of marker movements and the closeness of adjacent markers.

When using a low capturing frequency, the time interval between one frame and the next is longer than with a high capturing frequency. The distance a marker can travel during a long period is therefore greater and the likelihood for its co-ordinates to fall within the volume of the cone obviously lower. Even with a high capturing frequency, a marker that does not travel steadily but undergoes jerky movements is less likely to be located as its co-ordinates may be, again, outside the cone. Confusion can also be triggered with closely clustered markers, so that, despite a high capturing frequency and smooth, non-abrupt movements, the software detects more than one marker co-ordinates within the cone, thus opening up the possibility for a different marker to be considered the one in question from the previous frame. Choosing the correct dimension for the cone is therefore dependent on the type of recording to be made and it needs to be adjusted accordingly.

Figure 5.3: Background idea for predictor errors
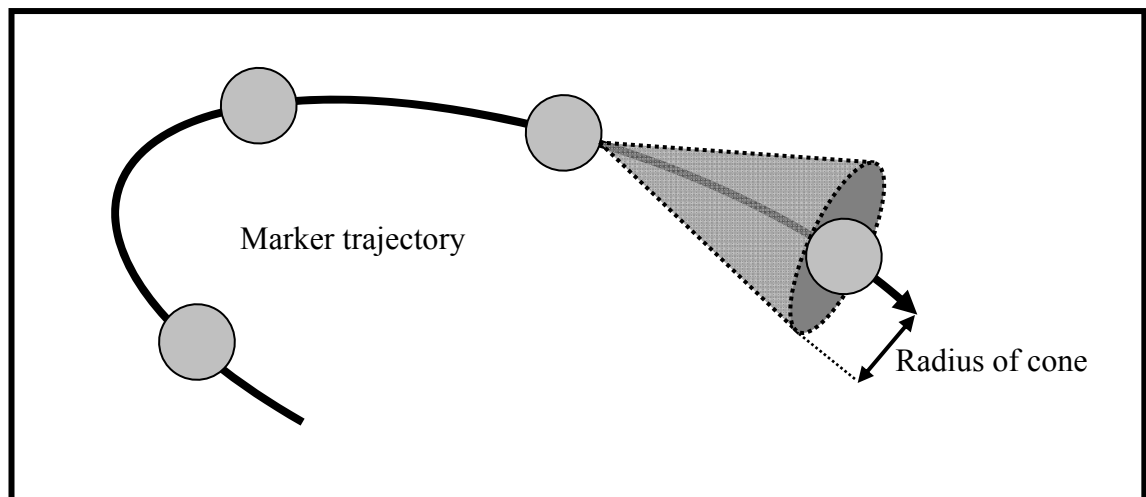
Another factor that affects the accuracy of mathematical image conversions is the maximum residual. As explained earlier in Section 5.1.1.5, the actual captured image of markers makes them appear disc-shaped and the centre of these discs determines the markers' co-ordinates in 2D, whereby imperfections in marker surfaces can lead to minor deflections of the reflected infra red light beams from their actual paths. The marker co-ordinates in 3D are then determined from the mean value of the co-ordinates obtained from all the cameras in operation. This implies that the co-ordinates for the centre of each marker's disc, as determined in 2D by each camera, may not exactly coincide with the calculated co-ordinates for the centre of the markers in 3D, as illustrated in Figure 5.4.

Figure 5.4:   Background idea for maximum residuals
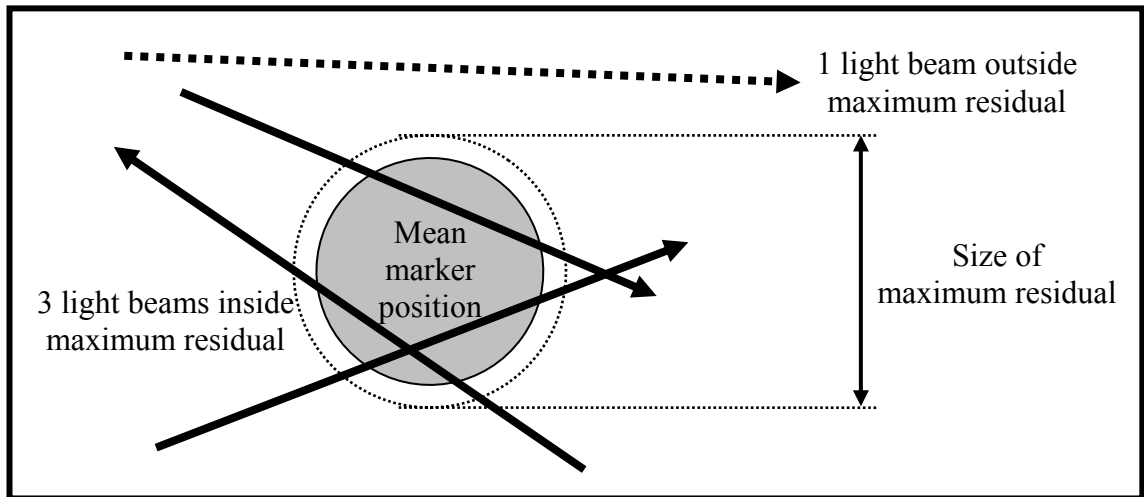
The maximum residual represents the distance between the centre of a disc and the calculated centre of the corresponding marker. Once this distance exceeds the actual value to which the maximum residual is adjusted, then the image captured by the camera in question will be disregarded for this particular frame. If this is the case for the majority of cameras, then the marker will not be recognised over the duration of frames that its image was properly detected by less than two cameras. The higher the maximum residual is being set, the more likely it therefore becomes for co-ordinates of discs to fall within the boundaries of this value. This obviously increases the number of images that are not being disregarded, or rather that are acceptable, and the larger this number becomes, the more accurate the calculation for a marker's mean co-ordinates in 3D will be.

However, it must be taken into consideration that the reason for these images to be accepted in the first place is because of a large value for the maximum residual. By allowing this parameter to exceed a certain dimension, even if such an adjustment increases the number of accepted images, larger errors will consequently be introduced into the calculation of a marker's mean co-ordinates in 3D. To obtain high accuracy recordings, it is therefore important that the value for the maximum residual is not too large or too small in order keep the error during data conversions as low as possible without reducing the number of acceptable images for accurately calculating the mean marker position.

Figure 5.5:   Background idea for acceleration factors
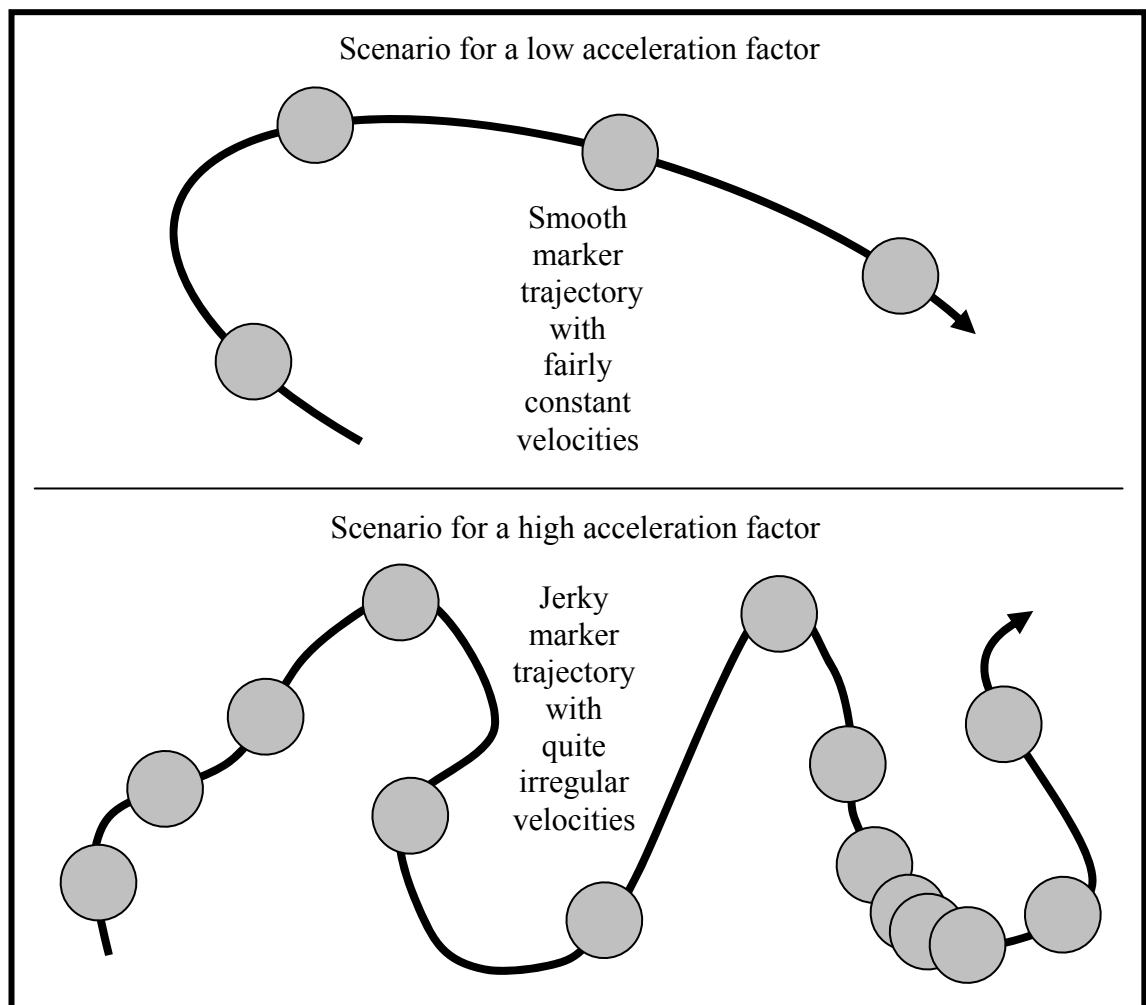
Unlike the predictor error and maximum residual, the acceleration factor is a parameter that determines the level of permitted irregularities for creating continuous marker trajectories. Depending on the value that this parameter is adjusted to, the software can establish whether an irregular motion pattern is acceptable or not. For instance, for motion patterns that are characterised by frequent changes in the direction as well as the

velocity of marker displacements, the value for the acceleration factor has to be set high. In turn, if marker displacements are fairly smooth with only slight changes in direction and velocity, then the value for the acceleration factor can be set low. Differences in marker displacements due to changes in direction and velocity are depicted in Figure 5.5. As markers rarely move at a fairly constant velocity, it appears reasonable to generally decide on a high acceleration factor, so that all the markers will be detected.

The final parameter that has an impact on the data processing procedure is the noise factor. This parameter is similar to the acceleration factor, but instead of determining fluctuations in the direction and velocity of marker travel, as induced by the actual manoeuvres to be performed, the noise factor focuses on marker displacements due to noise, like vibrations. Although adjustment of this parameter depends on the capture volume, an average setting is supposed to promote successful marker detection in most cases.

If a marker cannot be detected, either due to inappropriate settings of the predictor error, maximum residual, acceleration factor or noise factor or simply as a result of camera mal-positioning and marker obstruction, a rising number of consecutive frames without the marker being detected increases the likelihood for the software not to recognise a redetected marker as the same from the previous marker segment. This implies that the total number of marker segments produced during the initial data processing procedure for converting images in 2D into the required image in 3D may be a multiple of the actual number of markers used while recording data. It therefore re-emphasises the importance of adjusting the entire system correctly by tailoring the set-up to the circumstances required for the tests. Otherwise the resultant marker segments will be broken up into small and perhaps meaningless trajectories. If marker trajectories are already fragmented during smooth marker displacements, they will most certainly be further fragmented during irregular movements. A mathematical reconstruction of missing parts during irregular movements would therefore render the results useless as the true sequence of events will never be known.

5.1.1.8. *Software for processing data*

The actual recordings are taken using QTrac Capture, which is a data acquisition and processing software package. Once the information from individual cameras is converted into an overall 3D image, the marker segments can be inspected using QTrac

View. Both types of software are commercially available from Qualisys AB, Sävedalen, Sweden and can be downloaded onto a personal computer (PC) with at least a Pentium I processor or better and a minimum of 16MB random access memory (RAM).

Once the estimated duration of a recording is determined, data collection can be commenced with an external start button at a point in time that is convenient for capturing the required manoeuvres. Using batch recordings makes data collection very time efficient, as the computer is ready to receive the triggering signal from the start button almost immediately after the duration of the last recording expires.

When using the ProReflex^{TM} system for recording human motion, the objective is to determine the location of body segments in space from marker co-ordinates in 3D. This procedure requires further processing of those marker co-ordinates for calculating relevant gait parameters, whereby the most indicative ones are probably inter-segmental angles or joint angles. In addition to that, it is possible to use the obtained marker co-ordinates for calculating spatial and temporal parameters, including travelling distances, durations, velocities and accelerations. To determine the location of segments and relative positions between them, it is necessary to decide upon appropriate positions for markers to be mounted onto. Such positions should be relevant to the underlying anatomy in order to indicate segments themselves as well as the location of their inter-connections, namely the joints.

Although the actual recordings are followed by an immediate processing of the data in 2D to create the required co-ordinates in 3D, before proceeding with the calculation of the gait parameters, it is necessary to take an intermediate step and digitise the newly obtained co-ordinates. This process involves denoting virtual marker trajectories to actual, real life marker positions that represent relevant anatomic landmarks as identified during the recordings.

5.1.1.9. *Digitisation process for the data*

Using QTrac View, algorithms within this software allocate different colours to each calculated marker segment, thus making it easier to differentiate between fragmented parts. Preferably starting at a frame where the number of markers on the screen matches the number of actual markers used during the recordings, each virtual marker has to be denoted to its corresponding real life marker. To make this process easier, it is possible

to import a previously created text file that contains a list of meaningful names for all the markers used. Orientation on the screen can be difficult when only the coloured markers and the grid representing the floor are visible. Therefore, the software allows the image in 3D to be translated up and down and from side to side, to be zoomed in and out and to be rotated around by up to 360° in all directions. The latter also helps to reveal markers obscured by other markers. Once every virtual marker is named, it is useful to interconnect them by drawing straight lines or bones, particularly if the markers are clustered. This makes orientation around the otherwise more or less featureless image easier.

When progressing to the next frame it may be possible for several previously named markers to disappear. This means that the images in 2D are acceptable from less than two cameras. The disappearance of markers also comes to attention by the loss of bones between the missing markers and the ones they were connected to. There is no other option but to progress to the next few frames until a frame is reached where the markers reappear. If the software recognised those markers as the same from before the gap, then it will give them the same colour and the same name as previously allocated. However, sometimes the software does not recognise reappearing markers. These are then shown in different colours than before and they do not have a name or bones. In this instance, those markers have to be manually denoted the same name as the previous segment. Following this denotation, the two segments will have matching colours again and the bones will also reappear.

Identifying reappearing markers can be difficult particularly if the number of frames between one segment and the next is high. This re-emphasises the advantage of bones, because if a certain redetected marker is denoted with the wrong name then the bones will be incorrect, and a typical pattern of bones, as encountered in clusters of markers, may appear unrecognisable due to a stray marker and corresponding stray bones. The described naming process has to continue until all relevant markers are named over a large enough a number of frames to cover a sufficiently long duration of the capturing period.

Sometimes additional virtual markers randomly appear on the screen, which are the result of other reflective objects. These markers do not correspond with the actual real life marker set that was used. They are referred to as ghost markers and can be deleted.

The remaining relevant markers can then be saved in a segment file to provide the possibility for revisiting the final digitised data in the future. Saving these data creates an additional text file that contains not only a list of the markers, but of the bones also. Importing this file during subsequent digitisations makes the process of denoting marker names much easier, because the software automatically creates bones between their corresponding markers, so that stray bones immediately indicate markers with the wrong name.

Another way of saving marker information is by exporting the digitised data as a tab separated values (TSV) file. This process allows the total number of frames to be reduced to a lesser recording duration, thus utilising less hard disc space. When exporting a TSV file, the spline fill option can be set to a certain value, so that absent marker segments can be mathematically reconstructed by stringing fragmented marker segments together into complete trajectories. However, this only works if the absence of markers is less than the number of frames stipulated by the spline fill value. When deciding upon this value it is important not to set it too high, as mathematical reconstructions using interpolation may otherwise falsify the information and render the digitised data different from the true displacements of the actual real life markers. TSV files separate each marker's co-ordinates into three columns according to their X, Y and Z axes components, so that the actual numeric data of the markers can then be manipulated as required using spread sheets like Excel (Microsoft Corporation, Redmond Oregon, USA).

5.1.1.10. *Alternative software for processing the data*

The ease or difficulty of digitising data is dependent on the quality of the recorded information. Naming a large number of marker segments from recordings with high fragmentations of trajectories can be a tedious and exceedingly time consuming process that can easily lead to operating fatigue and consequently errors from denoting wrong marker names due to a drop in concentration. This is particularly the case when using a lot of markers as the likelihood for fragmentation increases.

During the initial part of this study, there was no other option than to use QTrac View in the way it was just explained for digitising the data that were captured with the ProReflex^{TM} system. However, almost immediately following completion of the gait laboratory tests, Qualisys AB, Sävedalen, Sweden started distributing a new version of

QTrac View named Qualisys Track Manager (QTM). QTM creates exceedingly detailed graphics and its operation is very user friendly, which implies that the hardware requirements for this software have to be a lot more powerful than they were for QTrac View. A PC with at least a Pentium III processor or better is needed as well as a minimum of 128MB RAM.

Although the overall digitising procedure is the same for QTM as it is for QTrac View, the advantage of QTM over QTrac View is that it recognises marker arrangements or biomechanical models from previous digitisations. Having finished digitising one trial of a particular subject, QTM can store the pattern of marker locations and marker names in a file by taking a snapshot of an arbitrary frame with a complete marker set, as recorded during that trial. Subsequent undigitised trials that are based on the same manoeuvres by the same subject with the same marker set can be digitised by opening the file that contains the snapshot of the pattern of marker locations and marker names. By applying the snapshot from the first trial onto an undigitised trial, the software then identifies similar marker patterns and allocates names and bones to the marker set whenever a recording frame contains a recognisable marker pattern.

5.1.1.11.   *Manipulation of marker trajectories*

As before with QTrac View, a completed digitisation procedure can be stored in a segment file and then be exported as a TSV file, but unlike QTrac View, the spline fill option can already be taken advantage of during the digitising process. This demonstrates a tremendous advantage over the old software with which it was not possible to view the results from interpolations of the data.

In QTM it is possible, for instance, to divide a marker segment before and after a part of its trajectory that appears unusual, therefore cutting it into three parts. By discarding the middle part that contains the unusual trajectory, the spline fill option can be applied to mathematically reconstruct the missing data between the first and third part of the trajectory, providing that the gap is not greater than the number of frames stipulated in the spline fill option. The new part and the two already existing ones can then be merged and the restrung trajectory can be inspected on the screen. It is obviously important to handle features like this with caution as interpolations can falsify the true data if applied under inappropriate circumstances.

With regard to the snapshot feature, it is not always possible to identify and name exactly all of the markers and, in addition to the very first digitisation that needs to be undertaken without automatic marker recognition, subsequent trials still require additional, manual digitising to refine the data. Also, being able to manipulate data by cutting, discarding and reconstructing trajectories is extremely useful and the fact that the results can be observed immediately demonstrates that, by using this option, it is more likely to improve the data than it is to deteriorate them.

Despite having been able to use the new software on time for the current study, the digitising procedure was still, in terms of time consumption, a large part of this investigation and obviously vital for providing a sound foundation for subsequent data processing. However, with QTM, this reduced the overall duration for digitising to approximately a quarter of the time it would have otherwise taken with QTrac View. Also, due to ongoing collaboration with the University of Salford and Qualisys AB, Sävedalen, Sweden, the investigators of the current study were granted unlimited and free access to the new software, which was beneficial so not to exceed the limit of the budget for this investigation, as there was no need to purchase other software.

5.1.1.12. *Definitive capture volume*

Having established all the parameters for adjusting the system and considered subsequent procedures for processing the data, it was now necessary to decide upon the size of the capture volume to establish the system's true accuracy for a customised set-up. Although too large a calibration volume can make it difficult for the cameras to be arranged in a way permitting detection of all the markers, too small a calibration volume would also be disadvantageous, in that insufficient amounts of data may render the results inconclusive. It is therefore important to find a balance between large enough a volume to capture all of the performed manoeuvres and small enough a volume so not to approach the limitations for camera arrangements imposed upon by the gait laboratory environment.

The minimum dimensions of the capture volume were decided to cover a range that permits subjects the completion of one full gait cycle on each the left and right side plus half a step prior to the first and another half step following the second gait cycle for good measure to ensure the entire walk is being recorded. The length of a full gait cycle was established empirically by one of the investigators walking with long steps. The

width of the volume was considered large enough if a person with a wide walking width and perhaps a slight sway during walking fits into the capture space. As only lower limb motions were to be captured, a volume height just above the pelvis was assumed to be sufficient. This led to the conclusion that a capture volume of 4.6m length, 1.1m width and 1.3m height would be sufficient.

5.1.1.13.   *Definition of the co-ordinate system*

Before taking recordings, it was necessary to define an axis arrangement for the Cartesian co-ordinate system that describes marker positions in 3D. The axis arrangement was chosen according to the recommendations made by the International Society of Biomechanics (ISB) (Wu & Cavanagh 1995).

These authors suggested for the X-axis to point in the anterior-posterior direction and parallel to the walking path with positive values representing forward orientation, for the Y-axis to point in the vertical direction and parallel to the field of gravity with positive values representing upward orientation and for the Z-axis to point in the medial-lateral direction, so that it is perpendicular to the X and Y axes with positive values representing rightward orientation. This is the same axis arrangement as in the example given in Section 5.1.1.3, which is based on a right handed system and rotations around these axes obey the right hand rule. This implies that with the thumb of the right hand pointing along an axis in positive direction, the fingers then curl around that axis and point in the direction a positive rotation is occurring in, as depicted in Figure 5.6.

Figure 5.6:   Right handed Cartesian co-ordinate system
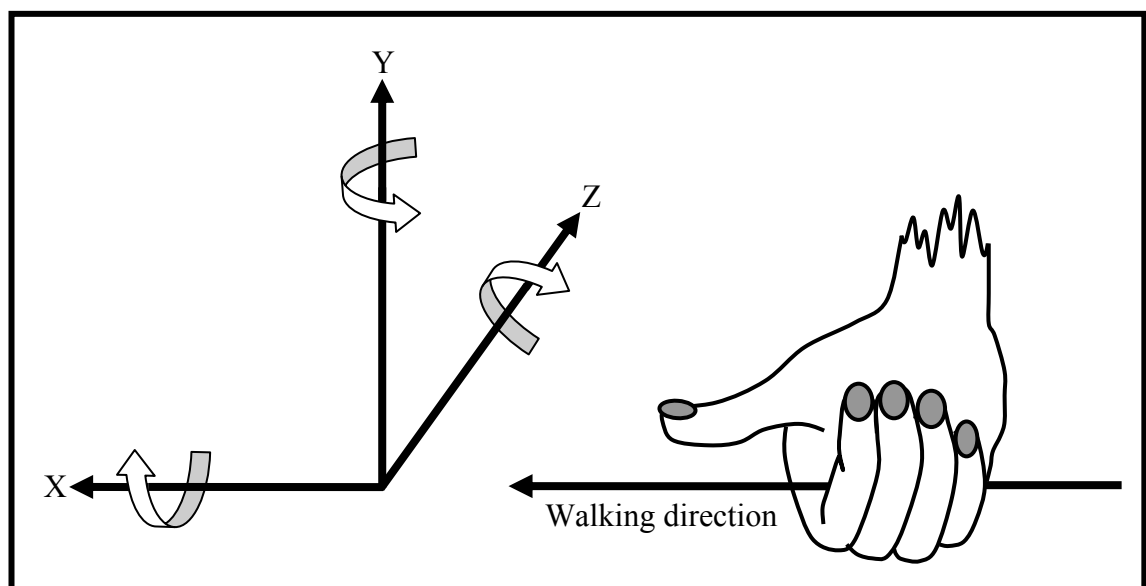
5.1.1.14.   *Analogue data capturing*

Apart from set-up guidelines and accuracy levels to be reached for recording motion of markers, another aspect worth taking into consideration is the fact that the ProReflex^{TM} system's versatility extends beyond kinematic data capturing and that it can be converted into a multi-functional data acquisition facility. In addition to its connection to the six infra red cameras, the computer that was used to run this system was also connected to a sixty-four channel analogue/digital (A/D) board. After setting up the appropriate tab in the hardware setup window of the QTrac Capture software, it was possible to use this system for synchronous motion and analogue voltage data retrieval.

This feature makes it possible to monitor external voltage producing devices, which is a key feature for running the motion analysis system in conjunction with additional data capturing equipment that was necessary for this study, as will be explained in subsequent Sections and Chapters. Using a standard A/D board that is supported by QTrac Capture, the voltage or analogue data and the kinematic data from the ProReflex^{TM} system are being captured simultaneously and can be inspected in QTrac View. When exporting the captured parameters, QTrac View automatically creates two TSV files. One of them contains the digitised data, as explained before in Section 5.1.1.9, and the other contains purely the analogue data. The latter is arranged in columns according to the amount of analogue channels available, and this data can then be further manipulated using spread sheets, as with TSV files for kinematic data.

5.1.2.   <u>Floor force plates</u>

5.1.2.1.   *Functional background*

Probably one of the most common kinetic data capturing devices for motion analyses, force plates measure the body's responses to gravitational forces and the extent to which the body's dynamic actions vary at floor level. Force plates that are mounted onto the floor are designed for walking on. In order to prevent people from tripping, the plates' entire chassis is generally located below the ground or walking platform, so that their upper surface is at floor level.

Rigidly fixed to the floor to prevent them from moving, force plates represent an interface between the body and the ground. At the instant contact is established, forces exerted onto the plates are transmitted from the body onto the earth. Because the plates

act in exactly the same manner as the earth does in accordance with Newton's third law by returning forces in equal and opposite direction back onto the body (Shames 1970), the measurements recorded with these sorts of devices are consequently termed ground reaction forces (GRFs).

5.1.2.2. *Force plate locations to each other*

The gait laboratory within the department at the University of Salford where the current study was undertaken has two force plates (Type 9281B, Kistler Instrumente AG, Winterthur, Switzerland) permanently embedded in the middle of an approximately 8m long walking path. As explained in Section 5.1.1.12, the overall length of the capture volume was set at 4.6m, but an additional travelling distance of approximately 3.4m, or 1.7m before and after the recording space, respectively, helped subjects to maintain a fairly constant walking velocity without having to speed up and slow down while being confined within the capture volume. When measuring GRFs, it is necessary to hit the plates in the centre with the entire shoe or foot and not to step too far sideward, forward or backward, because some of the forces are otherwise transmitted directly onto the ground, adjacent to the plates, which would falsify the readings. Being able to take a few extra steps before entering and after leaving the capture volume can make it easier to hit the plates accurately, because more time is available to find a comfortable walking rhythm for a better judgement as to where the next step may reach to.

The likelihood for stepping onto the central aspect of force plates is dependent on a number of other factors including the walking width and step length, which have to fall within the plates' dimensional boundaries as defined by their size and location. Each plate's upper surface measures 400mm in width and 600mm in length. Their rectangular shape therefore conforms to the longitudinal shape of the foot. Both plates are slightly offset from the centre of the walking path, so that the first plate's position to the left and the second plate's position to the right correspond with the laterally positioned left and right foot, respectively.

With an offset of approximately 85mm between one plate and the other and with an average shoe width of say 140mm, this allows a walking width of up to 345mm (400mm plate width minus 140mm shoe width plus 85mm offset), before stepping too far sideward. The walking width is determined by the distance between both feet's heel centres and is measured perpendicular to the walking direction (Trew & Everett 2001).

As mentioned in Section 2.6.1, the anatomic foot is rarely pointing straight forward, but is usually characterised by slight external rotation. It may therefore be possible for a forefoot with an excessively large toe out angle to step over the borders of its force plate, although the distance between both heels is not exceeding the maximum walking width. In such cases it is obviously necessary to decrease the maximum walking width accordingly to ensure that both feet hit their respective force plate in their entirety.

Figure 5.7: Dimensional boundaries of force plates
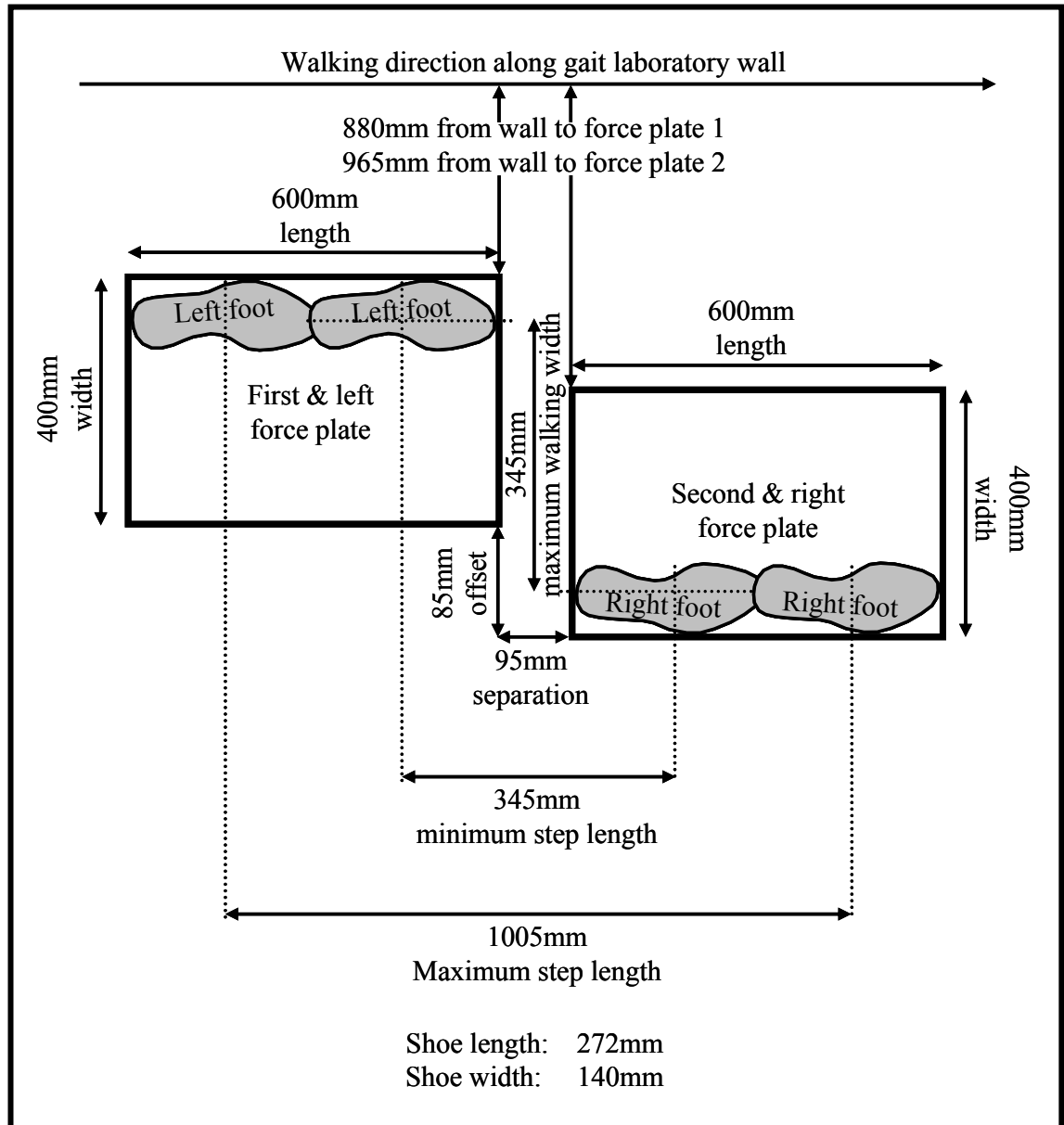
With respect to the walking direction, both plates are separated by approximately 95mm. The step length is determined by the distance between the heel centres of both feet and, unlike the walking width, measured parallel to the walking direction (Durward et al 1999). As may be seen in Table 4.2, the smallest and largest foot length of all ten

subjects measured 250mm and 290mm, respectively. Therefore, the step length could range from 345mm (250mm minimum foot length plus 95mm separation) up to 1005mm (1200mm two plate lengths minus 290mm maximum foot length plus 95mm separation) before stepping too far backward or forward.

It should be taken into consideration that during normal walking, an average walking width measures approximately 70mm (Trew & Everett 2001) and a step length approximately 700mm (Durward et al 1999). The corresponding parameters obtained from the plates' dimensional boundaries therefore seem to fall within an acceptable range, as illustrated in Figure 5.7.

5.1.2.3.   *Force plate locations within capture volume*

Despite a decent size walking path and fairly generous dimensions for the gait laboratory, the location of the force plates was rather awkward, in that they were not positioned centrally, but instead along one of the long walls of the rectangular laboratory environment. The capture volume obviously had to be positioned exactly over the plates for both the kinematic and kinetic data to be recorded simultaneously. However, with only approximately 880mm and 965mm between the wall and the first and second force plate, respectively, as depicted in Figure 5.7, this made it difficult to arrange the ProReflex^{TM} cameras evenly around the recording space. The likelihood for the markers to be captured on the side that is adjacent to that particular wall was therefore lower than for the remaining markers.

As described in Section 5.1.1.12, the data to be recorded was supposed to entail at least one full gait cycle on each the left and right side plus half a step before the first, and another half a step after, the second gait cycle. When considering the location of the capture volume with respect to the force plates, it may be helpful to split the gait cycle up into its two major phases, namely stance and swing phase as defined in Section 2.2.4.

Stance phase is the duration when the body is in contact with the force plates. For both the left and right gait cycle to be fully recorded, the capture volume must not be located centrally over the plates. Instead it should extend further towards the end of the walking path and not as far towards the beginning of it, as swing phase, the final gait cycle part of the limb in contact with the second plate, would otherwise occur outside the capture

Figure 5.8:   Photograph selection and drawings of gait laboratory set-up
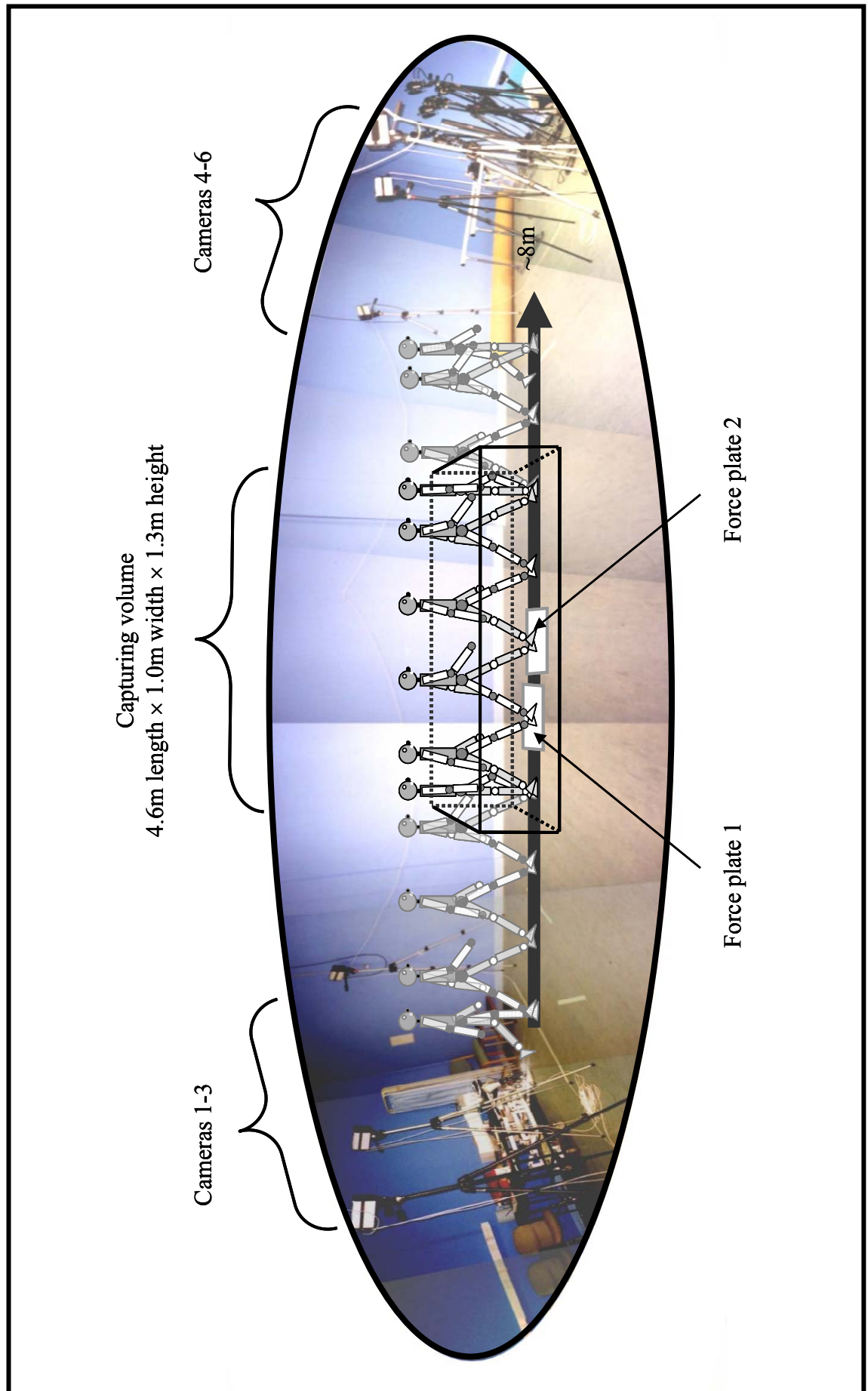
space. As mentioned in Section 4.2.2, data were to be captured of the subjects' left and right sides without prioritising one side over the other, and in this respect, the direction in which to travel along the walking path would not matter. However, the situation when the travelling direction did matter was related to camera positions, in that they obviously had to be arranged non-symmetrically around the plates to gain a complete view of the eccentrically located capture volume with respect to the force plates. It meant that the walking path was limited for travelling in one direction only, namely towards the side where the majority of the capture volume was located.

Figure 5.9: Schematic drawing of the gait laboratory set-up
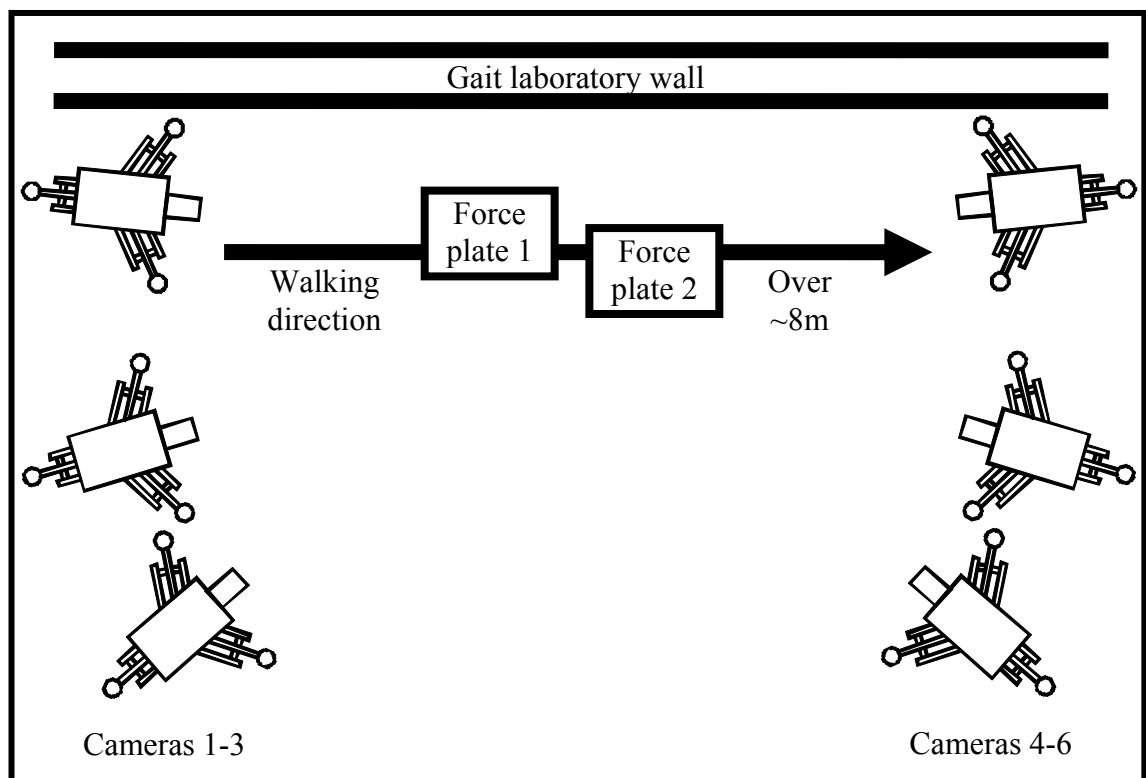
5.1.2.4. ***Camera locations around force plates***

The walking direction was decided upon arbitrarily to extend, as illustrated in Figure 5.8, from left to right when looking towards the wall that was nearest to the force plates. The cameras were adjusted accordingly, so that the capture volume was shifted towards the right side. The subjects' left side was therefore adjacent to the wall and the right side was facing the open part of the gait laboratory. Because the plates could not be moved, to increase the chances for the markers on the left side to be captured, it was necessary for at least two cameras to be positioned as close to the wall in question as possible, so that sufficient amounts of data would be gathered to create an image in 3D.

The remaining cameras were distributed as evenly as possible. Although it would have been desirable to locate at least one camera perpendicular to the walking path in order to capture motion from a greater variety of angles, this was not possible. The reason for that is, because even though there was plenty of room on the open side of the gait laboratory, the capture volume was too long for any camera to detect the entire space from such an angle, as becomes clear from the illustration in Figure 5.9. To prevent opposing cameras from detecting each other's infrared light, their tripods were adjusted to maximum height, which, in turn, was also advantageous as this improved the cameras' viewing angle for detecting markers.

5.1.2.5.   Force plates' internal components

The actual parts responsible for detecting GRFs are multi-component transducers and each of them contains three piezoelectric elements out of quartz. These are orientated to correspond with the force plates' Cartesian co-ordinate system based on axes that are parallel and perpendicular to the plates' rectangular chassis for measuring GRFs in anterior-posterior, medial-lateral and vertical directions. A force plate contains four of these piezoelectric transducers with one of them in every corner of each plate. The transducers are rigidly bonded to, and sandwiched between, the force plates' upper and lower surface. The upper surface forms the part of the force plates that will be in contact with the foot and the lower surface serves to anchor the plates to the ground. Both surfaces have the tendency to move relative to one another in response to GRFs, but the transducers resist this tendency due to their stiff properties. The forces acting upon the transducers put them under stresses and strains. The resultant compressions and elongations the transducers undergo trigger the release of an electric charge in response and proportional to those forces.

As each transducer's individual charges do not provide a complete picture that describes the overall force pattern inflicted upon its force plate, the charges from each plate's four transducers are combined in a particular configuration, so that the resultant signals contain information with regard to the magnitude and direction of GRFs. For obtaining accurate GRF data, it is vital to take into consideration the location of piezoelectric transducers within each force plate and the fact that the transducers' positive or negative outputs are dependent on the direction of forces.

Figure 5.10:   Output channel arrangements and positive readings for GRFs
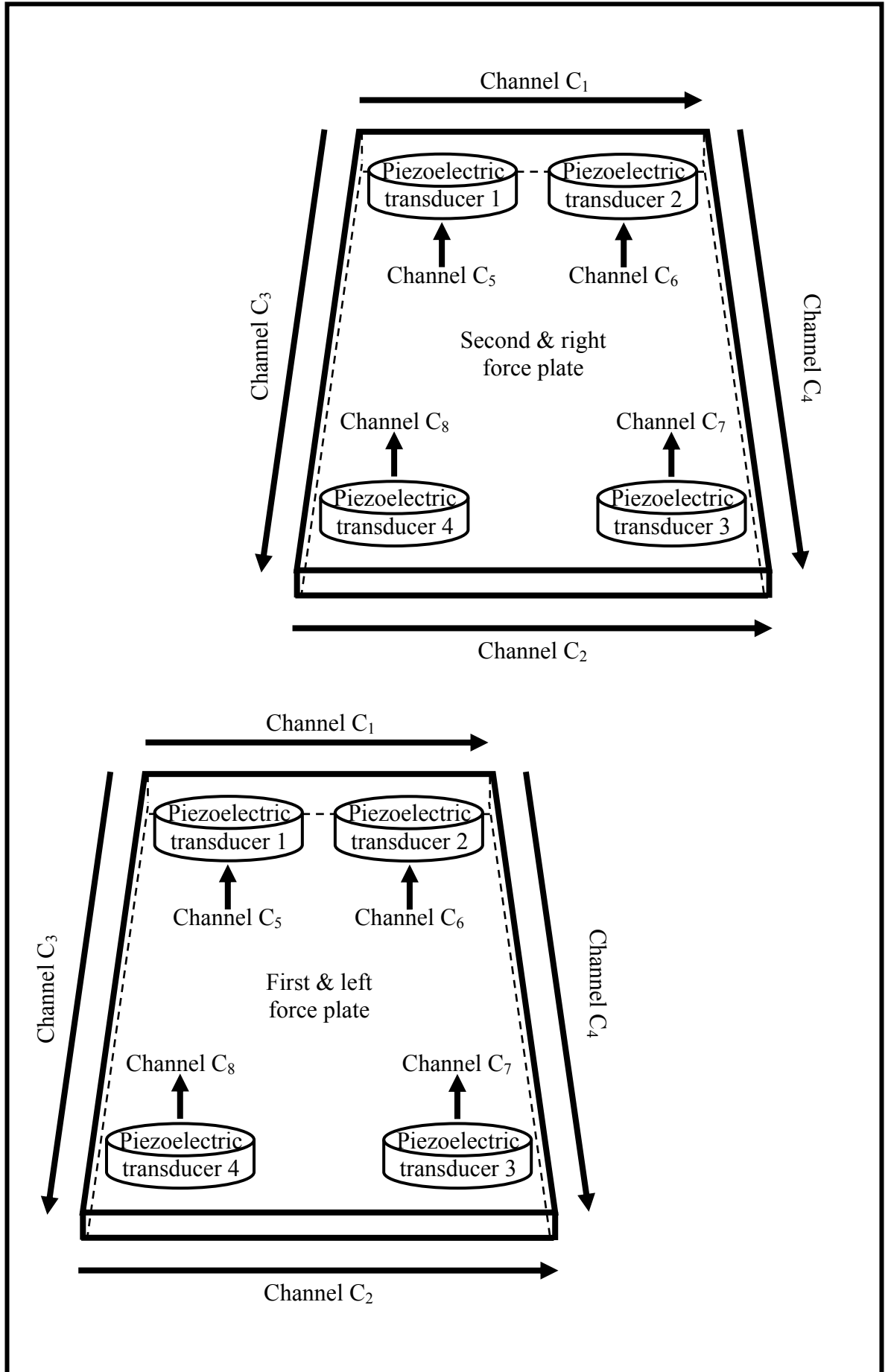
Each force plate's four transducers are arranged in a clockwise manner, and when seen from the start of the walking path, with the nearest wall to the left, the first transducer is located at its plate's far end left hand corner. Positive readings can be obtained when forcing a plate to the left, forward or downward, so that the GRFs are obviously orientated to the right, backward or upward, respectively. The axes arrangement of the plates' co-ordinate system is therefore similar to those described in Section 5.1.1.13, except that the X-axis is pointing in the opposite direction.

Each force plate has eight output channels that convey the signals from the four piezoelectric transducers. Medial-lateral GRFs from transducer one and two are transmitted via channel C_1 and from transducer three and four via channel C_2. Anterior-posterior GRFs from transducer one and four are transmitted via channel C_3 and from transducer two and three via channel C_4. Vertical GRFs from transducer one to four are transmitted via channels C_5-C_8, respectively. Channel allocations were the same for both force plates, as depicted in Figure 5.10.

Another aspect that needs to be taken into consideration when combining the output signals from the piezoelectric transducers is that they are not located in the very corner of their force plate, but slightly away from the plate's edges. Pushing down onto a force plates' central region compresses all four transducers, but when pushing onto a plate's outer region, then the transducers near that region will act as a fulcrum on which the plate rocks like a seesaw. The transducers located near the region that is being pushed onto will therefore be compressed, and the transducers on the opposite side will not be compressed anymore, but elongated instead.

The distance between each transducer's central aspect and the centre of their respective force plate is, as shown in Figure 5.11, 120mm in medial-lateral direction, 200mm in anterior-posterior direction and 63mm in proximal-distal direction, with the latter obviously not referring to the transducers' location above but below the plate's upper surface. As explained in Section 5.1.2.2 and shown in Figure 5.7, with the force plates' dimensions of 400mm width and 600mm length, each transducer's central aspect is therefore 80mm and 100mm away from its force plate's nearest side and front or back edge, respectively.

Figure 5.11:   Piezoelectric transducers' location under their force plate
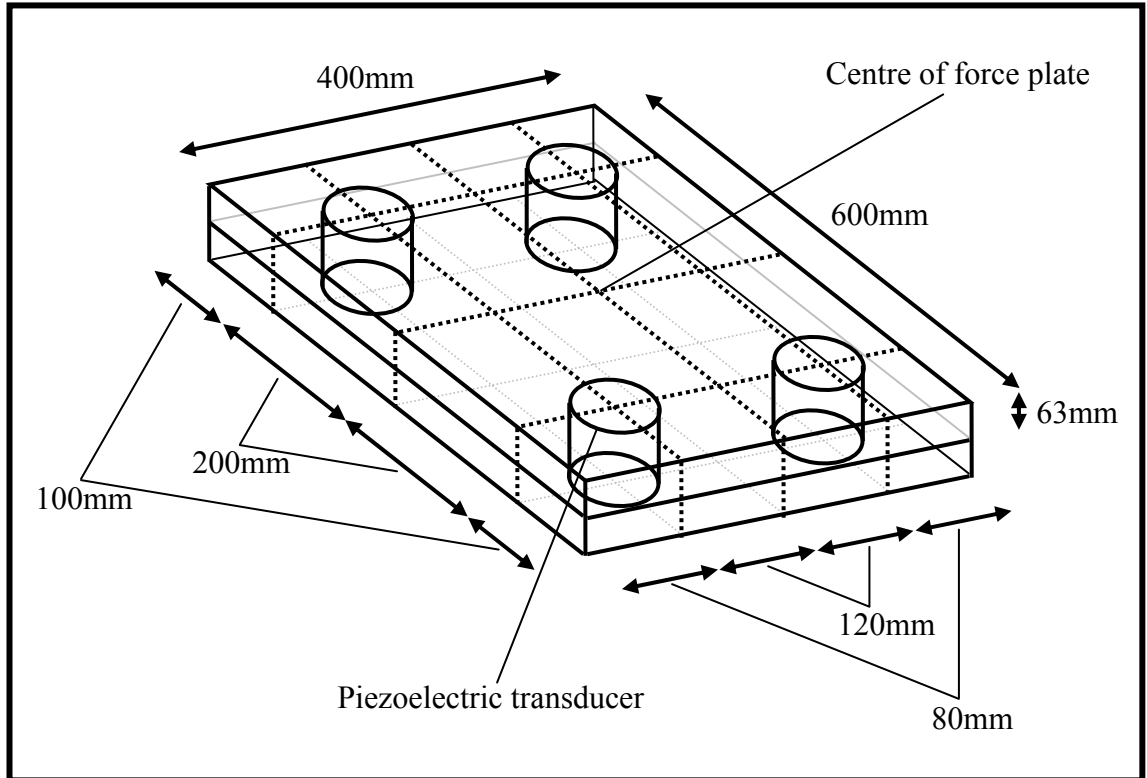
The way the output from a force plate is influenced by the location of its piezoelectric transducers and the location where a force is being applied to, becomes clear from the following examples. When applying, for instance, a force of 30N vertically downward and exactly in the centre between piezoelectric transducer one and two, then they both share the same force, namely 15N, as they are both the same distance away from the point of application (POA), which is the location where a force is being applied to, as depicted in Figure 5.12.

Figure 5.12:   Reaction forces from piezoelectric transducers: Part A
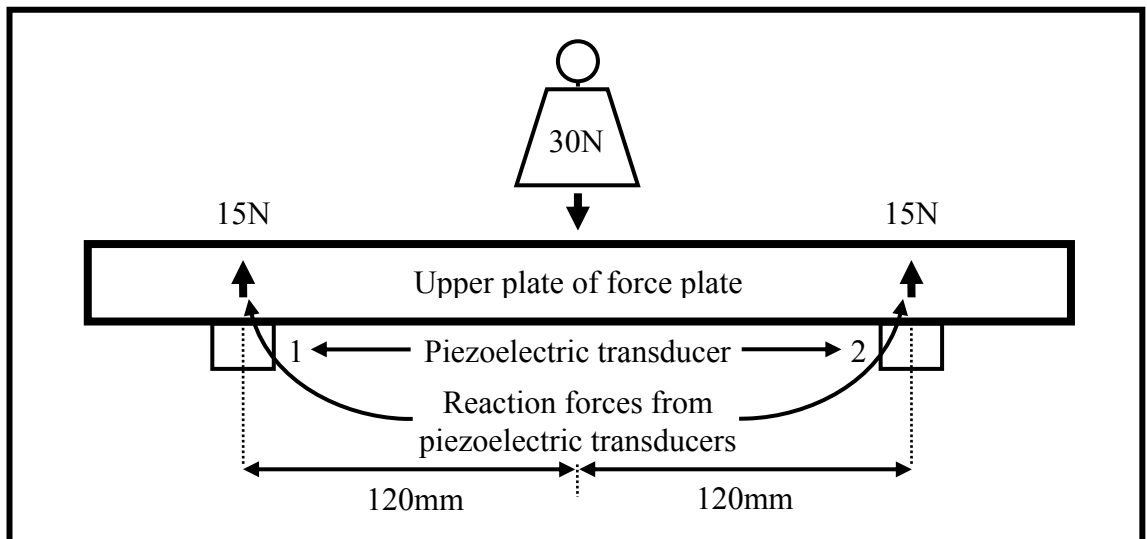
In turn, when applying a force of 30N vertically downward and exactly onto the force plate's left hand edge and in line with transducer one and two, then transducer one would act as a fulcrum, because of its location between transducer two and the POA, as displayed in Figure 5.13. Transducer two would be strained by 10N, which is only a third of the applied force of 30N, because of different lengths of lever arms as the distance between transducer one and two is 240mm and therefore three times the distance between transducer one and the POA, namely 80mm. Transducer one would be stressed by 40N, as it has to bear the resultant force, which is composed of 30N from the applied force and 10N from transducer two. This demonstrates quite clearly that the forces exerted onto both piezoelectric transducers are, as illustrated in Figure 5.12 and Figure 5.13, quite different for the two scenarios, and that the measurements depend upon the location of the POA, which underlines the necessity for combining transducer outputs accurately.

Figure 5.13:   Reaction forces from piezoelectric transducers: Part B
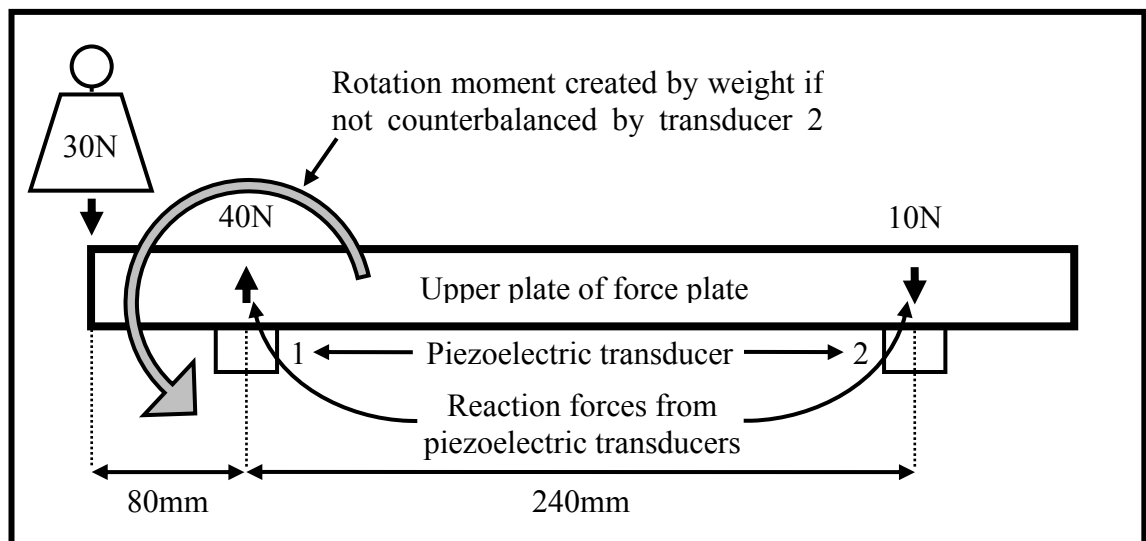
The POA not only influences the distribution of forces between the piezoelectric transducers, it also has a big influence on the plates' rotational aspect. Although the plates are anchored to the ground and cannot move, pushing down on them anywhere else but their centre will create a rotation moment, because the forces exerted onto the transducers are not the same for the two transducers in the example depicted in Figure 5.13. Rotation moments can therefore be created about axes in all three planes and they represent a useful indicator for detecting gait patterns.

5.1.2.6.   Output from force plates

Because charges from piezoelectric transducers are very small and fall within only fractions of a Volt (V), each force plate's outputs are being sent to their respective charge amplifier (Type 9865B, Kistler Instrumente AG, Winterthur, Switzerland) where the signals from that plate's eight channels C_{1-8} are boosted up for reaching values within a range of ±10V. From there, the signals from both charge amplifiers' accumulated sixteen channels C_{1-16} are being conducted to the A/D board for recording the outputs from the force plates as voltages or as analogue data in conjunction with the kinematic data from the ProReflex[TM] system, as explained in Section 5.1.1.14. Force plate one and two were allocated to channels C_{1-8} and to channels C_{9-16}, respectively.

5.1.2.7.   Calibration procedure for GRFs

Unlike the ProReflex[TM] system, which, as explained in Section 5.1.1.3, needs calibrating every time its set-up with regard to camera location has been changed, the force plates only need calibrating after they were manufactured or before the first time they are used for data capturing, so to ensure they function accurately. The calibration procedure involves the application and removal of known forces, so that the output from the force plates and charge amplifiers can be compared with the actual values of applied forces.

Calibrating the plates with regard to vertical forces is fairly straightforward and can be undertaken with an object of known mass, which is positioned in the centre of the plate of interest and then vertically lifted off. In turn, calibrating the plates with regard to horizontal forces is a much more complex procedure and requires the installation of a pulley system that works in conjunction with two weights of known and different mass, as depicted in Figure 5.14. The heavier weight is placed in the centre of the force plate of interest and attached to a horizontally extending string, which is part of the pulley system. Suspended by the string, the lighter weight is attempting to pull the heavier weight horizontally, but due to their difference in mass and due to friction with the plate, the heavier weight remains stationary. The lighter weight is therefore indirectly attempting to pull the plate, but without success as the piezoelectric transducers' connections to the plate counterbalance this action, which, in turn, triggers the transducers to release a charge proportional to the amount of pull produced.

Figure 5.14:   Weight and pulley arrangement for force plate calibrations
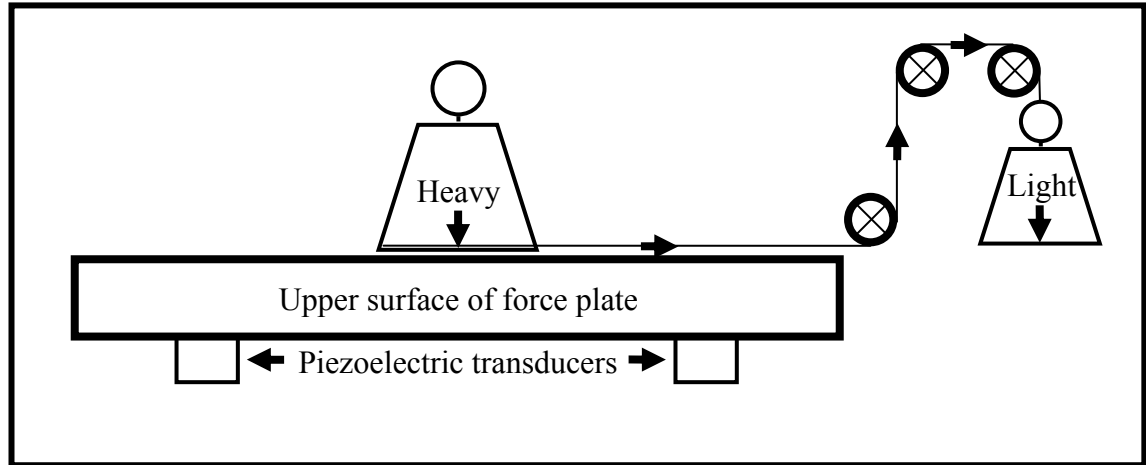
It is important during this procedure to align the string exactly horizontally, as the plate that is being calibrated is otherwise producing an output also related to vertical forces. To differentiate between horizontal forces in anterior-posterior and medial-lateral direction, the string should be parallel to two of the plate's opposing edges, and this process should be repeated with the string parallel to the force plate's other two opposing edges. To increase the accuracy of the calibration results, all three procedures for applying forces along the axes of the co-ordinate system, namely in vertical, anterior-posterior and medial-lateral directions, should be repeated several times.

Calibration procedures are usually undertaken by the manufacturer, because positioning the weights in the centre of each plate and aligning the string of the pulley system correctly is difficult, and if this is not done accurately then the calibration outcome will be affected. The calibration process can be completed prior to the installation of the plates in their definitive location, as long as they are positioned according to the manufacturer's guidelines. The most important factor for this is to make absolutely sure that the force plates are mounted horizontally, because data can otherwise become inaccurate as the plates' own weight will produce minor readings due to their tendency to shift under the influence of gravity.

During the calibration procedure, the manufacturer determines the sensitivity of each force plate with regard to forces applied in vertical and both horizontal directions. This sensitivity is defined as charge units and expressed in pC/N, as displayed in Table 5.1 where the corresponding values are arranged in accordance with the axis system defined in Section 5.1.1.13.

Table 5.1: Sensitivity of both force plates

Axes orientations of the co-ordinate system	First, left force plate (pC/N)	Second, right force plate (pC/N)
X-axis positive anterior	7.81	7.83
Y-axis positive upward	3.87	3.87
Z-axis positive rightward	7.90	7.88

Equations 5.1: Calculation of total measuring range of force plates

$$F_{x1} = 1000N \cdot 7.81pC/N = 7810pC$$

$$F_{y1} = 2000N \cdot 3.87pC/N = 7740pC$$

$$F_{z1} = 1000N \cdot 7.90pC/N = 7900pC$$

$$F_{x2} = 1000N \cdot 7.83pC/N = 7830pC$$

$$F_{y2} = 2000N \cdot 3.87pC/N = 7740pC$$

$$F_{z2} = 1000N \cdot 7.88pC/N = 7880pC$$

Definitions:

$F_{x1}...F_{z2}$ -   force plate 1&2 measuring range in X, Y, Z direction

Equations 5.2: Calculation of analogue signal outputs of force plates

$$F_{x1} = \frac{7810pC}{10000pC} \cdot 10V = 7.81V \,\hat{=}\, 1000N$$

$$F_{y1} = \frac{7740pC}{10000pC} \cdot 10V = 7.74V \,\hat{=}\, 2000N$$

$$F_{z1} = \frac{7900pC}{10000pC} \cdot 10V = 7.90V \,\hat{=}\, 1000N$$

$$F_{x2} = \frac{7830pC}{10000pC} \cdot 10V = 7.83V \,\hat{=}\, 1000N$$

$$F_{y2} = \frac{7740pC}{10000pC} \cdot 10V = 7.74V \,\hat{=}\, 2000N$$

$$F_{z2} = \frac{7880pC}{10000pC} \cdot 10V = 7.88V \,\hat{=}\, 1000N$$

Definitions:

$F_{x1}...F_{z2}$ -   force plate 1&2 analogue output in X, Y, Z direction

Both force plates' sensitivity level was determined by applying forces of up to ±2000N in vertical and ±1000N in each of the two horizontal directions. Therefore, the total measuring range for F_{x1}, F_{y1} and F_{z1} from force plate one and for F_{x2}, F_{y2} and F_{z2} from force plate two, as determined by the minimum and maximum value, fell within 7740pC and 7900pC, as calculated in Equations 5.1.

The charge amplifiers offer a choice of settings to which they can be adjusted, including 1000pC, 5000pC, 10000pC and 50000pC, whereby the maximum output they can produce at any of those settings is 10V. Because the force plates' were calibrated to their maximum measuring range of 7900pC, the charge amplifiers were, as recommended by the manufacturer, adjusted to the next highest setting for optimal signal-to-noise ratio, which, in this instance, was 10000pC. Taking into consideration the maximum forces that the plates were exposed to of ±2000N in vertical and ±1000N in each of the two horizontal directions, it was then possible to calculate the equivalent analogue signal output from the ratio of the plates' measuring ranges and the amplifier settings, which is detailed in Equations 5.2.

Equations 5.3: Calculation of voltage-force ratio of force plates

$$F_{x1} = \frac{7.81V}{7.81pC/N} \cdot \frac{10000pC}{10V} = 1000N$$

$$F_{y1} = \frac{7.74V}{3.87pC/N} \cdot \frac{10000pC}{10V} = 2000N$$

$$F_{z1} = \frac{7.90V}{7.90pC/N} \cdot \frac{10000pC}{10V} = 1000N$$

$$F_{x2} = \frac{7.83V}{7.83pC/N} \cdot \frac{10000pC}{10V} = 1000N$$

$$F_{y2} = \frac{7.74V}{3.87pC/N} \cdot \frac{10000pC}{10V} = 2000N$$

$$F_{z2} = \frac{7.88V}{7.88pC/N} \cdot \frac{10000pC}{10V} = 1000N$$

Definitions:

$F_{x1}...F_{z2}$　　　- force plate 1&2 voltage-force ratio in X, Y, Z direction

Having established the relationship between the analogue signal output or voltage and the corresponding force that was applied onto the calibrated plate, the next step was, as illustrated in Equations 5.3, to calculate the mathematical proportion of those two

values with respect to one another. This was undertaken by using the conversion factors of the plates, as mentioned in Table 5.1.

Equations 5.4:   Calculation of GRFs and GRMs of force plates

$$F_{x1} = \frac{(-C_3 - C_4)}{7.81 \text{pC}/\text{N}} \cdot 1000$$

$$F_{y1} = \frac{(C_5 + C_6 + C_7 + C_8)}{3.87 \text{pC}/\text{N}} \cdot 1000$$

$$F_{z1} = \frac{(C_1 + C_2)}{7.90 \text{pC}/\text{N}} \cdot 1000$$

$$M_{x1} = 120\text{mm} \cdot \frac{(C_5 - C_6 - C_7 + C_8)}{3.87 \text{pC}/\text{N}} \cdot 1000$$

$$M_{y1} = 120\text{mm} \cdot \frac{(C_3 - C_4)}{7.81 \text{pC}/\text{N}} \cdot 1000 + 200\text{mm} \cdot \frac{(C_2 - C_1)}{7.90 \text{pC}/\text{N}} \cdot 1000$$

$$M_{z1} = 200\text{mm} \cdot \frac{(C_5 + C_6 - C_7 - C_8)}{3.87 \text{pC}/\text{N}} \cdot 1000$$

$$F_{x2} = \frac{(-C_3 - C_4)}{7.83 \text{pC}/\text{N}} \cdot 1000$$

$$F_{y2} = \frac{(C_5 + C_6 + C_7 + C_8)}{3.87 \text{pC}/\text{N}} \cdot 1000$$

$$F_{z2} = \frac{(C_1 + C_2)}{7.88 \text{pC}/\text{N}} \cdot 1000$$

$$M_{x2} = 120\text{mm} \cdot \frac{(C_5 - C_6 - C_7 + C_8)}{3.87 \text{pC}/\text{N}} \cdot 1000$$

$$M_{y2} = 120\text{mm} \cdot \frac{(C_3 - C_4)}{7.81 \text{pC}/\text{N}} \cdot 1000 + 200\text{mm} \cdot \frac{(C_2 - C_1)}{7.90 \text{pC}/\text{N}} \cdot 1000$$

$$M_{z2} = 200\text{mm} \cdot \frac{(C_5 + C_6 - C_7 - C_8)}{3.87 \text{pC}/\text{N}} \cdot 1000$$

Definitions:

C_{1-8} - piezoelectric transducers' output channels

$F_{x1} \ldots F_{z2}$ - force plate 1&2 GRFs in X, Y, Z direction

$M_{x1} \ldots M_{z2}$ - force plate 1&2 moments about X, Y, Z-axes

Knowing the force plate conversion factors as described in Table 5.1, as well as the piezoelectric transducers' location under the force plates and output channels C_{1-8}, as detailed in Section 5.1.2.5, all the required information was available for calculating each force plate's GRFs F_{x1}, F_{y1}, F_{z1} and F_{x2}, F_{y2}, F_{z2} in all three directions and rotational moments or ground reaction moments (GRMs) M_{x1}, M_{y1}, M_{z1} and M_{x2}, M_{y2}, M_{z2} about all three axes. As explained in Section 5.1.2.5, the arrangements of axes for

the force plates are not identical to those described in Section 5.1.1.13, and calculations of GRFs and GRMs detailed in Equations 5.4 were based on a conversion to assimilate the co-ordinate system of the force plates to the one defined for the motion analysis system.

Figure 5.15: Determination of COP using GRFs and GRMs
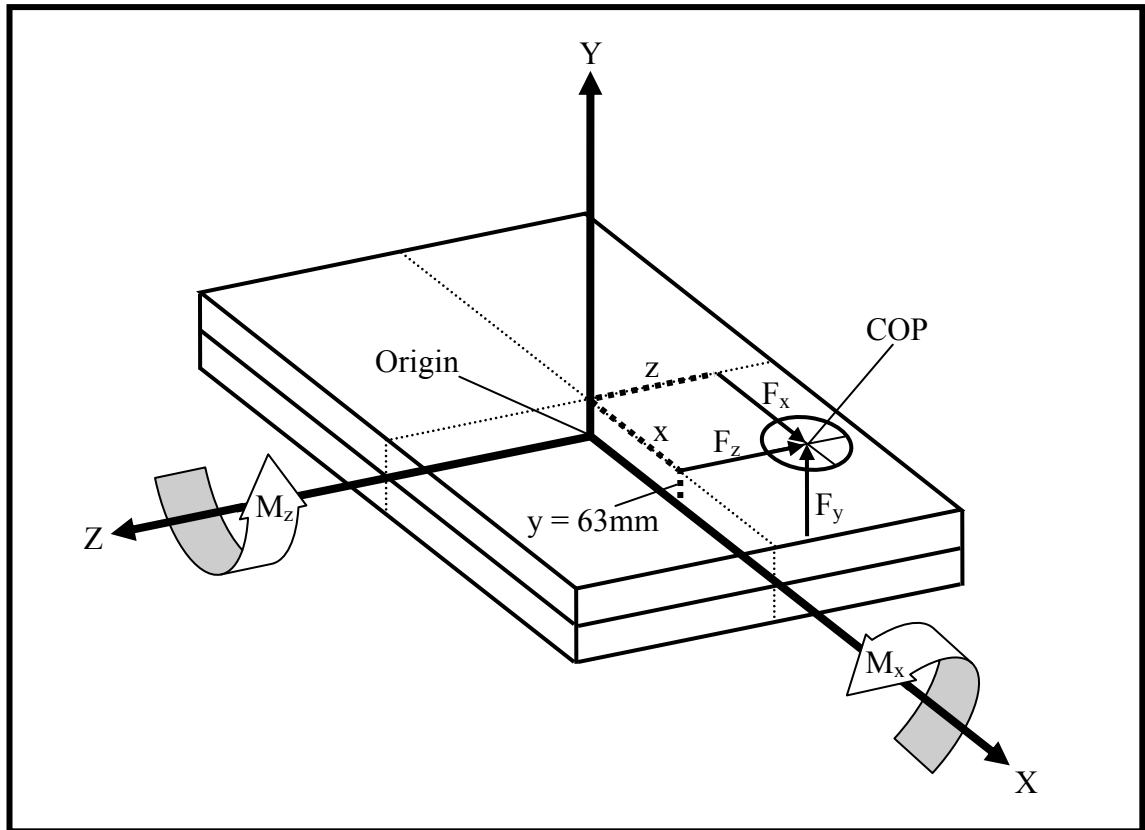
5.1.2.8. *Calibration procedure for COP*

In addition to measuring GRFs in all three directions and rotational moments about all three axes, force plates can also be used for calculating the centre of pressure (COP), which is the location where the forces that are applied onto a force plate are concentrated. However, this is not necessarily the same as the actual POA. For instance, when applying a force with a pointed object vertically onto the plate at a location where the centre of one of the piezoelectric transducers is positioned, then the COP coincides with the POA, namely the centre of that transducer. In turn, when applying a second force of equal magnitude with an identical pointed object vertically onto the plate at a location where the centre of another piezoelectric transducer is positioned, then the COP would be located exactly mid-way between the two points of application (PsOA), namely between the centres of both transducers. The horizontal plane defined by the X and Z-axes of the force plates' co-ordinate system coincides with the position of each

124

transducer's central aspect, which is 63mm below the plates' upper surface, as described in Section 5.1.2.5 and Figure 5.11.

Having established the GRFs and GRMs in Section 5.1.2.7, it is then possible to calculate the sum of moments about the origin of the co-ordinate system to determine the location of the COP in X and Z direction by substituting the appropriate parameters in Equations 5.5. The example given in Figure 5.15 demonstrates that the location of the COP with respect to the force plates' co-ordinate system determines whether the two components responsible for creating a moment are positive or negative.

Equations 5.5:   Calculation of COP using GRFs and GRMs

$$M_{x1} = z_1 \cdot F_{y1} - y_1 \cdot F_{z1}$$

$$\Leftrightarrow \quad z_1 = \frac{M_{x1} + y_1 \cdot F_{z1}}{F_{y1}}$$

$$M_{z1} = x_1 \cdot F_{y1} - y_1 \cdot F_{x1}$$

$$\Leftrightarrow \quad x_1 = \frac{M_{z1} + y_1 \cdot F_{x1}}{F_{y1}}$$

$$M_{x2} = z_2 \cdot F_{y2} - y_2 \cdot F_{z2}$$

$$\Leftrightarrow \quad z_2 = \frac{M_{x2} + y_2 \cdot F_{z2}}{F_{y2}}$$

$$M_{z2} = x_2 \cdot F_{y2} - y_2 \cdot F_{x2}$$

$$\Leftrightarrow \quad x_2 = \frac{M_{z2} + y_2 \cdot F_{x2}}{F_{y2}}$$

Definitions:

$F_{x1}...F_{z2}$ -   force acting on force plate 1&2 in X, Y, Z direction

$M_{x1}...M_{z2}$ -   force plate 1&2 moment about X and Z-axes

$x_1...z_2$ -   offset between COP and centre of force plate 1&2 in X, Y, Z direction

Force plates can be covered with a layer of vinyl or other materials for increased friction during walking thus making ambulation less slippery. This was the case in the gait laboratory at the University of Salford where the current study was undertaken. Such an extra layer on top of the force plates increases the distance y between the horizontal plane defined by the X and Z-axes and the force plates' raised upper surface, as illustrated in Figure 5.16.

Figure 5.16:   Error in calculating COP induced by force plate cover
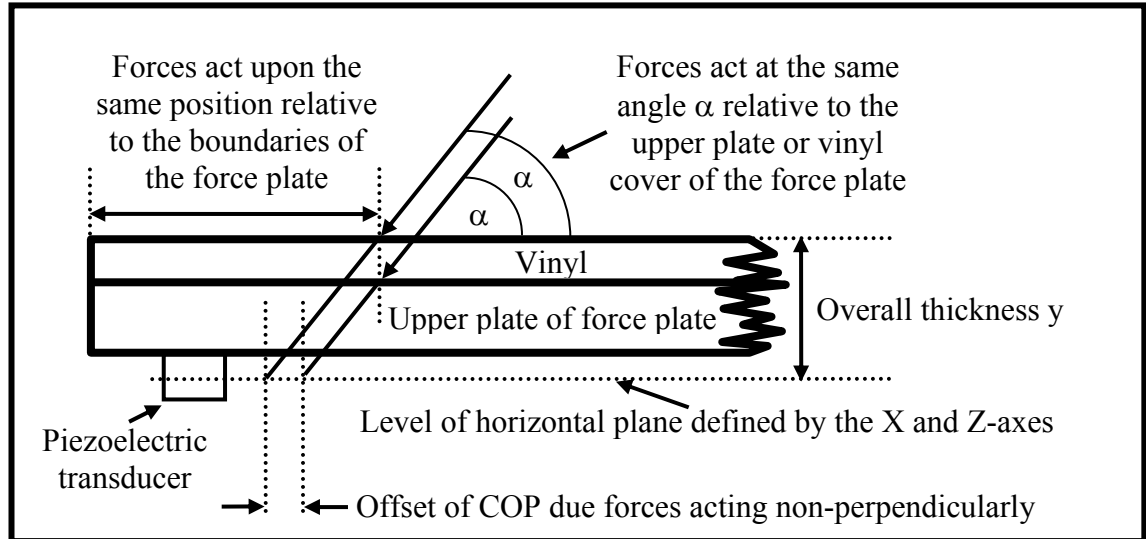
Problems when using an extra layer on top of the force plates evolve when forces are applied non-perpendicularly, because a larger vertical distance y between the origin of the co-ordinate system and the plates' raised upper surface affects the calculation of the COP. To counteract this scenario, the manufacturer of the force plates recommends a calibration procedure for determining the true distance y following the installation of a force plate cover. This calibration procedure can be undertaken by using a pointed object with which to push down at various angles onto a flat, thin plate with its countersunk hole located in the centre of the force plate in question. Calculations based on an incorrect distance y will reveal that the COP moves due to non-perpendicularly applied forces. In such cases the calibration procedure needs to be repeated with the distance y re-adjusted until a figure is found that leaves the COP stationary despite angular variations in applied forces. Tests conducted after installation of the force plates and their vinyl cover revealed that the distance y increased from 63mm, as illustrated in Figure 5.11 and Figure 5.15, to 66mm.

5.2.   Assessment of main capturing equipment

5.2.1.   Assessment of the computerised motion analysis system

After the definitive camera positions were determined in the way described in Section 5.1.2.4, the ProReflex™ system's quality of recorded information needed assessing to establish the level of performance that can be expected from data captures. The overall capture volume for the current study added up to 5.98m^3, which was determined from its length, width and height previously described in Section 5.1.1.12. When assessing

the ProReflex™ system, it must be taken into consideration that the force plates were located near one of the gait laboratory walls, as elaborated on in Section 5.1.2.3, which influences the quality of recorded information, because the cameras could not be evenly distributed around the capture volume.

To establish the system's performance, the two markers of the calibration wand were recorded over a duration of 5s at a sampling frequency of 100Hz while being displaced within part of the total capture volume of nearly 6m³. The resultant data were then used for calculating the distances between those two rigidly fixed markers for every one of the five hundred recording frames. It must be emphasised that establishing the system's performance was not based on a detailed investigation, because only two types of recordings were taken without introducing other variables into the test protocol. Conducting an in depth analysis would have gone beyond the scope of the overall study. Instead, the aim was to establish only a rough estimate as to what sort of level of performance could be expected from the ProReflex™ system.

Figure 5.17: Wand markers turned during type one recording
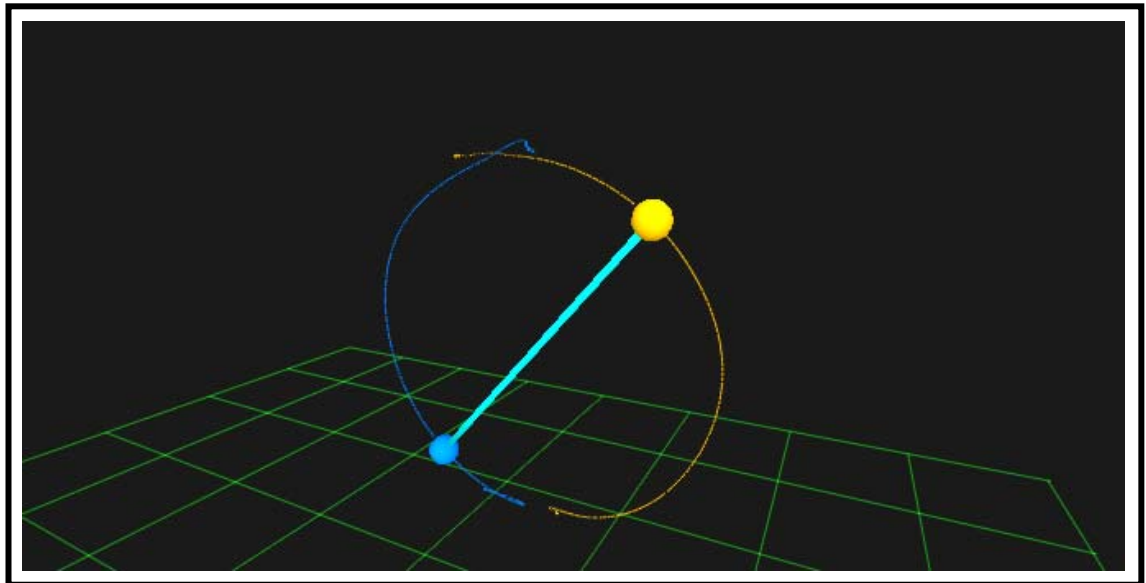
5.2.1.1. *Type one recording for inter-marker distances*

Type one recording was taken while holding the wand markers virtually stationary in the centre of the capture volume, after which they were turned around at 180° until they were held stationary again. The process for this is illustrated in Figure 5.17. A type one recording was based on a preliminary investigation and taken only once prior to the actual trials. The resultant data were split up into three sections A, B and C to

differentiate between frames when the wand was held still during section A and C and when it was turned around during section B, as illustrated in Figure 5.18.

Figure 5.18: Distances between wand markers from type one recording
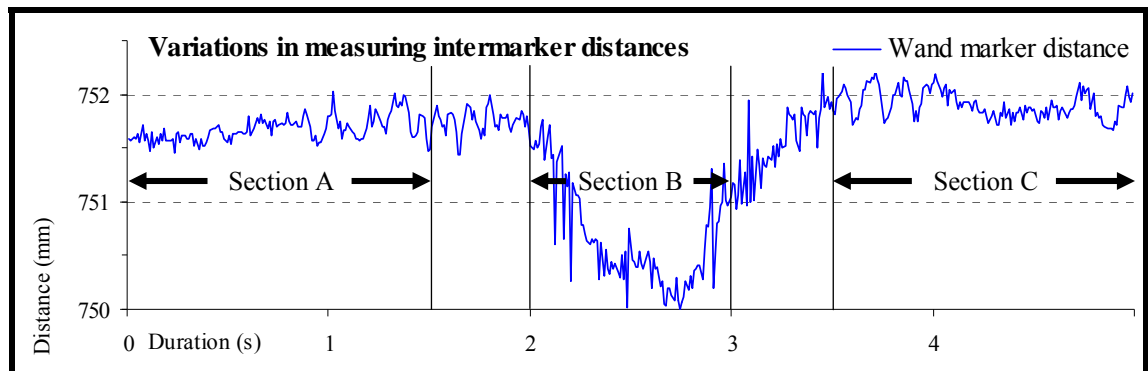
5.2.1.2. *Type two recording for inter-marker distances*

Type two recording was taken while slowly moving the wand markers around the centre of the capture volume at as near a constant velocity as was manually possible. The process for this is illustrated in Figure 5.19.

Figure 5.19: Wand markers moved during type two recording
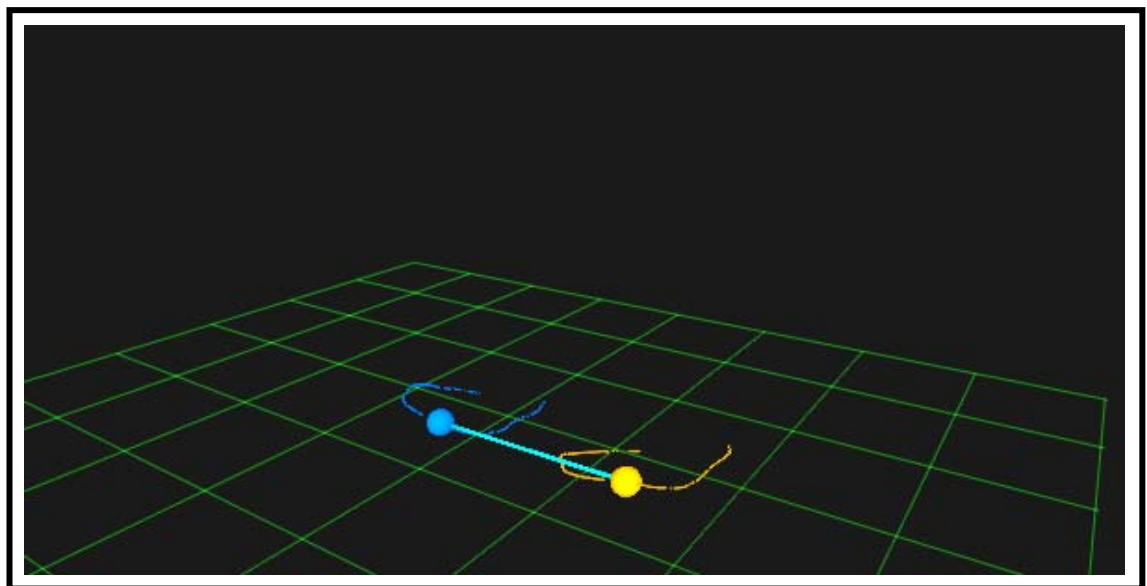
A type two recording was taken every time the gait laboratory was set up for capturing data during the actual trials with the recruited subjects. Therefore, unlike the type one recording, which was only taken once, the resultant number of type two recordings was equivalent to the number of subjects, namely ten. Each type two recording will be referred to as trial A-J, in accordance with each subject's respective alphabetic

representation. Although the camera arrangements were supposed to be the same for all ten subjects, setting up the system in an identical configuration is virtually impossible and slight variations in camera positions are common, thus making the test conditions for each of the ten trials slightly different from one another.

Motions of the wand markers during type two recordings were very regular, as can be seen in their graphic representations, which appear far less characteristic than those of type one recording. All ten trials show similarities in that they were lacking any particular pattern with specific characteristics, and an example based on a randomly chosen test is given in Figure 5.20, which represents trial D.

Figure 5.20:   Distances between wand markers from type two recording
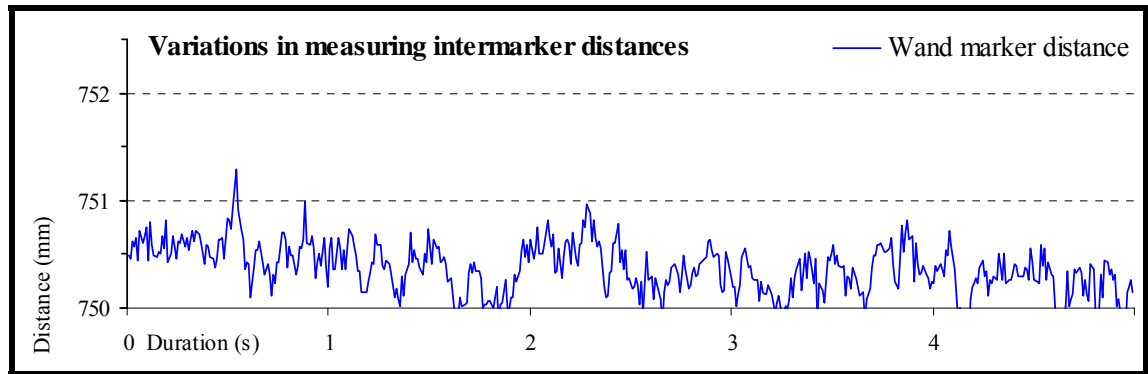
5.2.1.3.   *Assessment of inter-marker distances*

After the process of recording wand motions was completed, the data were, as described in Section 5.1.1.7 to Section 5.1.1.10, processed and digitised using QTrac Capture and QTM, respectively. The actual calculations for determining the inter-marker distance D were undertaken in Excel (Microsoft Corporation, Redmond Oregon, USA), by opening the TSV file that contained the stored data and substituting both markers' X, Y and Z co-ordinates X_{M1}, Y_{M1}, Z_{M1} and X_{M2}, Y_{M2}, Z_{M2} into Equations 5.6 for each recording frame.

Equations 5.6:   Calculation of inter-marker distances

$$D \;=\; \sqrt{(X_{M1} - X_{M2})^2 + (Y_{M1} - Y_{M2})^2 + (Z_{M1} - Z_{M2})^2}$$

Definitions:

D   -   inter-marker distance

$X_{M1}\ldots Z_{M2}$ -   marker co-ordinates in X, Y, Z direction

The results for type one and type two recordings are listed in Table 5.2 and Table 5.3, respectively. The statistical analysis for type one recording was summarised according to section A-C and for type two recording according to trial A-J. A number of factors were considered to be relevant for the assessment of the motion analysis system's performance characteristics including its precision, repeatability and accuracy.

The minimum, maximum and mean of each section or trial expresses the top, bottom and average of a measuring range, respectively. The dispersion of values from the average represents the precision of the equipment and was calculated as the standard deviation. Averaging the mean of measurements from each section or trial and establishing the dispersion of values from the average by calculating the standard deviation of the means of sections or trials, represents the repeatability of the system. The difference between the known inter-marker distance and the measured value represents the accuracy of the system, which was calculated as the root mean square (RMS) error, as shown in Equations 5.7.

Equations 5.7:   Calculation of RMS error

$$\text{RMS} \quad = \quad \sqrt{\frac{\sum\limits_{i=1}^{n} (D_{true} - D_i)^2}{n}}$$

Definitions:

D_i -   measured inter-marker distance

D_{true} -   actual inter-marker distance (750.3mm)

n   -   number of recording frames (500)

RMS   -   root mean square

5.2.1.4.   *Analysis of type one recording*

During the beginning and end parts of type one recording, namely section A and C, both wand markers were virtually stationary and inter-marker distances reached, as shown in Table 5.2, between 751.46-752.22mm. This is a range of 0.76mm. Comparing these figures with the actual, real life inter-marker distance of 750.3mm demonstrates that the measurements were 1.16-1.92mm larger. While the wand was being turned around during the middle part of the recording, namely section B, the measurements dropped as low as 750.00-751.76mm. This is much closer to the markers' actual real life distance, but quite different from the measurements taken while the markers were virtually static.

Table 5.2:   Wand marker motion data from type one recording

Section	Minimum (mm)	Maximum (mm)	Difference as in max-min (mm)	Mean (mm)	Standard deviation (mm)	RMS (mm)	RMS (% of 750.3mm wand)
A	751.46	752.03	0.57	751.68	0.11	1.38	0.18
B	750.00	751.76	1.76	750.69	0.49	0.62	0.08
C	751.67	752.22	0.55	751.91	0.13	1.62	0.22
	Minimum						
	750.00	751.76	0.55	750.69	0.11	0.62	0.08
	Maximum						
	751.67	752.22	1.76	751.91	0.49	1.62	0.22
	Difference as in max-min						
	1.67	0.46	1.21	1.22	0.38	1.00	0.14
	Mean						
	751.04	752.00	0.96	751.43	0.24	1.21	0.16
	Standard deviation						
	0.91	0.23	0.69	0.65	0.21	0.52	0.07

When looking at the differences between the minimum and maximum of measurements, it can be seen that the range for section B was 1.76mm, which is approximately 309% and 320% of the differences obtained for section A and C, namely 0.57mm and 0.55mm, respectively. A similar observation was made by looking at the standard deviations, because the value obtained for section B was 0.49mm, which is approximately 446% and 377% of the standard deviations for section A and C, namely 0.11mm and 0.13mm, respectively. This therefore indicates that the system's precision is lower when capturing relatively fast moving markers compared to slow or stationary markers.

When summarising the data, the mean and standard deviation of mean values from all three sections are 751.43mm and 0.65mm, respectively. It should be taken into consideration, however, that type one recording was based on one trial only and although splitting the data up in three sections is useful to distinguish between relatively

fast marker movements and slow or no marker movements, the statistical power is exceedingly low and the values obtained for the mean and standard deviation should therefore be interpreted with care when referring them to the system's repeatability.

Despite findings indicating that the precision during fast marker movements is a lot less compared to slow or no marker movement, the inter-marker measurements during rotation of the wand were, as explained previously in this Section, closer to the actual value than they were while the wand was stationary. This explains the results regarding the RMS error for section B of 0.62mm or 0.08% of the wand markers' known distance, which is approximately 50% and 38% of the RMS error for section A and C of 1.38mm and 1.62mm or 0.18% or 0.22% of the wand markers' known distance, respectively.

5.2.1.5. *Analysis of type two recording*

As shown in Table 5.3, inter-marker distances during this type of recording reached between 746.03-756.37mm for all ten trials, which represents a range of 10.34mm. Comparing these figures with the actual, real life inter-marker distance of 750.3mm demonstrates that the measurements were between 4.27mm smaller and 6.07mm larger.

Rather than looking at the overall figures, the range of measurements obtained from individual trials reach from 1.59-7.71mm. The mean values are quite similar for all ten trials ranging from 750.18-750.46mm, which is very close to the actual known inter-marker distance and only between 0.12mm smaller and 0.16mm larger. With regard to standard deviations, the inter-trial range extends from 0.24-0.88mm, which implies that the value for the highest precision is only approximately 27% of that obtained for the lowest precision.

When summarising the data, the average and standard deviation of mean values from all ten trials are 750.36mm and 0.08mm, respectively. Although the overall amount of trials used for this kind of statistical calculation was only ten, it is worth considering that each trial is composed of five hundred frames. This implies that the total number of entries from all ten trials is five thousand, which seems a fair representation of samples. The value obtained for the mean of those trials is 750.36mm, which is therefore only 0.06mm different from the actual known inter-marker distance of 750.3mm. The standard deviation from the mean value is 0.08mm, which is only 0.01% of the mean of trials of 750.36mm, thus indicating good repeatability.

Table 5.3:   Wand marker motion data from type two recording

Sub-ject	Minimum (mm)	Maximum (mm)	Difference as in max-min (mm)	Mean (mm)	Standard deviation (mm)	RMS (mm)	RMS (in % of 750.3mm wand)
A	747.45	754.99	7.54	750.40	0.88	0.88	0.12
B	749.53	753.37	3.84	750.36	0.50	0.51	0.07
C	747.29	753.56	6.27	750.31	0.60	0.60	0.08
D	749.70	751.29	1.59	750.37	0.24	0.25	0.03
E	747.73	752.85	5.12	750.40	0.55	0.55	0.07
F	749.60	756.37	6.77	750.46	0.51	0.54	0.07
G	748.59	752.32	3.73	750.36	0.36	0.37	0.05
H	746.03	753.70	7.67	750.18	0.65	0.66	0.09
I	749.09	752.81	3.72	750.44	0.47	0.48	0.06
J	747.17	754.88	7.71	750.27	0.72	0.72	0.10
	Minimum						
	746.03	751.29	1.59	750.18	0.24	0.25	0.03
	Maximum						
	749.70	756.37	7.71	750.46	0.88	0.88	0.12
	Difference as in max-min						
	3.67	5.08	6.12	0.28	0.64	0.63	0.09
	Mean						
	748.22	753.61	5.40	750.36	0.55	0.56	0.07
	Standard deviation						
	1.26	1.47	2.12	0.08	0.18	0.18	0.03

The range of RMS errors is similar to the range of standard deviations and extends from 0.25-0.88mm, which is the equivalent of 0.03-0.12% of the actual known inter-marker distance. Taking a walking path of approximately 8m into consideration and the fact that some of the cameras were therefore at least 50% of that distance or 4m away from the markers, an accuracy of at least 0.88mm represents approximately 0.02% of 4m, which seems quite reasonable.

5.2.1.6.   *Assessment considerations*

The two types of recordings that were used for assessing the system's performance characteristics differed. The markers were moved rapidly during section B of type one recording and the distances they travelled were considerably larger than during section A and C. However, despite fast movements of the markers and the inherent side effect of exposing markers to the upper regions of the capture volume due to rotation of the wand, the recordings were more accurate than they were during sections A and C. In turn, as can be seen in Figure 5.18, the inter-marker distances seem to vary a lot more when rotating the wand during type one recording than they did when the wand was stationary or only moved slowly during type two recordings, as demonstrated in Figure 5.20. The levels of precision, repeatability and accuracy from trials A-J were high. However, it must be taken into consideration that motion normally takes place at a fairly rapid pace over almost the entire capture volume. The true performance characteristics of the system are therefore more likely to be reflected by the total range of inter-marker measurements from all three combined sections of type one recording, which turned out to be 2.22mm.

As mentioned previously in Section 5.1.1.4, the manufacturer claimed the system's accuracy for a volume of $1m^3$ reached ±0.2mm, but it was not stipulated whether the markers were moving or not, nor were the locations of markers within the capture volume described. The quality of the data is, as explained throughout Section 5.1.1, dependent on numerous factors, and as the recording space used by the manufacturer was only approximately 17% of the volume used for the current study, this makes it difficult to compare their findings with those obtained here.

The literature is awash with publications that validate the performance characteristics of motion capturing systems. However, as demonstrated and elaborated on in this thesis, it may be more appropriate to assess each system's setup on its own merits, so that predictions for the quality of the data to be recorded are based on the specifications of the set-up in use and not on someone else's research findings of perhaps less relevance to the requirements for these particular testing conditions. The performance characteristics, as they were tested for the current study using the wand, may not entirely reflect the system's true capabilities, but it will at least give some insight into an estimated performance level that can be expected for this type of set-up and for a capture volume of approximately $6m^3$.

5.2.1.7.   Additional considerations

The ProReflex^{TM} system's marker capturing facilities are, as explained in Section 5.1.1.14, only one of its features and it can, in addition, also be used as a multi-functional data acquisition unit by taking advantage of its sixty-four channel A/D board for capturing analogue and kinematic data simultaneously.

This board was only acquired half way through the current study and the way simultaneous data captures were achieved prior to that was rather more complicated. The analogue data were recorded by using another, additional piece of software, namely ProVec 5.0 (MIE Medical Research Ltd, Leeds, UK), which was controlled by a different computer than the one used for the ProReflex^{TM} system. Inter-connecting both computers to create a link between ProVec 5.0 and the ProReflex^{TM} system made it possible to synchronise the two capturing processes. However, tests showed that the synchronisation was out of phase by a few milliseconds, and the additional problem was that the offset varied between recordings, which made it impossible to accurately compensate for the error mathematically.

The method used for testing data synchronisation was based on a metal marker of approximately 25mm diameter, which was covered with the same reflective coating as used for standard markers. Dropping the metal marker onto one of the force plates, while taking recordings with both systems, made it possible to determine the point in time when GRFs were triggered and when the orientation of the marker's displacement changed. As these two events did not coincide and it was impossible to make predictions with regard to the offset, it seemed inappropriate for this recording procedure to be used for the current investigation.

The University of Salford fortunately acquired the sixty-four channel A/D board in time for the gait laboratory tests. To determine whether the synchronisation of data with the help of this device is exact, it became necessary for the ProReflex^{TM} system's expanded capturing facilities to be tested, which was done in the same fashion as before by using the method with the metal marker. Recordings were taken at a sampling frequency of 100Hz. The resultant data revealed that the synchronisation with the ProReflex^{TM} system was not out of phase and that the results were repeatable, which deemed this capturing equipment suitable for the current investigation.

5.2.2.   Assessment of the floor force plates

It was necessary to assess the quality of information received from the force plates to establish the performance characteristics that can be expected when using them for capturing data.

5.2.2.1.   Analysis of calculations for GRFs and GRMs

The goal was to assess whether the algorithms described in Equations 5.4 are correct. Using data from a single walking trial, GRFs and GRMs were calculated in two ways. The first method was undertaken in Excel (Microsoft Corporation, Redmond Oregon, USA) where the required parameters were calculated as stipulated in those equations. The second method was based on commercially available software called ProVec 5.0 (MIE Medical Research Ltd, Leeds, UK), which was previously described in Section 5.2.1, whereby the algorithms for calculating these parameters are not accessible to the user. The processed data from both types of calculations were inserted into the same chart, but the resultant information was displayed as only one single graph. This meant that the two types of data were identical and they therefore overlapped completely. Assuming that the ProVec software operates accurately, proves that the algorithms described in Equations 5.4 are correct.

5.2.2.2.   Analysis of calibration procedure for GRFs

As mentioned in Section 5.1.2.7, calibrating the force plates with regard to GRFs is usually undertaken by the manufacturer, who uses a three-component calibration system that is based on precisely aligned hydraulic cylinders for applying forces in the direction of all three co-ordinate system axes. The environmental conditions acceptable for operating the force plates can range from -20-+70°C, whereby the actual temperature they were calibrated at was 20°C. This was similar to the temperature in the gait laboratory environment, which increases the likelihood for the output from the actual trials to be similar to those during force plate calibrations.

The sensitivity of the force plates is defined, as illustrated earlier in Table 5.1, by the output charges the piezoelectric transducers release in response to forces of up to ±2000N in vertical and ±1000N in each horizontal direction exerted onto them. The manufacturer gave no figures to define the accuracy of the force plates, but the results from the calibration processes reveal an output linearity of ±0.3% for all three

calibration ranges. The force plates' repeatability and the precision of measurements were not elaborated on either by the manufacturer, and a specifically devised method for determining these factors as part of this investigation may lead to inconclusive results, because the resources available for handling such an approach would probably be insufficiently exact. However, according to the manufacturer, the quartz sensors inside the piezoelectric transducers do not experience fatigue, ageing, creep or wear, which helps to obtain some insight into their performance characteristics.

With regard to the charge amplifiers, the accuracy from all eight channels is supposed to be less than ±1% and the drift less than ±0.03pC/s. Problems associated with hysteresis can be overcome by zeroing or resetting the charge amplifiers between trials.

Cross-talk between output channels is a common phenomenon with multi-purpose measuring equipment, which also affects data captures regarding GRFs. Cross-talk can originate from the arrangement of the three piezoelectric elements in each force plate's four transducers and from the electronic circuitries inside the charge amplifiers. However, the levels of cross-talk found during the calibration undertaken by the manufacturer were exceedingly low and summarised in Table 5.4.

Table 5.4:   Cross-talk between axes of force plates' co-ordinate systems

Force plate	Between x & y (%)	Between y & x (%)	Between x & z (%)	Between z & x (%)	Between y & z (%)	Between z & y (%)
First, left	0.3	0.7	0.7	0.3	1.0	-0.1
Second, right	0.3	0.7	0.8	0.4	1.0	-0.1

5.2.2.3.   Analysis of calibration procedure for COP

The calculated location of the COP may not necessarily reflect its true position and determining the accuracy and precision of measurements may help in establishing how exact the results would really be. The accuracy refers to the difference between the position of the COP obtained from force plate data and manually taken measurements, and the precision to the dispersion of measurements from the mean. Mickelborough 2001 conducted tests to establish these parameters with regard to one of the same two force plates used for the current study at the University of Salford. Instead of using the

entire force plate with its dimensions of 400mm in width and 600mm in length, as explained in Section 5.1.2.2, those tests were focused on a centrally located area of 400mm by 400mm only. This meant that the force plate's first and last 100mm were ignored.

Figure 5.21: Accuracy of COP calculated for one force plate

This diagram was adapted from Mickelborough 2001
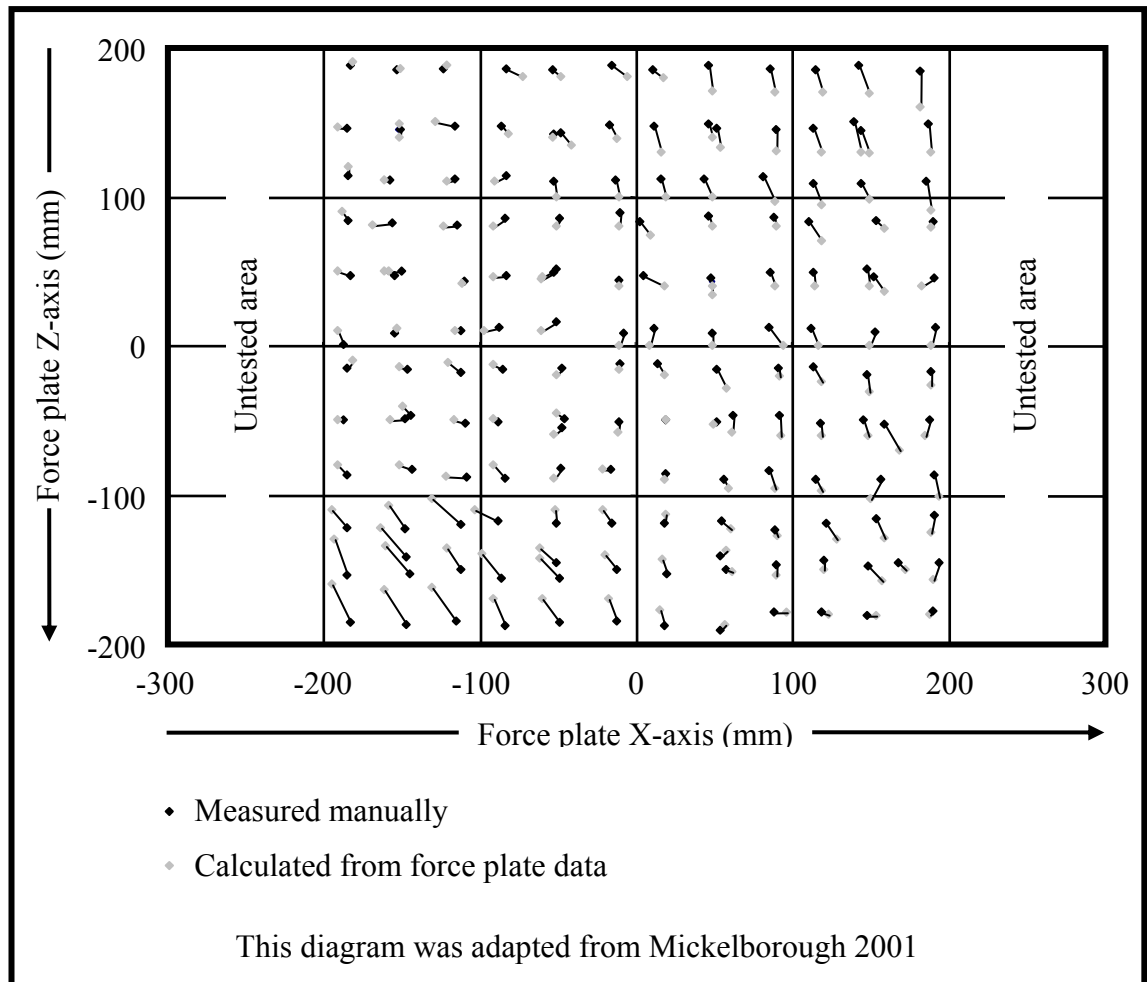
The chosen area was subdivided into a grid containing sixteen squares of 100mm length and width. Using a triangular board with a ball bearing located in each corner, the location of the COP was determined by placing part of this board onto the force plate, so that one of the ball bearings was located in one of the sixteen squares on the force plate and the other two ball bearings outside the force plate area. With the triangular board located in ten different positions per square while exposed to body weight, data were recorded over a duration of 2s at a sampling frequency of 500Hz for each of the hundred sixty positions. In addition to collecting force plate data for determining the position of the board and therefore the COP, each position the board was in was also identified using a tape measure and a set rule.

The force plate's accuracy for all ten trials per square is displayed in Figure 5.21, which is an illustration obtained from Mickelborough 2001, who gave permission for its reproduction, as confirmed by a letter in Appendix 5 of this thesis. The precision represented by the standard deviation for each trial ranged between 0-5mm. The mean and standard deviation of RMS errors was approximately 7.1mm and 4.0mm, respectively.

Compared to the force plate's overall dimensions, the statistical parameters Mickelborough 2001 obtained from the data analysis were very low. It can therefore be anticipated that the influences of these issues on the test results of the current study will only be minimal. Because Mickelborough 2001 tested only one of the force plates, it was assumed that outputs from the second one would be similar, particularly when the high quality manufacturing processes utilised during assembly of the force plates are taken into consideration.

CHAPTER 6.   <u>OTHER CAPTURING EQUIPMENT</u>

6.1.   <u>Considerations for other capturing equipment</u>

The computerised motion analysis system and the force plates are the main equipment for obtaining data that can be used to calculate the most commonly encountered gait parameters in motion analysis. However, additional information will be required to achieve the objectives outlined in Section 3.6.

One of the goals for this study was, as mentioned in Section 4.1.3.1, to establish the extent of displacement occurring at transverse rotation and longitudinal translation adapters. This requires a useful method from which accurate measurements with regard to angular and linear displacement between the TT Pylon housing and shin tube can be obtained.

The other goal was to establish whether this type of adapter has the potential for decreasing the magnitude of angular and linear displacements between the socket and the residual limb, so that shear stresses and peak impacts can be reduced to prevent tissue irritation and breakdown, as explained in Section 2.4.3. However, measuring angular and linear displacements at the residual limb-socket interface may be difficult due the intimate fit of the prosthesis. Instead, it seemed a more feasible option to measure the magnitude and duration of forces acting on the residual limb as these are the underlying factors that trigger shear stresses and peak impacts in the first place. Measuring forces rather than displacements inside the socket therefore represents a more direct approach in assessing the likelihood for tissue damage.

6.1.1.   <u>Radio telemetry system</u>

6.1.1.1.   Functional background

Motion analysis systems can optically gather information without having to be connected to the person performing a certain manoeuvre, and this is a similar scenario for floor force plates as they are only temporarily exposed to personal contact. Both types of systems represent standard equipment for obtaining relevant movement

parameters. However, in order to gain a more in-depth impression about the performance characteristics of a subject's motion pattern, it is sometimes necessary to record data from additional sensing devices.

The nature of the information to be gathered may require additional sensing devices to be continuously attached to the test subject. Using a cable for transferring the signals from those sensing devices to the computer used for storing data is a common solution. Because of the physical connection between test subjects and recording equipment, this cable is often being referred to as an umbilical cord. Such a connection can have practical implications in that the umbilical cord can knock markers off the landmarks to which they are attached or simply obstruct the view between markers and cameras. The extent of freedom to perform a certain task is also limited. Having a cable trailing behind amputees may cause them to trip, a problem exacerbated by their reduced ability to balance their body on a prosthesis compared to non-amputees.

It is therefore desirable to find an alternative solution for transferring information between subject-mounted sensing devices and the data storing computer to improve the manoeuvrability that test subjects should have for performing a task safely. In addition to the computerised motion analysis system and the two force plates, another data capturing unit available from the University of Salford that was considered potentially valuable for the current study was an analogue voltage data retrieval unit called MT8 (MIE Medical Research Ltd, Leeds, UK). This type of data capturing equipment does not rely on an umbilical cord, but transfers measurements telemetrically between a transmitter and a receiver.

6.1.1.2.   *Transmitter unit*

The transmitter has an adjustable fabric belt with a spring-loaded clasp for fastening it around the test subjects' waist. Electrical connections from the sensing devices can therefore be kept short, as they only need to reach the transmitter and do not have to be plugged into any stationary equipment. One 9V PP3 battery provides the power for the transmitter and this supply can last for up to 2.5 hours, depending on the type of sensing devices used. The dimensions of the transmitter are quite small, measuring 165×65×30mm with an overall weight of 550g including the belt and battery. This makes the transmitter exceedingly portable and minimises interference with the subjects' performance.

The transmitter possesses a total of eight channels for receiving information from the same number of sensing devices via eight four-pin Lemo^{TM} "OB" series plugs. These types of plugs are not only pushed into their female counterpart or socket, but they latch in. Taking them out again is therefore only possible by retracting part of the plugs' housing to unlock their connection. This holds a great advantage over plugs that rely on friction or spring mechanisms, as Lemo^{TM} plugs are less likely to become accidentally disconnected from their socket during the gait laboratory tests.

The transmitter has an aerial, approximately 100mm long, protruding from its housing, which is slightly flexible, so that knocking against it will not injure or hurt the subject nor break the aerial. The transmitter's operating frequency ranges in the UK between 173.7-174.0MHz with a band width of 15kHz narrow band and 90kHz wide band, whereby the channel band width is 165kHz narrow band and 1000kHz wide band. The transmitter has a power output of less than 10mW and a modulation voltage of 5V with high impedance.

6.1.1.3.   Receiver unit

Measuring approximately 400×300×100mm, the receiver is substantially bigger than the transmitter, but this is of little concern, as the test subjects are not in contact with this unit at all. Because portability is not an issue, the power for the receiver comes from the 220-240V mains supply.

The receiver has a built-in liquid crystal display (LCD) oscilloscope that can be used for individually observing the data from each of the eight channels. From there the signals are conducted to the A/D board for recording the outputs from the telemetry system as voltages or as analogue data in conjunction with the kinetic data from the force plates and the kinematic data from the ProReflex^{TM} system, as explained in Section 5.1.2.6 and Section 5.1.1.14, respectively. As channels C_{1-16} were occupied by the force plates, the data from the radio telemetry system were allocated to channels C_{17-24}.

6.1.2.   Equipment for measuring motion at the adapter

As the ProReflex^{TM} system is already part of the equipment to be used during the gait laboratory tests for recording the subjects' lower limb motions, it seemed logical to measure angular and linear displacements between the TT Pylon housing and shin tube

in the same way. This was the approach chosen by Linden van der et al 2002 who measured angular displacement at a transverse rotation adapter during trans-femoral gait. However, whether such a recording method is also applicable for the current study depends on the accuracy of the ProReflex^{TM} system and the amount of displacements at the TT Pylon.

6.1.2.1.   Considerations for measuring equipment

Optical tracking of slow moving markers within a capture volume of less than 1m^3 allows absolute position measurements to be made with sub-millimetre accuracy (Everaert et al 1999). In turn, Richards 1999 reported on errors well in excess of 1mm during fast motions within a capture volume that significantly exceeded 1m^3. The set-up for the current study required a capture volume of approximately 6m^3 and, as explained in Section 5.2.1.6, the level of accuracy was assumed to be around 2.22mm.

The extent of motion at the TT Pylon is, as described in Section 4.1.5.2, limited to a total of approximately 60° transverse rotation and 13mm longitudinal translation. Tracking reflective markers attached to the adapter is a possible solution for recording these motions, and although they are small in magnitude, the overall amount of displacements the markers may experience would be an accumulation of motion at the adapter and motion of the entire prosthesis. This implies that the recorded measurements would be rather inaccurate, because fluctuations in the system's output become larger with greater marker speed and more changes in position, as shown in Section 5.2.1.1.

The rapid pace at which markers travel and the long distance they cover are parameters that are significantly larger than they would be if purely motion at the adapter and not of the entire prosthesis were measured. Unless the walking speed is slowed down, those parameters will remain large. One method to overcome this problem would be to increase the amount that markers move in response to displacements at the adapter. Although this would have very little impact on the overall magnitude of marker travel, and a negligible effect on the motion capture system's accuracy, it would, however, alter the ratio between the amount that markers move in response to displacements at the adapter and the system's accuracy. Such an altered ratio would consequently lower the error in the recorded measurements.

The way this method could be put into practice is by using extension rods for attaching markers to the adapter. This locates them further away from the COR and increases the distance they travel during transverse rotation due to an increased length of perimeter arc. Depending on the size of extension rods used, a measurement error of 2.22mm might be a lot less than the amount of travel markers undergo, which makes optical tracking systems, in terms of measurement accuracies, a possible solution for recording transverse rotation.

In turn, the amount of marker travel during longitudinal translation will not be affected by varying the lengths of extension rods, which means that the system's error of 2.22mm is approximately 17% of 13mm maximum longitudinal translation. Also, the manufacturer of the ProReflex^{TM} system claimed that the nominal amount of travel can reach between approximately 5-8mm during normal walking, as previously described in Section 4.1.5.4, so that the system's error would increase to approximately 28-44% of longitudinal translation. Using the ProReflex^{TM} system for capturing longitudinal translation at the TT Pylon was therefore ruled out.

Although measurement accuracies for recording transverse rotation could be improved, the method for this to be accomplished by having extra length extension rods attached to the test-prosthesis did not seem a particularly practical solution. An additional constraint is that endoskeletal prosthetic designs leave little space for marker clusters, thus making individual detection difficult. It was therefore considered necessary to find an alternative method, not only for measuring longitudinal translation, but for measuring transverse rotation also.

Other approaches were considered including the possibility of capturing motion by using inertial sensors (Mayagoitia et al 2002), but this was considered inappropriate, because accurately measuring small relative displacements in a moving reference frame with this type of method remains difficult. More recent developments are based on computer vision techniques for extracting useful data from markerless video images of human motion (Cunado et al 2003), but this is not yet a mature field with accuracy remaining a problem. Another method thought of as plausible was the use of two rotary potentiometers for measuring motions at the adapter, but this would have required a mechanism with belts, chains, gears, links or similar means of transmission to convert

linear motions into rotational motions and to decouple the two types of motions, which seemed excessively complex.

6.1.2.2. *Measuring equipment selection*

The chosen design was based on a cam and two linear displacement transducers, as shown in Figure 6.2. The mechanical part of the system comprises a plate cam that is eccentrically mounted around the housing of the TT Pylon. Motion at the adapter is measured by recording the output from the two transducers, which are mounted orthogonal to one another and at the side of the adapter housing. Transverse rotation is measured using one of the displacement transducers with the long axis of its spring-loaded plunger located parallel to the transverse plane and against the eccentric perimeter of the cam. Longitudinal translation is measured using the other displacement transducer with the long axis of its spring-loaded plunger perpendicular to the transverse plane and against the distal, flat face of the cam. This orthogonal arrangement of transducers makes it possible to take decoupled measurements of transverse rotation and longitudinal translation. Either motion therefore only moves the plunger of its respective linear displacement transducer, thus allowing data to be recorded independently.

6.1.2.3. *Cam alignment*

Mounting the distal, flat face of the cam exactly perpendicular to the long axis of the adapter is vital for obtaining accurate measurements. This procedure is made easier by the shape of the TT Pylon housing, which helps in achieving the correct cam alignment. The circular dimensions of the TT Pylon housing expand proximally up to a point after which they decrease again, thus making the housing appear like two cones bonded together by their base.

The cam has four grub screws equidistantly spaced around its proximal body and a proximally expanding, conical cut-out with the same slope as the adapter housing. The dimensions of the cut-out allow the cam to be positioned around the largest diameter of the TT Pylon housing with the grub screws just proximal to it. Tightening them against the TT Pylon housing gives the cam the tendency to travel further proximally until its conical cut-out is jammed against the adapter housing, which ensures that the cam is aligned correctly.

6.1.2.4.   *Transducer selection*

In addition to the requirement for the transducers to be spring-loaded and linear, they also had to be light and small, so that the influence they might have had on the subjects' gait pattern was minimal. Adequate performance characteristics were additional design criteria the transducers needed to have. In turn, they also had to be low in cost to ensure that expenses remained within the remits of the research budget. Both transducers needed to be identical to provide the possibility for inter-changing them, so they could be used for detecting the motion previously measured by the other transducer.

Another crucial selection criterion was for the transducers' spring-loaded plunger to have an adequate ROM. This was governed by the operational characteristics of the adapter, in that the amount of longitudinal translation that takes place during normal walking should be similar to the maximum amount of plunger travel. Maximum longitudinal translation at the TT Pylon is 13mm, as previously described in Section 4.1.5.4, whereby the manufacturer claimed that no more displacement than 5-8mm would take place during normal walking. As 13mm was considered excessively large a displacement and 5-8mm too small, it was decided that the amount of travel to be expected during the gait laboratory tests would be a total of 10mm. This seemed a more realistic figure and it also determined the amount of plunger displacement the transducers should have.

The chosen transducers, referred to as linear position sensors (RS Components, Northamptonshire, UK), are resistance-based and therefore suitable to be used in conjunction with the radio telemetry system MT8, previously described in Section 6.1.1. They have an electrical and mechanical stroke of 10mm and 12.5mm, respectively, which requires an operating force of 2-7.5N. Their mechanical life is supposed to last over the duration of 5×10^6 full cycles, and they have a resistance of 5kΩ and a linearity of ±2%, but no information was available on the displacement of the plunger with respect to off-axis loading.

6.1.2.5.   *Cam geometry selection*

The depth of the cam was set at 20mm, which was directly determined by the estimated maximum longitudinal translation of 10mm plus an additional 10mm depth to allow for the plunger's diameter. That way the plunger of the transducer tracking the cam

perimeter for measuring transverse rotation cannot move beyond the cam's geometrical boundaries. Because the transducers' mechanical stroke of 12.5mm is 0.5mm less than the adapter's 13mm maximum longitudinal translation, accidentally causing full displacement during donning of the prosthesis or while getting accustomed to it would therefore destroy the transducer. To prevent this, a 4g light and 3mm thick aluminium ring was inserted between the internal aspect of the TT Pylon housing and the shin tube, so that longitudinal translations were limited to the estimated maximum of 10mm.

The perimeter geometry of the cam was based on the goal for the relationship between transverse rotation and travel of the respective displacement transducer's plunger to be linear. For this condition to be implemented, the ideal perimeter geometry would have to be an arc of a spiral. The adapter's maximum transverse rotation of 60° or ±30° was considered excessive, whereby a total of 30° or ±15° seemed a more realistic figure. Over this range, the transducer output can have an almost linear response, even if the ideal cam geometry is approximated to an arc of a circle. A cam with a circular geometry can be manufactured very precisely with a lathe. Such a process represents a more cost effective alternative than that of producing an accurately shaped spiral.

An approximation of the cam geometry to the arc of a circle can be derived from the ideal cam geometry, which implies that the shape of the spiral needed to be established first. With the transducers' 10mm maximum electrical stroke and an anticipated maximum of 30° or ±15° transverse rotation, increments of 1mm plunger displacement would be the equivalent of 3° cam rotation.

Although measurements were only to be taken over the estimated range of 30° or ±15°, as the transducers' mechanical stroke is 12.5mm and therefore 2.5mm larger than the electrical stroke, it was possible to increase the perimeter to 36° or ±18° without exceeding the maximum plunger displacement. Similar to preventative measures taken when deciding upon the cam depth, a slightly longer perimeter provides a larger cam surface to allow for the diameter of the plunger. That way, the full cam perimeter can be tracked without the plunger moving beyond the geometrical boundaries of the cam. Also, to prevent accidental damage to the edges of the cam perimeter, its arc was lengthened even further, but without exceeding the maximum radius, as the plunger would otherwise be pushed too far into the housing of its transducer. Despite this arc

Figure 6.1: Cam geometry and dimensions viewed from proximally
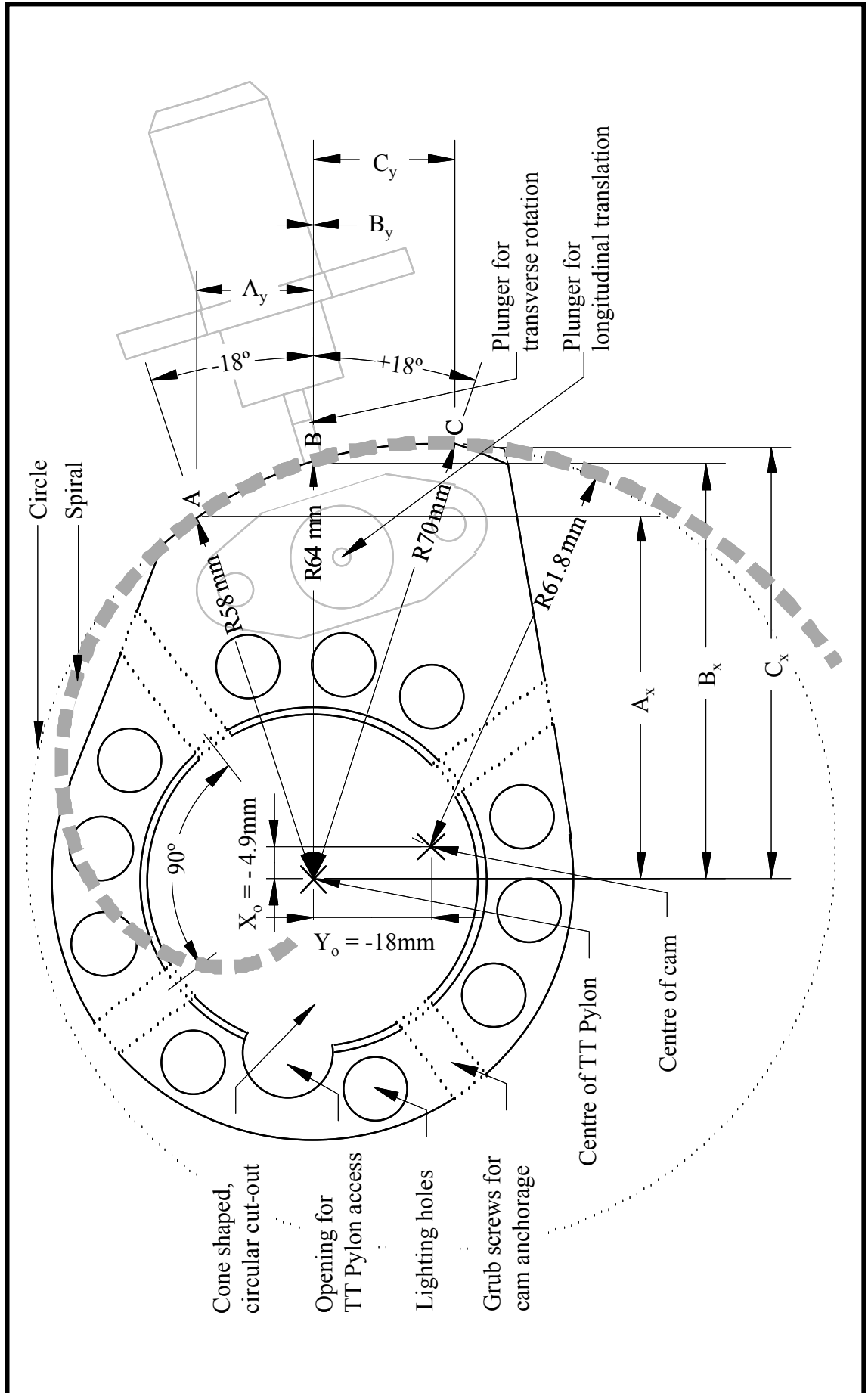
extension being useful for properly operating the cam, the magnitude by which the arc was lengthened was irrelevant for the calculation of the approximated cam geometry.

Taking the ratio of plunger stroke and cam rotation into consideration, the spiral would consequently need to have a geometry that is characterised by an arc with radii, which, from the adapter's neutral position of 0° transverse rotation, change by increments of 1mm every 3°, thus reaching a 6mm extension at +18° and a 6mm shortening at -18°. Having determined the increments of the radii, it was necessary to find their overall length. The shortest radius of the perimeter was set at 58mm, as it not only had to be larger than the radius of the cam's largest, cone shaped, circular cut-out of 26.6mm to prevent it from interfering with the boundaries of the adapter housing, it also needed to give the cam enough thickness for installation around the adapter. Knowing the length of the shortest perimeter radius and therefore the location of three points A, B and C at -18, 0 and +18° with radii of 58, 64 and 70mm from the centre of the adapter, it was possible to determine a circle that coincides with those three points, as depicted in Figure 6.1.

Equations 6.1: Calculation of dimension and location of circle

$$R_A{}^2 = (X_o + A_x)^2 + (Y_o + A_y)^2$$

$$= (X_o + \cos{-18} \cdot 58\text{mm})^2 + (Y_o + \sin{-18} \cdot 58\text{mm})^2$$

$$R_B{}^2 = (X_o + B_x)^2 + (Y_o + B_y)^2$$

$$= (X_o + \cos 0 \cdot 64\text{mm})^2 + (Y_o + \sin 0 \cdot 64\text{mm})^2$$

$$R_C{}^2 = (X_o + C_x)^2 + (Y_o + C_y)^2$$

$$= (X_o + \cos 18 \cdot 70\text{mm})^2 + (Y_o + \sin 18 \cdot 70\text{mm})^2$$

Definitions:

$A_x \ldots C_y$	-	offset between cam centre and points A, B, C
$R_A \ldots R_C$	-	radius from the cam centre to points A, B, C
X_o, Y_o	-	offset between cam centre and centre of circle

The calculation of the cam geometry, which is based on a spiral perimeter that coincides with a circle in three points A, B and C can be undertaken by using Equations 6.1. This calculation was aimed at determining the radius of the circle and the distance of its centre from the centre of the adapter. The actual computations were undertaken in Mathcad 2000 Professional (MathSoft Engineering & Education Inc, Cambridge Massachusetts, USA).

6.1.2.6. *Cam specifications*

Mountings were manufactured and attached to the TT Pylon shin tube via a 10mm thick clamp for rigidly securing both transducers while they are bolted into their corresponding position. The cam and mountings were made out of aluminium, so that the design is hardwearing yet low in weight. Lightening holes were drilled wherever possible for additional weight reductions. The combined weight of the cam, transducer mountings and the two transducers was 406g. Figure 6.2 illustrates the entire mechanism mounted into position around the TT Pylon.

Figure 6.2: TT Pylon with cam, transducers and transducer mountings
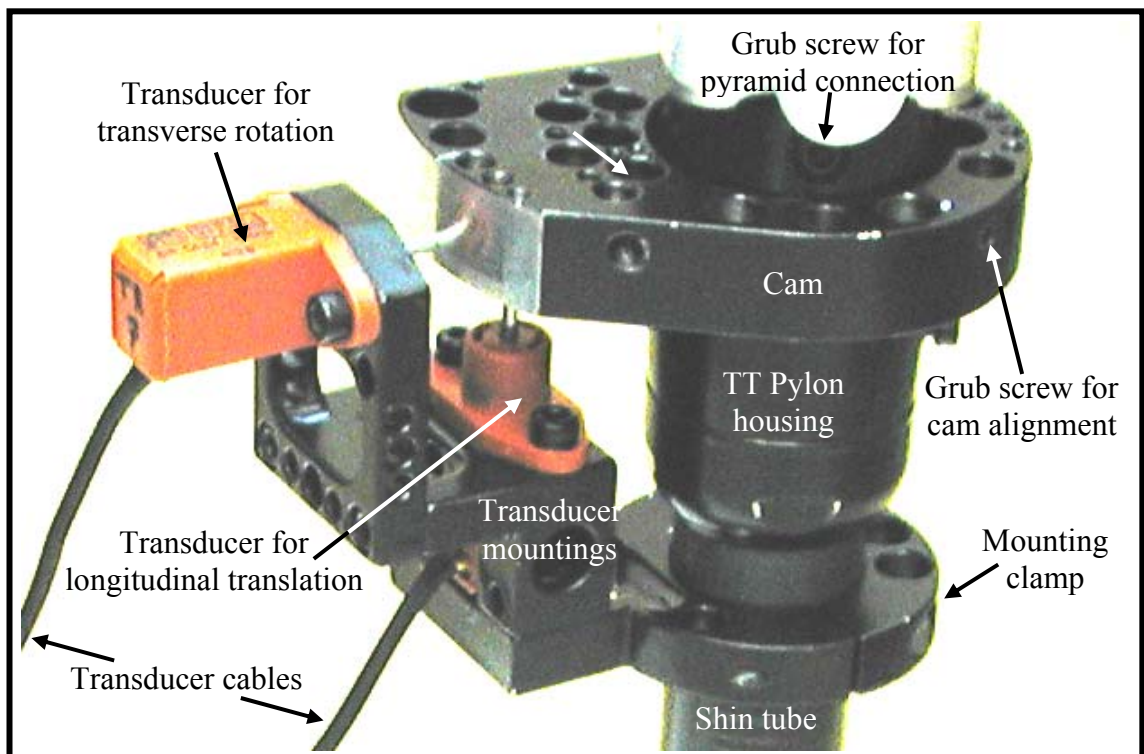
Each transducer's plunger had a stainless steel, domed rivet glued to its end to prevent the cam surfaces from getting scored. Friction between the rivet and the cam was

reduced by attaching a piece of lubricated smooth tape to the relevant cam surfaces, which also minimised off-axis loading.

As the cam and transducer mountings were made out of aluminium, they posed a risk of being mistaken for a marker due to their shiny surfaces that may reflect infra red beams back to the cameras. To reduce the chances for this to happen, all the surfaces were sprayed with matt, black paint, except for the cam perimeter and the distal face of the cam, because a layer of paint may affect the sliding action of the two displacement transducers' spring-loaded plunger. However, the fact that these two surfaces were not painted did not cause any problems with regard to infra red beams being reflected back to the cameras during the actual recordings.

6.1.2.7.   *Transducer alignment*

The transducer measuring transverse rotation and the other measuring longitudinal translation was aligned in such a way that the long axis of its plunger was perpendicular to the tangent of the cam's perimeter and perpendicular to the cam's distal, flat face, respectively. In addition to this, further alignment procedures were necessary to ensure that the full electrical stroke falls within the entire range of cam displacements.

The transducer measuring transverse rotation was adjusted by manually turning the slightly slackened mounting clamp around the shin tube until the centre of the respective plunger lined up with a mark that indicated the middle of the cam perimeter. Once in the correct position, it was necessary to adjust the distance between this transducer and the cam, so that the plunger is pushed exactly half way inward with respect to the electrical stroke. This was undertaken by adding shims between the transducer and its mounting until the transducer's resistance, measured with an Ohmmeter (0-40MΩ maximum range, ±0.9% accuracy), falls exactly mid-way between the top and bottom electrical stroke range.

The transducer measuring longitudinal translation was adjusted by gradually pushing the slightly slackened mounting clamp proximally until the respective plunger was moved far enough inward to trigger a change in the transducer's resistance, which indicated that the plunger was positioned where the range of the electrical stroke started. An additional clamp, which is illustrated in Figure 6.3, was temporarily fastened around the shin tube. This represented the tool for creating the required push. It has three

adjuster bolts that can be tightened against the distal aspect of the transducer mountings, thus moving them proximally.

Figure 6.3:   Clamp for adjusting the longitudinal translation transducer
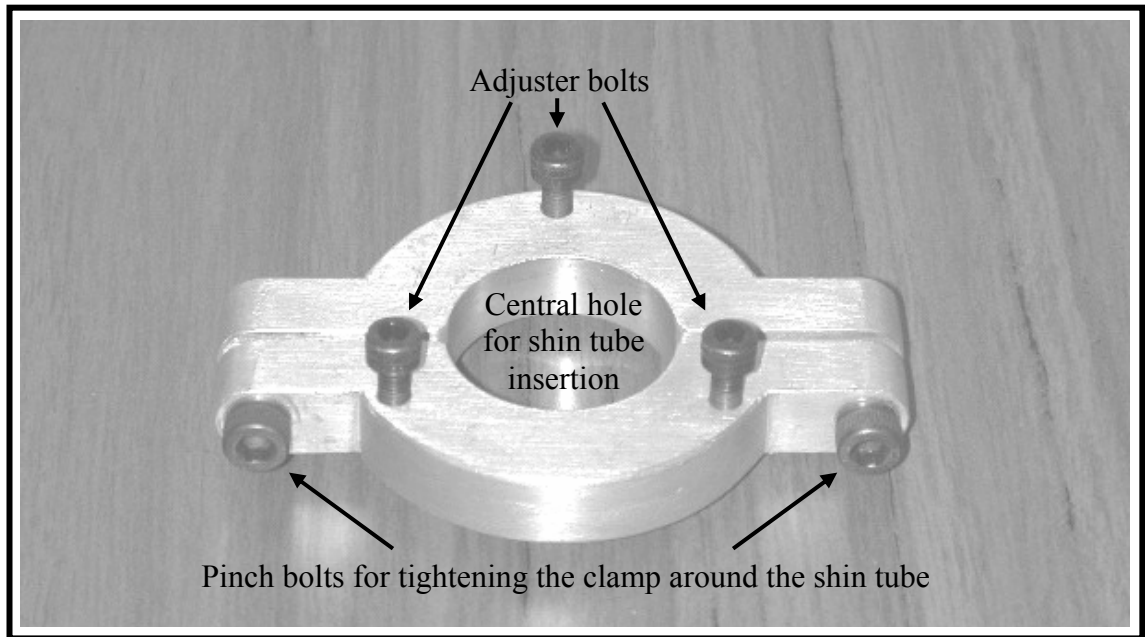
The position of each transducer may be affected by the other one's alignment procedure, so that these processes needed repeating a few times until the transducers' optimum locations were found. As the prosthetic foot was already anteriorly orientated, it was considered the least protrusive arrangement to align the entire cam system in such a way that it pointed anteriorly also.

6.1.3.   Equipment for measuring forces inside the socket

Problems associated with residual limb-socket interface forces have triggered a world-wide interest for research in this field, and various approaches were taken to quantify the magnitude and distribution of forces during amputee gait. However, prior to exploring these aspects, it was decided to gain an insight into critical levels of forces that underlying soft tissues can tolerate before the blood ceases circulating.

6.1.3.1.   *Force tolerances in tissues*

Excessive pressures and shear forces acting on the skin can cause discomfort and lead to a reduction in blood flow, whereby a combination of both pressures and shear forces can lead to capillary occlusion (Bennett et al 1979). The resultant lack of blood supply

reduces the oxygen level in tissues, thus causing necrosis if this condition is sustained for prolonged periods of time.

Amputations are often the result of underlying pathologies, like arterial hypertension and diabetes, or induced by external influences, like tobacco intoxication (Casillas et al 1993). The reason why these conditions can lead to amputations is, because of side effects including reduced blood supply. To promote healing of the residual limb after amputation, the transcutaneous oxygen tension has to be above approximately 2kPa, although this is not sufficient for prosthetic fitting where a pressure of at least approximately 5.3kPa for transcutaneous oxygen tension has to be reached (Casillas et al 1993). These figures obviously refer to the internal pressure within blood vessels, and it must be emphasised that external influences triggering capillary occlusion are not just dependent on pressure, but on the ratio of pressures and shear forces (Bennett et al 1979).

During an investigation into the effects a prosthetic socket has on the residual limb, the dual effect of pressure and shear forces therefore has to be decoupled, so that forces acting perpendicular and non-perpendicular onto the skin can be analysed separately. However, before deciding upon a method for measuring these parameters as part of the current investigation, it may prove sensible to search the literature for reports on previous research findings in this field. Mak et al 1996 and Silver-Thorn et al 1996 conducted a review of literature based on residual limb-socket interface measurements, and some of the most relevant ones are summarised below.

6.1.3.2. *Pressure measurements*

The majority of studies seem to concentrate on measuring the influence of forces acting perpendicular to the skin only. Some investigators used force sensing resistors (FSRs) for taking measurements, and because they knew the dimensions of the sensing area, it was possible for them to calculate the pressure from the ratio between force and area. Although in those instances it was forces that were measured, these studies as well as the majority of studies that were conducted with other types of sensing devices reported on pressures instead of forces acting on the residual limb, which was presumably done for making it easier to relate those findings to blood flow and capillary occlusion.

Sonck et al 1970 measured residual limb-socket interface pressures at the patellar tendon, the anterior-distal aspect of the tibia and the medial and lateral tibial condyle in three different types of PTB prostheses, but without specifying the equipment used for taking the readings. They found that the peak pressures were lowest for the prosthesis with a gel liner reaching 483kPa, highest for the prosthesis without insert reaching 827kPa and in between for the prosthesis with a Kemblo insert. Meier et al 1973 used dye-impregnated socks as a pressure indicator and measured pressures in excess of 379kPa in PTB sockets without insert and up to 310kPa in those with a Kemblo insert, but the landmarks exposed to those pressures were not identified.

Engsberg et al 1992 measured pressures with a Tekscan system that consisted of fairly large sensing mats. Peak pressures reached up to 90kPa and low pressures up to 60kPa. The reason why these measurements were so low seemed to be linked to the size of sensors these investigators used, as the pressure over the entire sensing area was averaged. Simpson & Convery 1997 established pressures of 190-290kPa at the patellar tendon and the anterior-distal aspect of the tibia. They used FSRs for taking the measurements, but specifications of the capturing equipment were not given. Convery & Buis 1998 also used FSRs, which were made by Tekscan and contained three hundred and fifty sensor cells for measuring interface pressures in a trans-tibial prosthesis at the anterior, posterior, medial and lateral aspect of a PTB socket. Pressures at the patellar tendon, proximal popliteal area, posterior-medial flare and fibula head were found in excess of 100kPa with a maximum output of 417kPa obtained from only one load cell at the patellar tendon.

Beil et al 2002 investigated the pressures exerted onto the residual limb of nine trans-tibial amputees. Measurements were taken with Interlink Electronics force sensing resistors that were located on five unspecified landmarks. These investigators used vacuum assisted sockets and they found peak pressures of 83.5kPa. Shem et al 1998 studied residual limb-socket interface pressures in thirteen trans-tibial amputees using six Rincoe SFS strips located at the anterior, posterior, anterior-medial, anterior-lateral, posterior-medial and posterior-lateral aspects of the socket. In prostheses with side steels and a thigh corset, the average pressure reached 13.6kPa and measurements without it revealed an average pressure of 17.2kPa. Zhang & Roberts 2000 used finite element analysis for establishing the pressures within a PTB socket, which were predicted to reach up to 226kPa over the patellar tendon. Also based on finite element

analysis, a study by Silver-Thorn et al 1996 reported on various pressures, which were related to a number of variables that those investigators incorporated in their computation to reflect typical characteristics for different residual limb-socket interface conditions.

6.1.3.3.   *Shear force measurements*

In addition to pressure measurements, other types of studies were undertaken to establish the amount of shear forces acting on the residual limb. However, the overall amount of research output is less than it is in fields related to measuring perpendicular forces. The reason for this may be because the required sensors need a far more complex design structure for detecting non-perpendicular forces with multi-directional orientations.

Williams et al 1992 designed a tri-axial transducer, which was based on a diaphragm strain gauge that functions in a similar fashion as FSRs for measuring perpendicular forces. An additional design aspect involved two semiconductor field coils that operate in conjunction with a magnet for measuring shear stresses. The magnet was located over the semiconductors and it was secured in this position with an elastic element. Non-perpendicular forces would move the magnet, which alters the resistance of the semiconductors. Taking into consideration that the amount of movement is proportional to the counterforce from the elastic element, the change in resistance of the semiconductors would therefore be an indicator of the amount of shear stresses exerted on the transducer. Sanders & Daly 1993 reported on a transducer design that was, like the one by Williams et al 1992, also based on a diaphragm strain gauge for measuring perpendicular forces. However, the method for measuring shear forces differed in that the transducer was relying on two strain gauges and a Wheatstone bridge, which produced outputs proportional to the shear forces acting on the transducer. In a later study, Sanders 1995 investigated various techniques that were used in the past for measuring shear stresses, but some of these were, due to the bulkier electronic components available in those days, probably less applicable than newer technology.

6.1.3.4.   *Considerations for measurements*

In the studies reporting on pressures, the measuring sites and techniques, as well as socket types, varied between studies, but the findings were still considered useful as a

rough guide for providing an estimate into the amount of forces or pressures that can be expected. However, it is important to keep in mind that these parameters are dependent on a number of factors including, amongst others, the measuring sites within the socket, the contouring of the socket, the quality of underlying tissues and the activity level of the amputee. As identified in the literature, pressures within these variables can reach up to 828kPa. Although these values greatly exceed the transcutaneous oxygen tension required for healing, forces from the socket are applied intermittently during the gait cycle, allowing blood briefly to return back into the capillaries, thus causing the oxygen levels to increase again.

A lot of commercially available force or pressure sensors are very thin. This is particularly the case for FSRs, which quite often only consist of a thin strip of material with less than 1mm thickness. Such dimensions allow the transducers to easily slide between the residual limb and socket or Iceross liner and socket, so that no additional socket modifications are required. It is also easy with FSRs to locate them on the desired landmark, because they can be taped into their required position on the residual limb prior to donning the socket. Instead of using FSRs with up to fifty millimetre width or more that may crease as they are being forced into concavities inside the socket, it may be better to choose a larger number of individual, narrower sensors to minimise creasing.

Although shear forces have a major influence on the reduction of blood flow, an investigation of existing techniques for measuring such a parameter revealed that the required transducers would be far more intricate than force or pressure transducers, which may also make them more susceptible to breaking down. Transducers like, for instance, the ones previously described by Williams et al 1992 and Sanders & Daly 1993 are, compared to FSRs, rather bulky and need to be mounted on the external aspect of the socket, which implies that the socket itself needs adapting to provide holes through which the transducers can protrude for establishing contact with the skin or Iceross liner. Mounting those transducers externally makes it difficult to locate them flush with the interior of the socket. This is particularly so if the socket contours are curved, which the tri-axial transducers' rigid sensing surfaces cannot adapt to, unlike flexible FSRs. This implies, as illustrated in Figure 6.4, that part of the sensing surface either protrudes too far into the interior of the socket, thus increasing force or pressure measurements or it retracts too far into the exterior of the socket, thus reducing skin

contact and therefore shear forces on the transducer. Also, sockets that are created from a pressure casting technique and to be worn in conjunction with an Iceross liner appear, as explained in Section 2.5.2.4, rather round in cross-section. This makes it difficult to identify individual anatomic landmarks from the interior of the socket for locating the transducers accurately.

Figure 6.4:   Problems associated with mounting of tri-axial transducers

Tri-axial transducer

Tri-axial transducer

Protrusion of sensing surface
into the interior of the socket

Retraction of sensing surface
into the exterior of the socket

Tri-axial transducer

Tri-axial transducer

Remark:
The geometrical representation of the interior part of the socket (∾) is only an example for a confined environment and is not supposed to represent a typical socket shape.

Despite the possibility that both forces or pressures and shear stresses may provide a better insight into motion at the residual limb-socket interface than only pressures, the practical implications for measuring shear stresses seemed too complex. Therefore, the likelihood is high that pressure measurements would be less accurate with tri-axial transducers or similar devices than they would be with the type of FSRs described previously. It was worth investigating the possibility of incorporating those measurements, but a logical deselection process lead to the conclusion that, with regard to residual limb-socket interface measurements, only perpendicular forces or pressures will be recorded.

6.1.3.5.   *Sensor selection*

As the research budget was limited, the sensors to be used for this investigation had to be inexpensive yet accurate and reliable. Initial investigations revealed a FSR available from Biometrics Ltd, Ladysmith Virginia, USA, a company specialised in equipment for motion analysis. However, the sensor's specifications did not seem to fall within the remits of the stipulated selection criteria. This type of device was therefore considered inappropriate for the current study.

Further investigations revealed a fairly recently developed type of FSR called FlexiForce® sensor (Tekscan, Boston Massachusetts, USA), which is depicted in Figure 6.5. Distributed amongst a wide range of customers, this sensor is particularly attractive for the current study due to its low cost and suitable specifications. Made out of two layers of thin polyester film with an additional layer of pressure sensitive ink sandwiched in-between, the sensor is a long, flat strip with a round sensing area of 9.53mm diameter at one end and a male three pin standard Berg connector at the other end. Thin silver tracks along the border of the sensor conduct the signal from the sensing area to the connector, whereby only the outer two of the three pins are occupied. One of the sensor's main features are it's dimensional properties, as it is only 0.127mm thick and 14mm wide, which makes it virtually ideal for wearing it inside the socket. Also, with an overall length of 203mm, the connector plug can remain outside the socket to prevent it from digging into the residual limb tissues, thereby avoiding injury to the subjects.

Figure 6.5:   Overall dimensions of FlexiForce sensor
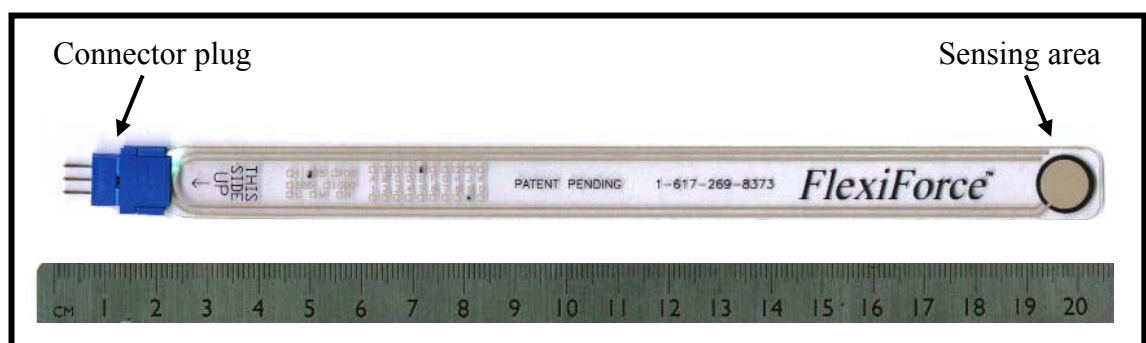
Three different types of sensors are available for measuring forces of up to 4.4N, 111N and 444N, which is the equivalent in pressure measurements of approximately 62kPa, 1556kPa and 6223kPa, as calculated over the aforementioned diameter of the sensing

area. Taking into consideration the in-socket pressure measurements described in Section 6.1.3.2, the sensor chosen for the current investigation was that designed for measuring intermediate magnitudes of pressures of up to 111N.

6.1.3.6.   Anatomic landmark selection

The radio telemetry system was the chosen equipment for transferring information from the FlexiForce® sensors to the computer used for data storage. Two of the transmitter's eight channels were already occupied by the linear displacement transducers for measuring motions at the TT Pylon. This therefore left six channels spare for six FlexiForce® sensors, which needed to be allocated to specific anatomic landmarks on the residual limb.

The thickness of residual limb tissues over bone prominences is minimal. These areas represent anatomic landmarks prone to capillary occlusion. They are therefore of interest for measuring the amount of forces exerted onto them. The three main spots are the fibula head, the tibial tuberosity and the anterior-distal aspect of the tibia where the remaining part of the bone was removed.

In turn, anatomic landmarks where the underlying bone is deeply embedded in the residual limb are less prone to capillary occlusion, as the tissues should experience greater freedom for moving away from the source of pressures. However, this is contradictory to the principles governed by hydrostatic conditions within total contact sockets, as elaborated on in Section 2.5.2.4, which implies that the forces exerted onto the residual limb should be fairly uniform. It was therefore decided to also measure the pressures in those soft tissue areas in order to determine whether these are exposed to lesser magnitudes of pressures than bone prominences are. Having already allocated three out of the six FlexiForce® sensors, this meant that another three sensors were left for allocation to the same number of landmarks. These were decided to be the medial and lateral tibial flare and the calf.

6.1.4.   <u>Miscellaneous electronic hardware</u>

6.1.4.1.   Connections to the A/D board

The sixty-four channel A/D board described in Section 5.2.1.7, was a fairly recent addition to the gait laboratory equipment within the department at the University of Salford

where the current investigation was undertaken. The board's sixty-four channels were divided into eight groups of eight channels each. The set-up for linking other data capturing facilities, including the force plates and the radio telemetry unit, to the A/D board required individual and customised connections. A specially designed and manufactured distributor box was used for conveying the signals from those pieces of equipment to the box that contained the A/D board.

Figure 6.6:   Distributor box and analogue board housing
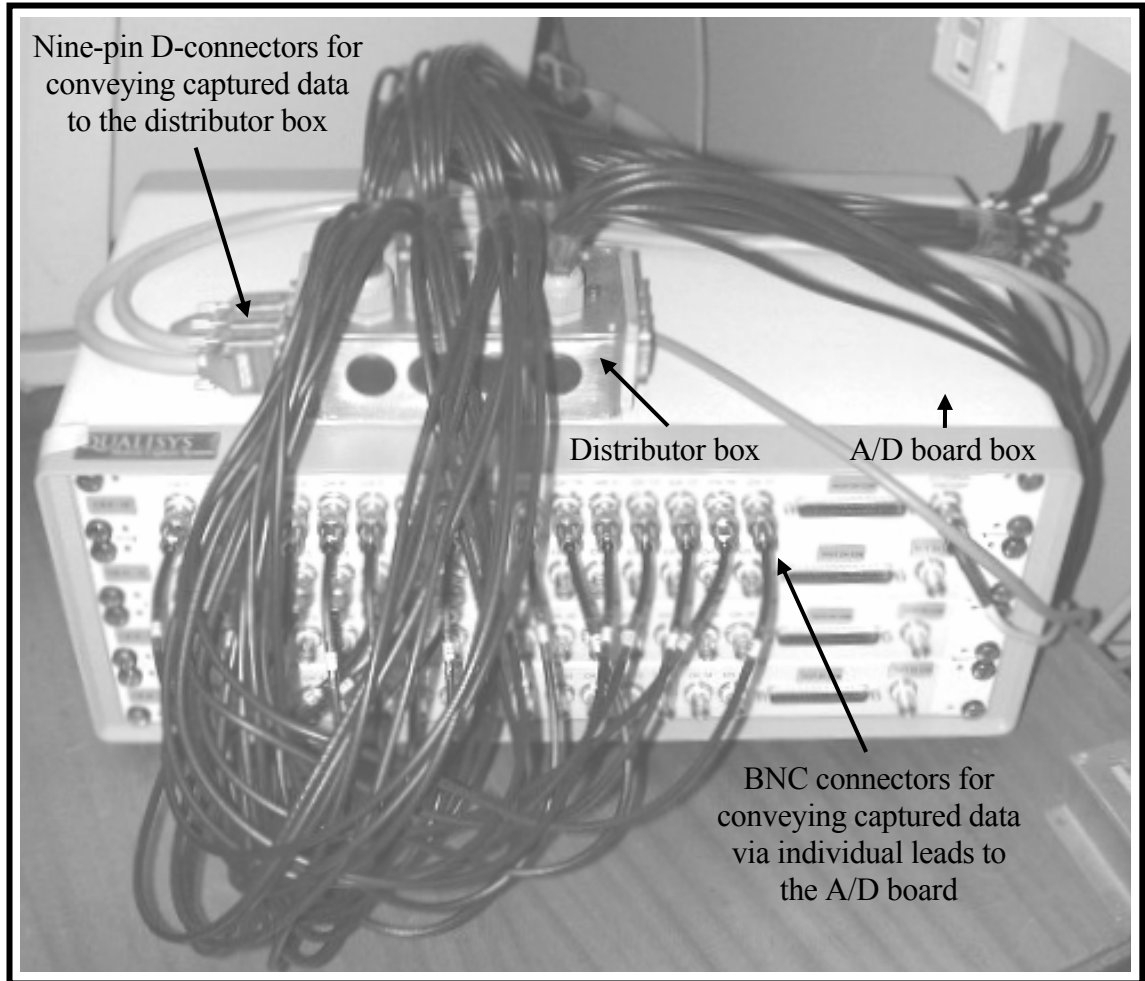
The incoming signals from each of the eight groups of channels entered the distributor box via a nine-pin D-connector (RS Components, Northamptonshire, UK). All the required D-connectors were secured by bolting them into the housing of the distributor box to prevent accidental loss of conductivity. From there, each group's outgoing signals exited the distributor box via cables that were rigidly secured into the housing of the distributor box with grommets. The other end of every exiting cable had a Bayonet Neill Concelman (BNC) connector for plugging it into the housing of the A/D board. All the components, including the distributor box, cables and connectors, were shielded to prevent the signals

from being distorted by interference. Both the distributor box and the housing of the A/D board are illustrated in Figure 6.6.

6.1.4.2.   Connections to the MT8 transmitter

It was decided, as elaborated on in Section 6.1.2.4 and Section 6.1.3.6, for the radio telemetry system MT8 to be the chosen analogue voltage data retrieval unit for conveying information from the two linear displacement transducers and the six force sensors to the computer that controls the ProReflex^{TM} system. Appropriate connections were therefore required to link the transducers and sensors from their location at prosthesis level to the MT8 transmitter around the subjects' waist.

Futuba Servo connectors (Maplin Electronics, Barnsley, UK) were used to extend individual leads from the transducers' flying wires and from the sensors' male three-pin standard Berg connectors into a socket-mounted junction box. Using this kind of connector rather than permanently bonded leads allowed the subjects to don their test-prosthesis without having to take care of additional wiring, which could be set up once the prosthesis was in place. From the junction box, all the signals were conducted proximally via only one cable to reduce the total amount of wiring and the likelihood for the reflective markers to be obstructed from the cameras' view. The junction box, which was made out of plastic for weight minimisation and simply taped to the socket, therefore not only served as a distributor to feed individual leads into one cable, it also took up any strain on that cable to prevent the Futuba Servo connectors from getting detached from the transducers and sensors.

The proximally extending cable was just long enough to reach the waist level. Any possible spare length could be wound around the MT8 transmitter's adjustable fabric belt to prevent markers from being knocked off by excessive slackness and dangling of the cable. At its proximal end, the cable entered another junction box that was attached to the MT8 transmitter with a velcro strap. Split back up into eight leads, the signals from each displacement transducer and force sensor were then individually fed into the MT8 transmitter, illustrated in Figure 6.7, via the four-pin Lemo^{TM} "OB" series plug (RS Components, Northamptonshire, UK), described in Section 6.1.1.2. All the leads and cables that entered or exited the socket-mounted and MT8-mounted junction box were permanently secured in place with grommets, because it was not necessary for any of them to be removed.

Figure 6.7:   MT8 transmitter with junction box and associated cables
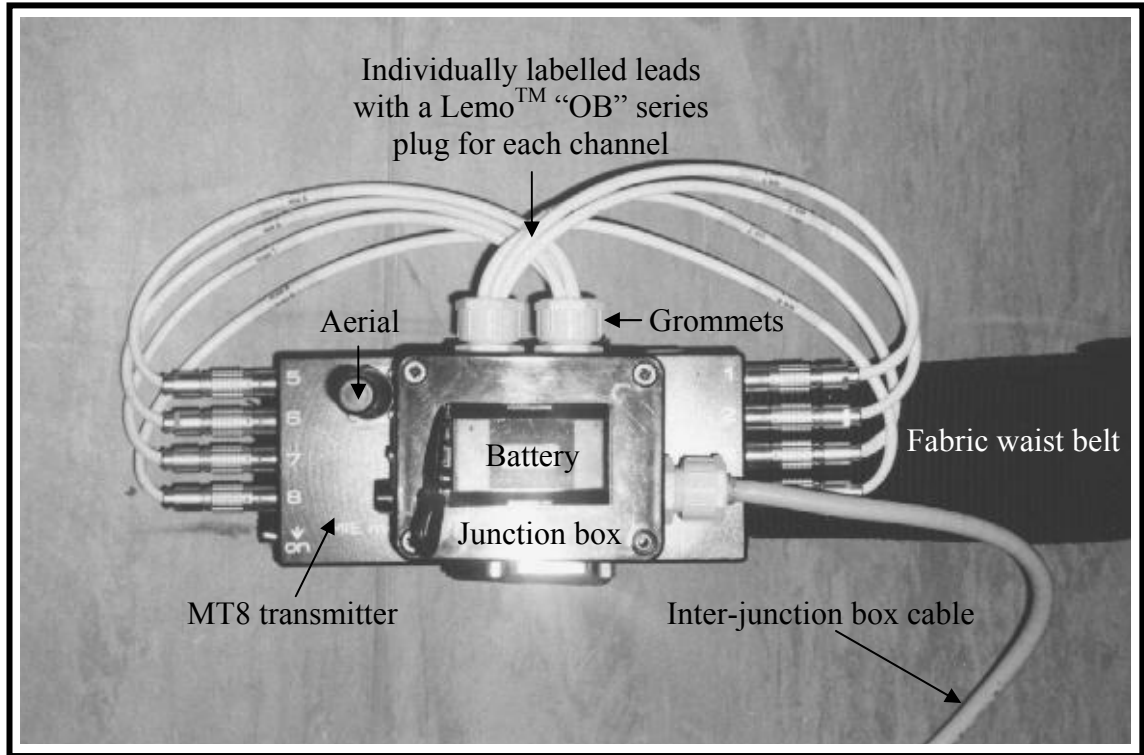
6.1.4.3.   *Electronics for the displacement transducers*

The displacement transducers were, as mentioned in Section 6.1.2.4, resistance-based and therefore classified as potentiometers. This made the connection between their internal slider with its opposing resistive surface and the radio telemetry system straightforward.

All of the MT8 transmitter's eight channels were configured in the same fashion with only three of each Lemo^{TM} "OB" series plug's four pins being occupied. One of them supplied a positive potential, another provided a connection to ground and the third one received the output signal. A flow of current was triggered by connecting one end of a transducer's internal resistive surface to the transmitter's positive potential and the other to ground. The slider then divided the potential and fed one part of it back to the transmitter thus creating the output signal. This output signal was proportional to the position of the slider relative to its opposing resistive surface, which, in turn, depended on the transducer's amount of plunger displacement.

6.1.4.4.   *Electronics for the force sensors*

Unlike the method used for connecting the displacement transducers to the radio telemetry system, the connection for the FlexiForce$^{®}$ sensors was less straightforward,

because each sensor required an electronic circuit that was based on an operational amplifier for signal processing and a variable resistor to control the gain of the output.

The circuit diagram that the manufacturer of the force sensors designed was a useful guide, but the specifications were not quite appropriate for the current circumstances and needed to be adapted to suit the electronics of the MT8 transmitter. Figure 6.8 illustrates the altered circuit diagram with all the necessary components and wiring for measuring one FlexiForce® sensor's output. The letters and numbers indicate the locations of component contacts.

Figure 6.8: Circuit diagram for one FlexiForce sensor
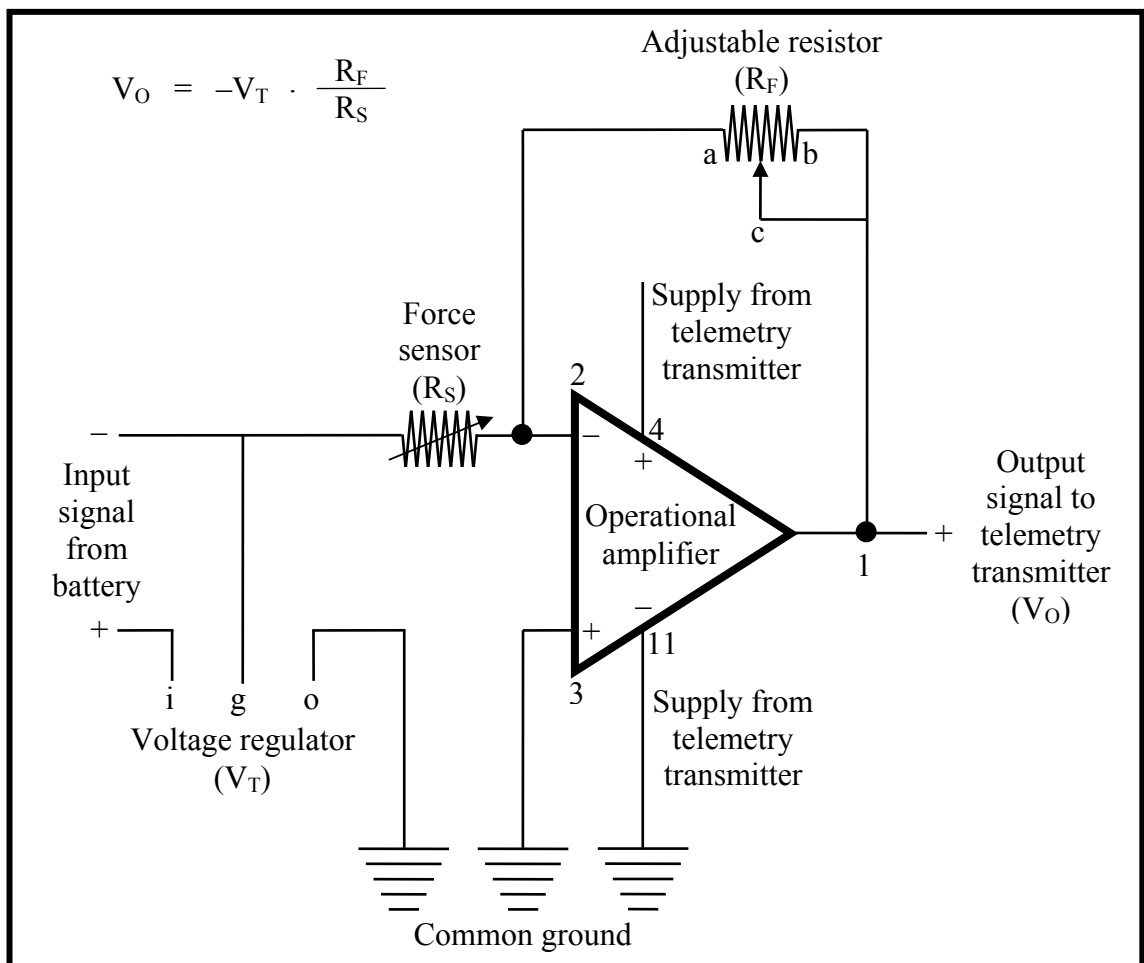
The next step was to compact the distribution of components, depicted in Figure 6.8, by creating a layout that accommodates the components and wiring for all six force sensors, as well as the wiring for the displacement transducers inside the MT8-mounted junction box. Instead of using individual leads it was considered a neater solution to use a strip board. This is a prefabricated, printed circuit board (PCB) with rows of copper strips and a matrix of equidistantly spaced holes where the required components can be soldered into,

for combining the entire electronic set-up, as illustrated in Figure 6.9. The letters and numbers previously used in Figure 6.8 to indicate the locations of component contacts correspond with the letters and numbers depicted in Figure 6.9. All of these electronic components were installed into the MT8-mounted junction box rather than the socket-mounted one to minimise the weight of the prosthesis. The power from the telemetry unit drove each sensor's operational amplifier, whereby a 9V PP3 battery provided additional power for the input signal. Secured in a clamp on top of the MT8-mounted junction box, the battery was easily accessible for a quick exchange with a fully charged one. An LED indicated whether the power switch on the side of the junction box was on or off, to avoid the battery from getting drained while the system was not being operated.

The chosen variable resistors were 22-turn Cermet Preset type trimmers (Maplin Electronics, Barnsley, UK), which are adjustable within a range of 0-1MΩ. Setting them to their required resistance was a process for which the junction box needed opening up, so that a screw driver could be inserted in order to turn the resistor's adjuster. The optimum setting was established empirically prior to each subject's gait laboratory tests. Having located each sensor in its respective position on the residual limb, the subjects were asked to walk, so that output readings could be checked. The threshold from the force sensors was, due to the operational amplifiers' functional characteristics, only approximately 4.4V and not the full 5V that the telemetry transmitter supplied. The aim was to adjust the resistors in such a way that each sensor produced a satisfactory signal with a maximum output just below their threshold of approximately 4.4V. That way the measurements at the top end of the scale would not flatten out and neither would they become too small to be interpretable.

It was considered useful to establish the actual value of each variable resistor, so that a record was kept, from which the same set-up could be recreated if necessary. This required all the sensors, transducers and external leads to be labelled appropriately. Unlike adjusting the resistors, measuring their settings was easier and could be undertaken from outside of the junction box. Integrated into the exterior of the junction box's housing was a fifteen-pin D-connector (RS Components, Northamptonshire, UK), which was connected to the soldered-in contacts of the variable resistors. That way, an Ohmmeter could simply be plugged into each resistor's corresponding pair of known pins at the D-connector in order to measure its resistance.

Figure 6.9:   Components for FlexiForce sensors and transducers
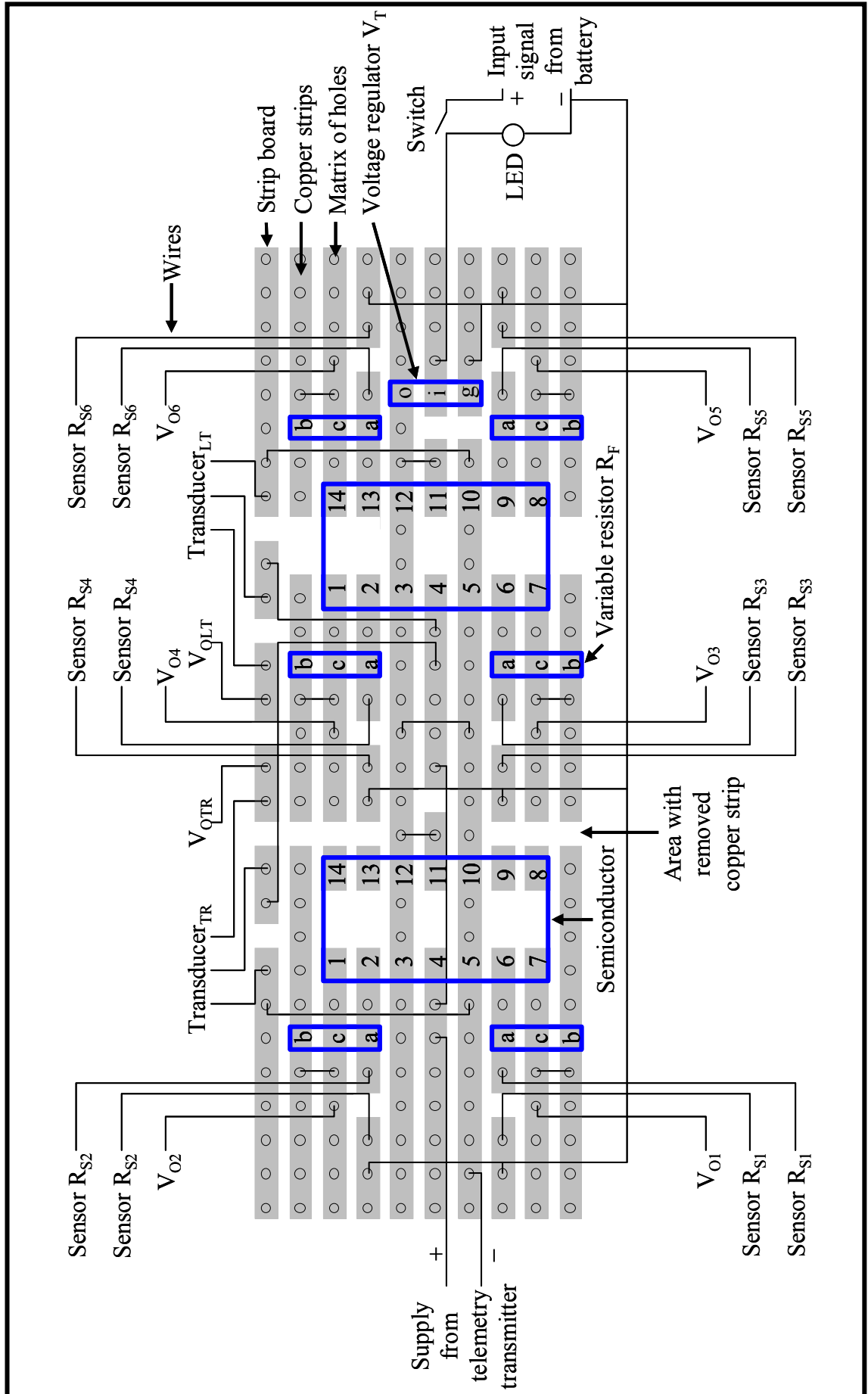
All the wiring and connections took up a lot of the junction box's internal volume, as depicted in Figure 6.10. Instead of using even more individual components than already accommodated for, it was considered less space consuming to install just two semiconductors with four operational amplifiers each rather than six individual semiconductors. Force sensors R_{S1-4} were connected to one of the semiconductors and force sensors R_{S5-6} to the other, thus leaving two operational amplifiers unused. Both semiconductors were designed to have all operational amplifiers powered by the same supply source. They were of type LM324N (Maplin Electronics, Barnsley, UK) with 1MHz unity gain bandwidth, 120dB channel separation, virtually no cross-over and an operating voltage between +3V and +32V.

Figure 6.10: Electronic hardware inside the MT8-mounted junction box
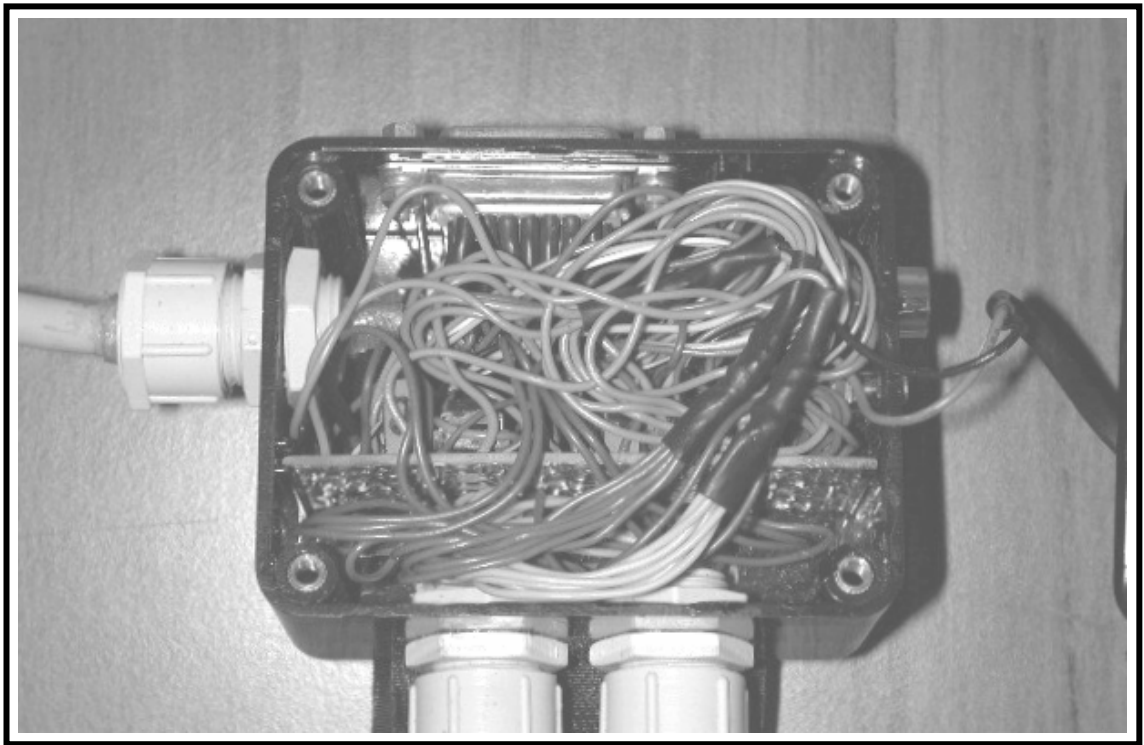
Minor output fluctuations from the telemetry transmitter were not considered to have a noticeable influence on the performance of the operational amplifiers, as these were designed to cope with a range of operating voltages. However, a high draw of current can trigger voltage fluctuations in the output of the battery, and this might affect the readings from all six force sensors. The problem was solved by stabilising the battery's potential with a voltage regulator (RS Components, Northamptonshire, UK), which had a maximum output tolerance of ±2%.

6.2.   Assessment of other capturing equipment

6.2.1.   Assessment of the radio telemetry system

The main issue that was considered relevant regarding the performance characteristics of the radio telemetry system was how prone the unit was to cross-talk between channels. To establish this, both displacement transducers and all six force sensors were connected to the transmitter via the necessary electronics, so that tests could be conducted with all sensing devices in situ.

Quantifying the magnitude of cross-talk between channels was difficult, as this depended on a number of factors. It was observed that cross-talk increased with larger amounts of sensing devices from which a change in output was being produced, whereby an increased size of output signal and a quicker rate of change also seemed to generate more cross-talk. Impact loading would therefore be one of the worst scenarios, as it triggers maximum output at the force sensors and displacement transducers in a very short period of time.

The radio telemetry system was tested for cross-talk by pushing onto the force sensors and by moving the displacement transducers' plunger inward. Once the output signals reached their maximum, it was important to maintain the push for at least 2s, so that the signals, in the event of cross-talk, could stabilise again, before the pressure was released again. This process was undertaken three times to generate cross-talk by operating different amounts and combinations of sensing devices. The first push was applied onto force sensors S_{1-5}, the second onto sensors S_{1-5} as well as both displacement transducers and the third onto force sensor S_6 only. Simultaneous force applications were possible by stacking sensors S_{1-5} and both transducers together and securing each group of sensing devices with tape.

A reflective marker needed to be placed within sight of the cameras, as the ProReflex^{TM} system needed to register at least one marker in order to make a capture process valid. Recordings were taken at 100Hz over the duration of 15s. The results from this capture are illustrated in Figure 6.11. The data contained some degree of noise and the graphs representing the output signals from each sensor are fairly close together. This is why only every fifteenth recording frame was used, so that the interval between one frame and the next was prolonged from 0.01s to 0.15s for an improved clarity of the display.

Also, the chart was reduced at levels where the output signals rapidly increased or decreased, so that levels where measurements occurred in response to maximum force or no force could be magnified, as focusing on these was more relevant for the assessment of inter-channel cross-talk.

Figure 6.11:   Operation of all eight sensing devices triggered MT8 cross-talk
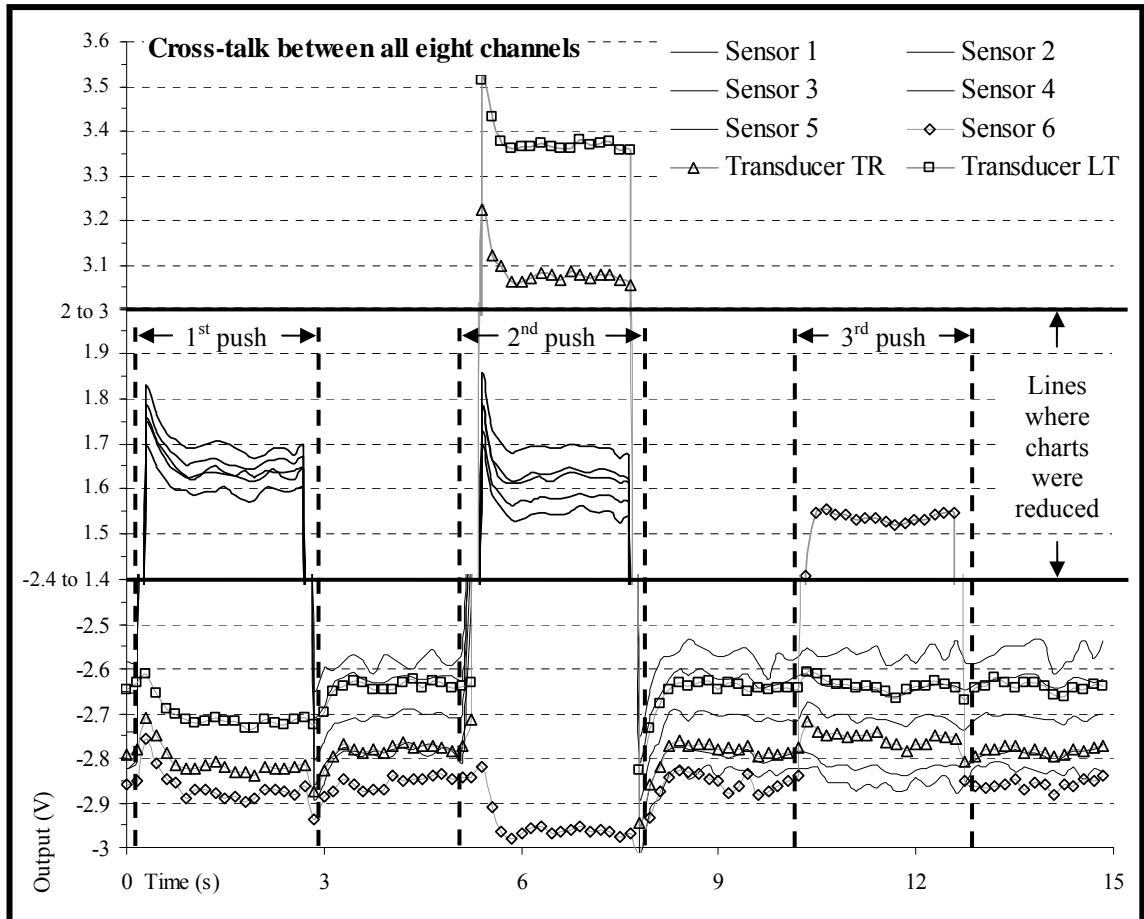
6.2.1.1.   *Analysis of the radio telemetry system*

Applying maximum forces by pushing hard onto sensors S_{1-5} drastically increased the output signals until they reached a peak. Immediately after that they lowered slightly, which took approximately less than 0.5s, until the signals settled at a certain level. The drop in output voltages was approximately 0.12V. This was similar when these five sensors and the two displacement transducers were operated simultaneously. In turn, operating force sensor S_6 on its own triggered a drop in voltage of only approximately 0.03V. Whether several sensing devices were operated together or just one of them was operated independently, the drop in their output voltage was reflected in the output from sensing devices that were not being operated, in that they also experienced a drop of similar magnitude and rate.

Abruptly terminating the application of forces had a reverse effect, which triggered the output voltages of sensing devices that were being operated to drastically decrease below their initial level before any forces were applied. Immediately after that, the signals went up again until they settled at their initial level. The effect the sensing devices that were no longer being operated had on those that were not being operated at all at the end of the particular push in question, was the reverse of what happened when forces just started to increase at the beginning of that push. This meant that the resultant rise in voltage that followed the abrupt drop in output signals due to the push being terminated was similar in magnitude and rate for all the other sensors.

The largest potential difference produced between minimum and maximum outputs from each sensor was approximately 4.4V and approximately 5V from each transducer. This meant that a drop of 0.12V and 0.03V was approximately 2.7% and 0.7% of the total sensor outputs and approximately 2.4% and 0.6% of the total transducer outputs, respectively.

As these figures are very small, it was not anticipated that the amount of cross-talk between channels of the radio telemetry system would have a noticeable influence on the captured data. This was particularly so, because the conditions for testing inter-channel cross-talk represented one of the worst scenarios that could happen. It was therefore unlikely for these sorts of conditions to occur during the actual gait laboratory tests. Instead, the rates of sensor and transducer loading during the actual tests were much more likely to be far less abrupt than the rates during cross-talk tests. Also, the magnitudes of output signals should be lower than the threshold of the sensing devices, as previously explained in Section 6.1.4.4. Therefore, with the rates of voltage increases and decreases reduced and with the magnitude of voltages being lowered, the resultant output signals would be more gradual and without flattening out at the top end of the scale.

6.2.2. Assessment of the displacement transducers

The performance characteristics of the cam were determined by the error related to the approximation of the perimeter geometry to an arc of a circle and by the output of the transducers. Knowing the radius and location of the circle, the predicted cam error can be established mathematically. In turn, the transducers' output needed assessing in a different manner, which was accomplished by calibrating them in two ways, so that

their output when operated on their own can be related to their output when operated in conjunction with the cam.

6.2.2.1.   Predicted cam error

The distance between each point on the spiral and the centre of the adapter was determined in Section 6.1.2.5, and the offset X_o and Y_o between the centre of the adapter and the centre of the circle was established in Equations 5.1. It was therefore possible to calculate the distance between each point on the spiral and the centre of the circle, by using standard trigonometric algorithms for non-right-angled triangles (Barth et al 1985). The cam error could then be determined as the difference between those distances and the radius of the circle for every degree over a range of 36° or ±18°.

6.2.2.2.   Transducer and cam calibrations

Although power sources can be stabilised, slight fluctuations in output voltages can introduce errors, which is why the displacement transducers were calibrated by measuring their resistance with the same Ohmmeter used for determining the optimum transducer alignment, as described in Section 6.1.2.7.

The first calibration method was based on a set-up that involved a flat, metal plate to which a micrometer (0-25mm range, 0.01mm accuracy) was rigidly attached, as illustrated in Figure 6.12. While both transducers were consecutively mounted opposite the micrometer, readings were taken every 0.2mm over ten trials per transducer covering the full range of their 12.5mm mechanical stroke.

The second calibration method was based on a procedure during which the transducers were calibrated by measuring their output in response to displacement at the adapter and therefore at the cam also. This calibration was not relevant for measuring longitudinal translation, because the geometry of the distal, flat cam surface was exact and not approximated to any other shape. However, it was necessary for this calibration to be performed with respect to transverse rotation measurements, because the geometry of the cam perimeter was approximated and not exact, so that the output from the respective transducer is dependent on the characteristics of the cam perimeter shape. The equipment needed for the calibration process was a flat board onto which the TT

Pylon was vertically erected together with the cam, transducer mountings and one of the transducers, as shown in Figure 6.13.

Figure 6.12:   Micrometer-mounted apparatus for transducer calibrations
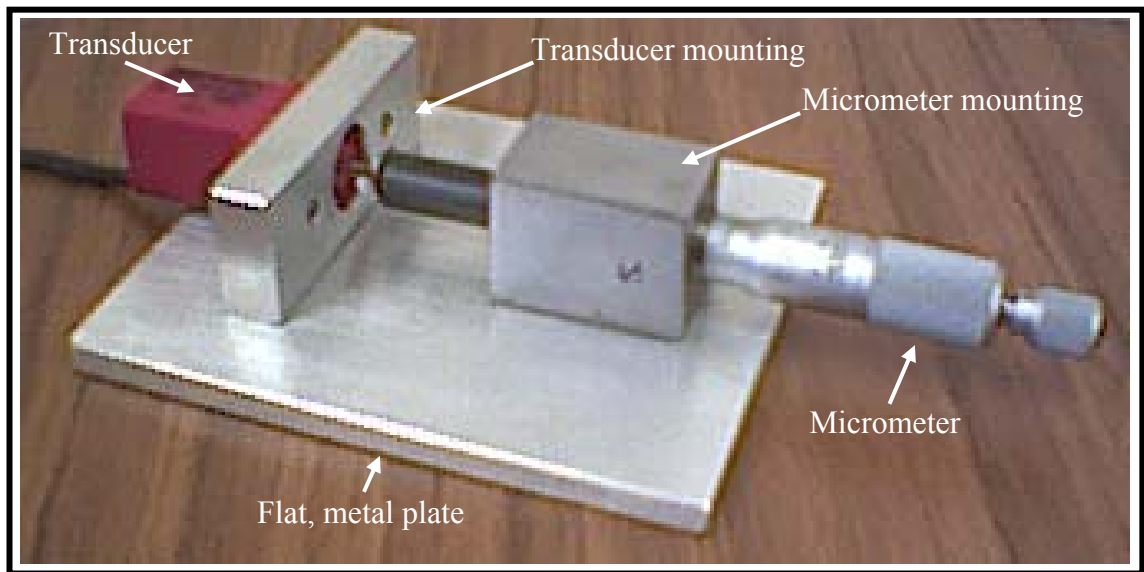
Figure 6.13:   Dial-mounted apparatus for transducer-cam calibrations
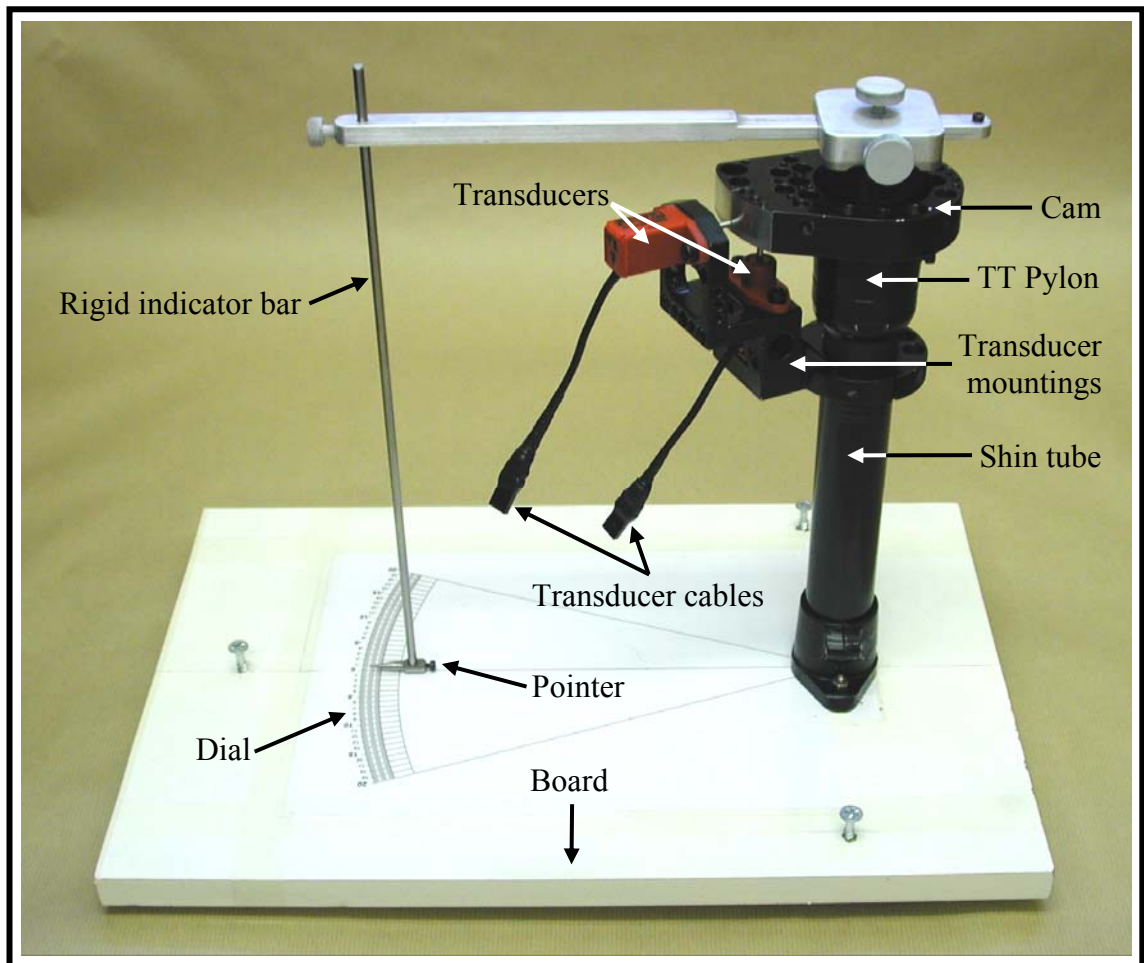
Instead of using a standard protractor, it was decided to design a customised dial for taking accurate measurements. The incremental divisions, displayed in Figure 6.14, were drawn within life size, global co-ordinates, using TurboCad version 9 (IMSI Inc, Novato California, USA). The resultant drawing was then printed out with a LaserJet 1200 series printer (Hewlet-Packard Company, Palo Alto California, USA). Laminated into a transparent cover to prevent it from getting stained, the dial was glued onto the flat board to fix it into its required position. The outer perimeter of the dial was located exactly 250mm from the adapter's COR, which was the maximum distance for printing the image on a standard A4 sheet of paper. Over this distance the arc between each angular increment is much longer than it would be with a dial located nearer the adapter. It makes it therefore more accurate for the pointer on the rigid indicator bar that extends from the pyramid connecting system at the proximal aspect of the adapter to be aligned with each increment on the dial.

Figure 6.14:   A customised dial for transverse rotation calibrations
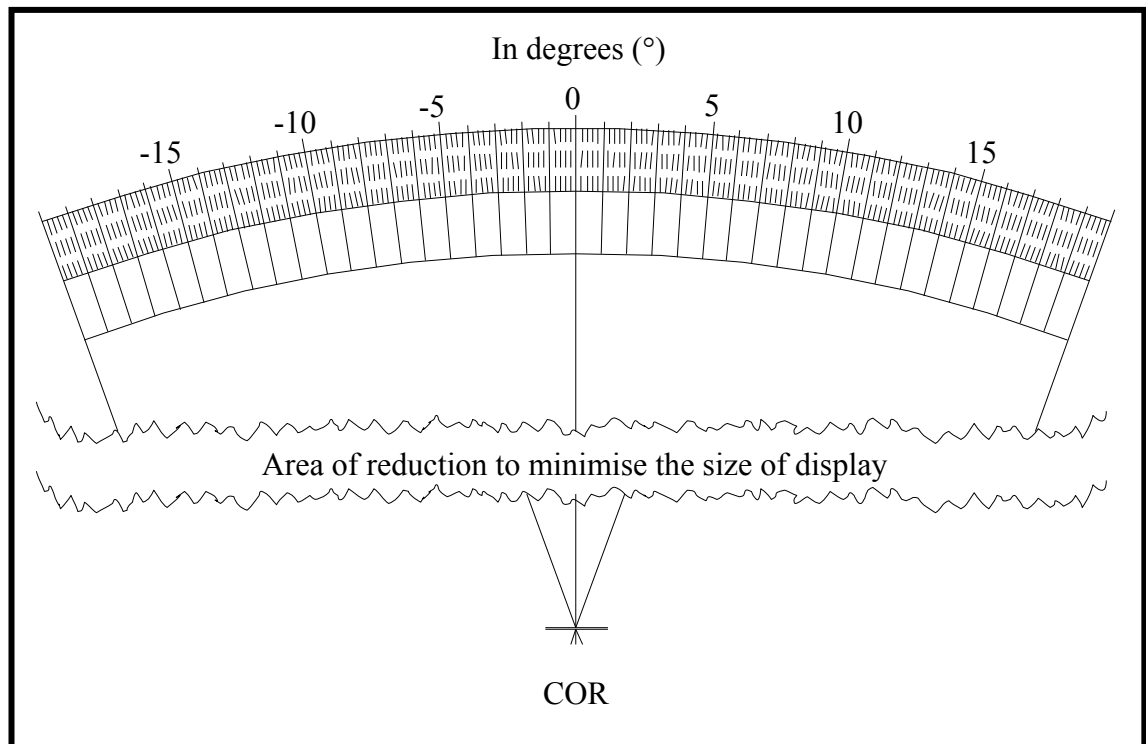
With the adapter in its neutral position, the rigid indicator bar was aligned in such a way that it pointed at 0°. Both types of return units were removed, so that the adapter would remain in its required position while the transducer output was being measured. Readings were taken every 1° over ten trials covering the full range of the 36° or ±18° perimeter. To support these data, this process was also repeated using the second

transducer. Finally, both transducers were mounted simultaneously into their corresponding position against the cam to establish possible cross-talk in transducer outputs while measuring longitudinal translation during transverse rotation and vice versa.

The following two Sections, namely 6.2.2.3 and 6.2.2.4, contain some of the results previously presented by the author of this thesis at national and international meetings. These include the Seventh International Symposium on the 3D Analysis of Human Movement from 10-12 July 2002 in Newcastle upon Tyne UK, the International Society of Biomechanics XIXth Congress from 6-11 July 2003 in Dunedin New Zealand and the Conference of Biomechanics of the Lower Limb in Health, Disease and Rehabilitation from 1-3 September 2003 in Salford UK. Some of these results were also published in a peer-reviewed journal, Medical Engineering & Physics. The publisher gave consent for the described paper to be integrated as part of this thesis. Additionally, an abstract was accepted for presentation at the 11th World Congress of the International Society for Prosthetics and Orthotics from 1-6 August 2004 in Hong Kong China, which focuses on similar findings as those that follow. All of the above publications are referenced at the end of this thesis.

6.2.2.3.   Analysis of predicted cam error

The minimum and maximum predicted error that was introduced by the approximation of the cam geometry to an arc of a circle was found between B and A at -10° and between B and C at +10° measuring approximately -0.0442mm and +0.0472mm, respectively. Increments of 1mm plunger motion are, as described in Section 6.1.2.5, the equivalent of 3° angular displacement of the cam. The errors from calculating the differences between the radius of the circle and the distances of each point on the spiral with respect to the centre of the circle can therefore be related to errors in measuring transverse rotation. These errors range, as depicted by the dotted graph in Figure 6.15, between approximately -0.1326° and +0.1416°.

Rotating the cam clockwise relative to the transducer mountings, as viewed from proximally, forces the respective transducer to slide between B and A, so that transverse rotation measurements at -10° will be approximately -10.1326°. In turn, during an anti-clockwise rotation of the cam relative to the transducer mountings, the same

transducer will be sliding between B and C, so that transverse rotation measurements at +10° will be approximately +10.1416°. As the measurements for clockwise and anti-clockwise rotations differ, it is necessary to investigate the influence those measurements can have during tests with amputees. A left sided amputee's 10° of internal cam rotation would measure 10.1326°, whereby a right sided amputee's 10° of internal cam rotation would measure 10.1416°, because the former is rotating the cam in a clockwise manner and the latter in an anti-clockwise manner. Turning the cam upside down between left and right sided recordings would solve the problem associated with differences in measurements, but this is not possible due to the cam's proximally expanding, conical cut-out for fitting it around the cam, as described in Section 6.1.2.3.

Figure 6.15:   Errors from approximating the cam geometry
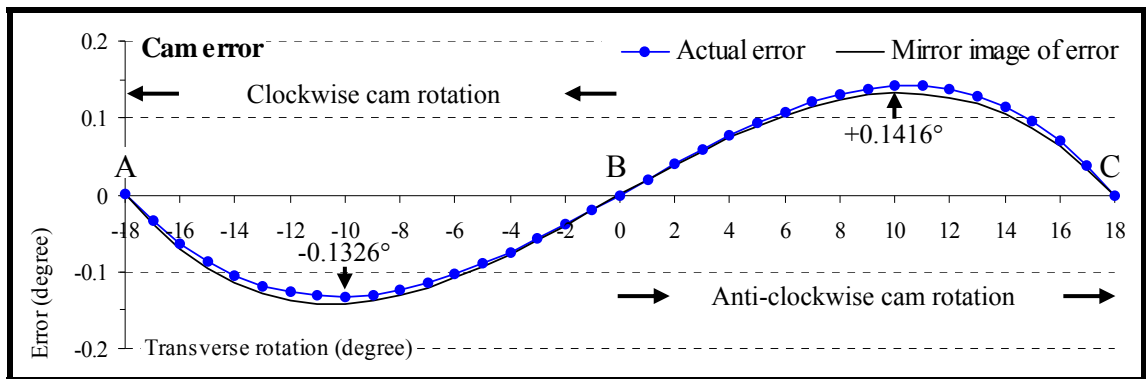
The example therefore shows that the measurements would not only be larger than the actual cam displacement, variations would also be dependent on the amputation side and on the direction in which transverse rotations occur. The maximum difference between errors during a clockwise and anti-clockwise rotation is approximately 0.003mm or 0.009°. The second graph in Figure 6.15, which is non-dotted, represents the reversed data of the main, dotted graph and the distances between those two graphs illustrate the difference between errors during incremental measurements that oppose one another with regard to the cam's neutral position of 0°.

A maximum cam error of only -0.0442mm and +0.0472mm is, on average, approximately ±0.46% of the transducers' 10mm electrical stroke and therefore less than a quarter of the value for the transducers' linearity of ±2%. Also, the maximum difference between errors for either side of the cam's neutral position of 0° is even smaller than the actual cam errors, which is why this aspect can be regarded as negligible and was anticipated not to have noticeable implications on the accuracy of

the gait laboratory tests. Manufacturing a second cam with a reversed geometry to the current one, so that both the left or right side have their own cam allocated to them, was, due to negligible cam errors, not regarded as necessary. Considering that one of the key specifications of the cam design was high accuracy, the approximations for simplifying cam manufacture were acceptable on the basis that the resultant cam error was so small.

6.2.2.4.   Analysis of transducer and cam calibrations

The mean values of the transducers' plunger displacements measured with an Ohmmeter were calculated over all ten calibration trials. They were plotted, as displayed in Figure 6.16, against actual, micrometer induced plunger displacements. The denotations "1" and "2" refer to transducer 1 and 2. The corresponding graphs that represent the results from calibrating both displacement transducers in conjunction with the cam are shown in Figure 6.17.

Figure 6.16:   Calibrations of both transducers using the micrometer
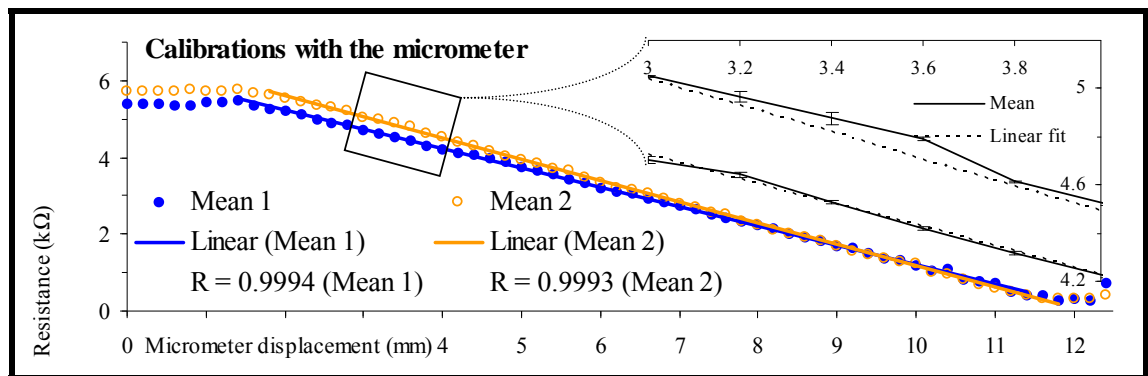
Figure 6.17:   Calibrations of both transducers using the cam
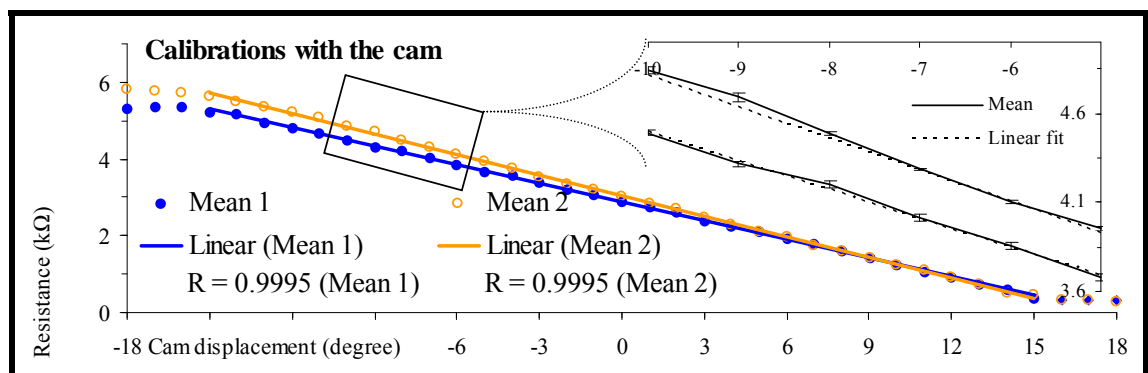
Due to minor imperfections within the transducers that were presumably introduced during their manufacture, the exact location of the electrical stroke relative to the mechanical stroke is slightly different for each transducer. Although readings were

taken to cover the transducers' entire stroke, a linear trendline was fitted over the range of their electrical stroke only, which was undertaken in Excel (Microsoft Corporation, Redmond Oregon, USA). Outside the electrical stroke the transducers' resistance measurements appear slightly random, so that the actual electrical stroke could be identified as the range where the graphs are characterised by a gradual slope. The locations of the trendlines in Figure 6.16 clearly show an offset between the start and finish of the two transducers' electrical stroke, which measured only 0.4mm. This offset, however, did not appear in Figure 6.17, because each transducer was, as described in Section 6.1.2.7, aligned accurately against the cam perimeter to take into account the location of the electrical stroke.

Figure 6.18:   Transducer 1 output errors from linear calibration method
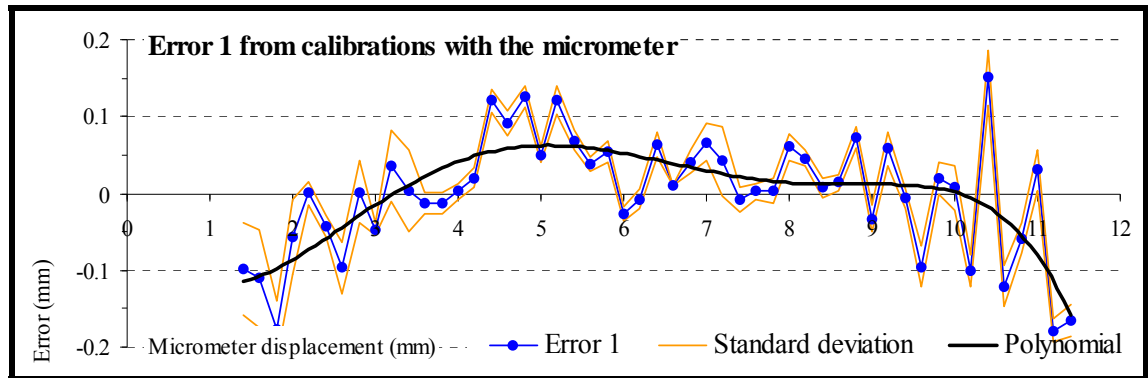
Figure 6.19:   Transducer 2 output errors from linear calibration method
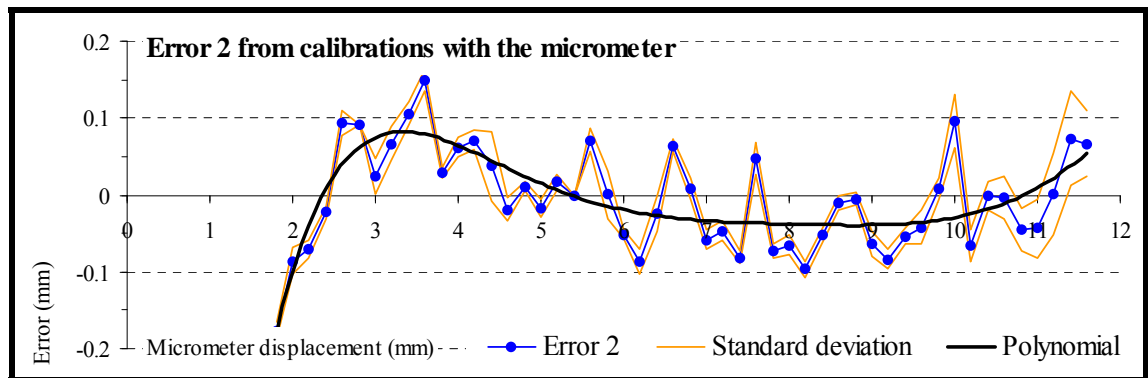
The correlation co-efficient R from the two transducers' output during both calibration methods ranged between 0.9993 and 0.9995, as calculated over the entire range of the electrical stroke. This indicates a very high degree of correlation and therefore a low dispersion from a truly linear output. The magnified areas display the full results from each of the ten trials over a limited range of 1mm linear displacement of the micrometer's movable part and 5° rotation of the cam to illustrate the repeatability of

the readings. Inter-trial measurements had a maximum standard deviation of approximately 0.034mm for calibrations with the micrometer and approximately 0.04° for calibrations with the cam. This is very low and only approximately 0.34% of the transducers' 10mm full electrical stroke and approximately 0.13% of 30° or ±15° cam rotation.

Knowing the gradient and intercept on the Y-axis of all four linear trendlines, it was possible to calculate the differences between actual measurements and each point on the respective trendline. These differences, illustrated in Figure 6.18 and Figure 6.19, represent the errors from each displacement transducer's calibration procedure with the micrometer.

The corresponding graphs that represent the errors from calibrating each displacement transducer in conjunction with the cam are shown in Figure 6.20 and Figure 6.21.

Figure 6.20:   Transducer 1 output errors from angular calibration method
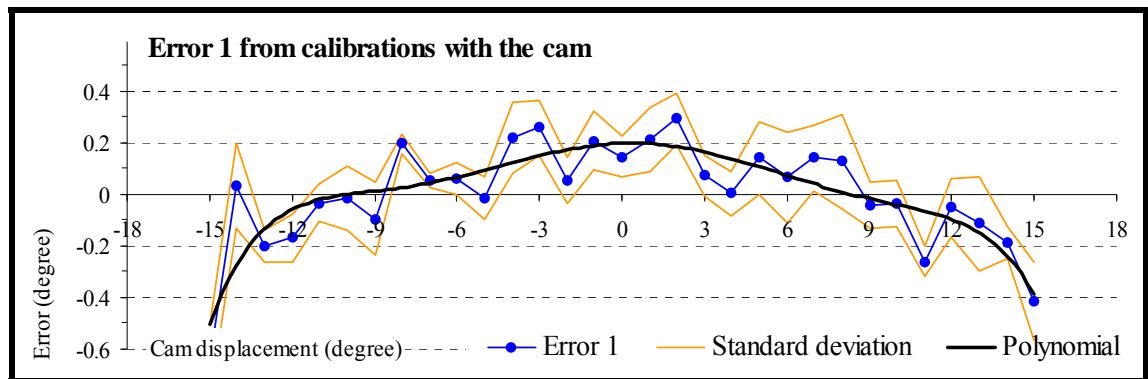
Figure 6.21:   Transducer 2 output errors from angular calibration method
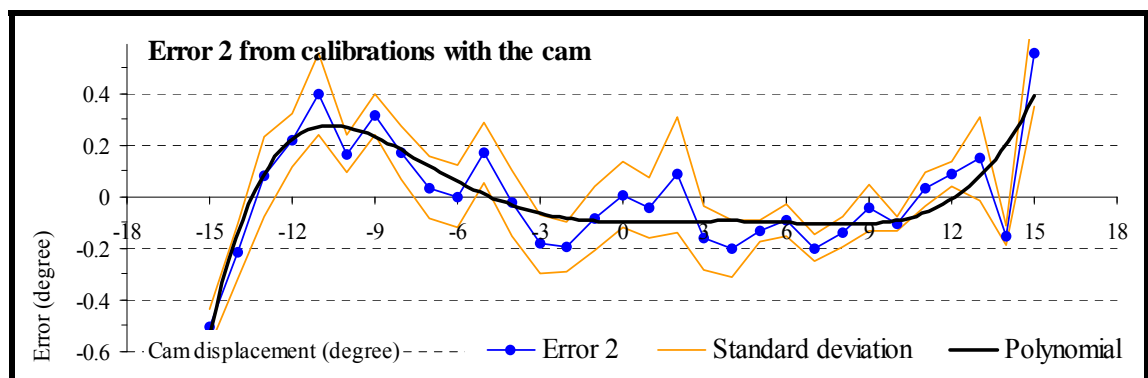
Determining the general trend of the data was initially difficult due the scattered appearance of the errors. However, fitting a sixth order polynomial to the data made it

easier to visualise the extent of error fluctuations. This was the highest order polynomial available within Excel, and it indicates the general trend of the data in a lot more detail than a lower order polynomial would have done.

It can be seen that errors in transducer measurements during calibrations with the micrometer and cam did not exceed ±0.18mm and ±0.5°, respectively, and the magnitude of those errors was even less within the middle measuring ranges. The ratio between errors from calibrations with the micrometer and those from calibrations with the cam is therefore approximately 1:3. The same ratio exists between linear plunger motion and angular cam displacement, namely 1mm translation for every 3°, as it was intended during the design of the cam geometry, previously described in Section 6.1.2.5. The fact that the ratio for calculations of measurement errors remained unchanged after the actual calibrations indicates that the level of recording accuracies is virtually the same for both types of calibrations methods.

The standard deviations were calculated over the differences between the linear trendline and each of the ten recordings for every incremental measurement. The maximum value obtained for calibrations with the micrometer was approximately 0.064mm or 0.192°, which is just over 85% of the maximum value obtained for calibrations with the cam of approximately 0.225° and therefore quite similar. However, the mean of those standard deviations for calibrations with the micrometer was only approximately 0.020mm or 0.060°, which is just over 56% of the mean standard deviation for calibrations with the cam of approximately 0.106° and therefore considerably lower. The dispersion of errors away from the trendline was therefore less with the micrometer than it was with cam and this is reflected by a narrower band width of standard deviations in Figure 6.18 and Figure 6.19 compared to the band width in Figure 6.20 and Figure 6.21. However, this did not appear to have a noticeable effect on the mean measurements and was therefore not considered of relevance for the assessment of the system's performance.

The patterns of errors found during the calibrations with the micrometer are reflected in the calibrations with the cam. This suggests that the predominant error came from the transducers themselves, rather than from the design or manufacture of the cam or transducer mountings. Also, the magnitudes of errors compare favourably with those found in measurements from static or slow moving markers in small capture volumes,

as reported on by Everaert et al 1999. However, compared to the errors reported by Richards 1999 and those described in Section 5.2.1 for fast moving markers within large capture volumes, the errors from measurements with the cam seem very small. The system's performance characteristics are therefore sufficient, which justifies the use of this type of alternative data capturing device during the current study.

Both transducers needed to be simultaneously located in their corresponding position, so that the sensitivity of the system's decoupled measuring characteristics could be established. The rigid substitute return units, previously described in Section 4.1.5.3, were used to permit one type of displacement at the adapter, but not the other. Depending on the type of return unit used, the mounting of the transducer that recorded the restricted type of displacement was aligned in such a way that the transducer's plunger was pushed far enough inward to be within the range of the electrical stroke. In both cases, changes in measurements were only significant from the transducer recording the displacement at the adapter. The other transducer measured only very slight fluctuations with a maximum of less than $\pm0.005\text{k}\Omega$ deviation from its output when the adapter was stationary. As the transducers' maximum resistance is $5\text{k}\Omega$, this amount of deviation is, when calculated over 10mm longitudinal translation and 30° or $\pm15°$ transverse rotation, approximately 0.01mm and 0.03°, respectively. The extent of mechanical cross-talk between the transducer measuring linear displacement and the other measuring angular displacement could therefore be considered negligible.

Output fluctuations from power sources were deliberately avoided by calibrating the transducers with an Ohmmeter, as explained in Section 6.1.2.7. However, having obtained satisfactory data from measuring the transducers' resistance, it was decided to repeat the entire calibration process by recording the output from the radio telemetry system in response to plunger motion at the transducers. The data were very similar to those obtained from measurements with an Ohmmeter, which not only consolidates the calibration results, but it also reconfirms the radio telemetry system's high performance characteristics. The second set of calibration results therefore provided evidence that this part of the measuring equipment had reached a sufficiently high level of sophistication. In addition to that, calibrating the cam and transducers with the radio telemetry system was vital for the data processing procedure following the gait laboratory tests. This was in order to convert the transducers' output from the actual trials in response to transverse rotation and longitudinal translation at the adapter into

units of angular and linear displacements, namely degrees (°) and millimetres (mm), respectively.

Despite satisfactory results when using the cam system for measuring displacements at the motion adapter, there were a number of improvements that could be undertaken during future work. Improvements could be made by using transducers with an even higher accuracy. An alternative approach would be to use an algorithm that rectifies the measurements by compensating for the systematic component of the errors, but this was not considered necessary for the current study as the magnitude of errors was already very small. Subsequent, newer models of the cam should have an improved perimeter geometry, which can be achieved by spacing the three points A, B, C closer together at, say, -12, 0, +12°. This would introduce errors in response to the cam design at the outer and perhaps less frequently used measurement regions of -18° and +18°. In turn, it would reduce the maximum error in perhaps more frequently used measurement regions, as currently found at the two apices of the dotted graph in Figure 6.15 namely at -10° and +10°.

At the completion of the current study it may show that the overall measurement range could be reduced, which in itself should also reduce the cam error, particularly if the three points A, B, C would, over the already smaller range, be spaced even closer together. Another possibility would be to increase the incremental radii of the spiral and therefore the radius of the approximated circle, which also reduces the error. However, this, in turn, would make the device heavier and bulkier, so that the gained advantage may not necessarily outweigh the disadvantages.

6.2.3. <u>Assessment of the force sensors</u>

The performance characteristics of FlexiForce® sensors are dependent on a number of factors. These needed to be established, so that the circumstances, during which the sensors produce an optimised output, are known.

6.2.3.1. Sensor conditioning

The measurements obtained from FlexiForce® sensors were, according to their manufacturer, supposed to improve with prolonged applications of forces. Better results can be obtained after conditioning the sensors, which is a procedure that requires them

to be repetitively exposed to approximately 110% of the maximum load that is to be forced upon them. This procedure should be undertaken prior to every data recording session to ensure consistency of results. Conditioning the sensors should improve the repeatability of measurements and lessen the effects of drift and hysteresis.

A rig, as illustrated in Figure 6.22, was designed and manufactured to make the conditioning process easier. Made out of aluminium, it measured approximately 330mm in length, 40mm in width and 12mm in depth. Placing the sensors into the rig's longitudinally orientated groove of approximately 5mm depth prevented them from moving sideward. It was also important to stop the sensors from shifting within the groove, which was achieved by pushing the aspect where the sensing area was located against a central, upward protruding bolt at one end of the groove. Two additional upward protruding bolts on either side of the groove acted as guides onto which a cube-shaped platform with matching holes was fitted. The purpose was to position the platform exactly over the sensing area, so that a disc at the bottom of the platform and another, precisely opposing disc at the bottom of the groove and therefore underneath the sensor would sandwich the sensing area.

Resting some weights on top of the platform therefore pushed the two discs together, which occurred in a parallel fashion as the alignment of the platform was governed by the two upward protruding bolts on either side of the groove, so that the forces were applied over the discs' entire area. With a diameter of 8mm, the discs were large enough to cover approximately 70.5% of the 9.53mm diameter sensing area, yet small enough not to spread the forces to the neighbouring surfaces outside the sensing area, which would negate the conditioning procedure. Both discs were made out of semi-rigid polypropylene rather than metal to prevent their edges from damaging the sensors.

The maximum residual limb-socket interface forces or pressures that needed measuring during the gait laboratory tests were, at this stage, still unknown. However, it was known that the maximum value identified from the literature reached up to 828kPa, as explained in Section 6.1.3.4. It made therefore sense to use this as the threshold for the conditioning procedure, whereby the 110% limit would consequently calculate as 910.8kPa. With a disc size of 8mm diameter and an area of approximately 50.27mm^2, the amount of force that would have to be applied was approximately 45.78N or 4.67kg. The increments of standard weights available from the University of Salford that could

be used for conditioning the sensors were 0.1kg. It was therefore decided to condition them with 4.7kg rather than 4.67kg, which was, with regard to the diameter of the disc, the equivalent of approximately 917.3kPa. When regarding this as 110% pressure then the equivalent value for 100% pressure would be 833.9kPa, which is only 5.9kPa more than the maximum value of 828kPa from the literature.

Figure 6.22: FlexiForce sensor calibration rig with different disc sizes
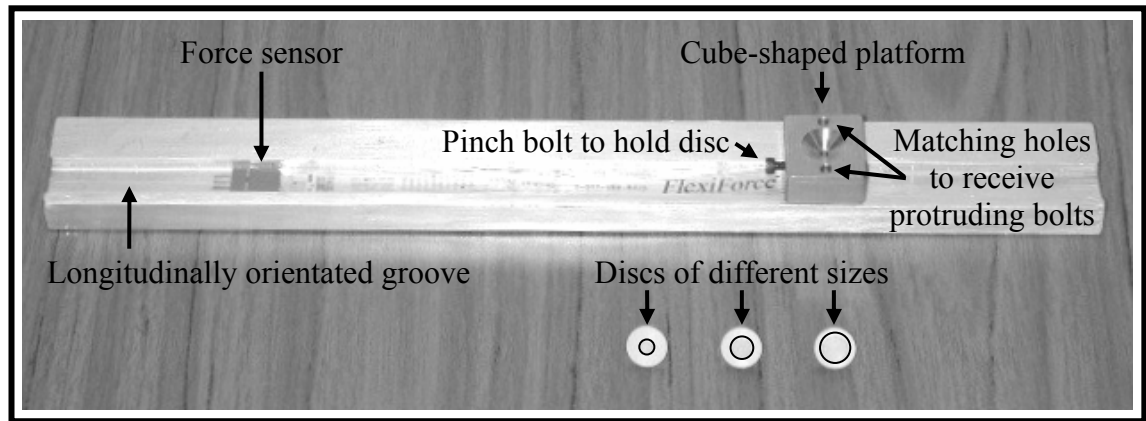
The manufacturer did not specify an exact figure for the amount of times a force should be applied during the conditioning procedure of the sensors, except that this should be "repeated a few times". It seemed therefore reasonable to repeat this process ten times per sensor for approximately 10s during each loading procedure and not more than two hours before the gait laboratory tests.

6.2.3.2. *Sensor specifications*

The sensors have a resistance of over 5MΩ without a load and approximately 5kΩ at full load. The manufacturer claimed that, providing the conditioning procedure was undertaken, the sensors have a linearity of less than ±5% and a repeatability within 2.5%. When applying 50% of the full force range, hysteresis is supposed to be less than 4.5% of the full scale, whereby the drift with a constant load is less than 3% over logarithmic time and the rise time below 20μs at impact load.

Whether the specifications given by the manufacturer were correct needed to be established. Ferguson-Pell et al 2000 tested FlexiForce[®] sensors in a number of ways. These authors obtained slightly different results, as they repeated the tests with a range of different magnitudes of forces. The linearity varied between 1.9% and 9.9% and they established that the output improved after ten minutes of loading, as the coefficient of

variation decreased. The repeatability was 2.3-6.6%, which meant that most of these measurements were larger than the figure stipulated by the manufacturer. Hysteresis was 5.4% and this was not obtained during tests with 50% of the full force range, but instead was calculated as the average of results from trials with different weights. Drift was 1.7-2.5% over logarithmic time and therefore less than the manufacturer's findings.

Although Ferguson-Pell et al 2000 did not provide any figures with regard to rise time at impact load, they did, in turn, investigate the effect that curved surfaces have on the output of the sensors, which the manufacturer failed to give any specifications for. Decreasing radii triggered an increase in output offset and a decreased sensitivity. The threshold for those radii was determined to be 32mm, whereby measurements on surfaces with radii greater than that were considered acceptable. The effect spherical surfaces have on pressure measurements was an aspect that the authors have not yet dealt with, but regarded it as worthy for further research.

The general performance characteristics of FlexiForce® sensors appeared acceptable for the current investigation. One factor that triggered a slight cause for concern was the fact that curved surfaces can affect measurements. However, the radii had to be less than 32mm for this to have a significant effect on the results. Although three of the chosen landmarks, previously described in Section 6.1.3.6, are generally not flat, namely the fibula head, the tibial tuberosity and the anterior-distal aspect of the tibia, they are covered by soft tissue, which should reduce the amount by which the sensors have to bend.

6.2.3.3.   Sensor calibrations

Another procedure that needed to be undertaken was the calibration of the sensors. This was necessary to be able to convert their voltage output into pressures. Calibrating each sensor, rather than just one of them, was important, as suggested by the manufacturer, because generalising the measurements can lead to inaccuracies due to slight variations between sensors.

Calibration procedures were undertaken after each subject's gait laboratory tests, so that variations in sensor outputs on different days could be accounted for. The reason for calibrating after, rather than before the tests was, because the forces acting on the sensors during walking can be regarded as further conditioning of the sensors and may

render their outputs slightly different to those just prior to the tests. It could be argued that an additional conditioning induced during walking might also affect the test results themselves. However, this was not considered to be the case, as the subjects were given some time to get accustomed to their test-prosthesis prior to the actual tests. Therefore, by the time the actual tests commenced the sensors should have been sufficiently conditioned.

The apparatus for calibrating the sensors was the rig for sensor conditioning, as described in Section 6.2.3.1. Because the force plates, described in Section 5.2.2.2, were probably the most accurate equipment available, it was decided to utilise these as the measuring device for sensor calibrations. With the rig placed in the centre of the first force plate, each FlexiForce® sensor was consecutively placed in its required position at the bottom of the groove along the rig.

Once everything was in place and the appropriate lead was connected to the sensor in question, the force plate's charge amplifier could be zeroed, so that the weight of all the equipment on top of the force plate was eliminated from the measurements. The rig's cube-shaped platform was then located onto the respective sensor, which meant that both the force plate and the sensor would register the weight of the platform. All the settings of the variable resistors for the sensors' electronic circuit remained the same as they were during the gait laboratory tests. This emphasises the importance for appropriate labelling, as explained in Section 6.1.4.4, to ensure that each sensor was connected to its respective lead. A reflective marker was, as described in Section 6.2.1.1, within sight of the cameras, as the ProReflex^{TM} system needed to register at least one marker in order to make a capture process valid. Figure 6.23 shows the entire set-up for sensor calibrations in relation to one of the force plates

Recordings were taken at 100Hz over a duration of 20s, during which the cube-shaped platform was pushed down ten times by hand. With the telemetry receiver, described in Section 6.1.1.3, positioned near by, it was possible to view its LCD oscilloscope. This made it possible to inspect that each downward push was hard enough for the measurements at the top end of the scale to flatten out, and therefore to trigger maximum sensor output, so that the entire measuring range was calibrated. Attempts were made for each push to fade in and out gradually rather than abruptly in order to

provide a greater capturing resolution in response to a larger number of measurements between the incident of minimum and maximum output.

Figure 6.23:   Arrangement of equipment for sensor calibrations
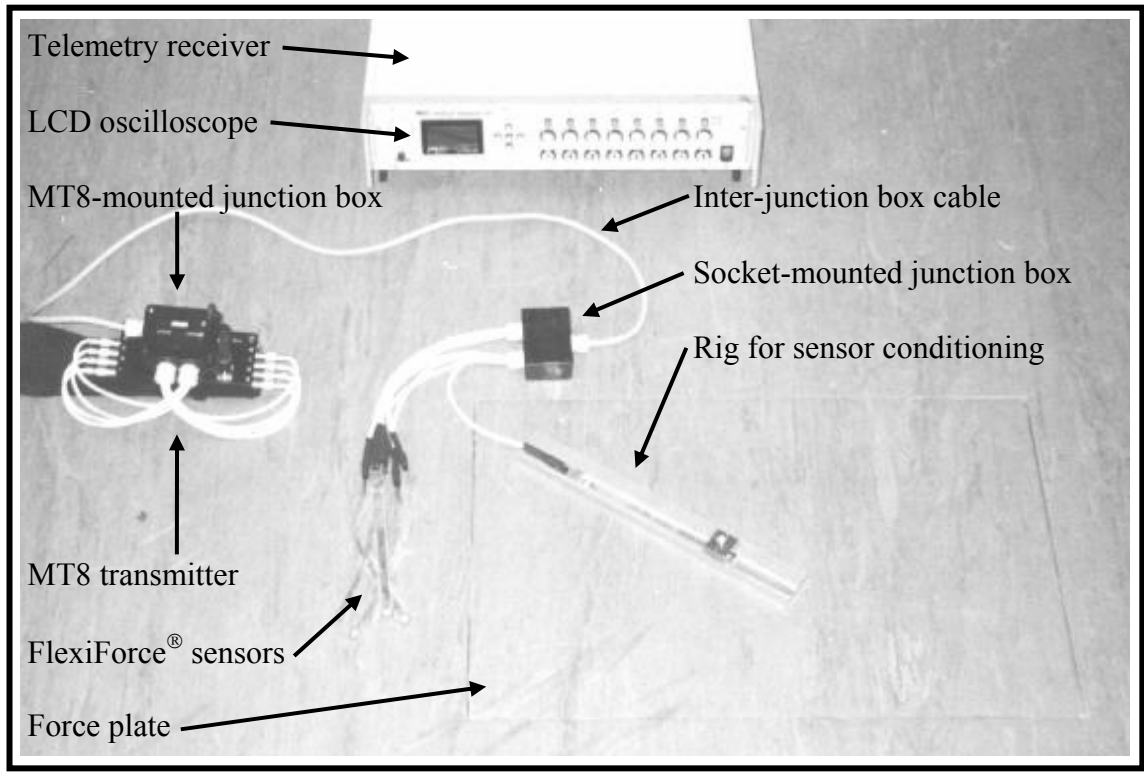
The calibrations were undertaken at room temperature of around 20°C, whereby the temperature within a socket was likely to be nearer to body temperature and therefore at approximately 37°C. The FlexiForce® sensors' operating temperature ranged, according to their manufacturer, between -9°C and +60°C with a change in force readings of approximately 0.36% for every 1°C. The resulting temperature difference of 17°C between the gait laboratory environment and the interior of the socket therefore meant that the sensor output changed by 6.12%. Warming the gait laboratory up for the sensor calibrations in an attempt to lower the temperature difference relative to the socket environment was difficult due to local heating facilities. In turn, cooling the interior of the socket down did not seem a feasible option either. An alternative solution would be to compensate for the difference in sensor output mathematically, but this was also not applicable as the manufacturer failed to specify whether an altered temperature triggers a positive or negative change in sensor output.

6.2.3.4.   *Additional sensor calibrations*

Ferguson-Pell et al 2000 suggested further research into the performance characteristics of the sensors to establish their output while applying forces over areas of different sizes. This was considered a valuable idea, because bone prominences may exert forces onto only part of the sensing area. If the sensor output would vary according to the size of surface onto which forces were transmitted, then such fluctuations must be evaluated to improve subsequent data analyses. The two opposing discs that sandwiched the sensors during the calibration procedure were, with a diameter of 8mm, the same as those used during the conditioning process. It was therefore decided to repeat the same sensor calibrations by using two additional pairs of discs with a 6mm and 4mm diameter. When using three different disc sizes, the three indented areas on the force sensors occupied approximately 70.5%, 39.6% and 17.6% of the sensors' total sensing area.

6.2.3.5.   *Processing of the data from sensor calibrations*

Prior to converting the sensor outputs into pressure, it was necessary to digitise all the calibration files by naming the single marker that needed recording to make a capture process valid. Once completed, the files were exported as TSV files.

The next step was to relate measurements from the force sensors to those from the force plate. As each of the six force sensors in use was calibrated with three different disc sizes, the total number of calibrations for all ten subjects added up to one hundred and eighty. Having obtained two thousand recording frames for each of those calibrations, it was necessary to devise a method that made it possible only to extract the frames recorded over the durations when the force sensor outputs faded in and out in response to the ten consecutive pushes onto the sensors, as mentioned in Section 6.2.3.3. Doing this manually was, due to the vast amount of data, far too time consuming, and the likelihood for making mistakes would have been high. It was therefore decided to write a program in Matlab (The MathWorks Inc, Natick Massachusetts, USA) that could identify the points in time when the signals from each push started and stopped increasing and decreasing.

Having digitised each data recording, the ProReflex^{TM} system automatically created headers at the top of the exported TSV files. As Matlab was incapable of opening files

with a header, the first step was to write a specific routine that removed the headers in order to make the files accessible. After that it was necessary to eliminate noise from the data by filtering them, so that it became easier for the Matlab program to determine the start and end of a gradually increasing and decreasing output.

Smoothing the data was undertaken with a low-pass Butterworth filter. To establish the optimum setting that the filter should have for this particular application, one set of data was processed with different orders of filters and different cut-off frequencies. Output fluctuations between each push and between commencing and terminating a maximum push were smoothed out too much if the order of filter and the cut-off frequency was too low. In turn, the most satisfactory results were obtained with a sixth order low-pass Butterworth filter and a cut-off frequency of 10Hz, as the graphs that represented the filtered and unfiltered data turned out to be very similar, except the filtered data were without noise. Also, filtering the output predominantly affected the data just before and after a push. This meant that the relatively regular rise and fall in sensor outputs, while increasing and decreasing the magnitude of a push, remained virtually unaffected by the filtering.

The next step was to establish an easily identifiable point in time during an increasing and decreasing force sensor output for each of the ten pushes. This was determined to be a data point that was mid-way in magnitude between the minimum and maximum force sensor output from each push. It was then possible to find the point in time when the output reached a minimum and maximum value before and after each mid-way measurement. The first and last of ten consecutive pushes were not used, because the start of the first and finish of the last push appeared slightly different to the other eight pushes, which made it difficult to identify the frames when the sensor outputs were at their minimum.

Figure 6.24 illustrates a typical output from a force sensor and force plate during the described calibration procedure. In order to make the two graphs appear similar in size, the force sensor and force plate data were, purely for demonstration purposes, divided and multiplied by a factor of five, respectively, as shown in the legend of that chart. It can be seen that the output from the force sensor clearly reached a threshold, as intended, which is indicated by the broadened and flattened-out apex of the graph representing the force sensor data. In turn, the output from the force plate is much more

pointed and obviously did not reach a threshold, because the applied forces still fell within the force plate's measuring range.

Despite filtering, the data fluctuated at the top and bottom end of the force sensors' output scale. This is why the minimum force sensor measurements before commencing and after terminating each push were determined to be slightly larger than the smallest signal. In turn, the maximum force sensor measurements before and after reaching the apex of each push were determined to be slightly lower than the largest signal. The vertical and horizontal parts of the square graph over the second to ninth push indicate the cut-off level when the output from the force sensors reached a minimum and maximum, respectively.

Figure 6.24:   Force sensor and force plate output from the calibration process
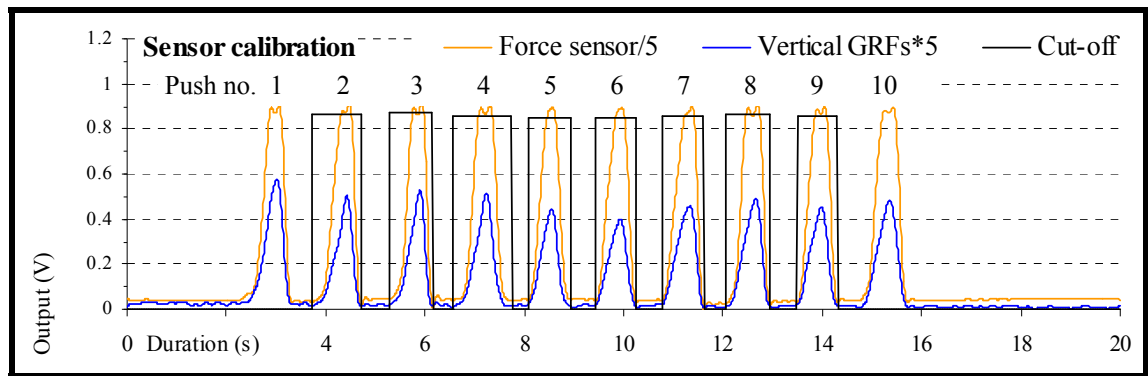
Having determined the start and end points of each slope, the force sensor data over these durations could then be related to the output from the force plate. To be able to summarise data from all eight pushes, the output between every start and end point of a slope needed normalising. This was done by using interpolation, so that every slope contained exactly one hundred measurements. The data between the maximum and minimum of each downward slope from the force sensors and the force plate were reversed, so that it was possible to calculate the mean from the data of all eight upward and all eight altered downward slopes.

Due to the anchorage of the cube-shaped platform onto the two protruding bolts on the sensor conditioning rig, the force sensors only experienced vertical forces. The output from the force plates could therefore be calculated as the sum of the piezoelectric transducers' signals from channels C_5-C_8, because these were responsible for conducting the output in response to vertical forces, as previously explained in Section

5.1.2.5. The values for the respective force plate's level of sensitivity, as illustrated in Table 5.1, were then used to convert this plate's output voltage into units of pressure (kPa) before finally saving the processed data as text files.

Both the force sensor data and the converted force plate data were plotted against each other. A sixth order polynomial was fitted to the calibration data, which was, as described in Section 6.2.2.4, the highest order polynomial available within Excel (Microsoft Corporation, Redmond Oregon, USA). Knowing the gradient and intercept on the Y-axis therefore provided a virtually exact numeric representation of the calibration data for converting a sensor's voltage output from the actual tests into pressures.

6.2.3.6.   Analysis of sensor calibrations

The gain of each sensor's operational amplifier was, as explained in Section 6.1.4.4, individually adjusted to obtain a suitably sized signal of slightly lower magnitude than the output threshold. This meant that the gain not only differed for every single one of each subject's six sensors, none of the settings for any of all ten subjects were the same either. As each subject acted as their own control, it was impossible to compare the results from the ten subjects and draw statistically based conclusions, so that an analysis similar that undertaken by Ferguson-Pell et al 2000 was not realistic. The reason for having chosen this particular calibration procedure was purely out of necessity for each sensor's voltage output to be converted into pressures. The fact that the results cannot be used for other types of analyses is unfortunate, but unavoidable.

Each of the six sensors needed calibrating with all three discs and this process had to be repeated for all ten subjects, which meant that the total number of calibrations added up to one hundred and eighty or sixty sets of three types of calibrations. Rather than displaying every single one of them, it was, due to this large number, considered a more concise option to provide examples of the data by choosing only two extreme sets of calibrations instead. Figure 6.25 contains data with the highest spread between all three calibration methods and Figure 6.26 contains data with the lowest spread. Both charts also display the mean of all three calibration methods.

As mentioned previously, each sensor's individually adjusted gain influenced its own sensitivity to the applied forces, which made it difficult to compare the spread of data

between the two sets of calibrations. It was therefore decided for each of the two chosen sets to have their data normalised to 100%, but only for the calibration with a disc that produced the largest output. The outputs from the other two discs were therefore smaller, as they were expressed in relation to the output that was normalised to 100%.

Figure 6.25:   A high spread of results from calibrations with all three discs
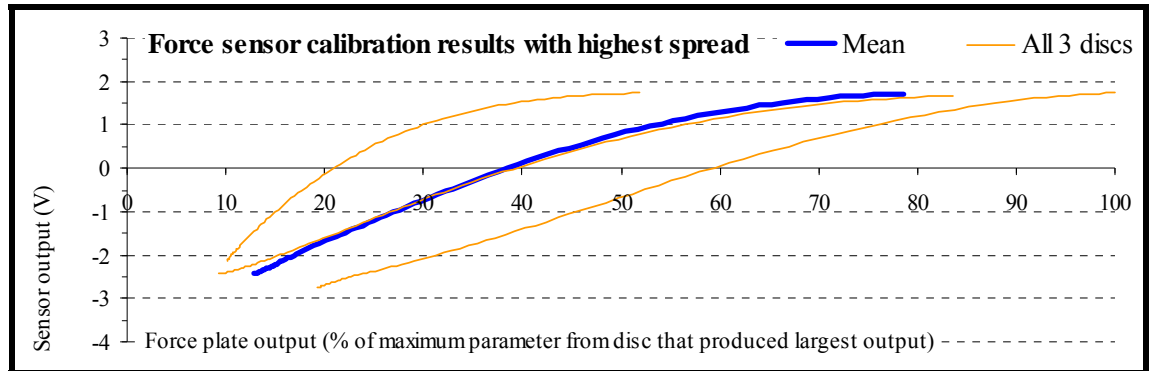
Figure 6.26:   A low spread of results from calibrations with all three discs
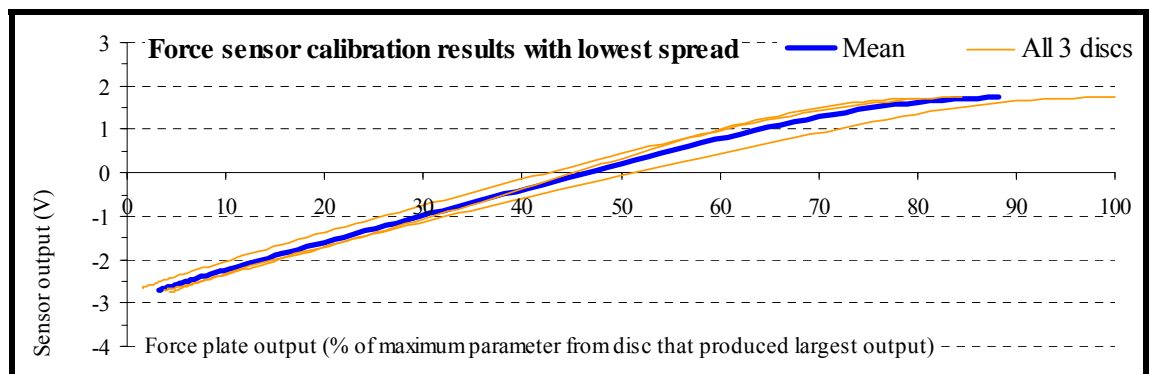
The results in Figure 6.25 and Figure 6.26 show that the FlexiForce® sensors' outputs varied depending on the size of area over which forces were exerted onto the sensing area. Calculating the mean from all three calibration results rather than using the data from only one calibration method therefore seemed to produce more representative parameters for converting the sensors' voltage outputs into pressures. Also, the scenario created during the calibration procedures by using three different sizes of discs may even be applicable during the actual measurements in that a bone prominence, for instance, could exert forces onto only part of the sensing area. It was difficult, if not impossible, to predict whether an anatomic landmark may or may not be in full contact with the sensing area, and the possibility that only part of it may be loaded reinforces the decision for combining the data from all three calibration methods.

CHAPTER 7.   GAIT LABORATORY TEST SET-UP

In order to make the gait laboratory tests successful, it was necessary to consider additional factors that contributed to the influence different types of equipment can have on the outcome of the capture processes.

7.1.   Markers for the ProReflex^{TM} system

7.1.1.   Definition of the global reference system

The calibration frame defined the position and orientation of the ProReflex^{TM} system's Cartesian co-ordinate system, which can be referred to as the global reference system. The location of the frame for the calibrations prior to the actual gait laboratory tests was arranged in the same fashion as described in Section 5.1.1.3. Therefore, with identical software parameters and parameter arrangements, the X-axis pointed forward, the Y-axis pointed upward and the Z-axis pointed to the right, as recommended by (Wu & Cavanagh 1995). The L-shaped frame's short bar was located exactly between force plate one and two and its long bar was just to the right of force plate two with the two markers on the short bar equidistantly spaced from their nearest force plate, as illustrated in Figure 7.1.

The origin of the global reference system was, according to the parameters in Figure 5.1, located in the corner of the L-shaped frame, and the capture volume was, as explained in Section 5.1.2.3, supposed to extend further towards the end of the walking path, so that its boundaries allow both the left and right gait cycle to be fully recorded. Taking the dimensions of 4.6m length, 1.1m width and 1.3m height, as stipulated in Section 5.1.1.12, into consideration, it was possible for the capture volume's bounding co-ordinates to be determined by defining the parameters illustrated in Table 7.1. To ensure that all distally located markers can be captured, the value for the Y-axis needed to be negative. This was because at zero the origin of the capture volume would be above the floor, as the distance between the centroid of the markers on the calibration frame and the ground is defined by the markers' radius and the thickness of the frame.

Figure 7.1:   Location of the calibration frame with respect to force plates
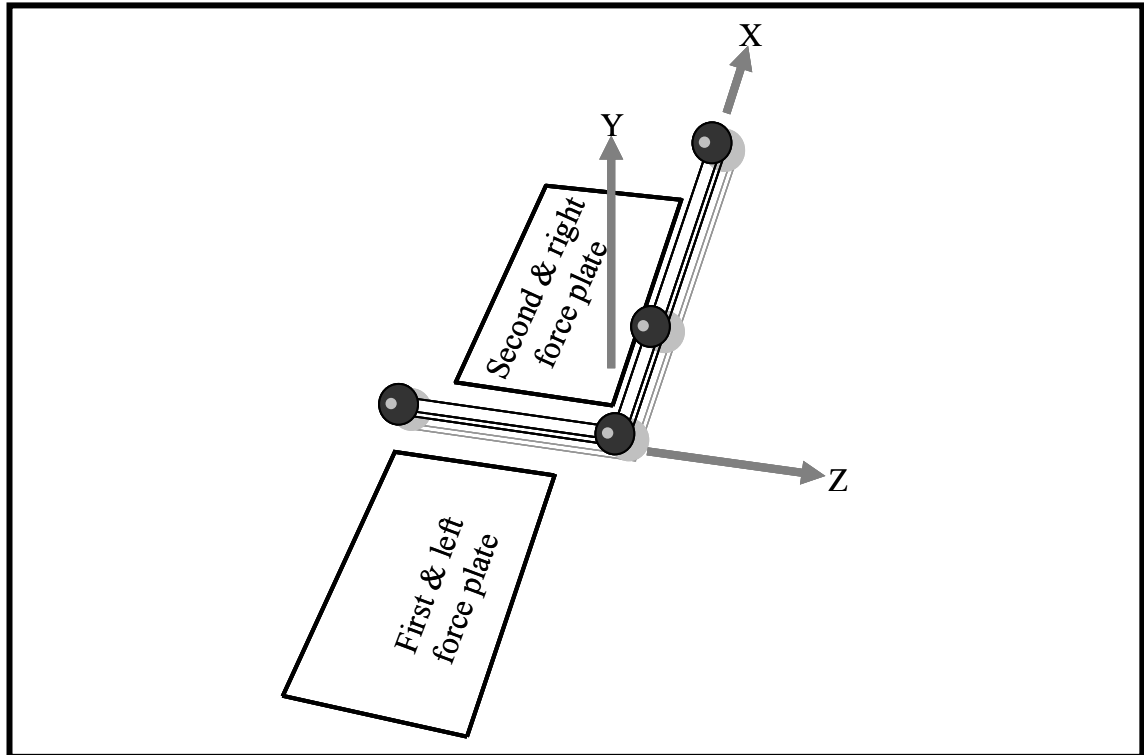
Table 7.1:   Bounding co-ordinates for the capture volume

Axes orientations of the co-ordinate system	Minimum (mm)	Maximum (mm)
X-axis positive anterior	-1800	2800
Y-axis positive upward	-30	1300
Z-axis positive rightward	-825	275

7.1.2.   Definition of the local reference systems

Using the ProReflex^{TM} system for capturing motion of each subject's test-prosthesis and both their lower limbs required reflective markers to be mounted in specific patterns and at certain locations, in order for each segment's position and orientation in space to be determined. A segment's location, as well as its linear and angular displacements relative to the origin and axes arrangements within the global reference system, can be calculated from the recorded positions of markers located on the segment in question.

A segment's markers defined an additional co-ordinate system, which was, as the global reference system, a right-handed type and can be referred to as the local reference system. All the other segments therefore also needed a set of markers to define their

own local reference system for calculating the location and displacement of each segment separately. In addition to the markers that identified the segments, it was necessary to have extra markers for determining the location and orientation of axes around which the segments rotate.

7.1.3.   <u>Considerations for biomechanical models</u>

At least three non-co-linear markers are required to define the three axes of a Cartesian co-ordinate system and two markers for identifying a rotation axis. This implies that, in theory, eight markers would be needed for calculating the relative position and displacement in 3D of two inter-connected segments, namely three markers per segment and two markers whose centre define two points on the rotation axis. Inter-connected segments share the same joint, which means that the rotation axis is either located at both segments' adjacent ends or it forms, as with the knee joint for instance, part of one segment, namely the femur, and represents an extension of the other, namely the tibia. The two markers for defining the rotation axis can therefore also be regarded as markers for defining part of each segment's local reference system. This means that, in addition to the two joint markers, only one additional marker would be required per segment, thus reducing the total number of markers for this type of scenario from eight down to four.

Some joints, including the knee and ankle, have a superficially embedded bone structure with anatomic landmarks that can easily be palpated. Finding relevant marker positions for indicating an approximated location of these joints' rotation axis is therefore not particularly difficult. However, such methods are less applicable for identifying the rotation axis of joints that are deeply embedded in the body and surrounded by thick layers of soft tissue, as, for instance, with the hip joint, because corresponding anatomic landmarks cannot be palpated so easily.

An additional problem is that, although the location of a rotation axis remains stationary during a static set-up, it can, in a dynamic situation, displace relative to the proximal and distal segment, due to the geometry of the underlying joint structure. Skin movement artefacts, as reported on by Cappozzo 1991 and Cappozzo et al 1996, cause displacements between markers relative to the underlying bone anatomy of up to 40mm. Such movements also have a major influence on identifying rotation axes during

motion, and they are one of the main contributors for introducing errors into the captured data.

Displacements of rotation axes relative to the proximal and distal segment, as well as skin movement artefacts, present problems in motion analysis that are not easy to overcome. Probably one of the most secure methods for tracking the location of the bone anatomy is by using markers mounted onto transcutaneous, bone-embedded rods, as previously described by Levens et al 1948. This requires surgical intervention and represents a highly invasive method that would, in many countries, not be possible due to ethical issues. Using skin-mounted markers is therefore, for the time being, the most applicable method for capturing motion. Despite the fact that tracking displacements of rotation axes still remains difficult, problems associated with skin movement artefacts, however, are less of a worry, as certain methods exist for these to be minimised.

Cappozzo et al 1996 discovered that the displacement of skin-mounted markers is greater when the thickness of tissues covering the bone structure is thin. Using markers for identifying joint centres is therefore likely to introduce large errors into the test procedure due to the joints' superficially located bone structure, which deems this method as fairly unreliable. However, mounting markers onto the middle part of segments should consequently be better, because the tissues are a lot thicker, as is often the case with, for instance, the thigh, so that errors introduced by these markers should be smaller.

Cappozzo et al 1995 elaborated on a static calibration procedure, referred to as "calibration anatomical systems technique" (CAST), with which the position of the joint centres during dynamic set-ups can be determined by using segment-mounted markers only. Apart from problems associated with displacements of rotation axes and skin movement artefacts, the position and orientation of joint-mounted markers should, in relation to the local reference systems of adjacent segments, remain the same during a static calibration procedure. It is therefore possible for the relationship between joint and segment-mounted markers during a static calibration set-up to be mathematically determined, and once the joint-mounted markers were removed, this information can be used to derive their original position from the segment-mounted markers during a dynamic situation.

This became the chosen method for arranging markers and determining rotation axes, whereby the initial procedure for identifying joint centres during static calibration set-ups can be undertaken in two ways. Markers can either be mounted directly onto the joint, which requires a fairly large amount of markers to capture the location of all joint centres. An alternative to this is to use a wand with two markers mounted on it at known distances, for consecutively pointing at each side of all the joint centres.

The procedure with the joint-mounted markers can be disadvantageous, as some markers may be obscured from the cameras' view. However, as the distances between the wand and segment-mounted markers are greater than those between joint and segment-mounted markers, the likelihood for introducing errors into the measurements is higher with the wand and was therefore not considered appropriate for the current study. With regard to the procedure that involves joint-mounted markers, if it was not possible to capture all of them, then the static calibration process needed repeating while the subject in question stood in a slightly different location within the capture volume, so that previously obscured markers fell into the cameras' view.

7.1.4.　　　Customisation of reflective markers

Commercially available markers can be purchased in a variety of sizes and they come attached to a flat, circular base to secure them with double sided tape to persons or objects that need capturing. Because these markers are very costly it was decided to manufacture new markers rather than purchasing ready-made ones, as this seemed a much more economical option to remain within the limits of the research budget, particularly when taking into account the large number of markers that were required.

The construction of the markers' spherical body was based on wooden beads. As explained in Section 5.1.1.5, too small a diameter of markers decreases the recording accuracy, and too large a diameter increases the likelihood for them to obstruct one another from the cameras' view. The chosen diameter was 25mm, which seemed an appropriate size for the required capture volume. Using paper or polystyrene for the markers' body represented a much lighter option to reduce the shaking they experience as a result of their own inertia and elasticity of the skin onto which they are mounted. This therefore should improve the tracking with the ProReflex^{TM} system due to less marker movements. However, the risk of accidentally denting the markers was high and

this would destroy their spherical shape, thus rendering them useless for capturing accurate data, which is why wooden beads represented a more suitable option.

Manufacturing customised markers instead of purchasing commercially available ones appeared to be a method frequently utilised amongst scientists who are involved in capturing motion with equipment for which reflective markers are required. Biomch-L is an internet-based discussion forum that forms part of the ISB website (www.isbweb.org), where a plenitude of ideas exchanged with regard to optimisation of marker constructions is archived. As there is a fairly high interest for alternative solutions, this demonstrates that the prices for commercially available markers and their design characteristics are generally not looked upon favourably. Coating spherical bodies in reflective material seemed to be the main difficulty during the construction of customised markers. The majority of people who sent their comments on this subject to the ISB website used sheets of reflective material, which they cut into individual strips for covering the marker spheres.

This became the chosen construction method during the current study, for which low-cost, self-adhesive sheets were purchased, called Scotchlite^{TM} Reflective Materials from 3M United Kingdom PLC, Bracknell, UK. One way of preventing individual strips from overlapping in order to maintain the wooden beads' spherical shape, is by shaping them elliptically, but this was considered far too complex a procedure. Instead, a paper guillotine was used for accurately cutting out strips of 6mm width, which were glued onto the beads in a regular configuration, as illustrated in Figure 7.2. Although this changed the beads' original shape, the likelihood that reflected light beams deviated from their intended path, due to the overlapping of individual strips, was for most of a sphere's surface therefore similarly low, particularly because each layer measured less than 0.02mm in thickness.

Using double-sided tape for mounting markers directly onto the test-subjects was not an option as their spherical body provided too small a contact area to make them stay securely in their intended location. Also, upon removal, the adhesion of the tape would put the markers at risk of ripping the reflective strips off. One way of mounting the markers was by providing a flat, circular base similar to those attached to commercially available markers. These were made out of 3mm thick semi-rigid leather with a fairly large diameter of 40mm to make them conform to curved surfaces yet provide the

markers with plenty of support that counteracted the likelihood for them to shake during motion of the body. Light-weight aluminium rivets were pushed through the centre of the leather base and jammed into an aluminium tube of approximately 10mm length and 6mm external diameter, which was tightly inserted into the central hole of the wooden beads for connecting them to the leather base. Individual markers, when covered with reflective strips, weighed approximately 5.5g and just over 15g when attached to their leather base.

Figure 7.2:   Configuration of evenly spaced, overlapping, reflective strips
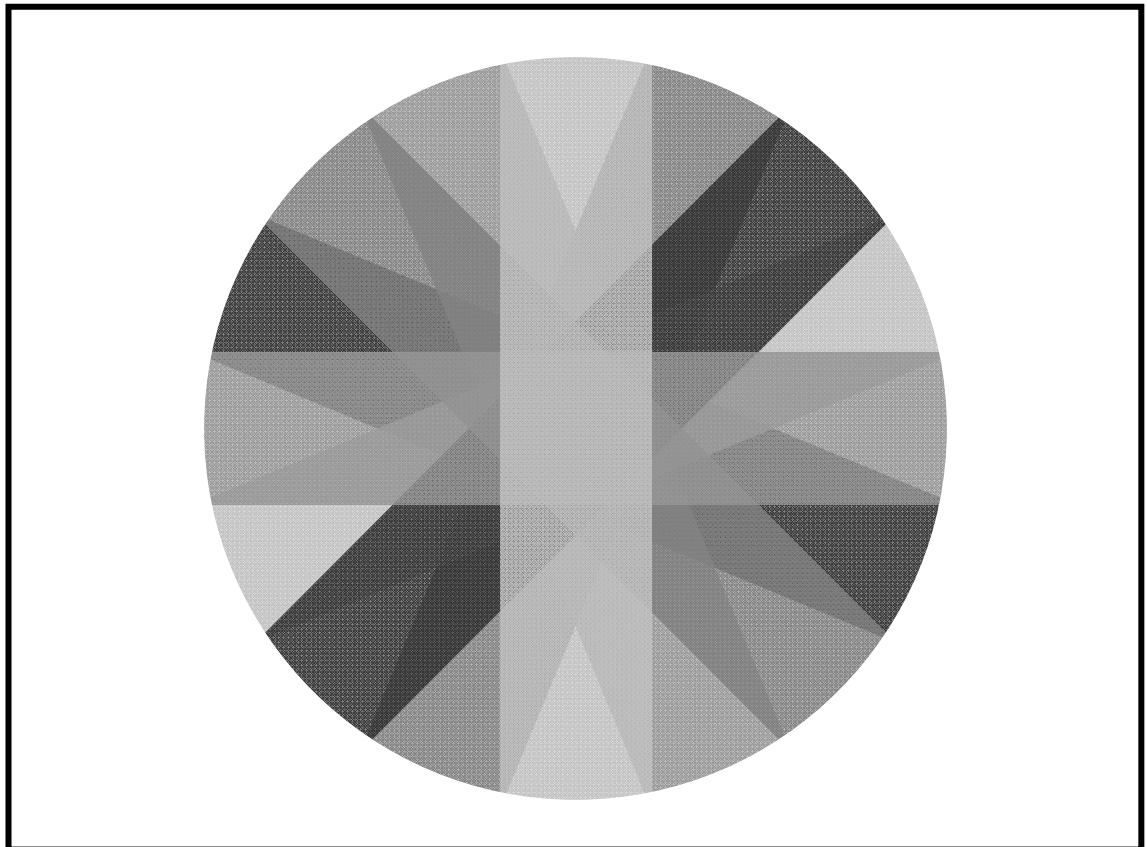
Another way of mounting the markers was by inserting light-weight aluminium extension rods into their central hole to increase the distance between markers and therefore improve their chances for being detected by the cameras. The extension rods were either rigidly attached to the test-prostheses via clamps or fixed with self-tapping screws onto semi-rigid cuffs out of polypropylene. These cuffs can be fastened around the required body segment by using riveted, adjustable fabric belts with spring-loaded clasps. The cuffs contained lightening holes and were lined with a layer of approximately 5mm thick plastazote, a closed-cell polyethylene soft foam, to improve comfort during skin contact.

The shiny surfaces of aluminium rods, clamps and polypropylene cuffs were at risk of being mistaken for a marker by reflecting infra red beams back to the cameras. This is why they were sprayed with matt, black paint, as with the cam and transducer mountings previously described in Section 6.1.2.6.

7.1.5. <u>Markers for the pelvis section</u>

The pelvis area is fairly wide and, compared to the thigh, shin and foot sections, it undergoes motion of much smaller magnitudes, because it does not have to swing back and forth, so that less marker clustering and displacement consequently improves marker detection. Co-ordinates from markers just below the waist not only identified the pelvis, they were also necessary for deriving the hip joint centres from. It was decided not to have any more markers than the absolute minimum required for defining a segment's local reference system, namely three non-co-linear markers, as explained in Section 7.1.3. Nevertheless, the likelihood for detecting all of them was considered high, because of the aforementioned reasons concerning less pelvis marker clustering and displacements.

Despite the discovery by Cappozzo et al 1996, described in Section 7.1.3, that the displacements of skin-mounted markers are greater when the thickness of tissues covering the bone structure is thin, this was not considered applicable for the identification of the pelvis. The reason for that was, because breathing and filling of the bladder over the course of the gait laboratory tests were factors likely to increase skin movement artefacts, as those physiological effects predominantly influence areas around the abdomen where layers of soft tissues are thick. The three pelvis markers were therefore located on bone prominences, despite the findings by Cappozzo et al 1996. Bone prominences that are quite easy to palpate, even in moderately obese people, are the sacrum and the left and right anterior superior iliac spines (ASIS).

The concavity created by the lumbar lordotic curvature may slightly conceal a skin-mounted sacral marker, so the likelihood for its detection was increased by attaching it onto a cuff-mounted extension rod. Measuring approximately 150×200mm, the sacral cuff carried an extension rod that located the centre of the sacral marker approximately 150mm away from the skin. A single, riveted, adjustable fabric belt with one anteriorly located, spring-loaded clasp provided a means for fastening the cuff around the pelvis area. Its two stitched-on, adjustable, fabric shoulder straps and pieces

of double-sided tape glued between the belt and all three bone landmarks helped to ensure that the sacral cuff and belt would not migrate distally in response to a prominent abdomen. After adjusting the belt and straps, any additional lengths were secured in place with safety-pins to prevent them from dangling loosely. The cuff with its belt, two shoulder straps and single extension rod weighed only approximately 400g. Its structure is illustrated in Figure 7.3.

Figure 7.3:   Sacral cuff with extension rod, shoulder straps and belt
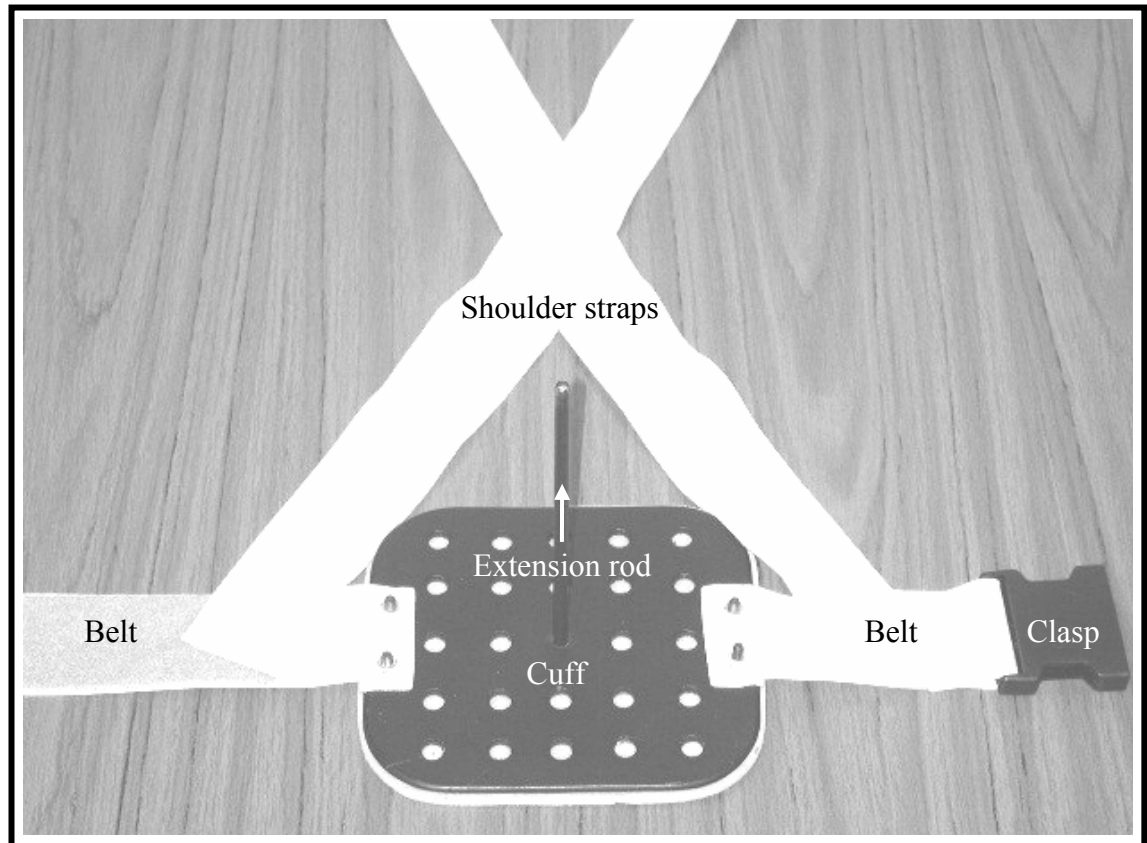
Marks made with a ball pen indicated the apices of the two ASISs and the centre of the sacrum at the height of the posterior superior iliac spines (PSISs), to ensure that the markers were correctly located. Once fastened around the pelvis area, the fabric belt with its stitched-on velcro hooks also served as an attachment for the two ASIS markers, which were mounted by using counterfitting velcro loops on their leather base. Preliminary trials proved that the visibility of all three markers was satisfactory. As the radio telemetry transmitter, described in Section 6.1.1.2, was supposed to be worn around the waist, there was no danger for this to interfere with either the sacral or ASIS markers. The three markers that define the local reference system for the pelvis section are illustrated in Figure 7.6 to Figure 7.8.

7.1.6. Markers for the thigh and shin section

Although using the bare minimum of markers might be an applicable solution for the pelvis, in other cases it might be better to have more than that, because if, for whatever reason, only two markers were detected, then the required calculations for determining a segment's position and orientation in 3D within the global reference system would be impossible. The thigh and shin sections are narrower than the pelvis area, but, compared to the foot, still relatively large, which allowed markers to be spread out, so that they were not clustered and therefore more likely to be detected by the cameras. Despite good exposure, using four rather than only three markers on each thigh and shin section seemed, due to the lower limbs' relatively quick swinging action, more secure, as it provided a spare marker in case one of them disappeared from view. In addition to the need for identifying every segment, making sure that at any point in time there would always be at least three markers was also necessary, because the knee and ankle joint centres were derived from marker co-ordinates of the thigh and shin sections, respectively. If all four rather than just the necessary three markers were detected than one of them was ignored during the subsequent data processing.

Cuffs, onto which extension rods were fixed, needed to be securely fastened around their corresponding body segment. However, due to their conical appearance, the shape of the thighs made it difficult to fasten cuffs around, as circumferentially tightened belts developed the tendency to migrate distally. Using extension rods for attaching markers to the thighs was consequently not only impractical due to lack of grip from the suspension, their protruding appearance also interfered with the pendulum action of the arms. It was therefore considered more appropriate to use the flat, circular leather bases for attaching markers directly onto the skin with double-sided tape.

Preliminary trials proved that the visibility of each thigh section's four markers was satisfactory when two of them were located anterior-proximally and anterior-distally and the other two located posterior-proximally and posterior-distally. An abundance of body hair can make double-sided tape, used for bonding the leather bases onto the skin, come loose, particularly when the skin moistens as a result of perspiration. To ensure that all the markers remained in place, additional tape was circumferentially strapped around the thighs, which was elastic for expansion in response to contracting and bulging muscles. All the surfaces that tapes needed to adhere to were cleaned with surgical wipes prior to mounting the markers, as oily skin can otherwise prevent the

tapes' adhesive substances from bonding. However, the amount of adhesion was not excessively strong, so that the removal of markers after completion of the gait laboratory tests could be undertaken quite easily without creating discomfort.

Mounting the markers onto the shin sections was, unlike the scenario with the thighs, comparatively simple. Not only did the arms not reach far enough distally for their pendulum action to interfere with any equipment located at that level, the shape of the non-amputated side made it possible for one riveted, adjustable, fabric belt with a spring-loaded clasp to be fastened just proximal, and a second just distal to the bulbous calf muscles. That way, the cuff-mounted extension rods could be securely held in place. Preliminary trials proved that the visibility of the non-amputated side's four markers was satisfactory when two of them were located anterior-laterally and posterior-laterally and the other two located laterally and lateral-distally. The entire calf cuff with its two belts and four extension rods, which located the centre of markers approximately 90mm away from the skin, weighed only approximately 180g. Its structure is illustrated in Figure 7.4.

Figure 7.4:   Calf cuff with extension rods and straps
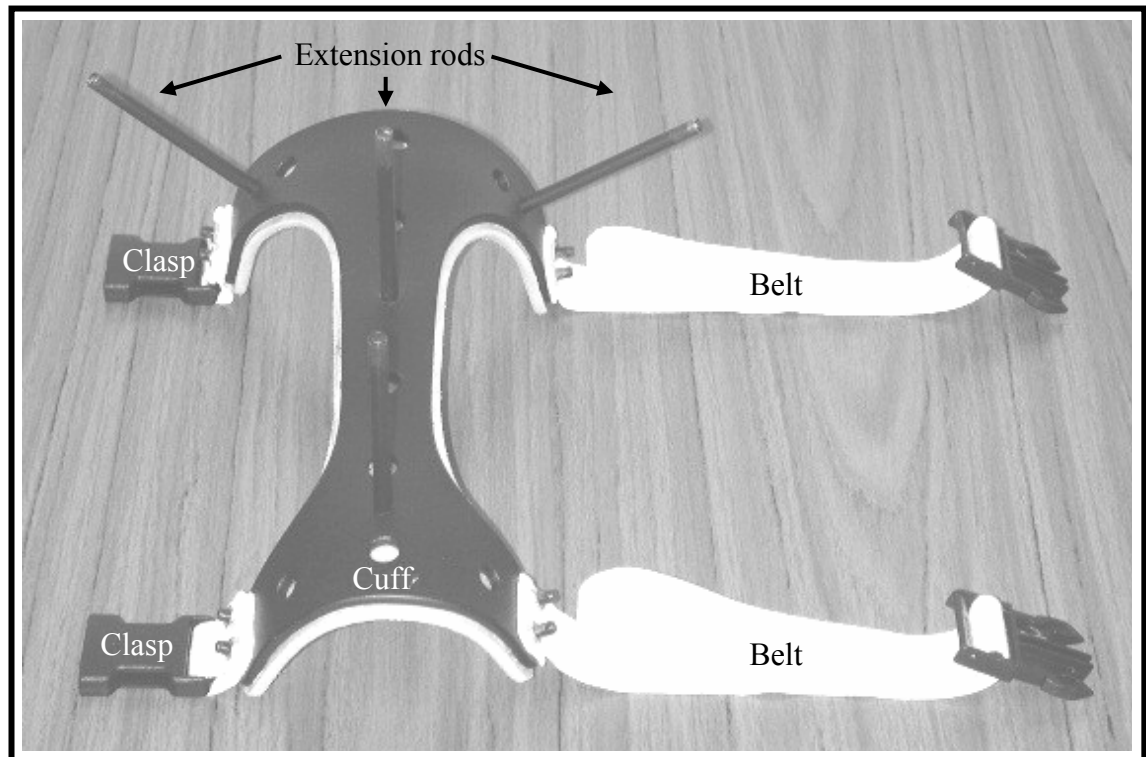
Extension rods were also used for the shin section of the amputated side, but instead of strapping a cuff just proximal and distal to the socket, it seemed even more secure for

all four extension rods to be bonded into a clamp. This clamp was, with its four equidistantly space grub screws, bolted around the PyraLok, previously described in Section 4.1.4.2. While the clamp took up part of the PyraLok's outer housing, its body obstructed the lock's release button, which therefore needed reducing in size, so that it could extend past the clamp, as it would otherwise not be possible to doff the test-prostheses without having to take the clamp off first. Covered with lightening holes, the prosthesis clamp and four extension rods weighed only approximately 80g. Its structure is illustrated in Figure 7.5.

The cam and displacement transducer mountings were, as explained in Section 6.1.2.7, located at the anterior aspect of the test-prostheses, which made it impossible for the extension rods to be positioned in the same place simultaneously. Also, medially orientated extension rods would interfere with the contra lateral non-amputated side. Therefore, the clamp needed aligning in such a way that the four markers were located lateral-proximally, lateral-distally, posterior-proximally and posterior-distally.

Figure 7.5: PyraLok-mounted prosthesis clamp with extension rods
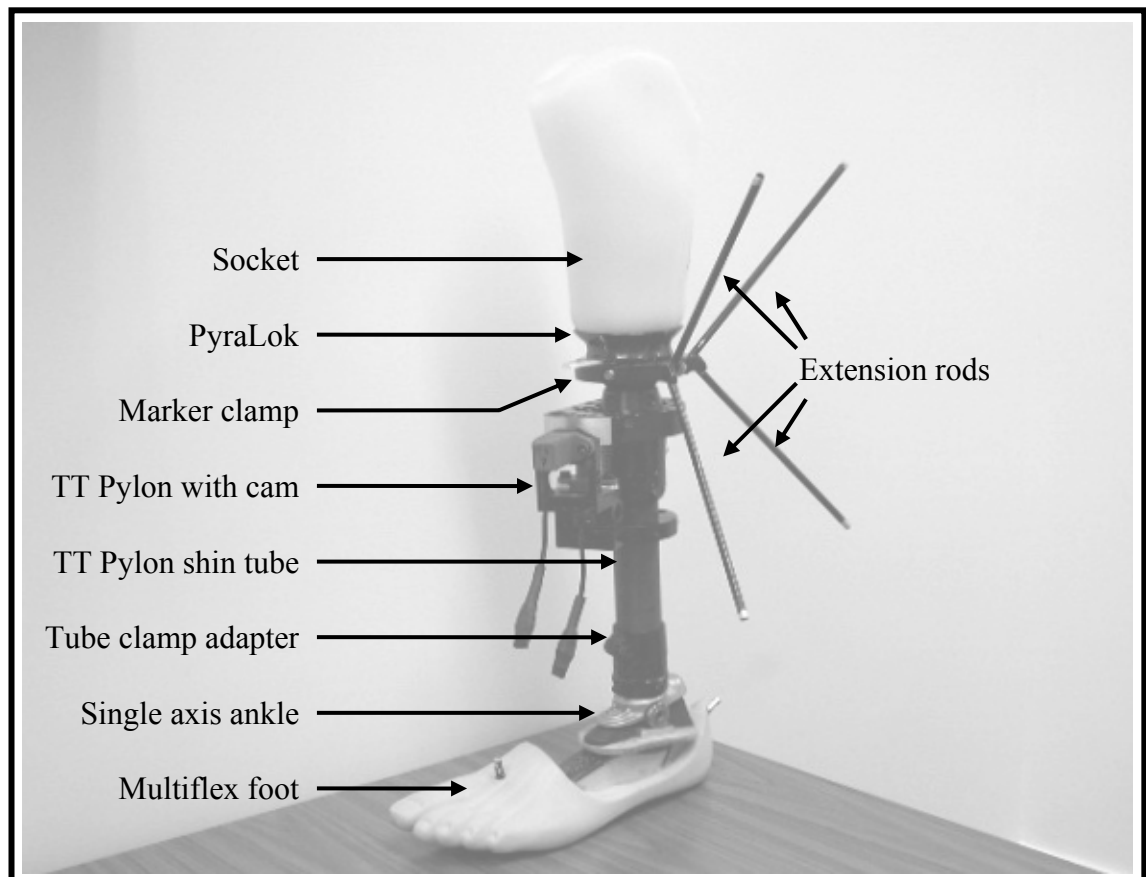
Unlike extension rods for the non-amputated shin section, which were near perpendicular to the skin, the design of the clamp required the extension rods for the test-prostheses to be orientated obliquely with respect to the shin tube. A distance of approximately 90mm between the centre of markers and the skin seemed, as explained before, appropriate for the non-amputated shin section. Therefore, the centre of markers on the amputated sided were located at approximately the same distance from the shin tube. This meant that the extension rods needed to be even longer due to their oblique orientation. The final location of the markers relative to the test-prostheses turned out to work favourably in conjunction with the ProReflex^{TM} system, as the visibility of the markers was satisfactory. The four markers that define the local reference system for each, the two thigh sections and the two shin sections, are illustrated in Figure 7.6 to Figure 7.8.

7.1.7.   Markers for the foot section

Because the foot is the last division in the chain of lower limb segments, its marker co-ordinates were solely required for determining its local reference system and not for any other purpose, such as the derivation of another joint centre. Failing to detect at least three markers would be unfortunate, but, compared to the thigh or shin sections, less crucial for the overall calculations. Using only the minimum amount of markers was therefore justifiable, particularly because an additional marker would cause clustering. This clustering would decrease the likelihood for detecting the other markers due to the foot's relatively small surface, thus negating the reason for mounting an additional marker in the first instance. In fact, only two instead of three markers needed mounting onto the foot, as the ankle joint centre, which was to be derived from the marker co-ordinates of the shin section, remained part of the foot. The ankle joint centre therefore represented the required third set of co-ordinates for calculating the foot's third axis of its local reference system.

The two foot-mounted markers needed to be separated as far away from one another as possible to maximise their visibility. Although some movement was likely to take place between the forefoot and hindfoot, the magnitude of this motion was considerably small, particularly when compared to the amount of displacement that takes place between the toes and forefoot. To obtain accurate measurements with regard to motion of the combined forefoot and hindfoot, it was therefore vital not to attach any of the two markers to the toes, as large quantities of toe displacements would otherwise introduce

errors into the data. It was decided for one of the markers to be attached to the centre of the heel's posterior aspect. This meant that the other marker had to be located at the junction between the forefoot and toes in order to be furthest away from the heel marker. Locating it fairly centrally on the dorsal aspect of the foot improved its visibility. The appropriate location for this was determined to be between the second and third metatarsal head.

As mentioned in Section 4.1.6.6, the subjects were not supposed to wear a shoe on their test-prosthesis, but they needed to wear one on their sound side. Using double-sided tape for gluing the required two markers to each shoe and prosthetic foot did not seem to ensure that they stayed on, which is why alternative and more secure methods of suspending those markers were required.

To make the test conditions as uniform as possible, several pairs of standard training shoes were purchased, so that each subject's anatomic foot could be dressed with the same shoe type of suitable size. Because these were not the subjects' own property, adapting the shoes, for fastening the markers on, was acceptable. Punching a hole where the markers were supposed to be located made it possible for a bolt and nut to sandwich the shoe's outer fabric cover, so that the two markers could be threaded onto their respective, outward protruding bolt. Despite this adaptation, the inside of the training shoes remained smooth as the countersunk bolts were squashed into the plush fabric cover. A similar method was used for the prosthetic feet, except that the bolts were not secured with a nut, but threaded directly into specially drilled holes at the appropriate locations that could be identified from the feet's outer foam cover. The two markers that define the local reference system for each foot section are illustrated in Figure 7.6 to Figure 7.8.

7.1.8. Markers for the hip joint centre

The hip joints are, as described in Section 7.1.3, deeply embedded in the body and surrounded by thick layers of soft tissue that make it difficult to palpate bone prominences located in the joints' vicinity. A number of methods exist for estimating the position of the hip joint centre. Probably one of the most accurate procedures was described in a publication by Seidel et al 1995, who conducted tests with de-fleshed pelves from thirty male and thirty-five female cadavers.

Dimensional boundaries of the pelvis were stipulated as the straight distance between both ASISs for pelvis width, the oblique distance between an ASIS and PSIS of the same side for pelvis depth and the perpendicular distance between the pubic centre and the inter-ASIS line for pelvis height. As the average depth of the acetabulum turned out to be approximately 49% of its own diameter, Seidel et al 1995 concluded that the shape of this bone concavity is hemispherical, which implied that the hip joint centre must be positioned in the centre of it.

Using the dimensional boundaries of the pelvis, the exact location of the hip joint was described as 14% of pelvis width medial, 34% of pelvis depth posterior and 79% of pelvis height inferior relative to the corresponding ASIS, with a mean error of 58mm, 30mm and 35mm, respectively. However, it was also possible for the hip joint location to be related to pelvis width alone as 24% posterior and 30% inferior to the corresponding ASIS with a mean error of 49mm and 75mm, respectively, whereby the medial offset remained obviously the same. This demonstrated that, by using solely the pelvis width for determining the hip joint centres, the error is 19mm larger in anterior-posterior direction and 40mm larger in proximal-distal direction, so that this method should only be used if really necessary. The ratio between pelvis width and the hip joint centre location in all three directions varied by only 1% between male and female pelves without any statistically significant differences.

Establishing the pelvis width seemed to be straightforward. This could easily be achieved by using markers located on both ASISs. As previously described in Section 7.1.5, two of the three markers for identifying the local reference system of the pelvis were already located there.

In turn, establishing the pelvis depth, in the same way Seidel et al 1995 did, seemed challenging, because the PSISs are not necessarily easy to palpate, thus making their identification with reflective markers difficult. The sacrum, however, is easier to palpate, and the fact that its posterior aspect is located slightly further anterior than the PSISs makes measurements of the oblique distance between the ASISs and the sacrum represent a fairly close approximation of the oblique distance between the ASISs and corresponding PSISs. As described in Section 7.1.5, the sacrum was identified by a marker that was mounted onto an extension rod. Therefore, determining the location of the sacrum was undertaken by measuring the perpendicular distance between the

inter-ASIS line and the sacral marker minus 150mm for the extension rod. Knowing the co-ordinates of all three pelvis landmarks, the depth of this segment could be determined.

Establishing the pelvis height during the gait laboratory tests was considered inappropriate, as this either required measurements to be taken manually or by placing a marker on the pubic centre for calculating the perpendicular distance from there up to the inter-ASIS line. Both methods deemed unacceptable as they were too invasive. Despite less accurate results when calculating the inferior offset of the hip joint centre as a percentage of pelvis width, this became, because of the aforementioned reasons, the chosen method for relating each hip joint centre position to its corresponding ASIS.

As explained previously, the markers for identifying the local reference system of the pelvis section were the same in number and in the same location as those required for determining the hip joint centres. Therefore, there was no need to use additional, temporary markers during the static calibration process for this body segment. The three markers from which both hip joint centres can be derived are illustrated in Figure 7.6 to Figure 7.8.

7.1.9.   Markers for the knee joint centre

The anatomic knee is not just a single axis, but a polycentric joint that, in addition to its main degree of freedom in the sagittal plane, also allows some movement in the coronal and transverse plane (Williams et al 1989). During motion at the knee, the medial and lateral femoral condyles slide relative to the tibia. Due to difficulties in tracing the displacement of rotation axes during motion, as explained in Section 7.1.3, it was decided that both condyles become the location for the knee joint markers during the static calibration process.

Because the femoral condyles are relatively large in size, the markers' precise location needed further identification. Tibiale is "the most proximal point on the medial margin of the head of the tibia", and the sphyrion is "the distal tip of the tibia", as explained by De Leva 1996. This author suggested that the position of the knee joint markers in proximal-distal direction should be determined as 7.4% of the distance between the tibiale and sphyrion proximal to the tibiale. In anterior-posterior direction, the markers' position should be located on the most prominent aspect of the femoral condyles. This

way of identifying the knee joint centre was the method adopted for the current investigation. Having determined the marker location for the knee joint centre on the medial aspect of the knee, the marker location for the lateral aspect of the knee was assumed to be at the same height from the ground as the medial marker location.

On the amputated side, the distal aspect of the tibia was missing. It was therefore necessary to use the measurement taken on the sound side regarding the distance between the tibiale and sphyrion in order to determine the marker location on the amputated side. Also, unlike the marker positions on the sound side, which could easily be identified, this was not the case for the amputated side, as most parts of the knee were inside the socket. Therefore, prior to wearing the prosthesis, a straight ball pen line was drawn of known length that originated where the markers would be if they were placed directly onto the skin. This line reached far enough proximally to extend beyond the area on the thigh where the trimlines of the socket would be. After donning the test-prosthesis, the marker positions were retraceable with a ruler for identifying their position on the outside of the socket where they were then mounted in their corresponding position.

For both the sound and amputated side, all four knee joint markers were attached with double-sided tape. The actual joint centres were then calculated as the distance mid-way between each medial and lateral marker. The four markers from which both knee joint centres can be derived are illustrated in Figure 7.6 to Figure 7.8.

7.1.10.   Markers for the ankle joint centre

The anatomic ankle is, like the knee, not just a single axis but a polycentric joint. It allows motion in all three planes with its main degree-of-freedom in the sagittal plane (Williams et al 1989).

Following roentgen stereophotogrammetry of the ankle or talo-crural joint, Lundberg et al 1989 discovered that the orientation of its axis constantly changes during movements. They also discovered that throughout those changes the axis remained close to the mid-point between the apices of both malleolei. Although it may not be possible during the gait laboratory tests to trace the orientation of the rotation axis, it did seem, however, feasible to locate its position. This could be done fairly accurately, because attaching the two ankle markers to the medial and lateral malleolei and calculating the

actual joint centre as the distance mid-way between both markers would therefore locate the axis in a position similar to the one identified by Lundberg et al 1989.

Compared to the anatomic ankle, determining the COR on the ankle of the test-prosthesis was even easier. This was because the markers could simply be mounted onto the central axle of the single-axis joint, described in Section 4.1.6.5.

For both the sound and amputated side, all four markers were attached with double-sided tape. As explained previously, the actual joint centre on the sound side was calculated as the distance mid-way between each medial and lateral marker, and this was also the case for the amputated side. The four markers from which both ankle joint centres can be derived are illustrated in Figure 7.6 to Figure 7.8.

7.1.11. Summary of dynamic and static set-ups

Three markers were used for identifying the pelvic section, four for each thigh and shin section and two for each foot section. Therefore, the total number of markers during dynamic set-ups added up to twenty-three. The way they were configured is displayed in Figure 7.6.

The illustration in Figure 7.7 shows the marker positions during a dynamic set-up, as viewed in QTM after the digitisation process was completed. Differently shaded discs represent the location of various marker groups for each lower limb section. Linear lines between discs are the bones, described in Section 5.1.1.9, that give the viewer a better orientation around the otherwise more or less featureless image. Obtaining a better orientation was also made easier by displaying a grid, which represents the floor of the capture volume. Non-linear lines represent the markers' trajectories that help to identify where marker segments might be missing.

The displayed image was obtained from recordings of one of the ten recruited test-subjects. The discs that represent the markers within that image are orientated in such a way as if to see the subject from his anterior, right-hand perspective. This was similar to the orientation that was used to show the same subject's walking performance inside the gait laboratory, as displayed in the top right hand corner of Figure 7.7.

Figure 7.6:   Schematic representation of marker configuration
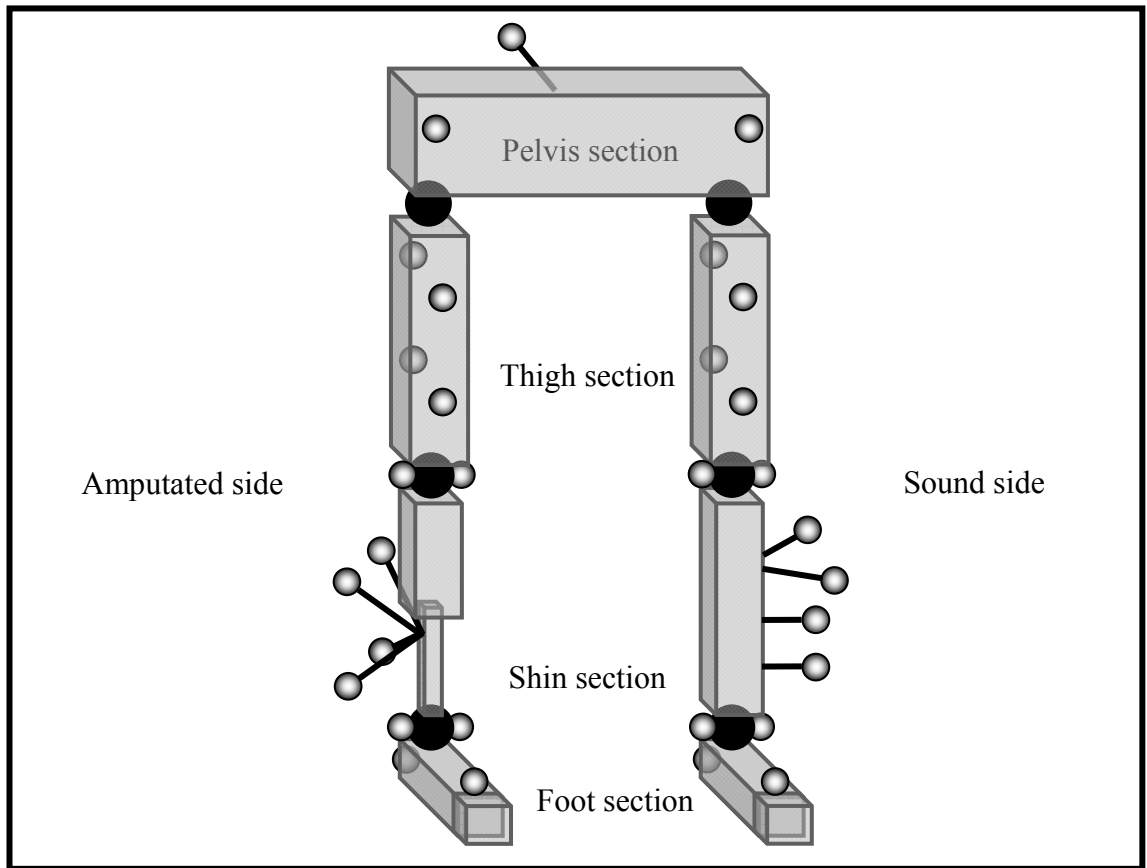
Figure 7.7:   Digitised marker positions during dynamic set-ups
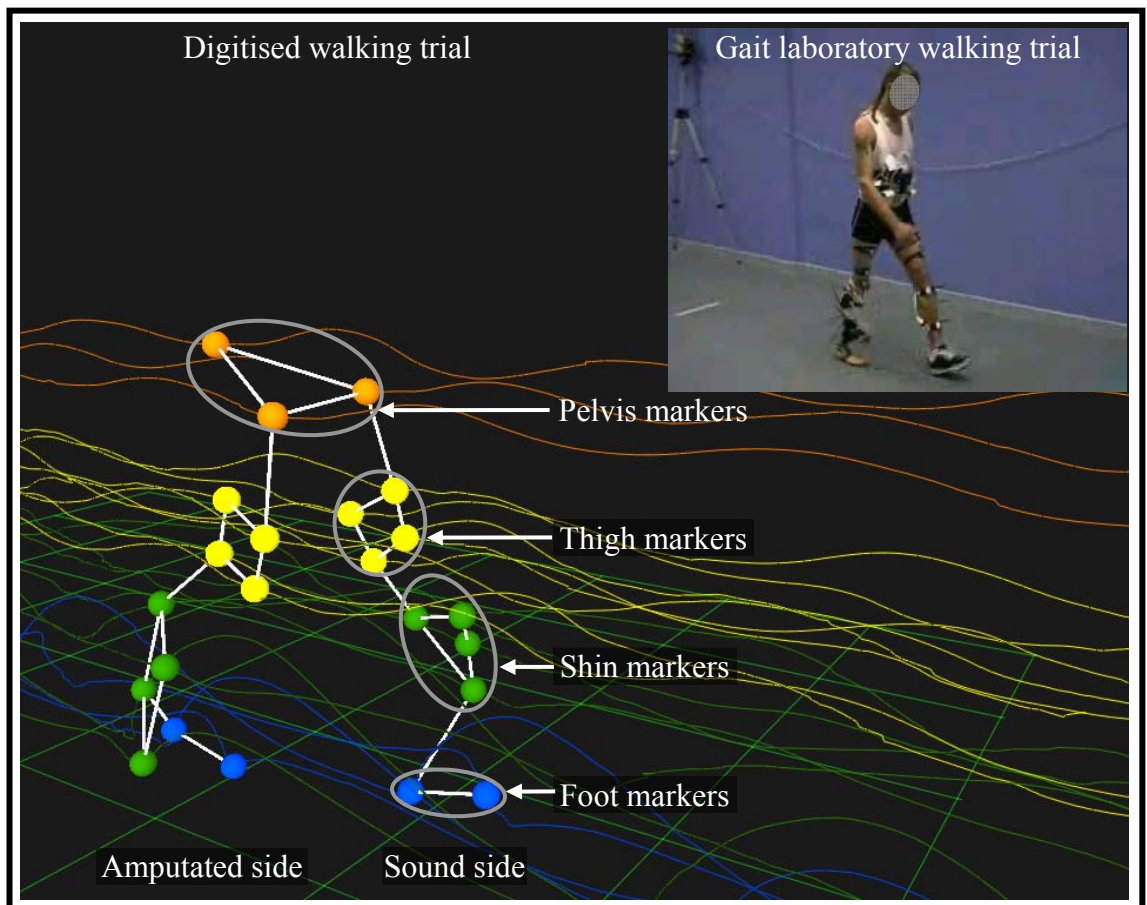
The number of markers that were required for static set-ups was obviously greater compared to dynamic set-ups, as additional markers were required to identify joint centres. Although this was not necessary for the hip, two extra markers were needed for each knee and ankle joint. Therefore, the total number of extra markers added up to eight, thus making it, together with those twenty-three markers from dynamic set-ups, on overall of thirty-one markers. Static calibrations were undertaken while the subjects stood still. This is why the image, illustrated in Figure 7.8, displaying marker configurations for the calibration set-up does not show any marker trajectories. Both the subject and the perspective of this image were the same as in Figure 7.7.

Figure 7.8:   Digitised marker positions during static set-ups
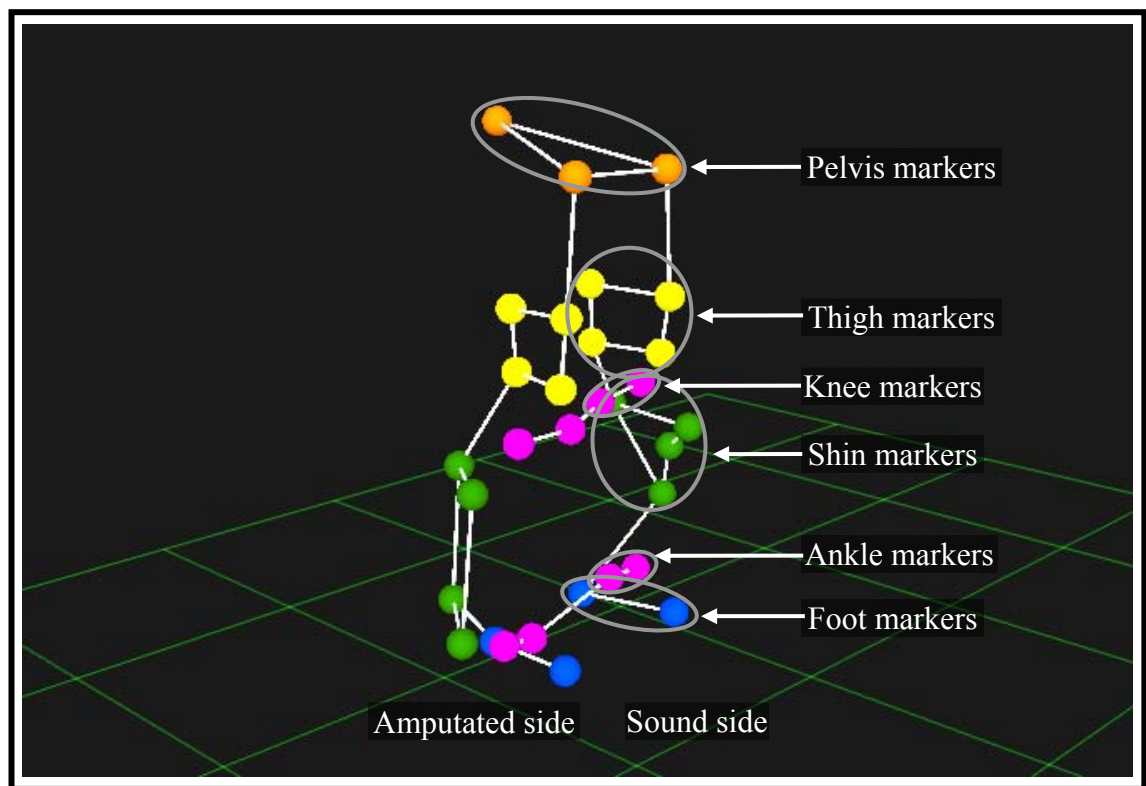
7.2.   Conduct of gait laboratory tests

7.2.1.   Introducing the subjects

Every time an appointment was made for a subject to be tested, the gait laboratory was prepared the day before to ensure that all the equipment was in good working order and set up properly, and that all the cables were either removed from the floor or taped down for safety reasons. The force sensors needed to be conditioned, as described in Section 6.2.3.1, to improve the quality of their output, which was undertaken just prior to the tests. Only one subject was invited per test-day, as the time interval between the

arrival and departure of an attending subject was estimated to be around four hours. Once inside the gait laboratory, the subjects were familiarised with the test-procedure, so that they felt comfortable and were aware of events throughout the entire session.

While the subjects were still wearing their own prosthesis, they were asked to practise walking along the path where the force plates were embedded, because one of the important factors during the tests was to step accurately within the boundaries of each plate, as described in Section 5.1.2.2. After they established a starting position that allowed them to perform the required task with regular step lengths, the location of this position was marked with a piece of tape on the floor, so that they could repeat the same walk over again. Once happy with their performance, they were guided to an area within the gait laboratory that was allocated only to them, where they could get changed, in private, behind a partition.

7.2.2.   Preparing the subjects

All the clothes and the shoe for their sound side were, as explained in Section 4.2.5, provided for them. Around their torso they wore a vest that was thin enough to prevent them from getting too hot while performing their walking tasks. As the lower limbs needed exposing to have the reflective markers, described in Section 7.1.6, mounted onto them, the subjects were asked to wear a pair of shorts that were cut high enough to show most of the thighs. Some subjects wore boxer shorts, which were too big to fit underneath the shorts and therefore needed to be exchanged against a pair of snug fitting underpants instead. Standard socks had to be removed and, rather than wearing nothing, they were swapped for a very short sports sock. This prevented the subjects from perspiring excessively inside the customised training shoe, described in Section 7.1.7, and also ensured that the ankle and shin section of the sound side was completely exposed.

Once fully dressed, the previously sterilised Iceross liner was donned in a standard fashion, as described in Section 2.5.2.1. This procedure was made easier by applying talcum powder to the side of the liner that is away from the skin to make the overlapping walls slide relative to one another while the liner was rolled onto the residual limb. With the distal, notched pin, described in Section 4.1.4.5, securely threaded into the liner, the subjects were asked to push their residual limb into the socket of their customised test-prosthesis. This was followed by standard alignment

procedures, previously outlined in Section 2.6. These alignment procedures were undertaken by the author of this thesis, who is an experienced prosthetist, to ensure that the subjects felt comfortable and the test-prosthesis functioned in the required manner. With the set-up of the test-prosthesis optimised, all the connections and adjustment facilities were tightened up for safety purposes.

In addition to the time the subjects had during the alignment procedure, they were given a few extra minutes to get even more familiar with their new artificial limb. However, this was the maximum time allowance available, as the overall duration of the entire testing session was already very long, and it was not desirable for the subjects to prolong their stay even further. An extended walking practice over the duration of a few days or more would have been ideal, but this meant that the subjects had to take their test-prosthesis home. This was, due to the customisation of components, not possible, as liability factors, previously outlined in Section 4.1.1, had to be taken into consideration.

As all the subjects were used to wearing a locking liner, the main difference between the test-prostheses and their own artificial limbs was the Multiflex foot, described in Section 4.1.6.5, with its adapted single axis ankle. The other aspect that made the test-prostheses different was the TT Pylon and the displacements it permitted. However, these newly introduced motions were the subject of this investigation, and unfamiliarity was not considered to be detrimental, as this meant that the volunteers were still objective towards the TT Pylon. In fact, neither of them ever tried this component before. The reason for most of the subjects to participate in the tests was curiosity, because they were keen on experiencing the influence of motions at the TT Pylon on their gait pattern. If they consider it to be beneficial, the possibility exists that their consultant might agree to prescribe such a device to have it installed into the subjects' own prostheses.

The next stage was to equip the subjects with all the required measuring devices. This meant that the test-prosthesis and Iceross liner had to be taken off again, so that the six FlexiForce® sensors, described in Section 6.1.3.5, could be positioned directly onto their respective landmark. Each sensor was fixed in place with adhesive tape, which needed to be located next to the sensing area and not directly on it, as this might otherwise affect the output of the sensors. With all of the sensors securely positioned, the Iceross liner was carefully rolled over the fixed sensors and back onto the residual limb, so that

the test-prosthesis could be donned again. Once fully on, it was necessary for only the proximal aspect of the Iceross liner to be rolled distally and down to a level just low enough to expose the sensors' standard Berg connectors.

Figure 7.9: Fully equipped test-subject

Anonymity cover

Shoulder straps

Vest

MT8 transmitter

Pelvis markers

Shorts

Inter-junction box cable

Thigh markers

Shin markers

Cam system

Training shoe

Foot markers
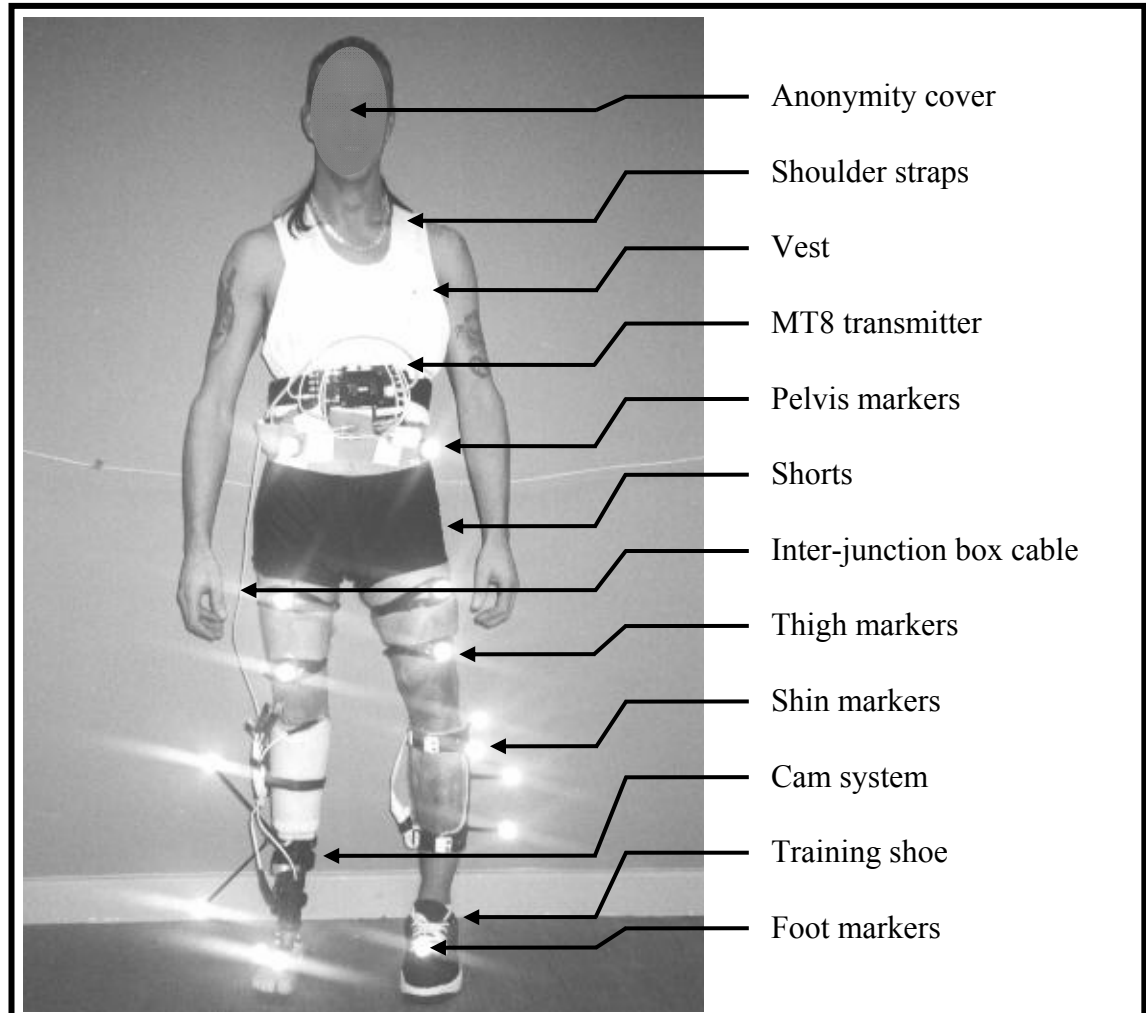
Having mounted the cam device, described in Section 6.1.2, with all its components into their corresponding positions, the force sensors and displacement transducers could be plugged into their respective Futuba Servo connectors. After that the junction box, described in Section 6.1.4.2, was taped just distal to the socket's lateral trimline. Fully recharged batteries were connected to both the MT8-mounted junction box and the telemetry transmitter, described in Section 6.1.1.2, so that they could be strapped together and fastened around the subjects' waist. With the marker cuffs in place, all thirty-one markers, including those for the static calibration procedure, were positioned in their respective locations, as elaborated on in Section 7.1. Safety pins secured excess lengths of straps and a check list was ticked to ensure that all the equipment was where it belonged. Figure 7.9 shows one of the ten subjects with all the equipment mounted into place. The

bright spots in the image are flashlight reflections from markers, which demonstrates how highly reflective the markers were.

7.2.3. Preparing the tests

The next step was to switch on the MT8-mounted junction box. With all the electronic circuitry fully operational, the variable resistors could be adjusted for optimising the force sensors' output gain, as elaborated on in Section 6.1.4.4. Also, having positioned the calibration frame and all six cameras in their required location and adjusted all the parameters within QTrac Capture, the ProReflex^{TM} system, described in Section 5.1.1, was ready to be calibrated.

In order to relate data obtained from the force plates to those from the ProReflex^{TM} system, it was necessary to determine the plates' position within the capture volume. For this, eight markers were distributed in such a way that both plates had one of them in each corner, as displayed in Figure 7.10, which is an illustration of the digitised plate markers viewed in QTM. The recordings could then be used to express the plates' position as co-ordinates within the global reference system.

Figure 7.10:   Markers for determining the force plates' location
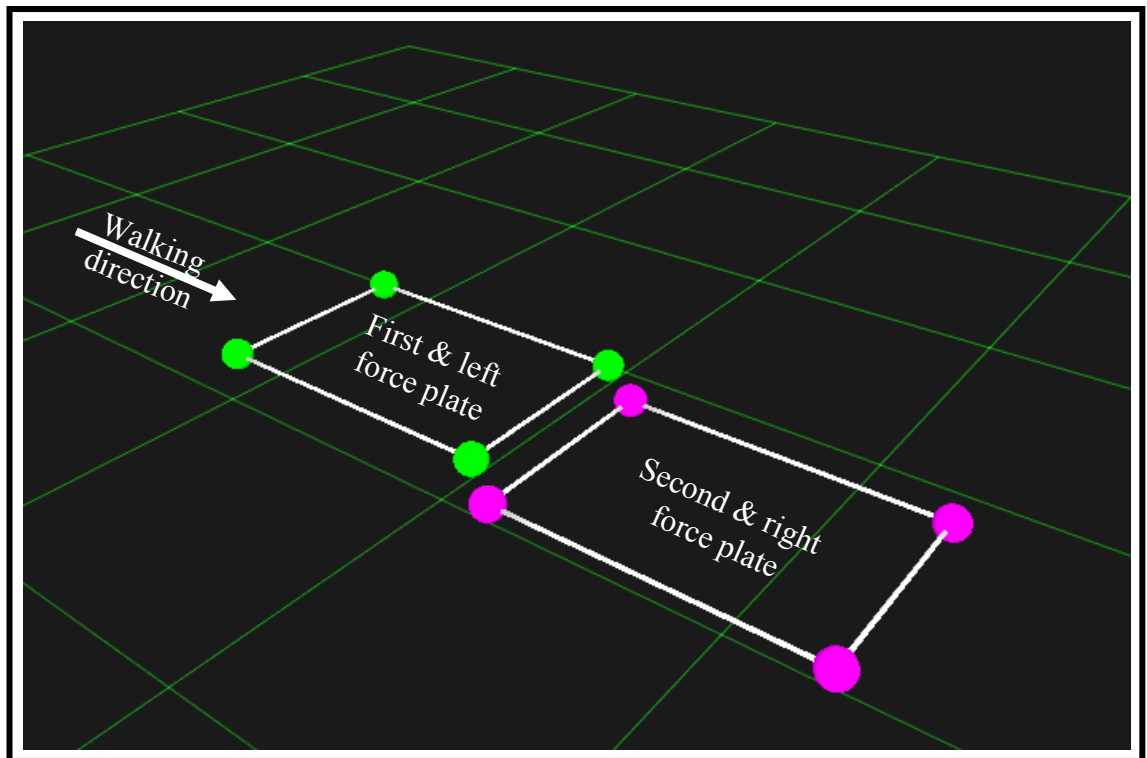
Having recorded and then removed the plate markers, the subjects were asked to step into the centre of the capture volume for undertaking the static calibration procedure, while all twenty-three segment markers and eight joint markers were in position. Recordings were taken at 100Hz over 1s, during which the subjects were supposed to stand in a normal, upright posture, so that the captured angles at the hip, knee and ankle could later be referred to as the joints' neutral position. Once it was checked that all thirty-one dynamic and static markers were detected, the eight joint markers could be removed again. While the subjects were fully equipped, they were asked to stand on one force plate for the purpose of weighing them, as previously explained in Section 4.2.5.

7.2.4.   Conducting the tests

The effects that transverse rotation and longitudinal translation have on the gait of the recruited subjects were to be established by permitting these motions separately, together and neither of them, as stipulated in Section 3.6. This added up to a total four different set-ups.

Chances that not all of the recordings could be considered appropriate for inclusion in subsequent data analyses were high, because of reasons including a visually unstable or unusual appearing walking pattern, a foot not stepping entirely within the boundaries of its force plate or the subjects themselves feeling they made a mistake. Notes were taken throughout the entire recording session to nominate trials of sub-standard calibre. Taking twenty recordings during each set-up appeared a reasonable figure. Therefore, after discarding recordings obtained from low quality performances, the number of useful trials would not be lower than ten, because this was, from the statistical point of view, deemed the necessary amount of data collections per set-up.

None of the subjects previously experienced walking on a prosthesis with the TT Pylon or similar adapter incorporated. This is why the initial set-up was based on restricting both transverse rotation and longitudinal translation simultaneously, as this made the test-prostheses feel most similar to their own artificial limb, due to absent motion at the adapter. The second set-up was based on permitting transverse rotation and restricting longitudinal translation, the third on restricting transverse rotation and permitting longitudinal translation and the fourth on permitting both transverse rotation and longitudinal translation simultaneously, as illustrated in Figure 7.11.

Figure 7.11:   Illustration of set-ups and order in which they occurred
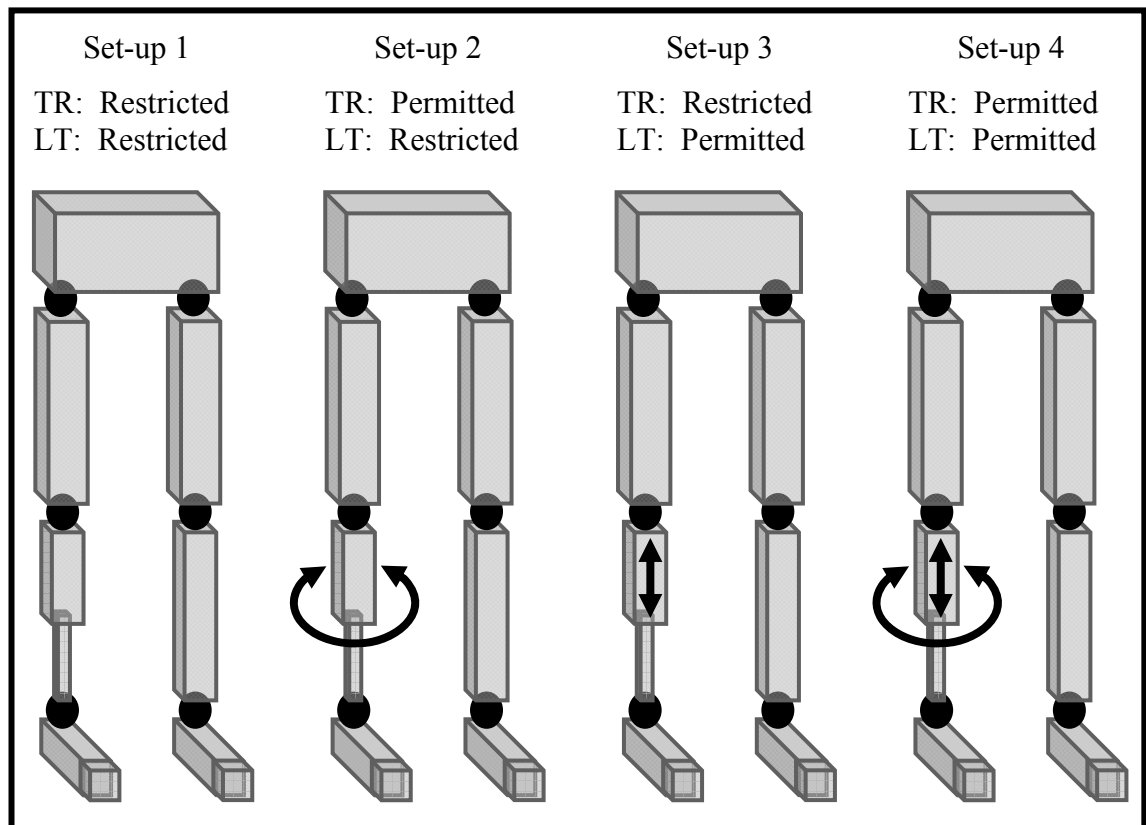
The actual gait laboratory tests were recorded at 100Hz over the duration of 6s. While the subjects stood where the starting position, identified in Section 7.2.1, was marked with a the piece of tape, a verbal prompt was given as soon as the QTrac Capture was ready for taking recordings. This prompt was the signal for the subjects to commence walking at a self-selected, comfortable speed. Once they were the length of approximately one gait cycle away from the first force plate, the person operating the recording systems pressed a trigger that started the data capturing process. After 6s the recordings automatically stopped and the subjects had time to walk back to their starting position.

It was considered good practice to check the first recording of each set-up before capturing the rest, to make certain that all twenty-three markers fell within the cameras' view and that the output signals from the force plates, force sensors and displacement transducers were received by all twenty-four analogue channels in operation. If everything worked as it was supposed to, then the remaining nineteen trials for the current set-up were recorded as a batch. This meant that the verbal prompt for the next trial was given as soon as the subjects were back at their starting position and had composed themselves.

216

Once the recordings of all twenty trials for a set-up were completed, the subjects had the opportunity to sit down and relax for a short period, while the return units and respective substitute return units, described in Section 4.1.5.2 to Section 4.1.5.5, were exchanged as necessary. Care had to be taken not to let the subjects sit on the entire seat of their chair, but only on its edge, to prevent skin-mounted markers and extension rods from getting dislodged or damaged. Once the necessary components were exchanged, the connections and adjustment facilities that needed undoing were tightened back up again, so that the new set-up was ready to be tested. The entire recording process and subsequent exchange of components continued until the required twenty trials were recorded for all four set-ups. After that, all the equipment mounted onto the subjects was taken off again, including the test-prosthesis.

Once the subjects got changed back into their own clothes and wore their own prosthesis, they were asked to fill in a questionnaire. This was based on a visual analogue scale that ranged from +100 to -100. The subjects were supposed to score a mark to express their level of satisfaction for each of the four set-ups, whereby positive and negative values meant satisfied and unsatisfied, respectively. Having measured the distance between zero and the location of all four marks, it was possible to calculate the ratio between each score and the full length of the scale from zero to ±100, which was expressed in percent. To prevent confusion, the questionnaire that the subjects were asked to fill in contained the expressions "rotation" and "shock absorption". These were only used because some of the subjects might not be familiar with the terminology, previously described in Section 3.1.1. An example of a blank questionnaire is given in Appendix 6 of this thesis.

Before departing, the subjects were finally reimbursed for their travel expenses. The amount they received was determined by the University of Salford in accordance with the distance the subjects had to travel from their home. This needed to be accurate, as the subjects' participation was voluntary and, according to the LREC, not encouraged by additional funding, as explained in Section 4.2.1.

CHAPTER 8.   <u>DATA PROCESSING</u>

All ten subjects needed to perform ten high quality walks for each of the four set-ups, as previously mentioned in Section 7.2.4, so that the total number of trials added up to four hundred. The data obtained from these trials were used for calculating the necessary gait parameters, which subsequently produced the foundation for the required gait analyses.

8.1.   <u>Considerations for data processing</u>

The first step was for the data to be digitised and then saved in TSV file format, as explained in Section 5.1.1.9. In addition to each of the ten subject's forty experimental trials, two further recordings needed digitising including the static calibration trial and the force plate marker trial. The raw data stored in those files could then be manipulated and processed by using appropriate algorithms. However, this would have been impossible without the help of a computer, due to the vast quantity of data that were recorded.

8.2.   <u>Preliminary procedures</u>

8.2.1.   <u>Software for data processing</u>

Commercially available software exists for calculating typical gait parameters including GRFs, inter-segmental angles as well as joint moments and powers. In most cases, however, such software will not be able to recognise the recorded data unless they are in a specific format. These formats are usually governed by a certain biomechanical model and by the number of markers that need to be used for the tests. As was the case during the current investigation, certain biomechanical models and the number of markers to be used may not be suitable for the required application. Under those circumstances, customised biomechanical models would be required. This also means that the resultant data need to be processed in a very specific manner, which may not be possible to undertake with commercially available software.

218

An additional problem was the customisation of the experimental set-up, which became very specific with the introduction of displacement transducers and force sensors, whereby commercially available software is, for the time being, not capable of dealing with such specialisations. It was therefore decided to write tailor made programs. This took up a major part of this study's overall duration. These programs were written in Matlab (The MathWorks Inc, Natick Massachusetts, USA) and were used for processing the entire set of data.

8.2.2.   Opening of the data-containing files

Accessing the TSV files within Matlab can cause difficulties, because they contain headers at the top of each data sheet that are irrelevant for the required computations. However, programmes previously written for processing the data from the calibrations of FlexiForce® sensors included a specific code that could handle problems associated with headers, as explained in Section 6.2.3.5. The algorithm that this code was based on was therefore adopted for the main data processing programs.

8.2.3.   Filtering of the data

Once the files were opened, it was necessary to eliminate noise from the raw data by filtering them. That way, the final graphic representations of the processed data appeared smooth and not riddled with jagged output fluctuations.

All four categories of measuring devices, namely the cameras, force plates, displacement transducers and force sensors, were responsible for capturing different aspects of gait. This meant that each of them needed their own specific filter settings to prevent excessive or insufficient smoothing from detrimentally affecting the data. The filtering was undertaken with a low-pass Butterworth filter. Its optimum settings were established empirically with different orders of filters and cut-off frequencies for each category of measuring device. This was a similar procedure to the one used during the smoothing of data from the force sensor calibrations, as previously described in Section 6.2.3.5.

The filter that made the graphs representing the processed data appear most similar to the raw data was of sixth order for all four measuring device categories. In turn, the cut-off frequency was not always the same. This needed to be adjusted to 12Hz for the

cameras and 20Hz for the force plates, displacement transducers and force sensors, as summarised in Table 8.1.

Table 8.1:   Filter settings for all four measuring device categories

Filter specifications	ProReflex^{TM} system cameras	Floor force plates	Linear displacement transducers	In-socket FlexiForce$^{®}$ sensors
Filter-type	Butterworth	Butterworth	Butterworth	Butterworth
Pass-type	Low-pass	Low-pass	Low-pass	Low-pass
Order	6th	6th	6th	6th
Cut-off (Hz)	12	20	20	20

8.2.4.   Reconstruction of missing markers

Data that were missing due to failure in detecting markers at one or several stages throughout the capture duration are the reason for introducing gaps into the processed parameters, which requires the missing information to be reconstructed. As explained in Section 5.1.1.11, QTM has a spline fill option that can be used to join split marker trajectories mathematically together. This means that after completing the digitisation process, the saved TSV files only contain a full set of data, so that interpolations for further mathematical reconstructions while running the Matlab programs are no longer necessary.

As it turned out, the quality of the recorded data was good enough that the fourth marker for the thigh and shin sections was not needed. This is a valuable discovery and should be taken into account during future gait laboratory tests, as a lesser number of total markers is likely to reduce the amount of time it takes for the digitising process.

8.3.   Mathematical background

8.3.1.   Definition of co-ordinate systems

Constructing the reference systems required at least three non-co-linear markers in order to define the necessary three axes of a Cartesian co-ordinate system, as explained in Section 7.1.3. Simply inter-connecting the three markers would result in three vectors that are all within one plane and unlikely to be perpendicular to one another. This

indicates the need for an alternative mathematical procedure that can be used to determine three vectors with orthogonal orientations relative to one another.

The global reference system G_R can be derived from three of the four markers that are mounted on the calibration frame, displayed in Figure 5.1, namely, for instance, marker M_1 in the corner of the L-shaped frame, marker M_2 at the end of the L's long bar and marker M_3 at the end of the L's short bar. Their position G_{R1}, G_{R2}, G_{R3} can be expressed in accordance with the definitions by Wu 1995, as shown in Equations 8.1.

Equations 8.1:   Calibration frame marker co-ordinates

$$G_{R1} = \begin{bmatrix} x_1 \\ y_1 \\ z_1 \end{bmatrix}, \quad G_{R2} = \begin{bmatrix} x_2 \\ y_2 \\ z_2 \end{bmatrix}, \quad G_{R3} = \begin{bmatrix} x_3 \\ y_3 \\ z_3 \end{bmatrix}$$

Definitions:

$G_{R1}...G_{R3}$ -   marker locations

$x_1...z_3$ -   marker co-ordinates

Those marker co-ordinates can then be used for subsequent calculations that determine the required three orthogonal vectors to define the global reference system G_R, as stipulated by Wu 1995. The way the first two vectors were determined is shown in Equations 8.2.

Equations 8.2:   Vectors based on calibration frame inter-marker distances

$$G_{R1,2} = G_{R1} - G_{R2}$$

$$G_{R1,3} = G_{R1} - G_{R3}$$

Definitions:

$G_{R1}...G_{R3}$ -   marker locations

$G_{R1,2}, G_{R1,3}$ -   inter-marker vectors

The global reference system's X-axis can be expressed as the unit vector X_{GR} from the inter-marker vector $G_{R1,2}$, the Y-axis as the unit vector Y_{GR} from the cross product between $G_{R1,2}$ and $G_{R1,3}$ and the Z-axis as the unit vector Z_{GR} from the cross product between X_{GR} and Y_{GR}. The calculation for this, and the way the resultant unit vectors are arranged, is illustrated in Equations 8.3 and Figure 8.1, respectively.

Equations 8.3:   Unit vectors for defining the global reference system axes

$$X_{GR} = \frac{G_{R1,2}}{|G_{R1,2}|}$$

$$Y_{GR} = \frac{G_{R1,2} \times G_{R1,3}}{|G_{R1,2} \times G_{R1,3}|}$$

$$Z_{GR} = X_{GR} \times Y_{GR}$$

Definitions:

$G_{R1,2}$, $G_{R1,3}$ -   inter-marker vectors

$X_{GR}...Z_{GR}$ -   unit vectors for the global reference system axes

Figure 8.1:   Unit vectors for defining the global reference system axes
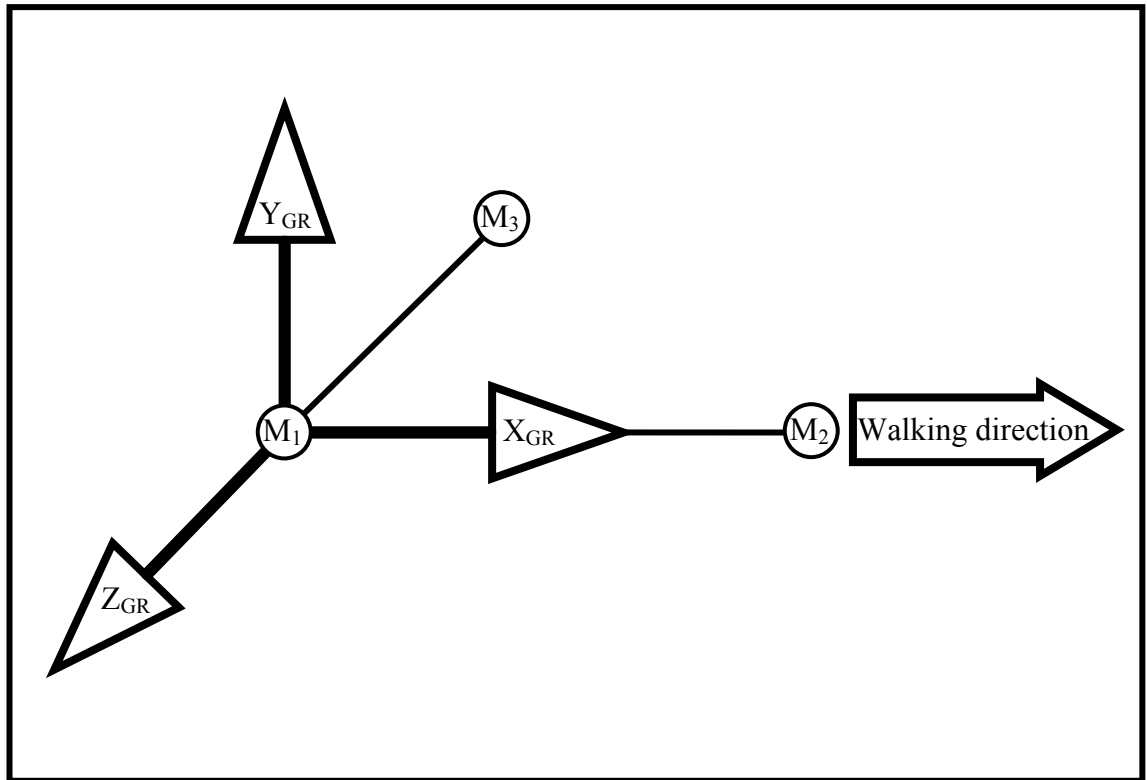
A segment's local reference system L_R can be determined in a similar manner. The calculations for this are based on the co-ordinates L_a, L_b, and L_c from the three markers M_a, M_b and M_c to obtain the three unit vectors X_{LR}, Y_{LR} and Z_{LR}.

8.3.2.   Rotational transformations in 2D

Movements of a segment's local reference system relative to the global reference system are defined as a combination of rotational and/or linear transformations. These

can occur along and/or around each of the Cartesian co-ordinate system's three orthogonal axes for creating six degree of freedom.

Rotational transformations between co-ordinates systems are the first aspect that will be investigated, and for reasons of simplicity, the initial scenario to be analysed is given in 2D only. Figure 8.2 represents an example for an angular displacement of point P and point P' or P'' within the co-ordinate systems XY and XY''.

Figure 8.2: 2D rotational transformations of point P and point P' or P''
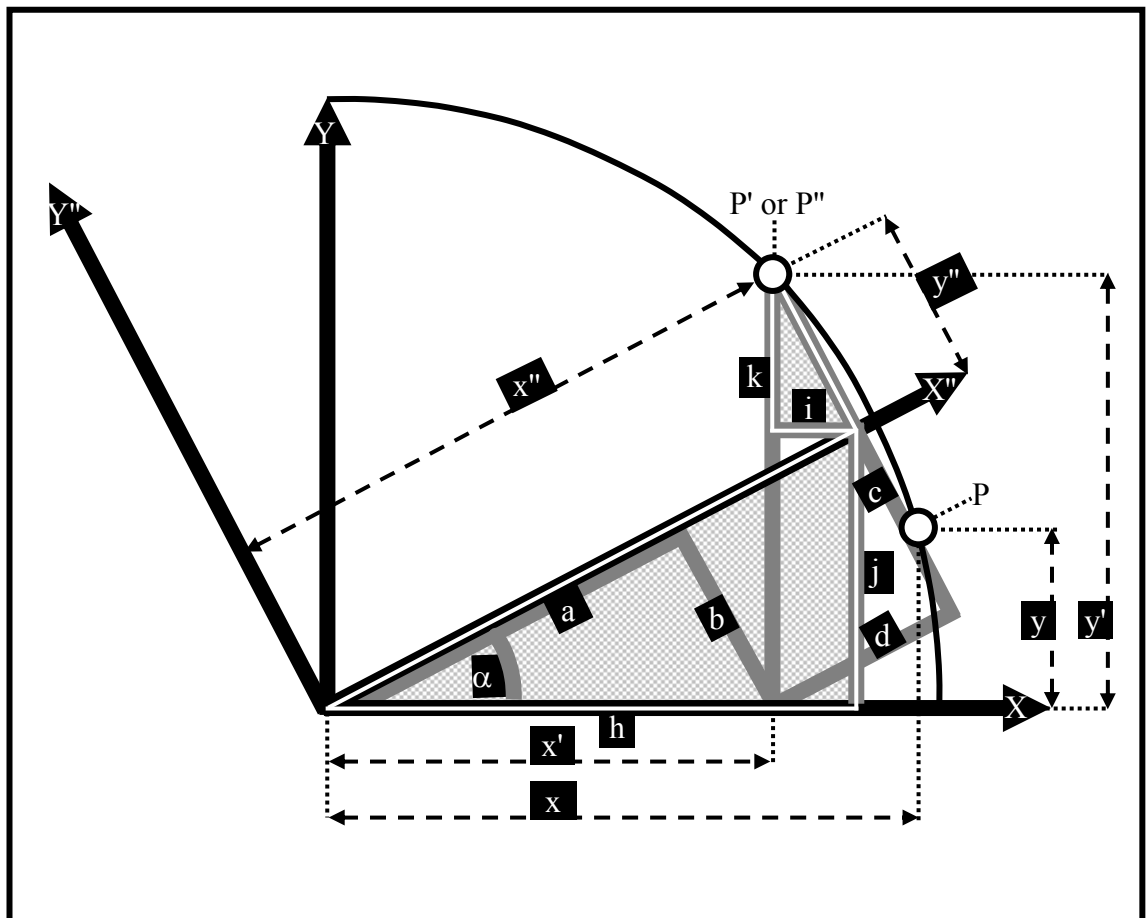
The point P' or P'' can be expressed in two ways, as described in Equations 8.4. For the sake of brevity, sine and cosine are abbreviated as s and c, respectively.

Knowing the co-ordinates of point P' or P'', it is possible to produce the corresponding rotation matrix. This can be undertaken in two ways depending on the reference system that the displacement is referring to, or the direction in which the rotation takes place, as illustrated in Equations 8.5.

Equations 8.4:   Formulae for expressing point P' or P"

$$x' \ = \ h - i \ = \ x'' c\alpha - y'' s\alpha$$

$$y' \ = \ j + k \ = \ x'' s\alpha + y'' c\alpha$$

or

$$x'' \ = \ a + d \ = \ x' c\alpha + y' s\alpha$$

$$y'' \ = \ -b + c \ = \ -x' s\alpha + y' c\alpha$$

Definitions:

any constant   -   certain distances or angles as depicted in Figure 8.2

Equations 8.5:   Rotation matrices for calculating point P and point P' or P"

$$\begin{bmatrix} P_{x''} \text{ or } P_x \\ P_{y''} \text{ or } P_y \end{bmatrix} = \begin{bmatrix} c(+\alpha) & : & s(+\alpha) \\ -s(+\alpha) & : & c(+\alpha) \end{bmatrix} \times \begin{bmatrix} P_{x'} \\ P_{y'} \end{bmatrix}$$

$$= \begin{bmatrix} c\alpha & : & s\alpha \\ -s\alpha & : & c\alpha \end{bmatrix} \times \begin{bmatrix} P_{x'} \\ P_{y'} \end{bmatrix}$$

or

$$\begin{bmatrix} P_{x'} \\ P_{y'} \end{bmatrix} = \begin{bmatrix} c(-\alpha) & : & s(-\alpha) \\ -s(-\alpha) & : & c(-\alpha) \end{bmatrix} \times \begin{bmatrix} P_{x''} & \text{or} & P_x \\ P_{y''} & & P_y \end{bmatrix}$$

$$= \begin{bmatrix} c\alpha & : & -s\alpha \\ s\alpha & : & c\alpha \end{bmatrix} \times \begin{bmatrix} P_{x''} & \text{or} & P_x \\ P_{y''} & & P_y \end{bmatrix}$$

Definitions:

α -   angle between reference system XY and XY"

$P_x \dots P_y''$ -   co-ordinates of a point in reference system XY, X'Y', X"Y"

The first method refers to point P' in the co-ordinate system XY. After rotation it becomes the point P" in the co-ordinate system X"Y" or point P in the co-ordinate system XY. The second method refers to point P" in the co-ordinate system X"Y" or point P in the co-ordinate system XY. After rotation it becomes the point P' in the co-ordinate system XY.

By using the examples in Equations 8.6, it can be seen that the first method is the reverse of the second method and vice versa. The figures that were substituted into the variables are as follows.

224

Fist method: $\alpha = 30°$ x = 56.0   y = 56.0

Second method: $\alpha = 30°$ x" or x = 76.5   y" or y = 20.5

Equations 8.6:   Examples for calculating point P, P' or P"

$$\begin{bmatrix} P_{x"} \text{ or } P_x \\ P_{y"} \text{ or } P_y \end{bmatrix} = \begin{bmatrix} \cos 30 & : & \sin 30 \\ -\sin 30 & : & \cos 30 \end{bmatrix} \times \begin{bmatrix} 56.0 \\ 56.0 \end{bmatrix} \hat{=} \begin{bmatrix} 76.5 \\ 20.5 \end{bmatrix}$$

or

$$\begin{bmatrix} P_{x'} \\ P_{y'} \end{bmatrix} = \begin{bmatrix} \cos 30 & : & -\sin 30 \\ \sin 30 & : & \cos 30 \end{bmatrix} \times \begin{bmatrix} 76.5 \\ 20.5 \end{bmatrix} \hat{=} \begin{bmatrix} 56.0 \\ 56.0 \end{bmatrix}$$

Definitions:

$P_x \ldots P_y"$ -   co-ordinates of a point in reference system XY, X'Y', X"Y"

8.3.3.   <u>Rotational transformations in 3D</u>

To obtain a better impression of the events during human motion, the transformations should take place in 3D. Previously described matrices in 2D therefore needed expanding to accommodate the additional, third dimension. When breaking motions down into three separate rotations, the respective co-ordinate that corresponds with the axis around which rotation takes place remains fixed until the next type of rotation occurs around another axis. A set of three rotations can be performed around the axes of a fixed or a moving Cartesian reference system, whereby transformations within the latter are derived from Euler angles (Craig 1989, Meglan & Todd 1994, Wu 1995).

Apart from Euler angles, alternative solutions exist, including motion around a screw displacement axis, which is based on the screw theory and described in terms of Plücker co-ordinates (Wu 1995). The rotational aspect of this type of transformation is often referred to as helical angles, but uncertainties in aligning segment-embedded axes during the static calibration procedure to an extent that the helical rotation is zero can lead to dependencies between rotations (Ramakrishnan & Kadaba 1991). Therefore, the screw theory method is rarely utilised in gait analysis (Wu 1995).

Similar to helical angles, Euler angles can also lead to dependencies between rotations due to uncertainties in defining segment-embedded axes (Kadaba et al 1990, Ramakrishnan & Kadaba 1991). However, rotational transformations with these types of angles seemed to be a much more frequently encountered method used for processing

data that are related to the field of gait analysis. Calculations of segment displacements during the current investigation were therefore based on Euler angles.

Figure 8.3:   Sequence of rotations affecting transformation outcome

Rotation around the Z-axis first and around the X-axis second

Rotation around the X-axis first and around the Z-axis second

This diagram was adapted from Sutherland et al 1994
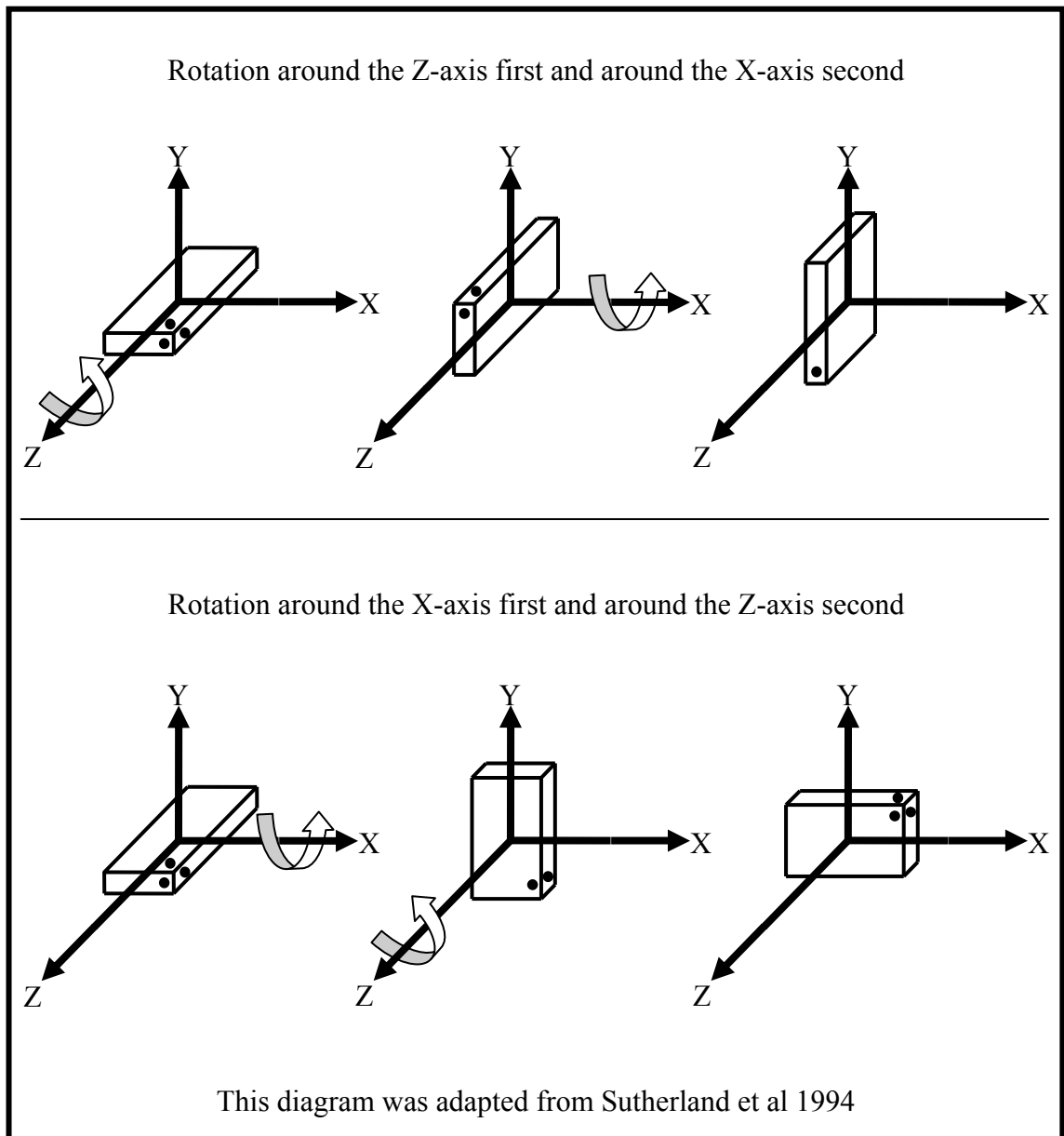
All three resultant angles are required for the calculation of a segment's total rotational transformations. To do this, the required matrix multiplications have to be undertaken in a constant fashion, because these types of mathematical conversions are not commutative (Barth et al 1985). It was therefore important to determine a sequence of rotations that will be maintained throughout the data processing, so that the calculations of the three angles occur in the same order for all seven segments. Figure 8.3 illustrates the effect two different rotation sequences can have on the outcome of the final transformation. It must be emphasised that the example is a simplification and does not

represent a true rotation sequence in 3D, as it only shows two, rather than all three, independent rotations.

Wu & Cavanagh 1995 recommended on behalf of the ISB the use of a rotation sequence of order ZXY for right handed co-ordinate systems with an axis orientation identical to the one previously defined in Section 5.1.1.13. The three independent rotations therefore occurred around the Z-axis first, around the X-axis second and around the Y-axis third, which became the adopted procedure for the current investigation. The way the rotation sequence took place is illustrated in Figure 8.4, which also displays the changes in orientation of the moving reference system. The reference system's Z-axis in this example is pointing upward, which is not its true alignment and only shown this way for display purposes, so that displacements of the reference system can be visualised easier.

Figure 8.4:   Rotation sequence ZXY within a moving reference system
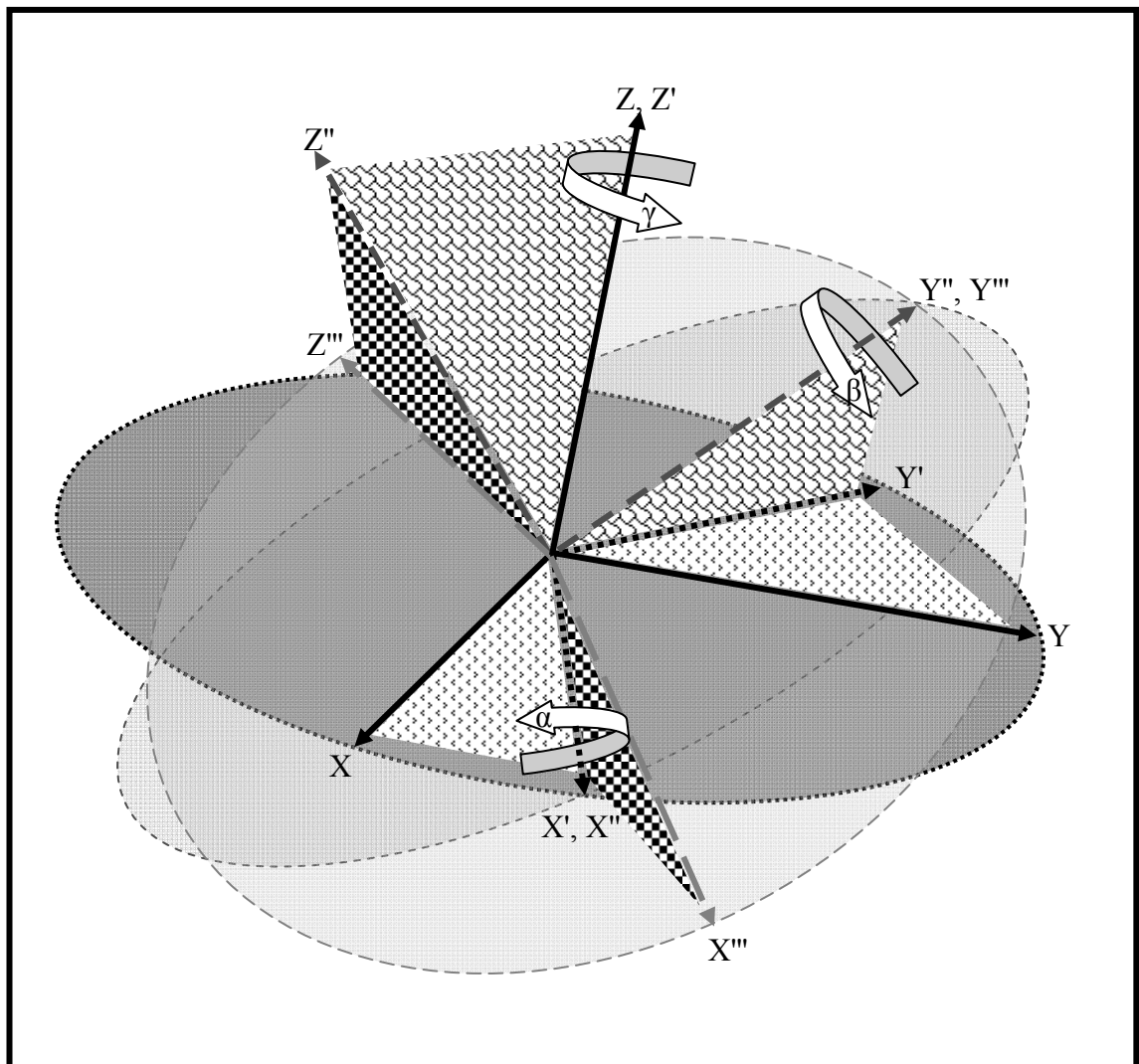
The mathematical representation for conducting a rotational transformation in 3D is a triad, or 3×3 rotation matrix, which is composed of three 3-row vectors. Each of them represents the projection of that vector onto the unit directions of the respective reference system. This is applicable for a fixed reference frame and the resultant rotation matrix can be written as a dot product between pairs of unit vectors, as depicted in Equations 8.7.

Equations 8.7: Rotation matrix for transformations between system A and B

$$x_B \cdot x_A \quad = \quad |x_B| \cdot |x_A| \, c\alpha \quad = \quad c\alpha$$

$$\vdots \quad \vdots \quad \vdots \quad = \quad \vdots \quad \vdots \quad \vdots \quad \vdots \quad = \quad \vdots \quad \text{because } x_A \ldots z_B \text{ are unit vectors and have the value 1}$$

$$z_B \cdot z_A \quad = \quad |z_B| \cdot |z_A| \, c\gamma \quad = \quad c\gamma$$

$$\Rightarrow R_{AB} \quad = \quad \left[x_{AB} \vdots y_{AB} \vdots z_{AB} \right] \quad = \quad \begin{bmatrix} x_B \cdot x_A & \vdots & y_B \cdot x_A & \vdots & z_B \cdot x_A \\ x_B \cdot y_A & \vdots & y_B \cdot y_A & \vdots & z_B \cdot y_A \\ x_B \cdot z_A & \vdots & y_B \cdot z_A & \vdots & z_B \cdot z_A \end{bmatrix}$$

Definitions:

R_{AB} -   rotation matrix
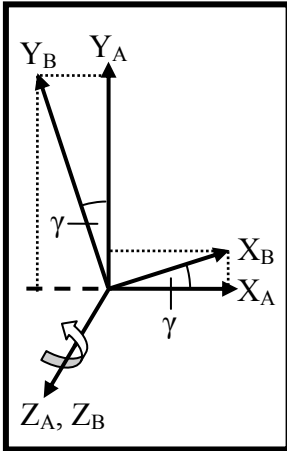
$x_A \ldots z_B$ -   unit vectors
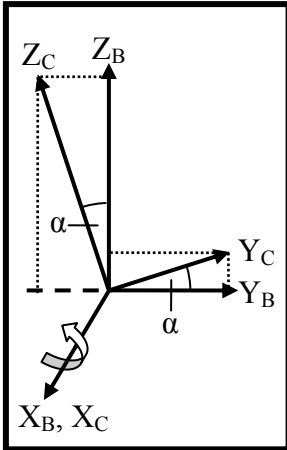
$x_{AB} \ldots z_{AB}$ -   dot product between unit vectors of reference system A and B
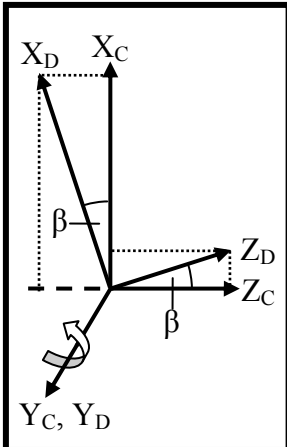
The principle of the rotation matrix R_{AB} is also applicable for rotating a segment within a moving reference system. A sequence of the entire transformation can then be broken down into individual rotations to establish the resulting rotation matrices for each of those displacements in a way as displayed in Equations 8.8. All three rotations are illustrated in the diagrams adjacent to the equations.

The next step was to combine all three individual rotation matrices into one. The way this was done is shown in Equations 8.9. Because the formula in that Equation is supposed to be applicable for a reference system with moving axes, it was necessary to swap all three factors into reverse order. That way the entire rotation sequence can be resolved from the left, as illustrated in Equations 8.10.

Equations 8.8: Rotation matrix for angular motion around the Z, X, Y-axes

$$
\begin{bmatrix} x' \\ y' \\ z' \end{bmatrix} = R_Z \cdot \begin{bmatrix} x \\ y \\ z \end{bmatrix} = \begin{bmatrix} x_B \cdot x_A & \vdots & y_B \cdot x_A & \vdots & 0 \\ x_B \cdot y_A & \vdots & y_B \cdot y_A & \vdots & 0 \\ 0 & \vdots & 0 & \vdots & 1 \end{bmatrix} \cdot \begin{bmatrix} x \\ y \\ z \end{bmatrix}
$$

$$
= \begin{bmatrix} c\gamma & \vdots & c(\gamma+90) & \vdots & 0 \\ c(90-\gamma) & \vdots & c\gamma & \vdots & 0 \\ 0 & \vdots & 0 & \vdots & 1 \end{bmatrix} \cdot \begin{bmatrix} x \\ y \\ z \end{bmatrix}
$$

$$
= \begin{bmatrix} c\gamma & \vdots & -s\gamma & \vdots & 0 \\ s\gamma & \vdots & c\gamma & \vdots & 0 \\ 0 & \vdots & 0 & \vdots & 1 \end{bmatrix} \cdot \begin{bmatrix} x \\ y \\ z \end{bmatrix}
$$

$$
\begin{bmatrix} x'' \\ y'' \\ z'' \end{bmatrix} = R_X \cdot \begin{bmatrix} x' \\ y' \\ z' \end{bmatrix} = \begin{bmatrix} 1 & \vdots & 0 & \vdots & 0 \\ 0 & \vdots & y_C \cdot y_B & \vdots & z_C \cdot y_B \\ 0 & \vdots & y_C \cdot z_B & \vdots & z_C \cdot z_B \end{bmatrix} \cdot \begin{bmatrix} x' \\ y' \\ z' \end{bmatrix}
$$

$$
= \begin{bmatrix} 1 & \vdots & 0 & \vdots & 0 \\ 0 & \vdots & c\alpha & \vdots & c(\alpha+90) \\ 0 & \vdots & c(90-\alpha) & \vdots & c\alpha \end{bmatrix} \cdot \begin{bmatrix} x' \\ y' \\ z' \end{bmatrix}
$$

$$
= \begin{bmatrix} 1 & \vdots & 0 & \vdots & 0 \\ 0 & \vdots & c\alpha & \vdots & -s\alpha \\ 0 & \vdots & s\alpha & \vdots & c\alpha \end{bmatrix} \cdot \begin{bmatrix} x' \\ y' \\ z' \end{bmatrix}
$$

$$
\begin{bmatrix} x''' \\ y''' \\ z''' \end{bmatrix} = R_Y \cdot \begin{bmatrix} x'' \\ y'' \\ z'' \end{bmatrix} = \begin{bmatrix} x_D \cdot x_C & \vdots & 0 & \vdots & z_D \cdot x_C \\ 0 & \vdots & 1 & \vdots & 0 \\ x_D \cdot z_C & \vdots & 0 & \vdots & z_D \cdot z_C \end{bmatrix} \cdot \begin{bmatrix} x'' \\ y'' \\ z'' \end{bmatrix}
$$

$$
= \begin{bmatrix} c\beta & \vdots & 0 & \vdots & c(90-\beta) \\ 0 & \vdots & 1 & \vdots & 0 \\ c(90+\beta) & \vdots & 0 & \vdots & c\beta \end{bmatrix} \cdot \begin{bmatrix} x'' \\ y'' \\ z'' \end{bmatrix}
$$

$$
= \begin{bmatrix} c\beta & \vdots & 0 & \vdots & s\beta \\ 0 & \vdots & 1 & \vdots & 0 \\ -s\beta & \vdots & 0 & \vdots & c\beta \end{bmatrix} \cdot \begin{bmatrix} x'' \\ y'' \\ z'' \end{bmatrix}
$$

Definitions:

$\alpha \ldots \gamma$ - angle of rotation

$R_X \ldots R_Z$ - rotation matrix

$x \ldots z'''$ - co-ordinates of a point within its respective reference system

$x_A \ldots z_D$ - unit vectors

Equations 8.9:   Combination of all three individual rotation matrices

$$
\begin{bmatrix} x''' \\ y''' \\ z''' \end{bmatrix} = R_Y \cdot \begin{bmatrix} x'' \\ y'' \\ z'' \end{bmatrix} = R_Y \cdot R_X \cdot \begin{bmatrix} x' \\ y' \\ z' \end{bmatrix} = R_Y \cdot R_X \cdot R_Z \cdot \begin{bmatrix} x \\ y \\ z \end{bmatrix} = R_{YXZ} \cdot \begin{bmatrix} x \\ y \\ z \end{bmatrix}
$$

Definitions:

$R_X \ldots R_Z$ -   rotation matrix

$x \ldots z'''$ -   co-ordinates of a point within its respective reference system

Equations 8.10: Resolving the entire rotation matrix

$$R_{ZXY} \quad = \qquad R_Z \qquad \cdot \qquad R_X \qquad \cdot \qquad R_Y$$

$$
= \begin{bmatrix} c\gamma & -s\gamma & 0 \\ s\gamma & c\gamma & 0 \\ 0 & 0 & 1 \end{bmatrix} \cdot \begin{bmatrix} 1 & 0 & 0 \\ 0 & c\alpha & -s\alpha \\ 0 & s\alpha & c\alpha \end{bmatrix} \cdot \begin{bmatrix} c\beta & 0 & s\beta \\ 0 & 1 & 0 \\ -s\beta & 0 & c\beta \end{bmatrix}
$$

$$
= \begin{bmatrix} c\gamma & -s\gamma c\alpha & s\gamma s\alpha \\ s\gamma & c\gamma c\alpha & -s\alpha c\gamma \\ 0 & s\alpha & c\alpha \end{bmatrix} \cdot \begin{bmatrix} c\beta & 0 & s\beta \\ 0 & 1 & 0 \\ -s\beta & 0 & c\beta \end{bmatrix}
$$

$$
= \begin{bmatrix} c\gamma c\beta - s\gamma s\alpha s\beta & -s\gamma c\alpha & c\gamma s\beta + s\gamma s\alpha c\beta \\ s\gamma c\beta + s\alpha c\gamma s\beta & c\gamma c\alpha & s\gamma s\beta - s\alpha c\gamma c\beta \\ -s\beta c\alpha & s\alpha & c\alpha c\beta \end{bmatrix}
$$

$$
= \begin{bmatrix} r_{11} & r_{12} & r_{13} \\ r_{21} & r_{22} & r_{23} \\ r_{31} & r_{32} & r_{33} \end{bmatrix}
$$

Definitions:

$\alpha \ldots \gamma$ -   angle of rotation

$r_{11} \ldots r_{33}$ -   elements of the triad

$R_X \ldots R_Z$ -   individual rotation matrix

R_{ZXY} -   total rotation matrix

Having established a complete rotation matrix, the next step was to solve each of the three angles α, β, γ. This was undertaken as described in Equations 8.11.

Equations 8.11: Calculations for solving each of the three angles α, β, γ

$$\alpha \;=\; \sin^{-1}(\quad R_{ZXY}(3,2)\,) \;=\; \arcsin(\quad r_{32}\;)$$

$$\beta \;=\; \sin^{-1}(\frac{-R_{ZXY}(3,1)}{\cos\alpha}) \;=\; \arcsin(\frac{-r_{31}}{\cos\alpha})$$

$$\gamma \;=\; \sin^{-1}(\frac{-R_{ZXY}(1,2)}{\cos\alpha}) \;=\; \arcsin(\frac{-r_{12}}{\cos\alpha})$$

Definitions:

α…γ   -   angle of rotation

$r_{11}…r_{33}$ -   elements of the triad

R_{ZXY} -   total rotation matrix

8.3.4.   <u>Rotational and linear transformations in 3D</u>

Having looked purely at rotational transformations in both 2D and 3D, the second aspect that will be investigated is the combined mathematical representation of rotational and linear transformations. A segment's orientation is identified by a matrix, as was previously shown in Section 8.3.3, and its position is identified by a vector as depicted in Figure 8.5.

Figure 8.5:   Relative displacement between two co-ordinate systems
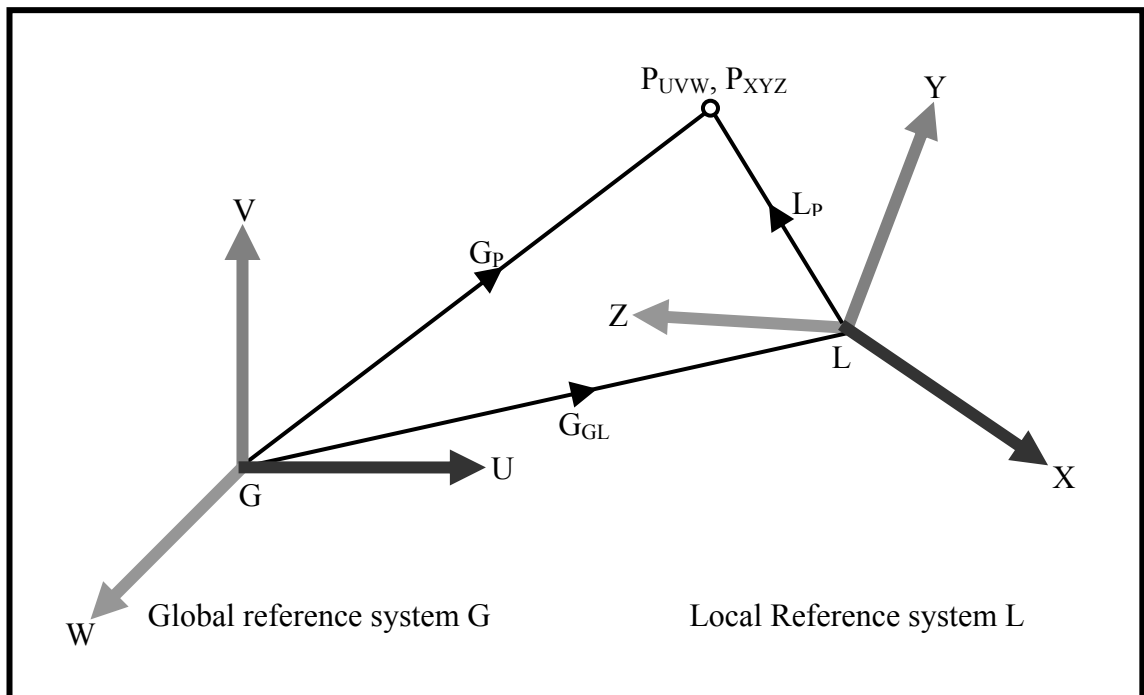
Although it is possible to calculate both types of displacements separately, using the homogenous transform (Craig 1989) is a method that contains both the rotation matrix

and the position vector in one quatrain or four-element vector (Wu 1995). Equations 8.12 contain formulae that express the final position of point P_{UVW}, as seen from global reference system G after the rotation and translation is completed.

Equations 8.12: Rotation and translation combined in a quatrain

$$G_P \quad = \quad R_{ZXY} \cdot L_P + G_{GL} \qquad\qquad \text{to be converted into a four-element vector}$$

$$G_P \quad = \quad \left[\begin{array}{ccc|c} & R_{ZXY} & & G_{GL} \\ \hline 0 & 0 & 0 & 1 \end{array} \right] \cdot \left[\begin{array}{c} L_{Px} \\ L_{Py} \\ L_{Pz} \\ 1 \end{array} \right]$$

$$= \left[\begin{array}{ccc:c:ccc:c} c\gamma c\beta & - & s\gamma s\alpha s\beta & -s\gamma c\alpha & c\gamma s\beta & + & s\gamma s\alpha c\beta & G_{GLu} \\ s\gamma c\beta & + & s\alpha c\gamma s\beta & c\gamma c\alpha & s\gamma s\beta & - & s\alpha c\gamma c\beta & G_{GLv} \\ & - & s\beta c\alpha & s\alpha & & + & c\alpha c\beta & G_{GLw} \\ & 0 & & 0 & & 0 & & 1 \end{array} \right] \cdot \left[\begin{array}{c} L_{Px} \\ L_{Py} \\ L_{Pz} \\ 1 \end{array} \right]$$

$$= \left[\begin{array}{c} c\gamma c\beta L_{Px} - s\gamma s\alpha s\beta L_{Px} - s\gamma c\alpha L_{Py} + c\gamma s\beta L_{Pz} + s\gamma s\alpha c\beta L_{Pz} + G_{GLu} \\ s\gamma c\beta L_{Px} + s\alpha c\gamma s\beta L_{Px} + c\gamma c\alpha L_{Py} + s\gamma s\beta L_{Pz} - s\alpha c\gamma c\beta L_{Pz} + G_{GLv} \\ - s\beta c\alpha L_{Px} + s\alpha L_{Py} \qquad\qquad + c\alpha c\beta L_{Pz} + G_{GLw} \\ 1 \end{array} \right]$$

Definitions:

$\alpha \ldots \gamma$	-	angle of rotation
G_{GL}	-	translation between reference system G and L
$G_{GLu} \ldots G_{GLw}$	-	co-ordinates of translation between reference system G and L
G_P, L_P	-	location of a point as seen from its respective reference system
$L_{Px} \ldots L_{Pz}$	-	co-ordinates of a point within reference system L
R_{ZXY}	-	total rotation matrix

Although such a method is mathematically correct, calculating the orientation and position of a segment from its three markers in this way can lead to small errors. This is, because the way the relationship between the markers is reflected in the stored data may not always remain the same for every recording frame. This can be caused by a number of factors including inter-marker displacements and failure of the cameras to correctly identify the centroid of each captured marker (Cappozzo et al 2003).

To overcome this problem, Veldpaus et al 1988 developed a least-square algorithm that reduces the error for defining a segment's local reference system by minimising the difference between the measured marker co-ordinates and those calculated during data processing. This algorithm was adapted by Linden van der 1999 for a study on amputee gait analysis, and it also became the chosen method for the current investigation. The resultant calculation of the total rotation matrix R_{ZXY} and the translation vector $S4_{bef-aft}$ is shown in Equations 8.13.

Equations 8.13: Calculation of total rotation matrix and translation vector

$$Sl_{aft} \quad = \quad R_{ZXY} \cdot (Sl_{bef} - S4_{bef}) + S4_{bef} + S4_{bef-aft}$$

Definitions:

R_{ZXY} - rotation matrix for one segment-mounted marker around tip of $S4_{bef}$

     - from before to after transformation

Sl_{aft} - position vector of one segment-mounted marker

     - after transformation

Sl_{bef} - position vector of one segment-mounted marker

     - before transformation

$S4_{bef-aft}$ - mean translation vector of four segment-mounted markers

     - from before to after transformation

$S4_{bef}$ - mean position vector of four segment-mounted markers

     - before transformation

The calculated rotation angles obey the rules of a right handed co-ordinate system. Positive measurements are therefore obtained for angular displacements from the X to Y-axis, from the Y to Z-axis and from the Z to X-axis, as previously illustrated in Figure 5.6. Each of the seven lower limb segments, namely the pelvis and both thigh, shin and foot sections, was identified by its own specific reference system. It was then possible to convert local co-ordinates into global co-ordinates.

8.4.   Calculating the gait parameters

8.4.1.   Reconstruction of joint markers

As previously described in Section 7.1.8, the markers for identifying the hip joint centres were the same as those for the pelvis section, so that the location of those

markers during the dynamic trials did not need to be re-calculated. The co-ordinates of both joint centres could therefore be related to the pelvis markers.

In turn, the rotation axes of the knees and ankles were, as explained in Section 7.1.3, only identified during the static calibration procedure, when all the segment-mounted and joint-mounted markers were captured simultaneously. The position of joint centres during dynamic trials without joint-mounted markers could then be derived solely from segment-mounted markers, using CAST in accordance with the study by Cappozzo et al 1995. Using matrix transformations, the process for this needed repeating for every recording frame of each dynamic trial. The calculations were based on the algorithm by Veldpaus et al 1988, described in Section 8.3.2, and could be expressed in the way illustrated by Equations 8.14.

Equations 8.14: Calculation of joint markers from segment-mounted markers

$$J_{dyn}(t) \quad = \quad R_{ZXY}(t) \cdot (J_{sta} - S4_{sta}) + S4_{sta} + S4_{sta-dyn}(t)$$

Definitions:

$J_{dyn}(t)$	-	position vector of a joint-mounted marker in frame t
	-	during a dynamic trial
J_{sta}	-	position vector of a joint-mounted marker
	-	during a static trial
$R_{ZXY}(t)$	-	rotation matrix of a segment
	-	from its orientation during a static trial to that of a dynamic trial
$S4_{sta}$	-	mean position vector of four segment-mounted markers
	-	during a static trial
$S4_{sta-dyn}(t)$	-	mean translation vector of four segment-mounted markers
	-	from its position during a static trial to that of a dynamic trial

Once the position of the two markers that were mounted onto each knee and ankle joint during the static trial were successfully transformed into every frame of all the dynamic trials, it was possible to determine the centre of each joint. This was undertaken in the way it was previously described in Section 7.1.9 and Section 7.1.10, by calculating the co-ordinates mid-way between a medial and its respective lateral marker, as shown in Equations 8.15.

Equations 8.15: Calculation of joint centres from joint markers

$$J_{cen} \quad = \quad J_{lat} + 0.5 \cdot (J_{lat} - J_{med})$$

Definitions:

J_{cen} -   position vector of joint centre

J_{lat} -   position vector of lateral joint marker

J_{mad} -   position vector of medial joint marker

8.4.2. <u>Calculation of inter-segmental joint angles</u>

After having determined the co-ordinates of every marker, defined all the local reference systems and reconstructed vital landmark positions, it was possible to determine the angles between inter-connected segments for every recording frame t. This was done by calculating the rotation matrix R_{ZXY} from local reference systems of two adjacent segments S_{dis} and S_{pro}, as shown in Equations 8.16 in accordance with Cappozzo et al 1990.

Equations 8.16: Calculation of angles between two adjacent segments

$$R_{ZXY}(t) \quad = \quad S_{pro}(t)^{-1} \quad \cdot \quad S_{dis}(t)$$

Definitions:

$R_{ZXY}(t)$ -   total rotation matrix in frame t

$S_{dis}(t)$ -   local reference system of a distal segment in frame t

$S_{pro}(t)$ -   local reference system of a proximal segment in frame t

The rotation matrix obtained from this calculation could then be resolved into its three angular components with the definitions given in Section 8.3.3. Using a rotation sequence of order ZXY for right-handed co-ordinate systems, the first, second and third angular displacements resulted in flexion-extension, abduction-adduction and internal-external rotation at the hips and knees, and dorsiflexion-platarflexion, eversion-inversion and internal-external rotation at the ankles, respectively. The zero position of all joint angles during dynamic trials was derived from their neutral position while the subjects' stood comfortably in a normal, upright posture during the static calibration trial, as previously explained in Section 7.2.3. Rotations in two opposite directions were therefore expressed using positive and negative values.

8.4.3.   Calculation of GRFs, GRMs and COP

As previously illustrated in Equations 5.4 and Equations 5.5, each force plate's GRFs F_{x1}, F_{y1}, F_{z1} and F_{x2}, F_{y2}, F_{z2} in all three directions, GRMs M_{x1}, M_{y1}, M_{z1} and M_{x2}, M_{y2}, M_{z2} about all three axes and the location of the COP in X and Z direction could be determined. Resetting the charge amplifiers between trials by zeroing their output should help to overcome problems associated with hysteresis, as explained in Section 5.2.2.2. However, following the filtering process, described in Section 8.2.3, GRF data may still contain minor fluctuations that are particularly detectable during periods when the force plates were not being touched, as their output should, under ideal circumstances, be zero. The fact that this was not always the case obviously indicated the presence of errors amongst the calculated force plate parameters. To overcome this problem, a code was written in Matlab (The MathWorks Inc, Natick Massachusetts, USA) as part of the data processing programs, which detected the point in time when GRFs started to drastically increase from, or decrease to, around zero. The threshold for this was set at 1N. Having approximated the onset and termination of the contact period with the force plate, which was the equivalent of stance phase, errors in GRF data were eliminated during periods before and after these two events by zeroing the force plate output.

8.4.4.   Calculation of inverse dynamics

Combining both the kinematic data from the ProReflex^{TM} system and the kinetic data from the force plates is a useful method for calculating additional gait parameters, like inter-segmental joint moments and power. These parameters were determined using inverse dynamics, and, in order for this approach to be applicable, certain variables needed to be considered including intra-segmental flexibility and the possibility of other, additional forces from external sources acting on the body. As it was difficult to establish these variables, it was decided that segments be assumed rigid and inter-connected by frictionless joints, and that any forces like air friction and slippage between the shoe, as well as prosthetic foot relative to the ground, were negligible.

The sum of all forces acting on a segment was composed of the gravitational pull in response to its own mass and the loads exerted by neighbouring segments onto its distal and proximal aspects. For the thigh, the neighbouring segments were the pelvis and shin and for the shin these were the foot and the thigh. With the foot being the most distal

part in the chain of lower limb segments, the source of forces acting upon it from distally was the ground. This therefore became the segment with which to commence solving the inverse dynamics. This was followed by the shin and then the thigh section.

Although the angles and positions of joints, GRFs and centres of pressure (CsOP) were already known, it was necessary to establish additional parameters for calculating inter-segmental joint moments and power. These included the PsOA, each segment's mass, COM location and radii of gyration (RiiOG), as well as their moment of inertia and acceleration. The way these parameters were obtained will be elaborated on in the following Sections.

8.4.5. <u>Calculation of PsOA</u>

The COP is related to the POA and this parameter has previously, in Section 5.1.2.8, been referred to as the location where a load was applied onto a force plate. Under certain circumstances the possibility exists that the POA and COP do not necessarily coincide. The given example was based on two PsOA that may locate the COP in between those points. This is the same scenario when considering the way GRFs are being exerted onto the foot, in that there may also be two or more PsOA.

During stance phase, for instance, forces are transmitted through both the heel and also through the ball of the foot, thus creating a simultaneous plantarflexion and dorsiflexion moment, respectively. The resultant moment can then be calculated as the difference between those two moments. This means that, if they were both of the same magnitude, the resultant moment would be zero, which would be the equivalent of having the COP directly underneath the ankle joint centre. It can therefore be concluded that a set of co-ordinates, which identifies the location of the force plates' COP relative to the foot, indicates the exact aspect on the foot's plantar surface onto which the epicentre of the GRFs act. Although there may be several, other locations where GRFs also act onto the foot, the COP is the resultant position of all those GRF locations. When the output from the force plates needs to be related to the position of anatomic and prosthetic segments, the COP can consequently be expressed as the POA, even if other PsOA may be exerting forces elsewhere.

In order to combine the data from the ProReflex[TM] system with the data from the force plates, it is necessary to determine the location of the force plates with respect to the

global reference system. This was achieved by recording eight markers M_{1-8} for identifying each corner of the two force plates, as previously described in Section 7.2.3. The COP can then be determined in relation to the centre of the plates, as elaborated on previously in Section 5.1.2.8. The next step therefore was to calculate each plate's central aspect from the position co-ordinates for the eight markers M_{1-8}, which was undertaken by using basic trigonometric algorithms (Barth et al 1985), as shown in Equations 8.17.

Equations 8.17: Calculation of force plates' centre from corner markers

$$F_{cen} \quad = \quad M_1 + 0.5 \cdot (M_1 - M_2)$$

Definitions:

F_{cen} -   position vector of force plate centre

M_1 -   position vector of a corner marker

M_2 -   position vector of other corner marker diagonally opposite from M_1

Because the COP is the location where forces are concentrated relative to the known centre of each force plate, it was possible to establish a relationship between analogue or kinetic data and the kinematic data. The COP could therefore be converted into the POA by expressing it in terms of global co-ordinates, as shown in Equations 8.18.

Equations 8.18: Calculation of COP or POA relative to the global system

$$x_1 \quad = \quad \frac{M_{z1} + y_1 \cdot F_{x1}}{F_{y1}} + D_{Gx1}$$

$$z_1 \quad = \quad \frac{M_{x1} + y_1 \cdot F_{z1}}{F_{y1}} + D_{Gz1}$$

$$x_2 \quad = \quad \frac{M_{z2} + y_2 \cdot F_{x2}}{F_{y2}} + D_{Gx2}$$

$$z_2 \quad = \quad \frac{M_{x2} + y_2 \cdot F_{z2}}{F_{y2}} + D_{Gz2}$$

Definitions:

$D_{Gx1/2}$, $D_{Gz1/2}$ -   offset between global origin and plates' centre in X and Z direction

$F_{x1}...F_{z2}$ -   force acting on the plates in X, Y, Z direction

$M_{x1}...M_{z2}$ -   force plates' moment about X and Z-axes

$x_1...z_2$ -   offset between COP and centre of force plate in X, Y, Z direction

Having determined the position of the POA in anterior-posterior and medial-lateral direction, the next step was to identify its location in proximal-distal direction. This was calculated as the vertical distance between the centroid of markers on the calibration frame and the bottom of that frame, described in Section 5.1.1.3, which lay level with the surface of the force plate where the POA was located.

Knowing the location of the POA and the position and orientation of each segment within the global reference system, it was possible to determine the loads F_{dis} exerted onto the distal aspect of the foot, shin and thigh section of both sides. The example given in Figure 8.6 illustrates typical calculations to determine the loads F_{dis}, which are shown here in 2D only.

Figure 8.6:   Force distribution onto the segments' distal end
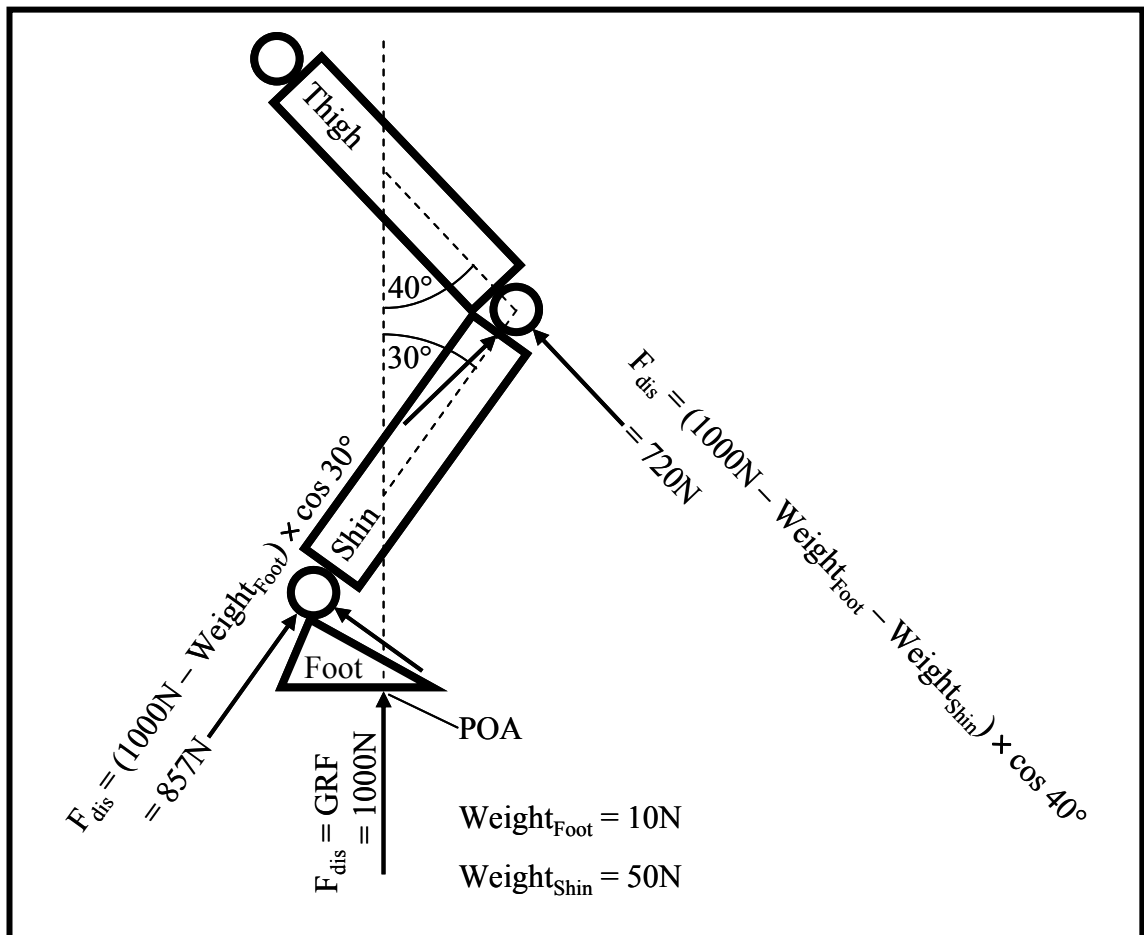
8.4.6.   <u>Anthropometry of anatomic segments</u>

De Leva 1996 conducted a study that was based on the adjustment of previously established anthropometric data regarding segments' mass, COM location and RiiOG from cadaver studies with college-aged Caucasians. Bone prominences were the

reference points in the original data, to which each segment's characteristics were related. However, most of these landmarks differed from joint centres that were typically encountered within research, similar to those defined in Section 7.1.8 to Section 7.1.10. This was the reason for De Leva 1996 to adjust the data in order to obtain parameters that can be used to express a segment's anthropometry with regard to its proximal and distal joint centre.

Table 8.2:   Details of segments' anthropometric data

Segments' characteristics	Thigh	Shin	Foot
Proximal endpoint (joint centre or bone boundary)	Hip joint	Knee joint	Posterior aspect of heel
Distal endpoint (joint centre or bone boundary)	Knee joint	Ankle joint	Tip of longest toe
Proximal joint (joint centre)	Hip joint	Knee joint	Ankle joint
Length (% of body height)	24.25	25.29	14.83
Mass (% of body mass)	14.16	4.33	1.37
COM from proximal endpoint (% of segment length)	40.95	43.95	44.15
ROG in the X-Y or sagittal plane (% of segment length)	32.90	25.10	25.70
ROG in the Y-Z or coronal plane (% of segment length)	32.90	24.60	24.50
ROG in the X-Z or transverse plane (% of segment length)	14.90	10.20	12.40

Having established the subjects' body height and mass, as explained in Section 4.2.4, Section 4.2.5 and Section 7.2.3, the data published by De Leva 1996 could then be used to express each segment's length and mass as a percentage of these measurements, whereby the location of the COM and RiiOG were calculated as a percentage of purely segment length rather than body height. All anthropometric details concerning the segments' mass, length, COM location and RiiOG, as well as the definition of joint centres are summarised in Table 8.2. These parameters were based on data from male

subjects whose body mass and height was normalised to 73.0kg and 1.741m, respectively.

To avoid confusion, it needed to be taken into consideration that the definition by De Leva 1996, regarding the anatomic planes of the foot, differed from those conventionally used with regard to the anatomic position, described in Section 2.1. The author of the referenced publication referred to what is commonly known as the anterior and posterior part of the foot, namely the toe and heel, as its distal and proximal aspects, respectively. Using such a description for this segment implies that its orientation within the sagittal plane can be regarded as perpendicular to the way it is during the anatomic position. The coronal plane and transverse plane are consequently the other way around. In order to make data interpretation for the current investigation easier, it was decided to adopt the convention used by De Leva 1996, but to implement it purely for descriptions concerning the foot's RiiOG.

8.4.7.   Anthropometry of prosthetic segments

The list of anthropometric parameters that De Leva 1996 published is vast and contains details for every major anatomic segment. Once the information required for the current investigation was extracted, the data needed adjusting. This was because the anthropometry of the left and right shin and foot sections were unlikely to be the same due to the artificial substitution of missing anatomic segments. In order for the data to be adjusted, it was necessary to first establish the anthropometry of the prosthetic shin and foot section.

To determine their length, mass, COM location and RiiOG, both segments needed separating by disconnecting the single axis ankle, described in Section 4.1.6.5, at its pyramid connecting system to the TT Pylon shin tube. For these parameters to be established, various procedures were undertaken that are described within the next three Sections 8.4.8 to 8.4.10 .

8.4.8.   Prosthetic segments' length and mass

Each section's length was measured with a ruler. Having indicated the location of the knee joint centre on the outside of the socket, as described in Section 7.1.9, the length of the shin section could be determined as the distance between those marks and the distal

end of the tube clamp adapter's female pyramid receiver. The length of the prosthetic foot was defined as the distance between the posterior aspect of the heel and the tip of the longest toe.

The subjects' anatomic foot section on the amputated side was completely replaced by the prosthetic foot, but the shin section on that side was only partially replaced as the residual limb still formed part of this segment. The anthropometry of the prosthetic shin section was consequently different without the residual limb embedded inside the socket. Therefore, the mass and mass distribution of the residual limb needed to be simulated inside the socket. This was achieved with the help of a water-containing latex bag that was filled just high enough for it to reach the lateral trimlines when inserted into the socket and secured in place with adhesive tape.

The entire shin section, namely the socket with a full latex bag, PyraLok, marker clamp, markers, TT Pylon, cam system, shin tube and tube clamp adapter was placed onto one of the force plates while taking a recording over 10s at 100Hz for the purpose of weighing it. A reflective marker was, as described in Section 6.2.1.1 and Section 6.2.3.3, within sight of the cameras, as the ProReflex[TM] system needed to register at least one marker in order to make a capture process valid. The same procedure was repeated with the foot including all its components, namely the single-axis ankle, Multiflex foot, markers and marker bolts.

Figure 8.7:   Force plate outputs from weighing a prosthetic segment
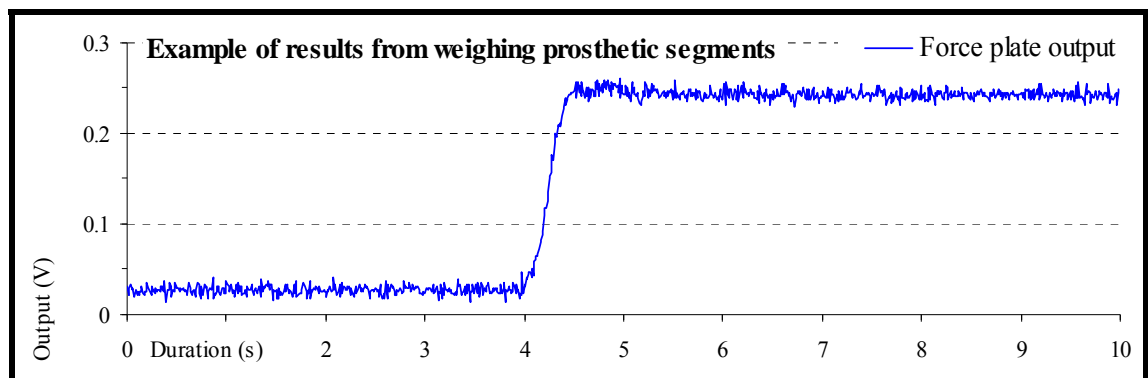
Having digitised the data, the force plate's output was processed in the same fashion as previously described in Section 6.2.3.5, by calculating the sum of the piezoelectric transducers' signals from channels C_5-C_8. Resultant voltages were converted into forces by using the force plate sensitivity levels, described in Table 5.1. The obtained

parameters were then divided by gravity's acceleration factor (9.81ms^{-2}) for further conversions into kg. Both segments' mass M_{seg} could be determined by calculating the difference between the mean of the raw data from their respective recordings' first and last three hundred frames. Figure 8.7 illustrates a typical output obtained from the weighing process.

8.4.9.   <u>Prosthetic segments' COM location</u>

Each segment's location of the COM was determined using a moment table, as described by Nigg 1994. The design used for the current study consisted of a wooden board that was resting horizontally on two knife edges located at either end of the board. Those knife edges were manufactured from the pointed tip of three self-tapping screws. They were sufficiently separated to consecutively fit in between the length and height of both the prosthetic shin and foot section. One of the knife edges contained two, and the other only one screw, so that the board formed a tripod base to ensure that it was stable and not rocking. The knife edge that was made from a pair of screws was orientated perpendicular with respect to the board's longitudinal axis, so that the distance between the two knife edges could be determined accurately using a ruler.

The board needed positioning in such a way that only one of the knife edges was located on a force plate. While taking recordings over 10s at 100Hz, each segment was positioned horizontally onto the board and secured in place by an anti-roll bar. Figure 8.8 illustrates the process of determining the COM for both the prosthetic shin and foot section using the described moment table.

Figure 8.8:   Determination of segments' COM through force plate output

| Tests with the shin section | Tests with the foot section |
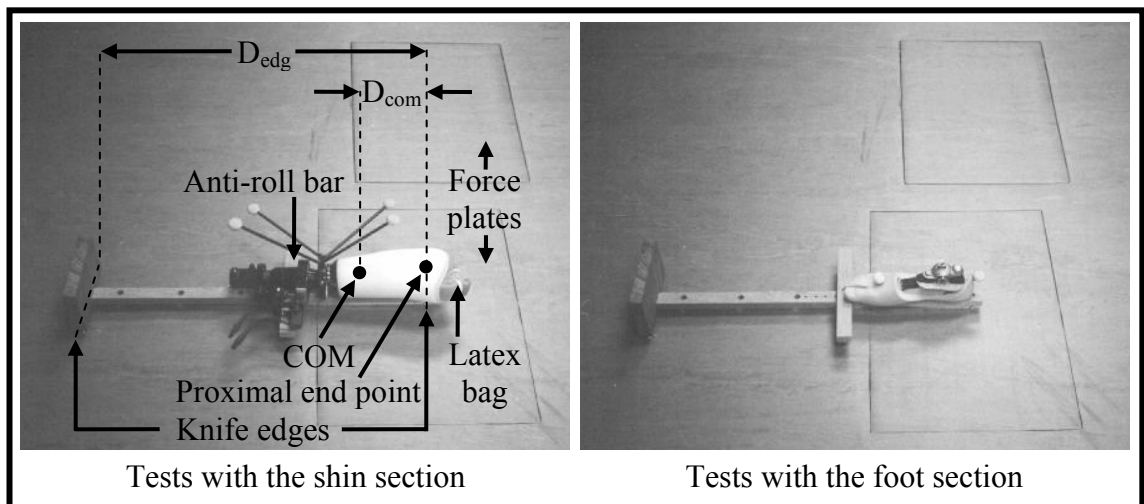
Having determined the force plate output F_{for}, the segments' mass M_{seg} and the distance D_{edg} between the two knife edges, it was possible to calculate the location of the COM relative to the force plate-mounted knife edge. Because one of each segment's previously defined endpoints, shown in Table 8.2, was positioned to coincide with the moment table's knife edge that was resting on the force plate, this knife edge was therefore also the starting pointfrom where the measurement D_{com} extended.

The way the calculations were undertaken is shown in Equations 8.19, which is the adapted form of the formula by Nigg 1994. This was done for determining the position of the COM in proximal-distal direction only. In turn, the COM position in anterior-posterior and medial-lateral direction was assumed to be in line with each segment's longitudinal axis, which was estimated to extend mid-way between the knee and ankle joint markers for the shin section and between the heel and metatarsal marker for the foot. To complete the calculations accurately, the force plate output needed to be converted into kg, as previously described in Section 8.4.8.

Equations 8.19: Calculation of COM location from knife edge

$$D_{com} \ = \ D_{edg} - (\, D_{edg} \cdot \frac{F_{for}}{M_{seg}} \,)$$

Definitions:

D_{com} - centre of mass location from knife edge or proximal endpoint

D_{edg} - distance between knife edges

F_{for} - sum of converted signals from force plate channels C_5-C_8

M_{seg} - mass of segment

8.4.10.   **Prosthetic segments' RiiOG**

The RiiOG represent the mass distribution of the prosthetic segments. This needed to be established from the segments' moments of inertia, which were determined via the pendulum approach, as described by Nigg 1994. Such a method relies on the gravitational pull that a suspended segment experiences. While swinging back and forth around a predetermined rotation axis, counting the amount of complete oscillation periods and measuring the time interval for these periods to be completed, provided the parameters that were still missing for calculating a segment's moment of inertia. This process needed repeating by letting each segment swing around different rotation axes to establish the moment of inertia about those axes within all three anatomic planes.

The hardware for the pendulum approach consisted of a metal bar that was rigidly clamped onto a table. Its free end contained a cross-bar onto which two L-shaped frames were mounted. Each of those L-shaped frames carried an adjustable pointer that opposed the pointer on the other frame. The two segments were consecutively suspended by pushing the two pointers together and clamping each segment between them. Friction while rotating the pointers was minimised by attaching them to their L-shaped frames with ball bearings. A round rod was pushed into a circular recess inside the rigidly clamped metal bar, which formed a connection to the cross-bar. Once each segment was securely held by both pointers, the round rod could rotate inside the recess until the suspended segment acquired an equilibrium position and was balanced. This was necessary in order to maximise the effect of gravity on its swing or pendulum action. A central bolt then needed tightening onto the round rod to lock it in place and prevent it from moving any further. The entire set-up, including both the suspended shin and foot section, is illustrated in Figure 8.9.

Figure 8.9:   Determination of segments' inertia through pendulum tests

Pendulum tests with the shin section   Pendulum tests with the foot section
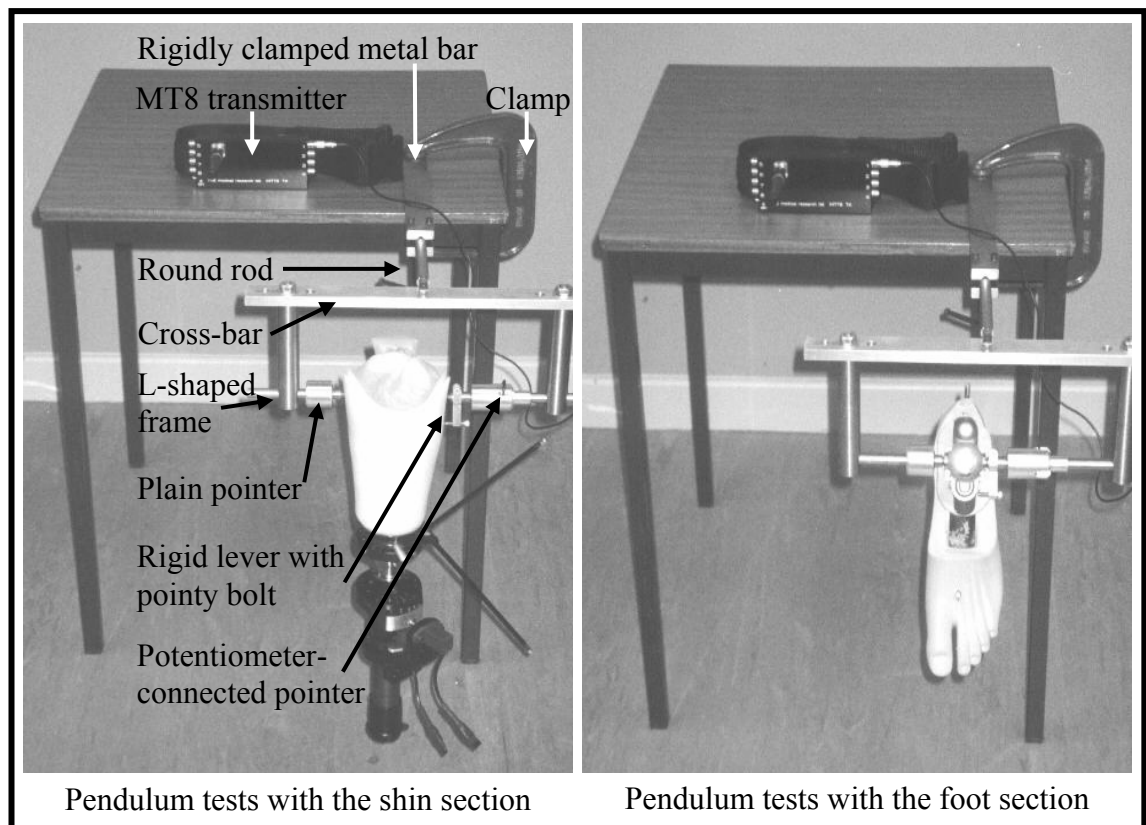
One of the pointers was directly connected to the central axle of a rotary potentiometer (RS Components, Northamptonshire, UK). This type of sensing device had an electrical and mechanical rotation of 340° and continuous 360°, respectively, which required a

starting torque of as low as 0.0028Nm. It had a virtually infinite resolution and a linearity of ±2%. The pointer that was connected to the rotary potentiometer needed to be fixed with respect to the prosthetic segment, in order for relative rotation between these two objects to be restricted, so that motion could only occur between the pointer and the cross-bar. That way, by letting the suspended segment swing back and forth between both pointers, its angular displacement also triggered motion of the rotary potentiometer's axle. As the potentiometer was plugged into the MT8 transmitter, described in Section 6.1.1.2, its signals, which constantly changed in response to the pendulum motion, were therefore transmitted to, and registered in, the data storage computer.

The way the pointer that was connected to the rotary potentiometer was fixed with respect to the prosthetic segment was by means of a sideward-protruding, rigid lever. This lever had a pointed bolt that was orientated in the same fashion as the pointer, so that it was parallel to it. Turning the head of the bolt towards the rigid lever tightened the bolt's pointed tip against the suspended segment. The pointed bolt together with its potentiometer-connected pointer was consequently pushed against one side of the segment and the plain pointer without the potentiometer against the segment's other side. Recordings were taken over 10s at 100Hz while the segments swung over an initial angle of approximately 90° or ±45°.

The first type of recording was taken while the two pointers were aligned parallel to the segments' coronal plane. The shin section was suspended from the knee joint centre indicated by the marks on either side of the socket and the foot section from the axle centre of the single axis ankle joint. The second type of recording was taken while the two pointers were aligned parallel to the segments' sagittal plane. Ideally, the two locations from which the two pointers suspended each segment should have been positioned in such a way that a line connecting the pointers during the second recording was perpendicular to a line connecting the pointers during the first recording, as well as perpendicular to the respective segment's longitudinal axis. To suspend a segment this way was possible for the prosthetic foot section, but not for the shin section, as the posterior trimline of the socket was too low for a pointer to push against. As the socket was fairly round in cross-section, it was considered that the affect on the pendulum action was negligible, if the socket remained in the same position, while only the components distal to the socket were turned by 90° at the PyraLok's pyramid system.

That way, the two pointers were left in the same position they were in during the first type of recording. The moment of inertia about the medial-lateral and anterior-posterior axis could then be determined from the data of the first and second type of recording, respectively.

Establishing the moment of inertia about a proximal-distal axis was more difficult, because, in order to do so using the pendulum approach, the segments' would have had to be suspended between two points that coincide with their longitudinal axis. Such a process seemed rather awkward, and so an alternative solution was required. Nigg 1994 reported on a number of methods, and the one most applicable is the torsional pendulum approach. When suspended by a spring or resting on a turntable with its fulcrum connected to opposing springs, a segment can oscillate around its own longitudinal axis. Similar to the pendulum approach, the amount of complete oscillation periods needs counting, and the time interval for these periods to be completed requires measuring. The only additional factor necessary for the required calculations is the rotational spring constant.

However, neither the method of suspending the segments by a spring nor that of involving the segments to stand on a turntable seemed particularly practical. Rotating the segments around their own longitudinal axis for determining their moment of inertia about that axis meant that one end of the segments was free to move away from this axis in response to centrifugal forces unbalancing the oscillations. A device that permits steady rotations without unbalancing the segments would need to be very intricate and was considered too complicated for construction during the current investigation. Also, the complexity of the design would increase further if an electronic device, like a potentiometer, was to be included for measuring the amount and duration of oscillations. Instead, adopting the data that De Leva 1996 published, seemed the most feasible way of approximating the prosthetic segments' moment of inertia about their longitudinal axis, particularly as the radius of gyration (RusOG) in a transverse plane is far smaller compared to the other two planes, which should therefore have a minimal affect on the calculations.

The data from the first and second type of recording for establishing the segments' moment of inertia about their medial-lateral and anterior-posterior axis was processed in

Excel (Microsoft Corporation, Redmond Oregon, USA). A typical output obtained from the pendulum tests is illustrated in Figure 8.10.

Figure 8.10:   Determination of RiiOG through pendulum tests
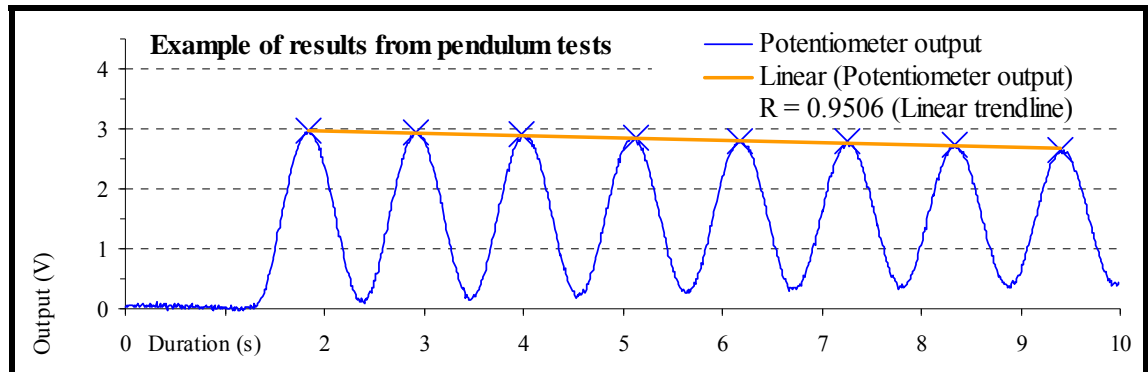
Decreasing magnitudes of the graph's individual apices indicate the pendulum's reducing amplitudes of oscillations as time progresses. The reduction in this example, as calculated over the period between the first and last peak and over only 1s, reached approximately 10.7% and just 1.42% of the maximum output during the first peak, respectively. This is a fairly low rate of reduction and demonstrates that the friction from the ball bearings as well as wind resistance was small. The correlation co-efficient R from the potentiometer output reached 0.9506, as calculated over the period between the first and last peak. Such a value indicates a very high degree of correlation and therefore a low dispersion from a truly linear reduction in oscillation amplitudes.

Equations 8.20: Calculation of one oscillation period

$$O_{cyc} = \frac{P_{las} - P_{fir}}{F_{sam} \cdot N_{tot}}$$

Definitions:

F_{sam} -   sampling frequency (100Hz)

N_{tot} -   total number of intervals between the first and last peak

P_{fir} -   recording frame number of the largest value during the first peak

P_{las} -   recording frame number of the largest value during the last peak

O_{cyc} -   duration of one oscillation period

Every complete oscillation period should, under ideal circumstances, extend over the same length of time. However, as this is rarely the case, the accuracy for determining the duration O_{cyc} of only one cycle can be increased by calculating the mean of all cycles. This was achieved by establishing the difference between the recording frame

number of the largest value during the first and last peak P_{fir} and P_{las}, which was divided by the product of the sampling frequency F_{sam} and the total number of intervals N_{tot} between the first and last peak, as shown in Equations 8.20.

The data obtained from swinging a segment around its predetermined rotation axes can be used for calculating the moment of inertia I_{axi} about those axes. This information can then be implemented to calculate the moment of inertia I_{com} about an axis through the COM by applying the parallel axis theorem. The formula for the pendulum approach is cited in Equations 8.21, which is the adapted form that incorporates the parallel axis theorem in accordance with Nigg 1994.

Equations 8.21: Calculation of moment of inertia about the COM

$$I_{com} = I_{axi} - M_{seg} \cdot D_{com}^{2}$$

$$\Rightarrow I_{com} = \frac{M_{seg} \cdot G \cdot D_{com} \cdot O_{cyc}}{4\pi^{2}} - M_{seg} \cdot D_{com}^{2}$$

Definitions:

D_{com}	-	distance from COM to segments' axis of rotation or proximal endpoint
G	-	gravity (9.81ms^{-2})
I_{axi}	-	moment of inertia about an axis through the proximal joint
I_{com}	-	moment of inertia about an axis through the COM
M_{seg}	-	mass of segment
O_{cyc}	-	duration of one oscillation period

For this to equate, it was necessary to determine the location of the segments' COM relative to their rotation axes. Previous calculations already established the distance D_{com} between the COM and the segments' proximal endpoint. In the case of the shin section, the longitudinal location of its proximal endpoint and those axes was identical, and the required distance between the COM and rotation axes was therefore already known. However, the proximal endpoint of the foot was in a different location to that of the rotation axes, so that the offset between these landmarks needed to be established. This was measured with a ruler parallel to the longitudinal axis of the foot, in order for the distance between the COM and rotation axes to be determined. Once the moment of inertia about three orthogonal axes through the COM was known, the RiiOG could be determined, as shown in Equations 8.22.

Equations 8.22: Calculation of RiiOG

$$I_{com} \quad = \quad M_{seg} \cdot K^2$$

$$\Leftrightarrow \quad K \quad = \quad \sqrt{\frac{I_{com}}{M_{seg}}}$$

Definitions:

I_{com} -   moment of inertia about an axis through the COM

K -   radius of gyration

M_{seg} -   mass of segment

8.4.11.   Summarised segments' anthropometry

All the parameters established in the last three Sections that represent the prosthetic segments' anthropometric data, are summarised in Table 8.3, except for the moment of inertia about the segments' longitudinal axis and their RusOG within the X-Z or transverse plane, as these were not determined experimentally. For purpose of comparison, the respective data from the study by De Leva 1996 are also included.

During data processing, the segments' anthropometry was expressed as percentages, as in Table 8.2. However, it was, for reasons of display and analysis, considered more comprehensive, if the parameters were converted into standard mass and length measurements, because the presented data would otherwise vary depending on how tall and heavy each subject was. Following the conversions, it became easier to relate the characteristics of prosthetic segments' to those of the anatomic segments.

It may be seen that the mean length of the recruited subject's prosthetic shin section was shorter than the anatomic shin section calculated by De Leva 1996. This happened because the prosthetic foot section was disconnected at the distal end of the tube clamp adapter's female pyramid receiver and not further distally at the axle of the single axis ankle, as disassembling this unit seemed impractical. In turn, the lengths of prosthetic and anatomic feet were very similar, but not quite identical. Small measurement differences have been introduced by the fact that prosthetic feet are manufactured in incremental sizes of 10mm, whereby the divisions for measurements of anatomic feet are obviously infinite.

Table 8.3: Summarised anthropometric data of prosthetic segments

Sub-ject	Segment length (mm)		Segment mass (kg)		COM from proximal end (mm)		ROG in X-Y / sagittal plane (mm)		ROG in Y-Z / coronal plane (mm)	
	Shin	Foot	Shin	Foot	Shin	Foot	Shin	Foot	Shin	Foot
A	450	280	2.90	0.74	163.7	111.8	143.1	74.2	143.1	84.0
B	390	270	3.20	0.73	143.9	110.3	132.6	72.4	134.6	80.7
C	350	270	2.80	0.73	149.9	110.3	140.0	73.7	132.3	77.8
D	350	250	3.20	0.71	161.1	108.8	144.9	73.8	141.8	76.0
E	440	260	3.30	0.72	144.3	109.4	143.0	69.9	138.6	76.2
F	460	290	3.20	0.75	176.1	112.5	156.4	74.2	158.2	79.8
G	410	270	3.10	0.73	139.2	110.3	135.7	80.7	133.7	80.7
H	400	270	3.20	0.73	147.3	110.3	128.4	79.7	128.4	77.5
I	400	280	3.60	0.74	147.8	111.8	146.8	78.1	141.2	78.1
J	410	280	3.00	0.74	130.8	111.8	128.3	83.7	128.3	81.5
	Minimum									
	350	250	2.80	0.71	130.8	108.8	128.3	69.9	128.3	76.0
	Maximum									
	460	290	3.60	0.75	176.1	112.5	156.4	83.7	158.2	84.0
	Difference as in max-min									
	110	40	0.80	0.04	45.3	3.7	28.1	13.8	29.9	8.0
	Mean									
	406	272	3.15	0.73	150.41	110.73	139.92	76.04	138.02	79.23
	Standard deviation									
	37.5	11.4	0.22	0.01	13.2	1.2	8.8	4.3	8.9	2.6
	Data by De Leva 1996									
	440.3	258.1	3.16	1.00	193.5	114.0	110.5	66.3	108.3	63.2
	Mean as % of data by De Leva 1996									
	92.21	105.4	99.68	73.00	77.73	97.13	126.62	114.69	127.44	125.36

As would have been expected, both the prosthetic shin and foot sections were a great deal lighter than their anatomic counterparts. This is because human tissue is larger in

volume than prosthetic components and in lot of cases, heavier than most man-made materials used in prostheses.

Another parameter that was smaller for the prosthetic segments compared to the anatomic ones was the distance between their proximal end point and the COM. This seemed particularly logical with respect to the shin section as the residual limb still formed part of this segment, whereby its distal aspect consisted predominantly of a light-weight carbon fibre shin tube, so that the main mass was located further proximally. A similar reason can be given with regard to the COM location within the foot section. Although this segment was completely replaced, the proximally located, metal ankle unit was a lot heavier than the remaining parts of the foot. This was especially true when the mass of the light-weight foot mould that formed part of this section's distal aspect was being taken into consideration, as this, again, located the foot's main mass proximally.

The prosthetic segments' moments of inertia that were established via the pendulum approach, namely those about anterior-posterior and medial-lateral axes, are summarised in Table 8.4. These were determined for rotations around both the proximal joint and the COM. For purpose of comparison, they were then expressed as a percentage of the respective parameters that were calculated from the data published by De Leva 1996.

Table 8.4:   Inertial properties of prosthetic segments

COR	Orientation of axis	Moment of inertia of prosthetic segment (% of moment of inertia of anatomic segments)	
		Shin	Foot
Proximal joint	medial-lateral	85.2	86.3
	anterior-posterior	85.0	98.1
COM	medial-lateral	160.7	96.5
	anterior-posterior	162.7	115.1

It can be seen that the prosthetic segments' inertial properties about axes through proximal joints were lower than those of their anatomic counterparts. This makes sense, because the prosthetic segments were lighter and the COM located closer to the COR.

In turn, such low inertial characteristics had an impact on the prosthetic segments' moment of inertia about their COM, as the values were, in most cases, a lot higher compared to the corresponding parameters for anatomic segments. As previously shown in Equations 8.22, the moment of inertia I_{com} about the COM is described by the product between the segments' mass M_{seg} and their respective RusOG K squared. Because the prosthetic components were lighter than the anatomic ones, the RusOG therefore needed to increase in magnitude, in order for the calculation to equate. This explains why the mean value of the RusOG was larger in both the sagittal and coronal plane for the prosthetic shin and foot compared to their anatomic counterparts.

8.4.12.   Adjustments of segments' anthropometry

Following amputation, the body mass had changed due to the artificial substitution of the anatomic shin and foot section. This was a factor that needed to be taken into consideration when expressing the ratio between the mass of a segment and the entire body, because the parameters by De Leva 1996 were calculated as a percentage of complete human bodies.

It was previously shown in Table 8.3 that the prosthetic shin and foot were lighter than their anatomic counterparts, which meant that the overall body mass was reduced when wearing a prosthesis. Results obtained from using the conversion factors published by De Leva 1996 for calculating the mass of segments would therefore be wrong if this calculation was based on the reduced body mass. The resultant error would therefore make the mass of individual segments appear lighter than they actually were.

Instead, an alternative approach was taken in the form of a compensatory algorithm. This reduced errors in calculating the mass of individual segments. The first step was to subtract the mass of the prosthetic shin M_{shi}, including the water-filled latex bag, as well as the mass of the prosthetic foot M_{foo} from the subjects' total body mass M_{amp}, which was weighed immediately prior to the tests. The obtained results resembled the subjects' mass M_{wit} without the test-prosthesis and residual limb. The true body mass M_{tru} they would have had, if part of their lower limb was not amputated, could then be mathematically approximated by establishing how heavy their missing anatomic segments, including the residual limb, would be. As previously described in Table 8.2, the mass of the anatomic shin and foot is, according to De Leva 1996, 4.33% and 1.37% of the total body mass, respectively. These conversion factors could then be used to

calculate the ratio between the subjects' mass M_{wit} without the prosthetic segments and residual limb, relative to the percentage body mass M_{per} without the anatomic shin and foot, as illustrated in Equations 8.23.

Equations 8.23: Calculation of true body mass without amputation

$$M_{tru} = \frac{M_{wit}}{M_{per}} \cdot 100$$

$$\Rightarrow \quad M_{tru} = \frac{M_{amp} - M_{shi} - M_{foo}}{100 - 4.33 - 1.37} \cdot 100$$

Definitions:

4.33	-	conversion factor for shin section, as stipulated in Table 8.2
1.37	-	conversion factor for foot section, as stipulated in Table 8.2
M_{amp}	-	total body mass with prosthetic segments and residual limb
M_{foo}	-	mass of prosthetic foot section
M_{per}	-	percentage body mass without the anatomic shin and foot
M_{shi}	-	mass of prosthetic shin section
M_{tru}	-	true body mass without amputation
M_{wit}	-	total body mass without prosthetic segments and residual limb

Knowing the true body mass, it was then possible to express the thigh, shin and foot of the sound side as a percentage of the true body mass. This was also possible for the thigh of the amputated side.

8.4.13.   Calculation of segments' velocity and acceleration

The angular velocity ϖ_L a segment experiences can be calculated as the first derivative of its displacement, using the filtered co-ordinates in 3D of the segment's COM location L_{seg} within the local reference system. After that, the angular acceleration α_L this segment experiences can be calculated as the first derivative of its angular velocity ϖ_L or its second derivative of the COM displacement. Cappozzo et al 1990 described a method for calculating those parameters and the mathematical algorithm for this was adapted by Linden van der 1999, as illustrated in Equations 8.24 for the angular velocity.

As the obtained angular velocity ϖ_L was referred to the segment's local reference system, this needed converting in order to establish its angular velocity ϖ_G relative to

the global reference system by multiplying ϖ_L with L_{seg}. The same procedure was also applicable for determining the angular acceleration α_G relative to the global reference system.

Equations 8.24: Calculation of segments' angular velocity

$$\varpi_L \quad = \quad L_{seg}{}^{-1} \cdot \frac{L_{seg}}{dt}$$

Definitions:

L_{seg}	-	local reference system of a segment
$\dfrac{L_{seg}}{dt}$	-	first derivative of local reference system L_{seg}
ϖ_L	-	angular velocity within local reference system L_{seg}

8.4.14.   Calculation of inter-segmental joint forces

The sum of all forces acting on a segment is, according to Newton's second law, equivalent to the product between a segment's mass and the acceleration it experiences about its COM, as described in Equations 8.25. Having determined the load F_{dis} exerted onto a segments' distal aspect, as shown in Section 8.4.5, and knowing its mass M_{seg} and angular acceleration α_{seg}, as established in Section 8.4.8 and Section 8.4.13, all the necessary variables were known for finding the unknown force F_{pro} that acts on the segment's proximal joint.

The output from the force plates was positive when GRFs were orientated upwards, but because the earth's pull was dragging the segment towards its centre, the parameter representing gravity had to be negative, which meant that the force plate data for these calculations needed multiplying by the factor -1. To maintain a consistent sign convention with regard to vector orientations, the remaining forces F_{dis} and F_{pro} consequently obtained positive and negative values, respectively.

8.4.15.   Calculation of inter-segmental joint moments

The sum of moments T that a segment experiences about its COM is composed of the moment T_{Edis} and T_{Epro}, due to linear acceleration and gravity about the segment's distal and proximal end, as well as the moment T_{Jdis} and T_{Jpro}, due to reaction forces produced by muscles about the segment's distal and proximal end, respectively. With the foot

being the most distal part in the chain of lower limb segments, this was where solving the inverse dynamics commenced, as mentioned in Section 8.4.4.

Equations 8.25: Calculation of a segment's sum of forces according to Newton

$$\sum F \quad = \quad M_{seg} \cdot G \quad + \quad F_{dis} \; + F_{pro}$$

also

$$\sum F \quad = \quad M_{seg} \cdot \alpha_{seg}$$

therefore

$$M_{seg} \cdot \alpha_{seg} \quad = \quad M_{seg} \cdot G \quad + \quad F_{dis} \; + F_{pro}$$

$$\Leftrightarrow \qquad F_{pro} \quad = \quad M_{seg} \cdot \alpha_{seg} \quad - \quad M_{seg} \cdot G \; - F_{dis}$$

$$= \quad M_{seg} \cdot (\quad \alpha_{seg} \quad - \quad G \;) \; - F_{dis}$$

Definitions:

α_{seg}	-	acceleration of a segment about its COM
F_{dis}	-	force acting on the distal joint (or plantar aspect of the foot)
F_{pro}	-	force acting on the proximal joint
$\sum F$	-	sum of forces acting on a segment
G	-	gravity ($-9.81 ms^{-2}$)
M_{seg}	-	segment's mass

The moment T_{Jdis}, due to reaction forces about a segment's distal end, was determined as the product between the force acting on its distal aspect F_{dis} and the difference between the co-ordinates of its distal joint G_{Jdis} and the co-ordinates of its COM G_{com}. Because the foot did not possess a distal joint due to its terminal position, the force acting on its distal aspect F_{dis} was the GRF and the co-ordinates of its non-existent, distal joint G_{Jdis}, were those of the POA.

In turn, the equation for the moment T_{Jpro}, due to reaction forces about a segment's proximal end, was defined as the product between the force F_{pro} acting on its proximal aspect and the difference between the co-ordinates of its proximal joint G_{Jpro} and the co-ordinates of the COM G_{com}. Because two inter-connected segments share the same

Equations 8.26: Calculation of segments' moment about their proximal end

$$\sum T \;=\; I_{com} \cdot \frac{d\omega_G}{dt}$$

$$=\; T_{Edis} + T_{Epro} + T_{Jdis} + T_{Jpro}$$

$$\Rightarrow\; T_{Epro} \;=\; I_{com} \cdot \frac{d\omega_G}{dt} - T_{Jdis} \qquad\qquad - T_{Jpro} \qquad\qquad - T_{Edis}$$

$$\Rightarrow\; T_{Epro} \;=\; I_{com} \cdot \frac{d\omega_G}{dt} - F_{dis} \cdot (G_{Jdis} - G_{com}) - F_{pro} \cdot (G_{Jpro} - G_{com}) - T_{Edis}$$

Definitions:

I_{com}	-	moment of inertia about an axis through the COM
F_{dis}	-	force acting on distal aspect
	-	from GRF (F), foot (S), shin (T)
F_{pro}	-	force acting on proximal aspect
	-	from shin (F), thigh (S), pelvis (T)
G_{com}	-	co-ordinates of COM
G_{Jdis}	-	co-ordinates of distal joint
	-	POA (F), ankle (S), knee (T)
G_{Jpro}	-	co-ordinates of proximal joint
	-	ankle (F), knee (S), hip (T)
$\sum T$	-	sum of moments about COM
T_{Edis}	-	moment due to linear acceleration and gravity about distal end
	-	zero (F), $-T_{Epro}$ from distal segment (S, T)
T_{Epro}	-	moment due to linear acceleration and gravity about proximal end
	-	ankle (F), knee (S), hip (T)
T_{Jdis}	-	moment due to reaction forces about distal end
		POA (F), ankle (S), knee (T)
T_{Jpro}	-	moment due to reaction forces about proximal end
		ankle (F), knee (S), hip (T)
ϖ_G	-	angular velocity within global reference system

joint, the moment T_{Edis}, due to linear acceleration and gravity about the proximal segment's distal end, was the same as the moment T_{Epro}, due to linear acceleration and gravity about the distal segment's proximal end. The only difference was that the moment T_{Edis} about the proximal segment's distal end was the reverse for the distal segment's proximal end, so that $T_{Edis} = -T_{Epro}$. As before, with regard to the force F_{dis}

acting on the distal aspect of the foot, the scenario concerning the moment T_{Edis}, due to linear acceleration and gravity about this segment's distal end, had to be treated differently than more proximal segments. Because the foot did not possess a distal joint, due to its terminal position, the moment T_{Edis} was therefore absent and for calculation purposes considered zero.

Inter-segmental joint moments were calculated in accordance with the algorithm reported by Hardt & Mann 1980, which was adapted by Linden van der 1999 and is shown in general form under Equations 8.26. This was re-arranged to solve the unknown inter-segmental moment T_{Jpro} that occurred due to reaction forces produced by muscles about each segment's proximal joint.

Denotations of variables are the same for all three lower limb segments, but the parameters or landmarks to which they refer can vary, due to previously described differences in calculating the moments about each joint. Explanations regarding these variations are given in the definitions of variables that follow Equations 8.26, by appending a bracketed "()" F, S and T for the foot, shin and thigh, respectively, as an indicator for a certain parameter or landmark and the segment to which it corresponds.

8.4.16.   Calculation of inter-segmental joint powers

The inter-segmental power P_{Joi} generated at each lower limb joint was calculated in accordance with the formula given by Meglan & Todd 1994, which was adapted to suit the current application and is displayed in Equations 8.27. This calculation was based on the dot product between the net inter-segmental moment T_{joi} and the net inter-segmental angular velocity ϖ_{joi}. The latter is defined as the difference between the angular velocity ϖ_{dis} and ϖ_{pro} of the distal and proximal segment, respectively.

When the inter-segmental angular velocity is very small, it may appear as if hardly any power is being generated. This may be the result of two antagonistic muscle groups contracting simultaneously, thus counteracting each other, which means that power is actually being generated, but because the changes in inter-segmental angles are very small, it appears as if the level of power is virtually absent. During an analysis of positive and negative power that is being generated at a joint, care has be taken for this parameter only to be interpreted with regard to action at the joint itself, and it should not

be related to muscle action, as such interpretations can, for the aforementioned reasons, be misleading or simply wrong.

Equations 8.27: Calculation of inter-segmental joint power

$$P_{joi} \quad = \quad T_{joi} \cdot (\varpi_{dis} - \varpi_{pro})$$

$$\Rightarrow \qquad = \quad T_{joi} \cdot \qquad \varpi_{joi}$$

Definitions:

P_{joi}	-	inter-segmental power
T_{joi}	-	inter-segmental moment
ϖ_{dis}	-	angular velocity of distal segment
ϖ_{joi}	-	inter-segmental angular velocity
ϖ_{pro}	-	angular velocity of proximal segment

8.4.17. <u>Calculation of the incident of gait cycle events</u>

Heel strike and toe off represented relevant events during the gait cycle when the force plate data increased from, or decreased to, zero, respectively. These two changes in output were used as indicators to determine the onset and termination of stance phase, as explained in Section 8.4.3. With a total of two force plates, both the left and right foot were able to make contact with only one plate each during a single, straight walk. The initial and final part of each foot's contact period with its respective plate was used as an indicator for heel strike and toe off, respectively. This defined the onset and termination of stance phase and the onset of swing phase. In turn, GRFs could not be used as an indicator for the second heel strike, as these could not be measured, because each foot established contact with the floor and not with another force plate. This meant that only the onset, but not the termination, of swing phase could be defined with GRFs. Therefore, an alternative solution that was different to measuring GRFs needed to be found, one with which the moment in time when the second heel strike occurred could be determined.

Mickelborough et al 2000 extracted relevant information from heel marker trajectories in order to determine the incident of heel strike. This method was based on the identification of a specific characteristic within each heel marker trajectory. The procedure for determination of heel strike required this characteristic to be manually

identified and marked, by moving the cursor on the computer screen to where that characteristic was located, while running a customised computer program. Such a method may be useful if GRFs cannot be measured.

With a total of forty trials for each of the ten subjects, it seemed rather time consuming to undertake the procedure reported on by Mickelborough et al 2000 for every single recording. Also, the likelihood for making a mistake is quite high when manually pointing the cursor to the required characteristic of each heel marker trajectory. It was therefore decided to write a code with which it was possible to relate force plate data from the first heel strike to heel marker displacements during the same heel strike. This code calculated the period between the incident of the first heel strike, as determined from GRFs, and the incident of a specific characteristic within each heel marker trajectory. It would then become possible to utilise the length of that period in the calculation for the approximation of the second heel strike.

The described code was written in Matlab (The MathWorks Inc, Natick Massachusetts, USA) and it formed part of the data processing programs. Having established the point in time or recording frame number amongst GRF data when the first heel strike took place, the next step was to identify a specific characteristic in the heel marker trajectory of the same foot that occurred within fractions of a second around the specified frame number. As described in Section 5.1.1.12, the size of the capture volume was set up in a manner that allowed half a step to be recorded prior to reaching the first force plate with the left foot. The characteristic to be identified was therefore estimated to occur within the initial 25% and 50% of the entire capture time for the left and right foot, respectively.

Preliminary data analyses showed that an appropriate characteristic in the heel marker trajectory occurred during the period specified above and within fractions of a second around the specified frame number from GRF data for the first heel strike. This characteristic was the lowest dip within the heel marker trajectory. This dip represented the incident when the heel marker was closest to the ground, due to its posterior location on the foot, which was at that stage dorsiflexed, as this segment was about to make contact with the floor. The apex of the described trajectory dip could be identified as the smallest value for the vertical distance between the centroid of the heel marker and the ground. Having determined the first heel strike for each foot, the second heel strike for

the left and right side had to occur after the initial 25% or 50% of the capture time, respectively. This gait cycle event was, like the first heel strike, determined by the apex of the trajectory dip during its respective period.

The next stage was to calculate the difference between the frame number of the first heel strike from GRF data and the frame number of the apex from the first heel marker trajectory dip. This difference was then deducted from the frame number of the second heel marker trajectory dip to approximate the occurrence of the second heel strike. Typical data representing vertical GRFs for the left and right side and simultaneously occurring heel marker trajectories of the same trial are illustrated in Figure 8.11 and Figure 8.12, respectively. To fit both sets of data into the same chart, the values for the GRFs were scaled down by dividing them by a factor of three, as indicated in the legend and the y-axis title of each chart.

Figure 8.11:   Typical data for vertical GRFs and left heel marker trajectory
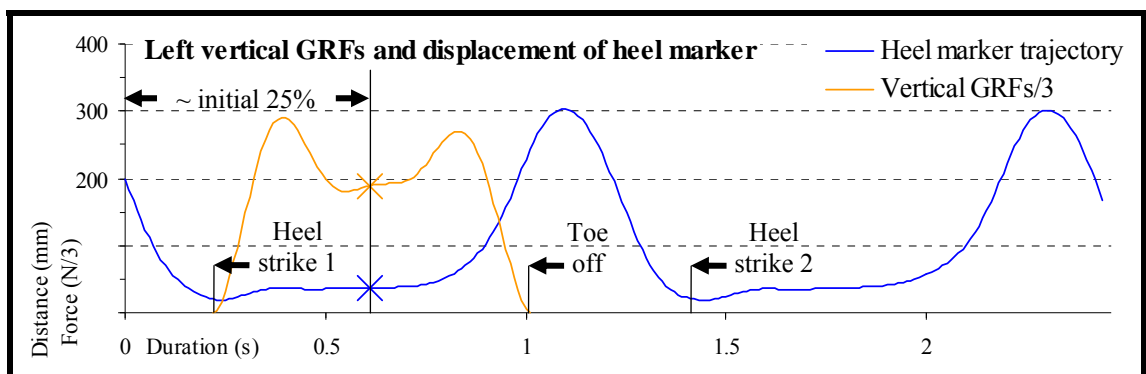
Figure 8.12:   Typical data for vertical GRFs and right heel marker trajectory
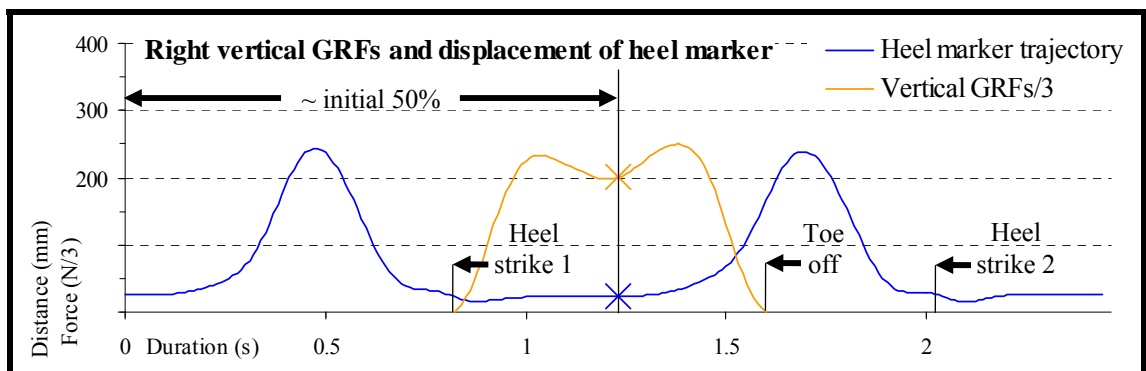
With exactly two force plate contacts per trial, namely one on the left and another on the right side, and ten trials for each of the four set-ups, the total number of force plate contacts added up to eighty for each subject. The data from each subject appeared similar with respect to the sound and amputated side, and also with respect to the four

261

types of set-ups that were based on permitting and restricting the two types of motions within the TT Pylon in various configurations. Although information showing such similarities was, for reasons of conciseness, not included in Table 8.5, the fact that the data were similar was why all eighty force plate contacts from each subject were summarised. This summary of all ten subjects' incidents concerning the first heel strike formed the basis for a statistical analysis with regard to the difference in determining this gait cycle event using GRF data and data from both heel marker trajectories.

Eighty is a relatively large number of measurements and lends the data analysis high statistical power. To indicate the order of the incident for the first heel strike with regard to the kinetic and kinematic measurements, negative values were used when the earlier incident of this gait cycle event was determined from GRF data, so that positive values were used when the earlier incident of this gait cycle event was determined from the heel marker trajectories.

Calculated differences between kinetic and kinematic data for the first heel strike ranged between 7-25 frames or 0.07-0.25s. Although this may appear fairly large, the minimum and maximum standard deviation from this range of differences was determined to be approximately 1.31 and 6.23 frames or 0.0131 to 0.0623s, respectively. This represented a very low dispersion of measurements, which meant that the precision for determining the first heel strike from the heel marker trajectories was high. The standard deviation of the mean of measurements from each subject reached only approximately 1.2 frames or 0.012s, thus indicating good repeatability. Also low was the RMS error, which was determined to be approximately 2.94 frames or 0.0294s, thus demonstrating a satisfactory level of accuracy. Because the mean values of all ten subjects' data were negative, it was concluded that heel strike, as calculated from the kinetic data, occurred in the majority of cases before the apex of the heel marker trajectory dip, as calculated from the kinematic data.

In conclusion, the analysis of the results from the actual gait laboratory tests showed that the aforementioned method of calculating the first heel strike from the heel marker trajectories is satisfactory. This is so, because the approximation of this event is very close to the actual incident of the first heel strike, as calculated from GRF data. It is therefore justifiable to apply this method for predicting the incident of the second heel strike, which can be undertaken with confidence.

Table 8.5:   Summary of timing differences for heel strike occurrence

Sub-ject	Minimum	Maximum	Difference as in max-min	Mean	Standard deviation
(difference in frame number between GRF data and heel marker trajectory) The values were calculated from each subject's eighty heel strikes (ten trials for each of the four set-ups for both the left and right side)					
A	-21	2	23	-4.00	6.23
B	-6	1	7	-2.96	1.31
C	-9	6	15	-1.48	3.35
D	-21	2	23	-3.23	3.14
E	-6	4	10	-2.25	3.22
F	-4	4	8	-0.85	1.62
G	-23	2	25	-3.48	4.60
H	-8	4	12	-2.71	3.54
I	-10	4	14	-0.19	2.45
J	-5	2	7	-2.55	2.21
	Minimum				
	-23	1	7	-4.00	1.31
	Maximum				
	-4	6	25	-0.19	6.23
	Difference as in min-max				
	19	5	18	3.81	4.92
	Mean				
	-11.30	3.10	14.40	-2.37	3.17
	Standard deviation				
	7.39	1.52	6.96	1.20	1.45

8.4.18.   Calculation of temporal and spatial parameters

Relative temporal and spatial gait parameters were established from the occurrence of the three gait cycle events previously determined in Section 8.4.17. These gait cycle events included heel strike one, toe off and heel strike two.

Table 8.6:   Definitions of temporal and spatial gait parameters

Temporal gait parameters:	Step time / stride time Double support time / stride time	
Definitions (time)	**From**	**To**
Stride (s)	L, _R_ - heel strike 1, _1_	L, _R_ - heel strike 2, _2_
Step (s)	L, _R_ - heel strike 1, _1_	R, _L_ - heel strike 1, _2_
Double support (s)	R, _L_ - heel strike 1, _2_	L, _R_ - toe off
Spatial gait parameters:	**Step length / stride length**	
Definitions (length)	**From**	**To**
Stride (m, x-direction)	L, _R_ - heel strike 1, _1_	L, _R_ - heel strike 2, _2_
Step (m, x-direction)	L, _R_ - heel strike 1, _1_	R, _L_ - heel strike 1, _2_
Temporal-spatial gait parameters:	**Walking speed (m/s)**	
Definitions (length/time)	**From**	**To**
Heel marker (m/s, x-direction)	L, _R_ - heel strike 1, _1_	L, _R_ - heel strike 2, _2_
	Left is abbreviated by an L Right is abbreviated by an R Regular digits represent the L side _Underlined & italic_ digits represent the R side	

The parameters chosen for the current investigation were step time, double support time, step length and walking velocity. The definitions for all four parameters are summarised in Table 8.6. In order to make inter-subject comparisons easier, step time, double support time and step length were expressed in relation to stride time and stride length as appropriate, because these parameters would otherwise vary greatly due to different body heights. In turn, each subject's walking velocity was expressed independently and not in relation to any other parameter. Because the table contains information with regard to both lower limbs, when interpreting the way each parameter was defined, it should be taken into account that the walking sequence commenced with the left side, due to the location of the first force plate.

8.4.19.   Conversion of data from the displacement transducers

The output from the displacement transducers needed converting in order to express transverse rotation and longitudinal translation in units of angular and linear displacements, namely degrees (°) and millimetres (mm), respectively.

As described in Section 6.2.2, calibrations were undertaken in two ways, by recording the transducers' output with them connected to an ohmmeter as well as with them connected to the radio telemetry system, while they were both consecutively mounted against a micrometer and against the cam perimeter. The first set of results, obtained from the calibrations with the ohmmeter, was purely used for establishing the performance characteristics of the transducers and cam. In turn, the purpose for the second set, obtained from the calibrations with the radio telemetry system, was twofold. Not only did it consolidate the results from the first set of calibrations, its main function was to provide relevant information that served for conducting the required conversions of the transducers' output. To distinguish between angular and linear displacements, signals from the transducer measuring transverse rotation needed to be related to the calibration results that involved the cam. In turn, the signals from the transducer measuring longitudinal translation needed to be related to those that involved the micrometer.

Errors in the transducers' output were, as shown in Section 6.2.2.4, exceedingly small. It was therefore not considered necessary to convert every incremental measurement individually in accordance with each transducer's data that were illustrated by their respective error charts in Figure 6.18 to Figure 6.21. Instead, using the data represented by each transducer's linear trendline was considered to be sufficient, as the correlation co-efficient R indicated a very low dispersion from a truly linear output. Knowing the gradient of each transducer's linear trendline and its intercept on the Y-axis, the actual conversions were undertaken by substituting the signals from the transducers into the equation from the respective trendline.

8.4.20.   Conversion of data from the force sensors

Similar to the data processing procedure undertaken for the displacement transducers' outputs, the signals recorded from the FlexiForce® sensors also needed converting. This

was necessary in order to express the forces applied onto certain areas on the residual limb in units of pressure, namely kilo Pascal (kPa).

As described in Section 6.2.3, calibrations were undertaken by simultaneously recording the outputs from one of the force plates, as well as the outputs from the force sensors while these were connected to, and powered by, the radio telemetry system. With all six force sensors consecutively positioned onto that force plate, forces were exerted onto each sensor via discs of three different sizes. The results were summarised as the mean from those three types of calibrations. Having converted the force plate's outputs into forces, it was possible to relate the obtained parameters to those from the force sensors. That way the force sensors' outputs from the calibrations were also converted into forces. Because the resultant correlations were not linear, each set of data was best traced by fitting a sixth order polynomial to it. The outputs from the calibrations of all six force sensors were then mathematically decoded by expressing each sensor's data conversions in terms of gradients that described the slopes of its polynomial and the intercept that described where its polynomial crossed the Y-axis.

The actual conversions of the data from the gait laboratory tests were undertaken by substituting the signals from the force sensors into the equations of the polynomials. Due to fluctuations in the sensors' outputs on different days, all six of these sensing devices needed calibrating every time a subject completed the designated gait laboratory session. This meant that each subject's data could only be processed accurately by introducing an individual set of six polynomials into the customised Matlab (The MathWorks Inc, Natick Massachusetts, USA) code. In comparison, this was different for the conversions of the displacement transducers' output, as the same calibration results from those sensing devices were applicable to all ten subjects.

8.4.21.   Data normalisation and adjustments

Having calculated all the required gait parameters, the processed data from the ProReflex^{TM} system, both force plates, both displacement transducers and the six force sensors were normalised to 100% over the period of one gait cycle, namely from the first heel strike to the second heel strike of the same lower limb for both the left and right side. As the left lower limb stepped onto the first force plate and the right lower limb onto the second force plate, this meant that the data of both lower limbs were not recorded simultaneously, but slightly earlier on the left side compared to the right. With

regard to the output produced by the displacement transducers and FlexiForce® sensors, once their signals were converted into relevant units, the processed data were normalised over the period of purely the amputated side's gait cycle, as this was the only side these sensing devices operated on. Normalisation to 100% is a procedure that was based on calculations during which the stipulated periods were divided up into one hundred equidistantly spaced readings. The resultant value that corresponded with each reading's new allocation within that period was mathematical reconstructed using interpolations.

With regard to analogue data from the displacement transducers, once the subjects commenced swing phase, the inertia and friction at the TT Pylon were the reason for hysteresis. This did not always allow the TT Pylon mechanism to fully return back to a neutral state following transverse rotation and longitudinal translation. In order to make inter-trial comparisons feasible, the data therefore needed adjusting. As transverse rotation occurred in either direction of the adapter's neutral state, the output during the first frame at heel strike was deducted from the output during every frame of the same trial. That way each gait cycle commenced with zero transverse rotation. In turn, because longitudinal translation occurred in just one direction from the adapter's neutral state, it was not necessarily the output during the first frame, but the lowest output during any frame within the entire measuring range that was deducted from the output during every frame of the same trial. That way, each gait cycle commenced with, or at least retuned to, zero longitudinal translation. Therefore, zeroing both displacement transducers' outputs helped to prevent the data from being affected by hysteresis at the adapter.

In order to make inter-subject comparisons easier, the parameters that depended on body mass were expressed as a ratio of this measurement, including GRFs, GRMs inter-segmental moments, power generated at joints and longitudinal translation of the socket. Although residual limb-socket interface pressures may be similarly affected by body mass, it was decided to leave this parameter as it was, namely in kPa, because anterior-posterior and medial-lateral movements were not necessarily mass dependent, but still likely to have an additional influence on in-socket measurements. In turn, displacements of the COP were expressed as a ratio of each subject's foot length, because these two measurements were closely related. Also, as may be seen in Section 8.4.15 and Section 8.4.16, GRFs represented one of the parameters that were needed for

calculating the GRMs, COP, joint moments and joint powers. Because these forces were absent during swing phase, the moments and powers reduced to zero during this part of the gait cycle.

In the majority of cases, the sign conventions used for the graphic representations of gait parameters were based on the recommendations made by Wu & Cavanagh 1995 on behalf of the ISB, in order for rotational displacements to follow the right hand rule within a right handed, global, Cartesian co-ordinate system. This was predominantly applicable for displacements within the sagittal plane as the directions of motions were the same for both lower limbs. Because GRMs and joint moments were based on extrinsic factors, namely GRFs, resultant angular displacements that would be triggered if no resistance at the joints existed were determined to occur in opposite direction to rotations used for describing the actual motion that the corresponding segments were experiencing.

Exceptions for the recommended and described sign conventions, however, were made in circumstances when this type of convention let a certain parameter that referred to one side appear inverted with respect to the other side. For instance, transverse angular motion of the socket in a clockwise direction, as viewed from proximally, can be described as internal rotation for the left side and as external rotation for the right. If the same sign convention was to be used for both sides, then the visual appearance of the respective data's graphic representations would make comparisons between the two sides difficult. To overcome this problem, such conditions were then assimilated by adapting the left side, so that its data were inverted and therefore similar to the right side, which, in turn, stayed the same as before and remained within the sign convention as recommended by Wu & Cavanagh 1995 on behalf of the ISB.

8.4.22.   Data selection

Over the course of the current investigation, equipment was available that could be used to determine kinematic data with respect to all three anatomic planes or all three axes within the global reference system for both lower limbs. In comparison to the coronal and transverse plane, however, sagittal plane displacements can be considered to have the greatest importance in terms of forward ambulation, as they are parallel to the line of progression. Also, in the context of prosthetic rehabilitation, the primary objective is to maintain sagittal plane movements at the joints on the sound side and the remaining

joints on the amputated side in order to permit as normal forward progression as possible. The primary interest, in terms of assessing prosthetic components, should therefore also relate to how these components affect sagittal plane limb motions. Based on this approach, the priority for the current study is to assess whether the adapter influences sagittal plane kinematics, as these are essential to the amputee for maintaining mobility. If those influences do exist, then it should be investigated how they manifest themselves in order to determine possible advantages that the adapter holds for amputee gait over more rigid prostheses without adapter mobility in terms of maintaining forward progression.

Although data regarding transverse and coronal plane motions may also contain useful findings, they are of secondary importance to amputees' rehabilitation processes. Also, these displacements are considerably smaller than sagittal plane motions. Relative displacements between markers and the underlying bone structure in response to skin movement artefacts (Cappozzo 1991, Cappozzo et al 1996) consequently have a much smaller influence on accurately capturing the far greater sagittal plane displacements. This implies that coronal and transverse plane kinematics are, due to their smaller magnitudes, a lot more error prone than sagittal plane kinematics. Also, the large volume of muscle bellies around the tibia and particularly the femur amplifies skin movement artefacts, especially in the transverse plane, due to rotation of the tissues relative to the inner bone structure.

Therefore, the chosen lower limb kinematics to be investigated during the current study are purely those within the sagittal plane. The only exceptions are the kinematics at the TT Pylon. These occur in the transverse plane and combined coronal and sagittal plane, but the chosen technique for capturing those displacements was based on the cam system, which is much less error prone than the ProReflex^{TM} system for tracking skin-mounted markers. Concerns regarding the plane in which motions occur are consequently unnecessary when using the cam, as this device was specifically designed for accurately capturing very small movements. Apart from the kinematics at both lower limbs and at the adapter, additional data to be captured include those from the floor force plates and in-socket pressure sensors. The gait parameters that were determined during the current investigation are described in Table 8.7, which also includes a summary of the chosen parameters' sign convention.

Table 8.7:   Chosen gait parameters and their sign conventions

Parameters	Involvement	Positive readings
Joint angles in the sagittal plane	Ankle Knee Hip	Plantarflexion Flexion Extension
Floor plate forces	Vertical GRFs Anterior-posterior GRFs Medial-lateral GRFs	Upward Anterior Lateral
Floor plate pressure and moment	Anterior-posterior COP Transverse plane GRM	Anterior External
Joint moments in the sagittal plane	Ankle Knee Hip	Plantarflexion Extension Flexion
Joint powers in the sagittal plane	Ankle Knee Hip	Generation Generation Generation
Temporal and spatial parameters	See Section 8.4.18	N/A
Displacement transducer and force sensor output	Transverse rotation Longitudinal translation In-socket pressures	Internal rotation of socket Distal translation of socket Increasing

8.4.23.   Statistical analysis and presentation of data

As previously mentioned in Section 7.2.4 and summarised at the beginning of Chapter 8, all ten subjects were asked to perform ten high quality walks for each of the four set-ups. This implied that the overall amount of data was therefore vast. In order to present the gait parameters, described in Table 8.6 and Table 8.7, in a logical and sensible manner, it was necessary to conduct a statistical analysis that produced a concise and meaningful representation of the processed data.

The initial step was to calculate the mean from each subject's ten walking trials and this procedure was repeated for all four set-ups. In most cases the standard deviations were very small, as can be seen from the band width of the two graphs on either side of the

mean in Figure 8.13. This is a typical example illustrating high repeatability or low inter-trial variability.

Figure 8.13:   Example for low inter-trial variability (subject D)
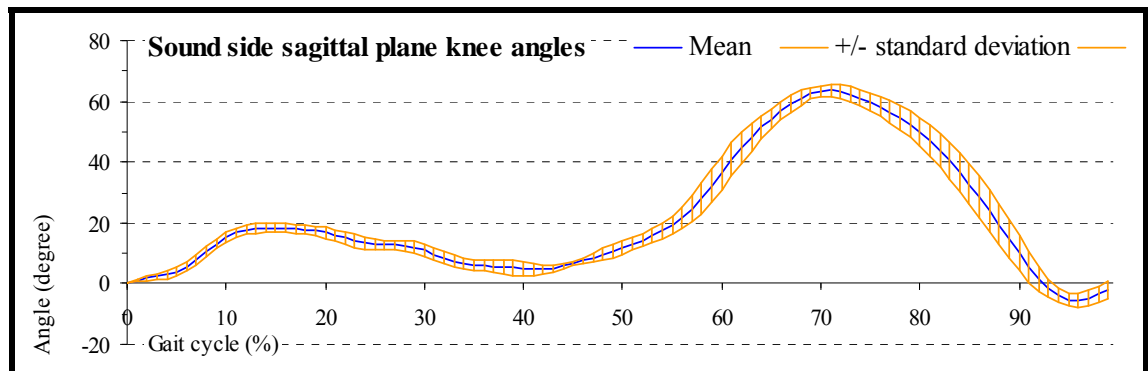
Only a few exceptions existed where the standard deviations were large, thus demonstrating that, for certain subjects, some parameters seemed less repeatable. The chart in Figure 8.14 is an example that represents one of the largest standard deviations encountered during the current investigation. This example therefore illustrates low repeatability or high inter-trial variability.

Figure 8.14:   Example for high inter-trial variability (subject D)
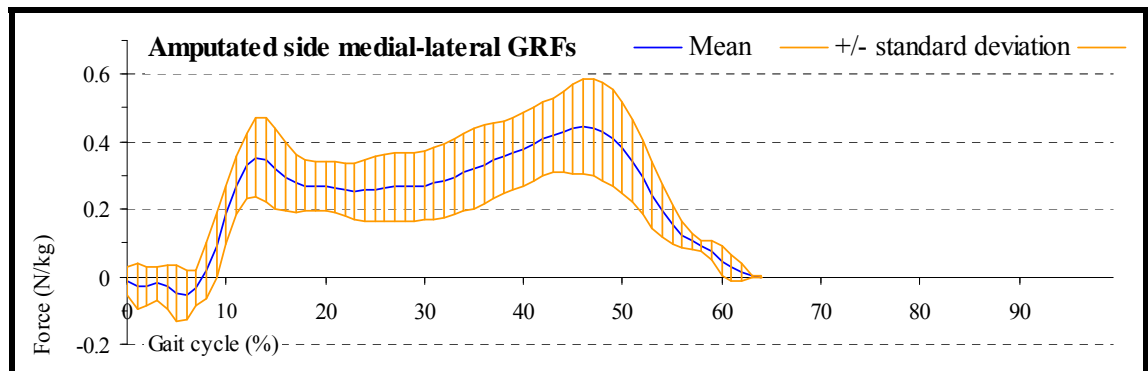
Because the total number of samples obtained was large, low repeatability simply signified that output fluctuations appeared to be typical amongst those parameters with larger standard deviations. This, however, was not considered detrimental, because a similar trend with regard to output fluctuations was usually not just inherent within the same parameters for only one set-up, but more frequently for all four set-ups. The decision was therefore made that for further statistical analysis, it would be justifiable to use only the mean of each subject's ten walking trials rather than every individual trial. Also, in an attempt to reduce the total amount of data even further, it would be more

concise a method to extract purely the values of certain characteristics within a graph and not every single mean value over the duration of the combined ten gait cycles.

Due to the extensive range of charts, the type and number of characteristics determined from each graph varied for the different parameters. Typical features included a maximum and minimum value within a particular part of the gait cycle, the incident of those values, as well as the incident of the graph crossing the x-axis. Because the entire data were normalised over 100% gait cycle, the incident of a characteristic within that cycle was expressed as a percentage and referred to as the duration since the first heel strike with which the gait cycle in question commenced. Additional characteristics, if applicable, were based on the total value, which was calculated as the difference between a maximum and minimum of a gait parameter. In some instances it also seemed appropriate to calculate the area under the graph. For instance, the maximum output from a force sensor may be lower during the first set-up compared to the second one, but the area under the graph may be larger during the first set-up, thus indicating that, despite a lesser peak force, the overall loading of the skin was greater.

Customised codes were written in Matlab (The MathWorks Inc, Natick Massachusetts, USA) for identifying the values of these characteristics. Not only did this increase the accuracy for correctly accomplishing such a procedure, it also reduced the time that it would have taken by doing this manually. Peak values and the incident of gait cycle events could easily be identified using standard Matlab commands. In turn, the more difficult aspect was to accurately calculate the area under the graph.

One way of tackling this task would be for the software to first of all determine a polynomial with which the original graph can be reconstructed. The problem with this method was that some of the graphs were fairly jagged due to the nature of the output, so that, after substitution of the required variables into the polynomial, the resultant graph did not quite resemble the shape of the original graph. Integrating the obtained data would therefore only be a rather rough approximation of the area under the graph. An alternative method would be to add up every single data point. However, following the normalisation procedure, only one hundred increments were available, so that the results regarding the area were unlikely to be more precise than those from the previously described integration method.

The definitive solution that was used to solve the problem was interpolation for mathematically constructing additional data points between already existing ones. The higher the resolution, the greater the approximation of the true area under the graphs became, whereby the change in area was less significant with greater numbers of increments. The threshold for interpolation was set at fifty thousand, which meant that four hundred and ninety-nine values were mathematically added between every pair of adjacent measurements as well as after the last measurement. With such a large number of data points, the resultant approximation of the true area under the graphs was considered satisfactorily. It should be noted that this large number of samples was purely used for calculating the area under the graphs, and, in turn, the presented charts were solely created from the original one hundred data points. Also, because the x-axis scale was not expressed as time but as percentages, the area under the graph could therefore not be described in terms of standard units, which is why the numeric values were displayed on their own without a unit.

Having extracted previously determined characteristics of the graphs, the next step was for these characteristics to be analysed. Using the statistical software package SPSS (SPSS Inc, Chicago Illinois, USA), individual groups of values were further processed by conducting a two-way analysis of variance (ANOVA), as described by Rowntree 1981. This involved a comparison between all four set-ups to obtain parameters that indicate whether or not the permission of transverse rotation or longitudinal translation or both types of motion significantly affected the values extracted from the calculated gait parameters.

The level of significance was expressed as a "p-value" and set at 5%, so that a parameter was interpreted to be significantly different from the set-up when the motion adapter was locked, if $p<0.05$. As it was of interest to explore the extent to which the gait parameters were affected by the permission of one or both types of motions, p-values were therefore not applicable for scenarios when neither of these motions took place. Also, every parameter had as many characteristics extracted as seemed feasible, in case those particular gait cycle events revealed any significant findings. This, however, did not mean that valuable conclusions could be drawn from every single one of them. In fact, differences between the various set-ups were often only very small and insignificant and in many cases absent altogether. But at least every opportunity to find significant differences was exploited.

In addition to a numeric analysis of the obtained gait parameters, it was decided that a graphic representation would be of similar importance to provide visual feedback also. For this purpose, further calculations were undertaken to establish the average of the data from all ten subjects' mean values. In most cases, these are illustrated in individual charts for each of the four set-ups. Based on the same chart principles as before in Figure 8.13 and Figure 8.14, the band width of the two graphs on either side of the average represents the standard deviation of all ten subjects' mean values and highlights the dispersion of parameters.

Both the numeric and graphic representations were then combined to maximise the potential for conducting data interpretations. The symbols " └─┬─┘ " and " ┌─┴─┐ " were used to indicate the range over which individual characteristics of the graphs extended due to variations between subjects. If these characteristics were peaks, then both, the mean maximum and/or minimum, as well as the mean incident of these values were appended, including their p-values. Characteristics indicating the crossing of the x-axis had solely their mean incident and their p-value added. Levels of significance below 5% were highlighted with a grey-shaded p-value. The total value and the total area under the graph was, together with its p-value, included in the bottom right-hand corner of each chart, if applicable.

Combining the numeric and graphic information can, in some instances, appear slightly confusing. For instance, the peak of a graph may reach a different value and occur at a different point in time than was indicated by the numeric value. The reason for this is because the incident of each peak was likely to be different for each subject. This feature is not as clearly expressed by the graphic representation, which emphasises the importance for the numeric data in order to provide a better understanding of the data and facilitate an easier data analysis.

To make comparisons easier, the charts were deliberately sized in such a way that each group of graphs fitted onto the same page to form a cohesive representation of gait parameters, whereby the sound and amputated side were treated separately. Verbal descriptions for different set-ups were abbreviated as shown in Table 8.8, and in such a manner displayed within each chart. Because some of the data were very similar for different set-ups, an extra, summary chart was added, which graphically contained nothing else but the averages. Their closely neighbouring values sometimes made it

difficult to distinguish between the various set-ups, as the graphs were often overlapping. Highlighting them with different colours and patterns would have increased the likelihood for overlaps, which is why all four averages were presented in the same way. The purpose for such charts was purely to illustrate, in a simple manner, a close or less close relationship between different set-ups. These charts also contained numeric information, which was restricted to the average of some characteristics' mean values from each individual graph. Although the aim was to distinguish between every single set-up for each side, the incorporation of average numeric data within the extra summary chart made comparisons between the sound and amputated side easier.

Table 8.8:   Abbreviations for the description of different set-ups

Abbreviation	Transverse rotation	Longitudinal translation
	(permitted / restricted or yes / no: ✓ / ✗)	
TRnLTn	✗	✗
TRyLTn	✓	✗
TRnLTy	✗	✓
TRyLTy	✓	✓

The graphs illustrating parameters like joint angles, GRFs, GRMs, COP, joint moments and joint powers were presented in five charts, including four for each set-up plus the extra, summary chart. Temporal and spatial parameters were incorporated in tabular format.

Because transverse rotation was individually permitted during only two set-ups, both outputs from the displacement transducer responsible for taking these measurements were summarised in just a single chart. This was also the same scenario for signals in response to longitudinal translation. Due to high inter-trial and inter-subject variability, the standard deviations for all ten amputees were large, and the incorporation of this information would distract from focusing on the overall trend of motion at the TT Pylon. Each of the two charts therefore purely contained the numeric values and the graphs for both corresponding set-ups' average of all ten subjects' mean transverse rotation and longitudinal translation, respectively.

In turn, signals from the force sensors were summarised in six charts. Each of them illustrate the numeric values and the graphs for the average of all ten subjects' mean in-socket pressures, as measured by one individual force sensor during all four set-ups. However, like the data from the displacement transducers, standard deviations were not included in the force sensor charts, as these would otherwise have been too cluttered. Spreading the data over a larger number of charts was not considered an option either, as this was not a sufficiently concise representation of information.

Having described the entire test set-up and elaborated on how the subsequent, resultant data would be processed, all relevant aspects necessary for the understanding of the test results and discussion during which the obtained data will be analysed were provided. The next Chapter is divided into three main parts. These will focus on the presentation and description of the results from the gait laboratory tests. Each of those Sections reflect one of the objectives outlined in Section 3.6, namely whether the motions at the adapter:

1)   have a major effect on the sound and amputated side gait parameters;
2)   change the kinematics between socket and prosthetic foot;
3)   reduce the loads on the residual limb.

For continuation purposes and because of the large volume of data, elements of the discussion are integrated with the presentation of results. This will be followed by a general discussion Chapter to focus on the merits of the various findings in relation to the aims and objectives of this study.

CHAPTER 9.   TEST RESULTS AND DISCUSSION

During the current investigation, the recruited subjects acted as their own control. This made it possible to analyse their gait on the amputated side with regard to gait of a non-amputated limb. Such a comparison does not imply that amputees' motion on their sound side was considered as normal. It merely allowed gait with a prosthesis to be compared to the gait of a limb that had not experienced any loss of segments, and such a comparison would still be justifiable even if this limb's motion pattern was dissimilar to that of non-amputees.

Also, as explained in Section 8.4.23, the three set-ups with the motion adapter partially or fully mobilised were compared to the situation when it was locked. If the data varied greatly then the resultant differences were being assessed by ranking them according to levels of significance set at 5%.

When interpreting levels of significance, it is important to see the obtained values in context with the type of motion that was possible and whether one or both types of displacements were being permitted during a set-up of interest. For instance, a certain gait parameter is, from the statistical point of view, considered significantly different with, say, set-up TRyLTn, because its magnitude is larger than when the adapter is locked. In addition, let's take into account that the same parameter was even greater with set-up TRyLTy, but only slightly, which nevertheless does not necessarily mean that the difference is significant as well. This is because both types of motions are permitted simultaneously and although the second one, namely longitudinal translation, is larger, too, its effect, when permitted on its own, is insignificant. In order for set-up TRyLTy to be significantly different, a possible scenario for this would be that the obtained value has to be hugely greater or smaller than the other two single motion set-ups.

9.1.   Sound and amputated side gait parameters

9.1.1.   Sagittal plane joint angles

9.1.1.1.   Inter-limb differences in ankle angles

Ankle angles of both the sound and amputated side are illustrated in Figure 9.1 and Figure 9.2, respectively. The standard deviation for the sound side was fairly consistent throughout the gait cycle, reaching a minimum and maximum of approximately 2.9° and 7.1°, which is around 9.3% and 22.8% of the 31.1° total mean ankle angular displacement, respectively. This was different for the amputated side, in that the standard deviation during swing phase was relatively low reaching a minimum of approximately 0.6°, but larger during stance phase reaching approximately 7.9° which is around 1.9% and 25.0% of the 31.6° total mean ankle angular displacement, respectively. Standard deviations during swing phase were low, due to absent GRFs, as the prosthetic ankle could not be actively moved and therefore remained near the same position for each subject's mean of ten trials.

On the sound side, the ankle angles changed from slight dorsiflexion at heel strike immediately over to plantarflexion within less than the first 10% of the gait cycle. Unlike landing flat footed, this gait cycle period can be thought of as a significant contributor to a reduction in shock impacts during the initial stages of stance phase by altering the force-time ratio. Once the initial forces were absorbed, the aim was to quickly reach full contact with the ground for increased stability and improved balance.

Ankle angles on the amputated side were different to those on the sound side in that the prosthetic joint at the instant of heel strike was not dorsiflexed, but in a neutral position, as this was its predetermined alignment when external forces were absent. Due to lack of control from muscles, the only source of resistance to the increasing GRFs while pushing the heel harder down onto the ground was the plantarflexion bumper, described in Section 4.1.6.5, at the posterior aspect of the prosthetic foot's rotation axle. The foot's plantar aspect therefore assumed full contact with the ground slightly earlier than the anatomic foot. The incident for this can be assumed to have occurred when plantarlflexion angles reached a peak at mean timing of approximately 8.2% and 7.6% of the gait cycle for the sound and amputated side, respectively. The magnitude of peak plantarflexion angles was consequently larger for the amputated side and nearly twice

278

Figure 9.1:   Ankle angles on sound side, plantarflexion +ve
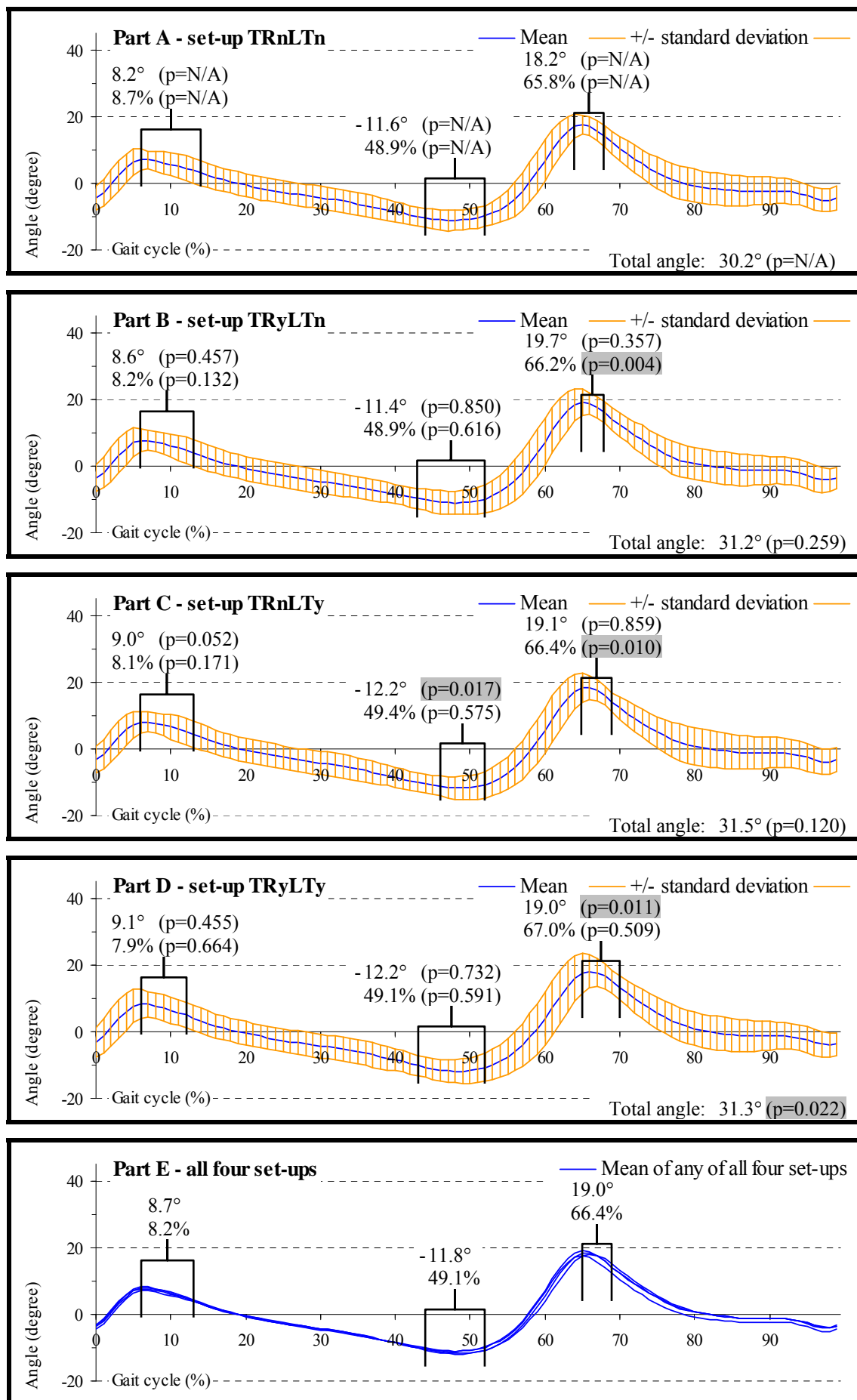
Figure 9.2: Ankle angles on amputated side, plantarflexion +ve

Part A - set-up TRnLTn — Mean — +/- standard deviation
16.2° (p=N/A)
7.2% (p=N/A)
-15.6° (p=N/A)
50.3% (p=N/A)
Angle (degree)
Gait cycle (%)
Total angle: 31.8° (p=N/A)

Part B - set-up TRyLTn — Mean — +/- standard deviation
16.1° (p=0.433)
7.7% (p=0.011)
-15.7° (p=0.836)
51.0% (p=0.074)
Angle (degree)
Gait cycle (%)
Total angle: 31.8° (p=0.438)

Part C - set-up TRnLTy — Mean — +/- standard deviation
15.9° (p=0.988)
7.5% (p=0.168)
-15.7° (p=0.783)
50.4% (p=0.223)
Angle (degree)
Gait cycle (%)
Total angle: 31.6° (p=0.885)

Part D - set-up TRyLTy — Mean — +/- standard deviation
16.4° (p=0.194)
7.8% (p=0.509)
-15.6° (p=0.636)
51.3% (p=0.764)
Angle (degree)
Gait cycle (%)
Total angle: 32.0° (p=0.355)

Part E - all four set-ups — Mean of any of all four set-ups
16.1°
7.6%
-15.7°
50.8%
Angle (degree)
Gait cycle (%)

280

the size of sound side ankle angles due to the still backward orientated prosthetic shin, reaching a mean value of approximately 8.7° and 16.1° for the sound and amputated side, respectively.

Following foot flat, the next approximately 40% of the gait cycle saw both the anatomic hindfoot and forefoot remain in contact with the floor simultaneously, but because the body shifted forward with respect to the now stationary anatomic foot, the ankle angles gradually changed again. This was triggered in response to motions of the shin, as its direction changed from leaning backward to leaning forward, so that the ankle reached a peak in dorsiflexion angles by the end of this period.

Changes on the amputated side were similar, except that peak dorsiflexion angles were over 30% larger than those on the sound side and they occurred fractionally later. For the sound and amputated side, peak dorsiflexion angles reached a mean value of approximately 11.8° and 15.7° and the incident of this peak occurred at a mean timing of approximately 49.1% and 50.8% of the gait cycle, respectively. It could therefore be assumed that the prosthetic heel remained on the ground for longer than the anatomic heel did, as the only source of resistance to GRFs acting on the prosthetic forefoot was the dorsiflexion bumper at the anterior aspect of the rotation axle.

During the next approximately 15% of the gait cycle, the heel on the sound side started to rise up and the ankle angles rapidly changed back from dorsiflexion until a peak in plantarflexion angles was reached. This phase was crucial for gaining forward propulsion and by the end of it the entire foot had taken off the ground.

On the amputated side, the push off period was much less forceful compared to the sound side. While GRFs acting on the prosthetic forefoot were slowly reducing, the dorsiflexion bumper managed to bring the foot back into a near plantigrade position with respect to the prosthetic shin. However, the forces from the bumper's compressed material were too small to provide active forward propulsion, which meant that the peak in plantarflexion angles was absent. Also, the interval for such a comparatively small change in ankle displacements was consequently slightly shorter than on the sound side. As no peak in plantarflexion angles occurred during this part of the amputated side gait cycle, it was difficult to determine the exact point in time when the ankle angles stopped

changing, which made it difficult to provide exact figures that allowed the changes in sound and amputated side ankle angles to be compared numerically.

Having terminated stance phase, the subsequent approximately 40% of the sound side gait cycle was characterised by swing phase. Initially, the ankle rapidly reduced its plantarflexion angles, in order for the foot to reach a near plantigrade orientation with respect to the anatomic shin. That way, the toes were no longer pointing distally, so that collision with the ground during mid-swing phase could be avoided. Just prior to the end of swing phase, the sound side ankle assumed a slight dorsiflexion angle again. This occurred in anticipation for cushioning during the landing period. That way, the ankle could experience a longer angular displacement until the foot was back flat on the ground, compared to when the foot was not dorsiflexed, but merely in a plantigrade position, which would have resulted in a shorter angular displacement until the foot was back flat on the ground.

Changes in ankle angles on the prosthetic side were, due to lack of GRFs, much smaller than they were on the sound side. Throughout swing phase, the artificial foot moved from a very slightly dorsiflexed position until it assumed a near neutral orientation. Part of the reason for the described angular changes may have been the foot's own inertia. While the prosthesis was being pulled forward, the forefoot, with its longer dimensions and therefore greater mass than the hindfoot, was lagging behind, particularly if some play developed at the ankle, thus reducing the dorsiflexion angle. Another possibility is that it was creep from the dorsiflexion bumper, which may have expanded slightly further following the release from full compression just before swing phase.

9.1.1.2. *Inter-set-up differences in ankle angles*

Towards the end of stance phase, peak sound side dorsiflexion angles were significantly greater with set-up TRnLTy reaching approximately 12.2° (p=0.017) compared to approximately 11.6° when the adapter was fully locked. This may have happened in anticipation of the amputated side's initial loading period, as the prosthesis was about to shorten. Dorsiflexing the anatomic ankle more than when the adapter was fully locked allowed the body to lean further forward, thus accommodating the expected downward travel in response to longitudinal translation. Those sound side peak dorsiflexion angles with set-up TRnLTy were equally large with set-up TRyLTy, but no significant differences were found compared to when the adapter was fully locked, due to virtually

absent changes with just transverse rotation being permitted, reaching approximately only 11.4°.

The other aspect with statistically significant findings was the peak in sound side plantarflexion angles around push off. This turned out to be larger and delayed when the motion adapter was partially mobilised compared to when it was fully locked. Such changes could have happened, because the subjects may have been perhaps less aware of when exactly they established ground contact on the amputated side, due to the cushioned feel from their prosthesis, so that movements at the sound side ankle continued.

During all four set-ups, peak sound side plantarflexion angles were largest with set-up TRyLTn and TRnLTy, reaching approximately 19.7° and 19.1°, respectively, compared to only approximately 18.2° when the adapter was fully locked. However, the only situation when a difference was significant occurred while the adapter was fully mobile, reaching approximately only 19.0° (p=0.011). This was because sound side peak plantarflexion angles were slightly lower than with the other two set-ups when the adapter was partially mobile. In turn, the incident of the sound side peak plantarflexion angles was most delayed with set-up TRyLTy, which occurred at approximately 67.0% of the gait cycle compared to approximately 65.8% of the gait cycle when the adapter was fully locked. However, the delay with set-up TRyLTy was only slightly greater compared to set-up TRyLTn and TRnLTy, during which peak plantarflexion angles occurred at approximately 66.2% (p=0.004) and 66.4% (p=0.010) of the gait cycle, respectively, thus rendering the delays as significant.

The final characteristic on the sound side with a significant difference was the total angle that represents the overall displacement at the anatomic ankle. With set-up TRyLTy, the magnitude of the total angle reached approximately 31.3° (p=0.022) compared to 30.2° when the adapter was fully locked. The reason the findings with set-up TRyLTy were significant was because the obtained value was slightly smaller and larger than it was for set-up TRyLTn and TRnLTy, respectively. This is unusual as the effects that transverse rotation and longitudinal translation individually had on the ankle kinematics were not cumulative when they were both being permitted simultaneously.

The effect of different set-ups on the amputated side ankle angles was very small, which can be attributed to the fact that this joint could only be moved passively. The sole incident significantly affected was for achieving peak plantarflexion angles following heel strike. This peak occurred later with set-up TRyLTn at approximately 7.7% (p=0.011) of the gait cycle compared to approximately 7.2% of the gait cycle when the adapter was fully locked. A possible explanation for such a delay is that most of the weight was predominantly carried by the contra lateral sound side, as the COM was still further towards that side. The prosthetic shin was therefore leaning medially and backward in particular, because the alignment procedure for the prosthesis, described in Section 2.6.2, was undertaken in such a way that a vertical orientation of the shin tube only occurred around mid-stance phase when the prosthesis carried the full body weight. Due to the leaning of the prosthesis, the downward momentum was therefore not only taken up by vertical motions, but may have been partly taken up by transverse rotation also, which, in turn, had an effect on vertical motions.

This could have occurred because the socket was slightly flexed relative to the prosthetic shin tube, as previously explained in Section 2.6.2, which put the proximal aspect of the socket slightly ahead of the shin tube while the prosthesis was upright. Therefore, while the shin tube was leaning backward, the proximal aspect of the socket could have been higher up than it would have been if it was not flexed relative to the shin tube. This meant that either internal or external transverse rotation would have allowed the proximal aspect of the socket to travel downward, even if only slightly. As a result of such downward travel of the socket, the distally directed push onto the ground became less forceful, or was at least delayed, which can be confirmed when inspecting the vertical GRFs, illustrated in Section 9.1.2.1. In turn, such a reduction and/or delay in downward travel would therefore have also affected the prosthetic peak plantarflexion angles during the weight acceptance period, which explains the delay in that peak.

A similar effect of shock absorption should consequently have also occurred with set-up TRnLTy, due to longitudinal translation at the adapter, and particularly with set-up TRyLTy, due to the combined effect of dual adapter mobility. This turned out to be the case, as the peak in plantarflexion angles occurred at approximately 7.5% and 7.8% of the gait cycle for set-up TRnLTy and TRyLTy, respectively, but the differences compared to when the adapter was fully locked were insignificant.

9.1.1.3.   Inter-limb differences in knee angles

Knee angles of both the sound and amputated side are illustrated in Figure 9.3 and Figure 9.4, respectively. The standard deviation for the sound side was fairly consistent throughout the gait cycle, reaching a minimum and maximum of approximately 0.9° and 9.0°, which is around 1.3% and 13.4% of the 67.2° total mean knee angular displacement, respectively. This was similar for the amputated side, in that the standard deviation reached a minimum and maximum of approximately 0.5° and 8.9°, which is around 0.7% and 12.9% of the 69.1° total mean knee angular displacement, respectively. The smallest values for both sides were predominantly found at heel strike as every subject's knee was fully extended.

On the sound side, the knee angles during the weight acceptance period immediately changed from a fully extended position at heel strike to slight flexion just after heel strike. Flexion angles soon reached a peak within less than the first 15% of the gait cycle. Unlike landing while maintaining a straight knee, this way of accepting weight can be thought of as a significant contributor to a reduction in shock impacts during the beginning of stance phase by altering the force-time ratio. Once the initial forces were absorbed, the aim was to quickly extend the knee again in order to reduce the muscle power required for preventing the joint from collapsing. An extended position also pushed the knee further posterior, so that, by the time early stance phase expired, GRFs acted anterior to the knee, thus helping to avoid sound side flexion angles from increasing inadvertently.

The behaviour on the amputated side was similar, in that the incident for the peak in stance phase knee flexion angles was reached only fractionally later, namely at a mean timing of approximately 14.9% of the gait cycle compared to approximately 14.7% of the gait cycle for the sound side. The aspect that differed more turned out to be the magnitude of amputated side knee flexion, reaching a mean value of approximately 8.5°, which is only half the angle achieved by the sound side of approximately 17.0°. Such comparatively small rotational displacements on the amputated side could therefore be considered a source for insufficient shock absorption. Following the peak in amputated side knee flexion during the weight acceptance period, the angles quickly reduced during the middle part of stance phase. This was likely to occur for similar reasons as explained previously regarding the sound side, in that the reduction of

Figure 9.3:   Knee angles on sound side, flexion +ve

Part A - set-up TRnLTn — Mean — +/- standard deviation

15.8° (p=N/A)
15.0% (p=N/A)

1.1°   (p=N/A)
39.2% (p=N/A)

58.7° (p=N/A)
72.7% (p=N/A)

Total angle: 66.6° (p=N/A)

Part B - set-up TRyLTn — Mean — +/- standard deviation

17.4° (p=0.002)
14.6% (p=0.217)

1.6° (p=0.149)
41.8% (p=0.139)

60.1° (p=0.020)
72.8% (p=0.196)

Total angle: 67.1° (p=0.280)

Part C - set-up TRnLTy — Mean — +/- standard deviation

16.8° (p=0.075)
14.7% (p=0.373)

1.4° (p=0.438)
41.5% (p=0.074)

60.1° (p=0.035)
73.2% (p=0.011)

Total angle: 67.4° (p=0.423)

Part D - set-up TRyLTy — Mean — +/- standard deviation

18.0° (p=0.573)
14.5% (p=0.443)

1.9° (p=0.995)
42.4% (p=0.169)

61.0° (p=0.370)
73.9% (p=0.239)

Total angle: 67.5° (p=0.700)

Part E - all four set-ups — Mean of any of all four set-ups

17.0°
14.7%

1.5°
41.2%

60.0°
73.2%

Figure 9.4: Knee angles on amputated side, flexion +ve
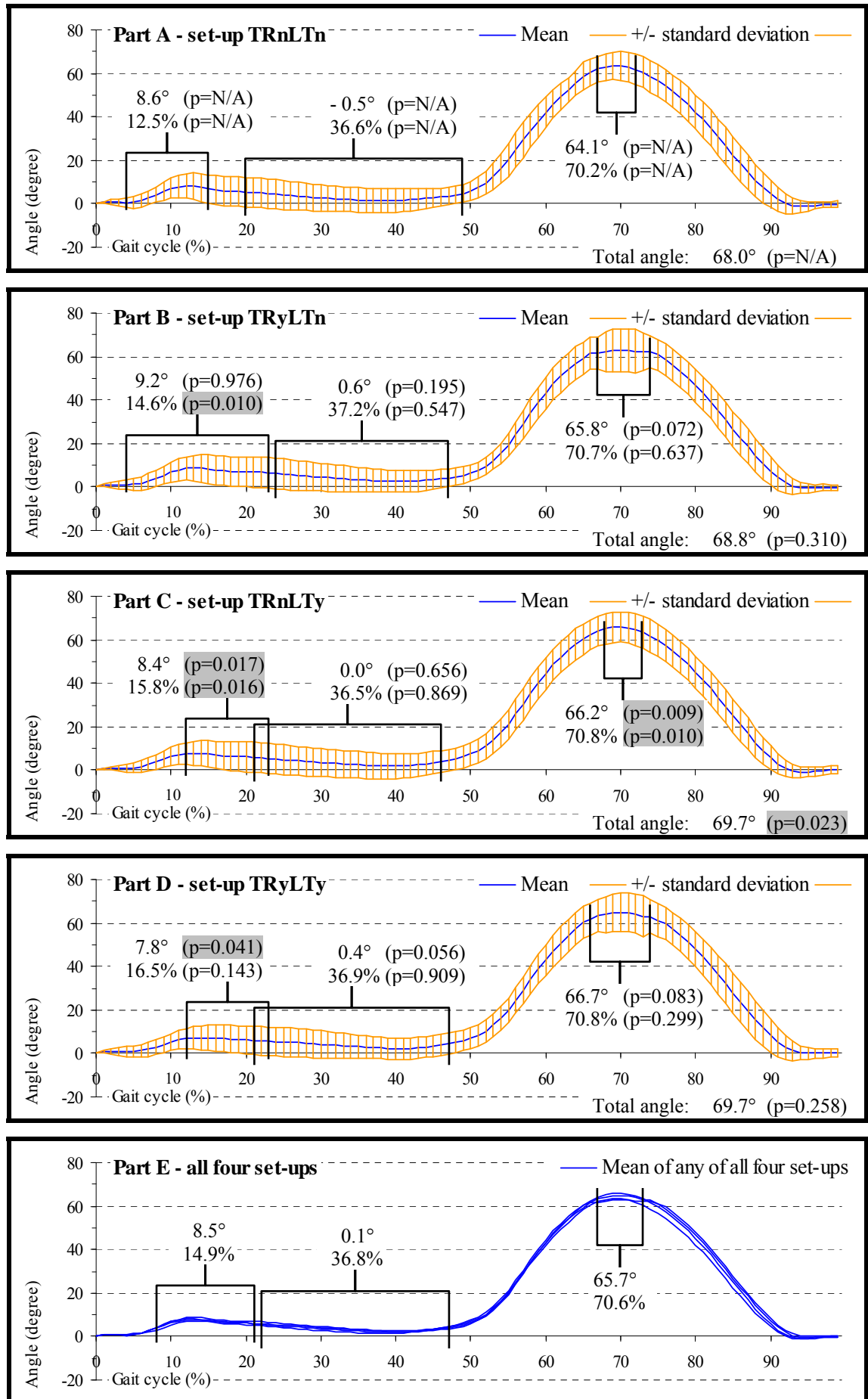
amputated side knee flexion angles helped pushing the knee posterior, so that the GRFs acted anterior to it, thus giving the knee greater stability.

Towards the later aspect of stance phase, the knee on the sound side started to flex again. At this stage of the gait cycle, the GRFs were located anterior to the knee, thus trying to push it back into extension and thereby making it more difficult to flex the knee. Despite counteracting GRFs, the initiation of knee flexion still took place and this already occurred during the end of stance phase and not just prior to swing phase, so that the knee could flex gradually rather than abruptly. A forward orientation of the anatomic shin, as a result of flexion induced at the knee, consequently provided the ankle with a larger magnitude of dorsiflexion. This posed a great advantage for forward propulsion, because the amount of angular displacement that the foot needed to undergo in order to reach peak plantarflexion angles became larger. The energy to be released was therefore concentrated in a more forward rather than upward direction due to the shin's forward orientation.

A similar behaviour to that of the sound side could also be observed on the amputated side. The main difference was that the initiation of amputated side knee flexion during the late stages of stance phase occurred slightly later compared to the sound side. Although the smallest flexion angles just prior to increasing them again occurred earlier on the amputated side at a mean timing of approximately 36.8% of the gait cycle compared to approximately 41.2% of the gait cycle for the sound side, initial amputated side angle changes that followed the incident of the near extended position were very small. Those small changes can therefore be considered as the delay in commencing more drastic increases in amputated side knee flexion. This could have happened in response to the relatively short residual limb and the resultant reduced lever arm that made it difficult to force the knee back into flexion, while GRFs were still trying to counteract this action by attempting to keep the knee extended. The period for building up to full knee flexion was, in response to a reduced lever arm, slightly shorter and the rate of increasing the flexion angles more drastic compared to the sound side.

During mid-swing phase, at a mean timing of approximately 73.2% of the gait cycle, peak sound side knee flexion occurred, which was immediately followed by a decrease in flexion angles. Such a reduction was so extreme that, by the time this process was completed, the joint even reached slight hyperextension at the end of swing phase. Only

marginally later, just before heel strike, the knee went back to a near neutral angle to be ready for flexion during the early part of the next sound side stance phase.

Peak flexion angles during mid-swing phase on the amputated side were larger than on the sound side, reaching a mean value of approximately 65.7° compared to approximately 60.0° on the sound side. This may be linked to the fact that the prosthetic ankle was a passive joint, as explained in Section 9.1.1.1, and unlike the anatomic ankle, not deliberately movable while in mid-swing phase, if normal walking is to be maintained. The fact that the prosthetic ankle could only be moved passively posed a danger for the toes to cuff the ground. One way of avoiding collision was by increasing the amputated side knee flexion angles to ensure that the artificial foot remained well clear from making ground contact. It must also be taken into consideration that virtually absent proprioception due to non-existing neural feedback from the prosthetic foot provided amputees with less spatial awareness compared to their sound side. Over-compensation by flexing the knee excessively may therefore be an alternative approach for allowing the prosthesis to swing forward safely. Following peak knee flexion during mid-swing phase, the amputated side went back to neutral just prior to heel strike and, unlike the anatomic limb, not into hyperextension.

9.1.1.4.   *Inter-set-up differences in knee angles*

The first characteristic with a significant difference amongst sound side knee angles was the peak in early stance phase flexion, which reached approximately 17.4° (p=0.002) with set-up TRyLTn compared to only approximately 15.8° when the adapter was fully locked. Immediately prior to that, while transverse rotation at the adapter was being permitted, the socket was in an externally rotated position around late stance phase of the amputated side, as will be shown in Section 9.2.1.1. As a result of this, the pelvis can be assumed to be also further externally rotated than without transverse rotation at the adapter, so that the aspect of the pelvis above the sound side was consequently displaced slightly more forward. This required additional knee flexion to accommodate the extra movement of the pelvis. With set-up TRyLTy, the magnitude in knee flexion was even greater than with set-up TRyLTn, reaching approximately 18.0°. However, the difference compared to when the adapter was fully locked was insignificant due to relatively small changes in sound side peak knee angles when purely longitudinal translation was being permitted, reaching a peak magnitude in stance phase flexion of approximately 16.8°.

The second characteristic with significant differences on the sound side was the peak in knee flexion angles during mid-swing phase. These differences were found with set-up TRyLTn and TRnLTy, in that the angles reached approximately 60.1° (p=0.020 and p=0.035) in both cases compared to approximately 58.7° with set-up TRnLTn. When the adapter could undergo longitudinal translation, the amputated limb was consequently shorter than when the adapter was fully locked, so that the sound side knee had to flex more in order to clear the ground. This also delayed the incident of the peak, which was reached at approximately 73.2% (p=0.011) of the gait cycle with set-up TRnLTy compared to approximately 72.7% of the gait cycle with set-up TRnLTn. Such a difference obviously turned out to be significant.

Although the shortening aspect during this part of the gait cycle was not the case while transverse rotation was being permitted, the subjects may still have reacted similarly by increasing sound side knee flexion due to the cushioned feel from the prosthesis. However, the delay with set-up TRyLTn was minimal, reaching peak knee flexion at approximately 72.8% of the gait cycle, which was only 0.1% later than with a locked adapter and therefore insignificant. Also, swing phase peak knee flexion was largest in magnitude and most delayed with set-up TRyLTy, reaching approximately 61.0° at 73.9% of the gait cycle, but the differences compared to when the adapter was fully locked were not significant either.

The first characteristic with significant differences on the amputated side was the peak in early stance knee flexion angles. With set-up TRnLTy and TRyLTy, the magnitude of those angles was small, reaching approximately 8.4° (p=0.017) and 7.8° (p=0.041), respectively, compared to 8.6° while the adapter was fully locked. The reason that peak knee flexion angles were smaller can be attributed to that fact that in both situations, longitudinal translation was being permitted, which reduced the shock impact, so that less flexion was required to achieve the same outcome. Also, if knee flexion angles were the same as when the adapter was fully locked, then the body would have tilted further towards the amputated side due to the shortening of the adapter.

Another aspect with significant differences during the initial amputated side stance phase was that the peak knee flexion angles were delayed with set-up TRyLTn and TRnLTy, which were reached at approximately 14.6% (p=0.010) and 15.8% (p=0.016) of the gait cycle, respectively, compared to 12.5% of the gait cycle while the adapter

was fully locked. This may have happened for similar reasons as previously explained in Section 9.1.1.2 with regard to initial amputated side peak plantarflexion angles, in that the downward momentum was partly taken up by the additional mobility at the motion adapter. With set-up TRyLTy the same delay was even longer, reaching the initial amputated side peak knee flexion angles at approximately 16.5% of the gait cycle. However, because the difference compared to when the adapter was fully locked was not drastically larger than when purely a single adapter motion was possible, the magnitude of such a difference was considered insignificant.

The second characteristic with significant differences on the amputated side was the peak knee flexion angles while swinging the limb forward. With set-up TRnLTy, differences were highly significant, in that the magnitude of these angles was approximately 66.2° (p=0.009), which was reached at approximately 70.8% (p=0.010) of the gait cycle compared to 64.1° and 70.2% of the gait cycle when the adapter was fully locked. A possible explanation for this may be that at late stance phase of the amputated side, the trunk and therefore the COM was closer to the ground due to the shortened adapter following longitudinal translation. Although the COM was quickly moving upwards due to weight acceptance on the sound side, even if the amount by which it moved upwards was the same as it was when longitudinal translation was restricted, the overall height the COM must have reached was consequently still smaller. This was because the initial position from which the COM started moving upwards was lower due to the shortened adapter compared to when the adapter was fully locked. The amputated side knee therefore had to flex more to prevent the prosthetic foot from catching the ground. For the same reason, this was also likely to be the case with set-up TRyLTy. However, although the peak in knee flexion angles was, as before, delayed, and the magnitude even further increased, reaching approximately 70.8° at exactly the same point in time as with set-up TRnLTy, differences compared to when the adapter was fully locked were nevertheless statistically insignificant, as changes with set-up TRnLTy were comparatively small.

The final characteristic with significant findings on the amputated side was the total knee flexion angle, which reached 69.7° (p=0.023) with set-up TRnLTy. This was in response to the large magnitudes of flexion angles around mid-swing phase. However, as the findings with just transverse rotation being permitted were not significant, the same was applicable when the adapter was fully mobilised.

9.1.1.5.   *Inter-limb differences in hip angles*

Hip angles of both the sound and amputated side are illustrated in Figure 9.5 and Figure 9.6, respectively. The standard deviation for the sound side was fairly consistent throughout the gait cycle, reaching a minimum and maximum of approximately 8.2° and 11.2°, which is around 18.6% and 25.3% of the 44.2° total hip mean angular displacement, respectively. This was slightly lower for the amputated side, in that the standard deviation reached a minimum and maximum of approximately 5.3° and 9.2°, which is around 11.8% and 20.4% of the 45.0° total mean hip angular displacement, respectively. Although every subject's total hip angular displacement was similar in magnitude, the reason for a relatively high standard deviation was, because subjects who had difficulties in extending the hip needed to obtain greater flexion angles instead. Such a compensatory movement simply displaced, rather than shortened, the entire ROM, hence the band width remained relatively even throughout the gait cycle.

Following heel strike, the first approximately 10% of the gait cycle saw the sound side hip remain nearly fully flexed. Within the middle of this first part of stance phase, the graphs showed minor fluctuations that were triggered by only momentarily reduced flexion angles. Fluctuations of this kind were likely to appear in response to the action at the sound side ankle and knee, described in Section 9.1.1.1 and Section 9.1.1.3. While these two joints seemed to help in reducing shock impacts during the initial floor contact, the hip took on the role as a compensatory mechanism. When the ankle became plantarflexed and the knee flexed, the hip's commencement to acquire a more extended posture was briefly interrupted, because one more slight increase in hip flexion was required, in order for the thigh to conform to the anteriorly moving shin. After this initial period, hip angles gradually changed from flexion to reach peak extension at a mean timing of approximately 54.8% of the gait cycle.

The behaviour of the amputated side was similar to that of the sound side, except that previously described fluctuations in sound side hip angles were virtually absent on the amputated side. Instead, the hip's rotational position started to change immediately after heel strike from flexion to extension, reaching peak extension angles at a mean timing of approximately 52.1% of the gait cycle and therefore before the sound side did. Considering that after heel strike the magnitude of amputated side knee flexion for shock absorbing purposes was small, this explained why the hip on this side did not have to experience fluctuations of similar scale as the sound side.

Figure 9.5:   Hip angles on sound side, extension +ve

Part A - set-up TRnLTn ———— Mean ——— +/- standard deviation ———

-18.2° (p=N/A)
8.9% (p=N/A)

23.4° (p=N/A)
54.5% (p=N/A)

-19.0° (p=N/A)
86.7% (p=N/A)

Total angle: 43.8° (p=N/A)

Part B - set-up TRyLTn ———— Mean ——— +/- standard deviation ———

-19.0° (p=0.038)
9.5% (p=0.168)

22.8° (p=0.774)
54.5% (p=0.343)

-20.2° (p=0.138)
87.3% (p=0.115)

Total angle: 44.0° (p=0.253)

Part C - set-up TRnLTy ———— Mean ——— +/- standard deviation ———

-19.3° (p=0.049)
9.1% (p=0.574)

22.4° (p=0.236)
54.9% (p=0.070)

-21.0° (p=0.032)
87.2% (p=0.040)

Total angle: 44.2° (p=0.114)

Part D - set-up TRyLTy ———— Mean ——— +/- standard deviation ———

-19.8° (p=0.557)
9.7% (p=0.100)

22.7° (p=0.171)
55.4% (p=0.343)

-21.1° (p=0.094)
87.9% (p=0.832)

Total angle: 44.8° (p=0.597)

Part E - all four set-ups ———— Mean of any of all four set-ups

-19.1°
9.3%

22.8°
54.8%

-20.3°
87.3%

Figure 9.6:   Hip angles on amputated side, extension +ve
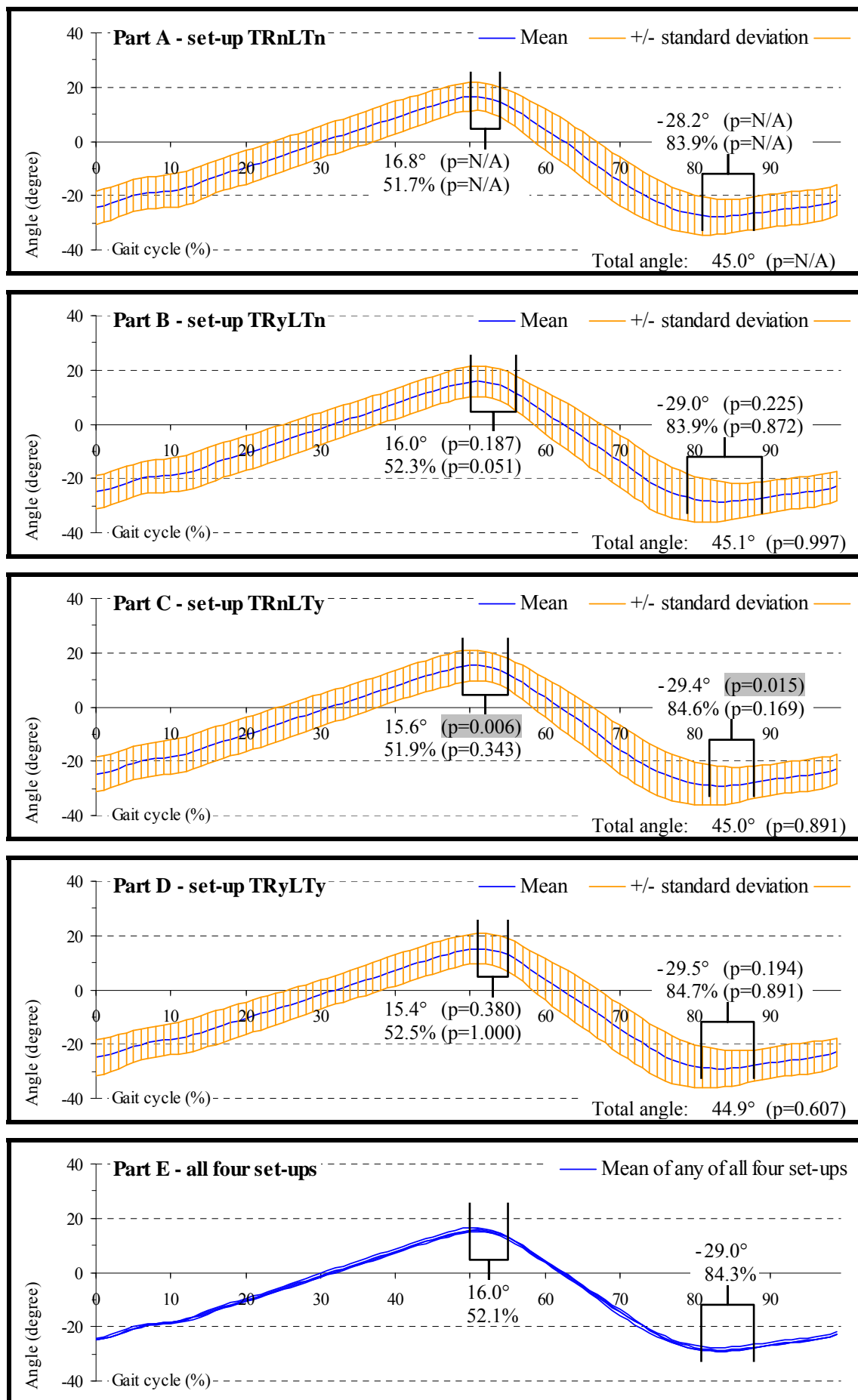
Near the end of stance phase, hip angles started to change back in order to return to full flexion by the time the later part of swing phase was reached. This process made the entire lower limb progress forward, which was the case for both the sound and amputated side during their respective period of the gait cycle. Accelerations triggered by this motion were one of the main contributors for large magnitudes of knee flexion. While the thigh was being pulled forward, the distal aspect of the shin lagged behind due to its own inertia. Only once the thigh started to decelerate was the shin catching up, as the kinetic energy from its pendulum action gave it sufficient propulsion. Having reached peak hip flexion at a similar point in time for the two sides, namely at a mean timing of approximately 87.3% and 84.3% for the sound and amputated side, respectively, the hip angles immediately began to reduce again.

On the sound side, this process of reducing hip flexion angles was very brief. Within only a few percent of the gait cycle, flexion of the hip increased again. Such a pattern may have occurred in response to the forward swinging shin, as this needed slowing down prior to full knee extension. The shin's own inertia was therefore opposing its required deceleration process, and the stored energy consequently dragged the thigh slightly forward again, hence the minor fluctuations in hip angles at the end of swing phase.

In turn, reductions in the amputated side hip angles following peak hip flexion during late swing phase occurred steadily. This may have been a preliminary procedure for helping to push the knee into extension once heel contact was achieved. Although shock absorption is desirable, encouraging knee extension would have helped the joint from flexing too drastically during early stance phase, thus preventing the residual limb from being exposed to an unusual force pattern transmitted by the socket in response to excessive knee flexion.

The largest hip flexion and extension angle that was obtained during the gait cycle reached a mean value of approximately 20.3° and 22.8° for the sound side and approximately 29.0° and 16.0° for the amputated side, respectively. This demonstrates that flexion angles were smaller and extension angles larger on the sound side compared to the amputated side, although the magnitude of total hip rotation was nearly the same for both sides, as previously explained in the opening paragraph of this Section.

Because the anatomic foot could actively be moved, there was no concern about cuffing the toes on the ground. This, however, was not the case on the amputated side, and the subjects may not have let the hip extend as much as on the sound side in order to pull the thigh forward abruptly and therefore initiate drastic knee flexion. Such a theory may be supported by the fact that the residual limb represents only a relatively short lever. Its dimensional limitations could have therefore made it difficult to achieve large magnitudes of knee flexion without the thigh giving the shin the necessary momentum for the required pendulum action. This which explains the smaller amputated side hip extension angles compared to the sound side.

In turn, the reason that hip flexion angles were larger on the amputated side than on the sound side may also have had something to do with the residual limb length, due to the potential for difficulties in actively achieving full knee extension prior to heel strike. By pulling the thigh of the amputated side backward while the shin swung forward, the knee flexion angles would reduce, thus pushing it into extension. This implied that the hip needed to be sufficiently flexed in the first place, so that there was enough scope for the necessary posterior motion of the thigh.

9.1.1.6.   *Inter-set-up differences in hip angles*

The first characteristic with significant differences amongst sound side hip angles was the peak in early stance phase flexion. With set-up TRyLTn and TRnLTy peak hip flexion reached approximately 19.0° (p=0.038) and 19.3° (p=0.049), respectively, compared to approximately 18.2° when the adapter was fully locked. With just transverse rotation possible, the reason for increased peak hip flexion angles was linked to the explanation previously given in Section 9.1.1.4 with regard to increased peak sound side knee flexion in response to transverse plane motion of the pelvis at that same instance. In turn, while only longitudinal translation was being permitted, shortening of the adapter due to push off on the amputated side required the sound side hip to increase its initial peak flexion angles. This was a compensatory action that occurred in conjunction with increased peak sound side knee flexion angles in order to shorten the overall length of the limb, thus preventing the COM, which was already lowered due to the shortening of the adapter, from being lifted upward excessively. In turn, with set-up TRyLTy, the peak sound side hip flexion angles were greatest, reaching approximately 19.8°, but the difference compared to peak hip flexion angles with the adapter fully locked was not significant.

The second characteristic with significant differences amongst sound side hip angles was the magnitude and timing for peak swing phase flexion. This was significantly different with just longitudinal translation possible, in that the angles reached approximately 21.0° (p=0.032), which occurred at approximately 87.2% (p=0.040) of the gait cycle compared to approximately 19.0° and 86.7% of the gait cycle when the adapter was fully locked. The reason for such an outcome was the same as that given previously concerning larger early stance phase peak hip flexion angles, so that the COM did not have to be lifted excessively, as its position was lower than without adapter motion due to shortening of the adapter. Also, despite having found the largest peak sound side hip flexion angles and delay in these angles with set-up TRyLTy, no significant differences were found compared to when the adapter was fully locked, as the changes with set-up TRnLTy were relatively small.

With regard to the amputated side, peak extension just before the end of stance phase significantly affected the peak hip angles with set-up TRnLTy, reaching approximately 15.6° (p=0.006) compared to approximately 16.8° with the adapter fully locked. This could have happened in response to the shortening of the adapter. Due to the reduced prosthetic shin length, the hip did not extend as far as without adapter mobility. This was to prevent the thigh from falling too far behind, thus ensuring that its forward motion would soon also trigger the required large amounts of knee flexion in order to clear the ground. Peak hip extension was even smaller with set-up TRyLTy, reaching approximately 15.4°, but the difference compared to when the adapter was fully locked was statistically insignificant, as the changes with set-up TRyLTn were relatively small.

The other characteristic with significant findings was that amputated side peak hip flexion angles during late swing phase reached approximately 29.4° (p=0.015) with set-up TRnLTy compared to approximately 28.2° with the adapter fully locked. This may have had something to do with the fact that at push off the extension angle was smaller than with a locked adapter, so that the hip had to flex more just before heel strike in order to maintain a similarly proportioned step length. With set-up TRyLTy the peak hip flexion angle was even larger, reaching approximately 29.5°, but the difference compared to when the adapter was fully locked was statistically insignificant, as the changes with set-up TRnLTy were relatively small.

9.1.2.   Floor plate forces

9.1.2.1.   *Inter-limb differences in vertical GRFs*

GRFs in vertical direction for both the sound and amputated side are illustrated in Figure 9.7 and Figure 9.8, respectively. The standard deviation for the sound side was fairly consistent throughout the gait cycle, reaching a minimum and maximum of approximately 0.8N/kg and 2.4N/kg, which is around 6.9% and 20.7% of the 11.6N/kg total mean vertical GRF, respectively. This was slightly lower for the amputated side, in that the standard deviation reached a minimum and maximum of approximately 0.2N/kg and 1.7N/kg, which is around 1.8% and 15.6% of the 10.9N/kg total mean vertical GRF, respectively. The smallest values for both sides were predominantly found at heel strike and toe off, as the magnitudes of forces were near zero.

Following heel strike, vertical GRFs immediately increased, whereby the pattern representing the first rise of these forces was different for the two sides. The graphs for the sound side appeared to be logarithmic, and for the amputated side they appeared exponential.

On the sound side, the logarithmic pattern of graphs was likely to occur in response to the fact that the anatomic ankle was capable of controlling its displacements. While the sound side resisted moving too quickly into a plantarflexed position, GRFs soon became larger. Only due to more gradual, controlled motions of the anatomic foot did the rate of increase start to slow down to finally reach a peak in vertical GRFs. This peak therefore presumably occurred at a slightly delayed stage due the controlled ankle motion, thus increasing the likelihood that the magnitude of peak vertical GRFs was slightly lowered.

On the amputated side, the exponential pattern of the graphs was likely to occur in response to a very soft plantarflexion bumper, previously described in Section 4.1.6.5. Resistance to vertical GRFs was therefore low, because the prosthetic ankle plantarflexed easily. Due to this compliance, the downward push from the heel onto the ground was initially not particularly strong, but the more the foot plantarflexed, the greater the resistance to plantarflexion from the increasingly compressed bumper became. This was reflected by a slight kink in the graphs at approximately 3-4% of the gait cycle, which developed due to a rapid rise in the magnitudes of forces as a result of large resistance to ankle motion from the compressed bumper.

Figure 9.7: Vertical GRFs on sound side, upward +ve
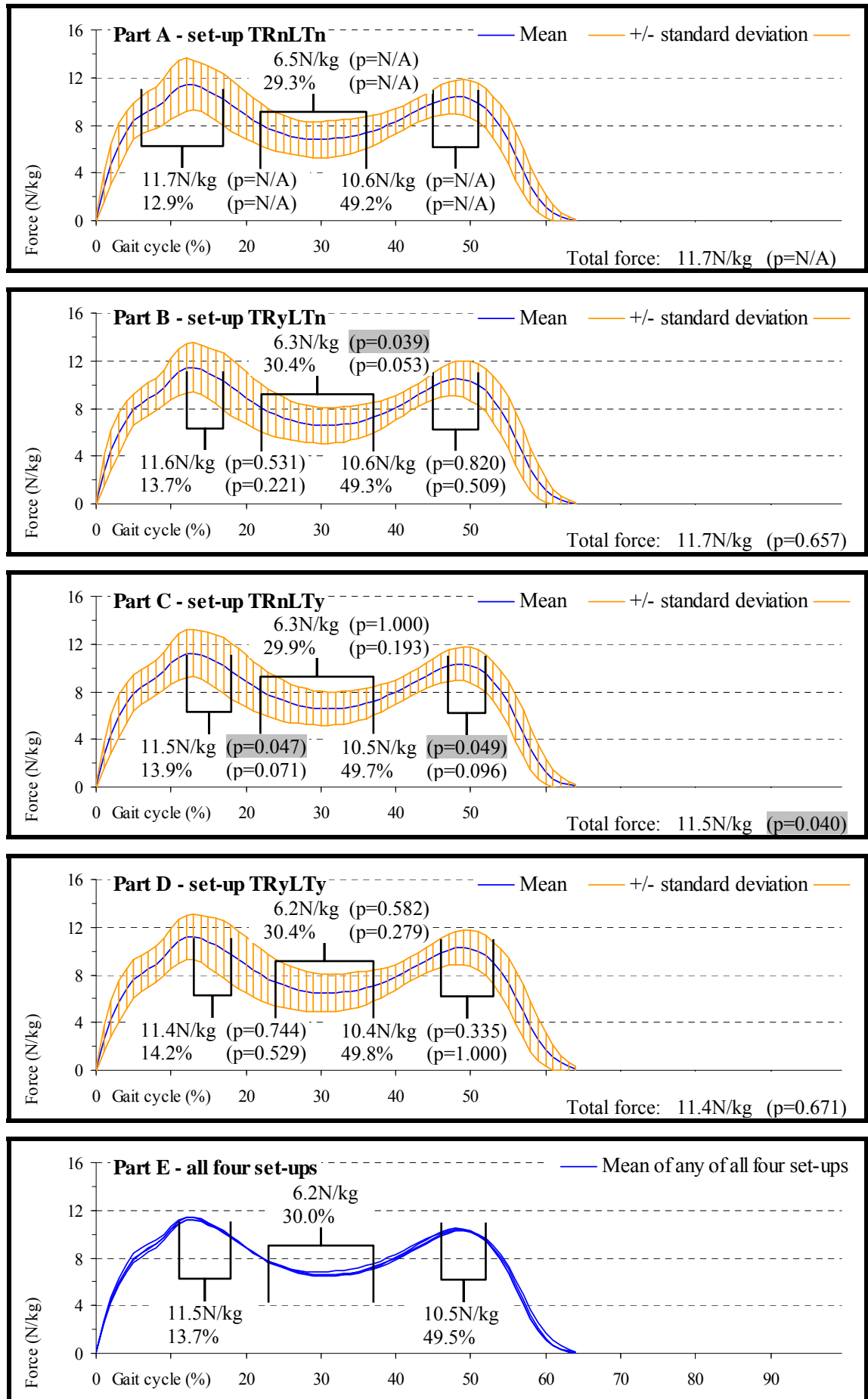
Figure 9.8:   Vertical GRFs on amputated side, upward +ve
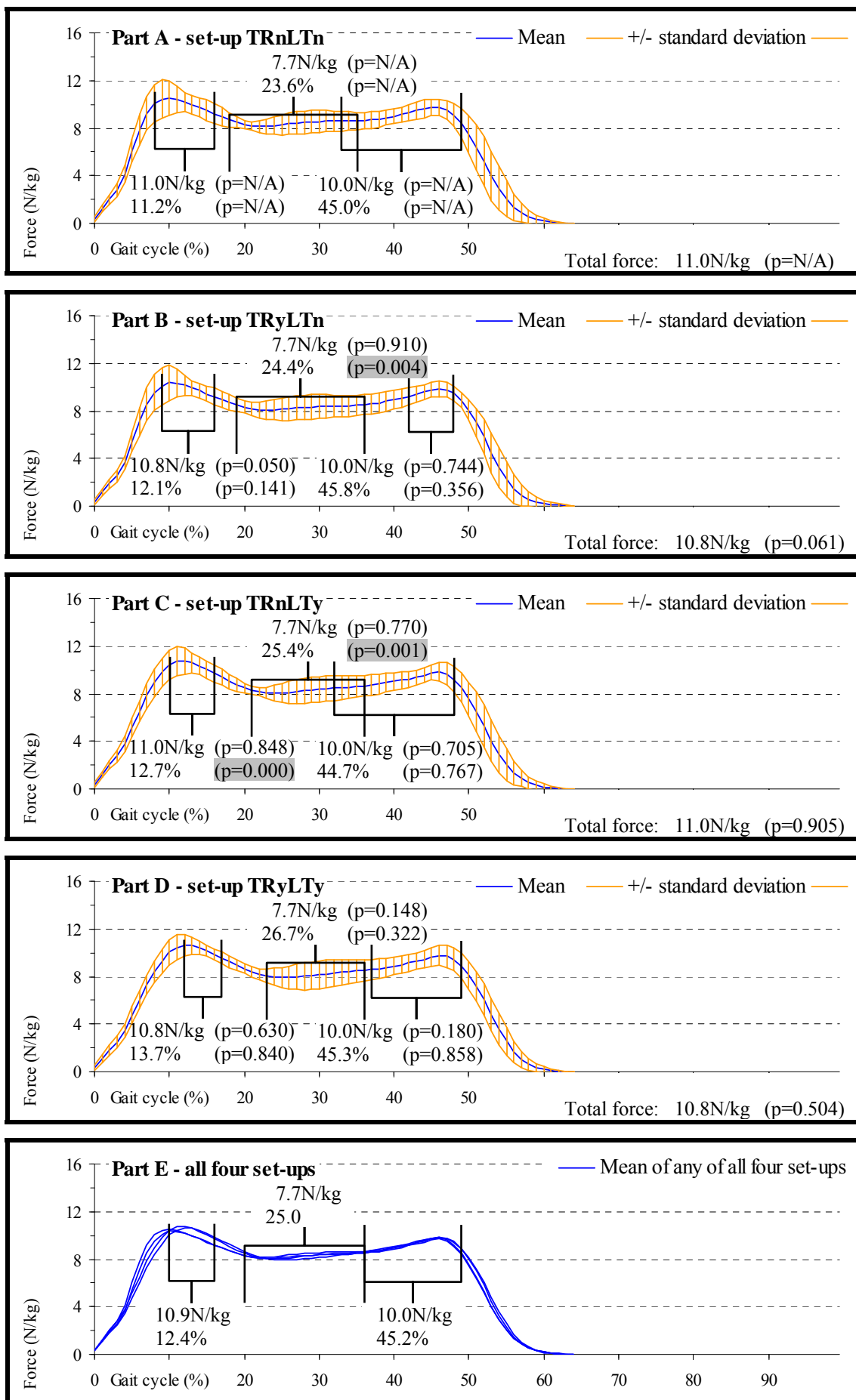
The incident of the peak in early vertical GRFs occurred fractionally earlier on the amputated side at a mean timing of approximately 12.4% of the gait cycle compared to approximately 13.7% of the gait cycle for the sound side. To understand the meaning of this, it is important to consider the ratio between the magnitudes of forces and the duration for these forces to cease increasing. In terms of shock absorption, a reduction of the period for vertical GRFs to reach the peak can therefore generally be considered as detrimental. This meant that the amputated side experienced less shock absorption, as the initial peak in vertical GRFs was reached quicker compared to the sound side. However, with a mean weight of 82.6kg for all ten subjects, as shown in Table 4.2, the forces exerted back onto the body by the ground were in the region of approximately 117% and 111% of mean subject body weight for the sound and amputated side, respectively.

Despite a shorter period to reach the peak of impact, it appeared as if the element of shock absorption was more beneficial for the amputated side, because the peak in initial vertical GRFs was smaller compared to the sound side. At this stage, it needs to be taken into account that both sides were fundamentally different, which meant that the behaviour of the amputated side may have affected the sound side. An explanation for a difference in the magnitude of peak vertical GRFs during the weight acceptance period could possibly be linked to the motion patterns at lower limb joints. Stance phase knee flexion was, as described in Section 9.1.1.3, only half the magnitude for the amputated side relative to the sound side. Therefore, the COM during this period must have been further upward than it was during the corresponding period for the sound side. Preparing for heel strike on the sound side consequently required the COM to travel downward over a longer vertical distance, in order for the foot to make contact with the ground. The amount of kinetic energy was, as a result of this, larger, so that the forces acting on the sound side limb were greater compared to the amputated side.

Despite an earlier incident for reaching the initial peak in amputated side vertical GRFs, the magnitude of this peak was, as just explained, lower compared to the sound side. Nevertheless, the actual method for absorbing shock impacts on the amputated side was likely to be less efficient overall than it was for the sound side due to insufficient action from the ankle and knee on the amputated side, as previously explained in Section 9.1.1.1 and Section 9.1.1.3. It therefore appears as if the prosthesis led to a non-optimised walking pattern in need of compensation from the sound side, which

explains the larger vertical GRFs exerted onto the anatomic foot during the weight acceptance period.

Following the weight acceptance period during the early part of the gait cycle, vertical GRFs quickly reduced again until they reached a minimum. The incident of this minimum occurred near the middle of stance phase for the sound side and slightly earlier for the amputated side at a mean timing of approximately 30.0% and 25.0% of the gait cycle, respectively. In turn, the difference in magnitudes of minimum vertical GRFs during mid-stance phase was more drastic than the timing of this event, reaching approximately 63% and 79% of mean subject body weight for the sound and amputated side, respectively.

Not only were vertical GRFs during sound side mid-stance phase smaller in magnitude, but when taking into consideration the high level of initial shock impacts the anatomic foot had to experience during the weight acceptance period, it becomes clear that the total lowering in forces between the initial peak in vertical GRFs and the minimum in vertical GRFs during mid-stance phase was far greater compared to the amputated side. This difference led to a reduction of nearly 50% of mean subject body weight on the sound side compared to just over 30% of mean subject body weight on the amputated side. The reason for a greater reduction of body weight on the sound side compared to the amputated side can be explained as follows.

Although the sound side experienced greater stance phase knee flexion than the amputated side, the overall magnitude in vertical GRFs during the initial weight acceptance period was greater for the anatomic limb, as explained previously. The initial upward propulsion was therefore stronger and the vertical shift of the COM likely to be greater for the sound side than it was for the amputated side. This means that mid-stance phase vertical GRFs could inevitably decrease more than they would have done if the COM had only shifted slightly, which explains why the minimum in vertical GRFs during mid-stance phase was smaller for sound side compared to the amputated side.

Towards the end of stance phase, vertical GRFs started to rise again. This was the result of the subjects pushing themselves off the ground in order to gain upward and forward propulsion. The magnitudes of forces were lower than during early stance phase, but

they still reached 107% and 102% of mean subject body weight for the sound and amputated side, respectively. As expected, vertical GRFs on the amputated side were lower, due to the lack of active plantarflexion from the prosthetic foot, as described in Section 9.1.1.1. Also, the incident of reaching late stance phase vertical GRFs occurred slightly earlier on the amputated side at a mean timing of approximately 45.2% of the gait cycle compared to approximately 49.5% of the gait cycle on the sound side. This reinforced the aspect regarding an early reduction in already comparatively low amputated side peak hip extension angles during terminal stance phase in an attempt to initiate drastic knee flexion, as previously elaborated on in Section 9.1.1.5. Following termination of stance phase, GRFs were absent as the foot on its respective side was off the floor.

9.1.2.2. *Inter-set-up differences in vertical GRFs*

The first characteristic with a significant difference was the sound side peak vertical GRFs during the initial weight acceptance period. The magnitude of this peak was reduced to approximately 11.5N/kg (p=0.047) with set-up TRnLTy compared to approximately 11.7N/kg with the adapter fully locked. Such a reduction occurred, because the shortening of the prosthesis lowered the pelvis in response to longitudinal translation at the adapter. To transfer the weight from the amputated side onto the sound side, the entire body therefore did not have to travel downward as far as when the adapter was fully locked, because the pelvis and the COM were already lower. The momentum of the COM was consequently smaller, so that the counteracting forces from the ground did not need to be quite as large. Although the lowest vertical GRFs of approximately 11.4N/kg occurred with set-up TRyLTy, the difference compared to when the adapter was fully locked was not significant.

The next characteristic with a significant difference was the minimum in vertical GRFs during mid-stance phase, which reached approximately 6.3N/kg (p=0.039) with set-up TRyLTn compared to approximately 6.5N/kg when the adapter was fully locked. Such a change may have occurred due to the sound side knee flexion angles, described in Section 9.1.1.3. As can be seen in Figure 9.3, the difference between early stance phase knee flexion and late stance phase knee extension was larger while transverse rotation was being permitted. This gave the body stronger upward propulsion and the COM a greater vertical lift, so that at mid-stance phase, vertical GRFs could inevitably decrease more than they would have done if the COM had only shifted slightly. Despite an even

greater reduction in vertical GRFs to approximately 6.2N/kg with set-up TRyLTy, findings remained insignificant as the difference between set-up TRnLTy and set-up TRnLTn was not at all significant.

Towards the end of stance phase, sound side peak vertical GRFs were significantly affected in that their magnitude was lowered to approximately 10.5N/kg (p=0.049) with set-up TRnLTy compared to approximately 10.6N/kg when the adapter was fully locked. This could have happened because less proximally directed propulsion was required during sound side push off, since the subjects did not have to travel upward as much when accepting weight on the amputated side due to the pending shortening of the adapter soon after heel strike with the prosthetic foot. GRFs were even lower with set-up TRyLTy, reaching approximately 10.4N/kg, but significant findings were absent.

For all four set-ups, the greatest vertical GRFs were found during the previously described initial weight acceptance period. As the only set-up with a significantly different value for this parameter compared to that when the adapter was fully locked was when longitudinal translation was possible, the same scenario therefore also occurred with regard to the total of vertical GRFs. This meant that the most significant findings occurred with set-up TRnLTy, reaching 11.5N/kg (p=0.040) compared to 11.7N/kg when the adapter was fully locked.

Concerning vertical GRFs on the amputated side, the first characteristic with a significant difference was the initial peak while loading all the weight onto the prosthesis. With set-up TRnLTy, the incident for this peak occurred at a mean timing of approximately 12.7% (p=0.000) of the gait cycle compared to approximately 11.2% of the gait cycle when the adapter was fully locked. This was highly significant and can be attributed to the shortening of the adapter. The magnitude of vertical GRFs was approximately the same as when the adapter was fully locked, but the delay in reaching the peak in these forces increased the deceleration of the body's COM, which meant that the period over which body mass was applied to the ground was prolonged. Although this was not associated with a lower magnitude in peak vertical GRFs, the delay of the incident for reaching peak vertical GRFs indicated a reduced loading rate.

The same peak occurred even later with set-up TRyLTy at a mean timing of approximately 13.7% of the gait cycle, but the difference compared to when the adapter

was fully locked was not significant, as transverse rotation only insignificantly delayed the peak. However, although the results seemed, from the statistical point of view, irrelevant, fully mobilising the adapter provided the prosthesis with the best shock absorbing properties. This was not only due to the delay of peak vertical GRFs, but also because the magnitude of those forces was reduced.

The other characteristic with significant differences on the amputated side was that around mid-stance phase the minimum in vertical GRFs was delayed. The incident of this event occurred at a mean timing of approximately 24.4% (p=0.004) and 25.4% (p=0.001) of the gait cycle with set-up TRyLTn and TRnLTy, respectively, compared to approximately 23.6% of the gait cycle when the adapter was fully locked. As the initial peak in vertical GRFs during the weight acceptance period occurred later for both these set-ups, the delay of the mid-stance phase minimum in vertical GRFs consequently seemed to be a knock on effect of this. The differences in the timing compared to when the adapter was fully locked were therefore, from the statistical point of view, highly significant. Such a delay, however, was not considered to have any meaningful effect on the gait in general. With set-up TRyLTy the incident of the minimum in vertical GRFs was also delayed and occurred at a mean timing of approximately 26.7% of the gait cycle, but the difference compared to when the adapter was fully locked was insignificant.

9.1.2.3. *Inter-limb differences in anterior-posterior GRFs*

GRFs in anterior-posterior direction for both the sound and amputated side are illustrated in Figure 9.9 and Figure 9.10, respectively. The standard deviation for the sound side was fairly consistent throughout the gait cycle, reaching a minimum and maximum of approximately 0.2N/kg and 0.6N/kg, which is around 4.9% and 14.6% of the 4.1N/kg total mean anterior-posterior GRF, respectively. This was slightly lower for the amputated side, in that the standard deviation reached a minimum and maximum of approximately 0.1N/kg and 0.5N/kg, which is around 2.9% and 14.9% of the 3.5N/kg total mean anterior-posterior GRF, respectively. The smallest values for both sides were predominantly found at heel strike and toe off, as the magnitudes of forces were near zero.

During the weight acceptance period, the leading foot hit the ground ahead of the remaining body, so that the entire lower limb of the same side was leaning backward.

Forward movement of the trunk in response to forward propulsion by the contra lateral trailing side therefore not only pushed the leading foot downward, but also forward. Due to friction with the ground, the tendency of the leading foot to migrate anteriorly was counteracted by posteriorly directed GRFs, which were quickly increasing. With a mean subject weight of 82.6kg, as shown in Table 4.2, posteriorly directed GRFs soon reached a peak of approximately 17% and 20% of mean subject body weight, which occurred at a mean timing of approximately 10.1% and 10.8% of the gait cycle for the sound and amputated side, respectively.

The reason that the peak in posteriorly directed GRFs was smaller in magnitude and its incident earlier for the sound side compared to the amputated side may be linked to the fact that the magnitude of early sound side stance phase knee flexion was larger than it was for the amputated side, as described in Section 9.1.1.3. While the knee flexed, the magnitude of anteriorly directed forces that were transmitted onto the force plate in response to the forward progressing trunk was reduced, and so therefore was the magnitude of posteriorly directed GRFs. This reduction occurred due to the compliance of the leading lower limb, which acted as a flexible link between the trunk and the force plate, because of flexion at the knee. A reduction in posteriorly directed GRFs and an increase in knee flexion angles were consequently co-related. Compared to the amputated side, such a relationship explains the positive effect of a smaller and quicker reducing peak in posteriorly directed GRFs on the sound side and the resultant decreased braking process with its negative effect of slowing down the required forward progression of the body.

While the trunk was moving further forward along the walking path, its horizontal distance in that direction steadily reduced relative to the stance foot. In turn, the magnitude of posteriorly directed forces also decreased until the trunk was slightly ahead of the stance foot. This was the point in time when the direction of GRFs changed, which occurred only fractionally later on the sound side at a mean timing of approximately 30.0% of the gait cycle compared to approximately 29.1% of the gait cycle for the amputated side.

Due to the weight of the trunk, the foot of the now forward leaning stance limb was being pushed posteriorly, thus triggering anteriorly directed GRFs. An additional

Figure 9.9:   Anterior-posterior GRFs on sound side, anterior +ve

Part A - set-up TRnLTn

— Mean   +/- standard deviation

- 1.7N/kg (p=N/A)
10.1%   (p=N/A)

2.4N/kg (p=N/A)
54.3%   (p=N/A)

30.0% (p=N/A)

Force (N/kg)

Gait cycle (%)

Total force: 4.1N/kg (p=N/A)

Part B - set-up TRyLTn

— Mean   +/- standard deviation

- 1.7N/kg (p=0.542)
9.6%   (p=0.173)

2.4N/kg (p=0.376)
54.3%   (p=0.168)

29.9% (p=0.462)

Force (N/kg)

Gait cycle (%)

Total force: 4.1N/kg (p=0.369)

Part C - set-up TRnLTy

— Mean   +/- standard deviation

- 1.7N/kg (p=0.487)
10.4%   (p=0.399)

2.4N/kg (p=0.952)
54.6%   (p=0.117)

29.1% (p=0.545)

Force (N/kg)

Gait cycle (%)

Total force: 4.1N/kg (p=0.710)

Part D - set-up TRyLTy

— Mean   +/- standard deviation

- 1.8N/kg (p=0.272)
10.2%   (p=0.541)

2.4N/kg (p=0.822)
55.0%   (p=0.037)

30.0% (p=0.229)

Force (N/kg)

Gait cycle (%)

Total force: 4.2N/kg (p=0.716)

Part E - all four set-ups

— Mean of any of all four set-ups

- 1.7N/kg
10.1%

2.4N/kg
55.0%

30.0%

Force (N/kg)

Gait cycle (%)

Figure 9.10: Anterior-posterior GRFs on amputated side, anterior +ve
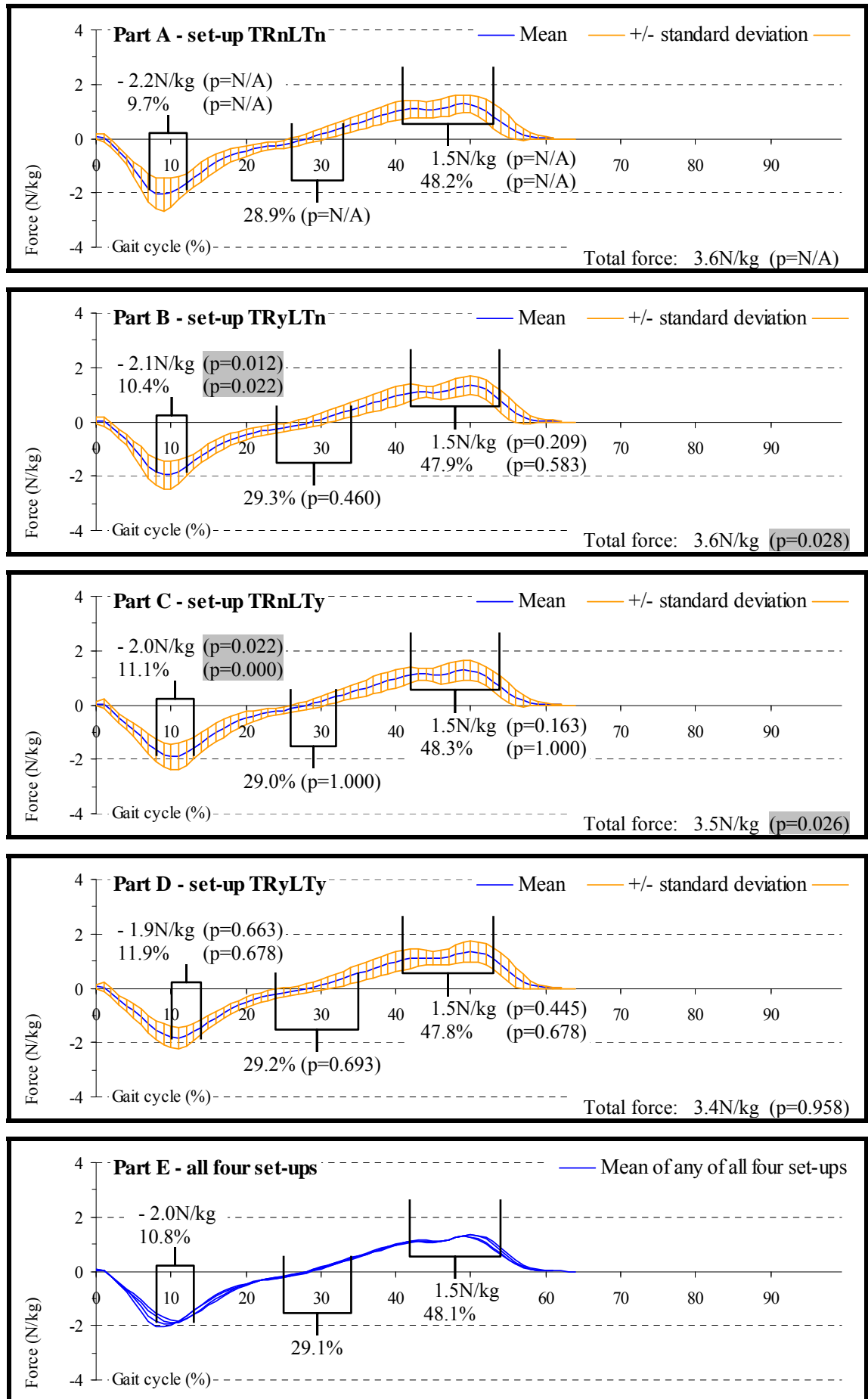
posteriorly directed push from the subjects was achieved by actively plantarflexing the sound side ankle to achieve the forward propulsion, previously emphasised in Section 9.1.1.1. As the prosthetic ankle could not be actively plantarflexed, the resultant peak in anteriorly directed GRFs was very small, reaching approximately only 15% of mean subject body weight compared to approximately 25% of mean subject body weight for the anatomic ankle. This demonstrates that the forward propulsion was considerably smaller when wearing a prosthesis. Also, the peak in anteriorly directed GRFs occurred at a mean timing of approximately 55.0% and 48.1% of the gait cycle for the sound and amputated side, respectively. Therefore, some of the time available for prolonged forward directed propulsion was clearly not utilised on the amputated side, as this action was terminated early. A possible reason for such a behaviour may be linked to the explanation previously given in Section 9.1.1.5 regarding low levels of hip extension in order to pull the thigh forward abruptly and therefore initiate drastic knee flexion.

9.1.2.4. *Inter-set-up differences in anterior-posterior GRFs*

Sound side GRFs were only significantly affected with regard to the timing of the peak in anteriorly directed GRFs around late stance phase. With the adapter fully mobile, the incident of this peak was delayed, as it occurred at approximately 55.0% (p=0.037) of the gait cycle compared to approximately 54.3% of the gait cycle when the adapter was fully locked. A possible reason for this may be linked to the explanation previously given in Section 9.1.1.2, in that the cushioned feel of the prosthesis, due to adapter mobility, left the subjects less aware of when exactly they established ground contact on the amputated side. Not knowing whether or not the prosthesis was safely in its correct position due to reduced proprioceptive feedback in response to shock absorption from the fully mobile adapter, peak anteriorly directed GRFs were therefore delayed. This would ensure that strong forward propulsion was only being transferred onto the amputated side at the appropriate point in time when the subjects were sure that the weight acceptance period on the amputated side had definitely started.

On the amputated side, significant findings amongst anterior-posterior GRF data turned out to be less sparse than they were on the sound side. The main characteristic with significant differences was the first peak in posteriorly directed GRFs following heel strike. The value obtained for this peak was in the region of approximately 2.1N/kg (p=0.012) and 2.0N/kg (p=0.022) with set-up TRyLTn and TRnLTy, which occurred at a mean timing of approximately 10.4% (p=0.022) and 11.1% (p=0.000) of the gait

cycle, respectively. Such findings were highly significant compared to a peak of approximately 2.2N/kg at approximately 9.7% of the gait cycle when the adapter was fully mobile. The reason for those differences may be explained as follows.

During the weight acceptance period, the prosthetic shin was, as previously suggested in Section 9.1.1.2, leaning backward and medially, because most of the weight was still predominantly carried by the trailing, contra lateral sound side. In the same way that some of the downward momentum might have been taken up by displacements at the adapter, the same could have been applicable with regard to the forward momentum, which was also likely to be partly taken up by displacements at the adapter due to the backward leaning shin. Such an outcome strongly suggests that the permission of socket displacements greatly contributed to an improved force-time ratio for greater shock absorption, particularly as inter-set-up differences were highly significant. This demonstrates that adapter mobility can be very advantageous for amputee gait, at least with respect to anteriorly directed GRFs on the amputated side. Also, an even further reduction of forces and a longer delay in reaching the peak occurred with set-up TRyLTy, thus providing even better shock absorption, but the findings were, from the statistical point of view, not significant.

The final characteristic that was significantly affected on the amputated side was the total of anterior-posterior GRFs. Due to the reduced initial peak in posteriorly directed GRFs with set-up TRyLTn and TRnLTy, the total value of anterior-posterior GRFs was also reduced to approximately 3.6N/kg (p=0.028) and 3.5N/kg (p=0.026) for the same two set-ups, respectively. This was a similar scenario for set-up TRyLTy, with which the total value of anterior-posterior GRFs was the lowest from all four set-ups, but the difference was insignificant compared to when the adapter was fully locked.

9.1.2.5.   Inter-limb differences in medial-lateral GRFs

GRFs in medial-lateral direction for both the sound and amputated side are illustrated in Figure 9.11 and Figure 9.12, respectively. The standard deviation for the sound side was fairly consistent throughout the gait cycle, reaching a minimum and maximum of approximately 0.1N/kg and 0.5N/kg, which is around 8.5% and 35.8% of the 1.4N/kg total mean medial-lateral GRF, respectively. This was slightly lower for the amputated side, in that the standard deviation reached a minimum and maximum of approximately 0.1N/kg and 0.3N/kg. However, the overall ratio was larger at around 14.3% and 42.9%

of the 0.7N/kg total mean medial-lateral GRF, respectively, because this value was much smaller compared to the sound side. The smallest values for both sides were predominantly found at heel strike and toe off, as the magnitudes of forces were near zero.

In order for the body to experience stable, unilateral support throughout the gait cycle, the COM needed constantly shifting from one weight bearing side to the other, while the contra lateral, forward swing limb took no part in maintaining the required upright posture. During mid-stance phase, such a reciprocating process meant that, with regard to a horizontal distance in the coronal plane, the centre of the trunk and therefore the COM was not located half way between both feet, but instead further over towards the support side. Accelerations and decelerations of the COM could therefore be monitored, as the forces responsible for triggering the resultant displacements of the COM were applied onto the ground.

When the support of the body was about to be transferred from the amputated side onto the sound side, the COM gradually shifted over nearer to a location above the anatomic foot. The required forces for this were transmitted to the floor by both the sound and amputated side during double support phase. The amputated side actively pushed the body over and at the same time the body was pulled by the sound side.

The resultant drag by the sound side, which was currently the leading limb, consequently gave the anatomic foot the tendency to migrate medially, thus briefly triggering laterally directed GRFs. With a mean subject weight of 82.6kg, as shown in Table 4.2, the peak magnitude of these forces reached approximately 5.1% of mean subject body weight. As the COM progressed moving over towards the sound side, the anatomic foot quickly changed its response by starting to push laterally after just over approximately 7% of the gait cycle, to increase the braking force in an attempt to slow the COM down.

In turn, for the amputated side's corresponding duration of the gait cycle when the support of the body was about to be transferred from the sound side onto the amputated side, the initial laterally directed GRFs did also occur. This was because the prosthetic foot developed the tendency to migrate medially in response to the drag that it generated

Figure 9.11: Medial-lateral GRFs on sound side, lateral +ve
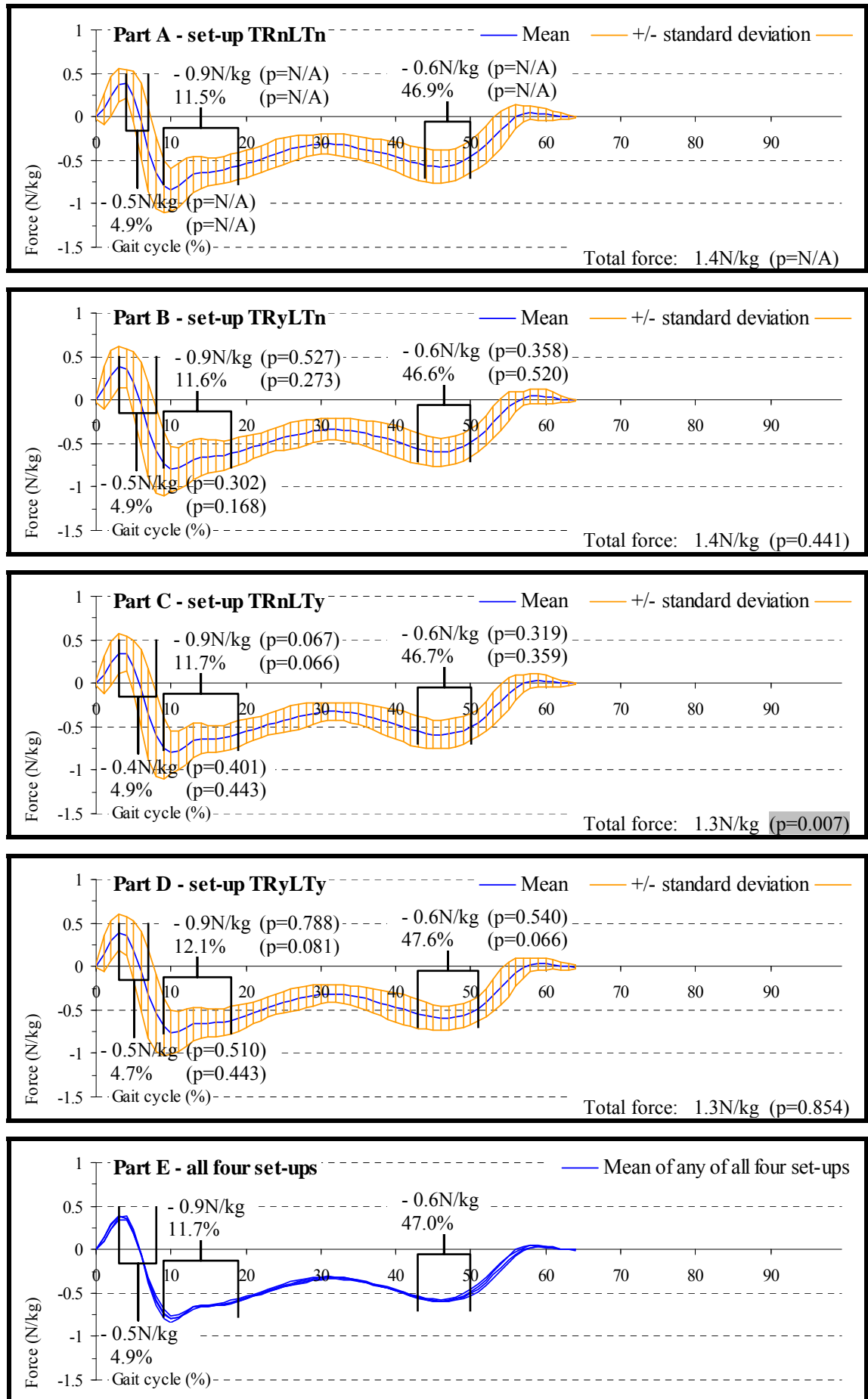
Figure 9.12:   Medial-lateral GRFs on amputated side, lateral +ve
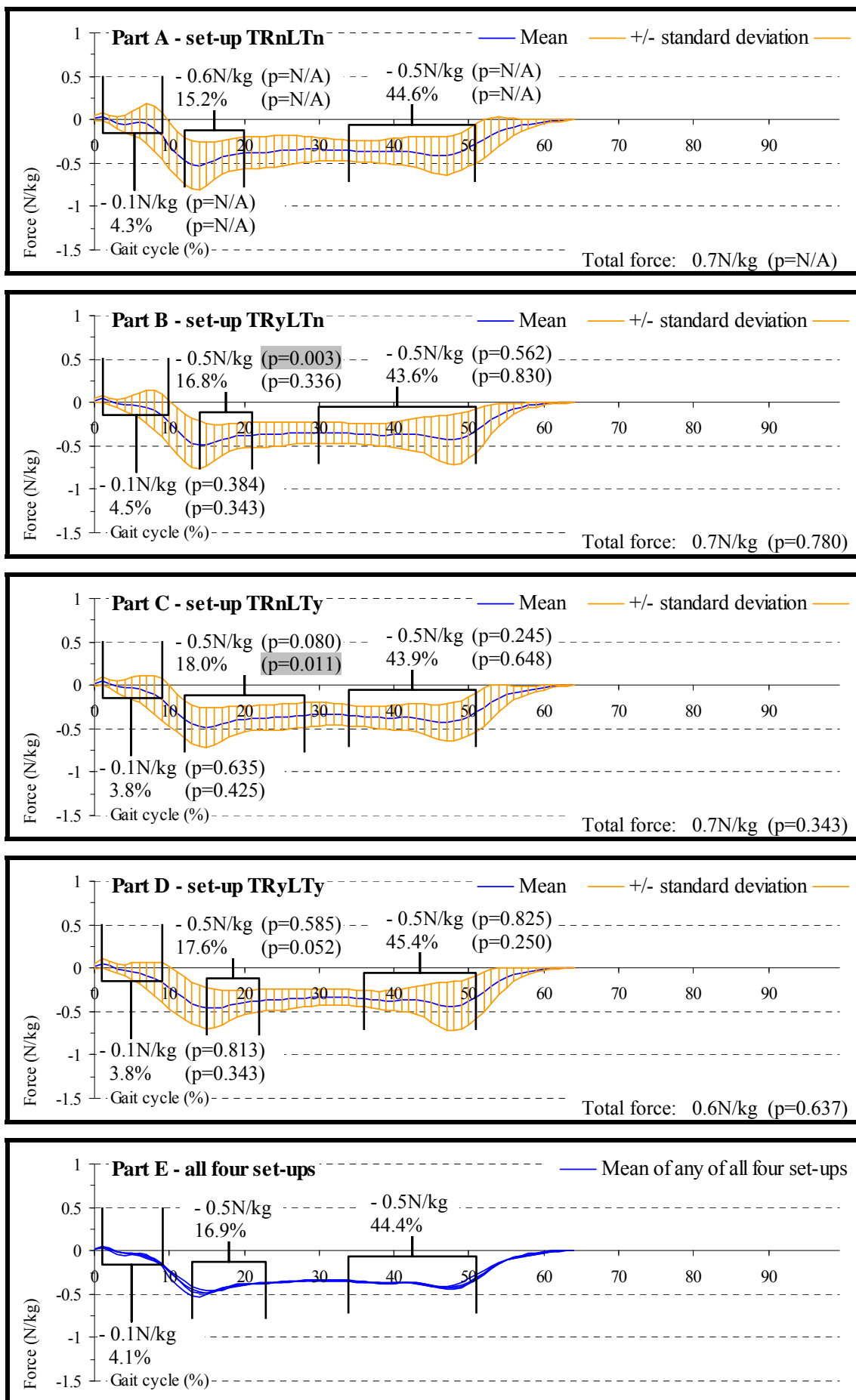
to pull the body over towards the amputated side. However, the magnitude in laterally directed GRFs was negligible, reaching a mean value of approximately 1.0% of mean subject body weight. This demonstrated that the required propulsion to shift the body over above the prosthesis came predominantly from the sound side.

As the anatomic foot was about to lift off the ground, the required braking force for slowing the COM down was entirely the responsibility of the amputated side. This turned out to be comparatively easy, because medially directed GRFs during the early part of amputated side stance phase were just above 55% of the value obtained during the equivalent period for the sound side, namely approximately 9.2% and 5.1% of mean subject body weight, respectively. Part of the reason for lower side-to-side braking forces on the amputated side could have been due to the fact that the incident of this event occurred later compared to the sound side at a mean timing of approximately 16.9% and 11.7% of the gait cycle, respectively. This meant that shock absorption on the amputated side was better as the force-time ratio was more advantageous compared to the sound side. Such a shock absorbing behaviour may have been triggered subconsciously in an attempt to reduce the magnitude of forces acting on the lateral aspect of the pressure sensitive, bony residual limb.

Following the initial peak in medially directed GRFs, the magnitudes of these forces immediately started to reduce during both lower limbs' respective part of the gait cycle until a minimum was reached at around mid-stance phase. From this point in time onward, the stance limb started to shift the body back over towards the still forward swinging contra lateral limb, in preparation for its weight acceptance. As a result of this, the now trailing foot of the stance limb needed to increase its laterally directed push, thus triggering a rise in medially directed GRFs again. These forces were slightly larger in magnitude and occurred marginally later for the sound side compared to the amputated side, reaching a mean value of approximately 6.1% and 5.1% of mean subject body weight at a mean timing of approximately 47.0% and 44.4% of the gait cycle, respectively. Such figures seemed to tie in with the previously described event during heel strike of the amputated side. Because the drag that the prosthesis applied onto the ground in order to pull the COM over to its side while accepting weight was only small, the main input for the required propulsion of the COM towards the amputated side therefore had to come from the sound side. This explains why medially

directed GRFs during late stance phase were slightly larger on the sound side compared to the amputated side.

9.1.2.6. *Inter-set-up differences in medial-lateral GRFs*

On the sound side, the only significant difference in medial-lateral GRFs was the total value these forces reached, which was highly significant at 1.3N/kg (p=0.007) with set-up TRnLTy compared to 1.4N/kg when the adapter was fully mobile. The total value of medial-lateral GRFs was composed of the largest forces in both medial and lateral direction, which occurred during the weight acceptance period. In medial direction, the GRFs reached virtually the same magnitude for all four set-ups, but in lateral direction the GRFs were different, in that they reached the smallest peak value with set-up TRnLTy, which explains the reduced total value in medial-lateral GRFs.

A typical situation that may result in smaller laterally directed GRFs would be larger medially directed GRFs during late stance phase of the amputated side. This would provide greater propulsion for shifting the COM over towards the sound side, so that the pull from the anatomic foot does not need to be as large as it would have to be if medially directed GRFs on the amputated side reached their normal, and not larger, level. However, this was not an applicable scenario for a reduction of the actual data from the gait laboratory tests regarding the peak in laterally directed sound side GRFs, because medially directed GRFs on the amputated side were virtually the same for all four set-ups. The true reason for the reduction in laterally directed sound side GRFs was not fully understood, hence an explanation for such an outcome could not be provided, except that it must have been linked to the fact that the adapter could shorten. Also, despite similar results with set-up TRyLTy, the difference compared to gait with a locked adapter was not significant.

On the amputated side, the only significantly affected characteristic was the peak in medially directed GRFs during the weight acceptance period. Compared to gait with no motion at the adapter, the magnitude of this peak was lower and its incident occurred later during all three dynamic set-ups. However, significant differences were only found on two occasions. With set-up TRyLTn, the peak in medially directed GRFs reached a magnitude of approximately 0.5N/kg (p=0.003), and with set-up TRnLTy the incident of this peak occurred at approximately 18.0% (p=0.011) of the gait cycle compared to 0.6N/kg and 15.2% of the gait cycle when the adapter was fully locked. Both

315

differences were highly significant. The reasons for such differences need explaining separately with regard to set-up TRyLTn and set-up TRnLTy.

The link between a reduction in peak medially directed GRFs during the weight acceptance period and transverse rotation at the adapter can be explained as follows. The lower limb is generally slightly externally rotated, so that the knee not only displaces anteriorly, but slightly laterally also, while it flexes together with the hip during the weight acceptance period. Despite the fact that at this part of the gait cycle the socket was internally rotated, as will be shown in Section 9.2.1, the magnitude of internal rotation was only small, so that the socket was still in a net position of external rotation, which was presumably the same for the knee. The lateral displacement of the knee during flexion of the knee and hip was consequently likely to counteract the braking forces from the prosthetic foot for slowing the COM down by pushing laterally and thereby triggering medially directed GRFs. It can be seen in Figure 9.4 that the peak amputated side knee flexion angle during the weight acceptance period increased with set-up TRyLTn compared to when the adapter was fully locked. The lateral displacement of the knee was therefore likely to increase also, which would reduce the peak in medially directed GRFs. Despite reduced medially directed GRFs with set-up TRyLTy, the difference compared to gait with a locked adapter was not significant.

The link between a delay of the peak in laterally directed GRFs during the weight acceptance period and longitudinal translation at the adapter can be explained as follows. The prosthesis was likely to lean slightly medially during the amputated side weight acceptance period, because the COM was still further over towards the contra lateral sound side, as previously elaborated on in Section 9.1.1.2. With regard to set-up TRnLTy and TRyLTy, if the prosthesis was leaning medially, this therefore made it possible for the force-time ratio to change due to the fact that longitudinal translation was being permitted, which took up some of the laterally directed momentum. As a result of this, shock absorption was greater, because of a reduced loading rate in response to a delayed peak in medially directed GRFs. This was similar to the scenario previously described in Section 9.1.2.4 regarding inter-set-up changes in anterior-posterior GRFs as a result of transverse rotation. Also, although the peak in medially directed GRFs was affected during all three set-ups, the only significant differences in its magnitude and timing were found with regard to set-up TRyLTn and TRnLTy, respectively and none with set-up TRyLTy.

9.1.3. Floor plate pressure and moment

9.1.3.1. Inter-limb differences in anterior-posterior COP

The COP in anterior-posterior direction for both the sound and amputated side is illustrated in Figure 9.13 and Figure 9.14, respectively. The standard deviation for the sound side was fairly consistent throughout the gait cycle, except that the band width was broader during mid-stance phase, reaching a minimum and maximum of approximately 0.10mm/mm and 0.19mm/mm, which is around 11.4% and 21.6% of the 0.88mm/mm total mean anterior-posterior COP displacement, respectively. This was very similar for the amputated side, in that the standard deviation reached a minimum and maximum of approximately 0.05mm/mm and 0.21mm/mm, which is around 7.1% and 30.0% of the 0.70mm/mm total mean anterior-posterior COP displacement, respectively. The smallest values for both sides were predominantly found at heel strike and toe off. Although every subject's total COP displacement was similar in magnitude, the reason for a relatively high standard deviation was because of variations in the location of the initial point of contact on each force plate. This simply displaced rather than altered the entire ROM, which is why the band width remained relatively even.

At the instant heel strike occurred, the COP of both the sound and amputated side immediately moved from the centre of the force plate to the posterior aspect of the foot in question. After that, the ankle started to plantarflex, so that more of the heel's plantar aspect touched the force plate, which allowed the COP to travel forward. In addition to the already established heel contact, once the ball of the foot was also placed onto the ground, the COP migrated even further anteriorly. From this point in time onwards, the travelling pattern of the COP differed for the two limbs.

In order to help resist sound side stance phase knee flexion, the anatomic ankle made attempts to plantarflex while the foot was flat on the ground. In addition to that, while the trunk became positioned above rather than behind the stance limb, the body weight was gradually being transferred to the anterior aspect of the foot. Both of these factors triggered a continuous forward shifting of the COP, as the reactive response from the ground was to provide resistance against the downward pushing foot. This process steadily carried on until late stance phase.

Figure 9.13:   Anterior-posterior COP on sound side, anterior +ve

Part A - set-up TRnLTn — Mean — +/- standard deviation
Shift (mm/mm)
Gait cycle (%)
Total shift: 0.89mm/mm   (p=N/A)

Part B - set-up TRyLTn — Mean — +/- standard deviation
Shift (mm/mm)
Gait cycle (%)
Total shift: 0.87mm/mm   (p=0.127)

Part C - set-up TRnLTy — Mean — +/- standard deviation
Shift (mm/mm)
Gait cycle (%)
Total shift: 0.90mm/mm   (p=0.934)

Part D - set-up TRyLTy — Mean — +/- standard deviation
Shift (mm/mm)
Gait cycle (%)
Total shift: 0.87mm/mm   (p=0.801)

Part E - all four set-ups — Mean of any of all four set-ups
Shift (mm/mm)
Gait cycle (%)

318

Figure 9.14:   Anterior-posterior COP on amputated side, anterior +ve
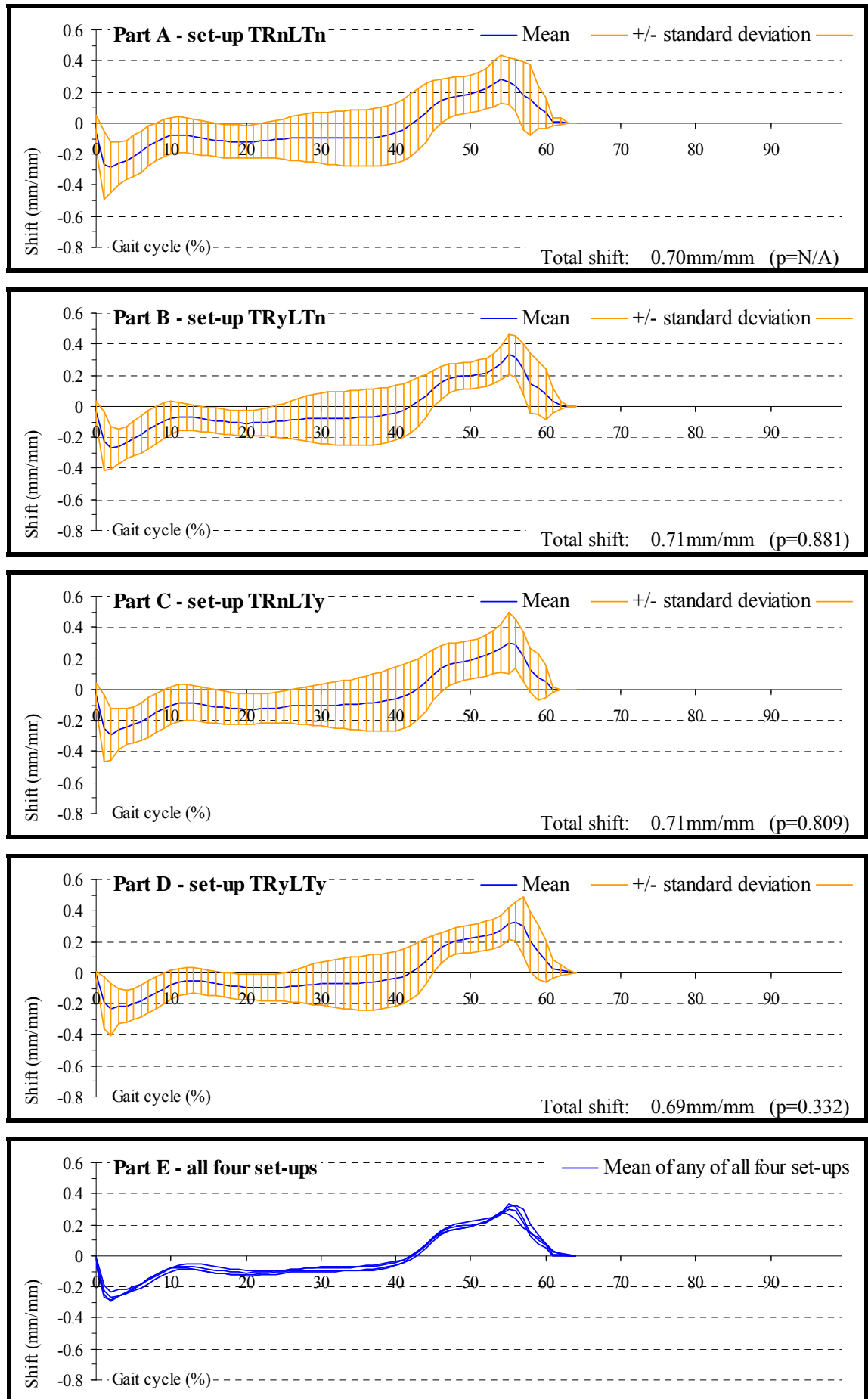
In turn, stance phase knee flexion during the weight acceptance period on the amputated side was, as described in Section 9.1.1.3, much smaller in magnitude compared to the sound side, which meant that less travel was required for returning the knee back into an extended position. Helping to create the required counteracting moment at the knee by generating power at distal articulations did not represent a viable option, because, as explained in Section 9.1.1.1, active plantarflexion of the prosthetic ankle was not possible. As it was only passive motion that was possible at the prosthetic ankle, this was not sufficient to trigger a further anterior displacement of the COP. Also, the dorsiflexion bumper only just started to become compressed by the ankle mechanism. Its resistance to the gradually forward rotating prosthetic shin in response to a continuous anteriorly directed transfer of body weight was therefore not sufficient to push the forefoot harder onto the ground. The COP was consequently not affected, so that its position in anterior-posterior direction remained more or less constant until the later part of mid-stance phase.

Once the sound side stance limb was positioned behind the trunk and the ankle became fully dorsiflexed, the heel started to lift off the floor. GRFs were therefore acting purely on the ball of the anatomic foot, which meant that the COP shifted even further forward. With plantarflexion angles quickly increasing, the COP was soon relocated again in that it was transferred to its most forward position, namely onto the toes, as these were the last parts of the anatomic foot that remained in contact with the ground.

A similar scenario could be observed on the amputated side. Having nearly fully compressed the dorsiflexion bumper, the heel was forced off the floor, so that the COP quickly shifted onto the ball of the prosthetic foot. As flexion at the knee and hip increased, the progressively more forward leaning prosthetic shin made the foot gradually tip forward onto its toes, so that this became the most anterior location for the COP. Once the prosthesis was fully in the air, GRFs were absent and the COP went back into the centre of the force plate where it started during heel strike, which was the same for the COP on the sound side.

The total mean displacement of the COP was larger on the sound side compared to the amputated side. This was so for a number of reasons. As explained in Section 4.1.6.6, the prosthetic foot was not covered by a shoe, so that its overall length was shorter than the sole of the footwear worn on the sound side, thus reducing the distance on the force

plate where contact was established. The other factor responsible for triggering a reduced COP displacement could have been because active plantarflexion on the amputated side was not possible. As a result of this, the distal aspect of the toes might have never touched the ground.

An additional aspect that could be observed was that the total mean displacement of the COP did not match the dimensions of the foot, but it only measured approximately 0.88mm/mm and 0.70mm/mm or 88% and 70% of each subject's foot length, respectively. This might have had something to do with the fact that the toes and heel of the prosthetic foot were curved when viewed from the side, as illustrated in Figure 4.6. Contact between its very anterior and posterior aspect and the force plate was therefore not possible without acquiring unusual angles at the ankle. This was a similar scenario for the anatomic side, because the type of footwear worn by the subjects was a standard training shoe of the same kind for all ten of them, as previously described in Section 7.1.7. Its heel and toe section had a curved appearance, which presumably served to provide some rocker action. The reason for a reduced displacement of the COP was therefore likely to be similar to the explanation previously given with respect to the prosthetic foot.

9.1.3.2.   Inter-set-up differences in anterior-posterior COP

The effect of different set-ups on the anterior-posterior displacement of the COP was minimal for both the sound and amputated side. The only characteristic extracted from these data was the total COP displacement, but this was not significantly different for the three set-ups when the adapter was at least partially mobile.

9.1.3.3.   Inter-limb differences in transverse plane GRMs

The GRMs in the transverse plane for both the sound and amputated side are illustrated in Figure 9.15 and Figure 9.16, respectively. The standard deviation for the sound side showed some fluctuations, in that the band width was fairly narrow at the beginning, middle and end of stance phase, but broader in between those events. The minimum and maximum standard deviation reached approximately 0.01Nm/kg and 0.07Nm/kg, which is around 4.6% and 31.8% of the 0.22Nm/kg total mean transverse plane GRM, respectively. This was similar for the amputated side, in that the standard deviation reached a minimum and maximum of approximately 0.01Nm/kg and 0.04Nm/kg, which

is around 6.7% and 26.7% of the 0.15Nm/kg total mean transverse plane GRM, respectively. The smallest values for both sides were predominantly found at heel strike and toe off, as the magnitude of GRFs was near zero.

GRFs in medial-lateral direction were the main aspect that influenced transverse plane GRMs, because each subject's anatomic and prosthetic foot was a lot narrower than it was long. Although medial-lateral GRFs were only approximately one third of the magnitude that anterior-posterior GRFs reached, the advantage for medial-lateral GRFs was an extended lever arm. By analysing the distance between the centre of the force plate and the POA, it can be seen that this separation was longer for pushing the force plate perpendicular to the walking direction than for pushing parallel to it, due to the dimensions of both the anatomic and prosthetic foot.

During the weight acceptance period of the sound side, the anatomic foot was pushing medially just after heel strike, as explained in Section 9.1.2.5. Because all the weight that the sound side carried was being transmitted through the heel, which was at this stage behind the centre of the force plate, the resulting laterally directed GRFs triggered an internal GRM. This was very short lived, because the foot soon started pushing laterally. Since the heel still remained the main weight bearing area, the now medially directed GRFs therefore introduced an external GRM with a mean peak value of approximately 0.12Nm/kg at a mean timing of approximately 12.6% of the gait cycle.

Events on the amputated side were similar, except that the initial internal GRM was virtually absent due to negligible amounts of laterally directed GRFs. In turn, the external GRM did become quite prominent, but not as large as on the sound side in response to smaller medially directed GRFs exerted onto the prosthesis. The magnitude of the external GRM reached consequently a mean value of only approximately 0.08Nm/kg, which calculated as 67% of the value reached by the anatomic foot. The incident of this peak occurred at approximately 11.9% of the gait cycle.

After that, although the GRFs maintained a medial direction, their magnitude started to reduce slightly. This process continued until mid-stance phase, whereby the external GRM therefore also lowered. The next stage was a repeated increase in medially directed GRFs. However, as the COP was about to shift onto the front half of the force

Figure 9.15:   Transverse plane GRMs on sound side, external +ve

Part A - set-up TRnLTn   — Mean   — +/- standard deviation —

-0.09Nm/kg (p=N/A)
50.8 %   (p=N/A)

0.13Nm/kg (p=N/A)
11.4 %   (p=N/A)

Total moment: 0.22Nm/kg (p=N/A)

Part B - set-up TRyLTn   — Mean   — +/- standard deviation —

-0.09Nm/kg (p=0.882)
50.5 %   (p=0.137)

0.12Nm/kg (p=0.205)
12.6 %   (p=0.048)

Total moment: 0.22Nm/kg (p=0.571)

Part C - set-up TRnLTy   — Mean   — +/- standard deviation —

-0.10Nm/kg (p=0.229)
51.5 %   (p=0.126)

0.13Nm/kg (p=1.000)
12.8 %   (p=0.028)

Total moment: 0.23Nm/kg (p=0.810)

Part D - set-up TRyLTy   — Mean   — +/- standard deviation —

-0.09Nm/kg (p=0.471)
51.0 %   (p=0.758)

0.11Nm/kg (p=0.483)
13.4 %   (p=0.509)

Total moment: 0.22Nm/kg (p=0.472)

Part E - all four set-ups   — Mean of any of all four set-ups

-0.09Nm/kg
51.0 %

0.12Nm/kg
12.6 %

323

Figure 9.16:   Transverse plane GRMs on amputated side, external +ve

Part A - set-up TRnLTn
— Mean — +/- standard deviation —
-0.07Nm/kg (p=N/A)
47.4 %   (p=N/A)
0.10Nm/kg (p=N/A)
11.3 %   (p=N/A)
Gait cycle (%)
Moment (Nm/kg)
Total moment: 0.17Nm/kg (p=N/A)

Part B - set-up TRyLTn
— Mean — +/- standard deviation —
-0.06Nm/kg (p=0.411)
47.7 %   (p=0.013)
0.08Nm/kg (p=0.098)
11.5 %   (p=0.223)
Gait cycle (%)
Moment (Nm/kg)
Total moment: 0.14Nm/kg (p=0.078)

Part C - set-up TRnLTy
— Mean — +/- standard deviation —
-0.06Nm/kg (p=0.653)
48.6 %   (p=0.332)
0.08Nm/kg (p=0.168)
12.2 %   (p=0.005)
Gait cycle (%)
Moment (Nm/kg)
Total moment: 0.14Nm/kg (p=0.308)

Part D - set-up TRyLTy
— Mean — +/- standard deviation —
-0.06Nm/kg (p=0.269)
49.5 %   (p=0.370)
0.07Nm/kg (p=0.251)
12.4 %   (p=1.000)
Gait cycle (%)
Moment (Nm/kg)
Total moment: 0.14Nm/kg (p=0.190)

Part E - all four set-ups
— Mean of any of all four set-ups
-0.06Nm/kg
48.3 %
0.08Nm/kg
11.9 %
Gait cycle (%)
Moment (Nm/kg)

plate, as described in Section 9.1.3.1, the rotational counteraction by this device was a change from an external to an internal GRM.

While the magnitude of medially directed GRFs continued rising, so did the internal GRM, particularly due to further forward migration of the COP and the resultant lengthened lever arm. Once the GRFs reached a peak, the same happened to the internal GRM. Its magnitude was greater for the sound side compared to the amputated side, reaching a mean value of approximately 0.09Nm/kg and 0.06Nm/kg, respectively. Although the COP on the sound side was not positioned as far forward as on the amputated side, the reason for a greater peak internal GRM on the sound side was because the magnitude of peak medially directed GRFs was approximately 20% larger than on the amputated side. The incidents of the peak internal GRMs were close together for both sides. They occurred at a mean timing of approximately 51.0% and 48.3% of the gait cycle for the sound and amputated side, respectively. The delay on the sound side was therefore only small, which was in response to a similar timing with regard to medial-lateral GRFs. Finally, the GRM went back to zero due to termination of contact with the ground.

9.1.3.4.   *Inter-set-up differences in transverse plane GRMs*

The incident for reaching the initial peak in the external GRM while transferring the weight onto the sound side was delayed during all three dynamic set-ups. At this stage of the gait cycle, the main forces responsible for triggering an external GRM were medially directed GRFs. These forces also occurred slightly later compared to when the adapter was fully locked, which explained the resultant delay in the peak external GRM. Although the incident of this event occurred latest with set-up TRyLTy, significant differences could only be found with set-up TRyLTn and TRnLTy, in that the peak was reached at approximately 12.6% (p=0.048) and 12.8% (p=0.028) of the gait cycle compared to approximately 11.4% of the gait cycle when the adapter was fully locked.

For the amputated side, the first characteristic in transverse plane GRMs that turned out to be significantly affected was the initial peak representing the force plate's peak external moment during the weight acceptance period. This peak was delayed during all three dynamic set-ups, but the differences were only significant with set-up TRnLTy. The incident when the peak was reached occurred at approximately 12.2% (p=0.005) of the gait cycle, which was highly significant compared to approximately 11.3% of the

gait cycle when the adapter was fully locked. The reason for such a delay was linked to the fact that with set-up TRnLTy medially directed GRFs were also delayed, as previously explained in Section 9.1.2.6. Also, the scenario when the peak external GRM was delayed the most occurred with set-up TRyLTy, but no significant difference was found compared to when the adapter was fully locked.

The other characteristic with significant findings concerning the amputated side GRMs was the incident in reaching the peak of the force plate's internal moment towards the end of stance phase. The largest differences occurred with set-up TRnLTy and TRyLTy, but the standard deviations between subjects were in these cases relatively small. In turn, the scenario was the opposite when only transverse rotation was possible, which meant that the data during this particular set-up were significantly different due to a greater dispersion of values. The point in time when the peak internal GRM was reached occurred at approximately 47.7% (p=0.013) of the gait cycle compared to approximately 47.4% of the gait cycle when the adapter was fully locked. The reason why the peak internal GRM was delayed with set-up TRyLTn might have been linked to the fact that the data representing medially directed GRFs were similarly dispersed as they were for the late stance phase internal GRM.

Despite having found only very few statistically significant differences, a general trend amongst GRM data could still be observed. This trend manifested itself in such a way that when the adapter was at least partially mobilised, peak internal and peak external GRMs were smaller in magnitude and delayed for both the sound and amputated side. This was the case for every single parameter, except for one, which was the incident of the peak internal GRM with set-up TRyLTn on the sound side, in that this parameter was not delayed, but fractionally early by only 0.3% of the gait cycle. The fact that in all other cases the peak GRMs were smaller in magnitude and delayed indicates a reduced loading rate.

The reason for such changes was partly because of transverse rotation, as this type of motion was being permitted during two out of the three dynamic set-ups. While the residual limb was trying to rotate in a transverse plane, the resultant moment was being transmitted via the socket down to the prosthetic foot, thus trying to rotate this segment in the same direction as the residual limb wanted to rotate. In response to that, the force plate applied a counteracting moment, the GRM, which resisted the tendency of the foot

to move. While transverse rotation was being permitted, rotation of the socket consequently twisted the elastic element of the torsion rod, and this prolonged the time it took for the GRM moment to reach its peak. The resultant delay therefore changed the moment-time ratio, which also lowered the peak that the GRM reached.

Although the transverse rotation aspect seemed a plausible explanation for changes in the moment-time ratio, it would be wrong to think that the entire reduction and delay of the GRM was the making of the torsion rod alone. In fact, there must have been another explanation for this, because those changes would otherwise have not occurred when purely longitudinal translation was being permitted. In order to find this additional explanation, it seemed logical to investigate the main source with the greatest influences on GRMs. This was medially directed GRFs, as these occurred throughout the majority of stance phase.

During mid-stance phase, the prosthesis would have been vertical as it was intended during the alignment procedure with the COM above it. In turn, at either end of stance phase, the prosthesis would have been leaning medially with the COM further over towards the sound side and no longer above the prosthesis, as previously alluded to in Section 9.1.1.2. Although medially directed GRFs were predominantly triggered by the tendency of the prosthesis to migrate laterally, a small part of them were likely to be the result of axial loading as the prosthesis was leaning medially. With the prosthetic foot located further laterally than the socket due to the medially leaning of the limb, medially directed GRFs therefore triggered some longitudinal translation at the adapter. In turn, this altered the force-time ratio at least during early and late stance phase, because the shortening of the adapter delayed the peak in medially directed GRFs. This therefore reduced and delayed the peak of the GRM. In conclusion, as the torque at the force plate was influenced by socket rotation and probably by the medially leaning prosthesis, this explained why the GRM was lowest and most delayed when the adapter was fully mobilised.

9.1.4. Sagittal plane joint moments

9.1.4.1. Inter-limb differences in ankle moments

Ankle moments of both the sound and amputated side are illustrated in Figure 9.17 and Figure 9.18, respectively. The standard deviation for the sound side was fairly

consistent throughout the gait cycle, reaching a minimum and maximum of approximately 0.1Nm/kg and 0.3Nm/kg, which is around 8.3% and 25.0% of the 1.2Nm/kg total mean ankle moment, respectively. This was different for the amputated side, in that the standard deviation varied greatly, particularly during mid-stance phase. The values reached a minimum and maximum of approximately 0.1Nm/kg and 0.4Nm/kg, which is around 10.0% and 40.0% of the 1.0Nm/kg total mean ankle moment, respectively. The smallest values for both sides were predominantly found at heel strike and toe off, as the magnitude of GRFs was near zero.

At the instant of stance phase, the part of the foot that established the initial contact with the ground was the heel. Its posterior position on the foot and its forward progressing tendency that triggered the posteriorly directed resultant GRFs, described in Section 9.1.2.3, were the factors responsible for locating the ankle anterior to those resultant GRFs. This momentarily triggered a very small plantarflexion moment for only approximately 2-3% of the gait cycle, thus helping to push both the anatomic and prosthetic foot further towards the floor during their respective gait cycles. As a more plantarflexed position was quickly acquired, resultant GRFs immediately commenced migrating anteriorly, thus locating them ahead of the ankle, which, in turn, triggered a dorsiflexion moment.

In Section 9.1.1.3, it was shown that during the sound side weight acceptance period, the knee experienced a number of degrees of flexion. This knee flexion was partially resisted by the knee extensors. The other source of resistance could have been the plantarflexors of the anatomic foot, thus transferring the body weight from the heel to the ball of the foot, so that the COP consequently moved further anterior, as illustrated in Section 9.1.3.1. At this stage of the gait cycle, the braking action following foot flat gradually lessened, as indicated by the reducing posteriorly directed GRFs. Because vertical GRFs also reduced, the combined resultant vector representation acquired a more vertical, and then forward leaning, orientation that consequently passed further anterior to the anatomic ankle. In addition to this, while the COP was continuously moving forward, the lever arm, defined by the distance between GRFs and the ankle, lengthened, thereby gradually increasing the dorsiflexion moment. This process continued until late stance phase.

Figure 9.17:   Ankle moments on sound side, dorsiflexion +ve
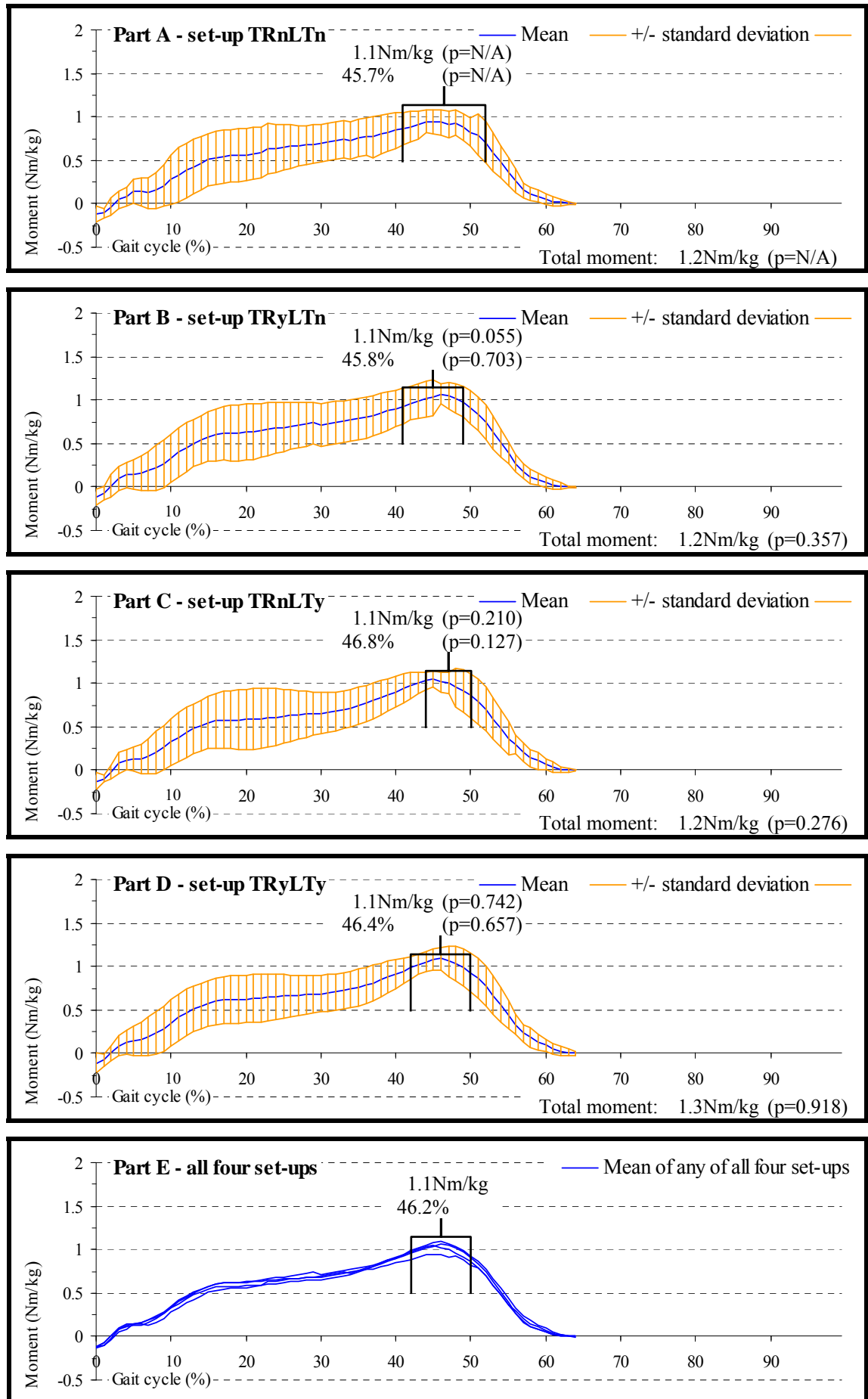
Figure 9.18:   Ankle moments on amputated side, dorsiflexion +ve
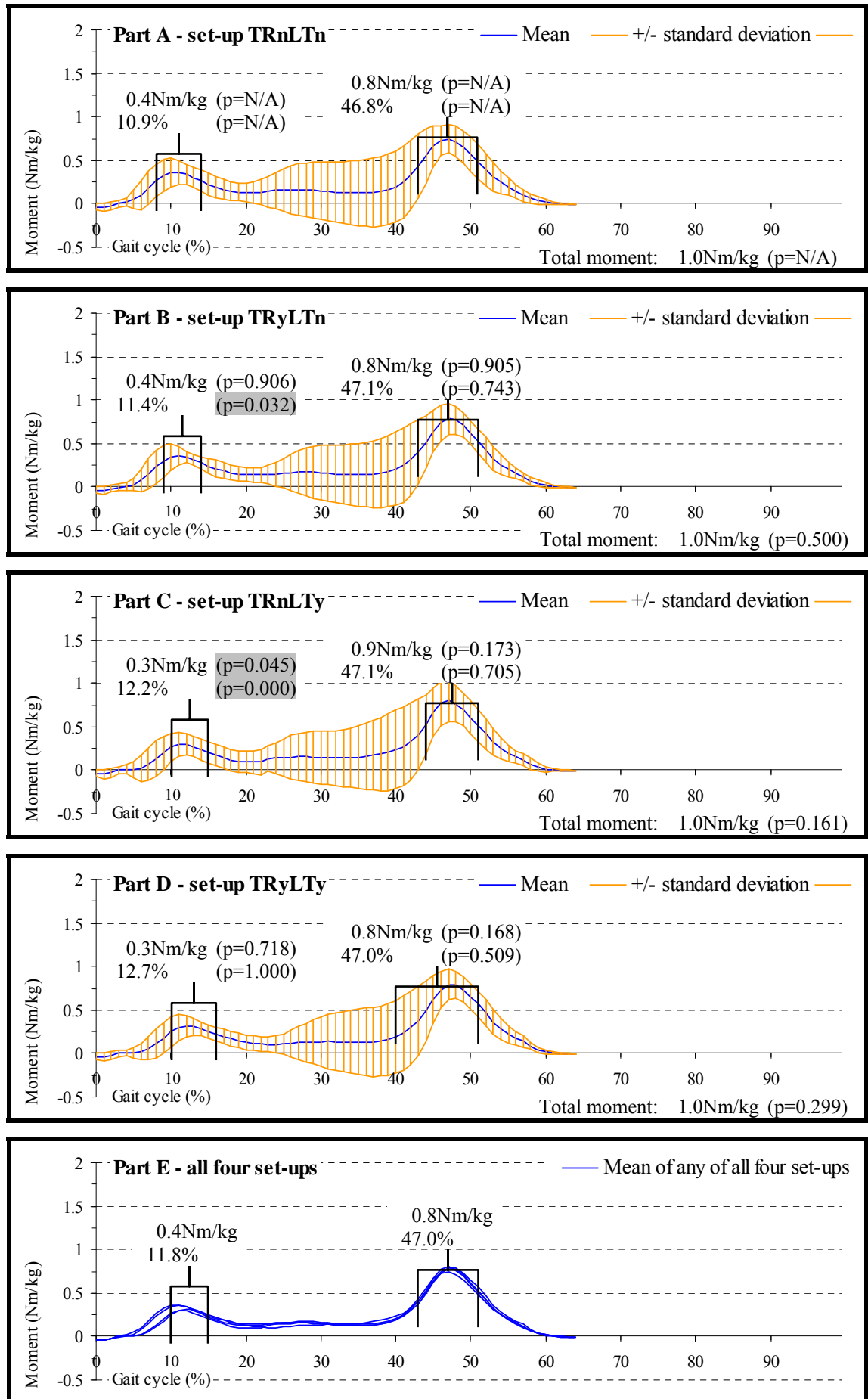
Although stance phase knee flexion on the amputated side was a lot smaller than on the sound side, once the prosthetic foot obtained full contact with the ground, the COP shifted further anterior, as with the anatomic limb, thus triggering a dorsiflexion moment. However, unlike the scenario on the sound side, the COP stayed in virtually the same position from around foot flat onwards until the end of mid-stance phase. As the lever arm therefore remained more or less constant and vertical GRFs were smaller during mid-stance phase than at heel strike, the resultant moment at the prosthetic ankle did not continue to increase, but soon decreased following early stance phase. Only after the prosthetic shin started to gradually lean forward beyond a vertical direction did the dorsiflexion bumper become compressed by the ankle mechanism. At the instant the compression was high enough, the generation of resistance to dorsiflexion reached sufficiently high levels. As a result of this, the COP moved further anterior, because the weight was being transmitted through the ball of the foot. This was also the point in time when the resultant GRFs increased again for creating the required forward propulsion, so that the dorsiflexion moment became greater until a peak was reached. In addition to an increase in resultant GRFs, the anterior position of the COP that was responsible for an extended lever arm between GRFs and the ankle also contributed to the increased dorsiflexion moment.

The incident when the dorsiflexion moment reached a peak was similar for both sides and only fractionally delayed on the amputated side. In turn, the main difference was the magnitude of late stance phase peak dorsiflexion moments, reaching a mean value of approximately 1.1Nm/kg and 0.8Nm/kg for the sound and amputated side, respectively. Such a difference was in response to the lower resultant GRFs exerted onto the prosthetic foot compared to the anatomic foot. This proved that the dorsiflexion moment's counteracting plantarflexion action was a lot lower on the amputated side compared to the sound side, thus indicating that forward propulsion must have been a lot less than that experienced by the sound side. Once the peak dorsiflexion moment was reached, it gradually dropped down to zero by the time toe off occurred, as the GRFs faded out, which was the same for both sides.

9.1.4.2.   *Inter-set-up differences in ankle moments*

On the sound side, the effect of different set-ups on the ankle moments was minimal. None of the characteristics extracted from these data were significantly different for the three set-ups compared to when the adapter was at least partially mobile.

In turn, on the amputated side, it was the first peak in the dorsiflexion moment during the weight acceptance period that was influenced by different set-ups. In all three cases when the adapter was at least partially mobilised, the initial dorsiflexion moment was delayed. However, significant differences were only found with set-up TRyLTn and TRnLTy, in that the described peak occurred at approximately 11.4% (p=0.032) and 12.2% (p=0.000) of the gait cycle, respectively, compared to approximately 10.9% of the gait cycle when the adapter was fully locked. A similar delay happened with regard to the early peak in amputated side plantarflexion angles, therefore it must have taken longer for the COP to move forward. Because of such a delayed displacement of the COP and the fact that both anterior-posterior and vertical GRFs were also delayed, this explains the delay in the dorsiflexion moment, as it took longer for the resultant GRF vector to move anterior to the prosthetic ankle.

In turn, with just longitudinal translation being permitted, the magnitude of the amputated side peak dorsiflexion moment was smaller reaching approximately 0.3Nm/kg (p=0.045) compared to approximately 0.4Nm/kg when the adapter was fully locked, which was a significant difference. Such an outcome can be attributed to a lower initial peak in posteriorly directed GRFs, because this was, as explained in Section 9.1.2.2, significant, too. With the magnitude of vertical GRFs reaching approximately the same value as when the adapter was fully locked, the resultant GRF vector therefore acquired a more backward leaning orientation. This vector consequently passed closer in front of the ankle and hence the lower dorsiflexion moment due to a reduced lever arm. This was similar with set-up TRyLTy, but no significant findings were revealed.

9.1.4.3.   Inter-limb differences in knee moments

Knee moments of both the sound and amputated side are illustrated in Figure 9.19 and Figure 9.20, respectively. The standard deviation for the sound side was fairly consistent throughout the gait cycle, reaching a minimum and maximum of approximately 0.2Nm/kg and 0.7Nm/kg, which is around 5.4% and 18.9% of the 3.7Nm/kg total mean knee moment, respectively. This was similar for the amputated side, in that the standard deviation reached a minimum and maximum of approximately 0.1Nm/kg and 0.7Nm/kg, which is around 2.6% and 18.0% of the 3.9Nm/kg total mean knee moment, respectively. The smallest values for both sides were predominantly found at heel strike and toe off, as the magnitude of GRFs was near zero.

Figure 9.19:   Knee moments on sound side, extension +ve
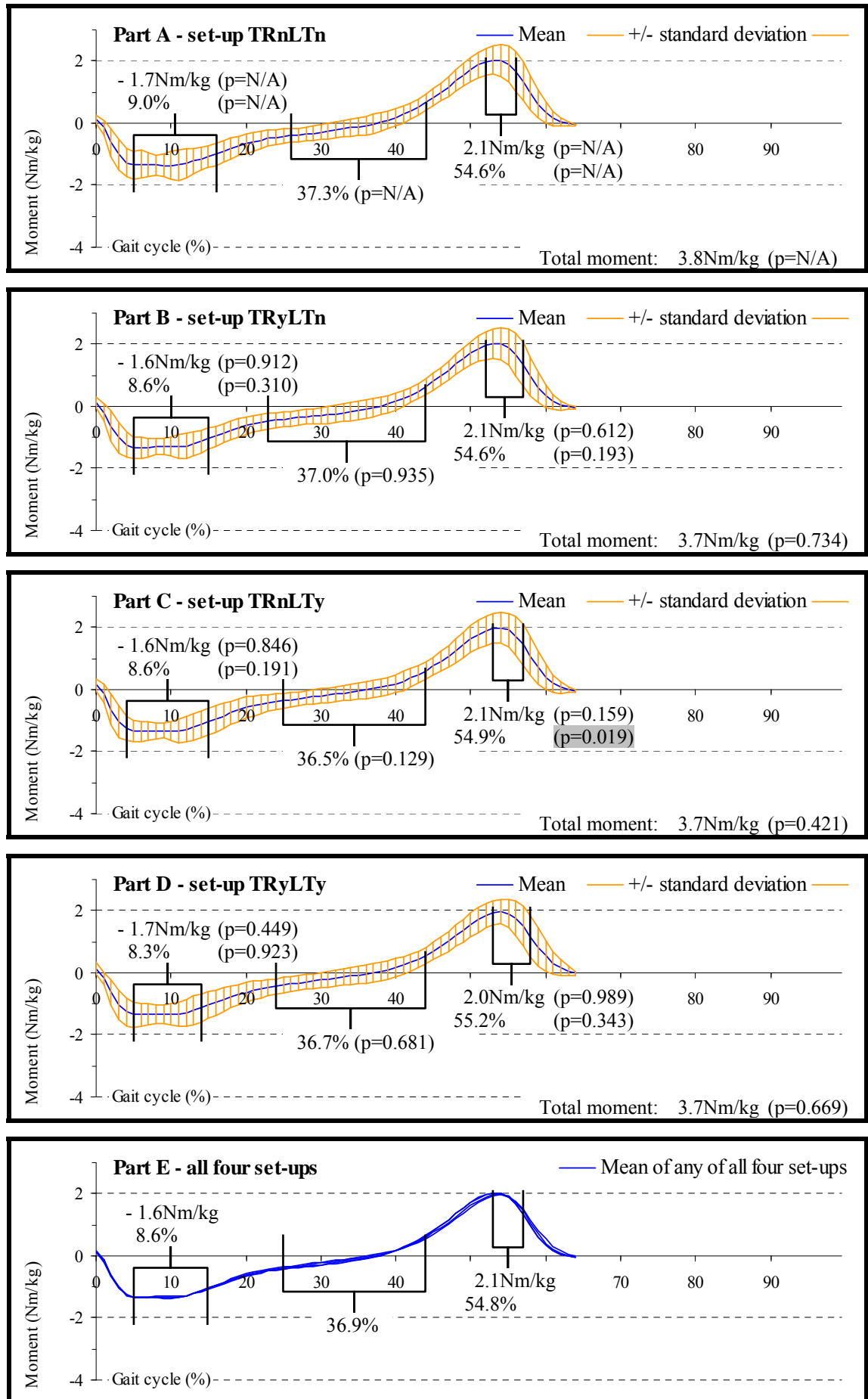
Figure 9.20:   Knee moments on amputated side, extension +ve

Part A - set-up TRnLTn — Mean — +/- standard deviation —

- 2.4Nm/kg (p=N/A)
9.3%   (p=N/A)
28.1% (p=N/A)
1.5Nm/kg (p=N/A)
46.7%   (p=N/A)
Total moment: 4.0Nm/kg (p=N/A)

Part B - set-up TRyLTn — Mean — +/- standard deviation —

- 2.3Nm/kg (p=0.009)
10.1%   (p=0.085)
28.0% (p=0.906)
1.5Nm/kg (p=0.327)
48.0%   (p=0.100)
Total moment: 3.9Nm/kg (p=0.025)

Part C - set-up TRnLTy — Mean — +/- standard deviation —

- 2.2Nm/kg (p=0.015)
11.0%   (p=0.001)
28.0% (p=0.823)
1.5Nm/kg (p=0.544)
47.7%   (p=0.377)
Total moment: 3.8Nm/kg (p=0.010)

Part D - set-up TRyLTy — Mean — +/- standard deviation —

- 2.1Nm/kg (p=0.794)
11.2%   (p=0.111)
28.2% (p=0.541)
1.5Nm/kg (p=0.806)
48.0%   (p=0.338)
Total moment: 3.7Nm/kg (p=0.677)

Part E - all four set-ups —— Mean of any of all four set-ups

- 2.3Nm/kg
10.4%
28.1%
1.5Nm/kg
47.6%

At the instant of heel strike, the posteriorly directed resultant GRF vector passed just anterior to the straight knee, thus momentarily triggering an extension moment. This extension moment was exceedingly brief and lasted only approximately 1% of the gait cycle for both the sound and amputated side. After that, the knee started flexing in order to absorb shock impacts, as previously described in Section 9.1.1.3. This placed the knee anterior to the GRFs, resulting in a flexion moment. Although the magnitude of early stance phase knee flexion was a lot smaller on the amputated side compared to the sound side, the peak of the flexion moment reached just under 144% of the value for the sound side, namely a mean value of approximately 2.3Nm/kg and 1.6Nm/kg, respectively. The reason for such a difference may have been linked to the fact that posteriorly directed GRFs acting on the prosthetic foot were larger, and vertical GRFs smaller, than for the anatomic foot. The combined vector representation therefore acquired a more backward leaning orientation for the amputated side, so that the lever arm, namely the distance between the GRF vector and the knee centre, became larger, thus increasing the flexion moment. This meant that the knee extensors had to work harder than on the sound side to prevent excessive knee flexion.

Following the initial peak flexion moment, the knee started to reduce its flexion angle, while the entire body shifted forward and above the stance limb. During this part of the gait cycle the resultant GRFs reduced, which was previously shown in Section 9.1.2, so that the flexion moment also decreased. As the force plate initiated pushing anteriorly, the upward directed and then forward leaning combined vector representation located itself anterior to the knee, thus triggering an extension moment. The point in time when the moment changed occurred nearly 9% of the gait cycle earlier on the amputated side, namely at a mean timing of approximately 28.2% of the gait cycle compared to approximately 36.7% of the gait cycle for the sound side. This was likely to occur in response to lower levels of amputated side stance phase knee flexion, which consequently shifted the knee centre quicker behind the resultant GRF vector than it did on the sound side. After that, due to continuous forward migration of the body the stance limb fell further behind, therefore increasing the moment, as the lever arm, namely the distance between the knee centre and the anteriorly positioned GRF vector, lengthened.

Towards the end of stance phase, it was time to initiate knee flexion in preparation for swing phase. While the knee and hip flexors were working hard to overcome the

counteracting knee extension moment, the magnitude of this moment was about to reduce, due to the currently reducing GRFs and the shortening lever arm. The incident for the start of such a change occurred slightly later on the sound side and the size of the peak value was larger compared to the amputated side. On the sound side, the peak extension moment reached a mean value of approximately 2.1Nm/kg at approximately 54.8% of the gait cycle, compared to approximately 1.5Nm/kg at approximately 47.6% of the gait cycle for the amputated side. This difference between the two lower limbs may have had something to do with the fact that peak hip extension angles were smaller and occurred slightly earlier on the amputated side in an attempt to bring the thigh forward quickly for triggering drastic knee flexion, as explained in Section 9.1.1.5. While the knee angle increased and hip extension decreased, the knee centre progressively shifted forward and the extension moment gradually reduced until toe off occurred. At this stage, the main extrinsic influences responsible for joint moments disappeared, namely the GRFs.

9.1.4.4.   *Inter-set-up differences in knee moments*

While approaching late stance phase, the incident for reaching the final peak in the sound side knee extension moment was delayed with set-up TRnLTy, which occurred at approximately 54.9% (p=0.019) of the gait cycle compared to approximately 47.7% of the gait cycle when the adapter was fully locked. This difference was significant and likely to be caused by a similar delay in vertical and anterior-posterior GRFs. Despite an even later incident for the peak knee moment with set-up TRyLTy, findings were not significant.

On the amputated side, it was the initial peak in the early stance phase knee flexion moment that was significantly affected. For set-up TRyLTn and TRnLTy, the magnitude of the peak knee flexion moment was significantly smaller, reaching approximately 2.3Nm/kg (p=0.009) and approximately 2.2Nm/kg (p=0.015), respectively, compared to approximately 2.4Nm/kg when the adapter was fully locked. With only transverse rotation being permitted, the reason for a reduced peak knee flexion moment can be attributed to a reduction in peak vertical GRFs during the same period. In turn, while purely longitudinal translation was possible, the factor that lowered the peak knee flexion moment was a reduced peak knee flexion angle, which placed the knee further backward and therefore closer to the resultant GRF vector.

Also significantly affected was the incident of the amputated side peak knee flexion moment with set-up TRnLTy. This was delayed, as it occurred at approximately 11.0% (p=0.001) of the gait cycle compared to approximately 9.3% of the gait cycle when the adapter was fully locked. Such a timing difference was triggered, because the early stance phase peak knee flexion angle also occurred significantly later, as previously reported in Section 9.1.1.4.

The other characteristic with inter-set-up differences was the total moment, which was significantly reduced with set-up TRyLTn and TRnLTy, reaching approximately 3.9Nm/kg (p=0.025) and approximately 3.8Nm/kg (p=0.010), respectively, compared to approximately 4.0Nm/kg when the adapter was fully locked. This was because, despite a similar magnitude for the peak extension moment compared to when the adapter was fully locked, the magnitude of the peak flexion moment, however, was smaller. Although the lowest total moment occurred with set-up TRyLTy, the difference was insignificant.

9.1.4.5. *Inter-limb differences in hip moments*

Hip moments of both the sound and amputated side are illustrated in Figure 9.21 and Figure 9.22, respectively. The standard deviation for the sound side was fairly consistent throughout the gait cycle, except that the band width was narrower during mid-stance phase. Values reached a minimum and maximum of approximately 0.4Nm/kg and 1.1Nm/kg, which is around 5.1% and 14.0% of the 7.9Nm/kg total mean hip moment, respectively. This was slightly lower for the amputated side, in that the standard deviation reached a minimum and maximum of approximately 0.1Nm/kg and 0.9Nm/kg, which is around 1.3% and 12.0% of the 7.5Nm/kg total mean hip moment, respectively. The smallest values for both sides were predominantly found at heel strike and toe off, as the magnitude of GRFs was near zero.

At the instant of heel strike, the backward directed resultant GRF vector passed just anterior to the hip, as the foot and the POA was located ahead of the trunk, thus triggering a hip flexion moment. While GRFs increased, so did the hip flexion moment, until it reached a peak. The incident for this occurred at a mean timing of approximately 10.3% of the gait cycle for the sound side, and only fractionally later for the amputated side at approximately 10.8% of the gait cycle. Also, the magnitude of the peak flexion

Figure 9.21:   Hip moments on sound side, flexion +ve
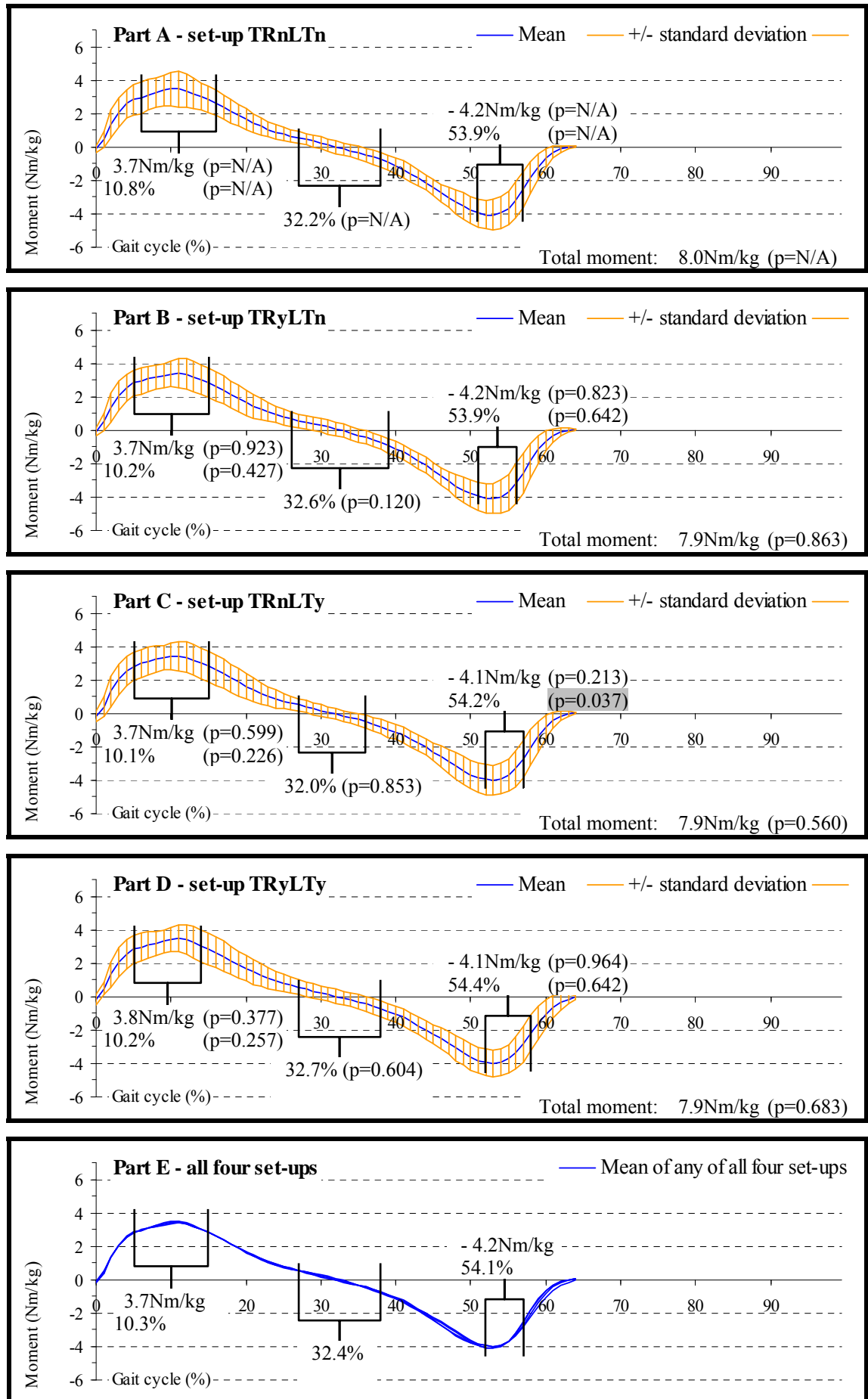
Figure 9.22:   Hip moments on amputated side, flexion +ve
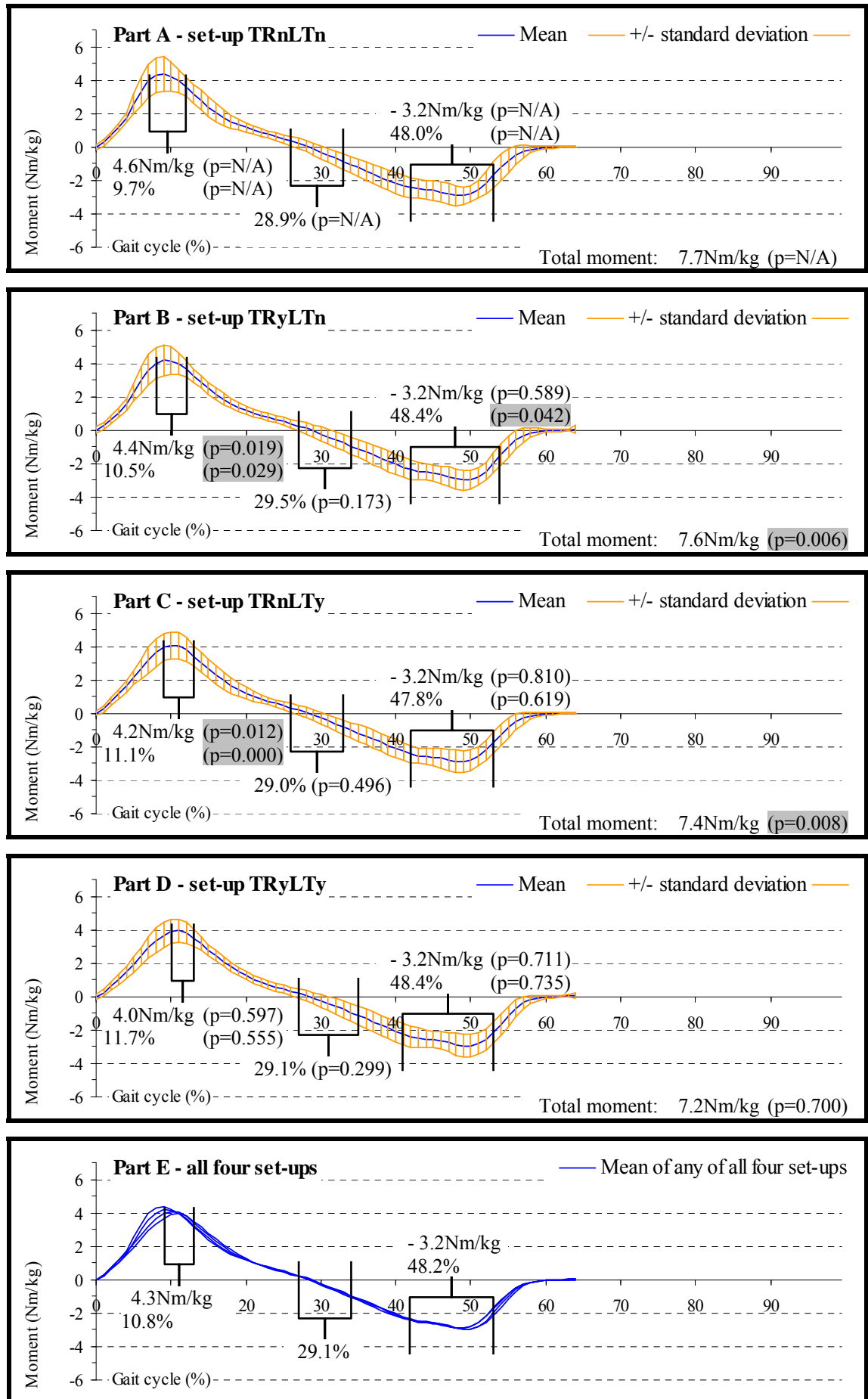
moment was smaller for the sound side, reaching a mean value of approximately 3.7Nm/kg compared to approximately 4.3Nm/kg for the sound side. The reason for such a difference may be linked to the fact that the amputated side hip was more flexed at heel strike than the sound side hip, as previously shown in Figure 9.5 and Figure 9.6. The prosthetic foot must therefore have been further ahead of the trunk than the anatomic foot during its respective weight acceptance period, and this also shifted the POA and GRFs forward. The lever arm, representing the distance between the force vector and hip centre, was consequently longer on the amputated side, thus increasing the moment. This meant that the amputated side hip extensors had to work harder than the sound side hip extensors to prevent excessive hip flexion.

Following the initial peak flexion moment, hip flexion angles started to reduce, while the entire body shifted forward and above the stance limb. It was previously shown in Section 9.1.2 that during this part of the gait cycle the vertical and anterior-posterior GRFs reduced, therefore the flexion moment also reduced. As the force plate started to push anteriorly, the combined resultant vector representation of GRFs acquired an upward direction and was later leaning forward. However, because the foot became now positioned posterior to the trunk, this obviously also affected the position of the POA. The resultant GRFs consequently located themselves posterior to the hip, thus triggering an extension moment. The point in time when the moment changed from flexion to extension was similar for both lower limbs at approximately 32.4% and 29.1% of the gait cycle for the sound and amputated side, respectively. After that, the resultant force vector representation was leaning forward even more, but due to continuous migration of the body, the stance limb fell even further behind, which was the same for the POA. This left the GRFs posterior to the hip and increased the extension moment even further. For the sound side, this was over 130% of the value that the amputated side experienced, namely a mean value of approximately 4.2Nm/kg and 3.2Nm/kg, respectively. Such a difference can be attributed to larger hip extension angles on the sound side, which left the POA further behind compared to the amputated side.

Towards the end of stance phase, it was time to initiate knee and hip flexion in preparation for swing phase. Once the magnitude of GRFs started to decrease in response to the uplifting foot, so did the moment acting on the hip. The incident for this occurred at a mean timing of approximately 54.1% and 48.2% of the gait cycle for the sound and amputated side, respectively. The reason for a timing difference between the

two sides was because the mean sound side peak hip extension angle occurred later than it did on the amputated limb. When toe off finally occurred, the main extrinsic influences responsible for joint moments disappeared, namely the GRFs.

9.1.4.6.   Inter-set-up differences in hip moments

On the sound side, the only significant finding was the incident of the peak hip extension moment around push off time with set-up TRnLTy. This peak extension moment occurred at approximately 54.2% (p=0.037) of the gait cycle compared to 53.9% of the gait cycle when the adapter was fully locked. Such a difference can be attributed to the fact that vertical and anterior-posterior GRFs were also delayed with set-up TRnLTy. A similar scenario happened with set-up TRyLTy, but the difference was insignificant.

On the amputated side, it was the initial peak hip flexion moment during the weight acceptance period that showed differences between set-ups. This peak hip flexion moment turned out to be smaller and delayed with set-up TRyLTn and TRnLTy, as it reached approximately 4.4Nm/kg (p=0.019) and 4.2Nm/kg (p=0.012) at approximately 10.5% (p=0.029) and 11.1% (p=0.000) of the gait cycle, respectively, compared to approximately 4.6Nm/kg and 9.7% of the gait cycle when the adapter was fully locked. Such differences could be explained by analysing the position of the amputated side hip relative to the prosthetic foot. With just transverse rotation being permitted, the socket internally rotated during the weight acceptance period, as will be shown in Section 9.2.1.1. It was therefore likely that the pelvis also internally rotated with respect to the amputated side, so that the hip on that side was displaced slightly more anteriorly. In turn, with just longitudinal translation being permitted, the shortening of the adapter decreased the overall length of the prosthesis. This shifted the hip a little further forward due to the limb's backward leaning orientation. In both cases, with transverse rotation or longitudinal translation being permitted, the distance between the resultant GRF vector and the hip centre was reduced, thus lowering the peak hip flexion moment, but also delaying its incident due to a delay in GRFs. This was a similar scenario with set-up TRyLTy, except that no significant difference was found.

Towards the end of stance phase, the peak amputated side hip extension moment occurred significantly late with set-up TRyLTn at approximately 48.4% (p=0.042) of the gait cycle compared to approximately 48.0% of the gait cycle when the adapter was

fully locked. The reason for such a difference was likely to be linked to a delayed peak in the resultant GRF. Although peak anteriorly directed GRFs were slightly early rather than late with set-up TRyLTn, the timing difference of 0.3% of the gait cycle compared to set-up TRnLTn was smaller than it was for the timing difference regarding the peak vertical GRFs, which was delayed by 0.8% of the gait cycle. Peak vertical GRFs can therefore be considered the main source that delayed the peak resultant GRF and this, in turn delayed the peak hip extension moment. With set-up TRyLTy, the incident of the peak hip extension moment also occurred at 48.0% of the gait cycle, but the difference compared to when the adapter was fully locked was not significant.

Finally, the last aspect that was affected by the permission of adapter mobility was the total hip moment. Although the smallest value could be found amongst data from set-up TRyLTy, significant differences only occurred with set-up TRyLTn and TRnLTy. This was because, despite a similar peak extension moment compared to when the adapter was fully locked, the peak flexion moment was smaller with set-up TRyLTn and TRnLTy, hence the lowering of the total moment to 7.6Nm/kg (p=0.006) and 7.4Nm/kg (p=0.008), respectively, compared to 7.7Nm/kg when the adapter was fully locked.

9.1.5.   Sagittal plane joint powers

9.1.5.1.   *Inter-limb differences in ankle power*

Ankle power of both the sound and amputated side is illustrated in Figure 9.23 and Figure 9.24, respectively. The standard deviation for the sound side was not particularly regular and showed fluctuations in its band width throughout the gait cycle. Values reached a minimum and maximum of approximately 0.1W/kg and 0.3W/kg, which is around 8.3% and 25.0% of the 1.2W/kg total mean ankle power, respectively. This was about the same for the amputated side, in that the standard deviation reached a minimum and maximum of approximately 0.1W/kg and 0.3W/kg. However, the overall ratio was a lot larger and around 16.7% and 50.0% of the 0.6W/kg total mean ankle power, respectively, because this value was so much smaller compared to the sound side. The smallest values for both sides were predominantly found at heel strike and toe off, as the magnitude of GRFs was near zero.

At heel strike, the sound side ankle absorbed power, but fractionally later it started to generate power, as its movement towards plantarflexion opposed the increasing

dorsiflexion moment. Power generation soon reached a peak, and once the increase in plantarflexion slowed down, the magnitude of power generation quickly dropped back down again. At the instant peak plantarflexion decreased, power started to be absorbed, because the ankle experienced an angular displacement in the same direction that GRFs were pushing it towards.

Events on the amputated side were slightly different in that the magnitude of initial power generation was virtually absent. The reason for lower power levels was because the initial ankle moment hardly changed at all and remained around zero. After the initial period during which there was virtually no power at the prosthetic ankle, this was followed by power absorption in response to the increasing dorsiflexion moment and decreasing plantarflexion angles.

With both lower limbs' dorsiflexion angles gradually becoming larger, the rate of increase in the sound side dorsiflexion moment was soon slowing down and for the amputated side it was even decreasing, as previously explained in Section 9.1.4.1. Power absorption therefore reached a peak, as it could not increase any further. This peak in power absorption reached a mean value of approximately 0.5W/kg and 0.4W/kg at approximately 13.5% and 11.3% of the gait cycle for the sound and amputated side, respectively. Despite a lower rate of change in ankle angles on the sound side compared to the amputated side, as illustrated in Figure 9.1 and Figure 9.2, the reason for more power absorption on the sound side was because the dorsiflexion moment was larger than it was for the amputated side, as shown in Section 9.1.4.1. Also, due to a continuously increasing sound side dorsiflexion moment, power at the anatomic ankle was absorbed throughout mid-stance phase. This was different for the amputated side as the moment remained exceedingly low, and so did the level of power at the prosthetic ankle.

Following mid-stance phase, the amount of power absorption started to increase again. This happened because the rate of increase in the dorsiflexion moment went up on both sides. Once the dorsiflexion moment reached a peak at late stance phase, it immediately started to reduce, thus also reducing the resultant peak in power absorption. This peak reached a mean value of approximately 0.5W/kg and 0.3W/kg at approximately 41.9% and 44.6% of the gait cycle for the sound and amputated side, respectively. Despite the

Figure 9.23: Ankle power on sound side, generation +ve

344
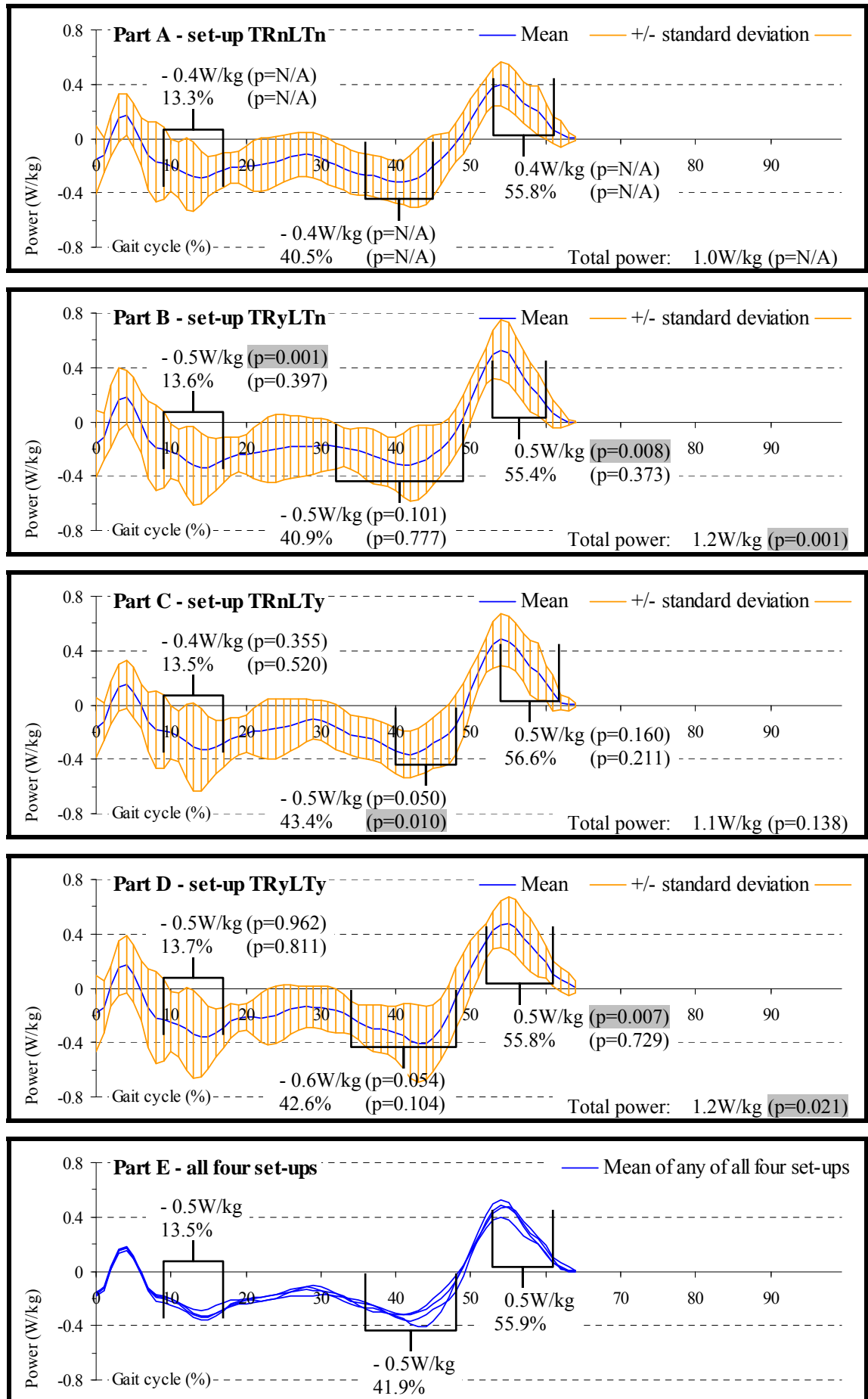
Figure 9.24:   Ankle power on amputated side, generation +ve
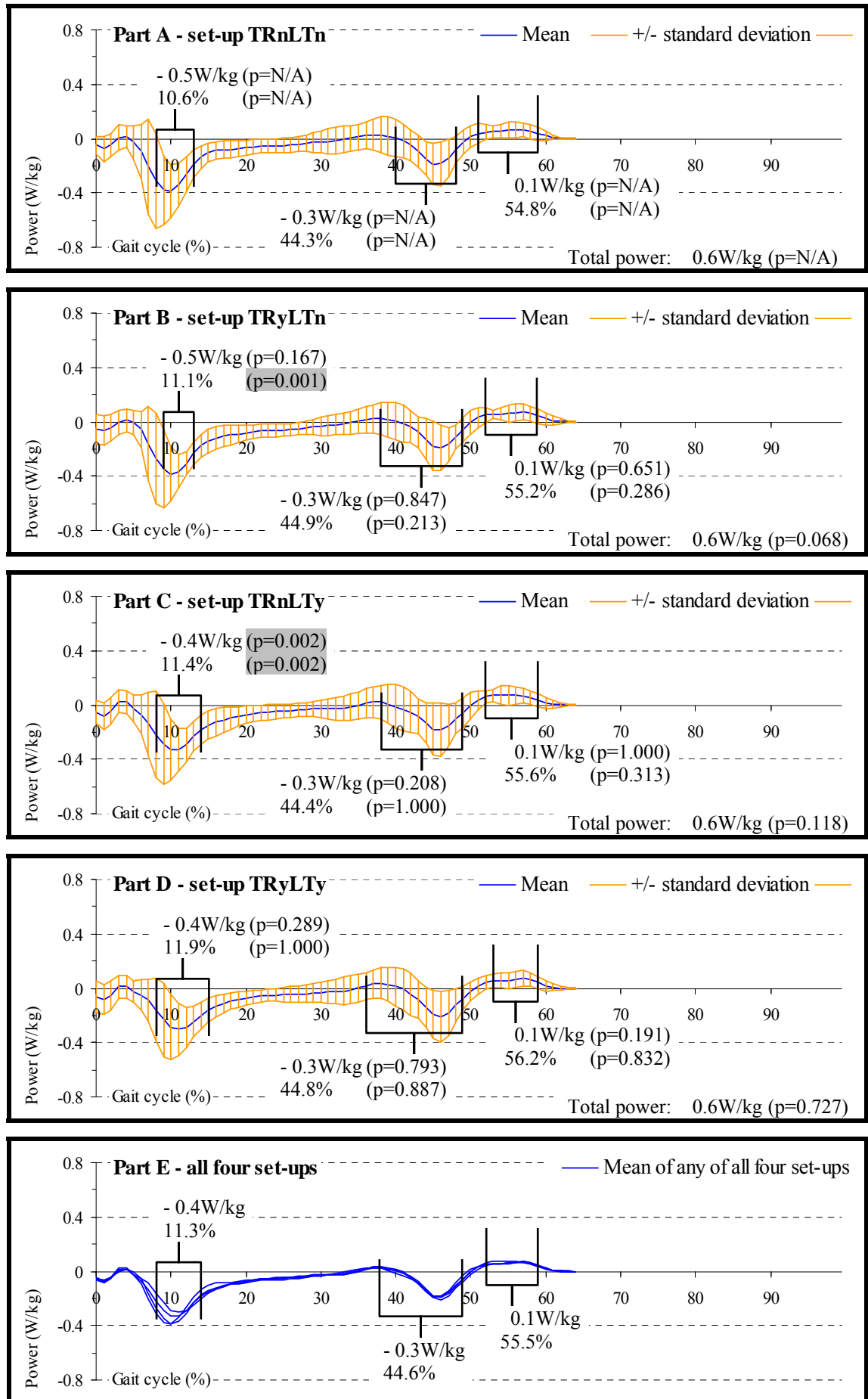
fact that the rate of angle changes for both sides was similar, the peak in power absorption happened to be greater in magnitude for the sound side, because the dorsiflexion moment reached a larger magnitude than it did on the amputated side.

As power absorption reduced, it soon reached zero. After that, power was being generated in response to plantarflexion at the ankle. On the sound side, while the dorsiflexion moment was drastically decreasing and the anatomic ankle rapidly plantarflexed, the magnitude of power generation was large, thus creating strong forward propulsion during the push off phase. In turn, on the amputated side, the prosthetic foot merely returned to a near plantigrade position with respect to the prosthetic shin, due to absent active plantarflexion, as described in Section 9.1.1.1. Small magnitudes of angular displacements over a similar duration as for the sound side ankle therefore meant that the angular velocity of the prosthetic ankle was small. Amputated side power generation was consequently very small, reaching a mean value of approximately 0.1W/kg at approximately 55.5% of the gait cycle. This was only 20% of the mean value reached by the sound side, namely approximately 0.5W/kg at approximately 55.9% of the gait cycle. It was therefore clear that forward propulsion on the amputated side was altogether very inefficient. After that, GRFs faded out, so that power absorption or generation in response to relevant extrinsic influences was no longer required.

9.1.5.2. *Inter-set-up differences in ankle power*

On the sound side, the first significantly affected characteristic was the peak in power absorption with set-up TRyLTn during the weight acceptance period, which reached approximately 0.5W/kg (p=0.001) compared to 0.4W/kg when the adapter was fully locked. The sound side ankle moment around that point in time did not reach a peak, as it continuously increased. It can nevertheless be seen that the value of the ankle moment, at the instant when power absorption reached its peak, was slightly greater with set-up TRyLTn compared to set-up TRnLTn, which directly influenced the extent of power absorption that the ankle experienced. Also, the peak value for power absorption that was reached with set-up TRyLTy was virtually the same as with set-up TRyLTn, but significant findings were absent.

The next characteristic with significant findings was the peak in power absorption towards late stance phase, which occurred at approximately 43.4% (p=0.010) with

set-up TRnLTy compared to approximately 40.5% of the gait cycle when the adapter was fully locked. The reason for such a delay seemed to be linked to the fact that the sound side peak dorsiflexion moment during late stance phase was also delayed.

Another characteristic with significant findings was the peak in power generation on the sound side just before push off, which reached approximately 0.5W/kg (p=0.008) and 0.5W/kg (p=0.007) with set-up TRyLTn and TRyLTy, respectively, compared to approximately 0.4W/kg when the adapter was fully locked. The exact reason that led to such an increase in power generation was difficult to determine. This was because neither the angles nor the moments at the ankle reached a peak, as the angles rapidly changed from peak dorsiflexion to peak plantarflexion and the moments faded out.

The final characteristic with significant findings regarding the sound side was the total power level at the anatomic ankle. Both the peak power absorption and generation were greatest mostly with set-up TRyLTn and TRyLTy. Therefore, the total power in those two cases was also the largest, reaching approximately 1.2W/kg (p=0.001) and 1.2W/kg (p=0.021) with set-up TRyLTn and TRyLTy, respectively. This was statistically different to the value obtained with set-up TRnLTn, namely approximately 1.0W/kg. In conclusion, it can be seen that the activity level of the sound side generally increased when at least partial mobilisation of the adapter was being permitted.

On the amputated side, the results were much less varied, which can be attributed to the fact that the prosthetic ankle could only be moved passively. The one characteristic with significantly different results compared to when the adapter was locked was the peak in early stance phase power absorption. With set-up TRnLTy, this peak was smaller than with set-up TRnLTn, reaching approximately 0.4W/kg (p=0.002) and 0.5W/kg, respectively. Also, with set-up TRyLTn and TRnLTy, the same peak in power absorption occurred at approximately 11.1% (p=0.001) and 11.4% (p=0.002) of the gait cycle, respectively, which was highly significant compared to approximately 10.6% of the gait cycle with set-up TRnLTn. The change in both the magnitude and the incident of early stance phase power absorption can be directly attributed to the fact that the scenario concerning the magnitude and timing of the initial peak dorsiflexion moment was similar for set-up TRyLTn and TRnLTy, which was also significantly different to set-up TRnLTn, as previously reported in Section 9.1.4.2.

9.1.5.3.   Inter-limb differences in knee power

Knee power of both the sound and amputated side are illustrated in Figure 9.25 and Figure 9.26, respectively. The standard deviation for the sound side was not particularly consistent in that its band width during mid-stance phase was very narrow, but broader at either end of this period. Values reached a minimum and maximum of approximately 0.1W/kg and 2.0W/kg, which is around 1.5% and 29.4% of the 6.8W/kg total mean knee power, respectively. This was slightly lower for the amputated side, in that the standard deviation reached a minimum and maximum of approximately 0.1W/kg and 1.0W/kg, which is around 2.3% and 23.3% of the 4.3W/kg total mean knee power, respectively. The smallest values for both sides were predominantly found at heel strike and toe off, as the magnitude of GRFs was near zero.

At the instant of heel strike, a very brief presence of power generation could be detected due to a momentarily encountered knee extension moment, while the knee was simultaneously flexing very slightly. After that, during the weight acceptance period, the knee immediately started to absorb power, as its flexion angle and flexion moment increased, as described in Section 9.1.1.3 and Section 9.1.4.3. Around the point in time, during each side's respective gait cycle, when the moment reached a peak, power absorption also came to a peak. The incident of this peak reached a mean value of approximately 2.9W/kg and 2.2W/kg at a mean timing of approximately 8.0% and 9.5% of the gait cycle for the sound and amputated side, respectively.

The fact that peak power absorption on the sound side was larger than on the amputated side seemed unusual, due to a smaller sound side knee flexion moment compared to the amputated side. The reason for that can be explained as follows. Although early stance phase peak flexion angles were reached around the same time for both knees, the magnitude of the displacement was greater for the sound side, so that the angular velocity must also have been greater compared to the amputated side. From this it becomes clear that the net shock impacts must therefore have been greater on the amputated side due to a smaller peak in power absorption, so that the resultant loads had to be transferred elsewhere.

Following the peak in power absorption, its magnitude immediately decreased, as the knee flexion moment also decreased and changes in angular displacements became

Figure 9.25:   Knee power on sound side, generation +ve

Part A - set-up TRnLTn   Mean   +/- standard deviation

- 3.0W/kg (p=N/A)
7.8%   (p=N/A)

3.8W/kg (p=N/A)
56.2%   (p=N/A)

Power (W/kg)
Gait cycle (%)
Total power: 6.8W/kg (p=N/A)

Part B - set-up TRyLTn   Mean   +/- standard deviation

- 2.9W/kg (p=0.566)
8.1%   (p=0.434)

3.7W/kg (p=0.915)
56.4%   (p=0.299)

Power (W/kg)
Gait cycle (%)
Total power: 6.6W/kg (p=0.695)

Part C - set-up TRnLTy   Mean   +/- standard deviation

- 2.8W/kg (p=0.795)
8.1%   (p=0.343)

3.8W/kg (p=0.237)
56.9%   (p=0.009)

Power (W/kg)
Gait cycle (%)
Total power: 6.7W/kg (p=0.586)

Part D - set-up TRyLTy   Mean   +/- standard deviation

- 3.0W/kg (p=0.185)
8.1%   (p=0.193)

3.9W/kg (p=0.618)
57.2%   (p=0.678)

Power (W/kg)
Gait cycle (%)
Total power: 6.9W/kg (p=0.313)

Part E - all four set-ups   Mean of any of all four set-ups

- 2.9W/kg
8.0%

3.8W/kg
56.7%

Power (W/kg)
Gait cycle (%)

349

Figure 9.26: Knee power on amputated side, generation +ve
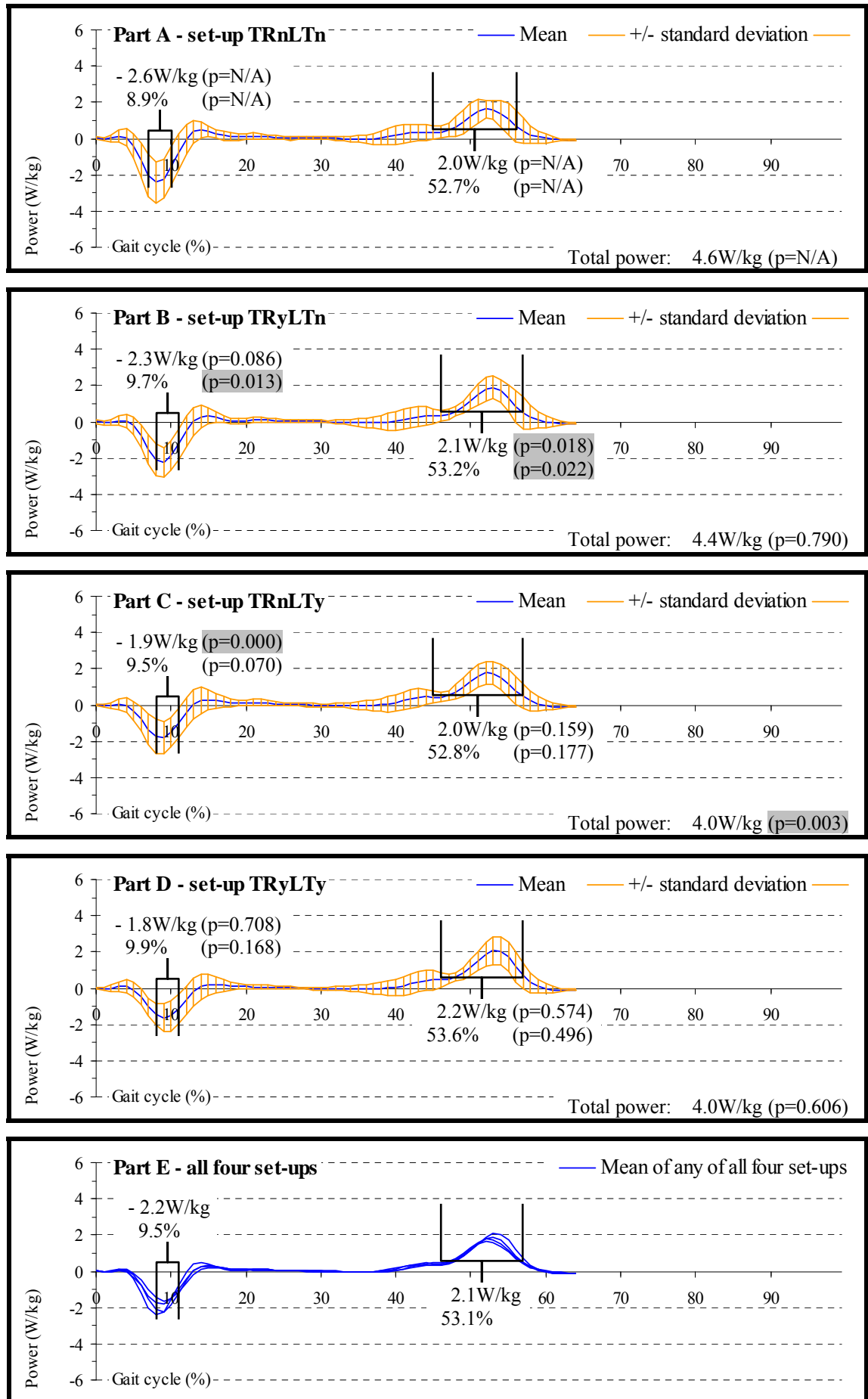
slower, hence a reduction in angular velocity. Once the knee reached peak stance phase flexion, it slowly started to extend again. This movement opposed the still present knee flexion moment, so that power was no longer absorbed, but was generated instead. However, because of minimal angular velocity due to a low rate for achieving a straight knee, the level of power generation was minute for both limbs, particularly as the already reduced knee flexion moment continued to decrease.

During the period when the moment changed from flexion to extension, the level of power at both the sound and amputated side knee was nearly zero, because the moment was also nearly zero and the knee angle approached full extension, so that the angular velocity was therefore virtually zero, too. In turn, while the extension moment started to increase, the knee started flexing again in preparation for swing phase. This response required power generation, because the angular displacement the knee experienced occurred in the opposite direction to where GRFs were attempting to push it.

At the time push off stage was reached, the moment at the knee started to reduce again, and so did the generation of power. The resultant peak in power generation reached a mean value of approximately 3.8W/kg and 2.1W/kg at a mean timing of approximately 56.7% and 53.1% of the gait cycle for the sound and amputated side, respectively. The fact that sound side peak power generation was greater and occurred slightly later compared to the amputated side could be directly related to the peak knee extension moment. This moment was characterised by a similar relationship concerning the magnitude and timing, so that the levels of power with regard to each lower limb were affected accordingly. Around toe off, the knee moment finally reduced down to zero, as GRFs faded out, so that the absorption or generation of power in response to relevant extrinsic influences was no longer required.

9.1.5.4. *Inter-set-up differences in knee power*

The only sound side characteristic amongst knee power data that was affected by adapter mobility was the incident of late stance phase peak power generation. With set-up TRnLTy, this peak was reached at approximately 56.9% (p=0.009) of the gait cycle compared to approximately 56.2% of the gait cycle when the adapter was fully locked. Such a delay was highly significant, which can be attributed to the fact that the peak knee extension moment around that time also occurred significantly later, as previously reported on in Section 9.1.4.4. Despite an even longer delay with set-up

TRyLTy, no significant differences were found compared to when the adapter was fully locked.

On the amputated side, the first characteristic with significant differences was the peak in power absorption at the knee during the weight acceptance period. With set-up TRyLTn, this peak was reached at approximately 9.7% (p=0.013) of the gait cycle compared to approximately 8.9% of the gait cycle when the adapter was fully locked. The reason for such a delay was likely to be triggered by a similar delay in reaching the peak flexion moment with set-up TRyLTn. Also, with set-up TRnLTy, it was the magnitude of the peak in power absorption that was affected, which reached approximately 1.9W/kg (p=0.000) compared to approximately 2.6W/kg when the adapter was fully locked. Such a finding was highly significant, and the reason for this can be attributed to a significantly smaller peak knee flexion moment, as previously described in Section 9.1.4.4. In turn, the magnitude and timing of the peak in power absorption at the knee was also smaller and delayed with set-up TRyLTy, but no significant differences could be found compared to set-up TRnLTn.

The other characteristic with significant findings was the peak in the amputated side knee power generation around push off time. With set-up TRyLTn this peak reached approximately 2.1W/kg (p=0.018) at approximately 53.2% (p=0.022) of the gait cycle compared to approximately 2.0W/kg at approximately 52.7% of the gait cycle when the adapter was fully locked. Considering purely the magnitude of this peak in knee power generation, because the peak knee extension moment was virtually identical compared to when the adapter was fully locked, the reason for more power absorption must be linked with the angular velocity at the knee. When calculating the difference between the peak extension and flexion angle before and after push off, it can be seen that this was larger when transverse rotation was being permitted, and the change occurred over a shorter period of time compared to when the adapter was fully locked. It can consequently be assumed that the angular velocity was greater with set-up TRyLTn compared to set-up TRnLTn, and hence the greater magnitude in peak power generation. With regard to the timing of this peak, its later incident seemed to be directly linked to the delay in the late stance phase peak knee extension moment. In turn, no significant difference was found with set-up TRyLTy compared to set-up TRnLTn, despite an even greater power generation and a longer delay than with set-up TRyLTn.

The final characteristic with significant findings was the level of total power that was reached at the knee on the amputated side. The lowest total power output occurred with set-up TRnLTy and TRyLTy, which was due to very low levels of the initial power absorption during the weight acceptance period. However, a significant difference could only be found with set-up TRnLTy, in that the total power reached approximately 4.0W/kg (p=0.003) compared to approximately 4.6W/kg when the adapter was fully locked. In conclusion, it can be seen that the activity level of the amputated side generally decreased the more mobile the adapter became.

9.1.5.5.   *Inter-limb differences in hip power*

Hip power of both the sound and amputated side are illustrated in Figure 9.27 and Figure 9.28, respectively. The standard deviation for the sound side was fairly consistent throughout the gait cycle, except that the band width was narrower during mid-stance phase. Values reached a minimum and maximum of approximately 0.3W/kg and 1.4W/kg, which is around 6.4% and 29.8% of the 4.7W/kg total mean hip power, respectively. This was slightly lower for the amputated side, in that the standard deviation reached a minimum and maximum of approximately 0.1W/kg and 1.2W/kg, which is around 2.3% and 27.9% of the 4.3W/kg total mean hip power, respectively. The smallest values for both sides were predominantly found at heel strike and toe off, as the magnitude of GRFs was near zero.

At the instant of sound side heel strike, the hip immediately started to generate power due to a decrease in hip flexion angles, which opposed the currently increasing flexion moment. Shortly after that, the sound side hip experienced some angular fluctuations, while the anatomic foot established full contact with the ground during the weight acceptance period, as previously explained in Section 9.1.1.5. These fluctuations were reflected by a rapid change in power levels that led to a very brief period of power absorption at the hip. Once the initial shock impacts were absorbed and the angular fluctuations had virtually ceased, the hip continued decreasing its flexion angles, which reversed the power levels as further power generation was required to counteract the still present flexion moment, previously described in Section 9.1.4.5.

The behaviour on the amputated side was similar, except that the first change in power levels was far less drastic. As on the sound side, increases in initial amputated side power generation also slowed down while the prosthetic foot established full contact

with the ground during the weight acceptance period. The magnitude of power generation even decreased again, but the drop was not low enough for power to be absorbed. The reason for that was, because after the reduction in hip flexion angles commenced, the continuation of this process was fairly steady, showing only minor fluctuations, and hence the less radical drop in amputated side power generation, unlike the power levels on the sound side.

Following the weight acceptance period, the hip was gradually decreasing its flexion angle in order to eventually acquire an extended position. While the hip flexion moment continued to increase, so did the power generation until the flexion moment reached a peak, which also triggered a peak in power generation. For the sound and amputated side, this peak in power generation reached a mean value of approximately 2.5W/kg and 2.4W/kg at a mean timing of approximately 15.1% and 14.1% of the gait cycle, respectively. The reason for a slightly larger magnitude in peak power generation on the sound side may be explained as follows.

As the period for changing the sound side hip angles from peak flexion during the weight acceptance period to peak extension during late stance phase was relatively short due to initial fluctuations in sound side hip angles rather than a continuous angular change, the angular velocity therefore needed to be relatively large. In turn, for the amputated side, this change showed only minor fluctuations and was consequently fairly continuous, thus prolonging the period between peak flexion and extension. This required a smaller angular velocity to achieve a change in hip angles of similar magnitude as for the sound side. A larger angular velocity at the sound side hip therefore resulted in a larger peak power generation despite a smaller peak hip flexion moment compared to the amputated side.

During the majority of mid-stance phase, the angular velocity of both the sound and amputated side hip remained fairly constant due to a gradual movement towards full extension, while the hip moment also steadily changed from flexion to extension. In response to both these parameters' relatively even changes, the power levels followed on in a similar fashion. Power generation therefore continuously decreased until it reached zero, after which power absorption increased, whereby the rate of change was similar to the scenario prior to crossing the x-axis. The reason for a change in power

Figure 9.27:   Hip power on sound side, generation +ve
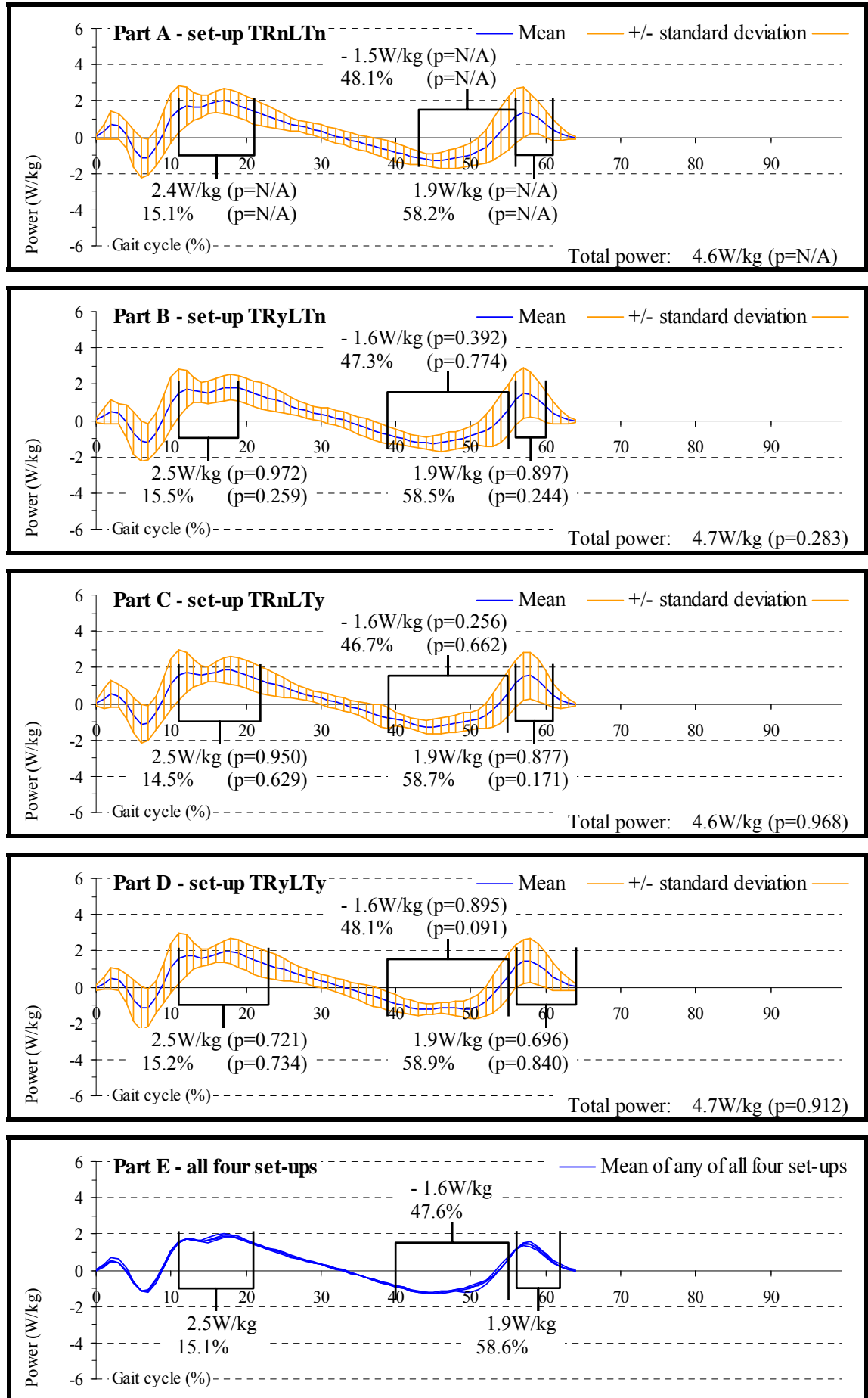
Figure 9.28: Hip power on amputated side, generation +ve
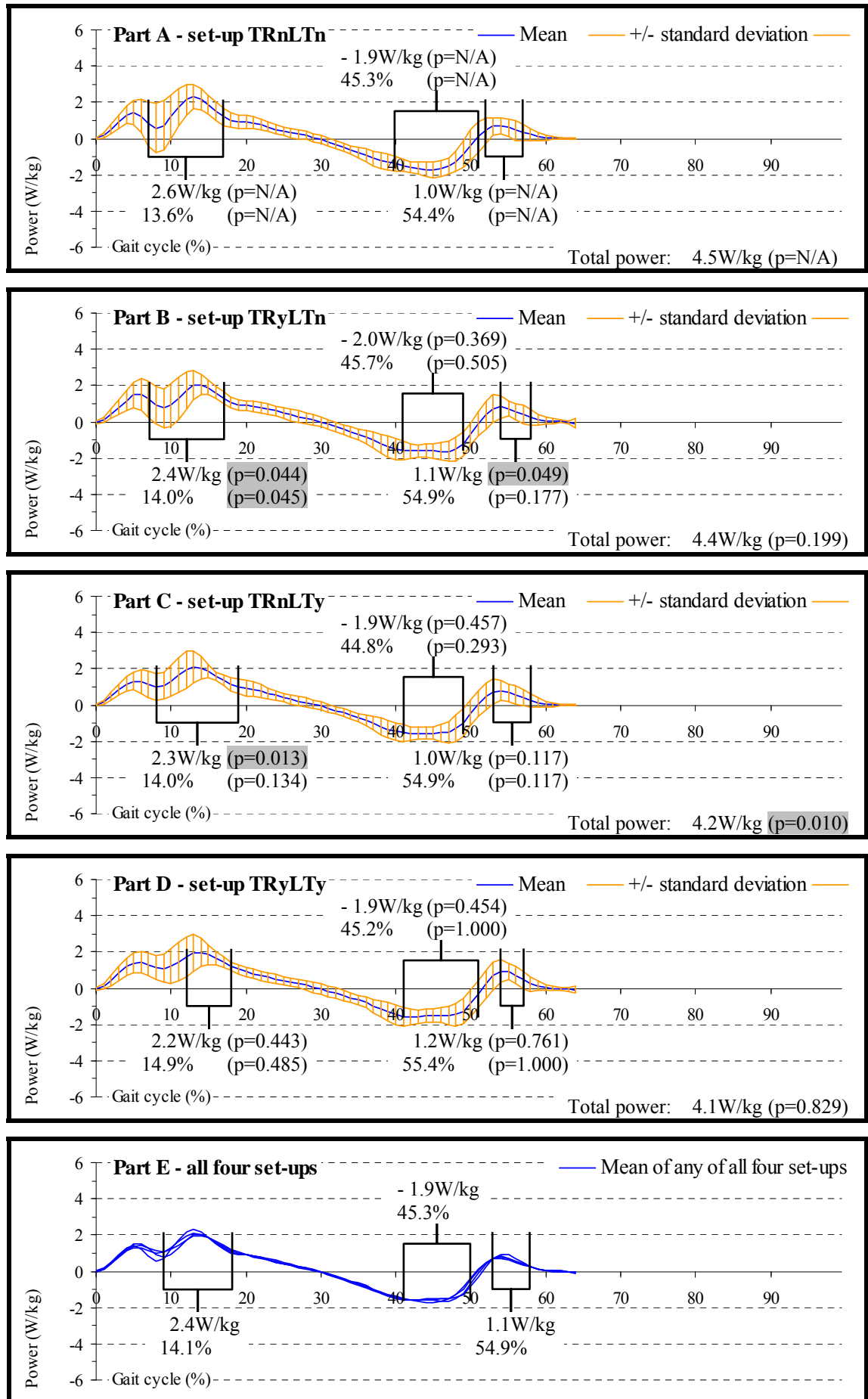
levels was because the hip passed its neutral position. It was therefore no longer decreasing its flexion moment and thereby still resisting a decrease in hip flexion, but instead the extension moment increased, which helped the simultaneously increasing hip extension angles.

With the thigh approaching its most backward orientated position during the gait cycle, motion at the hip started to slow down. This also slowed down the increase in power absorption until a peak was reached with a mean value of approximately 1.6W/kg and 1.9W/kg at a mean timing of approximately 47.6% and 45.3% of the gait cycle for the sound and amputated side, respectively. The reason why the peak in late stance phase power absorption was smaller on the sound side compared to the amputated side can be explained by analysing the displacement at the hip during this part of the gait cycle. The increase in hip extension just before reaching the peak extension angle appeared to be slowing down much earlier on the sound side compared to the amputated side, so that the angular velocity was smaller on the sound side around the time that power absorption reached a peak. A smaller angular velocity at the sound side hip therefore resulted in a smaller peak in power absorption compared to the amputated side.

While the increase in hip extension continued slowing down, power absorption started to decrease until it reached zero at the time peak hip extension was attained. After that, the thigh immediately started moving forward again due to the initiation of hip flexion. The resultant response was that small amounts of power were being generated, because the currently decreasing extension moment was still present and therefore opposing hip flexion. As the extension moment continued reducing, power generation soon reached a peak with a mean value of approximately 1.9W/kg and 1.1W/kg at a mean timing of approximately 58.6% and 54.9% of the gait cycle for the sound and amputated side, respectively. The reason why the magnitude in peak power generation reached nearly twice the size for the sound side was likely due to a larger peak extension moment during late stance phase compared to the amputated side. This extension moment therefore had to reduce more on the sound side, so that its magnitude was still larger than on the amputated side around the time when the peak in power generation was reached just before toe off. Once the hip moment was zero, absorption or generation of power in response to relevant extrinsic influences was no longer required.

9.1.5.6.   Inter-set-up differences in hip power

On the sound side, the effect of different set-ups on the hip power levels was minimal. None of the extracted characteristics were significantly different for the three set-ups compared to when the adapter was at least partially mobile.

On the amputated side, the first characteristic with significant findings was the initial peak in hip power generation during the weight acceptance period. With set-up TRyLTn and TRnLTy, the magnitude of this peak reached approximately 2.4W/kg (p=0.044) and 2.3W/kg (p=0.013) compared to approximately 2.6W/kg when the adapter was fully locked. Also significantly affected was the timing of this peak, which occurred at approximately 14.0% (p=0.045) of the gait cycle with set-TRyLTn compared to 13.6% of the gait cycle with set-up TRnLTn. Both the magnitude and the timing of peak power generation can be directly attributed to the fact that the scenario concerning the magnitude and timing of the initial peak hip flexion moment was very similar for those two set-ups and also significantly affected, as previously reported in Section 9.1.4.6.

The other characteristic with significant findings was the final peak in amputated side power generation at the hip towards the end of stance phase, reaching approximately 1.1W/kg (p=0.049) with set-up TRyLTn compared to approximately 1.0W/kg when the adapter was fully mobile. The exact reason that led to such an increase in power generation was difficult to determine. This was because neither the angles nor the moments at the hip reached a peak, as the angles rapidly changed from peak hip extension to peak flexion and the moments faded out.

The final characteristic with significant findings was the level of total power that was reached at the hip on the amputated side. The lowest total power output occurred with set-up TRnLTy and TRyLTy, which was due to very low levels of power generation during the weight acceptance period. However, a significant difference could only be found with set-up TRnLTy, reaching approximately 4.2W/kg (p=0.010) compared to approximately 4.5W/kg when the adapter was fully locked. In conclusion, it can be seen that the activity level of the amputated side generally decreased the more mobile the adapter became.

9.1.6. <u>Temporal and spatial parameters</u>

Table 9.1 contains the chosen data regarding temporal, spatial and combined temporal-spatial parameters. Those data are listed separately for both the sound and amputated side.

Table 9.1: Temporal and spatial gait parameters

Side	Set-up	Mean of **step time** divided by **contra lateral stride time**	Mean of **double support time** divided by **contra lateral stride time**	Mean of **step length** divided by **contra lateral stride length**	Mean of **walking velocity** (m/s)
Sound side	**TRnLTn**	0.49 (p=N/A)	0.12 (p=N/A)	0.54 (p=N/A)	1.20 (p=N/A)
	TRyLTn	0.49 (p=0.576)	0.12 (p=0.496)	0.53 (p=0.912)	1.23 (p=0.239)
	TRnLTy	0.49 (p=0.343)	0.12 (p=0.154)	0.53 (p=0.872)	1.22 (p=0.300)
	TRyLTy	0.49 (p=0.096)	0.12 (p=0.758)	0.54 (p=0.541)	1.23 (p=0.165)
	Mean	0.49	0.12	0.54	1.22
Amputated side	**TRnLTn**	0.49 (p=N/A)	0.11 (p=N/A)	0.46 (p=N/A)	1.22 (p=N/A)
	TRyLTn	0.50 (p=0.811)	0.11 (p=0.147)	0.46 (p=1.000)	1.24 (p=0.216)
	TRnLTy	0.49 (p=0.279)	0.11 (p=0.244)	0.46 (p=0.591)	1.24 (p=0.369)
	TRyLTy	0.49 (p=0.811)	0.11 (p=0.758)	0.46 (p=0.591)	1.24 (p=0.266)
	Mean	0.49	0.11	0.46	1.24

9.1.6.1. Inter-limb differences in temporal parameters

A stride is, as defined in Table 8.6, an interval that commences at heel strike on one side and terminates at the instant of the subsequent heel strike on the same side, whereby a step only covers the duration between heel strike on one side and the subsequent heel strike on the other side. This means that a stride is composed of two steps, or more precisely one step from each limb, so that the average stride time should be the same for the two sides (Sutherland et al 1994).

The mean ratio between the step times and respective contra lateral stride times turned out to be approximately 0.49 for both the sound and amputated side, which proved that

this parameter was quite evenly distributed between the two sides. One aspect that was unusual, however, was that the two step times added up to 0.98 and not to 1.00. Such an outcome may be explained in two ways. Firstly, despite fairly accurate results for calculating the incidents of the second heel strikes that are listed in Table 8.5, this calculation was, after all, based on an estimation technique. Therefore, resultant small errors in determining stride times, for which the incidents of the second heel strike were required, could have lead to discrepancies between the results for the step times of the two limbs. Secondly, the number of recordings that were taken for each of the ten subjects was relatively large, namely forty, or ten during each of the four set-ups. However, in terms of statistical power, a greater number of samples would obviously have been more advantageous for calculating step times that add up to 1.00 with an exactly equally shared distribution between the sound and amputated side.

Table 9.2:   The timing of temporal gait parameters
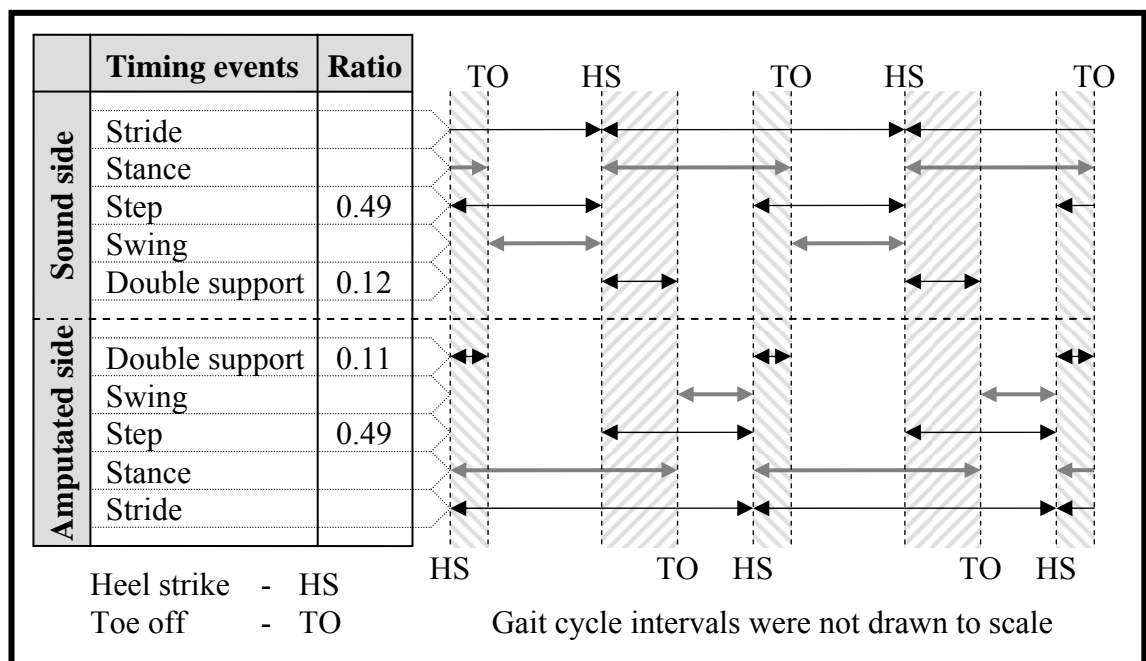
The results concerning the periods of double support times were also quite evenly distributed and in agreement with those reported by Sutherland et al 1994. Double support times reached a mean ratio with respect to the contra lateral stride times of approximately 0.12 and 0.11 for the sound and amputated side, respectively. On the one hand, a resultant difference of 0.01 could have simply developed due to previously described errors in calculating the incident of the second heel strike. On the other hand, if such a difference reflected the true variation between the durations of the two lower limbs' double support periods, then the duration of stance and swing phase would also

have been affected. Table 9.2 illustrates the timing of gait cycle events under certain circumstances, in that step times were the same and double support times different for the two sides. This illustration quite clearly demonstrates that stance times shorten and swing times lengthen for the sound side in response to longer double support times than during the amputated side gait cycle.

9.1.6.2.   *Inter-set-up differences in temporal parameters*

None of the four set-ups regarding different adapter configurations triggered any statistically significant differences in temporal parameters. This was because inter-set-up variations amongst the obtained values were virtually absent for both the sound and amputated side.

9.1.6.3.   *Inter-limb differences in spatial parameters*

The only spatial parameter included in the current Section was the step length. For the sound side, the ratio between step length and the contra lateral stride length was approximately 0.54. In turn, for the amputated side the same ratio reached only approximately 0.46.

This difference could have occurred in response to the differences in hip angles between the sound and amputated side, as previously described in Section 9.1.1.5. The magnitude of both sides' total hip angle was virtually the same for the two sides. However, following peak hip flexion just after mid-swing phase, the amputated side started to slightly move its thigh backward again in order to straighten the knee. In turn, the sound side did the opposite, in that a similar backward movement of the thigh was immediately followed by a further increase in hip flexion angles due to an additional forward movement of the thigh in response to the deceleration of the sound side shin section. This additional forward movement of the thigh therefore increased the distance between the location of the point of contact that was about to be made and the previous one at the end of the last stance phase, thus resulting in a longer step length for the sound side compared to the amputated side.

9.1.6.4.   *Inter-set-up differences in spatial parameters*

None of the four set-ups regarding different adapter configurations triggered any statistically significant differences in spatial parameters. This was because inter-set-up

variations amongst the obtained values were virtually absent for both the sound and amputated side.

9.1.6.5.   *Inter-limb differences in combined parameters*

The only combined temporal-spatial parameter included in the current Section was the mean walking velocity. Its value was very similar for both sides and only fractionally smaller during the sound side gait. The actual calculations of walking velocities were based on the ratio between each limb's stride lengths and stride times. Knowing that both of these parameters should theoretically be the same for the two sides, it seemed odd that this did not turn out to be the case. The reason for this could have been linked to the possibility of minor inherent errors for correctly calculating stride times, as previously described in Section 9.1.6.1, particularly because differences in velocities between the two sides were only very small.

In order to maximise the subjects' performance during the gait laboratory tests, they were asked to walk at a self-selected, comfortable speed, as explained in Section 7.2.4. The results Vitali et al 1986 reported revealed that the mean walking velocity during the gait of healthy adults is around 1.1m/s, as previously described in Section 2.2.4. Taking into consideration the slightly larger average value of approximately 1.23m/s from the subjects' recorded gait data, this demonstrated that their performances compared well to those by people without amputation. The reason as to why gait with a prosthesis was fractionally faster may have had something to do with the fact that the overall walking distance along the path inside the gait laboratory was very short. The subjects were therefore less likely to tire in response to an increased pace. If they would have had to walk over longer distances, then their mean velocity may have been lower than that achieved by non-amputees.

9.1.6.6.   *Inter-set-up differences in combined parameters*

None of the four set-ups regarding different adapter configurations triggered any statistically significant differences in combined temporal-spatial parameters. This was because inter-set-up variations amongst the obtained values were virtually absent for both the sound and amputated side.

9.2.   Kinematics between socket and prosthetic foot

Data from the two displacement transducers were purely recorded on the prosthesis and not on the anatomic shin. The current Section is therefore only applicable to the amputated side.

Transverse rotation was being permitted during only two of the four set-ups and this was the same for longitudinal translation, as explained in Section 8.4.23, which meant that during the other two remaining set-ups, each motion was therefore restricted. In theory, this should have kept the two respective displacement transducers' outputs constant, while the motion they were supposed to capture was being restricted. However, as explained in Section 6.2.1, the radio telemetry transmitter for capturing analogue signals was prone to small amounts of cross-talk between channels. Even when a specific adapter motion was locked, the channel that the corresponding displacement transducer was plugged into still produced varying output signals due to readings from the force sensors. Also, little play at the TT Pylon added further to fluctuations in those output signals, because these fluctuations triggered minor plunger movements at the displacement transducers.

As it was known that such outputs were just noise and not of relevance concerning gait analysis, the transducers' data were therefore zeroed for the two set-ups when a particular type of adapter motion was not being permitted, as the transducer outputs should have been zero if cross-talk and adapter play did not exist. It was therefore not surprising that during the other two set-ups when some adapter motion did take place, all the extracted characteristics amongst displacement transducer data were highly significant. This was due to much greater values regarding a particular type of adapter motion compared to when the adapter was fully locked and the transducer output was consequently zero.

9.2.1.   Transverse rotation at the motion adapter

9.2.1.1.   General descriptions of transverse rotations

Transverse plane angular displacements between the socket and the prosthetic foot are illustrated in Figure 9.29. This only includes the two set-ups when transverse rotation at the adapter was being permitted, namely set-up TRyLTn and TRyLTy.

At heel strike, the socket very briefly maintained its neutral position. This was then immediately followed by internal rotation of the socket. While progressing forward, the magnitude of internal rotation increased further until just before approximately 20% of the gait cycle was reached when internal rotation came to a peak. After that, the angular displacement changed direction due to a decrease in internal socket rotation. At approximately 30-35% of the gait cycle, the socket returned back to its neutral position. From this point in time onwards, external rotation angles started to increase until just before approximately 55% of the gait cycle was reached when external rotation came to a peak. While initiating the push off period, the socket reduced its externally rotated position as GRFs were fading out, and so was the moment that stopped the prosthetic foot from rotating together with the socket. Once the toes terminated contact with the floor, the socket regained virtually the same position again as the distal parts of its prosthesis.

Figure 9.29:   TT Pylon motion, internal rotation of socket +ve
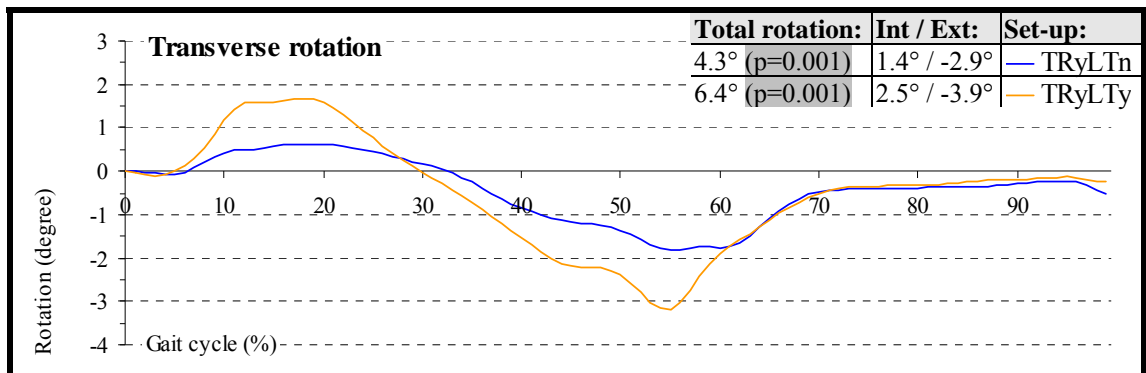
The reason that the socket did not fully return back to zero could have had something to do with the fact that the diameter of the torsion rod was reduced to make it easier for transverse rotation to occur, as described in Section 4.1.5.4. Therefore, due to inherent friction between the TT Pylon housing and its shin tube, the anti-rotational counterforce from the torsion rod might not have been sufficient, particularly when the angular displacement was small, as the moment from the torsion rod became smaller when twisted only slightly.

While the socket rotated one way, the internal resistance from the TT Pylon was attempting to pull the foot into the same direction. However, its friction with the floor prevented this from happening, which meant that the tendency for displacing the force plate must have triggered a GRM in the opposite direction to that in which the socket

was rotating. When comparing the results with regard to transverse rotation at the adapter to those previously explained in Section 9.1.3.3, it can be seen that the theory concerning GRMs was indeed correct. Nevertheless, taking into consideration that transverse plane socket rotations were predominantly triggered by rotations from the pelvis and lower limb segments, those changes in angular orientations were only one aspect responsible for the resultant GRMs. Additional aspects that influenced those moments, were already discussed in Section 9.1.3.3, namely anterior-posterior and medial-lateral GRFs, as well as the location of the COP.

The pattern of transverse rotations that the subjects experienced during the current investigation was very similar to the pattern reported by Levens et al 1948, which was previously illustrated in Figure 3.1. Because these authors predominantly recruited non-amputees, transverse rotations were not only detected during stance phase, but during swing phase also. Peak external rotation of the anatomic shin was reached at the beginning of swing phase and not around late stance phase as during the current investigation. After swing phase commenced, the anatomic shin was actively rotated back to a neutral position by the muscles while it swung forward. This was not possible on the amputated side during amputee gait, as the prosthesis could only be moved passively. Once GRFs were absent, the motion adapter quickly snapped back into a neutral position. However, due to the inertia of the prosthesis, this process was not quite instant. Instead, it took approximately 5% of the gait cycle, as becomes clear when comparing the data regarding transverse rotation with those regarding the last reading from vertical GRFs previously displayed in Figure 9.8.

Although the information published by Levens et al 1948 regarding transverse rotations and those found during the current study were similar in their pattern, the magnitudes reached very different levels. The maximum mean total amount of transverse rotation by the anatomic shin was approximately 18°, as extracted from the data by Levens et al 1948, but with the prosthesis this was only approximately 6.4°, as extracted from the data obtained during the current study. The reason for such a difference may be because the non-amputated, anatomic shin was longer than the residual limb, so that following amputation the now shortened muscles were no longer capable of generating similar forces to those on the non-amputated, anatomic shin. Another possibility would be lack of experience in walking on a prosthesis with a transverse rotation or combined transverse rotation and longitudinal translation adapter incorporated, because none of

the recruited subjects had previously used such a device, as can be seen in Table 4.1. Also, during both set-ups when transverse rotation was being permitted, external rotation was approximately twice the value for internal rotation, which was also similar to the findings by Levens et al 1948. This appeared to be a logical distribution, because external rotation of the entire trunk with respect to the stance limb helped bringing the currently swinging side forward.

As internal and external transverse rotations were unevenly distributed, with a maximum of approximately 3.9° in one direction, the overall ROM required at the TT Pylon would have to be at least 7.8°. This was a lot smaller and only approximately 13% of the TT Pylon's full range of 60° or 30° in each direction, as explained in Section 4.1.5.2. Despite having reduced the resistance to transverse rotation to a level below the lowest purchasable return unit, as described in Section 4.1.5.4, the overall amount of displacement still remained way below the available ROM. On the one hand, it was surprising that such a large discrepancy could occur, and this provoked the thought that the manufacturer's return units may be far too stiff. On the other hand, a large ROM gives amputees greater scope for high levels of activity that involve a lot of changes in the lower limb's orientational alignment.

With regard to capturing transverse rotation, an actual cam measuring range of 30° or ±15° seemed rather inappropriate, as only approximately 26% of its range was being used during walking in a straight line, therefore reducing the resolution of the recordings. Although the total range of the cam may be appropriate for other types of activities, when measuring transverse rotation during normal walking, it would be better to utilise a cam with a smaller measuring range, as previously considered in Section 6.2.2.4 a possibility for improving the cam geometry.

In conclusion, the main differences when utilising a trans-tibial prosthesis compared to gait without a prosthesis were that peak external rotation on the amputated side occurred slightly earlier and angular displacements were virtually absent throughout the majority of swing phase. With regard to the magnitude of transverse rotation, this was substantially smaller with a trans-tibial prosthesis, reaching a peak of approximately only 36% of the value for gait without a prosthesis. Also, further improvements in the cam geometry and/or a change of transducer to obtain a smaller maximum range for the

electrical stroke would be advantageous to accommodate the relatively small measuring range regarding transverse rotation.

9.2.1.2.   Inter-set-up differences in transverse rotations

Regarding the two set-ups when transverse rotation was being permitted, namely set-up TRyLTn and TRyLTy, it may be seen that the patterns of transverse rotation were very similar. In turn, the magnitudes of transverse rotation were very different reaching a mean total value of approximately 4.3° (p=0.001) and 6.4° (p=0.001) with set-up TRyLTn and TRyLTy, respectively. The exact reason as to why the two magnitudes were different remained unclear, but it obviously seemed to be linked to the fact that longitudinal translation was restricted with set-up TRyLTn and permitted with set-up TRyLTy.

A possible explanation for different magnitudes in transverse rotation, while restricting and permitting longitudinal translation, may be related to medially directed GRFs, as these had the greatest influence on resisting rotation of the prosthetic foot. This was because the longest dimensions of the prosthetic foot extended in anterior-posterior direction, as previously discussed in Section 9.1.3.3. At early and late stance phase, the prosthetic shin was leaning medially, as described in Section 9.1.3.4, so that longitudinal translation with set-up TRyLTy delayed the peak in medially directed GRFs. The tendency for the socket to rotate relative to the prosthetic foot was consequently granted for longer, due to an extended period between the point in time when the socket was in a neutral position and the later occurring peak in medially directed GRFs. In truth, the friction between the prosthesis and the floor was more than likely far exceeding the necessary level that prevented the foot from slipping and therefore rotating in the same direction as the socket. However, the delay in medially directed GRFs might have given the prosthesis a softer feel. As result of this, it may have subconsciously encouraged the subjects to increase the magnitude of transverse rotation when the adapter was fully mobile.

An alternative explanation for different magnitudes in transverse rotation, while restricting and permitting longitudinal translation, is that the coil spring was substituted by a rigid cylinder with set-up TRyLTn to prevent longitudinal translation from occurring, as described in Section 4.1.5.5. Despite the fact that the rigid cylinder had the same build height as the coil spring and the same lubricated plastic washers above and

below it for less friction, it may nevertheless have reduced the freedom for transverse rotation between the TT Pylon housing and its shin tube. This did not seem to be the case when the set-up was manually tested. However, upon weight bearing, the cylinder would obviously be clamped more tightly in between the adapter components, and due to the cylinder's rigidity, the friction inside the adapter would soon start to increase. Because of the careful machining of the cylinder and the lubrication of washers, this scenario seemed unlikely, but it still represents a possibility for a reduction in transverse rotation when longitudinal translation was restricted.

Another aspect worth considering when analysing the magnitudes of transverse rotations is that the peak in internal and external rotation reached a mean value of approximately 1.4° and 2.9° with set-up TRnLTy and approximately 2.5° and 3.9° with set-up TRyLTy, respectively. This meant that the ratio between internal and external rotation was approximately 0.483 with set-up TRyLTn and approximately 0.641 with set-up TRyLTy. In other words the amount of internal transverse rotation was less than 50% of external rotation with set-up TRyLTn and more than 50% with set-up TRyLTy.

In exactly which way the ratios were affected with regard to the magnitudes of transverse rotations that occurred in each direction was not quite clear. It can nevertheless be said that the changeover from transverse rotation in one direction to the other occurred later with set-up TRyLTn than it did with set-up TRyLTy. This meant that transverse plane motion with set-up TRyLTn was much less balanced, because the duration for internal rotation was longer, despite its percentage with regard to external rotation having been smaller compared to set-up TRyLTy. The reason that there was a difference between the changeover from internal to external socket rotation for the two set-ups was not fully understood. Also, the other aspect that could not be fully explained either was the question of which of the previously identified two ratios between internal and external rotation would be more beneficial for amputee gait.

In conclusion, transverse rotation reached a greater magnitude while the adapter could undergo both transverse rotation and longitudinal translation compared to when purely transverse rotation was being permitted. Also, with both types of adapter motions possible simultaneously, the amount of internal rotation was not quite as small when seen in proportion relative to external rotation as it turned out to be when purely transverse rotation was being permitted. In general, it can be seen that when transverse

rotation was possible, the residual limb had a similar tendency to rotate as the sound leg did during the study by Levens et al 1948, and by completely unlocking the adapter, this tendency was granted even more so.

9.2.2.   Longitudinal translation at the motion adapter

9.2.2.1.   *General descriptions of longitudinal translations*

Linear displacements along a longitudinal axis between the socket and the prosthetic foot are illustrated in Figure 9.30. This only includes the two set-ups when longitudinal translation was being permitted, namely set-up TRnLTy and TRyLTy.

At heel strike, the socket immediately started to travel distally, as the body weight was being transferred onto the prosthesis. Once the vertical GRFs reached the first peak, as illustrated in Figure 9.8, so did the magnitude of longitudinal translation. From this point in time onwards, the socket remained lower down until the vertical GRFs came to a second peak during late stance phase. This second peak in vertical GRFs was reflected in the magnitude of longitudinal translation, which also reached a second peak. As the subjects gained the necessary upward and forward propulsion, the counteracting response from the floor started to decrease in magnitude, so that the socket started to travel proximally. The more the GRFs reduced, the further proximally the socket moved, until it finally went back to its neutral position after the prosthetic foot lost contact with the floor.

Figure 9.30:   TT Pylon motion, distal translation of socket +ve
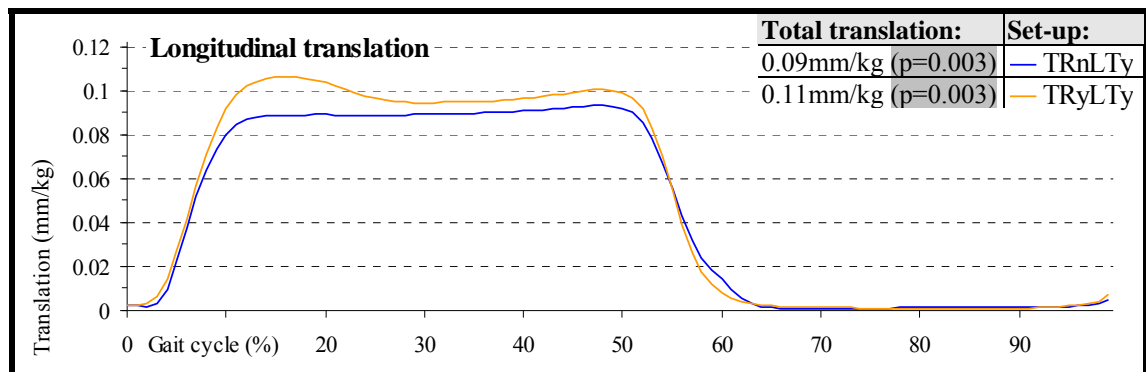
The maximum mean total amount of longitudinal translation was 0.11mm/kg. With an average body weight of 82.6kg, as shown in Table 4.2, the aforementioned figure of 0.11mm/kg converted to a total displacement of approximately 9.1mm. This was 3.9mm less than the 13mm maximum ROM that the TT Pylon can experience, as described in

Section 4.1.5.4. Also, the manufacturer of the TT Pylon stipulated a travel of approximately 5-8mm during normal walking, whereby the displacement achieved during the current investigation was 1.1mm greater than the top value of that range. The chosen return unit for this type of activity level was suitable for a body weight between 75-100kg, whereby none of the recruited subjects were heavier than 100kg. This meant that floor impacts were greater than what the manufacturer expected, so that the maximum value for the TT Pylon's ROM may also be an underestimation and not sufficient for high levels of activity.

With regard to capturing longitudinal translation, an electrical stroke of 10mm for the chosen displacement transducer's electrical stroke seemed appropriate. As this was only 0.9mm bigger than the largest measured displacement of approximately 9.1mm, it showed that most of the transducer's available range was utilised, thus increasing the resolution of the recordings without exceeding the maximum in the transducer's electrical stroke.

In conclusion, the results that were analysed in this Section could not be backed up by findings from the literature, because similar measurements have not been published elsewhere. However, considering the magnitudes of displacements that took place, it was therefore likely for the prosthesis to transmit less shock impacts onto the body. Also, as most of the transducer's measuring range was exploited, it was decided that the current cam geometry and maximum range of the transducer's electrical stroke was excellent for recording longitudinal translation.

9.2.2.2.   *Inter-set-up differences in longitudinal translations*

Regarding the two set-ups when longitudinal translation was being permitted, namely set-up TRnLTy and TRyLTy, it may be seen that the patterns of longitudinal translation were very similar. In turn, the magnitudes of longitudinal translation were very different reaching a mean total value of approximately 0.09mm/kg (p=0.003) and 0.11mm/kg (p=0.003) with set-up TRnLTy and TRyLTy, respectively. With an average body weight of 82.6kg, as shown in Table 4.2, the aforementioned figures of 0.09mm/kg and 0.11mm/kg converted to a total displacement of approximately 7.4mm and 9.1mm, respectively.

Although the general pattern of longitudinal translation was similar for the two set-ups, some of the output characteristics differed slightly. With set-up TRyLTy, the pattern of longitudinal translation resembled the M-shaped pattern of vertical GRFs, previously described in Section 9.1.2.2. In turn, the pattern of longitudinal translation obtained with set-up TRnLTy was less M-shaped, as the characteristic dip during mid-stance phase appeared to be negligible. The reason for that was because the weight acceptance period and the push off period hardly triggered a peak in longitudinal translation. Instead, the data reached approximately the same magnitude as the mid-stance phase dip did, thus giving it an upward sloping shape, due to slightly lower values at the beginning of stance phase than at the end.

As virtually no peaks were triggered with set-up TRnLTy, unlike with set-up TRyLTy, this meant that the magnitudes of longitudinal translation during the weight acceptance period and the push off period were greater with set-up TRyLTy compared to set-up TRnLTy. Such inter-set-up differences were reflected in the vertical GRF data. Although the second peak in vertical GRFs was approximately the same for the two set-ups, the first peak in vertical GRFs was smaller and the incident of both the first and second peak was delayed with set-up TRyLTy compared to set-up TRnLTy. This indicates that better shock absorption took place while transverse rotation and longitudinal translation was being permitted simultaneously rather than just longitudinal translation on its own.

Having seen that the magnitude of longitudinal translation turned out to be greater with set-up TRyLTy compared to set-up TRnLTy, the question therefore was why such a difference in adapter motion occurred in the first place. To answer this, it is necessary to refer back to Section 4.1.5.5 where the design of the torsion rod was being elaborated on. The quadrant of the torsion rod fitted into the square cut-out inside the TT Pylon shin tube, which meant that when longitudinal translation took place, there was constant friction between the quadrant and the square cut-out, even if only very small in magnitude. With set-up TRyLTy, this friction was fairly large when transverse rotation was also occurring, as the quadrant would be pushed harder against the surfaces inside the square cut-out while being displaced by transverse rotation. However, compared to set-up TRyLTy, the friction would be a lot further increased with set-up TRnLTy when the compliant torsion rod was replaced by the rigid substitute return unit, as the quadrant of this unit would not be displaced by transverse rotation. Therefore, lack of

compliance from the substitute return unit would eventually lead to the quadrant being jammed into the square cut-out, thus locking longitudinal translation, as the jamming of the quadrant prevents itself from sliding inside the square cut-out.

With set-up TRnLTy, the effect that the quadrant of the substitute return had on the locking and unlocking of longitudinal translation over the course of stance phase can be explained as follows. During the weight acceptance period, the socket internally rotated, as previously explained in Section 9.2.1.1, which soon jammed the quadrant and hence the reduced initial peak in longitudinal translation. During mid-stance phase, the residual limb's tendency to rotate in a transverse plane changed direction. This change momentarily unlocked the quadrant, because the adapter passed its neutral position. After that, the socket externally rotated, until the quadrant jammed again and hence the reduced final peak in longitudinal translation around push off.

For some subjects, the jamming was more severe than for others. Sometimes during the weight acceptance period, the adapter experienced only approximately three quarters of the peak in longitudinal translation that occurred during a subject's gait cycle due to the jamming of the quadrant. After that, at around mid-stance phase, the momentary unlocking of the jammed quadrant then allowed most of the remaining longitudinal translation to take place. The data therefore appeared to have an upward step rather than an upward slope or an M-shape. Despite a more skewed appearance, data that contained such an upward step obviously also needed to be included in the mean of all ten subjects' longitudinal translation. The occasional upward stepping characteristic with set-up TRnLTy can therefore be considered the reason for the mean graph to reach lower values during the weight acceptance period than it did during the push off period.

If the operational aspects of the TT Pylon were different, it might have happened that the pattern and magnitude of longitudinal translation became more similar for set-up TRnLTy and set-up TRyLTy. However, this type of adapter was obviously designed to be fully mobile and not to permit either one motion or the other. The information gained from the current investigation is therefore, if even only to a small extent, tarnished with small deviations from the true picture as to what happens when longitudinal translation occurs on its own as well as together with transverse rotation. Future studies should therefore address this point in order to obtain more accurate data.

In conclusion, it can be seen that longitudinal translation took place throughout stance phase, thus suggesting that the force-time ratio had changed. This can be confirmed when analysing GRF data and particularly those in vertical direction. Also, differences in longitudinal translation were found between a partial and full unlocking of the adapter. Those differences seemed to be triggered by the restriction of transverse rotation and the likelihood that this impeded the mechanics for longitudinal translation inside the adapter. If such a link is true, then it would not be possible to determine whether the influence of transverse rotation on the gait parameters also influenced longitudinal translation.

9.3. <u>Loads on the residual limb</u>

Data from the six force sensors were purely recorded on the prosthesis and not on the anatomic shin. The current Section is therefore only applicable to the amputated side.

9.3.1. <u>In-socket pressures</u>

9.3.1.1. *General descriptions of in-socket pressures*

Residual limb-socket interface pressure measurements taken with the six FlexiForce® sensors are illustrated in Figure 9.31 for all four set-ups. Recording signals from every one of the six force sensors were strongest during stance phase due to the presence of GRFs. However, unlike some of the previously described gait parameters that reduced to zero during swing phase, this was not the case with pressure measurements. Although the magnitudes greatly reduced while contact with the ground was absent, the subjects' snug fitting sockets and resultant counteracting forces from bones and muscles still triggered some force sensor outputs, even if no body weight was being transmitted through the prosthesis.

The pressures applied onto the six anatomic landmarks of the residual limb that were previously defined in Section 6.1.3.2, had a pattern very similar in appearance to the M-shaped graphs of vertical GRFs. This was particularly because of the two peak readings, namely one during the weight acceptance period and the other during the final push off period. These two peaks were present amongst the signals from all six sensors. However, large variations in the magnitudes of pressures between the first and second peak for the different measuring sites often gave the M-shaped graphs a rather skewed appearance.

The highest stance phase and swing phase total pressures were encountered on the fibular head, reaching a mean value of approximately 177.0kPa and 40kPa, respectively. Values of such magnitudes were not surprising, as the fibular is a superficially located bone landmark. Due to only thin tissue covers, such a landmark is not very pliable and it therefore easily resists externally applied forces, thus triggering increased total pressures. Also, not only are bones harder than soft tissues, the fibular head possesses an additional feature that makes it even more prone to high pressures, because it is not flat, but prominent instead, thus increasing the total pressure due to a reduced area for forces to be transmitted onto. Total pressures on the tibial tuberosity were lower than on the fibular head, but still amongst one of the highest recorded during the current investigation, due to an almost equally superficial and prominent bone structure as the fibular head. The tibial tuberosity therefore triggered the third highest mean total pressure of approximately 119.3kPa. In turn, the anterior-distal aspect of the tibia was an area that experienced by far the lowest total pressures of all six sites, despite this also being prominent and covered by only small quantities of soft tissues. Such low total pressures may have been recorded, because the anterior-distal aspect of the tibia was the most distally located landmark. As the material of the Iceross liner became thicker towards its distal, closed end, externally applied forces within the distal regions of the liner were consequently better cushioned than those within the liner's proximal regions. The mean total pressure on the anterior-distal aspect of the tibia therefore remained low and around only approximately 61.4kPa.

The remaining three of the six measuring sites were all characterised by thick layers of underlying soft tissues, but the total pressures measured here were, nevertheless, fairly high. Readings of total pressures taken around the medial tibial flare reached the second highest mean value of all six sensors, namely approximately 142.9kPa. In turn, the mean total pressure on the lateral tibial flare and the calf was slightly lower than that, reaching approximately 102.7kPa and 100.23kPa, respectively. The underlying bone structure at all of these three landmarks was deeply embedded within the residual limb, which should provide some degree of cushioning. However, each landmark contained the main intrinsic muscle groups that were partially responsible for controlling motion of the foot, so that these muscles may have been the source for the observed high pressures. Despite the fact that the foot no longer exists, the brain may still continue sending neural signals to those muscles as part of an automatic reflex secondary to a

Figure 9.31: Force sensor outputs from residual limb pressures, increasing +ve

Part A - fibular head	Total pressure:	Total area:	Set-up:
	189.8kPa (p=N/A)	5891 (p=N/A)	TRnLTn
	207.8kPa (p=0.851)	5848 (p=0.245)	TRyLTn
	169.0kPa (p=0.105)	6036 (p=0.378)	TRnLTy
	141.5kPa (p=0.302)	5468 (p=0.409)	TRyLTy
	177.0kPa mean (1*)	5811 mean (1*)	* ranking

Part B - tibial tuberosity	Total pressure:	Total area:	Set-up:
	139.8kPa (p=N/A)	5596 (p=N/A)	TRnLTn
	126.1kPa (p=0.224)	5089 (p=0.285)	TRyLTn
	118.7kPa (p=0.092)	5071 (p=0.101)	TRnLTy
	92.5kPa (p=0.568)	4155 (p=0.615)	TRyLTy
	119.3kPa mean (3*)	4978 mean (2*)	* ranking

Part C - anterior distal aspect of tibia	Total pressure:	Total area:	Set-up:
	66.6kPa (p=N/A)	2903 (p=N/A)	TRnLTn
	65.1kPa (p=0.973)	2983 (p=0.867)	TRyLTn
	56.7kPa (p=0.151)	2666 (p=0.089)	TRnLTy
	57.2kPa (p=0.641)	2714 (p=0.691)	TRyLTy
	61.4 kPa mean (6*)	2817 mean (6*)	* ranking

Part D - medial tibial flare	Total pressure:	Total area:	Set-up:
	172.1kPa (p=N/A)	4512 (p=N/A)	TRnLTn
	136.1kPa (p=0.101)	3797 (p=0.187)	TRyLTn
	154.3kPa (p=0.089)	4175 (p=0.083)	TRnLTy
	109.1kPa (p=0.317)	3385 (p=0.676)	TRyLTy
	142.9kPa mean (2*)	3967 mean (5*)	* ranking

Part E - lateral tibial flare	Total pressure:	Total area:	Set-up:
	107.3kPa (p=N/A)	4062 (p=N/A)	TRnLTn
	100.8kPa (p=0.474)	3965 (p=0.781)	TRyLTn
	104.4kPa (p=0.725)	4043 (p=0.917)	TRnLTy
	98.3kPa (p=0.955)	4021 (p=0.839)	TRyLTy
	102.7kPa mean (4*)	4023 mean (4*)	* ranking

Part F - calf	Total pressure:	Total area:	Set-up:
	107.9kPa (p=N/A)	5288 (p=N/A)	TRnLTn
	97.4kPa (p=0.347)	4661 (p=0.293)	TRyLTn
	98.9kPa (p=0.226)	4851 (p=0.124)	TRnLTy
	96.8kPa (p=0.374)	4749 (p=0.062)	TRyLTy
	100.2kPa mean (5*)	4875 mean (3*)	* ranking

habitual motor control. While the muscles contracted and therefore expanded, the socket fit consequently became more intimate, thus increasing the total pressures. In turn, if those contractions would not have occurred, these soft tissue sites may have experienced smaller total pressures, but then the magnitudes of forces exerted onto bone prominences might have consequently become larger.

Total pressures are extremely relevant in establishing the potential for skin damage. Nevertheless, the other factor of similar importance is the overall load exerted onto each landmark, as was previously emphasised in Section 8.4.23.

The fibular head not only experienced the highest mean total pressure, the total area under the graph or mean pressure throughout the gait cycle of approximately 5811 was also greatest at this site. In turn, although the medial tibial flare had to endure the second highest mean total pressure, the mean pressure throughout the gait cycle was the third highest of them all, reaching approximately 3967, due to a virtually absent second peak towards the end of stance phase. This was different for the lateral tibial flare, which experienced the fourth highest mean total pressure, but also the fourth highest mean pressure throughout the gait cycle of approximately 4023. Also, in spite of its prominence, the tibial tuberosity was not directly after the fibular head in the ranking list of mean total pressures, but only in third place. However, the dip in output signals during mid-stance phase was, unlike with other landmarks, not very low, so that the mean pressure throughout the gait cycle became the second largest, namely approximately 4978. Although the mean total pressure at the calf was the fifth highest, the mean pressure throughout the gait cycle was slightly higher up the list, in third place, reaching approximately 4875. Finally, the anterior-distal aspect of the tibia not only experienced the lowest mean total pressure, but the smallest mean pressure throughout the gait cycle also of approximately 2817. Similar to the reason for the lowest mean total pressure, this was likely to be attributed to the cushioning effect of the Iceross liner in that region of the residual limb.

Mean total pressures compared quite favourably with those previously described in Section 6.1.3.2, which appeared a lot higher than the results from the current investigation. However, it seemed alarming that two out of the three areas with only very thin tissue coverage, namely the fibular head and the tibial tuberosity, experienced the highest and third highest mean total pressure, as well as the highest and second

highest mean pressure throughout the gait cycle. This was unnerving, as the reduced cushioning effects that these landmarks experienced can easily lead to occlusion of superficially located blood vessels, and if sustained over prolonged durations, can ultimately also trigger skin damage.

In conclusion, despite some concerns regarding large mean total pressures, it was satisfying to reveal that these pressures dropped down drastically during swing phase. This provided a period of recovery, in order for blood and the required oxygen to at least momentarily return back to perhaps previously occluded parts. Also, the fact that there was a great resemblance of vertical GRF data amongst pressure readings meant that the way body weight was being transferred from one limb to the other played a huge part in influencing the exchange of forces and resultant pressures inside the socket. As it is obviously difficult to reduce the overall body weight, an alternative for lowering total pressures would be to change the force-time ratio. It can therefore be concluded that it is vital to facilitate a reduction of shock impacts with the ground in an attempt to lower the forces exerted onto the residual limb.

9.3.1.2.   *Inter-set-up differences in in-socket pressures*

From the two characteristics that were extracted out of the data of all six force sensors, namely the total pressure and the pressure throughout the gait cycle, no significant differences were found for any of the three dynamic set-ups compared to when the adapter was fully locked. This meant that, purely from the statistical point of view, the introduction of transverse rotation, longitudinal translation or both motions combined did not trigger any relevant changes in the pressures exerted onto the residual limb. Such findings seemed rather surprising, because the other gait parameters that were previously discussed in Section 9.1 and Section 9.2 did seem to be affected on a multitude of occasions.

Despite an absence of significant findings amongst in-socket pressures, it can still be observed that the pressure patterns varied greatly due to the locking and unlocking of the adapter in various configurations. For instance, during the first approximately 10-15% of the gait, more or less the same sequence of set-ups emerged from the pressures of four out of the six anatomic landmarks, namely the fibular head, tibial tuberosity, anterior-distal aspect of tibia and medial tibial flare. In those cases the

highest pressures were found with set-up TRnLTn, which was followed by set-up TRnLTy, then by set-up TRyLTn and finally by set-up TRyLTy.

Another aspect that can be observed was that, at the majority of landmarks, the pressure readings were amongst the highest, or the highest altogether, with set-up TRnLTn, even if only for part of the gait cycle. This was the opposite with set-up TRyLTy, in that pressure readings were amongst the lowest, or the lowest altogether, at the majority of landmarks. More precisely, at five out of the six landmarks, the mean total pressure was the highest with set-up TRnLTn and the lowest with set-up TRyLTy, as was summarised in Table 9.3 by using a ranking system for the mean total pressure on each landmark with each of the four set-ups.

Just one out of the six landmarks obtained a ranking with set-up TRnLTn and set-up TRyLTy that was different by only one position each in the ranking list of mean total pressures. This did not seem to coincide with the graphic representation of in-socket pressures, due to reasons that were previously explained in Section 8.4.23 regarding timing differences in peak pressures between set-ups. The reason that peak pressures were mentioned here was because the value of the largest peak pressure for each set-up represented the total pressure. The only reason that the mean total pressure for one of the six landmarks was not the highest with set-up TRnLTn and not the lowest with set-up TRyLTy was, because each of these two set-ups triggered a single extreme pressure reading during the trials of just one of the ten subjects. This single extreme pressure reading therefore changed the resultant mean total pressure for that one landmark, which, in turn, affected its ranking by just one position.

A similar consistency with regard to the ranking of mean total pressures was also found when the adapter was only partially unlocked. Set-up TRyLTn triggered the third highest mean total pressure three times, the second highest twice and the highest once. In turn, the ranking list of mean total pressures with set-up TRnLTy was a mirror image of that with set-up TRyLTn, as was the case with set-up TRnLTn and TRyLTy. Therefore, set-up TRnLTy triggered the second highest mean total pressure three times, the third highest twice and the lowest once. This meant that the ranking of mean total pressures was fairly regular with set-up TRyLTn and TRnLTy, but not as regular as with set-up TRnLTn and TRyLTy.

Table 9.3: Ranking of sensor outputs according to high and low pressures

Rank 1 = high 4 = low	Mean of							
	Total pressure				Pressure throughout the gait cycle			
	(number of landmarks where a certain rank in pressure was reached) (⌢ = weighted average)							
	TRnLTn	TRyLTn	TRnLTy	TRyLTy	TRnLTn	TRyLTn	TRnLTy	TRyLTy
1	5	1	---	---	4	1	1	---
2	1	2	3	---	2	1	3	---
3	---	3	2	1	---	2	1	3
4	---	---	1	5	---	2	1	3

Equally important as the analysis of total pressures in establishing the way different set-ups affected in-socket pressures was to analyse the pressures throughout the gait cycle that were exerted onto each of the six landmarks. Table 9.3 shows that the ranking of mean pressures throughout the gait cycle with set-up TRnLTn and TRyLTy was similar to the ranking found for the mean total pressures with the same two set-ups. With set-up TRnLTn, the mean pressure throughout the gait cycle was amongst the highest or the highest altogether. This was the opposite with set-up TRyLTy, in that the mean pressure throughout the gait cycle was amongst the lowest or the lowest altogether. More precisely, at four and three out of the six landmarks, the mean pressure throughout the gait cycle was the highest with set-up TRnLTn and lowest with set-up TRyLTy, respectively. The ranking for the remaining landmarks with set-up TRnLTn and set-up TRyLTy was different by only one position each in the ranking list of mean pressures throughout the gait cycle.

The ranking of mean pressures throughout the gait cycle with set-up TRyLTn and TRnLTy was also similar to the ranking found for the mean total pressures with the same two set-ups. Set-up TRyLTn triggered the lowest mean pressure throughout the gait cycle twice, the third highest twice, the second highest once and the highest once. In turn, the ranking list of mean pressures throughout the gait cycle for set-up TRnLTy was the mirror image of that for set-up TRyLTn, as was the case with set-up TRnLTn and TRyLTy. The only exception was that with set-up TRnLTy, one ranking was different, which meant that the overall ranking of its pressures was not quite a true mirror image of that for set-up TRyLTn. Set-up TRnLTy triggered the highest mean

pressure throughout the gait cycle once, the second highest three times, the third highest once and the lowest once. This meant that the ranking of mean pressures throughout the gait cycle was slightly more dispersed for set-up TRyLTn and TRnLTy compared to set-up TRnLTn and TRyLTy.

Concerning both, mean total pressures and mean pressures throughout the gait cycle, the values incorporated in Table 9.3 are useful for identifying the various rankings of individual force sensor outputs from the four set-ups. However, this information does not provide an insight into the overall ranking that each set-up reached with regard to all six force sensor outputs. In order to make inter-set-up comparisons easier, it was necessary to present the data in a different fashion. For this reason, the weighted averages were determined from the ranking values. Weighted averages were calculated as the sum of products between scores from each set-up and the corresponding ranking, divided by the total number of scores, namely six due to the same number of force sensors.

When inspecting the values and bar charts illustrated in Figure 9.32, it may be seen that the rankings with regard to mean total pressures gradually changed from high to lower pressures in relation to set-up TRnLTn, TRyLTn, TRnLTy and TRyLTy, respectively. This was very similar for the mean pressures throughout the gait cycle except that set-up TRyLTn and TRnLTy were the other way around. Also, for mean total pressures, the highest ranking was higher and the lowest ranking lower than it was for the mean pressures throughout the gait cycle, which indicated a greater diversity between set-ups for the former characteristic compared to the latter. The trendline incorporated in Table 9.3 is another way of illustrating the weighted averages to provide an even better understanding of pressure rankings for the four set-ups.

Figure 9.32:   Weighted averages for inter-set-up pressure ranking differences
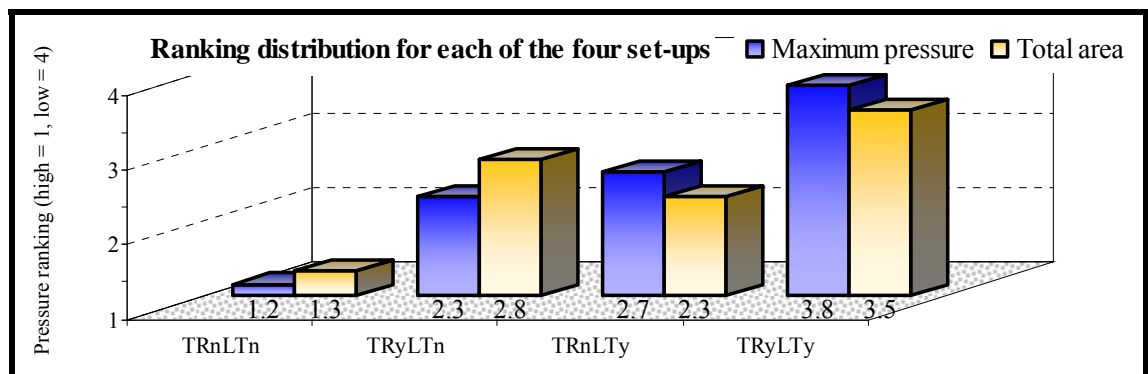
Returning once again to the actual force sensor outputs, another aspect that is notably different from the majority of measuring sites was that in some cases, the gaps between graphs from different set-ups seemed to be greater and remained that way over a longer duration of stance phase than for other cases. This was so for the tibial tuberosity and medial tibial flare, whereby the difference between a set-up with the highest total pressure and another set-up with the lowest, reached approximately 47.3kPa and 63.0kPa for those two sites, respectively. This meant, that in terms of the greatest inter-set-up measurement differences, the medial tibial flare was in second place and the tibial tuberosity in third. In both cases the two set-ups that led to those differences were TRnLTn and TRyLTy. In first place was the fibular head with an inter-set-up difference of approximately 66.3kPa, although the gaps between graphs were not sustained for very long. Also, unlike the scenario for the tibial tuberosity and medial tibial flare, the greatest difference between the highest and lowest total pressures on the fibular head was not triggered with set-up TRnLTn and TRyLTy, but instead with set-up TRyLTn and TRyLTy. Nevertheless, the difference between total pressures with set-up TRnLTn and TRyLTy still reached 48.3kPa, which is also an astonishing step in force sensor readings.

Inter-set-up differences for the remaining landmarks were lower and only around approximately 10kPa. Also, with respect to all six landmarks, the differences between pressures throughout the gait cycle were similarly affected as the differences between total pressures. However, the exception was that the types of set-ups involved in reaching the greatest differences were not necessarily the same for the total pressures, as becomes clear from the figures in Table 9.3.

Also, because the widest and longest sustained gaps between graphs were found amongst the charts representing the total pressures on the tibial tuberosity and medial tibial flare, these were therefore also the landmarks that experienced the greatest differences between pressures throughout the gait cycle, namely 1441 and 1127, respectively. Another aspect worth mentioning is inter-set-up differences during swing phase. These were exceedingly small if not absent, which can be attributed to the fact that GRFs were zero, so that the effects of adapter mobility were only minimal.

In conclusion, as touched upon previously in Section 9.3.1, it seemed alarming that different set-ups affected the pressures on bone landmarks to a great extent. This should

therefore be taken into consideration when prescribing motion adapters, as the combined permission of transverse rotation and longitudinal translation appeared to be most favourable for reducing the residual limb-socket interface pressures. Although no significant findings were revealed, the previous discussion demonstrated that inter-set-up differences still took place to a considerable extent, thereby influencing the way in-socket pressures were affected. It would therefore be justifiable to say that by completely unlocking the adapter, the likelihood for preventing vascular occlusion increases.

9.3.2.   Subjects' questionnaire

9.3.2.1.   *Inter-set-up differences in subjects' feedback*

The results from the questionnaire the subjects were asked to complete are given in Table 9.4. Six out of the ten subjects were least satisfied with set-up TRnLTn, whereby the other four thought of it as the second least favourable set-up. This was quite the opposite with set-up TRyLTy, which a total of eight subjects were most satisfied with. One of the other two subjects considered it the second most favourable and another the least favourable set-up. However, the latter person explained that the reason for considering set-up TRyLTy as the least favourable set-up was purely because he felt very unfamiliar with the softness during gait due to the fully mobilised adapter. However, he also reported that more practice might have a favourable effect on his opinion of the set-up, as he considered it to have great potential for improving his walking style and socket comfort.

Most subjects voted for set-up TRyLTn and TRnLTy as the second or third most favourable set-up, with a difference in the mean ranking score of only 0.2. Just one person considered each of those two set-ups the one they were most satisfied with. In turn, the most dissatisfied were two subjects with set-up TRyLTn and only one subject with set-up TRnLTy.

9.3.2.2.   *Interpretation of subjects' feedback*

The results from the questionnaires are very similar to those found with regard to pressures exerted onto the residual limb. The subjects' average least favourable and most favourable set-ups were TRnLTn and TRyLTy, respectively, which also

experienced the highest and lowest mean total pressure and the highest and lowest mean pressure throughout the gait cycle, respectively, as previously shown in Section 9.3.1.2.

Table 9.4:   Summary of subjects' feedback from questionnaires

Sub-ject	TRnLTn (%) 1…4 Best…worst (*Preference*)		TRyLTn (%) 1…4 Best…worst (*Preference*)		TRnLTy (%) 1…4 Best…worst (*Preference*)		TRyLTy (%) 1…4 Best…worst (*Preference*)	
A	-89	*4*	4	*3*	55	*2*	79	*1*
B	52	*3*	54	*1*	53	*2*	-41	*4*
C	50	*3*	41	*4*	86	*1*	67	*2*
D	77	*3*	78	*2*	74	*4*	95	*1*
E	11	*4*	84	*2*	29	*3*	99	*1*
F	65	*4*	69	*3*	75	*2*	77	*1*
G	0	*4*	2	*3*	83	*2*	85	*1*
H	38	*4*	77	*2*	61	*3*	88	*1*
I	-41	*4*	28	*2*	7	*3*	90	*1*
J	24	*3*	37	*2*	-43	*4*	39	*1*
Minimum								
	-89	*3*	2	*1*	-43	*1*	-41	*1*
Maximum								
	77	*4*	84	*4*	86	*4*	99	*4*
Difference as in max-min								
	166	*1*	82	*3*	129	*3*	140	*3*
Mean								
	18.7	*3.6*	47.4	*2.4*	48.0	*2.6*	67.8	*1.4*
Standard deviation								
	51.2	*0.5*	30.1	*0.8*	40.3	*1.0*	41.9	*1.0*

A similar situation was applicable with regard to set-up TRyLTn and TRnLTy, in that these were on average the second most favourable and third most favourable set-ups. The mean total pressure reached the second highest and third highest level with set-up

383

TRyLTn and TRnLTy and the mean pressure throughout the gait cycle the third highest and second highest levels for the same two set-ups, respectively. The subjects' questionnaire results may partly rely on proprioceptive feedback that is related to differences in gait parameters generally. In turn, as their residual limb was the part of their body that formed an interface with the prosthesis, the reason for the described outcome of the questionnaire was therefore more likely to be directly related to pressures inside the socket.

In conclusion, the questionnaire results emphasise that amputees' perception of comfort is extremely well developed, particularly because their residual limb is exposed to a force pattern that it is not naturally designed to cope with. More effort should therefore be made to rely on the opinion from prosthesis users, as it became apparent that the scientific evidence was to a great extent reflected in the recruited subjects' proprioceptive feedback.

CHAPTER 10. <u>GENERAL DISCUSSION</u>

As may be seen from the previous Chapter, the amount of data and the number of findings amongst those data was extensive. The purpose of the current Chapter is to extract only relevant results that provide an explanation as to what the benefits of motion adapters are for amputee gait. The Chapter will be concluded with a Section that lists the limitations of the study.

10.1. <u>Sound and amputated side gait parameters</u>

This Section deals with the question of whether the motions at the adapter had a major effect on the sound and amputated side gait parameters. The answer to that is yes, but the analysis as to what the adapter did and how it affected the sound and amputated side is complex.

The adapter is primarily designed to reduce the loads applied onto the lower limb, and the greatest component of those loads is vertical GRFs. Therefore, if the adapter has its proposed effects, there should be some clear evidence of reduced vertical GRFs. For both the sound and amputated side, the first peak in vertical GRFs during the weight acceptance period was smaller in magnitude with all three dynamic set-ups compared to when the adapter was fully locked. This was the case except on one occasion when longitudinal translation was being permitted on its own, in that the magnitude of amputated side vertical GRFs was the same as without adapter motion. However, the incident of peak vertical GRFs was delayed in all cases for both sides, thus indicating a reduced loading rate.

The lowering and/or delay of the peak in vertical GRFs indicates that the shock absorbing capacity of the limb was greater when the adapter was mobile. Such a reduction in shock impacts can be attributed to a greater freedom of motion at the adapter and to its deceleration effects, because the introduction of adapter mobility was the only aspect that was different with the three dynamic set-ups compared to when the adapter was fully locked. It can therefore be concluded that motions within the adapter

and the resultant displacements of the socket relative to the prosthetic foot reduced the loading on both limbs, and not just on the amputated side.

Explaining the decrease in shock impacts on both limbs requires an exploration of the possible relationships between adapter mobility and the reduction in vertical GRFs. These relationships are related to changes in sound and amputated side kinematics. On the sound side, the principal parameters that were influenced by motions at the adapter were the peak knee and hip kinematics during the weight acceptance period at approximately 0-15% of the gait cycle. This was the same scenario for the amputated side regarding peak knee kinematics, but there was little apparent effect on hip kinematics. An investigation into the effects of transverse rotation and longitudinal translation on vertical GRFs should focus on the mechanisms by which adapter mobility affected sound side knee and hip kinematics and amputated side knee kinematics, as these were the variables affected most.

For the sound side, both the peak knee and hip flexion angles during the weight acceptance period were greater with all three dynamic set-ups compared to when the adapter was fully locked, as depicted in Figure 9.3 and Figure 9.5, respectively. Since the effects on the sound side were during its weight acceptance period of the gait cycle, the influence of the adapter on the sound side limb is most likely to have occurred during, or just prior to, this period.

Regarding the effects of transverse rotation at the adapter without longitudinal translation compared to when the adapter was immobile, the socket was externally rotated relative to the amputated side at approximately heel strike of the sound side. The period during which the socket rotated externally coincided with the time that the sound limb was absorbing shock due to weight acceptance. During this weight acceptance period, the natural tendency of the pelvis is to externally rotate with respect to the amputated side in order to move the body forward and above the sound limb, as illustrated in Figure 10.1. As a result of greater freedom of motion at the adapter, it can be hypothesised that, while the socket rotated externally, the pelvis would also develop an increased tendency for further external rotation relative to the amputated side compared to when the adapter was immobile. This might be the case even when external rotation of the adapter soon started to reduce, because the socket was still in a position of external rotation.

Figure 10.1: Pelvis rotation to shift the body above the sound side

Heel strike on sound side

Push off on amputated side

External rotation of the pelvis with respect to the amputated side
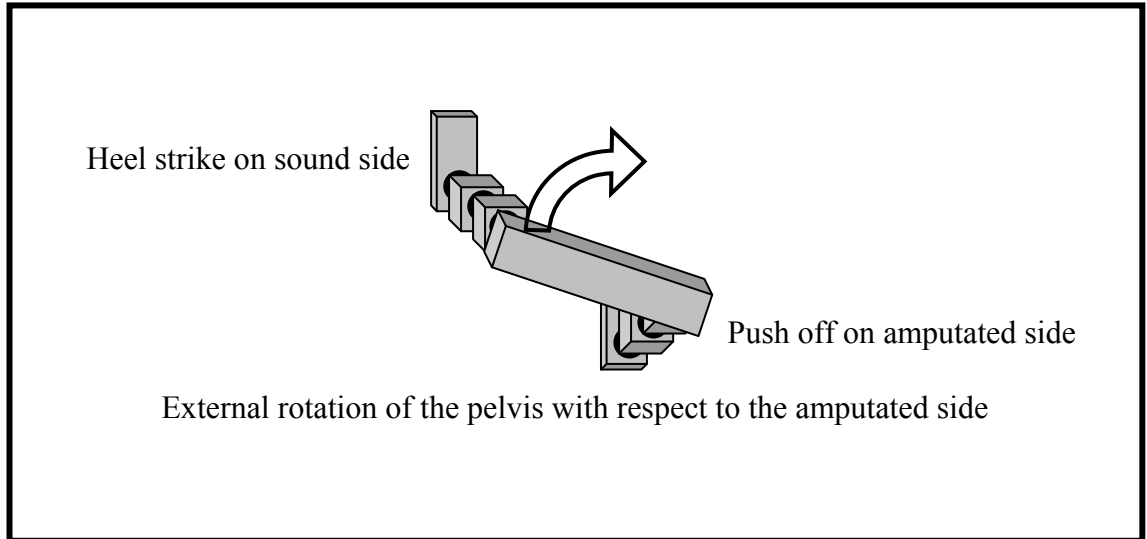
Figure 10.2: Sound side knee and hip kinematics due to pelvis rotation

Sound side weight acceptance period with adapter transverse rotation possible:

External rotation of the pelvis increases relative to the amputated side
Sound side pelvis moves anteriorly
Sound side knee and hip flexion increases

If the pelvis did rotate more relative to the amputated side, then the net anterior motion of the pelvis on the sound side would be greater during this period compared to when the adapter was immobile. Because the anatomic foot, which is stationary on the

ground, is connected to the moving pelvis by the shin and thigh section, the effect of increased external pelvic rotation would be a likelihood for increased sound side knee and hip flexion, as illustrated in Figure 10.2. This would explain the observed greater amputated side external rotation of the socket and subsequent increased sound side peak knee and hip flexion angles when adapter transverse rotation was being permitted compared to when it was fully locked. Increased sound side knee flexion can therefore be considered responsible for the reduction in vertical GRFs, as this is one of the usual mechanisms for shock absorption in the limb.

Regarding the effects of longitudinal translation at the adapter without transverse rotation compared to when the adapter was immobile, the socket was in a downward position at approximately late stance phase of the amputated side. This meant that the total length of the prosthetic limb was shortened and the pelvis located closer to the ground than without adapter mobility. While weight was gradually being transferred onto the sound side foot during its weight acceptance period, an increase in sound side knee and hip flexion angles occurred, which was greater than without longitudinal translation at the adapter.

A reason for this might be that in order to minimise vertical displacements of the COM and reduce energy consumption, the now lower position of the pelvis due to adapter longitudinal translation was maintained by increasing knee and hip flexion angles on the sound side. Although the overall vertical distance that the body's COM travelled may have been similar in magnitude compared to when longitudinal translation was immobilised, the maximum height that the pelvis and COM obtained while the prosthesis was shortened may have been less.

Conclusively, when each transverse rotation and longitudinal translation at the motion adapter was being permitted on its own, an increase in early stance phase peak knee and hip flexion angles on the sound side enabled a more gradual deceleration of the body's COM than without adapter motion. It was therefore the adapter motion in combination with subsequent changes in sound side kinematics and the deceleration of the COM that resulted in reduced peak vertical GRFs during the sound side weight acceptance period.

With both, transverse rotation and longitudinal translation at the adapter being permitted simultaneously, the effects that each of those motions had on knee and hip flexion

angles of the sound side, and therefore on vertical GRFs, were accumulative. This meant that the magnitude of both joints' peak flexion angles were greater when the two adapter motions were being permitted together than when either type of adapter motion was possible on its own. Corresponding to increased knee and hip flexion angles, the peak in vertical GRFs was further reduced when the adapter was fully mobile compared to when only one type of motion was permitted. This accumulated effect is perhaps evidence that both mechanisms by which peak knee and hip flexion angles increased could operate simultaneously, namely transverse plane motion at the pelvis due to transverse rotation at the adapter, as well as lowering of the pelvis due to longitudinal translation at the adapter.

For the amputated side, the mechanisms that affected the peak knee flexion angles during the weight acceptance period, illustrated in Figure 9.3, are most likely different compared to those on the sound side. In common with the sound side, changes in amputated side knee kinematics were found with all three dynamic set-ups compared to when the adapter was fully locked. However, the changes were slightly different than they were on the sound side, in that only knee flexion angles increased when just transverse rotation was possible, and conversely they decreased when just longitudinal translation was possible as well as when the adapter was fully unlocked. Since the effects on the amputated side knee were during the weight acceptance period of the gait cycle with the prosthesis, the influence is most likely to have occurred during or just prior to this period.

Regarding the effects of transverse rotation at the adapter without longitudinal translation compared to when the adapter was immobile, the socket rotated internally on the amputated side shortly after heel strike on that same side. The period during which the socket rotated internally occurred at a time when the amputated limb absorbed shock due to weight acceptance. During this weight acceptance period, the natural tendency of the pelvis is to internally rotate with respect to the amputated side in order to move the body forward and above the limb that is entering stance phase, namely the amputated side, as illustrated in Figure 10.3. As a result of greater freedom of motion at the adapter, it may be hypothesised that, while the socket rotated internally, the pelvis would also develop an increased tendency for further internal rotation on the amputated side compared to when the adapter was immobile.

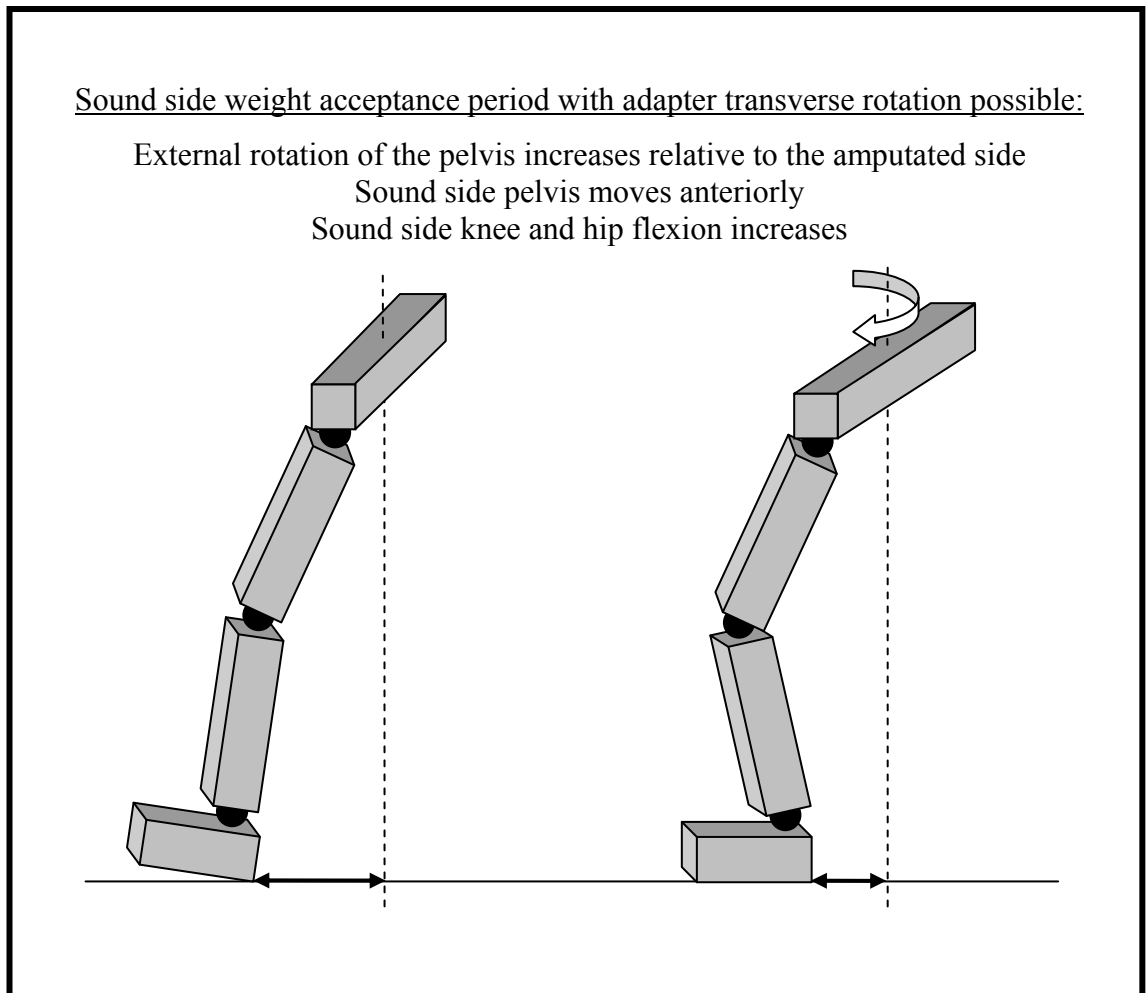**Figure 10.3:**   Pelvis rotation to shift the body above the amputated side
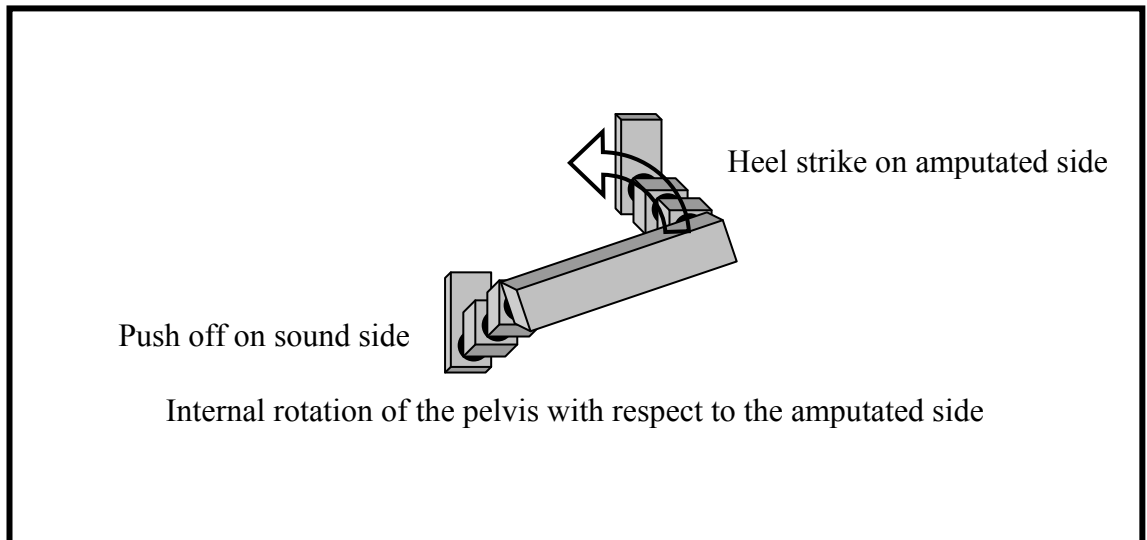

Figure 10.4:   Amputated side knee kinematics due to pelvis rotation
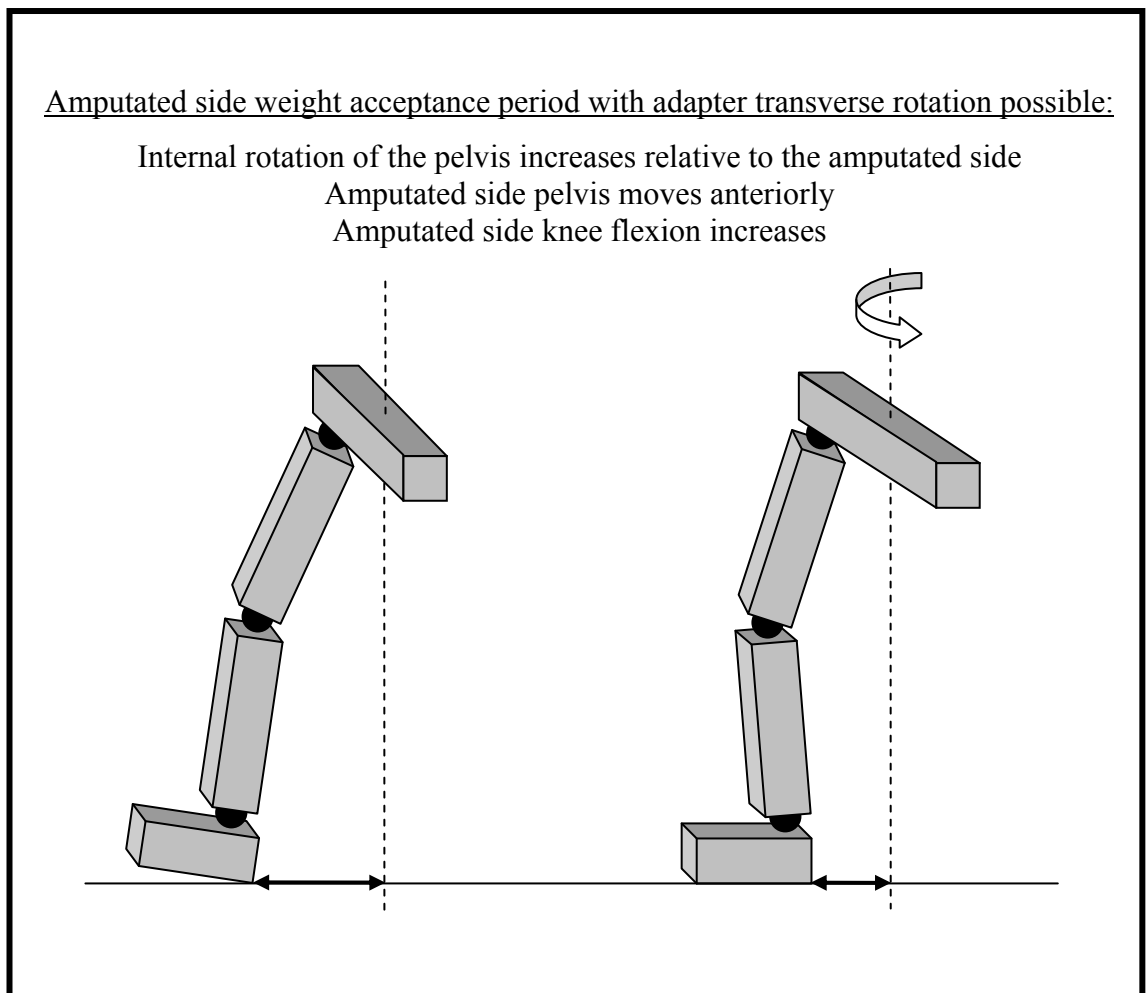
If the pelvis did rotate more relative to the amputated side, then the net anterior motion of the pelvis on that side would be greater during this period compared to when the adapter was immobile. Because the prosthetic foot, which is stationary on the ground, is

390

connected to the moving pelvis by the shin and thigh section, the effect of increased internal pelvic rotation would be a likelihood for increased knee flexion, as illustrated in Figure 10.4. This would explain the observed greater amputated side internal rotation of the socket and subsequent increased amputated side peak knee flexion angles when adapter transverse rotation was being permitted compared to when it was fully locked. Increased amputated side knee flexion can therefore be considered responsible for the reduction in vertical GRFs, as this is one of the usual mechanisms for shock absorption in the limb.

Regarding the effects of longitudinal translation at the adapter without transverse rotation compared to when the adapter was immobile, peak knee flexion angles were smaller compared to the scenario when the adapter was fully immobilised. As the adapter was allowed to shorten, this would facilitate some shock absorption, thereby decelerating the body's COM. It was therefore less necessary to flex the knee, which is one of the usual mechanisms for shock absorption in the limb. In fact, if additional knee flexion would have taken place, then the limb with the prosthesis may have shortened further overall, perhaps excessively, and may have forced the body to tilt more towards the amputated side.

Because the magnitude of knee flexion was reduced when longitudinal translation was being permitted compared to when it was restricted, one might have expected to observe an increase in vertical GRFs. However, this was not the case, because it was most likely that the effect of knee flexion on vertical GRFs was cancelled out by longitudinal translation with the net effect of no change in the magnitude of vertical GRFs. In turn, motion at the adapter and the deceleration of the body's COM would prolong the period over which body mass would be applied to the ground, and this corresponds to the observed delay in peak vertical GRFs.

Conclusively, it is known that at least early stance phase peak knee flexion angles increased on the amputated side, while transverse rotation was possible. This enabled a more gradual deceleration of the body's COM and therefore lowered vertical GRFs. Also, regarding longitudinal translation, the prosthesis shortened due to adapter mobility, so that the deceleration period of the COM was prolonged. Although this was not associated with a lower magnitude in peak vertical GRFs, the incident of that parameter was delayed, indicating a reduced loading rate.

In contrast to the sound side, with both, transverse rotation and longitudinal translation at the adapter being permitted simultaneously, the effects that each of those motions had on vertical GRFs were not accumulative. Knee flexion angles were increased when transverse rotation was being permitted, which would be associated with decreased vertical GRFs, whereby the knee flexion angles were decreased when purely longitudinal translation was possible, which would be associated with increased vertical GRFs. Therefore, with both types of adapter motions possible, the peak knee flexion angle would have been somewhere between the increased magnitude of knee flexion with only transverse rotation being permitted and the decreased magnitude of knee flexion with only longitudinal translation being permitted. Instead, peak knee flexion angles with the adapter fully mobile were reduced even more than when only longitudinal translation was being permitted, presumably because even less shock absorption was required from the knee, as more longitudinal translation was possible compared to when this type of motion was being permitted on its own. As would be expected with more longitudinal translation, there was an observed reduction in peak vertical GRFs, despite the magnitude of knee flexion being less.

As an overall conclusion, it is clear that adapter mobility affected knee and hip flexion angles on the sound side and knee flexion angles on the amputated side. The altered kinematics at these joints and at the adapter itself consequently affected vertical GRFs, which were reduced, delayed or both. As a result of this, the shock impact transmitted onto the weight bearing tissues must have been lowered, which was the hypothesised effect of the adapter. Whilst no data are presented to support any arguments regarding the influence of pelvis motion on the sound and amputated side knee and hip kinematics due to motion at the adapter, the explanations presented here represent a plausible justification of the observed differences in gait when adapter mobility was possible compared to when it was not.

10.2. Kinematics between socket and prosthetic foot

This Section deals with the question of whether the motions at the adapter changed the kinematics between socket and prosthetic foot. The answer to that is yes, as will become clear from the following discussion.

As expected, when purely transverse rotation was being permitted, the extent of mobility at the motion adapter increased drastically compared to when it was fully locked. Following heel strike, the socket rotated internally relative to the foot until mid-stance phase was reached, after which it rotated externally before returning back to a neutral position at the end of stance phase.

With regard to the amount of transverse rotation that took place, internal rotation reached only approximately half the magnitude of external rotation. Levens et al 1948 revealed similar findings from a study with predominantly non-amputees, which demonstrated that transverse plane angular motions during amputee gait represented normal physiological movements. The only abnormal aspect was that transverse rotation during amputee gait was only approximately one third in magnitude compared to that of non-amputee gait. Whether the reason for this was the reduced residual limb length compared to a non-amputated shin or unfamiliarity with transverse rotation remains unclear. However, the fact that transverse rotation took place demonstrated that at least some of the natural tendency for the residual limb to rotate was granted.

As expected, when purely longitudinal translation was being permitted, the extent of mobility at the motion adapter increased drastically compared to when it was fully locked. Following heel strike, the socket migrated distally and remained there until the end of stance phase after which it moved back proximally again. This shortening and lengthening of the prosthesis replicates the shock absorbing properties of the knee and hip and the subsequent lowering of the body's COM relative to the ground, which had consequences on the sound and amputated side kinematics, as described in Section 10.1.

The shortening action of the prosthesis has important deceleration effects on amputee gait. The force applied to the ground by the prosthesis is the product of mass and acceleration. Body mass is a constant, whereas acceleration can be affected by longitudinal translation at the adapter. Acceleration is the difference between the final and initial velocity of longitudinal translation, divided by the time it took for the changes in velocity to occur. While hitting the ground, the acceleration of the prosthesis was negative, because motion was slowing down. As the duration of time between impact and reaching zero velocity was longer while longitudinal translation was being permitted, the negative acceleration, or deceleration, was therefore more gradual compared to when longitudinal translation was restricted. Therefore, the limb

experienced a prolonged period of load acceptance, more gradual loading and reduced GRFs. All of these are likely to have clinical benefits.

While both transverse rotation and longitudinal translation was being permitted simultaneously, the magnitude of these two motions increased even further. The reason that each of the two motions was less in magnitude when being permitted on their own was considered to be a restriction within the adapter, due to this being partially locked.

10.3. <u>Loads on the residual limb</u>

This Section deals with the question of whether the motions at the adapter reduced the loads on the residual limb. The answer to that is yes, as will become clear from the following discussion.

The graphic representation of pressure measurements from all six landmarks on the residual limb resembled the M-shape appearance of vertical GRFs, even if sometimes curves were slightly skewed. Clearly, in-socket pressures are linked to vertical GRFs, and so, logically, the observed lowering in vertical GRFs when the adapter was mobile should correspond to a reduction in socket pressures. For the majority of anatomic landmarks, the greatest total pressures were found when the adapter was completely locked and the lowest when full adapter mobility was provided. This not only shows that the loads and therefore the likelihood for vascular occlusion are reduced the greatest when both types of motions are possible, but it also indicates that even partial adapter mobility can be advantageous for the residual limb. Apart from total pressures, similar findings were also revealed with regard to the pressures throughout the gait cycle. This is another important finding and adds to the argument that when adapter mobility was granted, the residual limb tissues were less likely to suffer from vascular occlusion.

In the amputees studied, the largest total pressures and pressures throughout the gait cycle were exerted on areas with thin tissue coverage. Those sites are, due to their reduced vascularisation, much more prone to tissue breakdown. Importantly, these same landmarks experienced the greatest reduction in pressures when adapter mobility was granted and in particular when both motions were being permitted.

Despite seemingly satisfactory results regarding the effect of adapter mobility on in-socket pressures, the obtained data have to be interpreted with caution, because none of the findings were, from the statistical point of view, significant. However, this might have happened, because when transverse rotation or longitudinal translation were being permitted on their own, the magnitudes of these motions were smaller than when the adapter was fully mobile, due to the possibility of a slight jamming of the mechanism with just one motion granted. If the jamming would not have occurred and individual motions, when permitted on their own, were equal to when both of them were being permitted, it might therefore be possible that the pressures during partial adapter mobility would be lower than they were observed. This, in turn, would also affect the ANOVA, as the differences in in-socket pressures from dynamic set-ups compared to the static set-up would be greater than they actually were, so that some significant differences between set-ups may be found. Nevertheless, the current results are still extremely useful in that they provide an insight into the level of pressure reduction to expect in response to adapter mobility.

10.4.   Limitations

- This study measured the loads on only six sites on the residual limb, which meant that the pressures in areas of critical loading may not have been captured.

- Residual limb pressures measured during the current study were slightly affected by varying sizes and shapes of measuring sites, but it may be possible to change this, by using sensors that are not affected by the size of the applied load.

- This study only captured forces perpendicular to the sensor surface and residual limb tissues, whereas shear forces are also known to be important factors that contribute to vessel occlusion and tissue damage.

- Determining the position of segments in space will remain relatively inaccurate as long as skin-mounted markers are being used due to inherent skin movement artefacts, which were unavoidable during the current study, because bone-mounted markers were, from an ethical point of view, unacceptable.

- The adapter appeared to jam when permitting only one type of motion, either rotation or translation, thus reducing the magnitude of motion compared to when the adapter was fully unlocked.

- Although it was difficult to find suitable amputees that matched all of the essential selection criteria, it would have given the results greater statistical power if the total number of recruited subjects was greater than ten.

- As none of the subjects who participated in the current study had previously used a motion adapter in their own prostheses, it would have been beneficial if they had the chance to get more accustomed with such a device prior to the actual tests.

- Walking in a straight line, as the recruited subjects did, represents only a small part of daily walking, which means that other activities, including turning corners and managing stairs and slopes, should also be tested, but this can be difficult due to limitations in camera set-ups within a constrained gait laboratory environment.

- Longitudinal gait data, like, for instance, walking for several minutes, would increase the number of gait cycles and quality of gait data obtained from each amputee, thus possibly providing greater insight into the effects of motion adapters on amputee gait.

- Incorporating a motion adapter in trans-tibial prostheses with a more standard socket design like, for instance, a PTB socket would make results from gait laboratory tests applicable to a larger group of amputees and not just those with specialised prostheses for high activity levels.

- The current study is cross-sectional in that it only provides a snapshot of the effects that the motion adapter has on the recruited subjects' gait, but it has not considered long-term clinical benefits.

CHAPTER 11.   <u>CONCLUSIONS</u>

This Chapter reports on general conclusions that were drawn with regard to all relevant aspects involved in completing the described investigation. This part of the thesis consists of three main Sections. The first Section focuses on specific conclusions in relation to the aims and objectives of the study. Subsequent to this follows a Section that highlights the innovations of this research project. Finally the Chapter finishes with a brief description of areas that may need to be investigated further and on which future work could focus.

11.1.   <u>Specific conclusions</u>

Considering that manufacturers of prosthetic hardware constantly introduce new components, it is worthwhile exploring whether any innovations in hardware improve amputee gait and reduce the chances of damage to residual limb tissues. This is the primary rationale for buying such hardware. The current study sought to assess the role of one aspect of hardware innovation, namely compliant elements that allow transverse rotation and longitudinal translation between the socket and the prosthetic foot in relation to the three main objectives of this study. Below is a list of the three main findings from the current investigation:

- Gait patterns were affected in a multitude of ways due to adapter mobility, whereby the greatest effects occurred in early stance phase peak vertical GRFs. These were reduced, delayed or both for the sound and amputated side, which can be attributed to partial or full adapter mobility and subsequent changes in knee and hip angles, thus indicating a beneficial decrease in loads applied onto the body.

- When completely unlocking the adapter, the socket internally rotated and moved distally in the first part of stance phase, and externally rotated and moved proximally during late stance phase relative to the prosthetic foot. The pattern of transverse rotation was similar to that of non-amputees, although the magnitude

was smaller, which meant that the lower limb could undergo more natural movements and the loading rates were reduced.

- Despite a lack of statistically significant findings regarding in-socket pressures, the general tendency that could be determined from all six measuring sites was that by fully allowing the adapter to move, the pressures exerted onto the residual limb tissues were reduced. This was particularly so on those landmarks where the largest peak readings were found, thus decreasing the likelihood for vascular occlusion.

11.2.   Innovations

- Despite a number of studies that investigated the effect of motion adapters on amputee gait, the majority of published literature focused on determining general gait parameters and only a few have reported on the magnitudes and patterns of motions that take place at the adapter itself. This means that the current study is therefore the first to fully quantify displacements within a motion adapter.

- Prior to the current investigation, no study has previously described the separate effects of transverse rotation and longitudinal translation on amputee gait. The current investigation has demonstrated that both are likely to contribute to maximising the benefit for amputees.

- The current investigation is the first to quantify the beneficial effects of the motion adapter on the actual residual limb-socket interface. The findings indicate that there is a reduced potential for tissue related clinical complications.

- The current study has designed and developed a cam mechanism for measuring the two different types of small motions at the adapter. The device was capable of decoupling both displacements, so that simultaneous yet independent and accurate motion capture could take place.

11.3.   Future work

The purpose of this study was to determine whether or not permitting motion at the adapter would affect amputees' gait parameters, change the kinematics at the adapter and reduce the loads on the residual limb. The next step in this process would be to conduct clinical trials in order to establish if the relative motion between the socket and

the prosthetic foot has, from a clinical perspective, positive long-term effects on the residual limb tissues, for example a reduction in the incidence of residual limb complications. In order that an understanding and evidence base to practice is advanced, further and more in depth studies in this field should focus on the following issues:

- Measuring devices for monitoring amputees' socket displacements and in-socket pressures over prolonged periods of time should be smaller. This would make the test-prostheses feel and appear as normal as possible for daily wear.

- Measuring the pressure on only six sites limits the picture regarding the pressure distribution across the residual limb surface. In turn, more detailed information could be obtained if flexible arrays of sensors were used that conform to the residual limb's topography.

- In-socket pressure sensors should be permanently embodied inside the socket of test-prostheses. Alternatively, in case the recruited subjects were to wear gel liners, then it may be possible to interweave pressure sensors within the liner's pliable material itself, which would make donning and doffing of the limb very easy.

- It may prove useful to locate additional sensors against the residual limb for measuring electromyographic (EMG) signals. These could then be used to identify possible interactions between the extent of muscle contractions within the residual limb and the pressure distribution on the tissues while alternatingly permitting and restricting adapter motions.

- Despite appropriate amounts of lubrication, the torsion rod seemed unable to fully overcome the resistance between the adapter housing and shin tube, and this prevented the motion adapter from completely returning back to its neutral state after transverse rotation. Therefore, future work would seek to identify the reason why such a recoiling action from the adapter was not entirely achieved and implement appropriate design changes.

- Because of previously described limitations when conducting tests with the TT Pylon, it can be concluded that future studies in this field would benefit from incorporating a different type of motion adapter. That way it may be possible to completely isolate individual adapter displacements without these being affected by the restricted movement.

- Incorporating a motion adapter in different types of prostheses for various levels of amputation, would provide a greater variety of test conditions. This would give an insight into the gait of a larger spectrum of amputees than was achieved with the current study.

- Conducting controlled, long-term gait tests would be advantageous to establish whether the incorporation of a motion adapter is beneficial for the condition of residual limb tissues in amputees with impaired blood circulation. The reason for this is because these, rather than just trauma cases, make up the majority of people who require prostheses.

- Future work would attempt to measure shear in addition to forces. This would provide a more complete picture of the biomechanics at the residual limb-socket interface.

APPENDICES

Appendix 1.   Consultants' approval for recruitments

<u>THE EFFECT OF TORQUE ABSORBERS AND TORQUE-SHOCK ABSORBERS ON THE GAIT OF TRANS-TIBIAL AMPUTEES</u>

I am writing to inform you that the investigators of this study would like to ask a few of your patients, whose details are given below, to participate in the above project. In order for those patients to participate, it will be necessary to obtain their consent.

Please find enclosed the patient information sheet describing the project, which aims to establish the effect of torque absorbers, shock absorbers and torque-shock absorbers on the gait of trans-tibial amputees. As you will notice the project does not interfere with the patients' ongoing treatment at the Manchester DSC and no particular medical problems or considerations are anticipated during this investigation.

If you think that these patients are suitable for participation in this project could you please sign the patients' covering letters so I can post them? I take it that patients whose covering letters you have not signed are not suitable for the trials.

Thank you very much for your help and please, do not hesitate to contact me if you have further queries.

Appendix 2.   <u>Invitation for potential subjects</u>

We would like to invite you to participate in gait laboratory tests at the University of Salford. The Manchester DSC is collaborating with the University of Salford for this study. The nature of the study and the process of the tests are explained in the attached INFORMATION SHEET. Participation in the tests is voluntary and travelling expenses incurred for participation in the tests will be reimbursed.

If you agree to take part in the trials, please sign the CONSENT FORM and tick the appropriate box below. Please use the pre-paid envelope to send both the section below and the CONSENT FORM back. If you decide not to take part in the tests, we would appreciate if you could tick the appropriate box below and send that section off, so we do not have to contact you for further arrangements.

If you have any queries please, do not hesitate to contact Martin Twiste, your prosthetist, your consultant or XXX for independent advice.

✂ ---

◯   I, XXX, **would like** to participate in the gait laboratory tests.

◯   I, XXX, **would not like** to participate in the gait laboratory tests.

Appendix 3.   Recruitment information for subjects

Introduction

In below-knee prostheses, the socket, which retains the residual limb, is usually connected directly to the prosthetic foot using a rigid shin tube. This means that there are no relative movements between the socket and the prosthetic foot. We assume that movements between the residual limb and the socket, however, cause friction, which can lead to tissue irritation and skin breakdown.

Torque absorbers, shock absorbers and torque-shock absorbers are prosthetic components that are inserted between the socket and the prosthetic foot to allow relative movements between the socket and the prosthetic foot. As a result, this is supposed to reduce the friction between the residual limb and the socket.

We would like to invite you to help us test the effect of torque absorbers, shock absorbers and torque-shock absorbers. We wish to establish if the incorporation of these prosthetic components in below-knee prostheses will reduce friction between the residual limb and the socket. Tests were already conducted with above-knee amputees who tested similar prosthetic components. The results showed that with the incorporation of these components in the prosthesis, motion between the residual limb and the socket was reduced. There are also a number of below-knee and above-knee amputees attending the Manchester DSC who already have had these components prescribed.

What will I have to do if I take part?

If you agree to take part it will be necessary for the investigator, who is a qualified prosthetist, to take a cast of your residual limb. For the tests you would be given a test-prosthesis with a socket, which will be manufactured from that cast and will have the same characteristics as your own socket to give you maximum comfort. This means that your own prosthesis will not be required for the tests. Reflective markers will be attached with double-sided tape to your pelvis and both the thighs, to the shin and foot of the non-amputated side and to the shin and foot of the test-prosthesis.

The tests will be conducted in a gait laboratory at the University of Salford and will take approximately four hours. You will be asked to walk along a path of approximately ten

meters. While you are walking, recordings will be taken, which capture the location of the markers. In between trials, you will have the opportunity to rest, while prosthetic components between the socket and the prosthetic foot of the test-prosthesis are exchanged. Once the tests are completed, the markers will be removed and you can wear your own prosthesis again. You will only be required to attend the University twice, first for measuring and casting and a second time for the tests.

What are the possible risks of taking part?

The test-prosthesis will have a socket with the same characteristics as the socket of your own prosthesis. However, because different types of prosthetic components will be attached to the socket of the test-prosthesis, walking with it may feel slightly different to walking with your own prosthesis. All the connections between prosthetic components will be tightened up to maximise safety from the test-prosthesis. If your consultant is concerned at any time, then he or she will withdraw you from the study.

Are there any possible benefits?

It is hoped that the incorporation of torque absorbers, shock absorbers and torque-shock absorbers will allow the socket to move with the residual limb. The information that we obtain from the study will help us gain some knowledge about optimising the prescription of prostheses for below-knee amputees in order to prevent tissue irritation and breakdown, and therefore to improve amputees' mobility and quality of life. A summary of your results will be filed in your DSC care notes.

Do I have to take part?

No, taking part is voluntary. If you would prefer not to take part you do not have to give a reason. Your consultant would not be upset and your treatment would not be affected. If you agree to take part, but later change your mind you can withdraw at any time from the study without hindrance or detriment to your future treatment. The investigator organising the study may inspect your medical records and the data other than your personal details may be given to prosthetic regulatory authorities. Also, your consultant will have to give consent prior to your participation in the tests.

What do I do now?

In case your consultant agrees for you to participate in the tests, an appointment will be arranged at your convenience for you to attend at the University of Salford where

measurements and a cast will be taken of your residual limb. Once the test-prosthesis is manufactured the investigator will make an appointment for you to attend at the University of Salford for the tests. If you have any questions, please do not hesitate to ask your investigator, prosthetist or your consultant and let them know if you are interested in taking part.

Thank you very much for considering taking part in our research. Please discuss this information with your family, friends or consultant if you wish. If you want to obtain independent advice about this research you may contact XXX.

Appendix 4. Consent form to be signed by subjects

○ I confirm that I have read and understand the information sheet and have had the opportunity to ask questions.

○ I understand that my participation is voluntary and that I am free to withdraw at any time, without giving any reason and without my medical care or legal rights being affected.

○ I understand that sections of any of my medical notes may be examined by responsible individuals from the Manchester DSC or from regulatory authorities if this is relevant to my taking part in research. I give permission for these individuals to have access to my records.

○ I agree that the investigator may withdraw me from the study in the interests of my health or welfare.

○ I have been informed of any compensation arrangements that have been made.

○ I understand that my participation in this study is conditional upon the agreement of my consultant and I give permission for the investigator of this study to contact my consultant.

○ I have had enough time to think about the study, talk to relatives and friends about it and I agree to take part in the above study.

Appendix 5.   Consent for using Figure 5.21

Written consent obtained from Mickelborough 2001

The University of Salford Salford Greater Manchester M6 6PU UK www.salford.ac.uk
Telephone 0161 295 2270 Facsimile 0161 295 2302
E-mail s.hutchins@salford.ac.uk
Steve Hutchins
Director
Directorate of Prosthetics & Orthotics

Mr M Twiste
University of Salford
Centre for Rehabilitation and Human Performance Research
Brian Blatchford Building
Frederick Road
Salford

Thursday, 12 June 2003

Dear Martin,

Re: Reproduction of Figure 3.9, Error vectors for COP, from my PhD Thesis "The biomechanics of gait initiation in normal elderly people and in patients with higher-level gait disorders associated with cerebral multi-infarct states" The University of Manchester, 2001

With regard to your request to reproduce the above figure in your PhD Thesis, I hereby give permission for you to use this figure, subject to the source being fully acknowledged.

Regards

Jane Mickelborough MCSP PhD.
Research Fellow
Centre for Rehabilitation and Human Performance Research
University of Salford
Frederick Road
Salford M6 6PU

J.Mickelborough@salford.ac.uk
Tel 0161 295 3487

THE QUEEN'S
ANNIVERSARY PRIZES
FOR HIGHER AND FURTHER EDUCATION
2000

Faculty of Health Care and Social Work Studies
School of Health Care Professions

Appendix 6. Questionnaire to be completed by subjects

A questionnaire for determining set-up satisfaction

Questionnaire

Please mark a vertical line where appropriate for each of the four set-ups

No rotation and no shock absorption

Satisfied   Unsatisfied

+10   +5   0   -5   -10

Rotation but no shock absorption

Satisfied   Unsatisfied

+10   +5   0   -5   -10

No rotation but shock absorption

Satisfied   Unsatisfied

+10   +5   0   -5   -10

Rotation and shock absorption

Satisfied   Unsatisfied

+10   +5   0   -5   -10

<u>REFERENCES</u>

Barth F, Mühlbauer P, Nikol F, Wörle K. In: Mathematische Formeln und Definitionen. *4. Auflage München: Bayerischer Schulbuch-Verlag*; 1985.

Beil TL, Street GM, Covey SJ. Interface pressures during ambulation using suction and vacuum-assisted prosthetic sockets. *J Rehab Res Dev* 2002;39(6):693-700.

Bennett L, Kavner D, Lee BK, Trainor FA. Shear vs pressure as causative factors in skin blood flow occlusion. *Arch Phys Med Rehabil* 1979;60:309-14.

Blakinston's pocket medical dictionary. *5th ed. New York: McGraw-Hill Inc*; 1980.

Blumentritt S. A new biomechanical method for determination of static prosthetic alignment. *Prosthet Orthot Int* 1997;21:107-13.

Blumentritt S, Scherer HW, Wellerhaus U, Michael JW. Design principles, biomechanical data and clinical experience with a polycentric knee offering controlled stance phase knee flexion: a preliminary report. *J Prosthet Orthot* 1997;9(1):18-24.

Board WJ, Street GM, Casper C. A comparison of trans-tibial amputee suction and vacuum socket conditions. *Prosthet Orthot Int* 2001;25(3):202-9.

Boonstra AM, Duin van W, Eisma W. Silicone suction socket (3S) versus supracondylar PTB prosthesis with pelite liner: transtibial amputees' preference. *J Prosthet Orth* 1996;8(3):96-9.

Boonstra AM, Fidler V, Spits GMA, Tuil P, Hof AL. Comparison of gait using a Multiflex foot versus a Quantum foot in knee disarticulation amputees. *Prosthet Orthot Int* 1993;17:90-4.

Buchold G. Der Multiflex-Fuß: erste klinische Erfahrungen. *Med Orthop Tech* 1991;111:96-9.

Buckley JG, Jones FJ, Birch KM. Oxygen consumption during ambulation: comparison of using a prosthesis with and without a tele-torsion pylon. *Arch Phys Med Rehab* 2002;83:576-81.

Brånemark R, Brånemark P-I, Rydevik B, Myers RR. Osseointegration in skeletal reconstruction and rehabilitation. *J Rehab Res Dev* 2001;38(2):175-81.

Cappozzo A. Three-dimensional analysis of human walking: experimental methods and associated artefacts. *Hum Mov Sci* 1991;10:589-602.

Cappozzo A, Berme N, Meglan D. Rigid body mechanics as applied to human movement studies: kinematics. In: Biomechanics of Human Movement: applications in Rehabilitation, Sports and Ergonomics. Berme N, Cappozzo A, editors. *Worthington: Bertec Corporation*; 1990:89-102.

Cappozzo A, Camomilla V, Donati M. High resolution human movement analysis. In: Nester C, Kenney L, editors. *Proceedings of the Conference of Biomechanics of the Lower Limb in Health, Disease and Rehabilitation;* 2003 Sep 1-3; Salford, UK. ISBN: 0-902896-51-2 p. 4-5.

Cappozzo A, Catani F, Della Croce U, Leardini A. Position and orientation in space of bones during movement: anatomical frame definition and determination. *Clin Biomech* 1995;10(4):171-8.

Cappozzo A, Catani F, Leardini A, Benedetti MG, Della Croce U. Position and orientation in space of bones during movement: experimental artefacts. *Clin Biomech* 1996;11(2):90-100.

Carlsson T. Applications of silicone sockets. *BACPAR Newsletter* 1997;6:10.

Casillas J-M, Michel C, Aurelle B, Becker F, Marcer I, Schultz S, Didier J-P. Transcutaneous oxygen pressure: an effective measure for prosthesis fitting on below-knee amputations. *Am J Phys Med Rehabil* 1993;72:29-32.

Chakraborty JK, Patil KM. A new modular six-bar linkage transfemoral prosthesis for walking and squatting. *Prosthet Orthot Int* 1994;18:98-108.

Chaudry KK, Guha SK, Verma SK. An improved above-knee prosthesis with functional versatility. *Prosthet Orthot Int* 1982:6:157-60.

Convery P, Buis AWP. Conventional patellar-tendon-bearing (PTB) socket/stump interface dynamic pressure distributions recorded during the prosthetic stance phase of gait of a trans-tibial amputee. *Prosthet Orthot Int* 1998;22:193-8.

Cook SD, Kester MA, Brunet ME. Shock absorption characteristics of running shoes. *Am J Sports Med* 1985;13:248-53.

Cunado D, Nixon MS, Carter JN. Automatic extraction and description of human gait models for recognition purposes. *Comput Vis Image Underst* 2003;90:1-41.

Craig JJ. In: Introduction to robotics: mechanics and control. *2nd ed. Reading: Addison-Wesley Publishing Company*; 1989.

Daniel DM, Malcom LL, Losse G, Stone ML, Sachs R, Burks R. Instrumented measurement of anterior laxity of the knee. *J Bone Joint Surg* 1985;67(5):720-6.

De Leva P. Joint centre longitudinal positions computed from a selected subset of Chandler's data. *J Biomech* 1996;29(9):1231-3.

De Leva P. Adjustments of Zatsiorsky-Seluyanov's segment inertia parameters. *J Biomech* 1996;29(9):1223-30.

DiAngeleo DJ, Winter DA, Ghista DN, Newcombe WR. Performance assessment of the Terry Fox jogging prosthesis for above-knee amputees. *J Biomech* 1989;22(6/7):543-58.

Durward BR, Baer GD, Rowe PJ. In: Functional human movement: measurement and analysis. *Oxford: Butterworth Heinemann*; 1999.

Edelstein JE. Current choices in prosthetic feet. *Crit Rev in Phys Rehab Med* 1991;2:213-26.

Engsberg JR, Springer MJN, Harder JA. Quantifying interface pressures in below-knee-amputee sockets. *J Assoc Child Prosthet Orthot Clin* 1992;27:81-8.

Esquenazi A, Torres MM. Prosthetic feet ankle mechanisms. *Phys Med Rehabil Clin North Am* 1991;2(2):299-309.

Everaert DG, Spaepen AJ, Wouters MJ, Stappaerts KH, Oostendorp RA. Measuring small linear displacements with a three-dimensional video motion analysis system: determining its accuracy and precision. *Arch Phys Med Rehabil* 1999;80(9):1082-9.

Fergason JR, Boone DA. Custom design in lower limb prosthetics for athletic activity. *Phys Med Rehabil Clin North Am* 2000;11,681-99.

Ferguson-Pell M, Hagisawa S, Bain D. Evaluation of a sensor for low interface pressure applications. *Med Eng Phys* 2000;22:657-63.

Fillauer CE, Pritham CH, Fillauer KD. Evolution and development of the Silicone Suction Socket (3S) for below-knee prostheses. *J Prosthet Orthot* 1989;1(2):92-103.

Fisher LD, Judge GW. Bouncy knee: a stance phase flex-extend knee unit. *Prosthet Orthot Int* 1985;9:129-36.

Fisher LD, Lord M. Bouncy knee in semi-automatic knee lock prosthesis. *Prosthet Orthot Int* 1986;10:35-9.

Gard SA, Childress DS, Uellendahl JE. The influence of four-bar linkage knees on prosthetic swing-phase floor clearance. *J Prosthet Orthot* 1996;8(2):34-40.

Gard SA, Konz RJ. The effect of a shock-absorbing pylon on the gait of persons with unilateral transtibial amputation. *J Rehab Res Dev* 2003;40(2):109-24.

Gard SA, Konz RJ. The influence of prosthetic shock absorbing pylons on transtibial amputee gait (abstract). *Gait Posture* 2001;13:303.

Gailey RS, Lawrence D, Burditt C, Spyropoulos C, Newell C, Nash MS. The CAT-CAM socket and quadrilateral socket: a comparison of energy cost during ambulation. *Prosthet Orthot Int* 1993;17:95-100.

Goh JCH, Solomonidis SE, Spence WD, Paul JP. Biomechanical evaluation of SACH and uniaxial feet. *Prosthet Orthot Int* 1984; 8:147-54.

Greene MP. Four bar linkage knee analysis. *Orth and Pros* 1983;37:15-24.

Hardt DE, Mann RW. A five body - three dimensional dynamic analysis of walking. *J Biomech* 1980;13:455-7.

Heim M, Wershavski M, Zwas ST, Sievner I, Nadvorna H, Azaria M. Silicone suspension of external prostheses: a new era in artificial limb usage. *J Bone Joint Surg* 1997; 79B(4):638-40.

Hsu M-J, Nielsen DH, Yack HJ, Schurr DG. Physiological measurements of gait during walking and running in trans-tibial amputees with conventional versus energy storing-releasing prosthesis (abstract). *Phys Ther* 1997;77(5):45.

Hsu M-J, Nielsen DH, Yack HJ, Schurr DG. Physiological measurement of walking and running in people with transtibial amputations with 3 different prostheses. *J Orthop Sports Phys Ther* 1999;29(9):526-33.

Hsu M-J, Nielsen DH, Yack J, Schurr DG, Lin S-J. Physiological comparisons of physically active persons with transtibial amputation using static and dynamic prostheses versus persons with nonpathological gait during multiple-speed walking. *J Prosthet Orthot* 2000;12(2),60-7.

Inman VT, Mann RA. In: DuVries' surgery of the foot. *St Louis: Mosby*; 1978.

Jøergensen U, Bojesen-Møller F. Shock absorbency of factors in the shoe/heel interaction - with special focus on role of the heel pad. *Foot Ankle* 1989;9(11):294-9.

Kadaba MP, Ramakrishnan HK, Measurement of lower extremity kinematics during level walking. *J Orthop Res* 1990;8(3):383-92.

Kaphingst W. Torsionseinheiten in Beinprothesen. *Orthop Tech* 1977;28:85-7.

Ker RF, Bennett MB, Bibby SR, Kester RC, Alexander RMcN. The spring in the arch of the human foot. *Nature* 1987;325(8):147-9.

Kinoshita H, Ogawa T, Arimoto Kkuzuhara K, Ikuta K. Shock absorbing characteristics of human heel properties (abstract). *J Biomech* 1992;25:806.

Knoche W. Welche Vorteile bringt der Einbau eines Torsionsadapters in Beinprothesen? (Erfahrungsbericht über die Otto-Bock-Torsionsadapter 4R39 und 4R40). *Orthop Tech* 1979;30:12-4.

Kristinsson Ö. The ICEROSS concept: a discussion of a philosophy. *Prosthet Orthot Int* 1993;17(1),49-55.

Lafortune MA, Cavanagh PR, Sommer HJ, Kalenak A. Foot inversion-eversion and knee kinematics during walking. *J Orthop Res* 1994;12:412-20.

Lamoureux LW, Radcliffe CW. Functional analysis of the UC-BL shank axial rotation device. *Prosthet Orthot Int* 1977;1:114-8.

Levens AS, Inman VT, Blosser JA. Transverse rotation of the segments of the lower extremity in locomotion. *J Bone and Joint Surg* 1948;30-A(4):859-72.

Linden van der M. Biomechanical and physiological effects of various prosthetic feet on amputee gait. *PhD thesis*, University of Strathclyde, Glasgow UK; 1999.

Linden van der M, Twiste M, Rithalia SVS. The biomechanical effects of the inclusion of a torque absorber and type of knee units on trans-femoral amputee gait. *Prosthet Orthot Int* 2002;26:35-43.

Lundberg A, Svensson OK, Németh G, Selvik G. The axis of rotation of the ankle joint. *J Bone Joint Surg* 1989;71-B:94-9.

Mak AFT, Zhang M, Boone DA. State-of-the-art research in lower-limb prosthetic biomechanics-socket interface. *J Rehab Res Dev* 2001;38(2):161-74.

Manter JT. Movements of the subtalar and transverse tarsal joints. *Anat Rec* 1941;80(4):397-410.

Martel G. Terry Fox running prosthesis - the prosthetist's vista. *Proceedings of the 5th World Congress of the International Society for Prosthetics & Orthotics*; 1986 Jun 29-Jul 04; Copenhagen, Denmark. p. 389-93.

Mayagoitia RE, Nene AV, Veltink PH. Accelerometer and rate gyroscope measurement of kinematics: an inexpensive alternative to optical motion analysis systems. *J Biomech* 2002;35(4):537-42.

May BJ. In: Amputations and Prosthetics - a case study approach. *Philadelphia: FA Davis Company;* 1996.

McPoil TG, Knecht HG. Biomechanics of the foot in walking: a functional approach. *J Orthop Sports Phys Ther* 1985;7:69-72.

Meglan D, Todd F. Kinetics of normal human walking. In: Human walking. Rose JR, Gamble JG, editors. *Baltimore: Williams & Wilkins;* 1994:73-99.

Meier RH, Meeks ED, Herman RM. Stump-socket fit of below-knee prostheses: comparison of 3 methods of measurement. *Arch Phys Med Rehabil* 1973;54:553-8.

Mickelborough J. The biomechanics of gait initiation in normal elderly people and in patients with higher-level gait disorders associated with cerebral multi-infarct states. *PhD thesis*, University of Manchester, Manchester UK; 2001.

Mickelborough J, Linden van der M, Richards J, Ennos AR. Validity and reliability of a kinematic protocol for determining foot contact events. *Gait Posture* 2000;11:32-7.

Miller L, Childress D. Vertical compliance in prosthetic feet: a preliminary investigation. *Proceedings of the 8th World Congress of the International Society for Prosthetics & Orthotics;* 1995 April 2-7; Melbourne, Australia. p. 217.

Miller LA, Childress DS. Analysis of a vertical compliance prosthetic foot. *J Rehabil Res Dev* 1997;34(1),52-7.

Mulby WC, Radcliffe CW. An ankle-rotation device for prostheses. *Biomechanics Laboratory, University of California, San Francisco and Berkeley* 1960; Tech. Rep. 37.

Nack JD, Phillips RD. Shock absorption. *Clin Podiatr Med Surg* 1990;7(2):391-7.

Narita H, Yokogushi K, Shii S, Kakizawa M, Nosaka T. Suspension effect and dynamic evaluation of the total surface bearing (TSB) trans-tibial prosthesis: a comparison with the patellar tendon bearing (PTB) trans-tibial prosthesis. *Prosthet Orthot Int* 1997;21:175-8.

Nester C. The relationship between transverse plane leg rotation and transverse plane motion at the knee and hip during normal walking. *Gait and Posture* 2000;12:251-6.

Nester CJ, Linden van der ML, Bowker P. Some effects of foot orthoses on joint motion and moments, and ground reaction forces. In: Kenney L, Mickelborough J, Nester C, Rithalia S, editors. *Proceedings of the Conference of Biomechanics of the Lower Limb in Health, Disease and Rehabilitation*; 2001 Sep 10-12; Salford, UK. ISBN: 0-902896-29-6 p. 134-5.

Nester C, Bowker P, Bowden P. Kinematics of the midtarsal joint during standing leg rotation. *J Am Podiatr Med Assoc* 2002;92(2):77-81.

Nester CJ, Findlow AF, Bowker P, Bowden P. Transverse plane motion at the ankle joint. *Foot Ankle Int* 2003;24(2):164-8.

Nigg BM. Inertial properties of the human or animal body. In: Biomechanics of the musculo-skeletal system. Nigg BM, Herzog W, editors. *Chichester: John Wiles & Sons Ltd*; 1994:337-64.

Noe DA, Voto SJ, Hoffman MS, Askew MJ, Gradisar IA. Role of the calcaneal heel pad and polymeric shock absorbers in attenuation of heel strike impact. *J Biomed Eng* 1993;15:23-6.

Oxford English Dictionary. *Oxford University Press.* 2003.

Quesada PM, VanNess WC, Rash GS, Williamson J. Below-knee amputee golf swing kinematics (abstract). *Gait Posture* 2000;11:160-1.

Radcliffe CW. Prosthetic knee mechanisms for above-knee amputees. In: Murdoch G, editor. Prosthetic and orthotic practical. *London: Edward Arnold & Co*; 1970:225-49.

Radcliffe CW. Above-knee prosthetics. *Prosthet Orthot Int* 1977;1:146-60.

Radcliffe CW. Four-bar linkage prosthetic knee mechanisms: kinematics, alignment and prescription criteria. *Prosthet Orthot Int* 1994;18:159-73.

Radcliffe CW, Foort J. The Patellar-Tendon-Bearing Below-Knee Prosthesis. *Berkeley, CA: University of California.* 1961;168-80.

Ramakrishnan HK, Kadaba MP. On the estimation of joint kinematics during gait. J Biomech 1991;24(10):969-77.

Reischl SF, Powers CM, Rao S, Perry J. Relationship between foot pronation and rotation of the tibia and femur during walking. *Foot Ankle Int* 1999;20(8):513-20.

Richards JG. The measurement of human motion: a comparison of commercially available systems. *Hum Mov Sci* 1999;18:589-602.

Ross J, Luff R, Ledger M. Study of telescopic pylon on lower limb amputees. *Orthop Tech, quarterly English edition* 2003;3:1-4.

Ross J, McLaren A. A clinical evaluation of vertical shock absorption for transfemoral amputees. *Proceedings of the 10th World Congress of the International Society for Prosthetics & Orthotics;* 2001 July 1-6; Glasgow, UK. p. THO1.4.

Rowntree D. In: Statistics without tears - a primer for non-mathematicians. *London: Penguin Books*; 1981.

Sanders JE. Interface mechanics in external prosthetics: review of interface stress measurement techniques. *Med Biol Eng Comput* 1995;33:509-16.

Sanders JE, Daly CH. Measurement of stresses in three orthogonal directions at the residual limb-prosthetic socket interface. *IEEE Trans Rehabil Eng* 1993;1:79-85.

Schmidl H. Torsionsadapter im Kunstbein aus der Sicht des Technikers und des Amputierten. *Orthop Tech* 1979;30:35-8.

Schuch M. Dynamic alignment options for the Flex-Foot™. *J Prosthet and Orthot* 1989;1(1):37-40.

Seidel GK, Marchinda DM, Dijkers M, Soutas-Little RW. Hip joint center location from palpable bony landmarks - a cadaver study. *J Biomech* 1995;28(8):995-8.

Sepin W. 3-S silicon suction socket - Eine Versorgungsmethode für Unterschenkelamputierte (the 3-S silicon suction socket - a special fitting technique for below-knee amputees). *Orthop Tech* 1993;44:594-7.

Shames IH. In: Engineering mechanics - statics and dynamics. *S I unit ed. London: Prentice-Hall International Inc*; 1970.

Shem KL, Breakey JW, Werner PC. Pressures at the residual limb-socket interface in transtibial amputes with thigh lacer-side joints. *J Prosthet Orthot* 1998;10(3):51-5.

Silver-Thorn MB, Dudley S, Childress DS. Parametric analysis using the finite element method to investigate prosthetic interface stresses for persons with trans-tibial amputation. *J Rehabil Res Dev* 1996;33:227-38.

Silver-Thorn MB, Steege JW, Childress DS. A review of prosthetic interface stress investigations. *J Rehabil Res Dev* 1996;33:253-66.

Simpson D, Convery P. Aspects of prosthetic socket design. *BACPAR Newsletter* 1997;6:8-9.

Sonck WA, Cockrell JL, Koepke GH. Effect of liner materials on interface pressures on below-knee prostheses. *Arch Phys Med Rehabil* 1970;51:666-9.

Subotnick SI. Biomechanics of the subtalar and midtarsal joint. *J Am Podiatr Assoc* 1975;65(8):756-64.

Sutherland DH, Kaufman KR, Moitoza JR. Kinematics of normal human walking. In: Human walking. Rose JR, Gamble JG, editors. *Baltimore: Williams & Wilkins;* 1994:23-44.

Staros A, Peizer E. Veterans Administration Prosthetics Centre Research Report. *Bull Pros Res* 1972;10(18):223-53.

Staros A, Peizer E. Veterans Administration Prosthetics Centre Research Report. *Bull Pros Res* 1973.19(19):146-188.

Stauf C. Untersuchung der Prothesen-Rotationsstoßdämpfer OS1 und US1 im Rahmen einer Biomechanik-Studie. *Orthop Tech* 2000;51:267-74.

Stein JL, Flowers WC. Stance-phase control of above-knee prostheses: knee control versus SACH foot design. *J Biomech* 1987; 20:19-28.

Thomsen W. Gelöste und ungelöste Fragen und Forderungen beim Bau von Kunstfüßen. *Orthop Tech* 1959;5:117-9.

Tortora GJ. In: Principles of human anatomy. *6th ed. New York: HarperCollins*; 1992.

Trew M, Everett T. In: Human movement: an introductory text. *4th ed. London: Churchill Livingstone*; 2001.

Trieb K, Lang T, Stulnig T, Kickinger W. Silicone soft socket system: its effect on the rehabilitation of geriatric patients with transfemoral amputations. *Arch Phys Med Rehabil* 1999;80:522-5.

Twiste M, Linden van der ML, Rithalia S. The effect of a torque absorber on prosthetic knee joints. *Proceedings of the 10th World Congress of the International Society for Prosthetics & Orthotics;* 2001 July 1-6; Glasgow, UK. p. THO1.5.

Twiste M, Rithalia SVS. Transverse rotation and longitudinal translation during prosthetic gait - a literature review. *J Rehab Res Dev* 2003;40(1);9-18.

Twiste M, Rithalia SVS, Kenney L. An electromechanical device for measuring intersegmental prosthetic motion. In: Nester C, Kenney L, editors. *Proceedings of the Conference of Biomechanics of the Lower Limb in Health, Disease and Rehabilitation;* 2003 Sep 1-3; Salford, UK. ISBN: 0-902896-51-2 p. 14-5.

Twiste M, Rithalia S, Linden van der ML. Investigation into torque absorber and prosthetic knee joints in transfemoral gait. In: Kenney L, Mickelborough J, Nester C, Rithalia S, editors. *Proceedings of the Conference of Biomechanics of the Lower Limb in Health, Disease and Rehabilitation;* 2001 Sep 10-12; Salford, UK. ISBN: 0-902896-29-6 p. 56-7.

Vandeven D. Versorgung von Amputierten mit maßgefertigen Silikonschäften unter Anwendung der zweiteiligen Vakuumtechnik (treatment of amputees with custom made silicone sockets by means of a double vacuum technique). *Orthop Tech* 1999;50:106-11.

VanNess WC, Quesada PM, Rash GS, Williamson J. Below-knee amputee golf swing kinematics (abstract). *Am J Phys Med Rehabil* 2000;79(2):208.

Veldpaus FE, Woltring HJ, Dortmans LJMG. A least-squares algorithm for the equiform transformation from spatial marker co-ordinates. *J Biomech* 1988;21(1):45-54.

Vitali M, Robinson KP, Andrews BG, Harris EE, Redhead RG. In: Amputations and Prostheses. *2nd ed. London: Bailière Tindall*; 1986.

Whittle MW. In: Gait analysis - an introduction. *Oxford: Butterworth-Heinemann Ltd;* 1991.

Williams PL, Warwick R, Dyson M, Bannister LH. In: Gray's anatomy. *37th ed. London: Churchill Livingstone;* 1989

Williams RB, Porter D, Roberts VC, Regan JF. Triaxial force transducer for investigating stresses at the stump/socket interface. *Med Biol Eng Comput* 1992;30:89-96.

Wosk J, Folman Y, Voloshin AS, Liberty S. Die Wirkung Stoßdämpfender Einlagen und Sohlen auf die axiale Belastung des Skeletts beim Fersenauftritt. *Med Orthop Tech* 1984;104:135-7.

Wu G. Kinematics theory. In: Craik RL, Oatis CA. Gait analysis - theory and application, editors. *St. Louis: Mosby;* 1995.

Wu G, Cavanagh PR. ISB recommendations for standardization in the reporting of kinematic data. *J Biomech* 1995;28(10):1257-61.

Yack HJ, Nielsen DH, Shurr DG. Kinetic patterns during stair ascent in patients with transtibial amputation using three different prostheses. *J Prosthet Orthot* 1999;11(3):57-62.

Zhang M, Roberts C. Comparison of computational analysis with clinical measurement of stresses on below-knee residual limb in a prosthetic socket. *Mech Eng and Phys* 2000;22:607-12.

PUBLICATIONS

Published material is listed in chronological order.

Academic publications

Twiste M. The effect of a torque absorber on various prosthetic knee joints. *MSc thesis*, University of Salford, Salford UK; 2000.

Peer-reviewed papers

Twiste M, Rithalia SVS, Kenney L. A cam-displacement transducer device for measuring bi-plane prosthetic motion. *Medical Engineering & Physics* 2004;26(4):335-40.

Twiste M, Rithalia SVS. Transverse rotation and longitudinal translation during prosthetic gait - a literature review. *J Rehab Res Dev* 2003,40(1);9-18.

Linden van der ML, Twiste M, Rithalia SVS. The biomechanical effects of the inclusion of a torque absorber and type of knee units on trans-femoral amputee gait. *Prosthet Orthot Int* 2002,26;35-43.

Abstracts of presentations

Twiste M, Rithalia SVS, Kenney L. An electromechanical device for measuring intersegmental prosthetic motion. In: Nester C, Kenney L, editors. *Proceedings of the Conference of Biomechanics of the Lower Limb in Health, Disease and Rehabilitation;* 2003 Sep 1-3; Salford, UK. ISBN: 0-902896-51-2 p. 14-5.

Twiste M, Rithalia S, Linden van der ML. Investigation into torque absorber and prosthetic knee joints in transfemoral gait. In: Kenney L, Mickelborough J, Nester C, Rithalia S, editors. *Proceedings of the Conference of Biomechanics of the Lower Limb in Health, Disease and Rehabilitation;* 2001 Sep 10-12; Salford, UK. ISBN: 0-902896-29-6 p. 56-7.

Paper presentations

Twiste M, Rithalia SVS, Kenney L. Displacement measurements at a torque-shock absorber during amputee gait. *The 11th World Congress of the International Society for Prosthetics & Orthotics*, 2004 Aug 1-6; Hong Kong, China (accepted).

Twiste M, Kenney L, Smith C, Rithalia SVS. Measuring intersegmental prosthetic motion during gait using a cam. *International Society of Biomechanics XIXth Congress*, 2003 Jul 6-11; Dunedin, New Zealand.

Twiste M, Kenney L, Rithalia SVS. A cam design for measuring displacement between prosthetic segments. *Seventh International Symposium on the 3-D Analysis of Human Movement*, 2002 Jul 10-12; Newcastle upon Tyne, UK.

Twiste M, Linden van der ML, Rithalia SVS. The effect of a torque absorber on prosthetic knee joints. *The 10th World Congress of the International Society for Prosthetics & Orthotics*, 2001 Jul 1-6; Glasgow, UK.

Twiste M, Rithalia SVS, Bowker P. The importance of transverse rotation during prosthetic gait. *Salford Postgraduate Annual Research Conference (SPARC)*, University of Salford, UK, 25-27 June 2001.

Twiste M, Linden van der ML, Rithalia SVS. What is the effect of torque absorber on prosthetic knee joints? *Sixth Annual Conference of the British Association of Prosthetists and Orthotists*, 2000 Mar 24-26; Glasgow, UK.